AUG 2 6 1981

982-D-23

TD 8.22:S.11/2

NHTSA Technical Report
DOT-HS-805 889

COMPLETED ORIGINAL
445

SIDE IMPACT SLED & PADDING DEVELOPMENT

February 1981

Prepared by

U.S. DEPARTMENT OF TRANSPORTATION
National Highway Traffic Safety Administration
Safety Research Laboratory
Washington, D.C. 20590

This document is disseminated under the sponsorship of the Department of Transportation in the interest of information exchange. The United States Government assumes no liability for its contents or use thereof.

BEST DOCUMENT AVAILABLE

Technical Report Documentation Page

1. Report No.	2. Government Accession No.	3. Recipient's Catalog No.
DOT-HS-805-889		

4. Title and Subtitle
SIDE IMPACT SLED & PADDING DEVELOPMENT

5. Report Date
February 1981

6. Performing Organization Code
NRD-52

7. Author(s)
Michael W. Monk, Lisa K. Sullivan

8. Performing Organization Report No.
SRL-17

9. Performing Organization Name and Address
Safety Research Laboratory
National Highway Traffic Safety Administration
P.O. Box 37
East Liberty, Ohio 43319

10. Work Unit No. (TRAIS)

11. Contract or Grant No.

12. Sponsoring Agency Name and Address
U.S. Department of Transportation
National Highway Traffic Safety Administration
Washington, D.C. 20590

13. Type of Report and Period Covered
FINAL
June 1979 - February 1981

14. Sponsoring Agency Code

15. Supplementary Notes

16. Abstract

A study was conducted to devise and fabricate a HYGE sled buck which could be used to simulate oblique side impact collisions. Once completed the buck was demonstrated by simulating the occupant and side door interactions of two separate laboratory car-to-car impacts. The degree of success of these two simulations is discussed.

Following the simulations, the sled buck was used to select padding materials which appeared promising for occupant protection in side impact collisions. The selection criteria and results are presented.

17. Key Words	18. Distribution Statement
Side Impact HYGE Sled Simulations Padding	Document is available to the U.S. public through the National Technical Information Service, Springfield, Virginia 22161

19. Security Classif. (of this report)	20. Security Classif. (of this page)	21. No. of Pages	22. Price
Unclassified	Unclassified	295	

Form DOT F 1700.7 (8-72) Reproduction authorized

BEST DOCUMENT AVAILABLE

METRIC CONVERSION FACTORS

Approximate Conversions to Metric Measures

Symbol	When You Know	Multiply by	To Find	Symbol
	LENGTH			
in	inches	*2.5	centimeters	cm
ft	feet	30	centimeters	cm
yd	yards	0.9	meters	m
mi	miles	1.6	kilometers	km
	AREA			
in^2	square inches	6.5	square centimeters	cm^2
ft^2	square feet	0.09	square meters	m^2
yd^2	square yards	0.8	square meters	m^2
mi^2	square miles	2.6	square kilometers	km^2
	acres	0.4	hectares	ha
	MASS (weight)			
oz	ounces	28	grams	g
lb	pounds	0.45	kilograms	kg
	short tons (2000 lb)	0.9	tonnes	t
	VOLUME			
tsp	teaspoons	5	milliliters	ml
Tbsp	tablespoons	15	milliliters	ml
fl oz	fluid ounces	30	milliliters	ml
c	cups	0.24	liters	l
pt	pints	0.47	liters	l
qt	quarts	0.96	liters	l
gal	gallons	3.8	liters	l
ft^3	cubic feet	0.03	cubic meters	m^3
yd^3	cubic yards	0.76	cubic meters	m^3
	TEMPERATURE (exact)			
°F	Fahrenheit temperature	5/9 (after subtracting 32)	Celsius temperature	°C

*1 in = 2.54 (exactly). For other exact conversions and more detailed tables, see NBS Misc. Publ. 286, Units of Weights and Measures, Price $2.25, SD Catalog No. C13.10:286.

Approximate Conversions from Metric Measures

Symbol	When You Know	Multiply by	To Find	Symbol
	LENGTH			
mm	millimeters	0.04	inches	in
cm	centimeters	0.4	inches	in
m	meters	3.3	feet	ft
m	meters	1.1	yards	yd
km	kilometers	0.6	miles	mi
	AREA			
cm^2	square centimeters	0.16	square inches	in^2
m^2	square meters	1.2	square yards	yd^2
km^2	square kilometers	0.4	square miles	mi^2
ha	hectares (10,000 m^2)	2.5	acres	
	MASS (weight)			
g	grams	0.035	ounces	oz
kg	kilograms	2.2	pounds	lb
t	tonnes (1000 kg)	1.1	short tons	
	VOLUME			
ml	milliliters	0.03	fluid ounces	fl oz
l	liters	2.1	pints	pt
l	liters	1.06	quarts	qt
l	liters	0.26	gallons	gal
m^3	cubic meters	35	cubic feet	ft^3
m^3	cubic meters	1.3	cubic yards	yd^3
	TEMPERATURE (exact)			
°C	Celsius temperature	9/5 (then add 32)	Fahrenheit temperature	°F

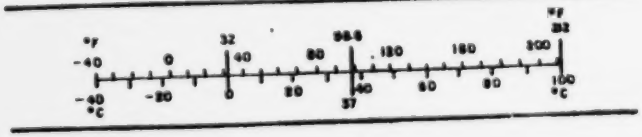

BEST DOCUMENT AVAILABLE

TABLE OF CONTENTS

		Page
	LIST OF TABLES	iii
	LIST OF FIGURES	iv
	LIST OF APPENDICES	vi
1.0	BACKGROUND	1
2.0	OBJECTIVES	1
3.0	PROJECT ELEMENT SUMMARY	2
4.0	PROJECT ELEMENT OVERVIEW	3
5.0	SIDE IMPACT SLED & PADDING DEVELOPMENT	9
5.1	RICSAC and Budd Cars and Data	9
5.2	New Dummy Computer Software	10
5.3	Prototype Side Impact Dummy	13
5.4	Analysis of RICSAC and Budd Test Data	14
5.5	Interior Door Crush Devices	26
5.6	Interior Door Crush Tests	37
5.7	Analysis of Dynamic Science Test	42
5.8	Definition of Interior Door Stiffness	49
5.9	Design and Fabrication of Sled Buck	52
5.10	HYGE Sled Simulation of Budd Test #11	56
5.11	HYGE Sled Simulation of Dynamic Science Test #8330-2	66
5.12	Review of Prior Padding Studies	77
5.13	Padding Component Tests	82
5.14	Padding Evaluation: HYGE Sled Tests	98
5.15	Tarriere Drop Tests	104
6.0	CONCLUSIONS AND RECOMMENDATIONS	105
	REFERENCES	107
	APPENDICES	

BEST DOCUMENT AVAILABLE

LIST OF TABLES

Table No.		Page
1	Interior Crush Test Matrix	38
2	Test Buck Parameter Variations Matrix for Budd Simulation	57
3	Budd Simulation Test Results	58
4	Test Buck Parameter Variations Matrix for DySci No. 8330-2 Simulation	69
5	DySci No. 8330-2 Simulation Test Results	70
6	List of Padding Materials	90
7	Component Level Phase I Test Results	91
8	Three-Point Padding Evaluation	94
9	Padding Materials for Component Level Phase II Tests	95
10	Component Level Phase II Test Results	97
11	HYGE Sled Padding Evaluation Test Results	99
12	Final Version/Prototype SID Comparison	102

BEST DOCUMENT AVAILABLE

LIST OF FIGURES

Figure No.		Page
1	Project Element Flow Chart	4
2	HSRI Data Processing Flow Chart	11
3	Budd Test No. 12 - Upper Door Acceleration	15
4	Crash Tests/Rigid Wall Comparison	17
5	Calspan Baseline Crash Test #5	18
6	Vehicle Accelerometer Placement Schematic	21
7	Force Direction By Film Analysis	22
8	RICSAC #2 Force Direction	23
9	Budd #7 Force Direction	23
10	Budd #4 Force Direction - Front	24
11	Budd #4 Force Direction - Rear	24
12	Budd #6 Force Direction - Front	25
13	Budd #6 Force Direction - Rear	25
14	Car-to-Car Impact Layout	27
15	Car-to-Car Holding Fixture	28
16	Upper Torso Body Form Drawing	30
17	Pelvis Body Form Drawing	31
18	Whole Body Form Drawing	32
19	Upper Torso Body Form - Photo	33
20	Pelvis Body Form - Photo	34
21	Whole Body Form - Photo	35
22	Static Crush Test Fixture	36
23	Dynamic Crush Test #7	39
24	Static Crush Test #17	39
25	DySci No. 8330-2 Upper Door/Thorax Acceleration	43
26	DySci No. 8330-2 Lower Door/Pelvis Acceleration	43
27	DySci No. 8330-2 Upper Door Velocity	44
28	DySci No. 8330-2 Lower Door Velocity	45
29	DySci No. 8330-2 Upper Door/Thorax Velocity	47

BEST DOCUMENT AVAILABLE

LIST OF FIGURES (Cont.)

Figure No.		Page
30	DySci No. 8330-2 Lower Door/Pelvis Velocity	47
31	DySci No. 8330-2 CG Force Direction	48
32	Static Crush Test No. 20	50
33	Static Crush Test No. 21	51
34	HYGE Sled Buck - Assembled View	54
35	HYGE Sled Buck - Exploded View	55
36	SRL Test No. 9 - Chest Acceleration	59
37	SRL Test No. 9 - Pelvis Acceleration	59
38	Time Sequence of Budd Crush Test No. 11	61
39	Time Sequence of Sled Test No. 6	62
40	Budd No. 11 - Lower Door/Pelvis Acceleration	63
41	SRL Test No. 6 - Lower Door/Pelvis Acceleration	63
42	Budd No. 11 - Upper Door/Chest Acceleration	64
43	SRL Test No. 6 - Upper Door/Chest Acceleration	64
44	Pendulum Calibration Test Set-up	67
45	Left Upper Rib Accel. - Test #8330-2/SRL Test #12	71
46	Pelvis Accel. - Test #8330-2/SRL Test #12	71
47	Right Upper Rib Accel. - Test #8330-2/SRL Test #12	72
48	Upper Spine Accel. - Test #8330-2/SRL Test #12	72
49	Lower Spine Accel. - Test #8330-2/SRL Test #12	73
50	Time Sequence of DySci Test No. 8330-2	75
51	Time Sequence of SRL Sled Test No. 16	76
52	Body Form and Sled Platform	83
53	View from Accelerator to Strike Plate	83
54	Strike Plate with Padding Samples	83
55	Strike Plate, Load Cells and Displacement Rod	83
56	Impact Accelerator Device	84
57	Rigid Drop vs. 10 mph Mini Sled Test	87
58	Drop Test vs. 15 mph Mini Sled - APR Padding	88

BEST DOCUMENT AVAILABLE

Appendices

A -	Interior Door Crush Test Results
B -	Interior Door Stiffness Trend Curves
C -	Discussion of Roller Tape Mechanisms
D -	Occupant/Door Comparisons from Budd #II Simulation
E -	Body Form Responses from Dynamic Science Test #8330-2 Simulation
F -	Force vs. Deflection Curves for Phase I Padding Component Tests
G -	Force vs. Deflection Curves for Phase II Padding Component Tests
H -	Body Form Responses from HYGE Sled Padding Evaluation Tests
I -	Drawing & Description of Fluid Impact Accelerator
J	Tarriere Drop Tests

ACKNOWLEDGMENTS

The views and findings of this report are those of the authors and do not necessarily reflect the policy of the NHTSA. The authors are grateful to the following for technical support in the fabrication of special hardware and the successful conduct of experiments:

Herb Litteral
Ed McGhee
Harvey Witter
Harry Mullins
Bob Esser

The authors wish to thank Mr. Richard M. Morgan for assistance in formulating the project objectives and Mr. Lee Stucki for coordination of the project with other NHTSA research efforts.

Also, special thanks go to Reva Blaker and Susan Weiser for the preparation of the manuscript.

BEST DOCUMENT AVAILABLE

1.0 Background:

Lateral accidents are responsible for an estimated 30 percent of motor vehicle occupant fatalities each year. Within the past 5 years, efforts have greatly increased toward understanding the side impact environment and interpreting side impact data. These studies form the basis for current efforts to provide improvements to the level of crash survivability of passenger cars.

Accident data gathered under the National Crash Severity Study indicates head and thoracic injuries caused by side rails and door contact are a major problem in side impact collisions.

As part of a larger effort to mitigate the deaths and injuries caused by door contact, the Agency initiated the search for producible, energy-absorbing interiors for installation into structurally modified vehicles. This report reviews the approach used in selecting a side impact cushioning material.

2.0 Objectives:

There were two main objectives to the overall project. The first objective was to design and fabricate a sled buck which accurately reproduced the environment of a modified Rabbit in a side impact collision. The test mode in which the Rabbit was evaluated was a 60 degree impact, with the impacting vehicle traveling at 30 mph and the Rabbit traveling at 15 mph. The second objective was to develop a suitable padding material for installation into the modified Rabbit structure.

BEST DOCUMENT AVAILABLE

3.0 Project Element Summary

The Safety Research Laboratory approach consisted of 17 project elements. The following is a brief description of the 17 elements.

Project Element	Summary Description
1	order and receive RICSAC cars
2	order and receive RICSAC data
3	order and receive Budd cars
4	install new dummy computer software
5	acquire new dummy
6	analyze RICSAC and Budd crash test data
7	design interior door crush device
8	conduct interior door crush tests
9	analyze crash test data from Dynamic Science 214 mode crashes
10	define interior door stiffness
11	design and build sled buck
12	conduct dynamic sled simulations of Budd data
13	conduct dynamic sled tests with new dummy
14	review prior padding studies
15	conduct padding component tests
16	conduct dynamic sled tests to evaluate padding
17	conduct Tarriere drop tests

BEST DOCUMENT AVAILABLE

4.0 Project Element Overview

The following is a brief description of each project element. A flow chart, providing easy reference to the sequence of the project elements, is shown in Figure 1.

Project Element 1 - Order and Receive RICSAC Cars

Project Element 2 - Order and Receive RICSAC Data

Project Element 3 - Order and Receive Budd Cars

The purpose of obtaining the RICSAC[1]* and Budd[2] cars and data was to aid the SRL in defining the side impact environment for HYGE sled testing.

Project Element 4 - New Dummy Computer Software

The purpose of installing the new dummy computer software was to provide a means of estimating the injury level to a human thorax based on the responses of the dummy during impact. The software provided as output the Abbreviated Injury Scale (AIS) based on four methods: B parameter of the left upper rib signal, Q parameter of the left upper rib signal, average power of the upper spine and average power of the lower spine.

Project Element 5 - Acquire New Side Impact Dummy

A new side impact dummy was developed for the Agency under Contract No. DOT-HS-4-00921. The production version of the dummy was desired for this project. However, only the prototype version was available for use during component level and HYGE sled testing.

*Numbers in parenthesis refer to references at the end of the text.

Blank Page

BEST DOCUMENT AVAILABLE

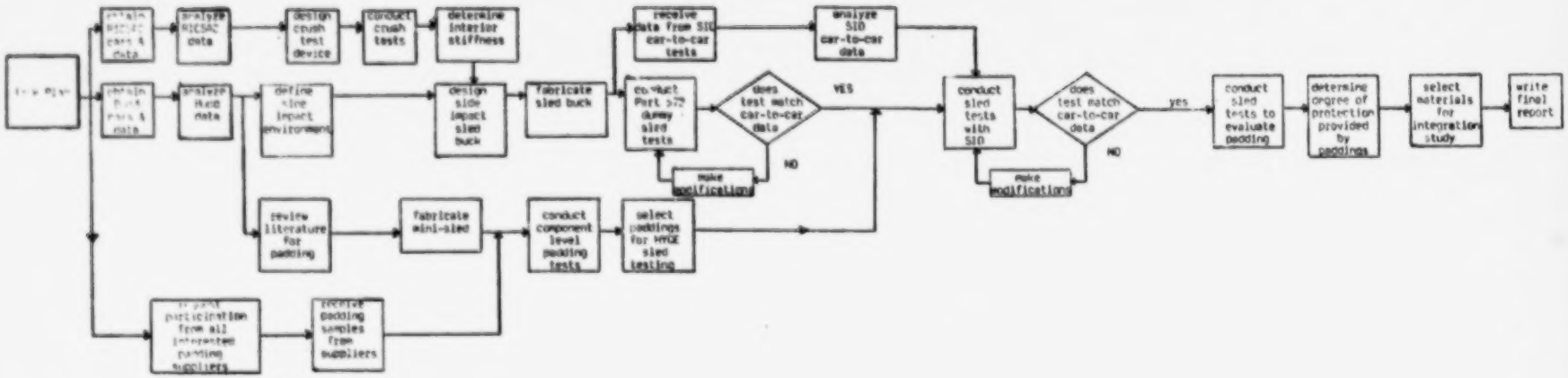

FIGURE 1

Project Element Flow Chart

BEST DOCUMENT AVAILABLE

Project Element 6 - RICSAC and Budd Crash Test Analysis

The RICSAC[1] and Budd[2] Crash Test data were analyzed to determine the necessary parameters for HYGE sled simulation of the side impact environment. The Budd tests utilized Part 572 dummies in a stationary VW Rabbit. The RICSAC tests utilized Part 572 dummies in two-car-moving side impacts.

Project Element 7 - Interior Door Crush Device

Two interior door crush test devices were devised to statically and dynamically impact the door interiors of previously impacted VW Rabbits obtained during project elements 1 and 3. The torso, pelvic and whole body regions of a 50th percentile male were represented by three rigid body forms fabricated for the interior door stiffness tests.

Project Element 8 - Interior Door Crush Tests

The purpose of the interior door crush tests was to determine the force-deflection properties of the Rabbit door interior. The stiffness that was desired was that experienced by the occupant when the door was pushed into him by an impacting vehicle. General trends in vehicle stiffness were investigated using several different VW Rabbits.

Project Element 9 - Dynamic Science 214 Mode Crash Test Analysis

Dynamic Science Test No. 8330-2[3] was performed under conditions being considered as candidate in the upgrade of the FMVSS No. 214 test procedure (60 degree side impact, both cars moving), using the prototype side impact dummy. The test data were analyzed to determine test conditions (dummy positioning, peak accelerations, etc) for HYGE sled simulation prior to conducting padding evaluation tests on the HYGE sled.

BEST DOCUMENT AVAILABLE

Project Element 10 - Definition of Interior Door Stiffness

Data from Budd Test No. 11[2] was examined along with the SRL static and dynamic crush tests of Element 8. The stiffness of the Rabbit interior door of Budd Test No. 11 was estimated. The amount of door intrusion into the passenger compartment and force levels of the upper and lower door were also estimated. The information was needed in order to simulate Budd Test No. 11 on the HYGE sled buck.

Project Element 11 - Design and Build Sled Buck

The sled buck was designed to reproduce the environment of a side impact collision as seen by the surrogate. This sled was demonstrated by correctly simulating (1) the velocity-time curve and motion of the interior Rabbit door, (2) the gross kinematics of the surrogate, and (3) the selected accelerations of the surrogate.

Project Element 12 - HYGE Sled Simulation of Budd Data

The purpose of simulating Budd Test No. 11[2] was to check out the sled buck with a Part 572 dummy, attempting to match the chest, pelvis, upper door and lower door responses, and the overall dummy kinematic response of the car-to-car collision.

Project Element 13 - HYGE Sled Simulation of Dynamic Science 214 Mode Test

Dynamic Science Test No. 8330-2[3] was the first Agency crash test conducted using a side impact dummy in the collision mode being considered in the FMVSS 214 upgrade. The simulation was intended to provide an independent check-out of the sled buck. Once simulation was achieved, the same sled test conditions were to be used to demonstrate the protection level provided by various padding materials.

BEST DOCUMENT AVAILABLE

Project Element 14 - Review of Prior Padding Studies

A limited literature search was conducted which identified only four studies directly related to the project. The four studies dealt with padding used in interior vehicle applications and were reviewed.

Project Element 15 - Component Level Padding Tests

The main purposes of the component level padding tests were (1) to identify padding materials viable for thorax protection and (2) to eliminate performing extensive HYGE sled tests using undesirable padding materials.

The padding materials were evaluated for their desirability as a thoracic restraint by three main criteria: (1) padding force-deflection properties, (2) body form AIS calculated from the B(LUR) parameter and (3) peak spinal acceleration.

The component level tests were performed in two phases. Phase I consisted of impacting the prototype SID thorax laterally into 5 inch padding samples at 15 mph. A number of the less desirable padding materials were eliminated during Phase I testing. Phase II consisted of impacting 3 inch padding samples at 15 mph. Those padding materials which passed the criteria during Phase II testing were then evaluated on the HYGE sled buck.

Project Element 16 - HYGE Sled Padding Evaluation Tests

Those padding materials which had been deemed viable candidates for thoracic protection, based on component level test results, were tested on the HYGE sled. The series of 17 tests, using the prototype SID, was performed to evaluate the protective capability of the padding materials. The door contacted the dummy at an impact velocity of 23.5 mph.

BEST DOCUMENT AVAILABLE

Project Element 17 - APR Drop Tests

The Laboratory of Physiology and Biomechanics, Association Peugeot-Renault, had conducted several lateral drop tests using cadavers and a mechanical surrogate developed in their laboratory[4]. It was of interest to the Agency to reproduce the tests using the mechanical surrogate developed by the NHTSA. The drop tests were conducted at the SRL using the SID. Lateral drops were conducted from a one meter drop height onto a rigid surface and from a two meter drop height onto padding samples supplied by the APR.

BEST DOCUMENT AVAILABLE

5.0 Side Impact Sled and Padding Development

5.1 RICSAC and Budd Cars and Data

The tentative test mode for the FMVSS No. 214 upgrade is as follows:

Bullet (striking) car velocity - 30 mph
Target (struck) car velocity - 15 mph
Impact angle - 60 degrees into vehicle compartment

Two previous side impact collision studies were chosen to be analyzed. The first study, "Research Input for Computer Simulation of Automobile Collisions"[1] (RICSAC), developed a library of experimental data to validate computer reconstruction techniques. In the study, four 60 degree side impact collisions with both cars moving were conducted. The second study, "Lightweight Subcompact Vehicle Side Structure Program"[2], (the Budd Study), included a number of 60 degree side impact collisions with only the bullet vehicle moving and the target vehicle stationary.

The films and hard copy reports from the four RICSAC tests and selected Budd tests were ordered and received. The two Rabbits, two Pintos and three Malibus crashed in the RICSAC Study were shipped from Buffalo, New York to the VRTC in East Liberty, Ohio. The purpose of obtaining the seven vehicles was to (1) help in the definition of the side impact environment (Section 5.4) and (2) provide vehicle interiors for interior stiffness testing (Section 5.6). Five Rabbits, crashed during the Budd Study, were also shipped from Buffalo to the VRTC. The purpose of obtaining these vehicles was (1) for use in the interior crush tests (Section 5.6) and (2) to help in designing the energy-absorbing material to fit the structurally modified Rabbits.

BEST DOCUMENT AVAILABLE

5.2 New Dummy Computer Software

Installation of the side impact injury prediction computer software at the VRTC was completed in November, 1979.

Throughout both HYGE and component sled testing, it was desired to have uniformity with the data processing procedures used by the Highway Safety Research Institute (HSRI) in their development work with a side impact dummy. Figure 2 is the previously published flow chart of the HSRI data processing. The characteristics of their "anti-alaising" filter were not originally described. It was revealed, through conversations with HSRI personnel, that their work utilized a 4-pole Bessel filter with characteristics similar to the SAE class 60, but their FM recorder is slowed to a 16:1 reduction during play back giving an effective band pass before cutoff of around 1600 Hz. For the processing of the component sled tests, the SRL used 2-pole Butterworth filters (100 Hz cutoff) and an 8:1 reduction in play back and a 3200 Hz digitizing rate. For the HYGE sled tests, the dummy data channels were digitized at 8000 Hz, while all other data channels (ie, sled acceleration, etc.) were digitized at 4000 Hz. Exact reproduction of the HSRI procedure was not possible but differences were believed to be negligible.

The side impact body form is instrumented to measure lateral accelerations of the left upper rib (LUR), right upper rib (RUR), upper spine and lower spine. The AP acceleration of the lower sternum (LS) is also measured.

The computer software calculates the AIS by two methods. One method is based on the Q(LUR). The Q parameter is the maximum value of the first integral (cm/sec) of the acceleration signal. The signal is first run through a time windowing algorithm to minimize sensitivity to signal bias. Q(LUR) means the Q parameter of the left upper rib acceleration signal. In order to compute AIS, two other parameters have been defined. VI5 is defined as the

BEST DOCUMENT AVAILABLE

FIGURE 2
HSRI Data Processing Flow Chart

BEST DOCUMENT AVAILABLE

time between achievement of 10% to 50% of the Q value. V19 is the time between achievement of 10% to 90% of Q. The AIS is then computed by the following equation.

$$\overline{AIS} = 3.19 + .00215*Q(LUR) - 43.56*V15(LS) - 68.27*V19(RUR)$$

The second method for computing AIS is based on the B parameter. The B parameter is defined as follows:

$$B = \ln[\text{maximum}(|F_1|,|F_2|)]$$

where F_1 is the net velocity change over 20 msec of positive acceleration and F_2 is the net velocity change over 20 msec of negative acceleration. From the B parameter, AIS is computed as follows:

$$\overline{AIS} = 1.5953*B(LUR) - 7.6$$

BEST DOCUMENT AVAILABLE

5.3 Prototype Side Impact Dummy

Under Contract No. DOT-HS-4-00921 with the HSRI, the Side Impact Dummy (SID) was developed for the Agency. Only a prototype version of the dummy was completed at the time of this project's initiation. This prototype was used in the second portion of the HYGE sled tests and a prototype thorax was used throughout the mini sled component tests.

During the final stages of this project, a production version of the SID became available and was utilized for HYGE sled simulations.

BEST DOCUMENT AVAILABLE

5.4 Analysis of RICSAC and Budd Crash Test Data

The RICSAC[1] and Budd[2] crash test data were analyzed for the purpose of defining the side impact environment and reproducing that environment as closely as possible in a sled test.

The following parameters were determined as necessary for simulating the impact environment on the sled buck:

1) the door acceleration/velocity time history
2) the relative displacement of upper and lower door prior to occupant contact
3) the stiffness of the upper and lower door (as seen by an occupant)
4) the direction of compartment motion (same as force direction)

The degree to which the sled reproduced the environment was measured by the following dummy response measures:

1) chest acceleration - time history
2) pelvis acceleration - time history
3) injury measure (AIS)
4) gross overall kinematics

The effect of the occupant-door interaction was taken into consideration when determining the door acceleration/velocity-time history. Figure 3 shows the upper door accelerometer reading from Crash No. 12 of the Budd Contract. A positive accelerometer reading indicates acceleration into the compartment. Note that at around 55 msec, the acceleration suddenly drops off and even tends negative for a short duration. Two explanations might be offered for the cause of this acceleration drop. One explanation is that it is a structural resonance vibration and/or tensioning of a structural member. The other explanation is that it is due to the interaction between the door and the occupant (in this case, a Part 572 dummy). The latter explanation appears

BEST DOCUMENT AVAILABLE

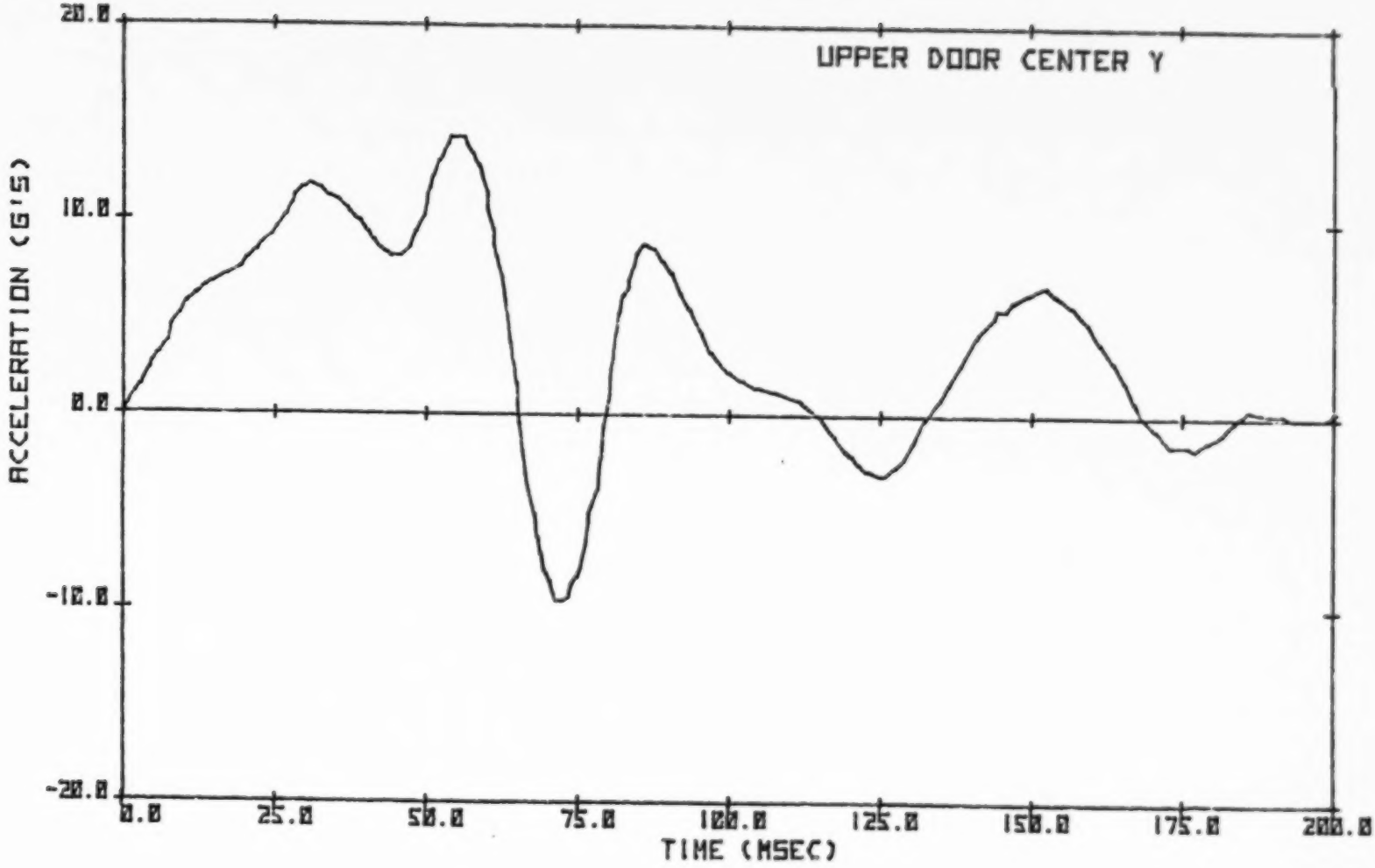

BUDD MOD RABBIT TEST #12 15HZ

FIGURE 3
Budd Test No. 12 - Upper Door Acceleration

BEST DOCUMENT AVAILABLE

more reasonable to the SRL. It is believed that the occupant is able to make a pronounced effect on the door response due to the finite stiffness of the door. The door deforms locally around the occupant's shoulder causing the sudden drop in door acceleration. The following discussion enlarges on this factor.

Vehicle Interior Side Stiffness

Indications that the interior door stiffness has an important effect on occupant loading are found in two areas: (1) comparisons between sled tests and actual car crashes, and (2) in-depth analysis of individual car crashes.

Comparisons of Part 572 dummy readings in actual car crashes and in rigid wall sled tests reveal differences. In Figure 4, the circles represent car crash data points from the Greene Study[5]. The triangles are from subsequent sled tests with a rigid wall[6]. The dissimilarities between the two sets of data suggest that an interior door panel cannot adequately be modeled by an inflexible wall.

Secondly, examination of the time history of the interior door panel suggests the door can yield. Figure 5 shows the velocities of key points during Calspan's baseline crash test No. 5[2]. A stationary 1973 Ford four-door sedan was struck perpendicularly [directly on the passenger door] by another Ford traveling at 37.3 mph. The test used a Part 572 dummy in the front passenger seat. The velocity of all of the key points progress toward a common velocity, Vf, which in this case is 19.4 mph.

The initial contact is between the striking vehicle's bumper (dotted line) and the near side [outer skin] of the struck vehicle. The force applied to the struck vehicle by the bumper causes the vehicle [or, more precisely, the vehicle compartment] to accelerate up to Vf relatively slowly. This same force, however, produces a much more dramatic increase in the velocity of the struck vehicle's door. The near-side front seat occupant, meanwhile, is not moving at all in the initial stages [0-24 msec] of the crash. At 24 msec into

BEST DOCUMENT AVAILABLE

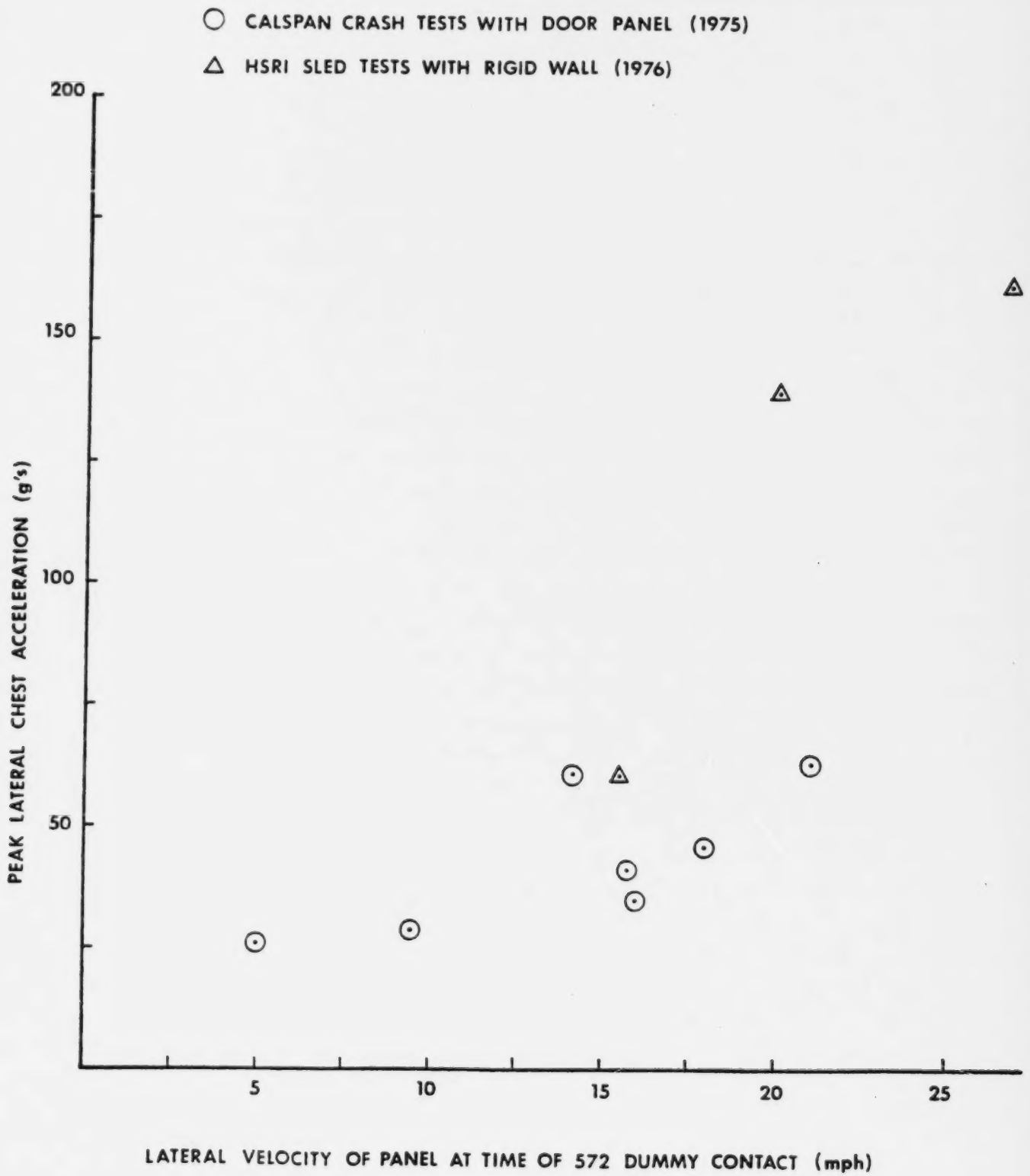

FIGURE 4 - Crash Tests/Rigid Wall Comparison

BEST DOCUMENT AVAILABLE

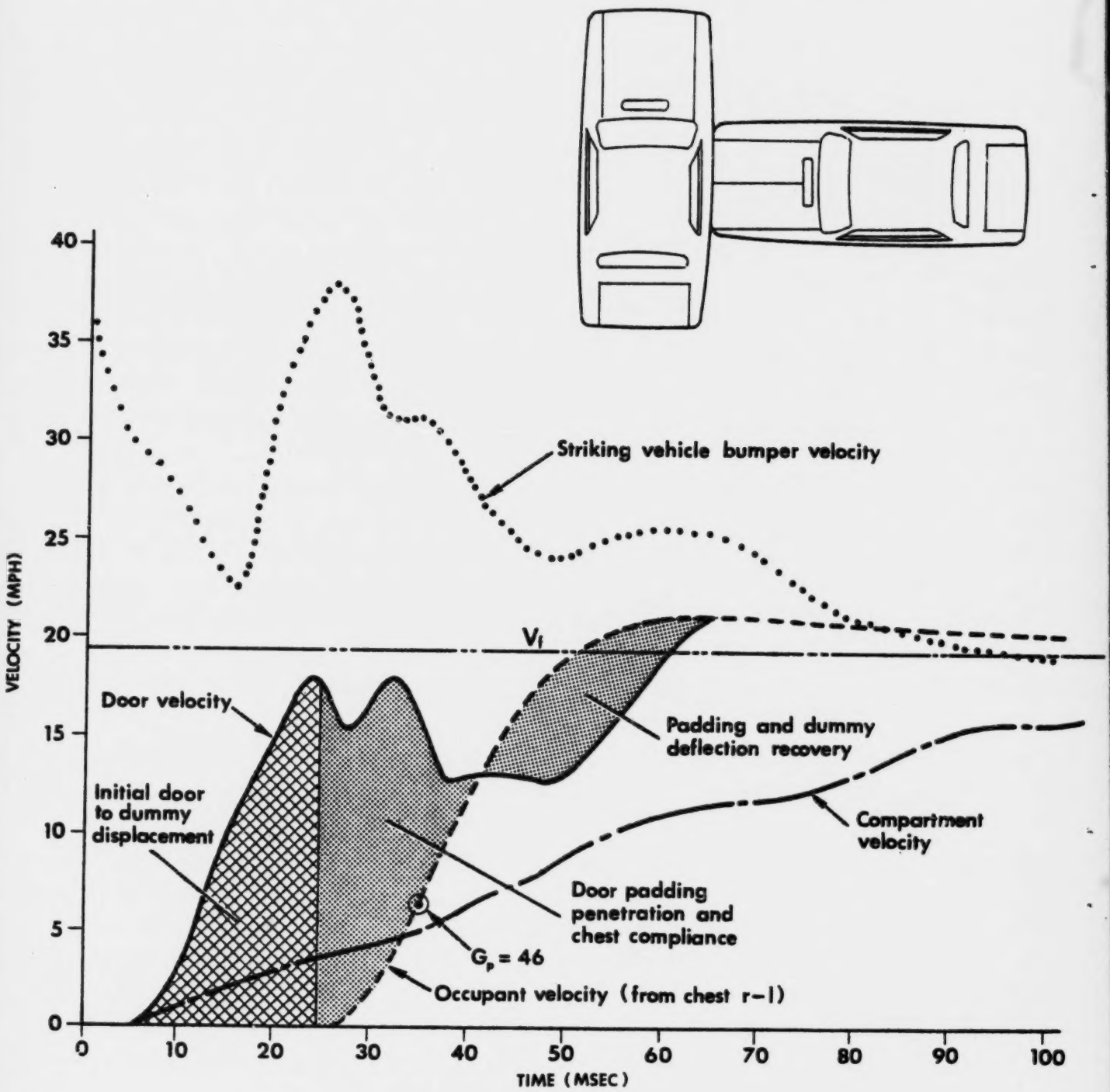

In Depth Analysis of Actual Side Impact Crash

FIGURE 5 - Calspan Baseline Crash Test #5

BEST DOCUMENT AVAILABLE

the crash the dummy impacts the struck door interior.

The door velocity does not continue to rise [after the 24 msec point] and approach the bumper velocity. The dummy impacts the door; and force builds up to interupt the velocity rise. While it is believed that the primary source of this force is the dummy impacting the door, other structural effects (such as the seat structure) may be contributing. The door was within 2 mph of Vf at the instant of dummy contact.

At 35 msec, the occupant's chest experiences it's maximum lateral acceleration of about 46 G [3 msec duration]. Assuming that the 50th percentile's upper body has an effective weight of 80 pounds, the dummy would be producing a decelerating force on the door of about 3700 pounds at this time.

At 40 msec the dummy and the door reach a common velocity of about 12 mph. By computing the area between the occupant and door velocity curves between 24 and 40 msec we can determine the extent of door padding penetration and dummy chest compliance. This calculation yields a prediction of 3 inches. The vehicle which is being tested has very little padding [less than one inch]. Therefore, it is likely that the upper door structure [the window sill area] is functioning essentially like padding, attentuating chest lateral G-levels by deforming under the inertial force of the dummy upper body. That is, the dummy may be making beneficial use of the full upper door depth to substitute for the padding that is not there. Note that at about 50 msec the interior door velocity again increases, indicating that the interior door has now bottomed out (stiffness increases) against the striking vehicle.

BEST DOCUMENT AVAILABLE

Force Direction

This discussion describes the methods by which the resultant force direction was determined.

The first approach to obtaining the direction of the resultant collision forces that are acting on the compartment utilizes the accelerometer traces. If an accelerometer were located at the c.g. of the vehicle, the vector sum of the X and Y accelerations is the force direction. For this analysis, the angle is referenced from the forward longitudinal axis. Figure 6 shows a schematic of a vehicle with 7 accelerometer locations, and a force vector at an instant of time. If the vehicle has rotational velocity during the collision then all the accelerometer readings will be affected since they are not located at the c.g. A partial compensation is obtained by using opposite corner readings and averaging the two at each time point.

A computer routine was written which computed the angle of the resultant acceleration at each time point and plotted the angle over the time considered. The routine yielded "noisy" results from high frequency accelerometer data.

The second approach attempted by the SRL to estimate force direction utilizes film data. A camera view from overhead is projected onto the digitizer table. Visible markers are tracked at fixed time intervals to determine the heading angle and c.g. position at each time. The heading angle and the initial velocity at the beginning of a time interval are used to predict where the c.g. will be at the beginning of the next time interval. Since collision forces act on the vehicle during the interval, the actual position at the next time is displaced in both the X and the Y direction (see Figure 7).

BEST DOCUMENT AVAILABLE

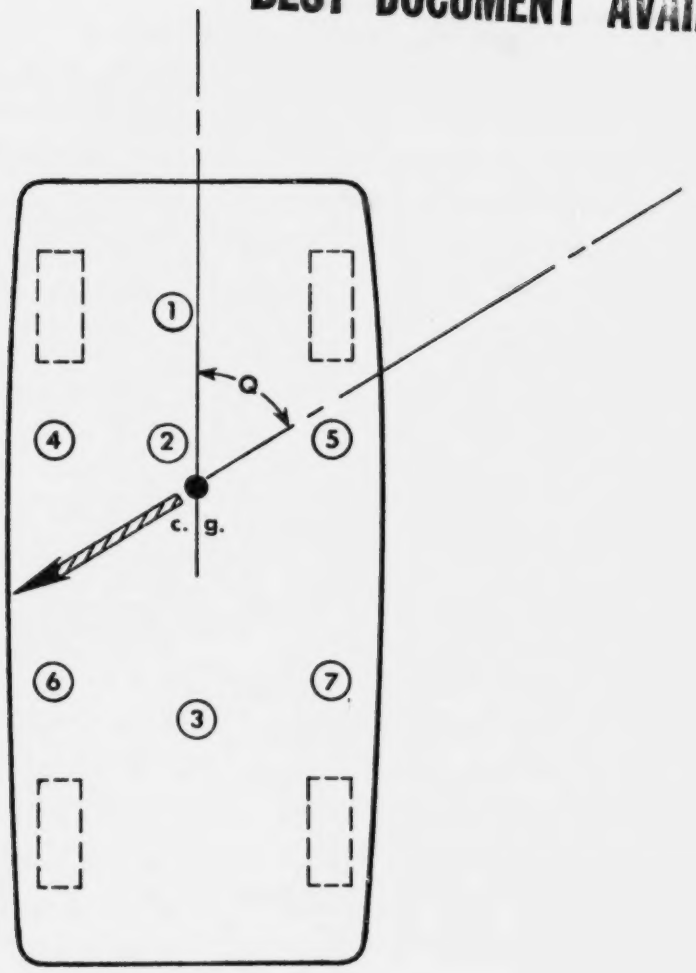

1. FIREWALL ACCELEROMETER
2. DRIVE TUNNEL ACCELEROMETER
3. REAR DECK ACCELEROMETER
4. LEFT FRONT COMPARTMENT ACCELEROMETER
5. RIGHT FRONT COMPARTMENT ACCELEROMETER
6. LEFT REAR COMPARTMENT ACCELEROMETER
7. RIGHT REAR COMPARTMENT ACCELEROMETER

FIGURE 6

VEHICLE ACCELEROMETER PLACEMENT SCHEMATIC

BEST DOCUMENT AVAILABLE

Problems were encountered in the quality of the films for this type of analysis. No ground references were present in most overhead views which made scaling difficult. The results had questionable repeatability, therefore, we relied on the accelerometer traces for determining force direction.

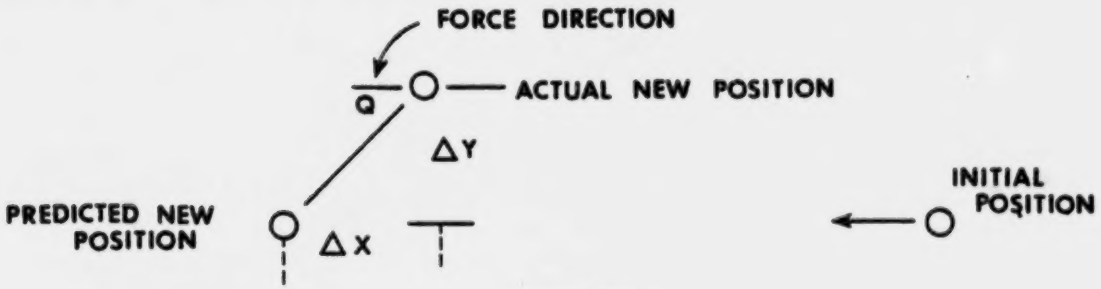

FIGURE 7

Force Direction by Film Analysis

Figures 8 and 9 illustrate the importance of filtering the data at a low frequency. A large difference is seen between Figure 8 taken from 60 Hz data and Figure 9 taken from 15 Hz data. It was found that rotational effects appear to be small. This is seen in comparing the front and rear corner accelerometer readings from Budd tests No. 4 and No. 6 (Figures 10 through 13).

BEST DOCUMENT AVAILABLE

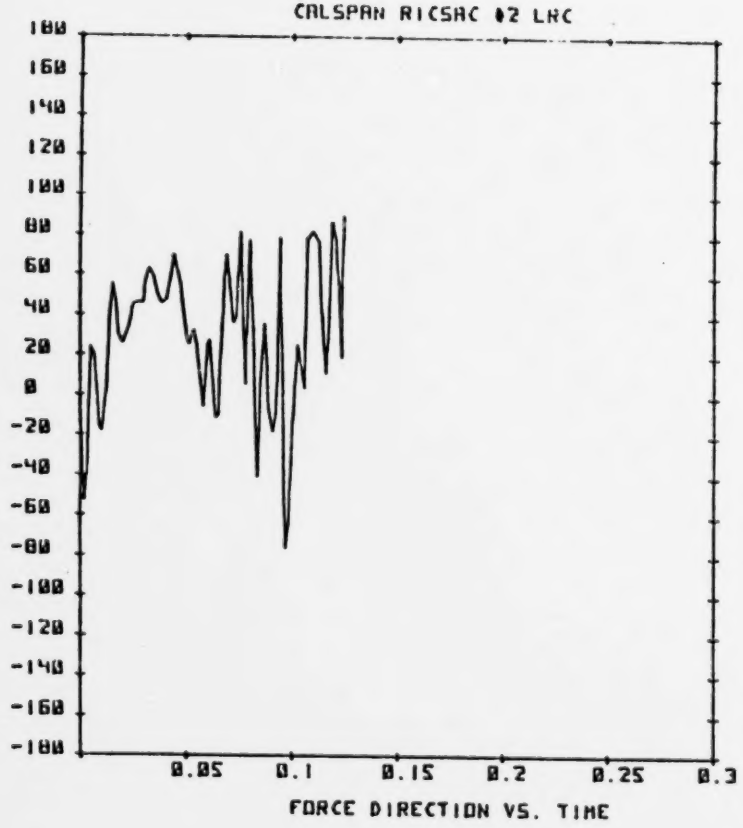

FIGURE 8
RICSAC #2 Force Direction

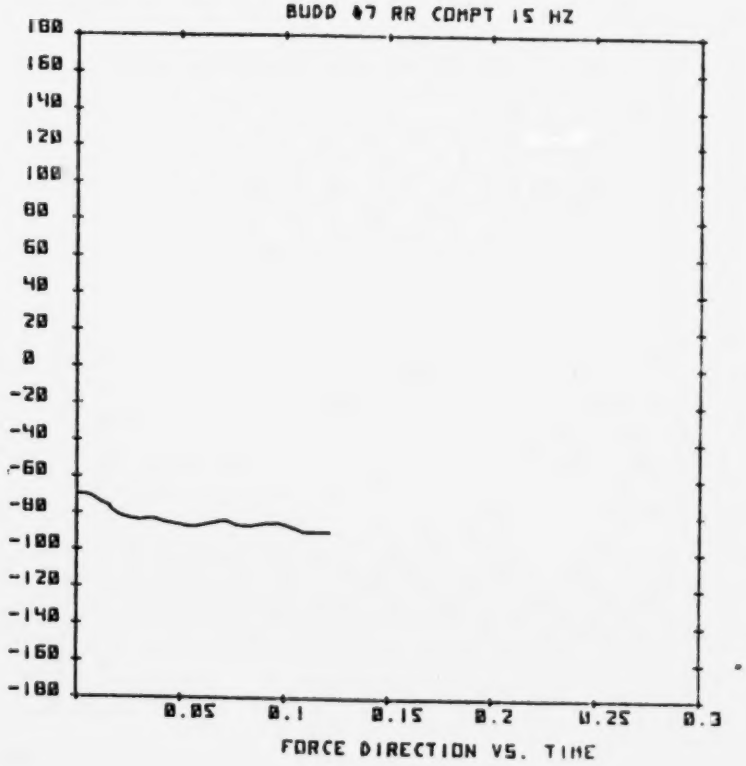

FIGURE 9
Budd #7 Force Direction - Rear

BEST DOCUMENT AVAILABLE

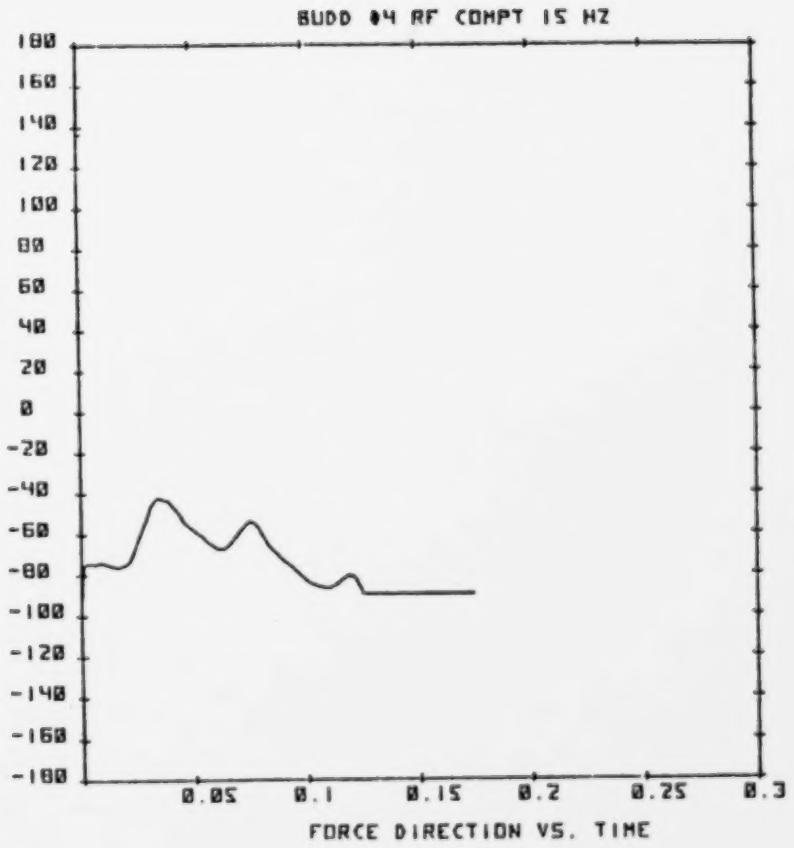

FIGURE 10
Budd #4 Force Direction - Front

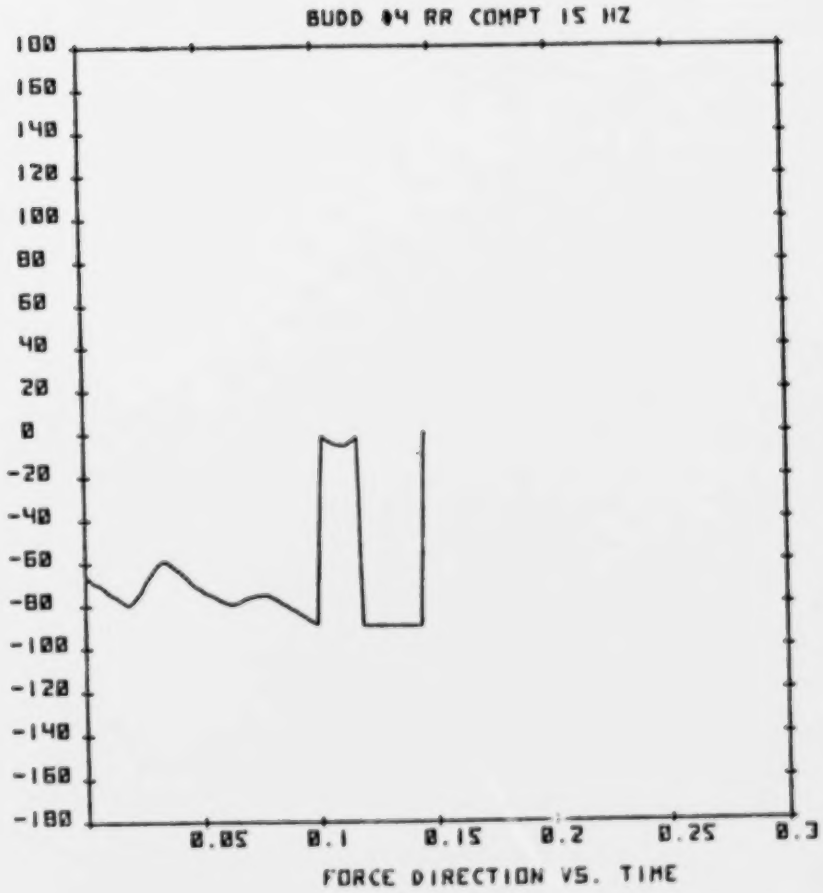

FIGURE 11
Budd #4 Force Direction - Rear

BEST DOCUMENT AVAILABLE

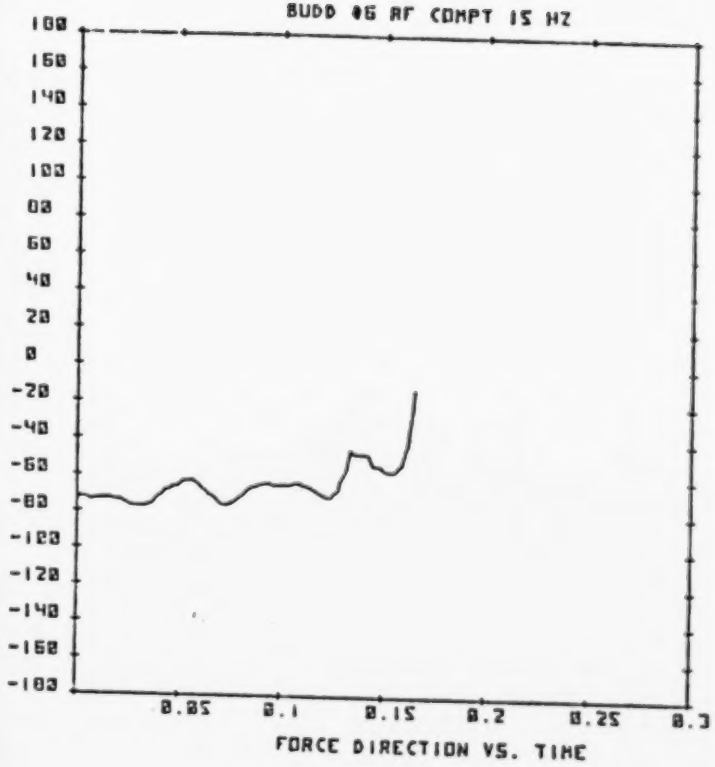

FIGURE 12

Budd #6 Force Direction - Front

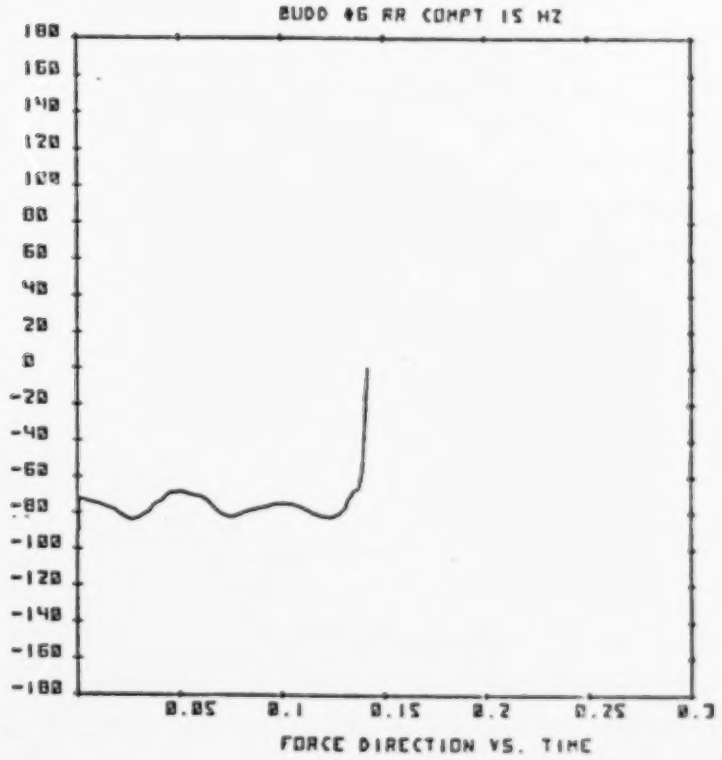

FIGURE 13

Budd #6 Force Direction - Rear

BEST DOCUMENT AVAILABLE

5.5 Interior Door Crush Devices

The purpose of the interior door crush tests was to find the force-deflection properties of the Rabbit door interior. The hardware necessary to conduct the tests consisted of:

- Bullet car into Rabbit dynamic crash test fixture
- Bullet car into Rabbit static crush test fixture
- Body forms to represent an occupant
- Body form into door static crush test fixture
- Body form into door dynamic crush test fixture

It was desired that most of the interior door stiffness tests be conducted on vehicles which (1) had been impacted in the side by a striking vehicle, and (2) had the striking vehicle still engaged.

Although only one or two specific collisions from the Budd study were to be later simulated, it was decided to investigate general trends in interior door stiffness. The factors chosen as variables were (1) the amount of penetration by the impacting vehicle, (2) the impact point (at the A-pillar or aligned with the occupant hip point), (3) the type of VW door (modified or unmodified), (4) the vertical elevation on the door (upper and lower door) and (5) the crush depth of the body form into the interior door panel.

In order to obtain various penetrations of the bullet car into the Rabbit, a simplified dynamic car-to-stationary car crash site was prepared. Tests were performed at 10, 15 and 20 mph with some impacts at the occupant hip point and some at the door opening reference point. Figure 14 is a schematic of the car-to-car crash site.

Prior to conducting the interior door stiffness tests, the striking car and struck car were drawn together into the impacting position and held in the laboratory. The equipment to accomplish this consisted of two (2) heavy chains and two (2) screw-type hand winch mechanisms. Figure 15 is a photograph of the test setup.

BEST DOCUMENT AVAILABLE

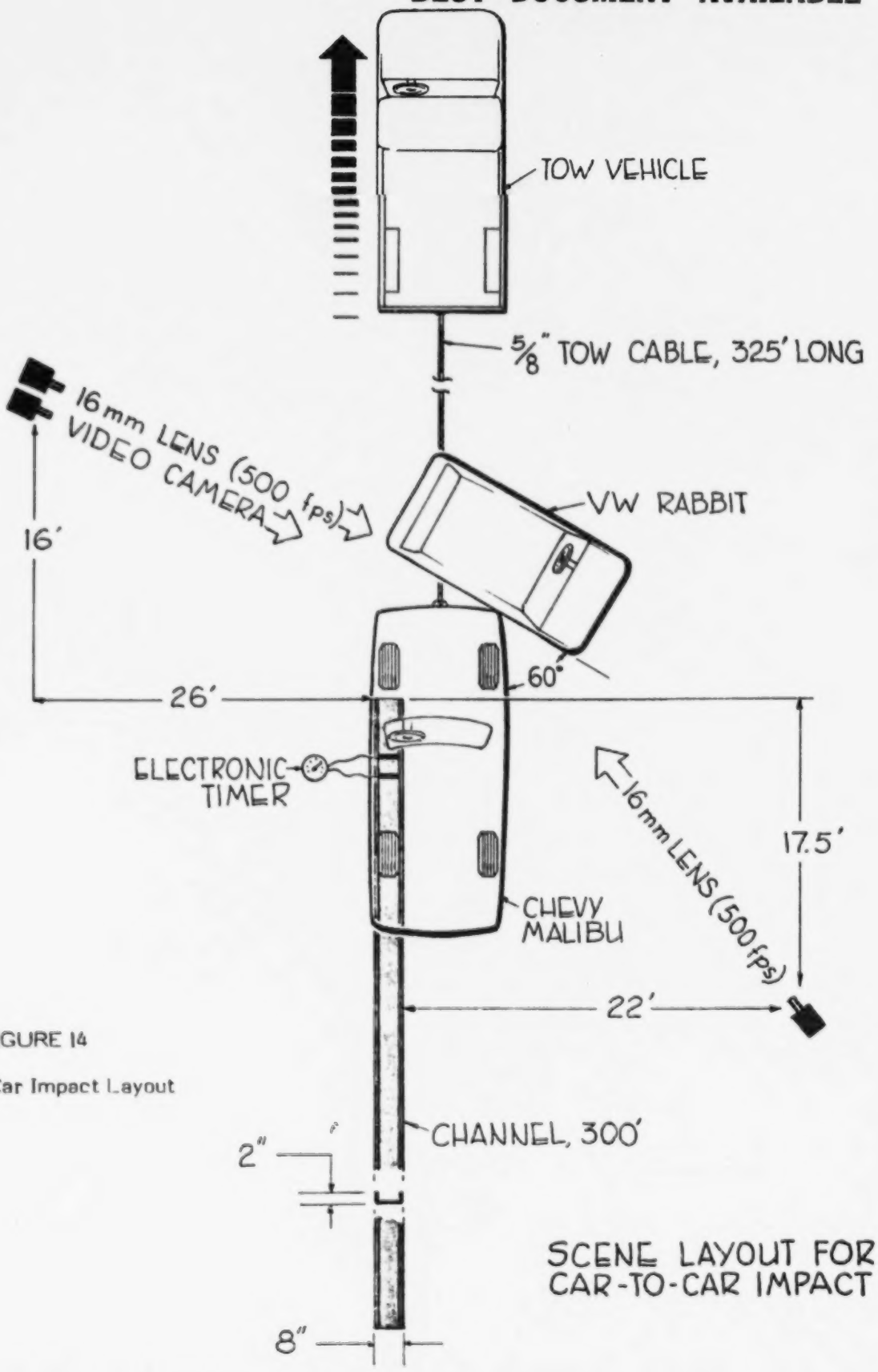

FIGURE 14

Car-to-Car Impact Layout

BEST DOCUMENT AVAILABLE

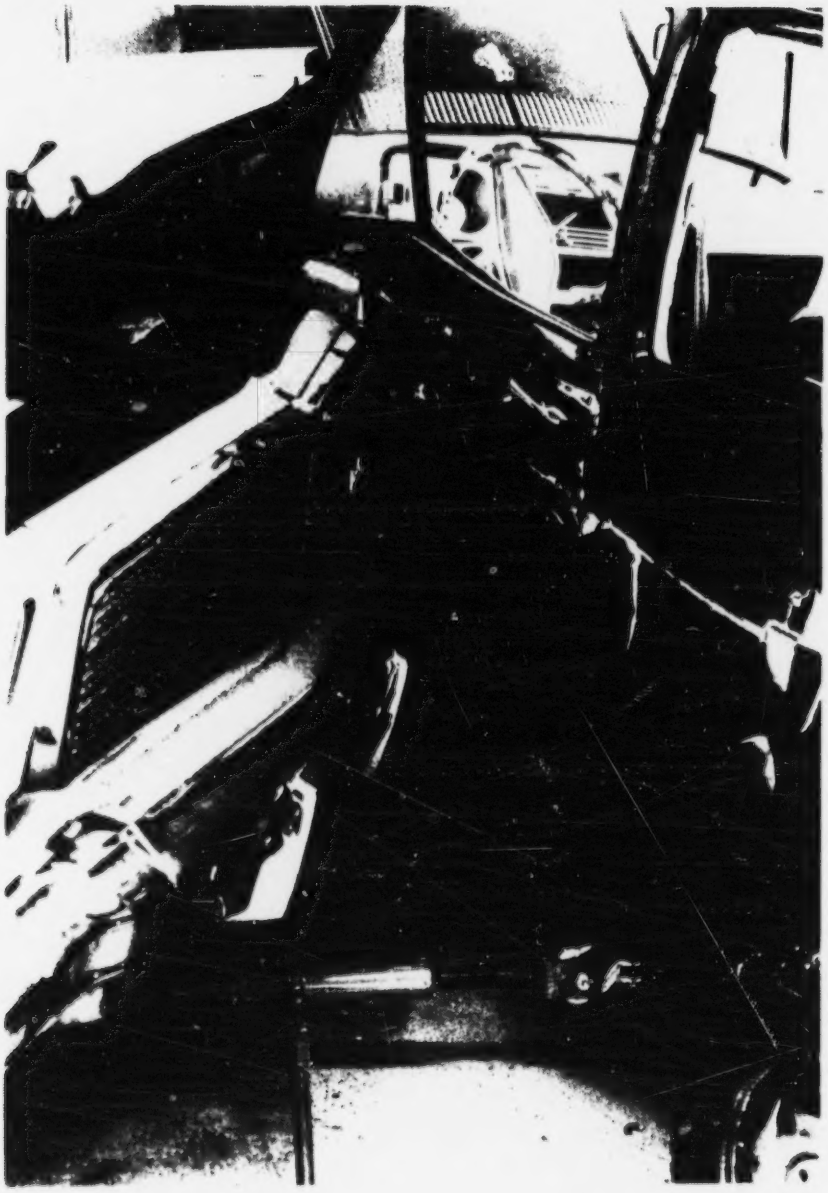

FIGURE 15

Car-to-Car Holding Fixture

BEST DOCUMENT AVAILABLE

The interior stiffness tests were performed using a rigid body form which represented the approximate surface area of a 50th percentile male. Three body forms were fabricated; an upper body form representing the torso area, a lower body form to represent the pelvic region, and a whole body form to represent the combined torso and pelvic areas. Figures 16 through 18 contain drawings of the body forms and photos are shown in Figures 19 through 21.

The static interior stiffness tests were performed by mounting the body forms on a static crush test fixture (Figure 22). The fixture consisted of a frame, a 10-ton hydraulic hand jack, and a 10,000 pound load cell. The frame was designed to be attached to a forklift. The fixture was designed to measure forces over a static deflection of around 2.0".

The dynamic crush tests were performed with the pedestrian impact device[7], utilizing the same body forms. The impact velocities were around 20 mph. The acceleration data was used to compute force and the displacement potentiometer gave the corresponding displacement.

BEST DOCUMENT AVAILABLE

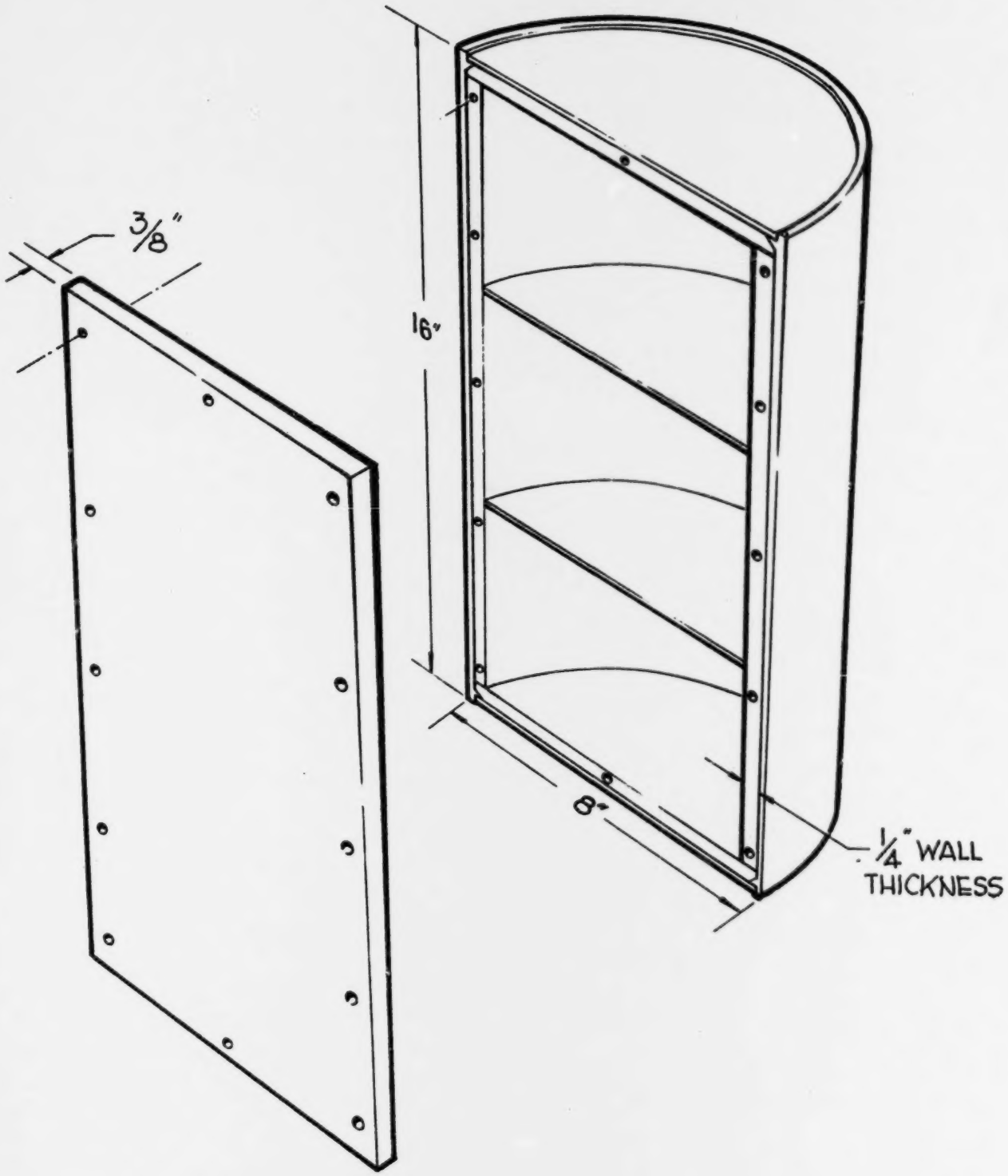

FORM No. 1

FIGURE 16
Upper Torso Body Form

BEST DOCUMENT AVAILABLE

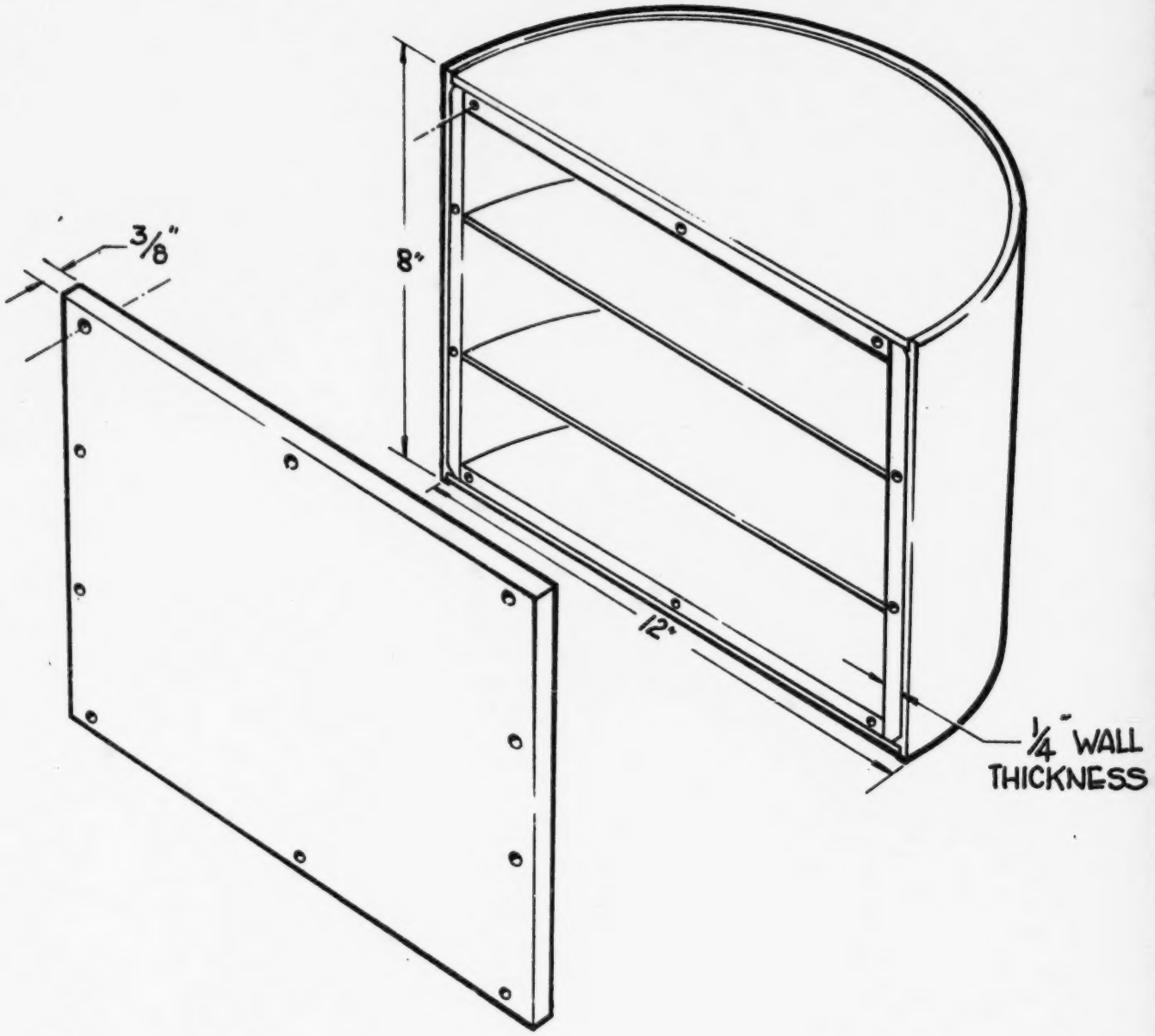

FORM No. 2

FIGURE 17
Pelvis Body Form

BEST DOCUMENT AVAILABLE

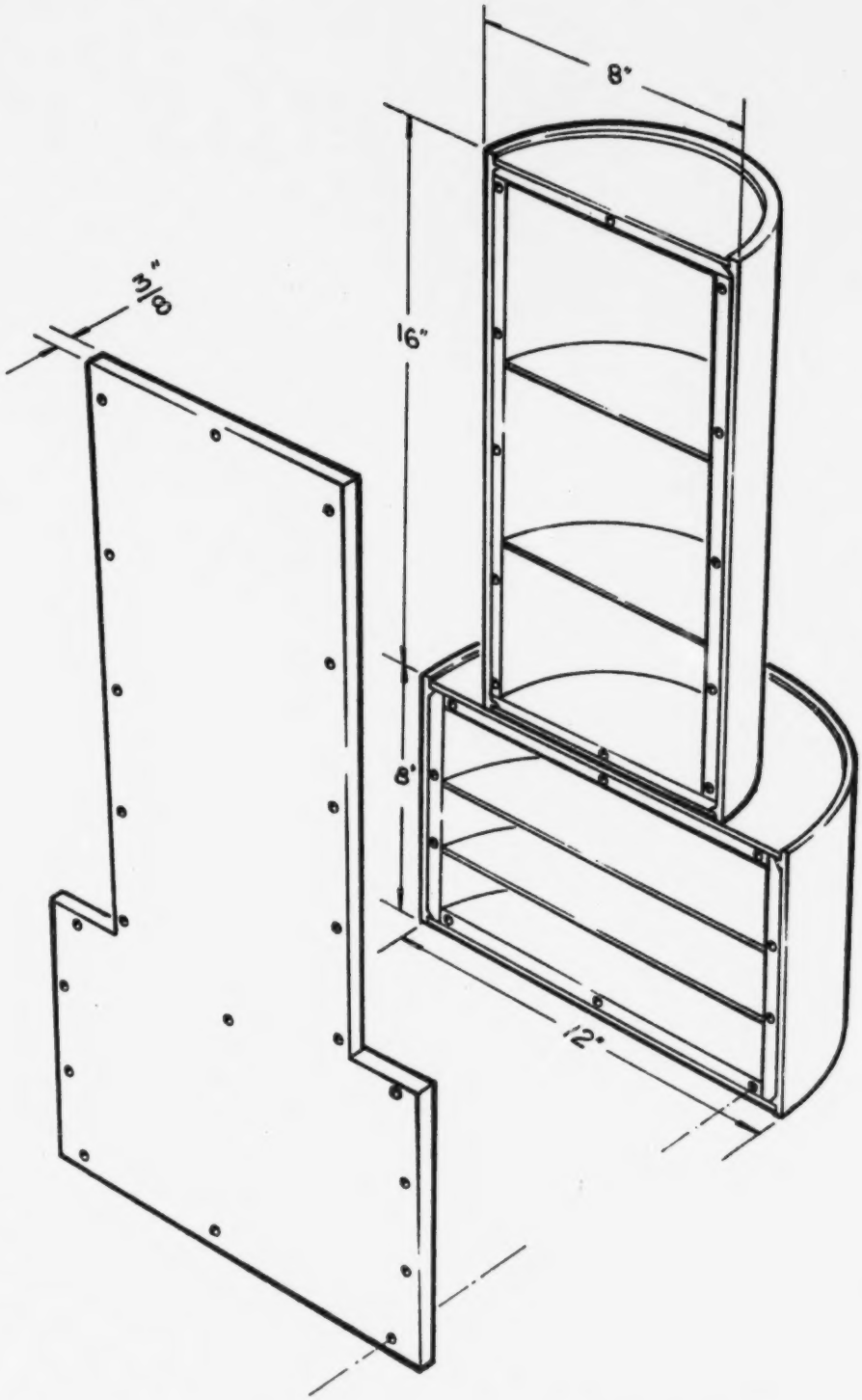

FORM No. 3

FIGURE 18
Whole Body Form

BEST DOCUMENT AVAILABLE

FIGURE 19

Upper Torso Body Form

BEST DOCUMENT AVAILABLE

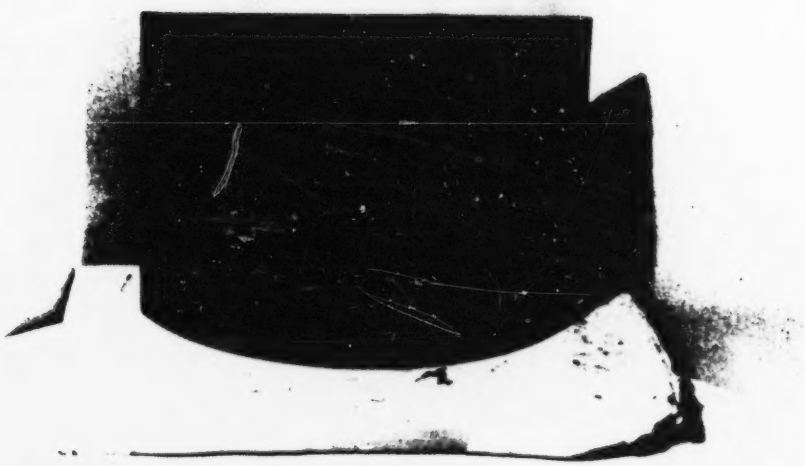

FIGURE 20

Pelvis Body Form

BEST DOCUMENT AVAILABLE

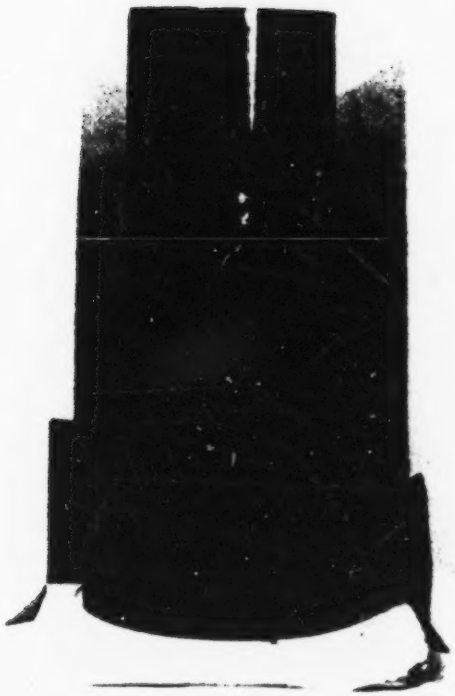

FIGURE 21

Whole Body Form

BEST DOCUMENT AVAILABLE

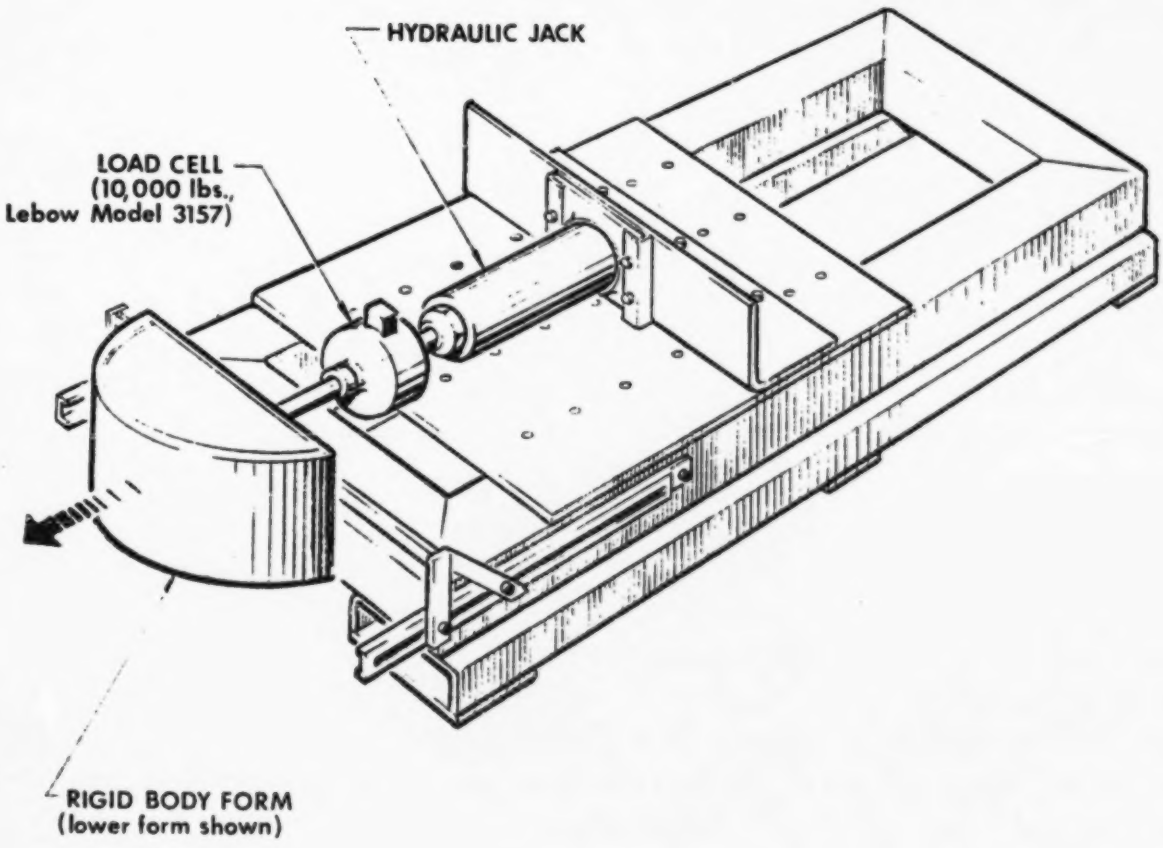

INTERIOR DOOR STATIC CRUSH FIXTURE

FIGURE 22

Static Crush Test Fixture

BEST DOCUMENT AVAILABLE

5.6 Interior Door Crush Tests

The purpose of the interior door crush tests was to determine the force-deflection properties of the Rabbit door interior.

Interior crush tests were conducted during October 1979. Table 1 is the test matrix. Tests No. 2 through No. 9 were performed using the pedestrian impact device to dynamically impact the door interior with the rigid body forms. Most of the vehicles had been previously impacted from the outside and the door was deformed into the compartment. The amount of this intrusion was noted with each test. Tests No. 4, No. 5 and No. 10 used the whole body form at 20 mph. All other tests were conducted with an upper and a lower body form separately, i.e., two tests on each door. Therefore, tests No. 2 & No. 3, No. 6 & No. 7 and No. 8 & No. 9 were pairs of impacts on the same doors with the separate body forms. The body forms' acceleration data and the displacement data were reduced to force-deflection curves using the Hewlett-Packard 9830 Calculator. Figure 23 is a photograph of the post test setup of test No. 7, which was a lower body form into the lower door area with the impacting car engaged near the D.O.R. point.

Tests No. 1 and No. 11 through No. 15 were car-to-car crash tests at 60 degrees. A Chevrolet Malibu was towed into the undeformed sides of the VW Rabbits at various impact speeds. The purpose of the crash tests was to pre-crush the doors of the Rabbits prior to conducting the static interior crush tests. Speeds of 10, 15 and 20 mph were arbitrarily chosen to provide 3 typical levels of penetration. This enabled the stiffness of the inner panel to be correlated with the amount of crush of the door caused by the impacting car. Some impacts were at the door opening reference point and some were at the occupant hip point as noted.

Tests No. 16 through No. 25 were static crush tests performed with the static crush fixture. Again, the tests were conducted using the three body forms and engaging the impacting car at one of the two points. Figure 24 is a photo of

BEST DOCUMENT AVAILABLE

INTERIOR CRUSH TEST MATRIX

Test Number	Test Description	Impact Speed (car-to-car)	Impact Point	Body Form
1	Car-to-car Impact	15 mph	Occupant Hip Point	-----
2	Dynamic Crush* (cars drawn together)	------	" " "	Lower
3	" " " " "	------	" " "	Upper
4	" " " " "	------	Door Opening Ref.Point	Whole
5	" " " " "	------	Occupant Hip Point	Whole
6	" " " " "	------	Door Opening Ref.Point	Upper
7	" " " " "	------	" " " "	Lower
8	" " " " "	------	Occupant Hip Point	Lower
9	" " " " "	------	" " "	Upper
10	Dynamic Crush (one car, alone)	------	-------	Whole
11	Car-to-Car Impact	15 mph	Occupant Hip Point	-----
12	" " " "	10 mph	" " "	-----
13	" " " "	20 mph	" " "	-----
14	" " " "	10 mph	Door Opening Ref. Point	-----
15	" " " "	20 mph	" " " "	-----
16	Static Crush (cars drawn together)	------	Occupant Hip Point	Upper
17	" " " " "	------	" " "	Lower
18	" " " " "	------	" " "	Upper
19	" " " " "	------	" " "	Lower
20	" " " " "	------	" " "	Upper
21	" " " " "	------	" " "	Lower
22	" " " " "	------	Door Opening Ref. Point	Upper
23	" " " " "	------	" " " "	Lower
24	" " " " "	------	" " " "	Upper
25	" " " " "	------	" " " "	Lower

*Pedestrian Impact Device

TABLE 1

BEST DOCUMENT AVAILABLE

FIGURE 23

Dynamic Crush Test #7

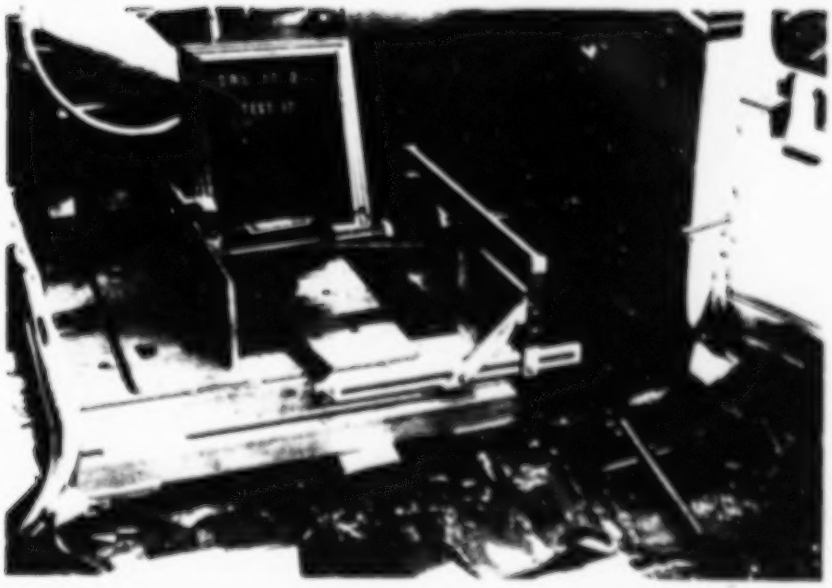

FIGURE 24

Static Crush Test #17

BEST DOCUMENT AVAILABLE

the static crush fixture. Data from the static crush tests were reduced to force-deflection curves in the same manner as the dynamic crush tests. Appendix A contains the force-deflection curves for both the dynamic and the static crush tests.

Appendix B contains trends observed from the crush tests. The crush tests performed at the SRL were done to show trends in stiffness and give approximate values. They should not be viewed as exact and reproduceable conditions. Some reasons for viewing the data with caution are:

1. The test fixture for holding the impacting car against the Rabbit was not as elaborate as desired due to cost constraints. This simple method of engaging cars effects the static data more than the dynamic data. Because the duration of the static tests was longer than that of the dynamic tests, it is highly probable that the cars did not remain solidly engaged. This would account for smaller forces than expected in the static tests.

2. Secondly, the SRL was not able to obtain the Impalas used in the previous Budd tests. Instead, Malibus were used for testing, leading to variation of test parameters for the dynamic tests.

3. The process of impacting and re-engaging the cars for the interior tests may have weakened the door's inner stiffness.

These last two factors may account for the unexpected trend seen for the upper door: at larger vehicle penetrations, smaller forces were recorded than those at smaller vehicle penetrations. All of the above must be taken into consideration when reviewing the data.

BEST DOCUMENT AVAILABLE

Three symbols were used in Appendix B to designate the type of door used. The type of door and its corresponding symbol are as follows:

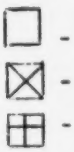

On each graph, the symbols designate specific points of data used in analysis. On certain graphs, a "?" appears. This is to signify our doubts about the validity of the data and to refer the reader to the preceeding paragraph.

The majority of test results exhibited the door properties that were believed to be present: larger forces with larger vehicle penetration, and larger forces on the lower body form than on the upper body form under the same test conditions.

The results showed that the lower door interior is much stiffer than the upper door during the collision. Lower door interior stiffness was seen to increase with increased penetration of the striking vehicle. The upper door sheet metal was established to be a relatively yielding surface for an occupant to interact with. Trends regarding variations in interior door stiffness due to the structural modifications or to the impact point are not felt to be conclusive.

BEST DOCUMENT AVAILABLE

5.7 Analysis of Dynamic Science Test

It was anticipated that when completed, the sled buck was to be checked out by simulating at least two types of laboratory car-to-car tests. The first type selected was a stationary Rabbit impacted by a mid-size vehicle. A Part 572 dummy was to be in the Rabbit. The Budd Test No. II[(2)] was selected. Section 5.8 contains the discussion of this data.

The second type of car-to-car test was chosen to represent more closely the intersection collision environment.

Such a test was performed under conditions being considered as candidate in the upgrade of the FMVSS No. 214 test procedure (60 degree side impact, both cars moving), using the prototype SID. The striking car was an Oldsmobile Cutlass, and the struck car was a VW Rabbit containing the middleweight modified door.

The vehicle accelerometer data, which were especially requested to have been filtered at 60 Hz and at 15 Hz, were received filtered at 100 Hz. Upon receipt, the 100 Hz data was digitized on the Hewlett-Packard 9830 from the report plots and filtered at 15 Hz for better analysis.

At 56 msec into the event, the SID thorax contacted the upper door. The pelvis contacted the lower door at approximately 45 msec. Figure 25 is a comparison of the thorax and upper door accelerations at 60 Hz and 15 Hz, respectively.

The peak acceleration for the thorax of 92.3 g's occurred at 79 msec. The upper door's peak acceleration of 37 g's occurred at 35 msec. Figure 26 is the corresponding comparison for the pelvis and lower door. The peak pelvis acceleration of 88.6 g's occurred at 55 msec. The lower door sustained a peak of 73 g's at 35 msec.

BEST DOCUMENT AVAILABLE

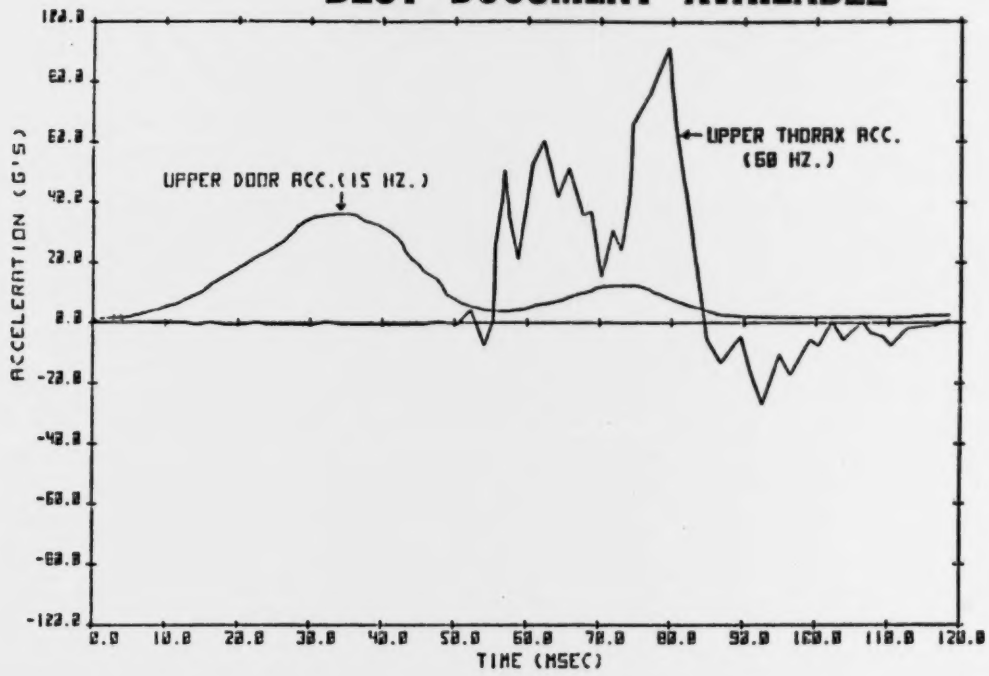

TEST NO. 8330-2 60 DEG. IMPACT

FIGURE 25 - Upper Door/Thorax Acceleraton

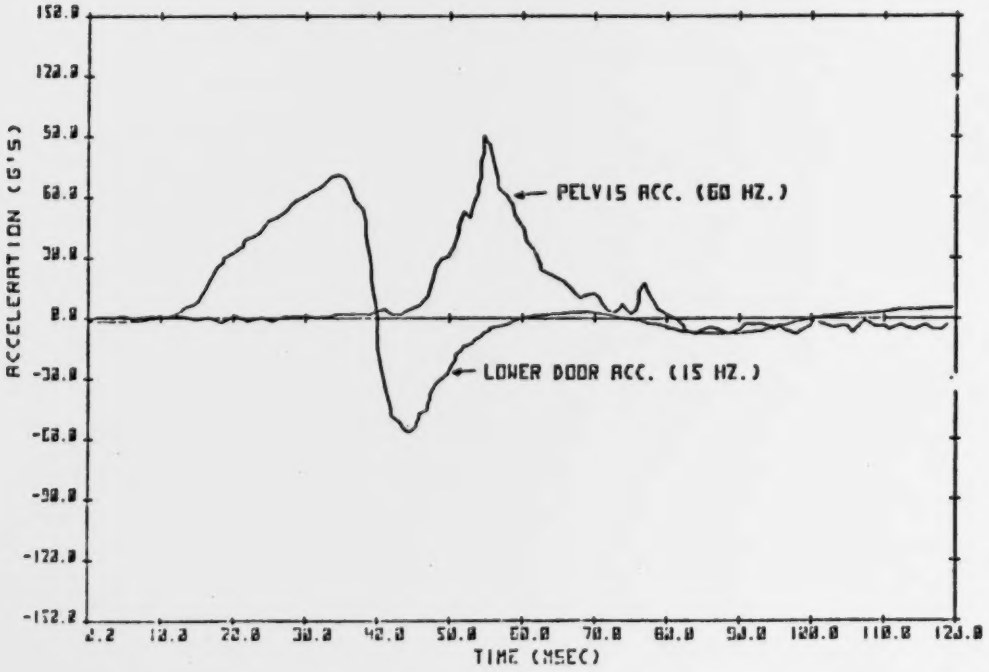

TEST NO. 8330-2 60 DEG. IMPACT

FIGURE 26 - Lower Door/Pelvis Acceleration

BEST DOCUMENT AVAILABLE

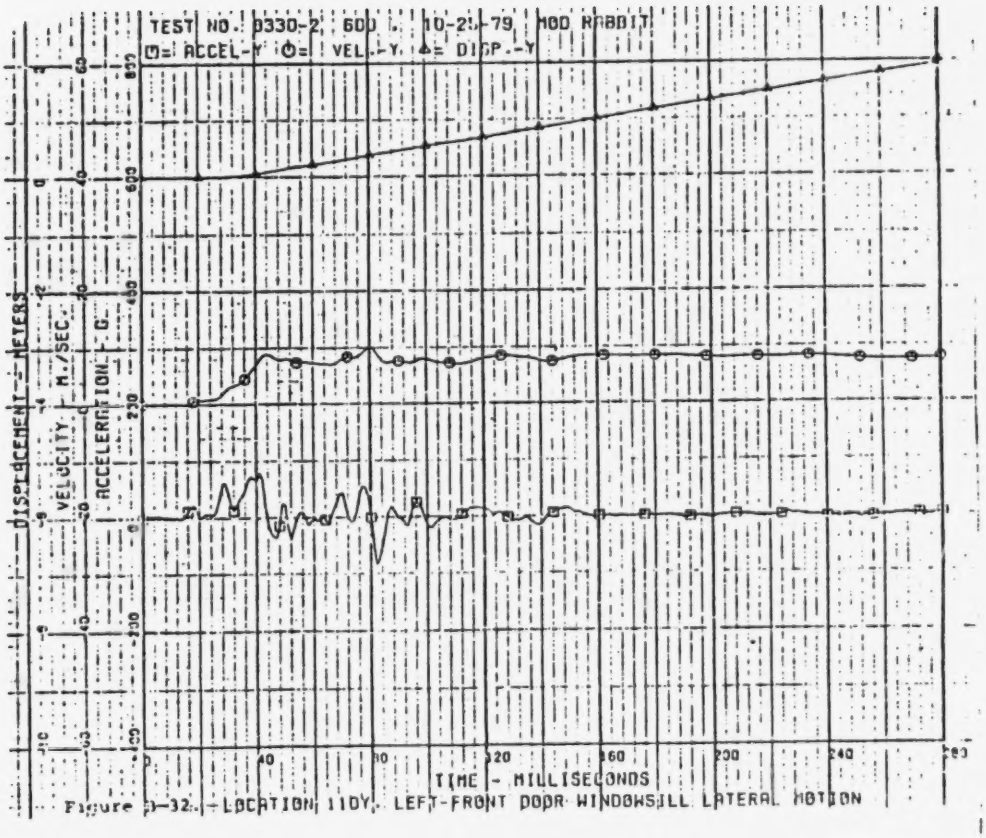
TEST NO. 8330-2 600 L 10-2[illegible]-79 HOD RABBIT
□= ACCEL-Y ○= VEL.-Y △= DISP.-Y
DISPLACEMENT - METERS
VELOCITY - M./SEC.
ACCELERATION - G.
TIME - MILLISECONDS
Figure [illegible]-32. - LOCATION 11DY, LEFT-FRONT DOOR WINDOWSILL LATERAL MOTION

FIGURE 27

DySci No. 8330-2 Upper Door Velocity

BEST DOCUMENT AVAILABLE

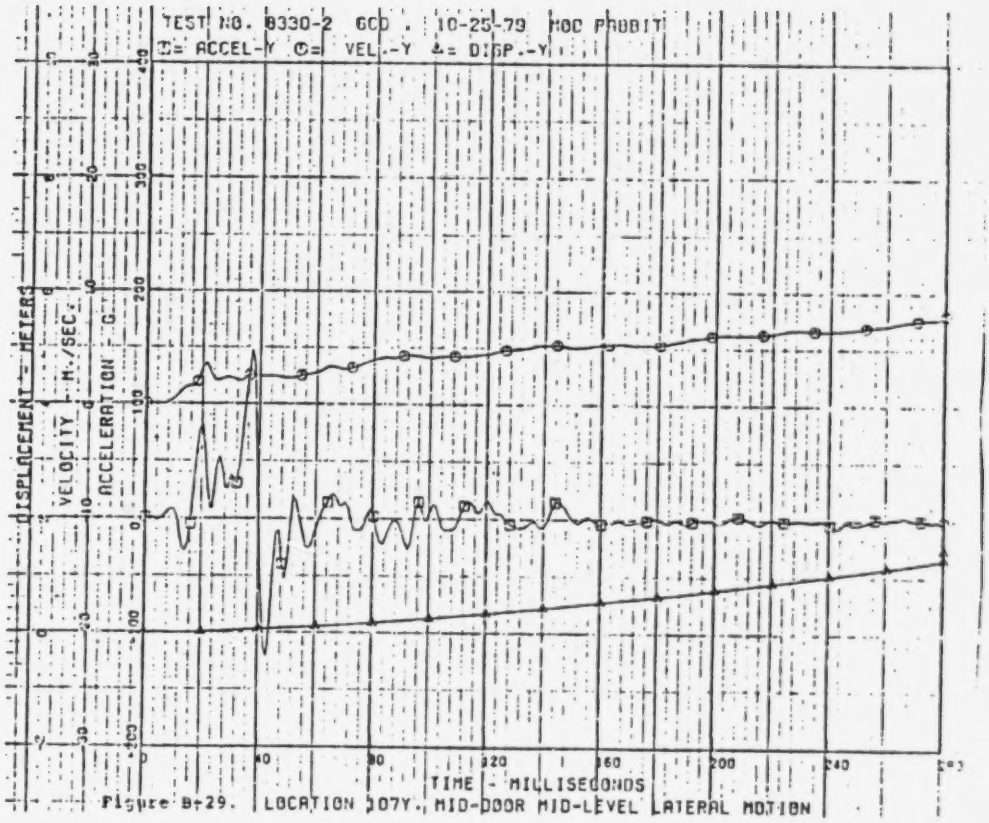
TEST NO. 8330-2 6CD . 10-25-79 HOC PROBIT
□= ACCEL-Y ○= VEL.-Y △= DISP.-Y
DISPLACEMENT - METERS
VELOCITY - M./SEC.
ACCELERATION - G.
TIME - MILLISECONDS
Figure B-29. LOCATION 107Y., MID-DOOR MID-LEVEL LATERAL MOTION

FIGURE 28

DySci No. 8330-2 Lower Door Velocity

BEST DOCUMENT AVAILABLE

Discrepancies were found in the velocity curve of the mid level door accelerometer. Figures 27 and 28 are the upper and mid level door responses reproduced from the Dynamic Science report. In Figure 28, the acceleration was positive until 40 msec, at which time it tended negative. The velocity should have been maximum at this time and begun dropping off. As illustrated, the velocity was only about 5 mph (2.3 meters/sec) at this time and still increasing. An integration using the HP 9830 was attempted from the reported accelerations in Figures 27 and 28.

Figures 29 and 30 are the velocity profiles obtained for the doors from our integration. In Figure 29, the upper door velocity agreed well in shape and magnitude with that reported in Figure 27. In Figure 30, the SRL integraton did not agree with that reported in Figure 28 but was more reasonable in shape and magnitude. The occupant chest and pelvis velocities are shown overlayed on Figures 29 and 30 and also appeared reasonable.

Figure 31 is a force direction vs. time graph for the Rabbit compartment's center of gravity. The initial force direction was approximatly 85 degrees. At approximately 56 msec (time of dummy-door contact), the force direction was 52 degrees.

BEST DOCUMENT AVAILABLE

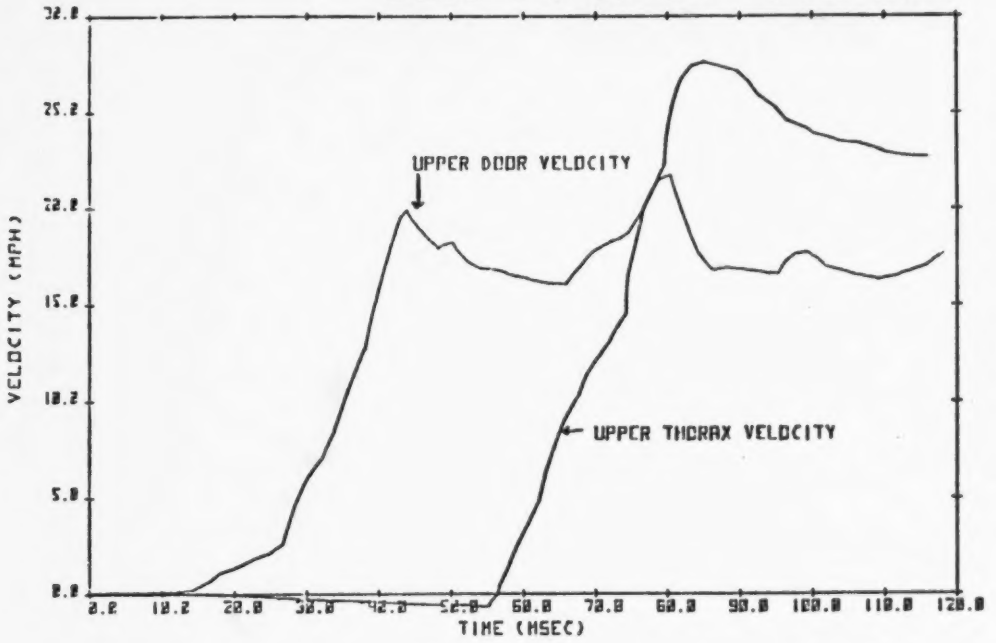

TEST NO. 8330-2 60 DEG. IMPACT

FIGURE 29 - Upper Door/Thorax Velocity

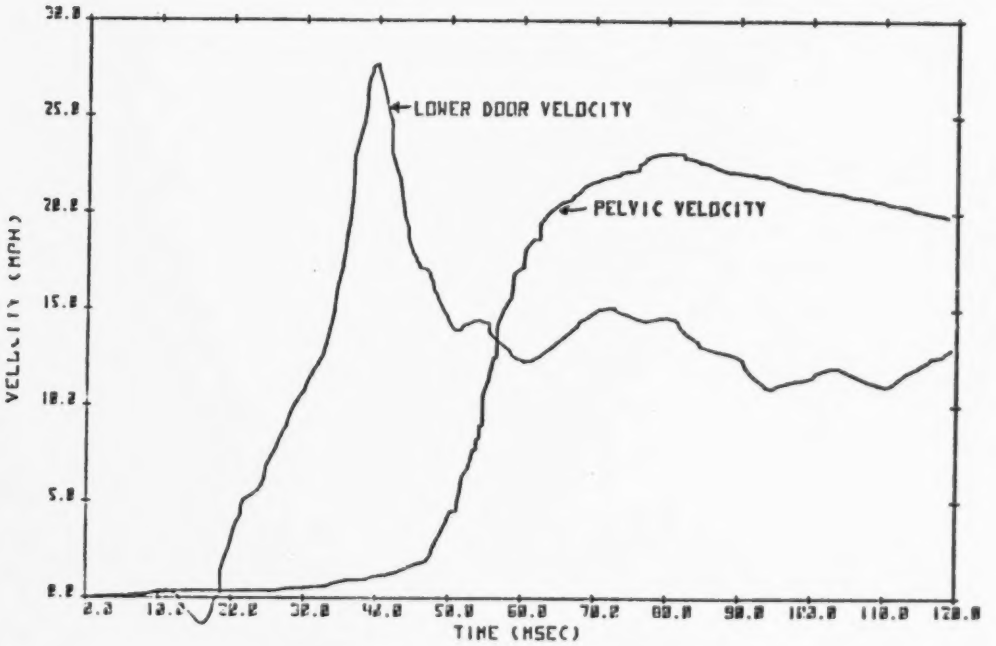

TEST NO. 8330-2 60 DEG. IMPACT

FIGURE 30 - Lower Door/Pelvis Velocity

BEST DOCUMENT AVAILABLE

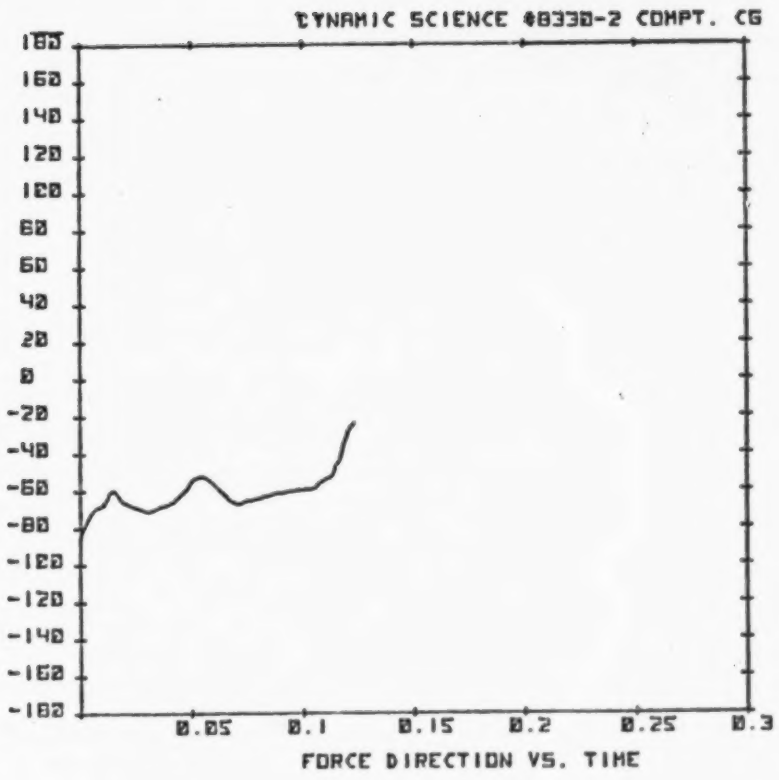

FIGURE 31

DySci No. 8330-2 CG Force Direction

BEST DOCUMENT AVAILABLE

5.8 Definition of Interior Door Stiffness

As mentioned in the previous section, the sled buck was to be demonstrated by reproducing two separate laboratory collisions. The first was to be of a stationary struck VW Rabbit with a Part 572 dummy in the front seat. The second was described in Section 5.7. Budd test No. II[(2)] was selected as the first because the revised middleweight door modification was tested and because the data appeared consistent. The stiffness of the interior door was to be determined from the information gathered in Section 5.6.

It was found from looking at the Budd data that the impacting vehicle intruded 12.4 inches into the compartment. The Part 572 dummy contacted the door at 50 msec into the event and the peak dummy-door interaction occurred at 60 msec. At 75 msec, the far side dummy contacted the near side dummy, preventing further analysis. The impacting car, at 60 msec, approached the seated position (hip point) of the dummy and intruded to near the maximum amount.

Figure 32 shows the force vs. deflection that was derived for the upper door panel on the HYGE sled and Figure 33 shows the lower door panel properties. Figures 32 and 33 reflect static properties of the door. Both static and dynamic force-vs-deflection data were derived for the VW interiors. It was judged to be more reliable to match the static properties of the door panels on the HYGE sled to the static properties of the actual vehicle, since static measurements were more easily made. It was understood that these were only starting points which could be adjusted during HYGE testing.

STATIC CRUSH PROPERTIES

BEST DOCUMENT AVAILABLE

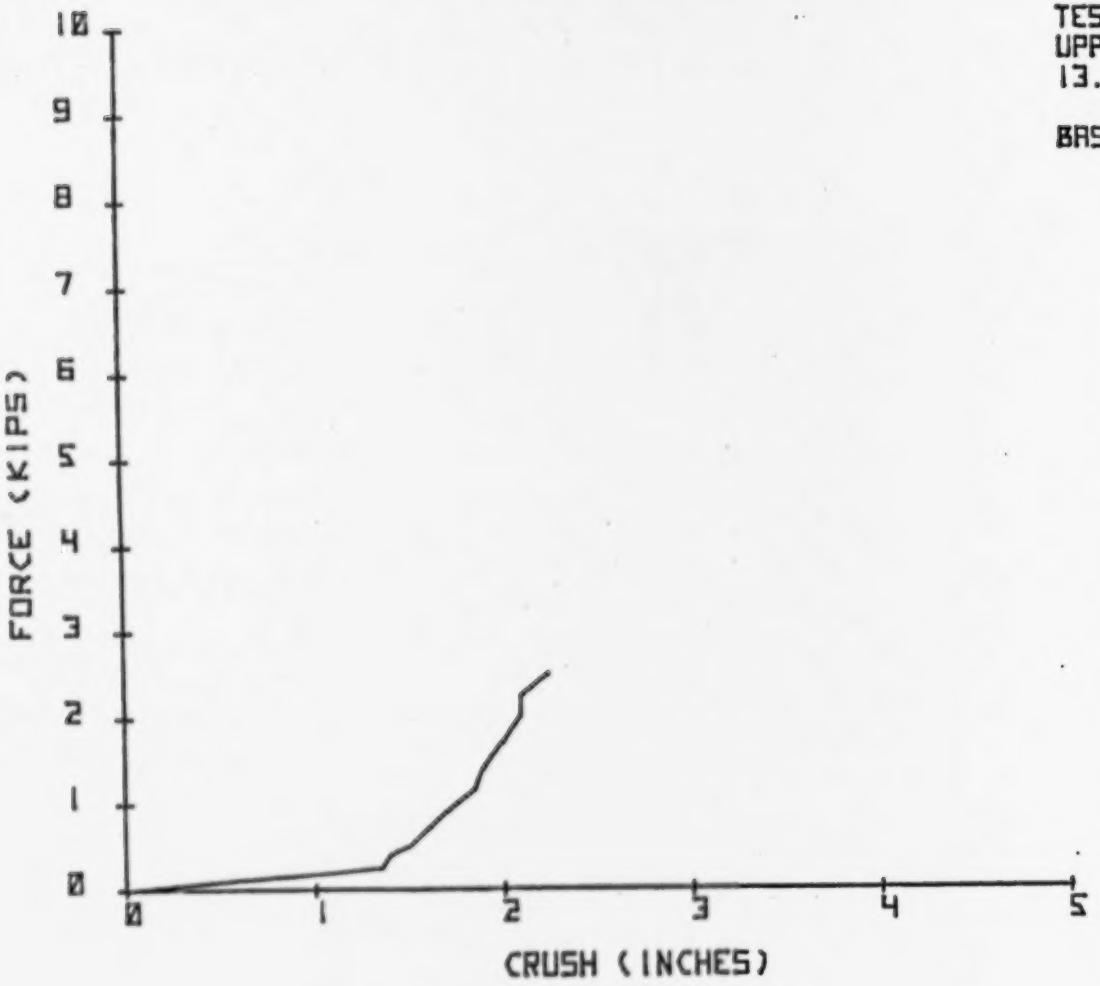

FIGURE 32

Static Crush Test No. 20

BEST DOCUMENT AVAILABLE

STATIC CRUSH PROPERTIES

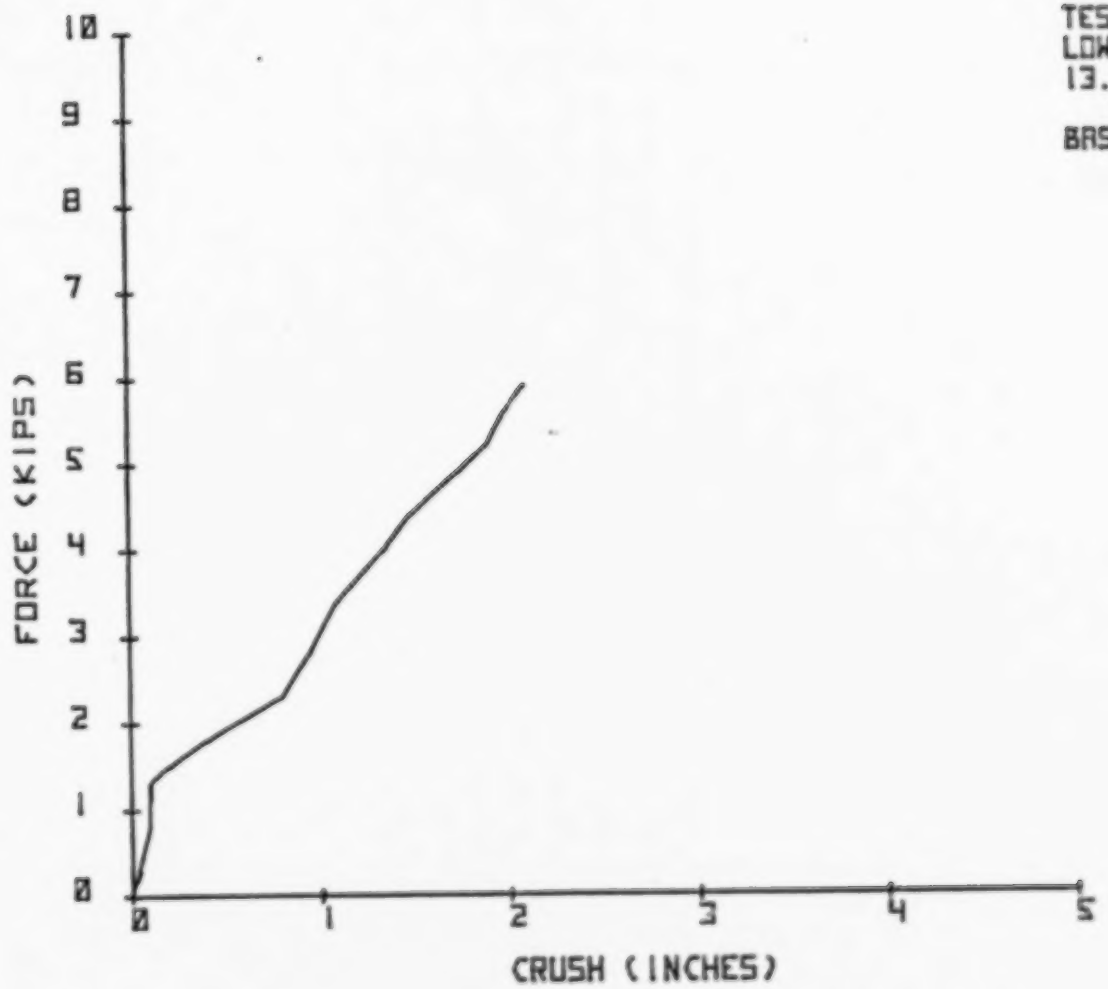

FIGURE 33

Static Crush Test No. 21

BEST DOCUMENT AVAILABLE

5.9 Design and Fabrication of Sled Buck

The sled buck was designed to reproduce the correct (1) velocity-time curve and motion of the interior Rabbit door, (2) kinematics of the surrogate, and (3) accelerations of the surrogate.

The door contact panels were fabricated from reinforced aluminum and were hinged at the A-pillar and attached to roller tape mechanisms at the B-pillars. This enabled separate positioning of each panel with respect to the dummy, based upon the dummy/door relationship in the actual crash tests.

Several experiments were conducted with roller tape mechanisms in the Instron Test Machine. Designs containing both one and three rollers were tested along with varying widths, thicknesses and types of tape materials. A one (1) roller mechanism was chosen for use because of the small travel length (2 inches) and the need to obtain force variations during the small distance. The tape material chosen was steel sheet metal in 0.11 inch and 0.08 inch gauges. Neither the upper door nor the lower door were exactly linear in static force-deflection properties but a linear shape was used for the steel tapes to avoid complicated machining. The force level was controlled by varying the width of the steel tape. The maximum force level to be attained determined the maximum width of the tape profile. The minimum level of force on Figures 32 and 33 is "zero" but this is not physically possible. Instead, the minimum width was determined such that the minimum cross section would not experience tensile fracture when the maximum width was being pulled through the roller. The physical width of the roller that was selected (2.5 inches) and the sheet metal gauges bounded the attainable roller tape forces to between 270 and 7500 pounds. The starting point was very near those of Figures 32 and 33 and variations were made during HYGE tests to "tune" the system to match the car-to-car results.

Appendix C contains a discussion of the mechanics of roller tape mechanisms prepared by Mike Fitzpatrick for the SRL.

BEST DOCUMENT AVAILABLE

The roller tape mechanisms provided achievement of separate force levels for each panel. A roof rail was positioned above the door panels. A left-front seat was positioned on the buck, with the seat track adjustable in the X and Y directions. The seat back was reinforced to the buck frame to prevent lateral motion of the seat.

The sled buck platform was designed to be adjustable to any desired angle. For our purpose, the buck was angled 15 degrees off of pure lateral to approximate the force direction of the 60 degree impact. The sled buck was instrumented to measure accelerations in the X, Y and Z directions. Accelerometers were mounted on each contact panel to measure its lateral acceleration. Potentiometers were also mounted behind each panel to measure the panel's relative displacement. Three high speed camera mounts were positioned on the buck in the following manner: on the front of the buck, outboard to the left, and directly overhead of the dummy.

Toward the end of the padding component testing, a sheet of Lexan was angled outboard from the door panels to simulate the impacting car's hood, which the dummy's head contacted during the Dynamic Science test[3].

Figure 34 is an assembled view of the sled buck. An exploded view is shown in Figure 35.

BEST DOCUMENT AVAILABLE

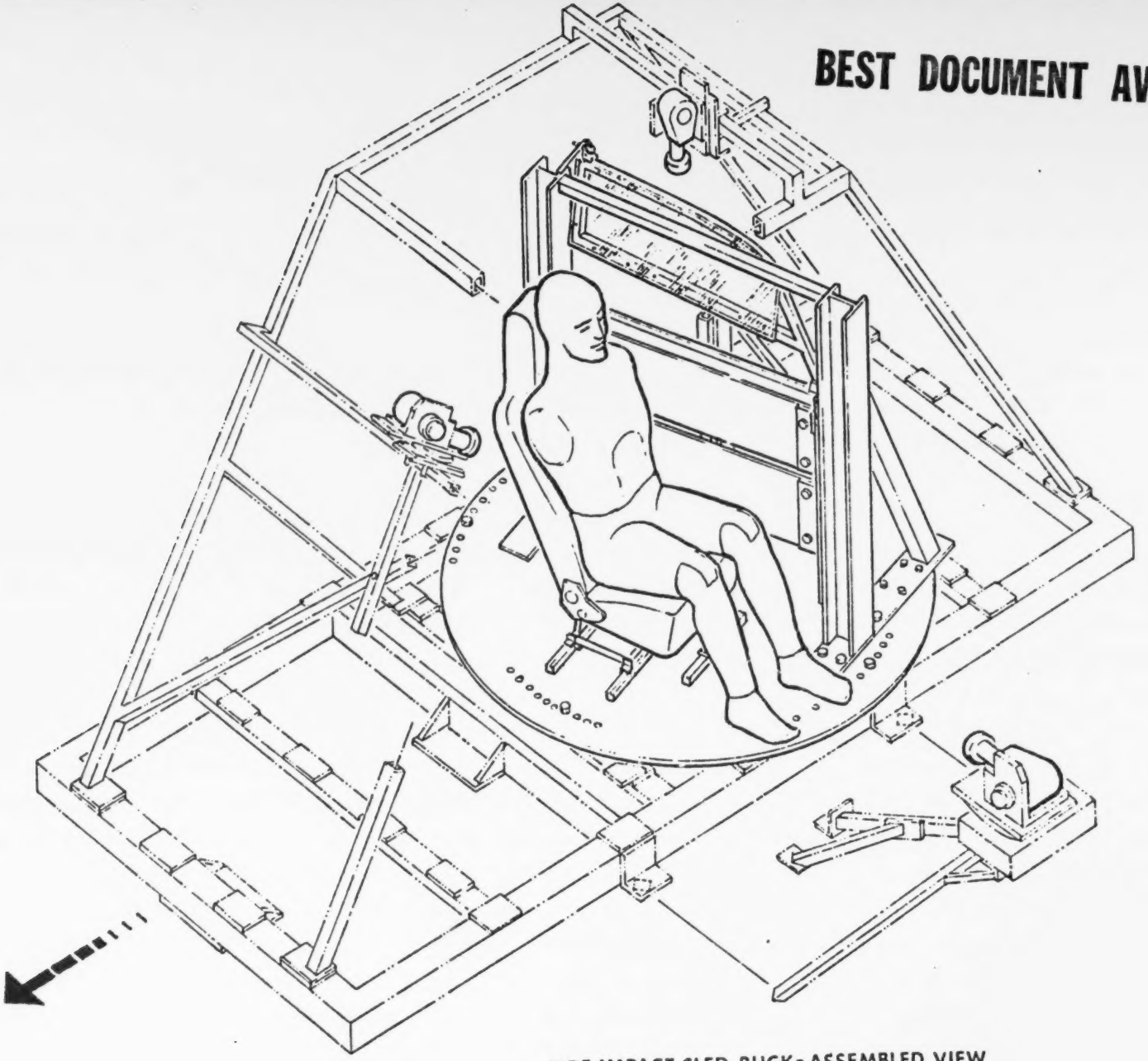

SIDE IMPACT SLED BUCK - ASSEMBLED VIEW

FIGURE 34

BEST DOCUMENT AVAILABLE

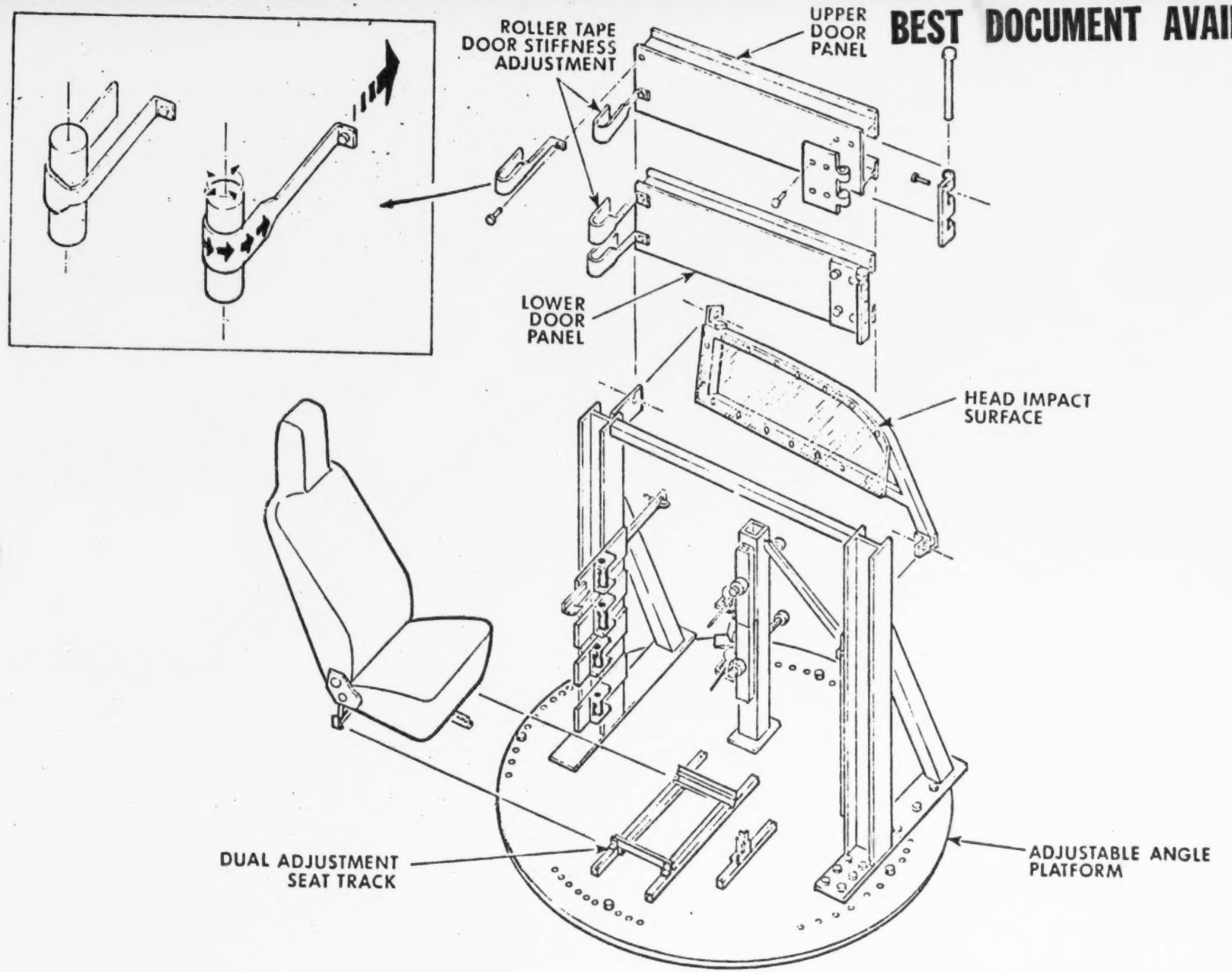

SIDE IMPACT SLED BUCK- EXPLODED VIEW

FIGURE 35

BEST DOCUMENT AVAILABLE

5.10 HYGE Sled Simulation of Budd Test No. II

The purpose for simulating Budd Test No. II[2] (a car-to-car impact) was to check out the sled with a Part 572 dummy, attempting to match the upper door and chest responses and the lower door and pelvis responses. Also, a matching of the over-all dummy kinematic response of the car-to-car collision was attempted. In Budd Test No. II, the bullet car was traveling at 30 mph, the modified Rabbit was stationary and the angle of impact was 60 degrees.

The sled buck platform was rotated to 15 degrees off of pure lateral to approximate the force direction of the impact. The lower door panel was initially 2 inches closer to the occupant than the upper panel to simulate the displacement caused by the striking vehicle bumper in the collision.

Nine sled tests were conducted with the Part 572 dummy. The test velocity was held constant at 22 mph for all tests. Five parameters were varied from test to test: dummy arm-to-door and pelvis-to-door distances, lower door panel offset, door reference position (to a specified point on buck frame) and roller tape dimensions.

Table 2 is a matrix of parameter variations made on the test buck. Table 3 is a corresponding matrix of post-test results for the 572 dummy and both door panels. Appendix D contains occupant/door comparisons for the Budd test simulations. During Tests No. 8 and No. 9, roller tape mechanisms were not used. Both door panels were braced from behind to prevent stroking. In Test No. 8, both panels were observed to bend outward because of the dummy. However, in Test No. 9, both panels were bolted to the frame of the test buck, approaching the rigid wall effect.

Test films revealed that even with the bracing, small deflections in the door occurred. This variation and that of Test No. 8 produced a marked increase in the dummy's peak chest and pelvis accelerations and chest severity index. Figures 36 and 37 are the chest and pelvis accelerations from Test No. 9.

BEST DOCUMENT AVAILABLE

TABLE 2

Test Buck Parameter Variations Matrix for Budd Simulation

Test #	Door Reference Position	Bottom Panel Offset	Max. Force Upper Panel (lbs)	Max. Force Lower Panel (lbs)	Upper Panel Max. Force Per Tape	Lower Panel Max. Force Per Tape	Length of Tape Profile	Min. Force Upper Panel (lbs)	Min. Force Lower Panel (lbs)	Door Arm to Door Distance	Door Pivot to Door Distance
1	0	0.75"	1160	5640	#1 - 580 lbs #2 - 580 lbs	#3 - 2820 lbs #4 - 2820 lbs	3.0"	753	1176	4.625"	6.75"
2	1.0"	1.5"	3000	6459	#1 - 2000 lbs #2 - 1000 lbs	#3 - 3760 lbs #4 - 2699 lbs	3.0"	753	2321	4.5"	6.125"
3	1.0"	2.5"	3000	6459	#1 - 2250 lbs #2 - 750 lbs	#3 - 3760 lbs #4 - 2699 lbs	2.0"	753	2909	4.5"	6.125"
4	1.0"	1.625"	3000	6459	#1 - 2499 lbs #2 - 501 lbs	#3 - 3760 lbs #4 - 2699 lbs	2.0"	753	2909	4.5"	6.125"
5	1.0"	2.625"	3000	6459	#1 - 2499 lbs #2 - 501 lbs	#3 - 3760 lbs #4 - 2699 lbs	2.0"	753	2909	5.0"	6.5"
6	1.0"	2.375"	3000	6459	#1 - 2499 lbs #2 - 501 lbs	#3 - 3760 lbs #4 - 2699 lbs	2.0"	753	2909	5.0"	6.625"
7	1.0"	2.625"	3000	6459	#1 - 2499 lbs #2 - 501 lbs	#3 - 3760 lbs #4 - 2699 lbs	2.0"	753	2909	5.0"	6.625"
8	1.0"	2.437"	(NO TAPES)	-	-	-	-	-	-	5.0"	6.625"
9	1.0"	2.437"	(NO TAPES)	-	-	-	-	-	-	5.0"	6.625"

BEST DOCUMENT AVAILABLE

TABLE 3

Budd Simulation Test Results

Test #	Chest Peak Acc. (G's)	Pelvis Peak Acc. (G's)	Upper Door Peak Acc. (G's)	Lower Door Peak Acc. (G's)	Upper Door Displacement	Lower Door Displacement	Chest Severity Index	Chest Peak Acc. (3 m sec)	Pelvis Peak Acc. (3 m sec)	Post Test: Tape Extensions
1	80.0	65.9	46.2	41.3	1.20"	0.54"	368.6	52.4	64.4	#1 - #2 - #3 - #4 -
2	68.5	66.3	45.1	43.2	1.52"	0.4"	307.5	48.9	64.8	#1 - 2.25" #2 - 1.475" #3 - 0.5" #4 - 0.2"
3	73.4	88.6	50.7	44.9	1.40"	0.46"	385.4	48.9	84.9	#1 - 2.0" #2 - 1.375" #3 - 0.25" #4 - 0.125"
4	76.3	77.5	46.5	41.4	1.37"	0.3"	416.5	56.8	73.5	#1 - 2.0" #2 - 1.5" #3 - 0.156" #4 - 0.1875"
5	71.1	95.3	45.1	42.6	1.18"	0.39"	422.1	60.2	90.3	#1 - 1.78" #2 - 1.156" #3 - 0.375" #4 - 0.156"
6	74.6	117.4	46.9	45.6	1.20"	0.37"	360.7	50.3	111.8	#1 - 1.75" #2 - 1.25" #3 - 0.5" #4 - 0.0"
7	70.2	65.8	40.7	37.2	1.12"	0.35"	337.5	53.0	56.3	#1 - 1.468" #2 - 1.094" #3 - 0.25" #4 - 0.125"
8	114.8	93.7	49.6	41.6	0.17"	0.32"	733.2	109.8	87.2	----------
9	129.9	137.0	42.7	37.5	0.62"	0.07"	1013.0	125.5	128.6	----------

BEST DOCUMENT AVAILABLE

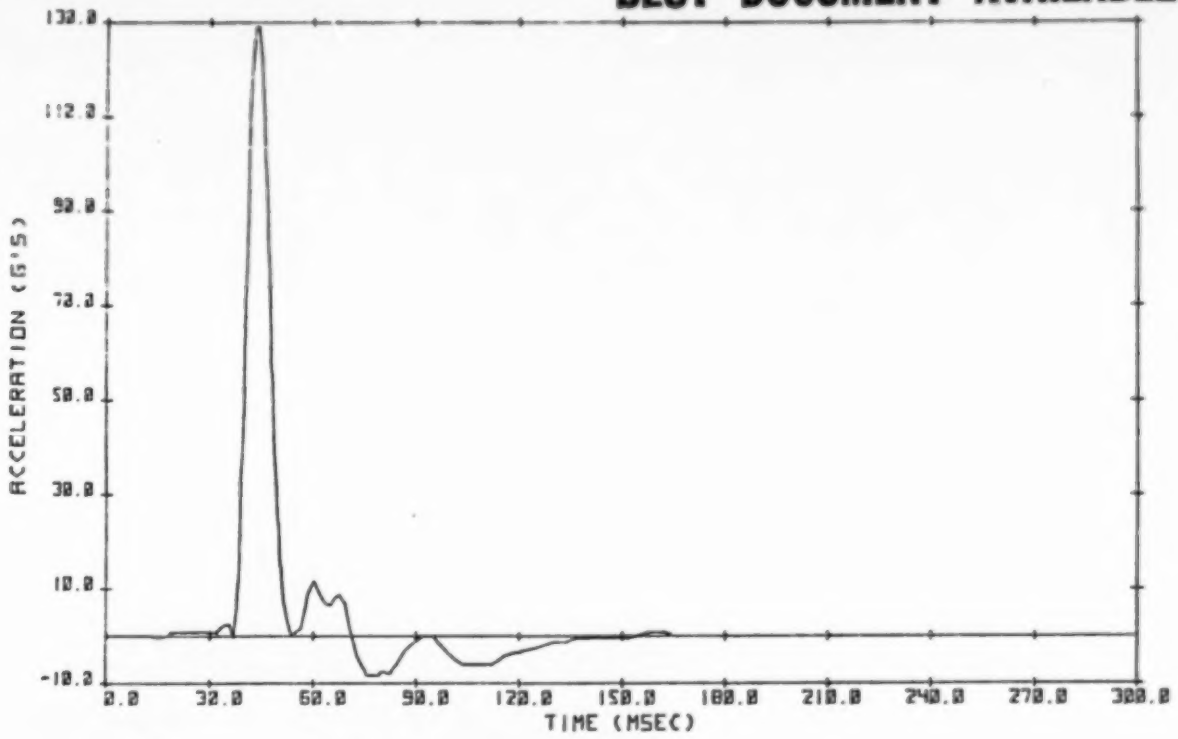

CHEST ACCELERATION (SRL 17-5 #9)

FIGURE 36

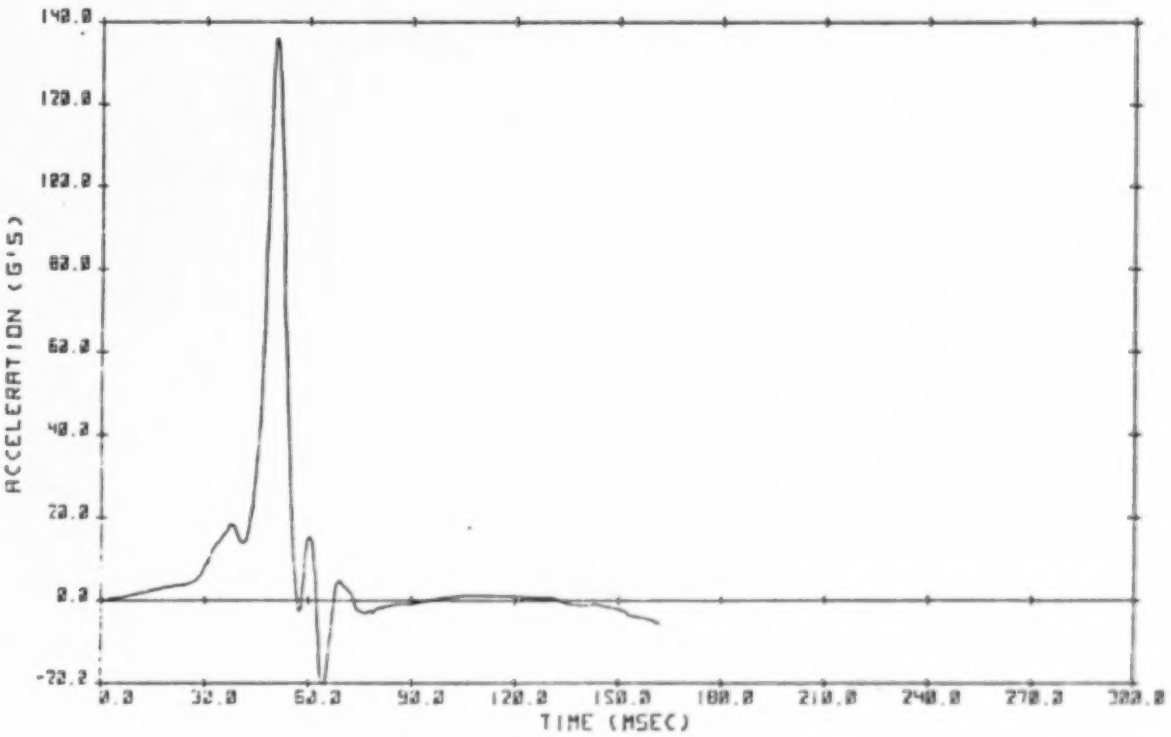

PELVIS ACCELERATION (SRL 17-5 #9)

FIGURE 37

BEST DOCUMENT AVAILABLE

In the car-to-car crash, the dummy's head just missed the roof rail as it went out the side window. After the shoulder and pelvis were struck by the door, the body rotated to face more into the door. The pelvis was thrown from the door ahead of the upper body area.

The kinematic comparison of sled test and car-to-car crash was best done by viewing the two movie films side by side. Figure 38 is a time sequence taken from the Budd crash test high speed films. The approximate time from dummy-door contact of each frame is shown. Figure 39 is a similar presentation for SRL sled test number 6. Note the similarity of motions as described earlier. In the car event, vehicle rotation during the time that the dummy was in free flight toward the opposite side (this is also after the vehicles have separated) gave the appearance that the dummy's trajectory was purely lateral in the compartment. In the absence of vehicle rotation, the dummy's trajectory would have taken it into the dashboard area. Since the sled does not rotate, the dummy had the appearance of being thrown forward in the compartment after the door contact.

In the car-to-car event, the direction of the dummy prior to door contact could not be determined from the films, so the angular setting of the sled could not be verified.

The second criteria for evaluating the sled was the acceleration responses of the dummy and door components. The dummy pelvis response and sled lower door response are coupled together in the sense that one affects the other. By varying the width profile of the two roller tapes on the lower door the car-to-car response of the pelvis was matched. Figures 40 and 41 are the comparisons of lower pelvis and door acceleration responses from the crash event and the sled event. Lower door accelerations were both on the order of 40 g's and pelvis accelerations both on the order of 110 g's. This was felt to be a good simulation.

The chest lateral acceleration and upper door responses are shown in Figures 42 and 43. The upper door acceleration was higher in the sled simulation than

Blank Page

BEST DOCUMENT AVAILABLE

0 ms

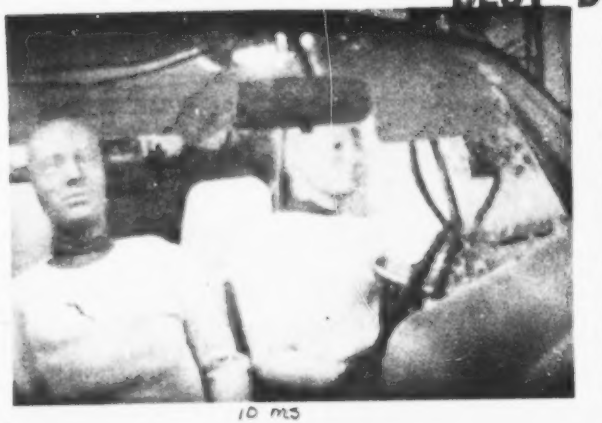
10 ms

20 ms

30 ms

40 ms

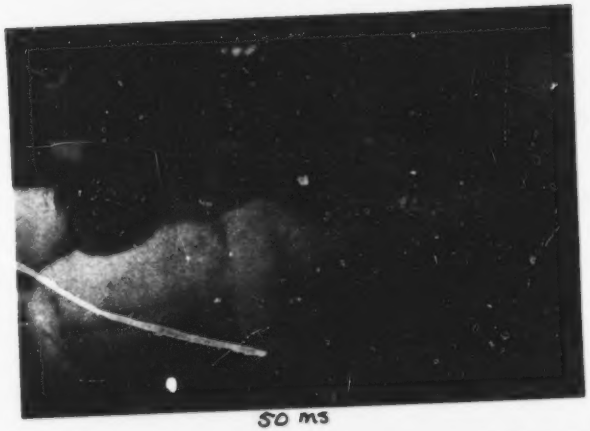
50 ms

60 ms

70 ms

80 ms

FIGURE 38 - Budd Test No. 11

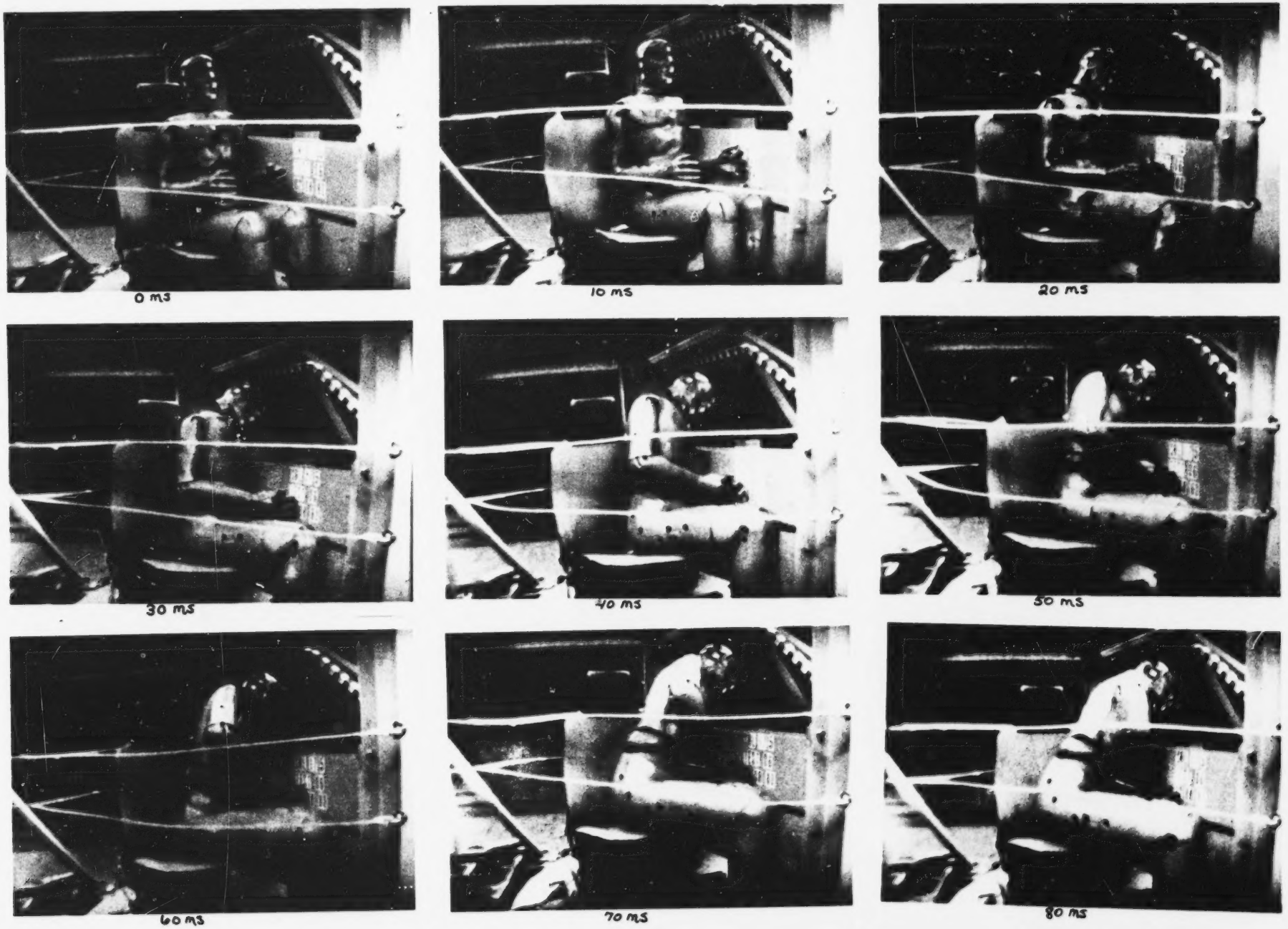

FIGURE 39 - SRL Test No. 6

BEST DOCUMENT AVAILABLE

BEST DOCUMENT AVAILABLE

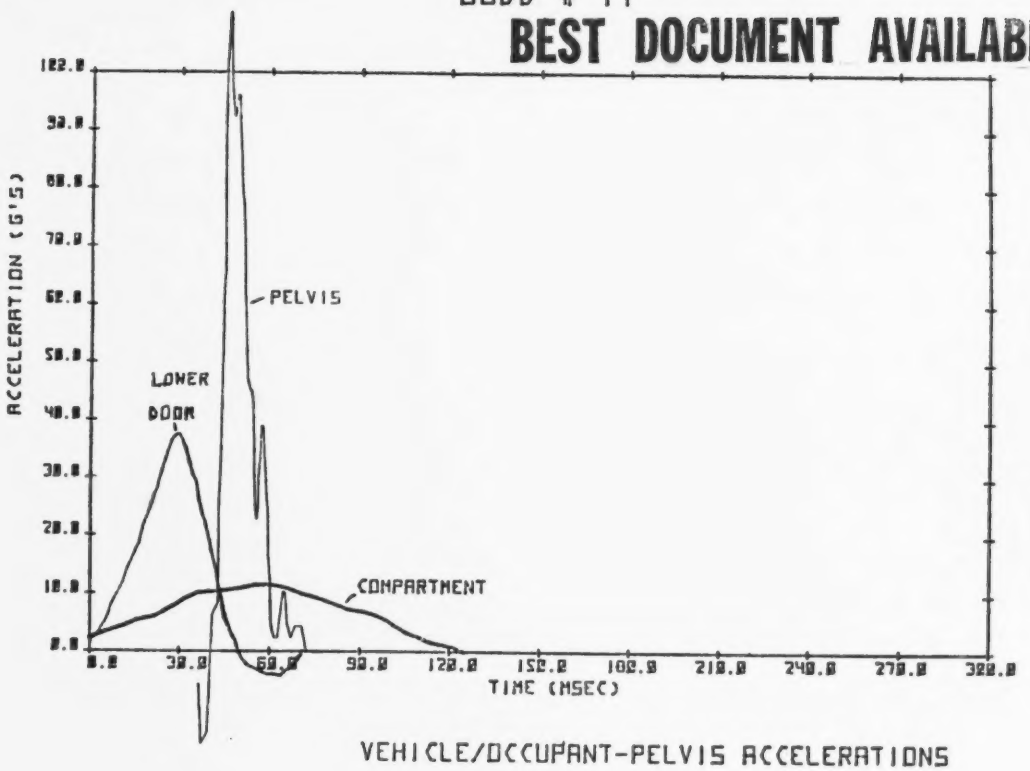

VEHICLE/OCCUPANT-PELVIS ACCELERATIONS

FIGURE 40
SRL 17-5 TEST #6

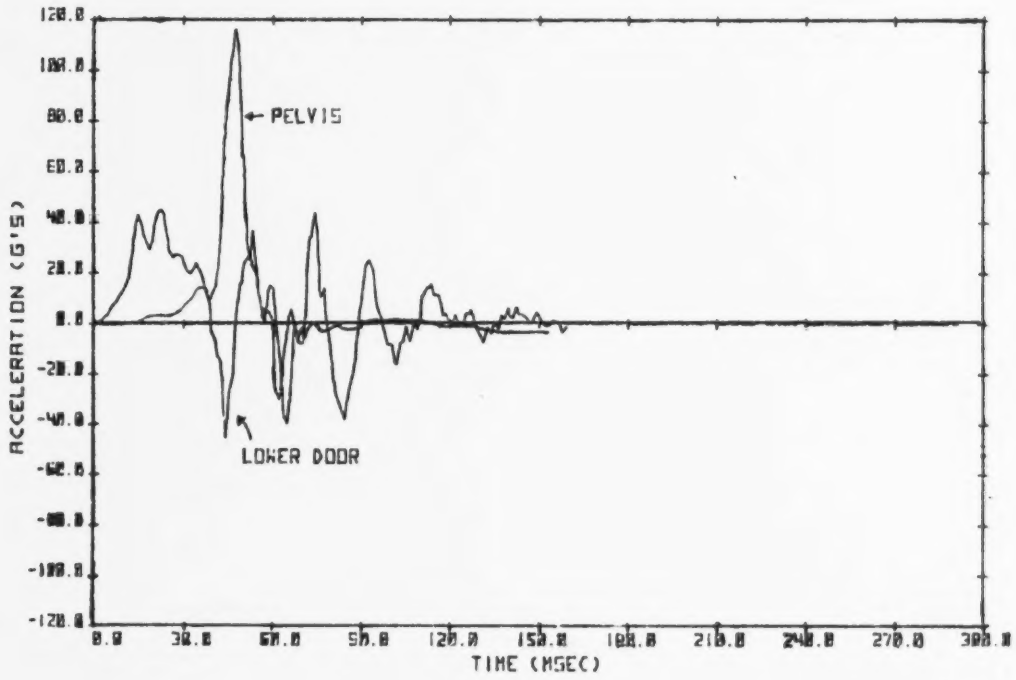

LOWER DOOR/OCCUPANT-PELVIS ACCELERATIONS

FIGURE 41

BEST DOCUMENT AVAILABLE

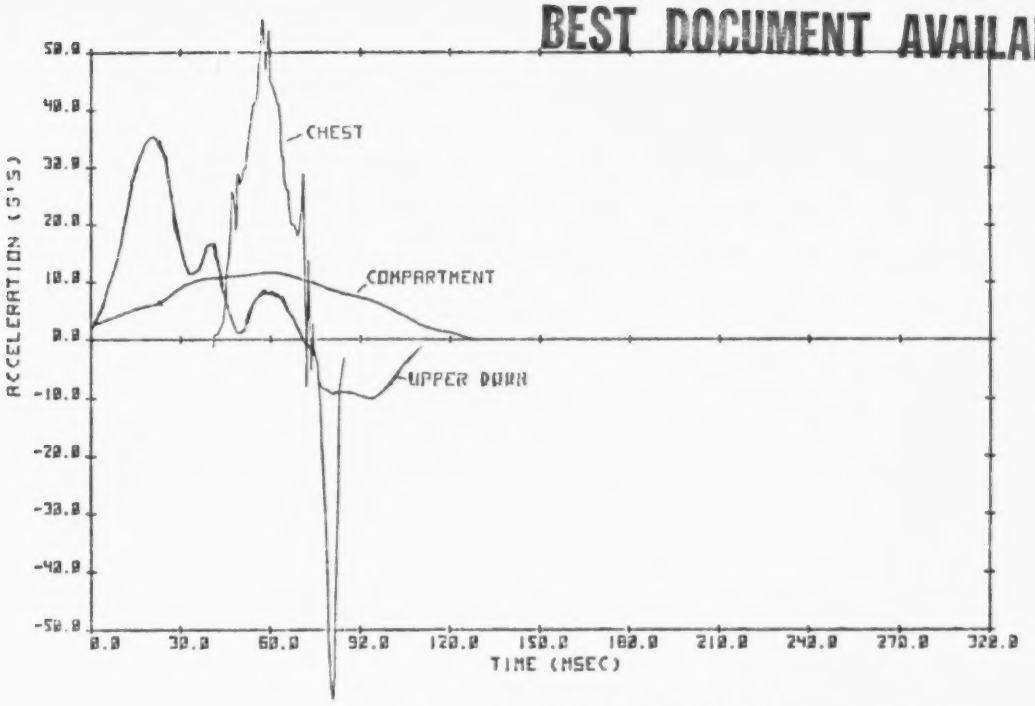

VEHICLE/OCCUPANT-CHEST ACCELERATIONS

FIGURE 42

SRL 17-5 TEST #5

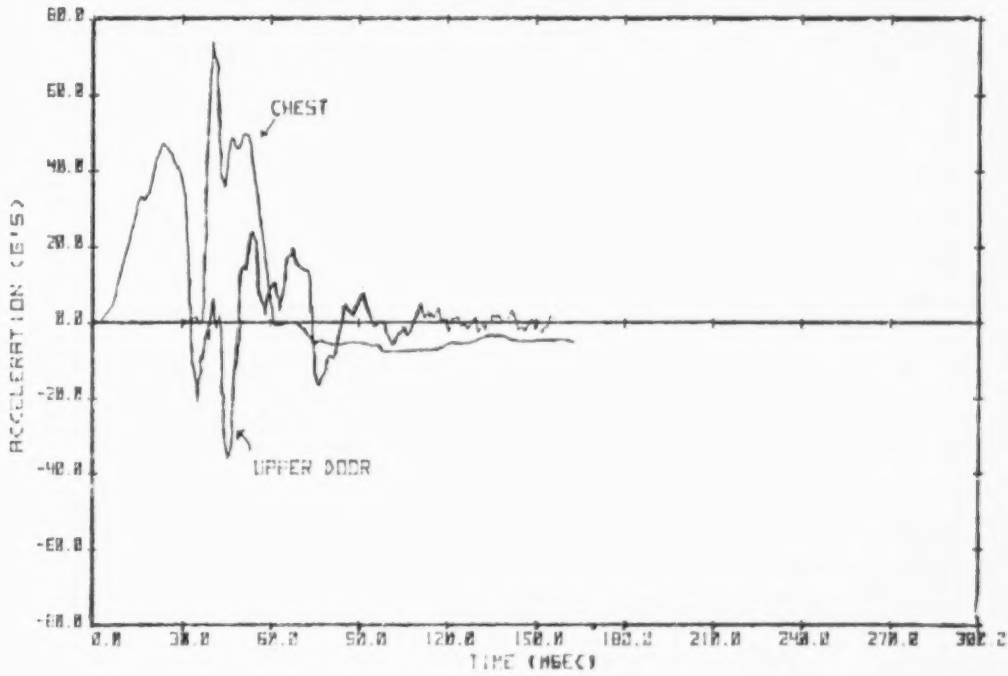

UPPER DOOR/OCCUPANT-CHEST ACCELERATIONS

FIGURE 43

BEST DOCUMENT AVAILABLE

in the car event. Also, the early inertial spike on the chest acceleration was higher in the simulation. The inertial spike indicated that the effective mass of the door was too high, but the doors could not be significantly lightened without losing needed strength. The roller tape profile was adjusted to accomplish an approximate match (average magnitude and pulse width) of the car event. The chest response of Figure 43 was felt to be a reasonable approximation of that of Figure 42.

BEST DOCUMENT AVAILABLE

5.11 HYGE Sled Simulation of Dynamic Science Test #8330-2

Dynamic Science Test No. 8330-2[3] was next selected to be simulated. The test mode for the car-to-car crash test was: bullet vehicle traveling at 30 mph, target vehicle (modified Rabbit) traveling at 15 mph, and a 60 degree impact angle into the Rabbit compartment. It was determined that the sled configuration and roller tapes of the Budd simulation were a reasonable starting point for the Dynamic Science crash test simulation.

The Side Impact Dummy (SID) developed by the Highway Safety Research Institute, University of Michigan, was used in the Rabbit. SID calibration was accomplished using the pendulum impact device built at the VRTC. Figure 44 is a photo of the test setup for the pendulum thorax calibration tests using the prototype SID. The impactor height was 17.7 inches above the seat as specified in the Part 572 calibration procedures. It was noted that the left upper rib accelerations were higher than the 40G average of the cadaver tests. Also, the spinal and left lower rib readings were lower than the desired average. This would imply that the impactor should be centered on the rib cage of the SID rather than 17.7 inches above the seat as with the Part 572 thorax.

The lateral velocity change at the mid level of the near side door in the subject test was around 20 mph at the time the dummy's thorax contacted it. The lower door velocity was above 25 mph in the reported data. Some concern existed as to the validity of the door accelerometer data. The SRL selected a sled velocity around 22 mph to attempt the simulation.

The test parameters used to determine goodness of fit were the same as those for the Budd No. II simulation: matching the chest and upper door responses, the pelvis and lower door responses, and the over-all dummy kinematic response of the car-to-car collision.

BEST DOCUMENT AVAILABLE

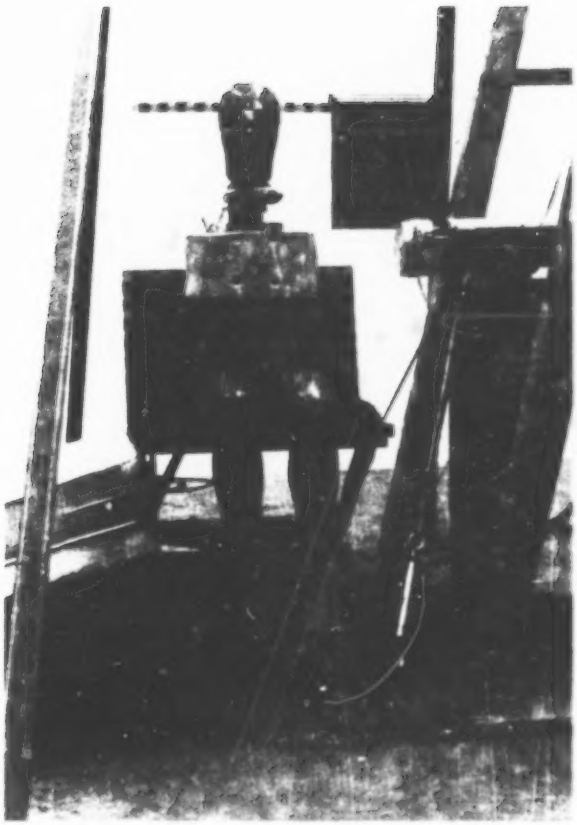

FIGURE 44

Pendulum Calibration Test Set-up

BEST DOCUMENT AVAILABLE

The pelvis acceleration from the car crash peaked at around 90 g's, which was lower than in the Budd test. This indicated that the door stiffness was less, probably because the striking car bumper was not at the pelvic area at the same time pelvic contact occurred.

The parameter values of relative distances, etc. became unknowns again in this new test configuration. Four parameters were varied from test-to-test: dummy arm-to-door and pelvis-to-door distances, lower panel offset and roller tape dimensions. The distance variations did not cause major response differences but rather subtle relative timing changes. Table 4 contains the list of parameters which were varied. Table 5 contains the results for the eight sled tests.

The HYGE sled test series with the SID was much more complicated than those with the Part 572 dummy due to the number of accelerometer time histories to match, and due to the frequency of breakage, and sensitivity of the left rib accelerometer to the inertial effect of the door. In addition, the car-to-car test being simulated was conducted with both vehicles in motion. This added motion may have been responsible for the unusual left upper rib acceleration (the peak was lower and the pulse much longer than expected). The motion definitely caused excessive vehicle rotation late in the contact event and during spinout.

Some rib bending resulted from each sled test in the baseline simulation series. Refurbishing was necessary after Test No. 12. Tests No. 10 through No. 13 were performed in an attempt to match the acceleration and gross kinematic responses of the car-to-car event. In Test No. 12, the left upper rib acceleration was much higher in the simulation than in the car (Figure 45). If the inertial spike were removed, it would have been a reasonable approximation. Figure 46 shows the pelvic response for Test No. 12 and the pelvic response from the car event. A reasonable match was attained. Figure 47 shows the right upper rib comparison. Both have a double peak and are around 60 g's in magnitude. This is also a reasonable match. Figures 48 and 49 show comparisons of the spinal accelerations. The two upper spine

BEST DOCUMENT AVAILABLE

TABLE 4

Test Data Parameter Variations Matrix for
DySCi No. 8330-2 Simulation

Test #	Bottom Panel Offset	Max. Force Upper Panel (lbs)	Max. Force Lower Panel (lbs)	Upper Panel Max. Force Per Tape	Lower Panel Max. Force Per Tape	Length of Tape Profile	Min. Force Upper Panel (lbs)	Min. Force Lower Panel (lbs)	Dummy Arm to Door Distance	Dummy Pelvis to Door Distance
10	1.25"	3000	6459	#1 - 2499 #2 - 501	#3 - 3760 #4 - 2699	2.0"	753	2909	6.0"	5.5"
11	1.75"	3500	6459	#1 - 2917 #2 - 583	#3 - 3760 #4 - 2699	2.0"	753	2909	6.5"	5.5"
12	1.75"	3500	5347	#1 - 2917 #2 - 583	#3 - 2673.5 #4 - 2673.5	2.0"	753	2374	6.5"	5.5"
13	0"	3500	5347	#1 - 2917 #2 - 583	#3 - 2673.5 #4 - 2673.5	2.0"	753	2374	6.5"	6.5"
14	1.0"	3500	4812.4	#1 - 2917 #2 - 583	#3 - 2406.2 #4 - 2406.2	2.0"	753	2139	6.5"	7.25"
15	1.0"	3724.6	4812.4	#1 - 2994.4 #2 - 730.2	#3 - 2406.2 #4 - 2406.2	1.0"	753	2139	6.5"	7.25"
16	1.0"	3671.1	4812.4	#1 - 2940.9 #2 - 730.2	#3 - 2406.2 #4 - 2406.2	1.0"	1020.7	2139	6.5"	7.25"
17	1.0"	3671.1	4812.4	#1 - 2940.9 #2 - 730.2	#3 - 2406.2 #4 - 2406.2	1.0"	1020.7	2139	6.5"	7.25"

BEST DOCUMENT AVAILABLE

TABLE 5

DySci No. 8330-2 Simulation Test Results

TEST NO.	PADDING: UPPER PANEL	PADDING: LOWER PANEL	AIS B PARAM.	PEAK UPPER SPINE (G)	PEAK LOWER SPINE (G)	PEAK PELVIS (G)	DAMPER DISPLACE-MENT (IN)
10	-	-	3.6	49.5	85.9	89.7	1.72
11	-	-	3.6	59.7	94.1	102.5	1.98
12	-	-	3.5	59.0	82.5	86.9	1.45
13	-	-	3.9	57.1	76.9	88.6	1.59
14	-	-	4.0	51.0	81.6	78.8	1.62
15	-	-	4.1	52.1	78.3	89.7	1.74
16	-	-	3.9	59.0	82.5	94.7	1.68
17	-	-	3.7	57.0	90.6	93.1	1.74

BEST DOCUMENT AVAILABLE

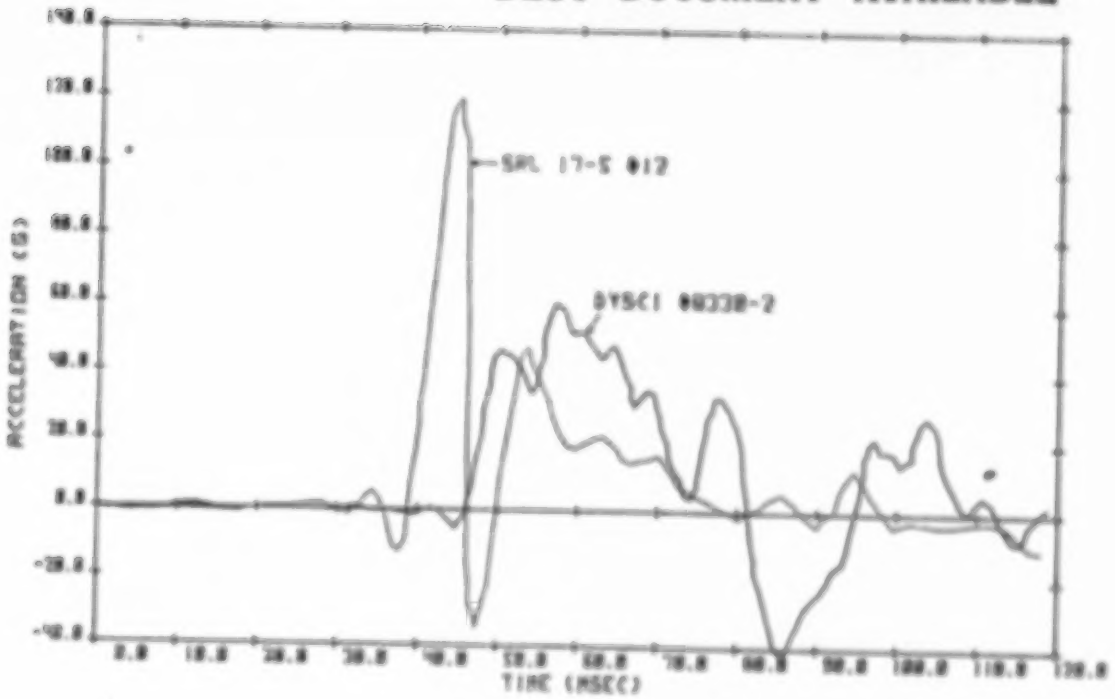

L. UPPER RIB ACCELERATION

FIGURE 45

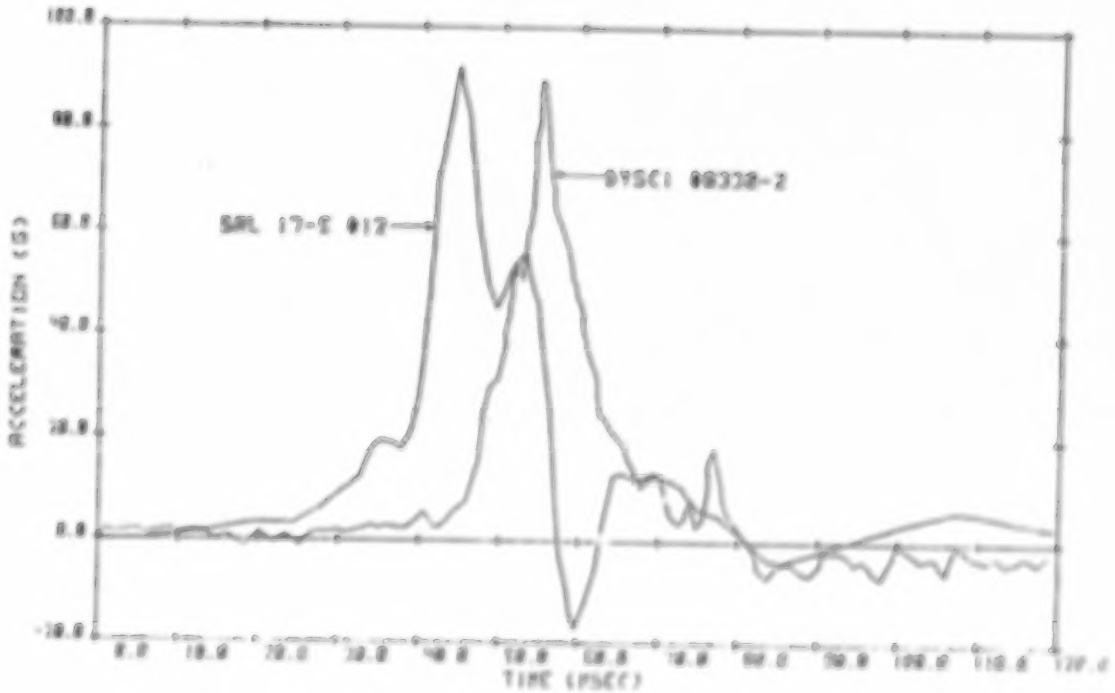

PELVIS ACCELERATION

FIGURE 46

BEST DOCUMENT AVAILABLE

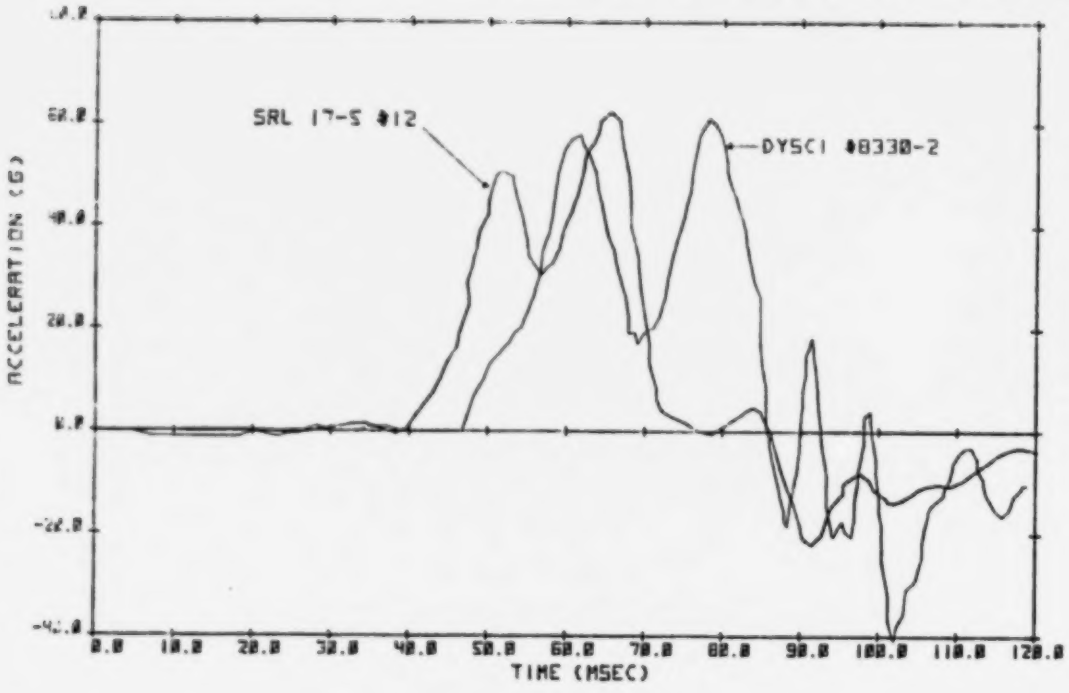

RIGHT UPPER RIB ACCELERATION

FIGURE 47

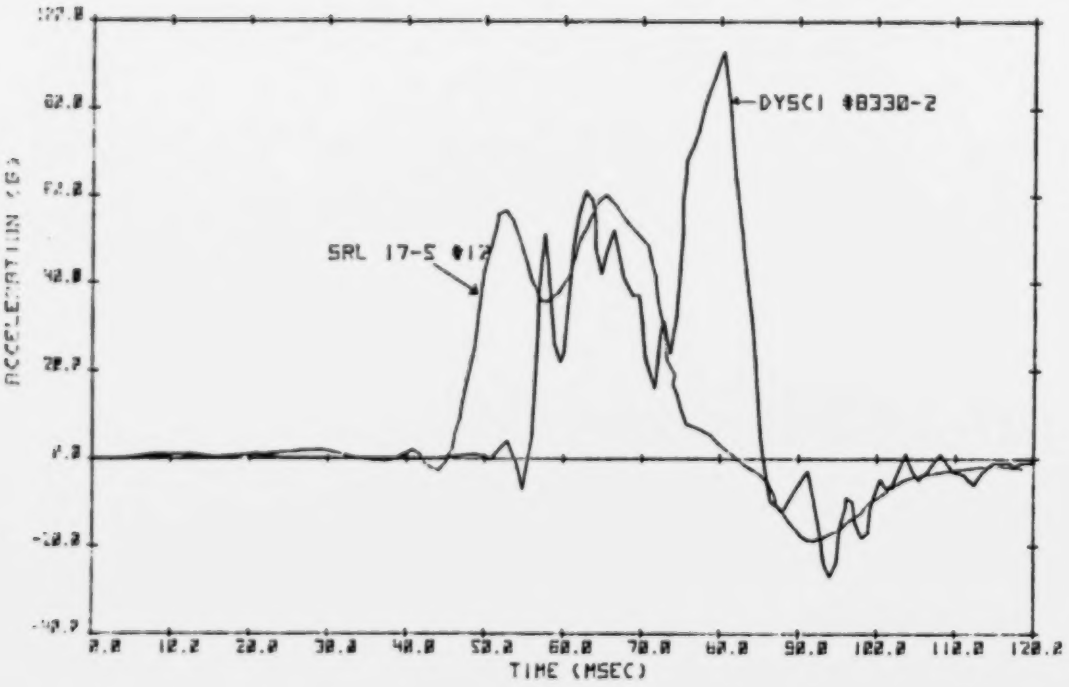

UPPER SPINE ACCELERATION

FIGURE 48

BEST DOCUMENT AVAILABLE

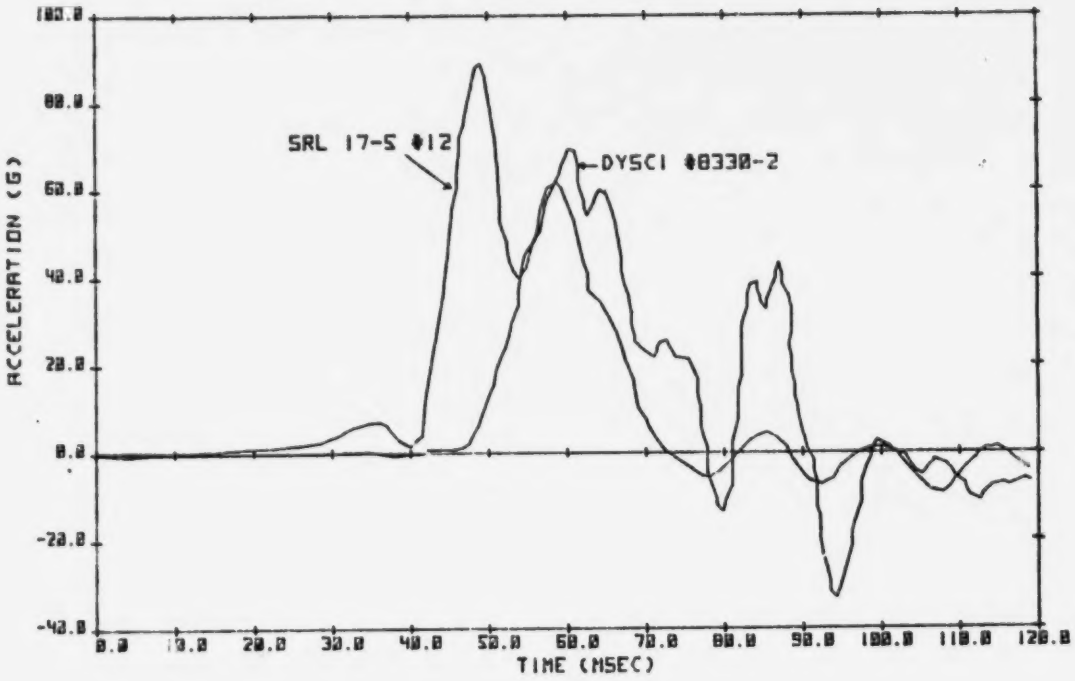

LOWER SPINE ACCELERATION

FIGURE 49

BEST DOCUMENT AVAILABLE

readings are in Figure 48 and the lower spine in Figure 49. In the car event, the upper spine had a double peak trace with a second peak about 90 g's. It is unusual to have a load applied through the upper rib to the spine and have the spinal acceleration higher than that of the rib. This might be an anomaly, but whether it is or not, the sled simulations were not acceptable approximations of the spinal accelerations. Tests No. 13 through 17 were intended for baseline data at a slightly higher speed prior to conducting the padded sled tests (see Section 5.14 for discussion of padded tests at increased sled velocity).

Up to Test 13, the kinematics were different in that the dummy leaned out the "window" on the sled and rebounded from the door panel with pelvis leading. The car event showed the dummy's head going only part way out the window and rebounding from the door in a nearly upright position (see Figure 50). A closer examination of the films of the vehicle impact showed that the hood of the Cutlass directly impacted the dummy's head. The hood edge may have struck the dummy in the neck region. This accounted for the kinematic difference and may have also been the explanation for the second spike of acceleration on the upper spine. It was not felt reasonable to attempt to reproduce this occurence on the sled, but the kinematics on the sled were improved by the addition of a lexan panel just outboard of the window area. The dummy's head impacting into the lexan approximated the effect of the hood impact and improved the kinematics. The time sequence of the dummy kinematics in sled Test 16 are shown in Figure 51. The attempted simulation of Dynamic Science Test 8330-2 resulted in a marginally successful simulation.

BEST DOCUMENT AVAILABLE

0 ms

10 ms

20 ms

30 ms

40 ms

50 ms

60 ms

70 ms

80 ms

FIGURE 50 - DySci Test No. 8330-2

FIGURE 51 - SRL Test No. 16

BEST DOCUMENT AVAILABLE

BEST DOCUMENT AVAILABLE

5.12 Review of Prior Padding Studies

The purpose of reviewing the literature on previous padding studies was to discover possible experiments with direct application to side impact thorax protection.

The literature on the mechanical and chemical properties of various foams is extensive. However, many of these studies involve specific paddings in special tests. As concluded by William R.S. Fan in his paper, "A Simulation of the Dynamic Properties of Energy Absorbing Materials,"[8] the dynamic behavior of various foams varies, depending on the test performed. A material judged favorably in one test might not perform well in another test. Therefore, in choosing previous padding studies to review, only those dealing with padding used in interior vehicle applications were considered. The four studies reviewed were James E. Greenes, "Basic Research in Crashworthiness II -- Development and Testing of Vehicle Side Structure Modifications"[9] and "Occupant Survivability in Lateral Collisions"[5], Mark Haffner's, "Dynamic Characteristics of Energy-Absorbing Materials" (study was not published), and L.S. Paul's "Energy Absorption and Shock Attenuation Characteristics of School Bus Padding Materials"[10].

James Greene's (Calspan), "Basic Research in Crashworthiness II - Development and Testing of Vehicle Side Structure Modifications"[9] dealt with the progressive structural modifications made on 1968(69) mid-sized Fords. However, some consideration was given to interior padding. Styrofoam, a 1PCF polystyrene, was tested in a 4 inch thickness with and without 1 inch diameter holes drilled to reduce the density. Also, a 3 inch thick sample of styrofoam with holes, covered with ensolite, and a 3 inch sample of ethafoam were tested.

The ethafoam static test results indicated poor energy absorption, and ethafoam was eliminated. The remaining three (3) combinations were tested dynamically at 10 mph using a 430 pound flat-bottomed impact weight. The

BEST DOCUMENT AVAILABLE

results showed that the 4 inch standard styrofoam dissipated 56 percent of the total kinetic energy, the 4 inch styrofoam with holes dissipated 55 percent of the energy and the styrofoam and ensolite combination dissipated 49 percent of the energy. Two additional materials manufactured by Scott Paper Company, Impac II and Impac III, were dynamically tested at 10 mph and 15 mph with a 205 pound flat impactor. Impac II and Impac III, both open-cell polyether foams, dissipated 84 percent and 87 percent respectively of the energy.

Five basic modifications were tested in the car-to-car crash test series, each one with different padding configurations and structural changes. In general, the structural modifications involved reinforcing the side pillars, doors, roof and 3rd and 4th frame cross-members up to 275 pounds in order to increase energy dissipation and lateral compartment strength.

The results of these tests showed a reduction in the peak accelerations in the test dummies and a reduction in intrusion. However, the extent of this reduction due to the padding is not clear.

In the second Greene study[5], thirteen side impact tests with 50th percentile anthropomorphic test dummies were performed in order to test the integrity of passenger compartments. The vehicles used (both as bullet cars and as target cars) were 1973 Ford 4-door automobiles.

In each modified case, the side door or vehicle was modified structurally and/or padded. The modifications which directly pertained to the side impact padding study involved the changes made to the door interiors. The choices considered for the padding modifications were 4 inch S-00230 expanded urethane and 0.5 inch, 7PCF, type AI Ensolite over 3/4 inch cell or 3/8 inch cell paper Honeycomb. Static tests and dynamic tests at 10 and 20 mph were run utilizing the body form impactor. From these results, a combination of 3/4 inch cell Honeycomb on the lower door panel and 3/8 inch cell Honeycomb on the upper door panel, both covered with 0.5 inch of ensolite, was chosen. Seven tests with the modified 1973 Ford vehicles were run. The results of the

BEST DOCUMENT AVAILABLE

tests showed that the padding and structural modifications did lower the acceleration levels of the dummies. However, the extent of the improvement due specifically to the padding and specifically to the structural modifications could not be clearly distinguished from these tests alone.

As pointed out in this study, the usefulness of paper Honeycomb in automotive applications is questionable. Prolonged exposure to high humidity reduces the crush strength up to 50 percent, water deteriorates the paper, the paper is readily flammable if not treated, and production tolerances allow a 20 percent range in crush strength values. Furthermore, the application of Honeycomb as an interior door padding is probably not compatible with current mass production techniques.

In 1977, Mark Haffner at the NHTSA, SRL, began a study entitled "The Dynamic Characterization of Energy Absorbing Materials". In this study, Haffner reviewed previous literature on energy absorbing materials, ran five tests to determine the effect of temperature on ethafoam (polyethylene) 220, and setup an experiment matrix with 15 experiments for 3 different thicknesses.

Unfortunately, prior to running the 15 experiments at 3 thicknesses of foam, the SRL was moved to Ohio and the group working on the project was separated. The project was never completed.

"Energy Absorption and Shock Attenuation Characteristics of School Bus Padding Materials"[10] was the most recent and informative study. The study evaluated seatback, side wall, and ceiling paddings. Various materials were judged in several areas: flammability, smoke emissions, toxicity, environmental resistiveness, and maintainability.

Based on results from the above methods of testing, five materials were chosen as core materials:

- Honeycomb ACG-I-.003 - an aluminum product

BEST DOCUMENT AVAILABLE

- Honeycomb HNCI-80(°) EDF - a Kraft paper material
- LS-Neoprene - not a good energy-absorber but a good load distributor
- Ensolite AH and AL
- Rubatex R-1800-FS and R-310-V

Temperfoam, a polyurethane foam, was retained for use as a baseline material. The two cover materials chosen were low carbon steel alloy sheets and Kydex 100.

Each combination was rated in such areas as cost, energy absorption, shock attentuation, and vandalism resistance. The rating heavily depended on the results of the dynamic drop tests that were run. These tests were performed on either 3 or 6 inches of padding and at approximately 72°F or 110°F. Various bodyforms were dropped at 10, 15 and 20 mph and deflection, energy absorption, force and other such parameters were measured or calculated.

The results of all of the padding tests and the results of the flammability tests were weighted to obtain the following ranking:

1) Kydex 100 cover - Low Smoke Neoprene over paper Honeycomb
2) Steel Sheet Cover - Low Smoke Neoprene over paper Honeycomb
3) Kydex 100 Cover - Low Smoke Neoprene over aluminum Honeycomb
4) Steel Sheet Cover - Low Smoke Neoprene over aluminum Honeycomb
5) Temperfoam
6) Steel Sheet Cover - Rubatex R-1800-FS cover
7) Kydex 100 Cover - Rubatex R-1800-FS cover

The top four padding configurations in this study include aluminum and paper honeycombs. The selection of either type of honeycomb for vehicle interior door application would require the development of new mass production techniques to shape or form the materials.

BEST DOCUMENT AVAILABLE

In conclusion, it was found that experiments directly applicable to side impact thorax protection (i.e., using current injury criteria and surrogate design) have not been performed. Although L.S. Pauls' school bus padding study did consider or test a large number of paddings, those materials chosen for extensive testing (paper honeycomb, etc.) generally are not well suited for the current mass production techniques used to fabricate such components for interior doors. These findings indicated a need for a padding study that focused on the specific application required.

BEST DOCUMENT AVAILABLE

5.13 Padding Component Tests

The main purposes of the component level padding tests were (1) to identify padding materials viable for thorax protection and (2) to eliminate performing extensive HYGE sled tests using undesirable padding materials.

The component test fixture consists of a body form (the SID prototype thorax) mounted on a sled platform, an accelerator device, and a strike plate. The sled travels along linear bearings on polished steel rails. Figure 52 is a photo of the sled and body form, as viewed from the back. The tooth pattern below the sled platform is for the magnetic velocity trap. This magnetic velocity trap is now replaced with a light trap velocity device. Figure 53 is a view down the track looking from the accelerator to the strike plate. Figure 54 shows a padding sample mounted on the strike plate. Two load cells behind the plate measure force, and a rod through the center of the plate attached to a washer on the padding surface measures padding deflection. The rod attaches to a string potentiometer behind the back up structure. Figure 55 is a photo of the strike plate, load cells and displacement measuring rod.

The energy source used to accelerate the mini sled to the desired impact velocity was built at the SRL. It is called the "fluid impact accelerator" because it utilizes silicone hydraulic oil as an energy storage medium rather than compressed air. The impact accelerator operates at working pressures up to 20,000 psi and has the capacity to accelerate 100 pounds to nearly 50 mph. Figure 56 is a photograph of the device along with the remote fire valve. Because it is felt to be an important "by product" of this project which has many useful applications, the design drawings and working description are contained in Appendix I.

The padding component tests were performed in two phases. The Phase I tests consisted of impacting the prototype SID thorax laterally into 5 inch padding samples at 15 mph. The reason for doing the "easy" tests first was to get an idea of the energy absorption properties and the relative protection potential

Blank Page

BEST DOCUMENT AVAILABLE

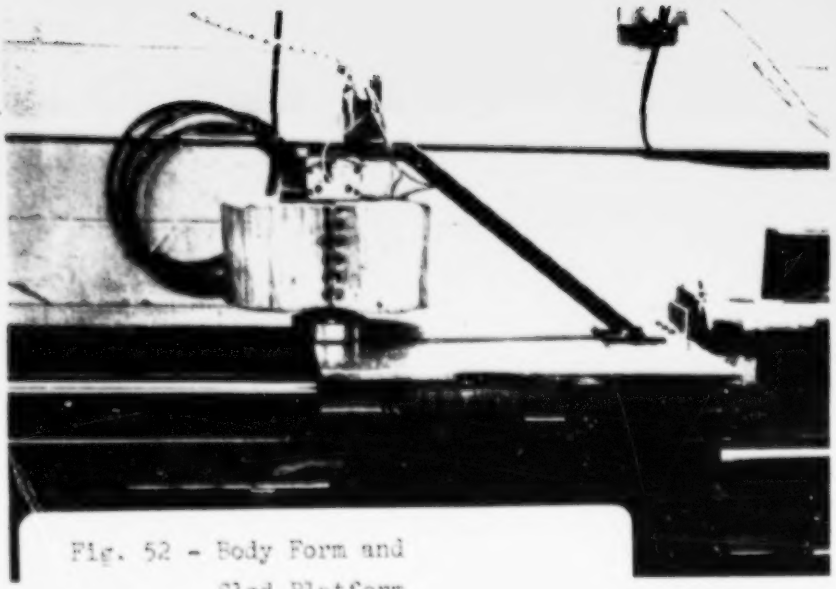

Fig. 52 - Body Form and Sled Platform

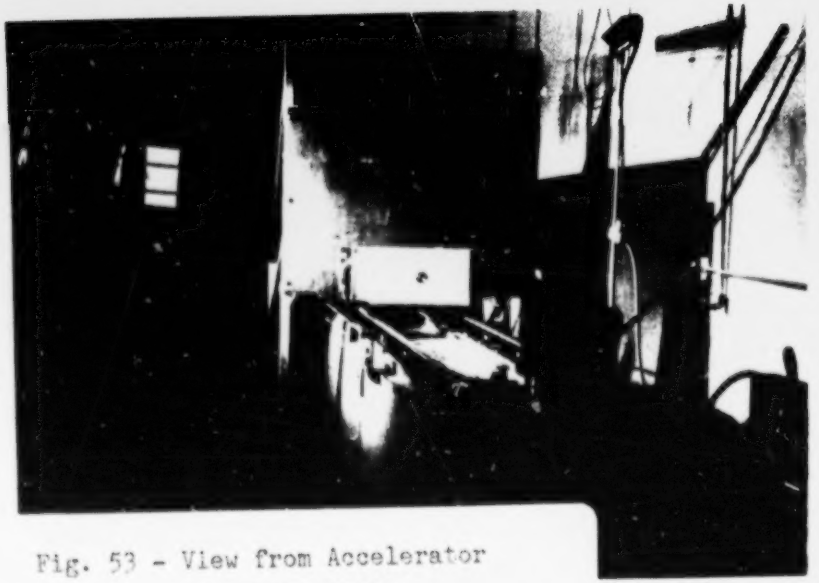

Fig. 53 - View from Accelerator to Strike Plate

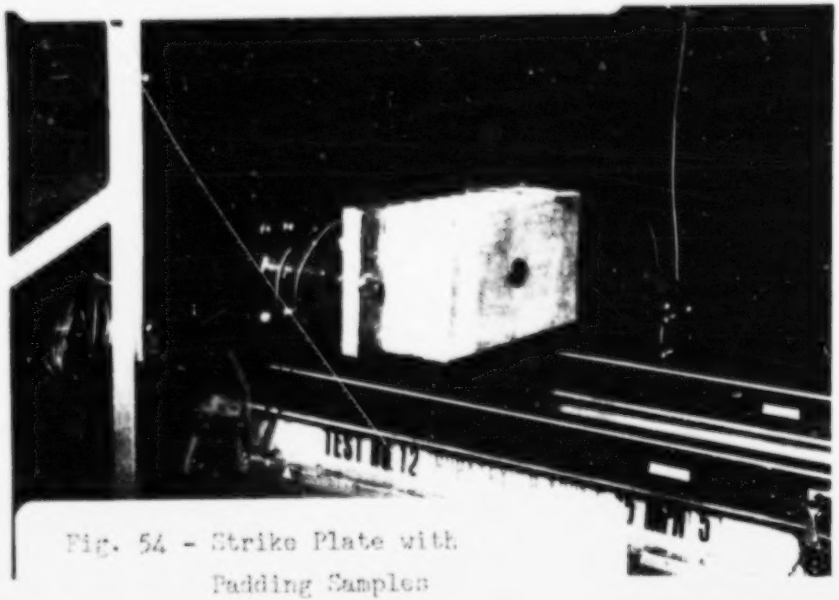

Fig. 54 - Strike Plate with Padding Samples

Fig. 55 - Strike Plate, Load Cells and Displacement Rod

BEST DOCUMENT AVAILABLE

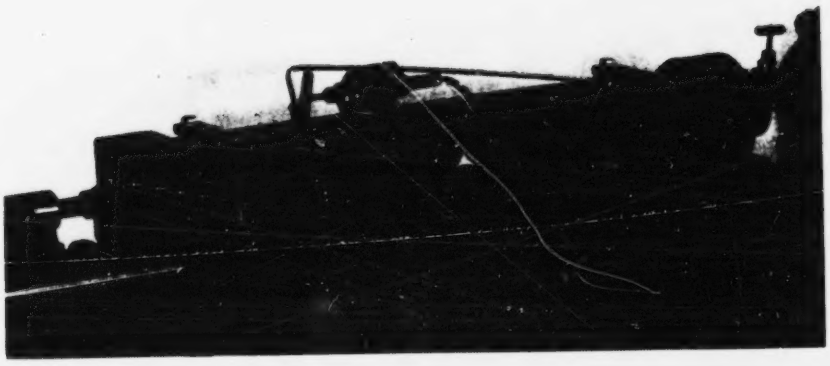

FIGURE 56

Impact Accelerator Device

BEST DOCUMENT AVAILABLE

of each material with the least amount of breakage. Upon completion of Phase I, many of the less desirable paddings were identified and were not used in more severe testing. Phase II testing consisted of impacting those paddings that passed Phase I criteria. The tests were performed using 3 inch padding samples with an impact velocity of 15 mph.

The paddings were judged as to their desireability for a thoracic restraint by three main criteria. These criteria were (1) the padding force-deflection properties, (2) the body form AIS calculated from the B(LUR) parameter, and (3) the peak spinal acceleration.

Data Recording: The data that were recorded included lateral accelerations of the left upper rib, right upper rib, and upper and lower spine; forward acceleration of the lower sternum; load cell readings for both load cells; sled velocity; and padding and thorax displacement. All data was recorded on FM tape except thorax displacement which was recorded on a strip chart. The thorax displacement measured was simply the displacement of the shock absorber in the thorax.

An overhead camera recorded 1000 fps movie coverage of the padding and thorax crush and provided a double check of the electronic data.

Data Processing: As stated in Element 4, the SRL used 2-pole Butterworth filters (100Hz cutoff) using an 8:1 reduction in play back and a 3200 Hz digitizing rate to maintain uniformity with data processing done by the HSRI.

All data processing (AIS calculations and plots) was performed on the PDP-11 minicomputers located at the VRTC. The two load cell readings and the displacement potentiometer reading for each test were digitized and combined to obtain force-deflection curves.

BEST DOCUMENT AVAILABLE

Check-out Testing

The first step in the component testing was to check out the body form response to see if it responded like the dummy. Since the SID had previously been used by the SRL for drop testing from one meter onto a rigid surface and from 2 meters onto a padded surface, similar tests were done on the component test device. A one meter drop is approximately a 10 mph test. The body form was accelerated into the strike plate at 10 mph with no padding. The test results (see Figure 57) indicated that the body form behaved like the dummy in this mode.

Next, a test into the APR padding sample at 15 mph (a 2 meter drop test is approximately 14 mph) was performed. A different left upper rib response resulted (see Figure 58). The following differences between the body form tests and the dummy drop tests were noted, which could account for the response difference.

1. The weight of the body form and sled is about 100 pounds which is about 10 pounds heavier than the corresponding dummy parts it is designed to represent. All of the extra weight is attached to the spine.

2. The motions of the thorax are not the same for the two types of tests. The motion of the body form is constrained by the rails of the minisled to be linear. The films of the 2 meter padded drop tests show a considerable amount of flexure between the pelvis and spinal connection which indicate that the motions are not linear.

Phase I Testing

Each Phase I test was performed at least twice. If more than one material sample was available in a 5 inch thickness, then the material was replaced between tests. For some, it was necessary to use the same sample for the repeat test. In such cases, the results of the first test were considered more valid since the first test may have degraded the sample for the second test.

BEST DOCUMENT AVAILABLE

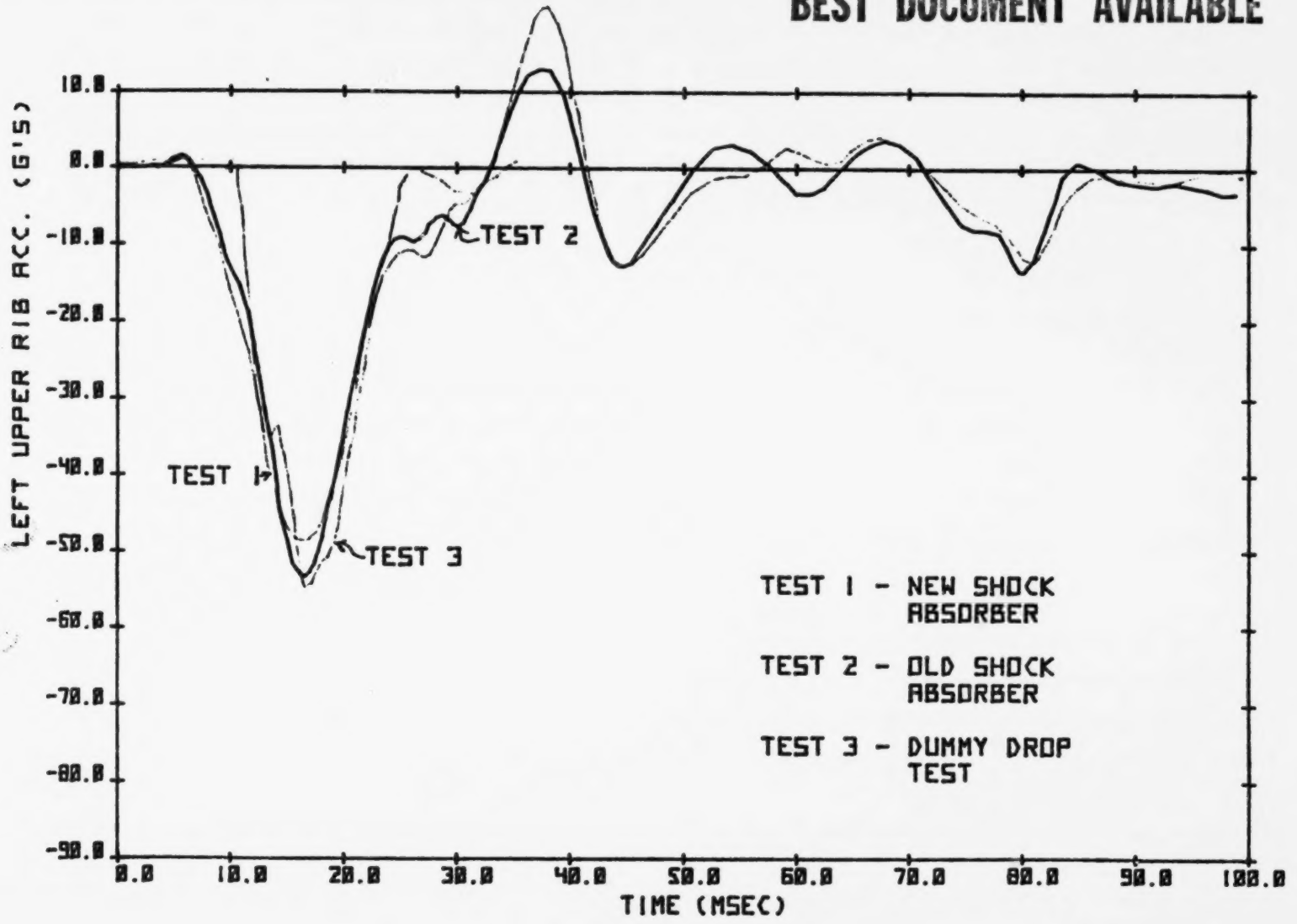

RIGID DUMMY DROP VS. 10 MPH MINISLED TESTS

FIGURE 57

BEST DOCUMENT AVAILABLE

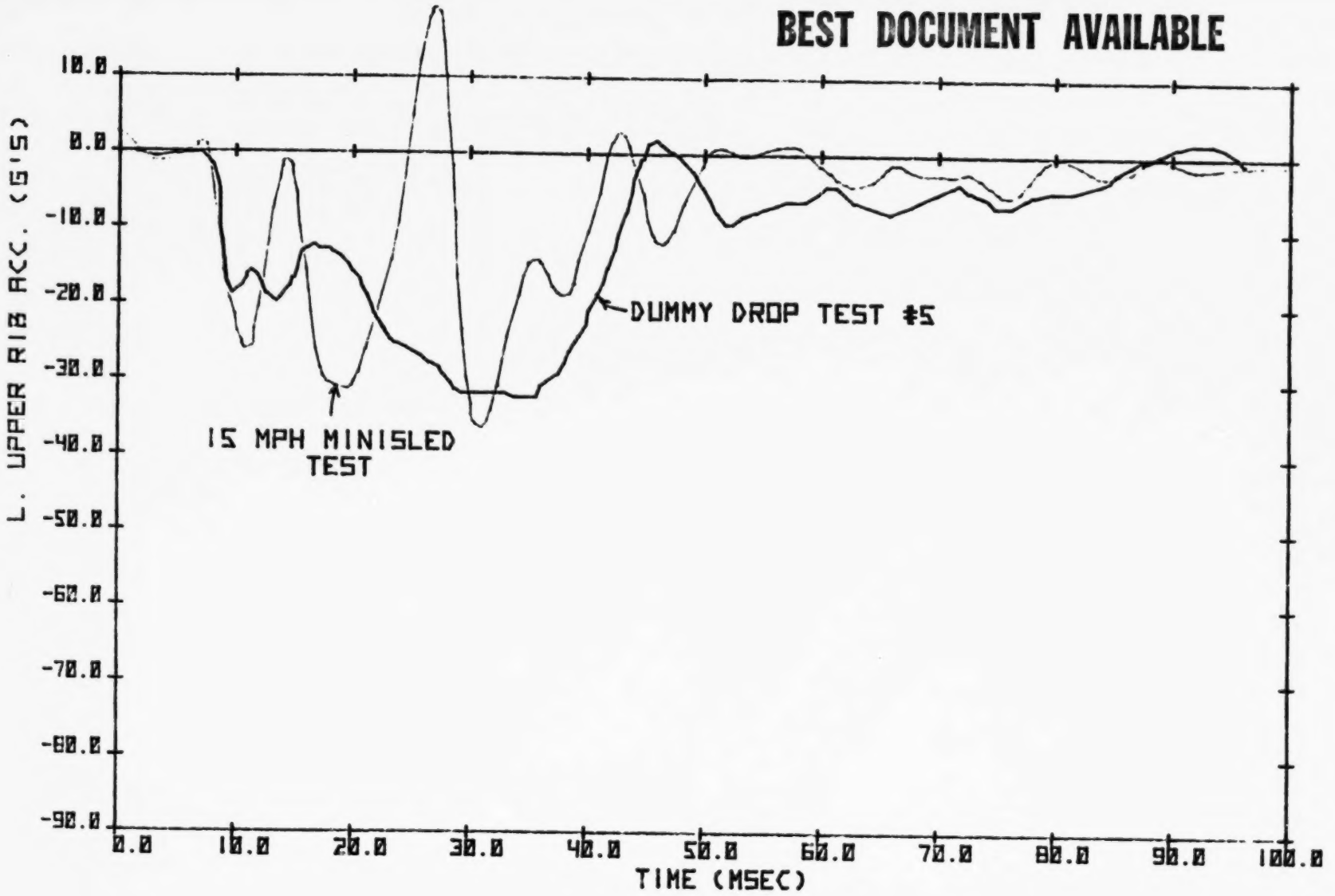

DROP TEST (2M) VS 15MPH MINISLED TEST-PADDED (APR PADDING)

FIGURE 58

BEST DOCUMENT AVAILABLE

The criteria for Phase I padding acceptance were as follows:

(1) AIS measurement less than or equal to 3.

(2) Peak upper spine (3 msec duration) acceleration less than or equal to 40 G's.

(3) Padding peak force of 3200 pounds or less.

Table 6 is a list of all materials tested in this Phase I. Table 7 summarizes test results for each material tested (duplicate tests on the materials are not shown). Appendix F contains the force vs. deflection plots for Phase I.

Rubatex R-310-V, Ensolite AAC and the APR padding were the more effective materials observed in Phase I testing. Table 8 shows the best 5 paddings within each of the 3 individual approaches. It was felt that each of these materials, coupled with the flexibility in the door structure, would provide protection up to the 20 mph range of occupant-door interaction. Table 9 shows the paddings that were selected for Phase II testing. (Subsequent to the Phase I testing, other materials and other variations of Phase I materials were supplied to the VRTC. These were tested in Phase II only.)

Phase II Testing (3" material samples; 15 mph; minisled)

Additional (those not on Table 9) materials and variations of materials included in the Phase II testing include the following:

- Fiberglas honeycomb (custom made by Owens Corning as per SRL's request)(called Fiberglas H_BC).
- Polyurethane foam supplied by General Tire and Rubber Co., in varying densities (called GTREM -" ").
- A layered variation of Ensolite consisting of 2 inches of Ensolite AAC fronted with 1 inch of Ensolite BCR (the composite was called Ensolite ABC).
- A layered variation of Rubatex consisting of 2 inches of Rubatex R-310-V fronted with 1 inch of R-8407-S (the composites was called Rubatex R-2VS).

BEST DOCUMENT AVAILABLE

TABLE 6

List of Padding Materials

APR (supplied by Dr. Claude Tarriere)
Ensolite AAC
Rubatex R-4991-T
Rubatex R-310-V
Ensolite HCR
Fiberglas Type G
Neoprene LS-200
Neoprene UDRP
Ethafoam 220
Ethafoam 600
Ethafoam 400
Neoprene JL
Rubatex R-8407-S
Ethafoam 900
Ensolite BCR
Durafoam C222A
Durafoam C111A
Durafoam C191XLDS
Durafoam C191LD
Fiberglas 4-5 pct
Fiberglas dual density
Fiberglas Type L
Fiberglas Type Q
Ensolite LPC
Ensolite MLC
Ensolite FBC

BEST DOCUMENT AVAILABLE

TABLE 7

Component Level Phase I Test Results

Test No.	Padding Type	Thickness (in.)	Velocity (mph)	Temp.	Peak Spinal Accel	AIS B	Chest Deflection	Padding Deflection (in.)	Load (Cells) (lbs.)
10	Tarriere	5.625	14.99	64°F	30.8	2.5	1.7"	3.27	2383
7	Ensolite AAC	5.625	14.99	63°F	33.2	2.3	1.9"	2.99	2739
13	Rubatex R-4991-T	5.25	15.15	64°F	34.2	2.7	1.7"	3.81	2700
15	Rubatex R-310-V	5.25	14.99	67°F	30.7	2.3	1.7"	3.03	2295
23	Ensolite HCR	5.25	14.76	64°F	34.5	2.6	1.625"	2.76	2955
25	Fiberglas Type G	5.25	14.99	64°F	49.0	3.2	1.7"	2.90	4110
26	Neoprene LS-200	5.0	14.82	69°F	59.0	3.1	1.85"	4.69	5466
28	Neoprene UDRP	5.0	15.15	70°F	59.5	3.3	1.75"	4.8	5339
30	Ethafoam (220)	5.0	14.99	71°F	37.2	2.5	1.65"	3.85	3398
32	Ethafoam (600)	5.13	14.92	72°F	39.0	2.9	1.55"	2.0	3643

Blank Page

BEST DOCUMENT AVAILABLE

TABLE 7 (Cont.)

Component Level Phase I Test Results

Test No.	Padding Type	Thickness (in.)	Velocity (mph)	Temp.	Peak Spinal Accel	AIS B	Chest Deflection	Padding Deflection (in.)	Load (Cells) (lbs.)
35	Ethafoam (400)	5.125	14.82	71°F	36.5	2.5	1.6"	3.45	3682
36	Neoprene JL	5.0	14.99	71°F	55.5	3.1	1.53"	4.65	5239
40	Rubatex R-8407-S	5.0	15.15	71°F	45.5	3.2	1.78"	0.95	3823
42	Ethafoam (900)	5.063	15.15	71°F	49.0	3.2	1.85"	0.84	4320
45	Ensolite BCR	5.125	15.25	71°F	38.6	2.7	-----	1.88	2817
47	Durafoam C222A	4.063	15.32	70°F	36.4	2.6	1.52"	2.51	2666
48	Durafoam C111A	4.125	15.25	69°F	33.5	2.8	1.70"	3.10	2739
51	Durafoam C191XLDS	4.25	15.32	71°F	50.5	3.1	1.65"	4.24	3276
52	Durafoam C191LD	4.063	15.15	71°F	48.5	3.1	1.51"	4.0	4067
54	Fiberglas 4-5 PCT	5.25	14.97	70°F	42.5	2.8	1.76"	3.75	3667

BEST DOCUMENT AVAILABLE

TABLE 7 (Cont.)

Component Level Phase I Test Results

Test No.	Padding Type	Thickness (in.)	Velocity (mph)	Temp.	Peak Spinal Accel	AIS B	Chest Deflection	Padding Deflection (in.)	Load (Cells) (lbs.)
57	Fiberglas Dual Density	4.25	14.20	70°F	45.5	3.0	1.5"	3.60	3486
58	Fiberglas Type L	4.75	15.25	69°F	51.5	3.2	1.4"	1.75	4561
59	Fiberglas Type Q	4.625	15.25	70°F	62.6	3.3	1.275"	1.45	6021
64	Ensolite MLC (white)	5.5"	14.75	70°F	44.0	2.8	1.65"	4.50	3613
65	Ensolite MLC White (20 mil)	5.5	14.75	70°F	44.4	2.9	1.50"	4.32	3940
68	Ensolite MLC (Blk)	5.5	14.75	67°F	42.6	2.9	1.575"	4.30	4287
69	Ensolite MLC (B-20)	5.5	15.15	66°F	46.9	3.0	1.75"	3.74	3774
72	Ensolite LPC	5.25	15.37	63°F	41.5	2.9	1.80"	3.84	3037
73	Ensolite LPC (20)	5.25	15.25	66°F	43.8	2.9	1.75"	3.79	3218
74	Ensolite FBC	5.25	15.25	67°F	45.1	3.0	1.65"	4.0	3931
75	Ensolite FBC (20)	5.25	15.25	67°F	46.8	3.0	1.65"	3.96	3774

BEST DOCUMENT AVAILABLE

TABLE 8
Three-Point Padding Evaluation

	FORCE DEFLECTION		B PARAMETER		PEAK SPINAL ACCELERATION	
	Material	Peak Load/ Deflection	Material	AIS	Material	Peak G's
1	Rubatex R-310-V	2295/3.0	Ensolite AAC	2.3	Rubatex R-310-V	30.7
2	APR	2383/3.3"	Rubatex R-310-V	2.3	APR	30.8
3	Durafoam C222A	2666/2.5"	APR	2.5	Ensolite AAC	33.2
4	Rubatex R-4991-T	2700/3.8"	Ethafoam 220	2.5	Durafoam C111A	33.5
5	Ensolite AAC	2739/3.0"	Ethafoam 400	2.6	Rubatex R-4991-T	34.2

Note: For equal peak loads, a material with less deflection was considered better

BEST DOCUMENT AVAILABLE

TABLE 9

Padding Materials for Component
Level Phase II Tests

Ensolite AAC

Rubatex R-310-V

Rubatex R-4991-T

Ethafoam 400

Durafoam C222A

Durafoam C111A

APR

BEST DOCUMENT AVAILABLE

The criteria used to evaluate the Phase II test results were relaxed somewhat from the Phase I tests since the padding thickness was reduced from 5" to 3". The criteria were as follows:

(1) AIS measurement (less than or equal to 3.5 was the goal)

(2) Peak upper spine (3 msec duration) acceleration (less than 53 g's was the goal to which is a rough estimate of the upper spinal g's corresponding to an AIS = 3.5 from the cadaver tests of Reference 6)

(3) Peak load (less than 4000 pounds was the goal)

Table 10 is a summary of the results of the Phase II tests. The Ensolite and Rubatex materials were tested twice to determine the response difference caused by bonding the 1 inch samples rather than merely stacking them. This result is summarized at the end of Appendix G.

On the basis of the criteria and goals for the mini sled testing, all six of the suppliers had materials which appeared acceptable. It was decided to conduct HYGE sled tests with all six material types. Appendix G contains a description of the concepts and use of force vs. deflection curves and the plots of the force vs. deflection from the Phase II tests.

The six main types of padding materials that passed the Phase II criteria were as follows:

Fiberglas Honeycomb (faced with 0.5 inch Ensolite BCR)
GTREM
Ensolite (both AAC and the composite ABC)
Rubatex R-310-V
Ethafoam 600
Durafoam C222A

BEST DOCUMENT AVAILABLE

TABLE 10

Component Level Phase II Test Results

TEST NO	PADDING TYPE	THICKNESS (IN)	VELOCITY (MPH)	TEMP (°F)	PEAK SPINAL ACCEL(G)	AIS B Parameter	CHEST DEFLECTION (IN)	PADDING DEFLECTION (IN)	LOAD CELLS (LBS)
60	Ensolite AAC	3.5	15.15	68	44.0	2.7	1.7	2.42	3579
61	Ensolite BCR	3.8	15.15	68	41.6	2.6	1.51	1.59	3320
62	Ensolite HCR	3.4	15.15	66	46.3	2.8	1.53	2.31	3682
63	Ethafoam 600	3.0	15.32	66	46.3	2.7	1.55	1.74	3740
77	Rubatex R-310-V	3.06	15.08	70	44.9	2.9	1.6	2.39	4209
78	Durafoam C111A	3.0	15.15	69	48.0	3.2	1.8	2.41	3476
79	Durafoam C222A	3.0	15.32	71	44.0	3.0	1.73	2.16	3433
80	Rubatex 2VS	3.0	15.08	70	47.9	2.9	1.63	1.65	3906
81	Ensolite ABC	3.0	15.15	69	40.1	2.7	1.75	2.25	3311
82	Fiberglas HBC	3.75	15.15	69	45.4	3.0	1.65	3.30	3857
84	Fiberglas HBC	3.19	15.32	67	46.5	3.0	1.4	2.75	3232
87	GTREM C41104	3.0	15.32	67	42.9	2.9	1.4	2.41	3305
88	GTREM 041101	3.0	15.15	69	46.5	3.1	1.33	2.0	3906
89	Ensolite ABC	3.0	15.22	65	41.6	2.8	1.60	2.70	2953
90	Rubatex R-310-V	3.19	15.15	68	50.6	3.1	1.53	2.83	3545
91	Tarriere APR	3.0	15.22	68	48.4	3.0	1.65	2.8	3916
92	Rubatex 2VS	3.0	15.15	67	52.5	3.0	1.45	2.13	4004
93	Fiberglas HBC	3.5	14.82	78	39.3	2.5	----	3.25	3804

BEST DOCUMENT AVAILABLE

5.14 Padding Evaluation - HYGE Sled Tests

A series of 17 tests on the HYGE sled, using the SID, was performed to evaluate the protective capability of the materials identified in Section 5.13.

The first test of this series (Test No. 18) was a baseline (unpadded) test. Tests No. 10 through No. 17 were an attempt to reproduce Dynamic Science Inc. Test No. 8330-2[3], with Tests No. 14 through No. 17 focusing primarily upon the occupant kinematics. Test No. 18 was actually the final variation of this series in which the placement of the lexan contact panel was altered slightly. The velocity had been increased to insure that the sled environment was as severe as the vehicle environment. The amount of velocity increase was arbitrary in that the pressure of the HYGE was increased holding the pulse width the same. The velocity increased from 22 mph to 23.5 mph. Initial test conditions for Test No. 18 were used throughout the remaining tests. The test conditions were as follows: dummy thorax to upper panel distance - 6.5 inches, dummy pelvis to lower panel distance - 7.75 inches, and bottom panel offset from upper panel - 1.5 inches. Control tapes on the upper panel provided a maximum force-deflection of 3671.1 lb/1". The maximum force-deflection for the lower panel was 4812.4 lb/1". Test No. 34 was another unpadded test performed after the padding tests to observe whether dummy responses varied substantially from the initial baseline test. The results were quite good considering that the ribs had sustained slight damage during the padding tests.

The tests were conducted with 3.0 inches of padding on the upper door and 1.0 inch on the lower door. The pelvic and lower spine accelerations were higher than expected, so the lower door padding was increased to 3.0 inches for a few exploratory tests. The better lower body responses seemed to result from the softer lower door paddings. Table II contains dummy data for Tests No. 18 through No. 34.

The majority of the test results were as expected, although a few unusual responses occurred. In Test No. 37, GTREM (low density) padding was used on

BEST DOCUMENT AVAILABLE

TABLE 11

HYGE Sled Padding Evaluation Test Results

TEST NO.	FILE NAME	PADDING: UPPER PANEL	PADDING: LOWER PANEL	AIS B PARAM.	PEAK UPPER SPINE (G)	PEAK LOWER SPINE (G)	PEAK PELVIS (G)	DAMPER DISPLACE-MENT (IN)
18	S17318	-	-	4.0	66.6	76.3	90.6	1.6
19	S17319	Ensolite ABC-3"	Ensolite BCR-1"	3.2	46.5	59.0	83.0	1.6
20	S17320	Fiberglas H2BC-3.13"	Ensolite BCR-1"	3.6	46.0	63.4	79.4	1.55
21	S17321	GTREM-3.0"	GTREM-3.0"	3.4	45.6	66.9	85.9	1.42
22	S17322	Rubatex 2VS-3"	Rubatex R-8407-S-1"	3.3	53.0	63.4	78.0	1.59
23	S17323	Fiberglas H3BC-3.5"	Ensolite BCR-1.0"	3.3	42.5	61.8	96.9	1.53
24	S17324	Durafoam C111A-3.0"	Durafoam C111A-1.0"	3.9	52.0	55.5	80.6	1.56
25	S17325	Durafoam C222A-3"	Durafoam C222A-1"	3.5	40.1	53.0	79.7	1.43
26	S17326	Rubatex R-310-V-3"	Rubatex R-310-V-1"	3.8	44.8	55.5	81.6	1.49
27	S17327	GTREM-3.0"	GTREM-3.0"	3.5	56.0	77.2	130.0	1.39
28	S17328	APR-3.0"	APR-2.0"	3.5	44.5	59.6	67.4	1.53
29	S17329	Durafoam C311A-3.0"	Durafoam C111A-3.0"	3.6	48.0	73.1	70.6	1.47
30	S17330	Ethafoam 400-3"	Ethafoam 400-3"	3.5	48.5	70.6	78.8	1.53
31	S17331	Rubatex R-310-V-3.25"	Rubatex R-310-V-3.25"	3.4	76.9	58.5	77.7	1.58
32	S17332	Ensolite AAC-3.0"	Ensolite AAC-3.0"	3.7	43.1	62.4	69.8	1.44
33	S17333	Fiberglas H2BC-3.5"	Fiberglas H2BC-3.5"	3.3	43.0	66.4	86.9	1.49
34	S17334	-	-	3.8	78.4	84.4	95.5	1.32

BEST DOCUMENT AVAILABLE

the upper panel and GTREM (high density) on the lower panel. Using the high density material, the peak pelvic acceleration was 40 g's greater than the pelvic acceleration in Test No. 18 with no padding. In Test No. 31 (Rubatex R-310-V), an abnormally high spike in the upper spine acceleration occurred. Had the spike not occurred, the peak acceleration would have been around 37 or 38 g's. Starting with Test No. 21, a spike occurred in the majority of the upper spine responses. One possible explanation is that the left ribs contacted the mounting bracket on the spinal column. Another possible explanation is that one of the ballast weights on the thorax contacted the spinal column.

Upon completion of testing, the paddings were ranked according to AIS ("B" parameter) and upper spine acceleration. The following 6 types of padding appear to be the best, ranked according to B(AIS):

Ensolite ABC	GTREM
Fiberglas H3BC	APR
Rubatex 2V5 & R-310-V	Durafoam C222A

The AIS values range from 3.2 to 3.5.

The following 6 padding types are ranked according to upper spine acceleration:

Durafoam C222A	APR
Fiberglas H3BC	Rubatex R-310-V
Ensolite AAC	GTREM

The spinal accelerations range from 40 G's to 45 G's.

Appendix H contains the bodyform responses for this series of 18 HYGE sled tests.

During the HYGE sled testing, the SRL received a production version of the SID. Differences were noted (the inertial weight distribution was different, etc.) from the prototype being used for the padded sled tests. Also, the production version had molded arms whereas the prototype was armless. Another 6 HYGE sled tests were performed, using the production version of the SID. The main purpose of these tests was to determine if dummy responses differed significantly from those of the prototype.

BEST DOCUMENT AVAILABLE

Tests No. 35 and No. 36 were baseline (unpadded) tests. The presence of the molded arms on the dummy raised the question whether to keep the original door positioning (used in Tests No. 18 through No. 34) the same or to keep the door to dummy distances the same. The change in dummy geometry made it impossible to do both. In Test No. 35, all test parameters, except the door panels' offset, remained the same as those in Tests No. 18 through No. 34. The offset was reduced from 1.5 inches to 1.0 inch. The dummy arm-to-door distance was 6.5 inches and the dummy pelvis-to-door distance was 7.75 inches. In Test No. 36, the door panels' offset was returned to the original position, decreasing the dummy arm-to-door distance to 4.75 inches. AIS (Blur) for Test No. 35 was 4.03 and for Test No. 36, AIS (Blur) was 4.12. Test No. 35 configuration was chosen for the padding tests due to the fact that its AIS was closest to that of Test No. 18 (4.01).

The paddings tested were GTREM, Fiberglas H2BC, Ensolite ABC and APR. The Rubatex and Fiberglas H3BC were temporarily out of stock. Each set of paddings was positioned in the same configuration as tested with the prototype dummy. The parameters used to make the comparisons were: AIS (Blur), peak (3 msec) upper spine acceleration, peak (3 msec) lower spine acceleration and peak (3 msec) pelvis acceleration. In all tests it was observed that the final version dummy predicts higher injury measures than did the prototype dummy in an identical test condition. As can be seen from Table 12, the only "acceptable" (AIS less than 3.5) injury reading on the production version dummy came from the "B" parameter on the left upper rib.

This test series finalized the HYGE sled testing.

Although it was intended that the best of the available paddings be selected after the HYGE sled testing, this final selection was not done. The reasons were as follows:

- The surrogate, which had changed mid-way through this study, was still not in final production form (not only was the SID

BEST DOCUMENT AVAILABLE

TABLE 12

Final Version/Prototype SID Comparison

	Final Version Side Impact Dummy								Prototype Side Impact Dummy						
Test No.	Padding: Upper Panel	Padding: Lower Panel	AIS (Blur)	Peak Upper Spine (G)	Peak Lower Spine (G)	Peak Pelvis (G)	Damper Displace-ment* (IN)	Test No.	Padding: Upper Panel	Padding: Lower Panel	AIS (Blur)	Peak Upper Spine (G)	Peak Lower Spine (G)	Peak Pelvis (G)	Damper Displace-ment (IN)
37	GTREM 3.0"	GTREM 3.0"	3.6	64.4	87.5	91.6	1.99	21	GTREM 3.0"	GTREM 3.0"	3.4	45.6	66.9	85.9	1.42
38	Fiberglas H2BC 3.0"	Ensolite BCR 1.0"	3.9	75.0	113.8	112.5	2.00	20	Fiberglas H2BC 3.13"	Ensolite BCR 1.0"	3.6	46.0	63.4	79.4	1.55
39	Ensolite ABC 3.0"	Ensolite BCR 1.0"	3.3	56.9	79.7	111.3	2.00	19	Ensolite ABC 3.0"	Ensolite BCR 1.0"	3.2	46.5	59.0	83.0	1.60
40	Tarriere APR 3.0"	Tarriere APR 2.5"	3.7	71.6	100.6	107.8	1.98	28	Tarriere APR 3.0"	Tarriere APR 2.5"	3.5	44.5	59.6	67.4	1.53

*It appears that the thorax damper bottomed out in every test

BEST DOCUMENT AVAILABLE

still under refinement, but discussions with headquarters personnel indicated that a dummy developed by the APR of France might be selected over the SID).

- The feasibility of actually molding or fabricating finished door components from the materials was unknown. The effect of such a procedure on the protective capability was also unknown.

- The final selection was judged to require other factors besides the protective capability (such as cost, weight, flammability, etc. of the finished panels).

It was decided to invite all six of the suppliers to participate in a study entitled "Side Impact Padding Integration Study". It was hoped that the surrogate would be finalized during the interim.

BEST DOCUMENT AVAILABLE

5.15 Tarriere Drop Tests

Dr. C. Tarriere of the Laboratory of Physiology and Biomechanics, Peugeot-Renault Association (France) made available a padding material which appeared to reduce injury to cadavers in lateral drop tests. The SRL agreed to duplicate two drop tests conducted by Dr. Tarriere[4], using the prototype SID. Because the drop tests were a parallel investigation to the project, the discussion of the tests are contained in Appendix J.

6.0 Conclusions and Recommendations

BEST DOCUMENT AVAILABLE

From this study, the following was concluded:

- A method of controlled component level testing was developed to identify padding materials that are suitable candidates for thoracic protection. Materials that were identified:

Fiberglas Honeycomb	(supplied by Owens Corning)
GTR	(supplied by General Tire & Rubber Co.)
Rubatex R-310-V	(supplied by Rubatex Corp.)
Ethafoam 600	(supplied by Dow Chemical)
Ensolite AAC, & BCR	(supplied by Uniroyal)
Durafoam CIIIA, &C222A	(supplied by Monmouth Rubber)

- A simple sled buck was developed which mimics the crash environment experienced by an occupant of a struck vehicle in an oblique side collision. The sled buck incorporates the following features:
  - upper and lower door panels with adjustable stiffness properties
  - adjustable base angle for oblique impact simulations
  - HYGE acceleration capablity to mimic the door acceleration pulse from a car-to-car impact

- Testing was conducted using the Part 572 dummy on the side impact sled buck which showed that a "rigid wall" impact is not a reasonable approximation of a car side impact environment. The rigid wall environment increased the chest acceleration from 75 g's to 130 g's at the same impact velocity.

- Using the prototype SID, in a simulation of an oblique side impact at impacting speeds of 30 mph and 15 mph for the striking and struck vehicles respectively, 3 inches of padding yielded thoracic injury levels of less than AIS 3.5 and upper spinal accelerations less than 53 g's (goals selected for the study).

BEST DOCUMENT AVAILABLE

Based on the above, it is recommended that another study be conducted after the side impact surrogate and injury criteria are finalized and that all of the above six suppliers be invited to furnish door panels in production form for testing. This future testing should include cost, flammability, weight and other parameters in the selection of the superior material.

BEST DOCUMENT AVAILABLE

References

1. Shoemaker, N.E., "Research Input for Computer Simulation of Automobile Collisions," Final Report for NHTSA Contract DOT-HS-7-01511, 1978

2. "Lightweight Subcompact Vehicle Side Structure Program," Monthly Progress Reports under NHTSA Contract DOT-HS-7-01588.

3. "Countermeasures for Side Impact," Monthly Progress Reports under NHTSA Contract DOT-HS-9-02177

4. Tarriere, C., et. al., "Synthesis of Human Tolerances Obtained From Lateral Impact Simulations", Proceedings of 7th International Technical Conference on Experimental Safety Vehicles, Paris, 1979.

5. Greene, J.E., "Occupant Survivability in Lateral Collisions," Volumes I and II, Report Nos. DOT-HS-801 801 and DOT-HS-801 802, January 1976.

6. Melvin, J.W., et al., "Side Impact Response and Injury," Sixth International Technical Conference on Experimental Safety Vehicles, October 1976.

7. Eppinger, R.H., and Pritz, H.B., "Development of a Simplified Vehicle Performance Requirement for Pedestrian Injury Mitigation", Seventh International Technical Conference on Experimental Safety Vehicles, DOT-HS-805-199, December 1979.

8. Fan, William R.S., "A Simulation of the Dynamic Properties of Energy Absorbing Material," SAE Report No. 700425, 1970.

9. Greene, J., "Basic Research in Crashworthiness II -- Development and Testing of Vehicle Side Structure Modifications," Final Report of Contract No. DOT-HS-800-879.

10. Paul, L.S., "Energy Absorption and Shock Attentuation Characteristics of School Bus Padding Materials Volume III - Appendices," Report No. DOT-HS-805-272, January 1980.

BEST DOCUMENT AVAILABLE

APPENDIX A

Interior Door Crush Tests Results

BEST DOCUMENT AVAILABLE

STATIC CRUSH PROPERTIES

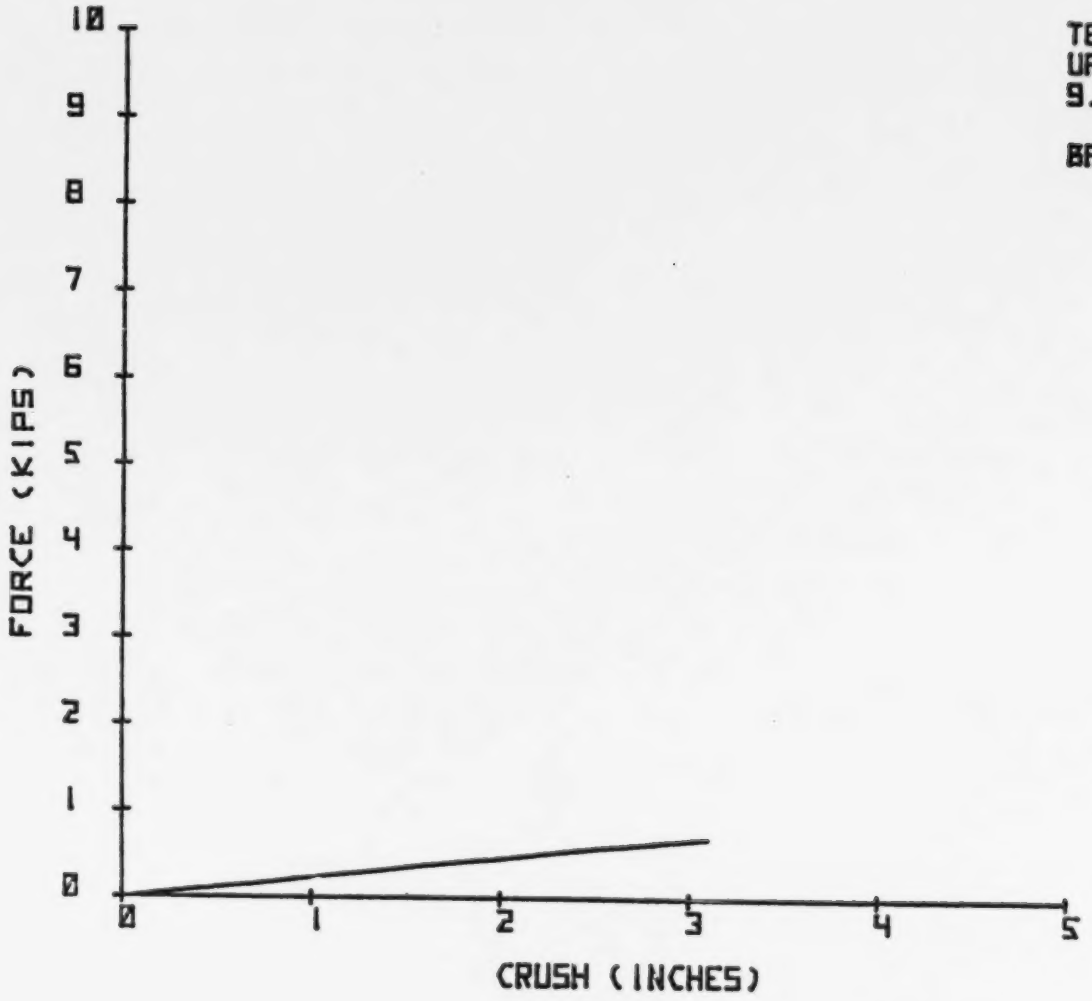

BEST DOCUMENT AVAILABLE

STATIC CRUSH PROPERTIES

TEST 17
LOWER BODY FORM
9.75 IN. CRUSH AT
THE HIP POINT
BASELINE DOOR

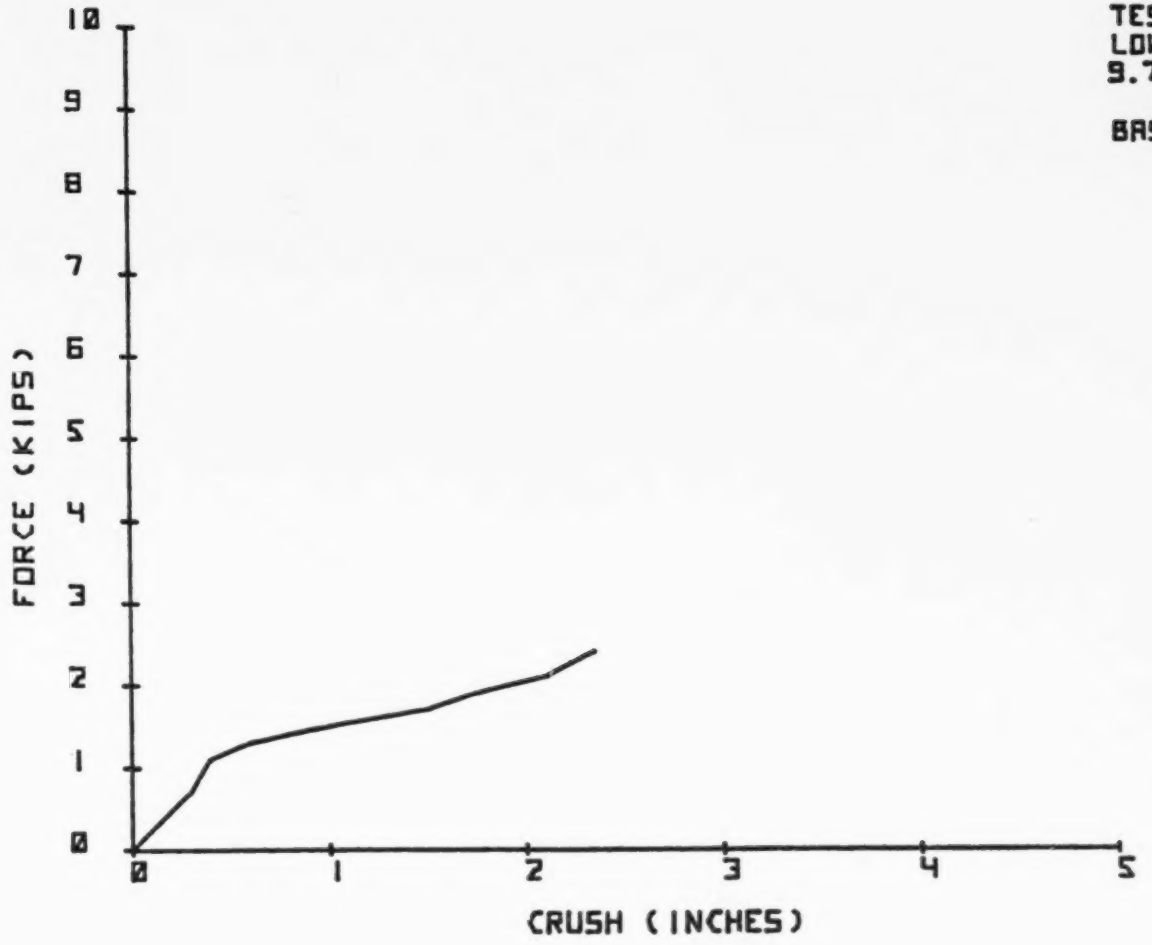

BEST DOCUMENT AVAILABLE

STATIC CRUSH PROPERTIES

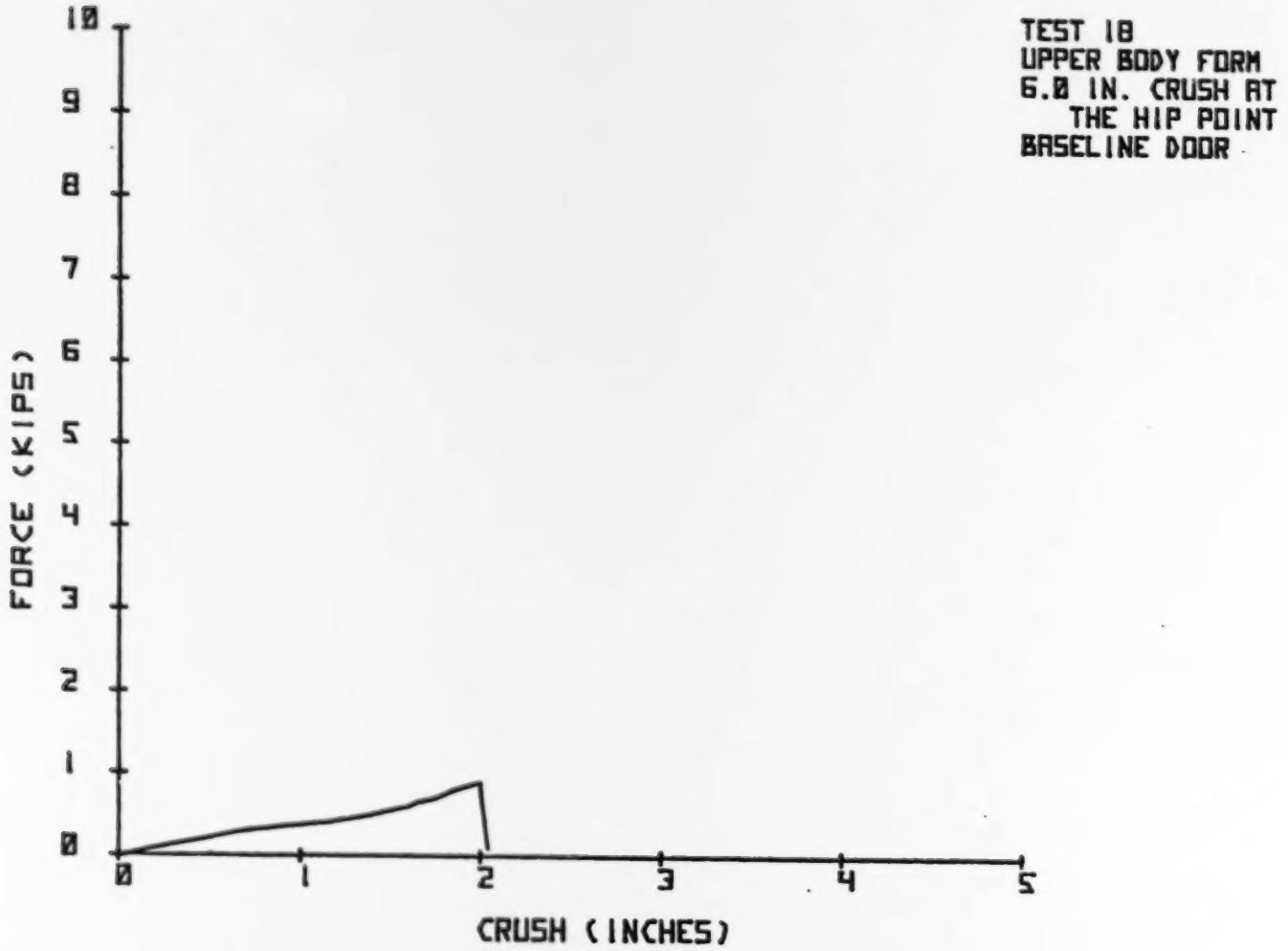

///

STATIC CRUSH PROPERTIES

BEST DOCUMENT AVAILABLE

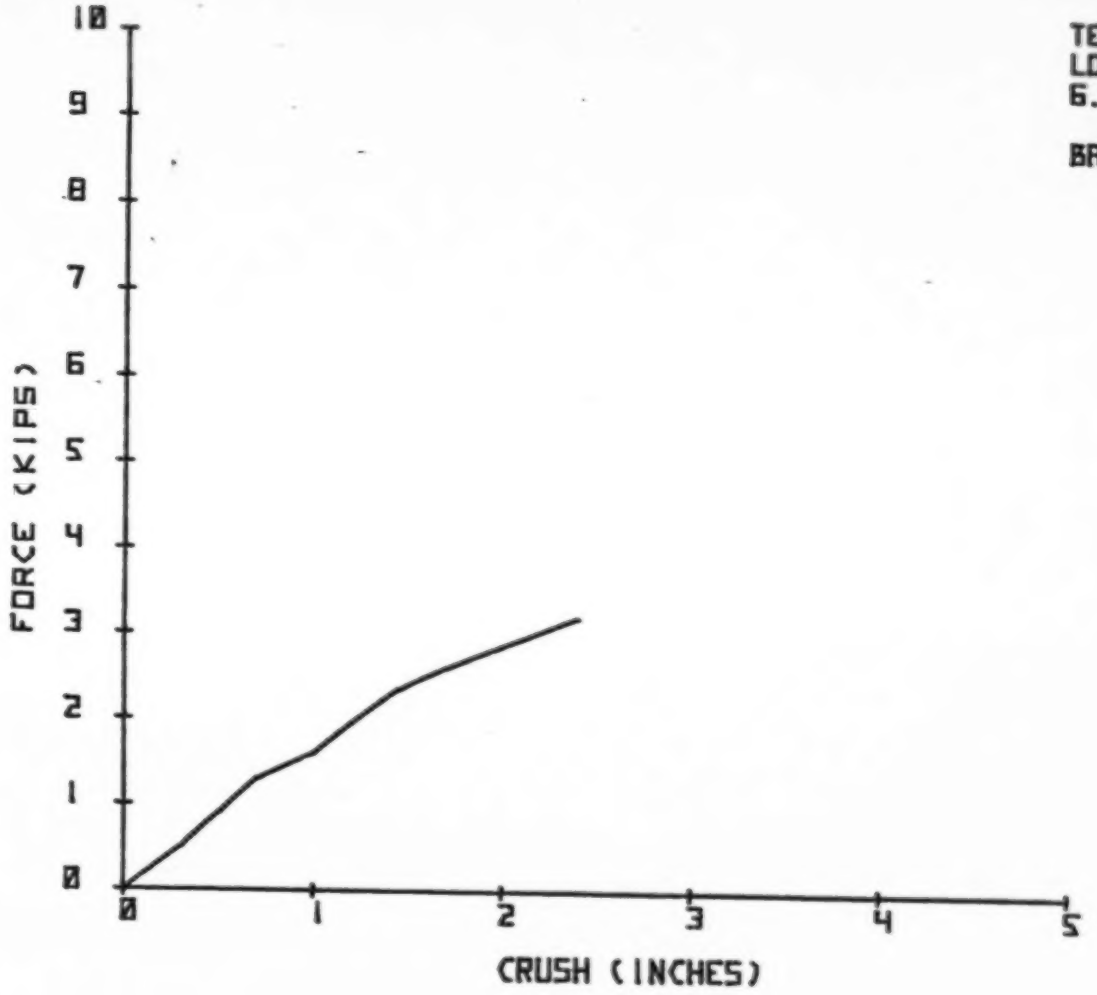

STATIC CRUSH PROPERTIES

BEST DOCUMENT AVAILABLE

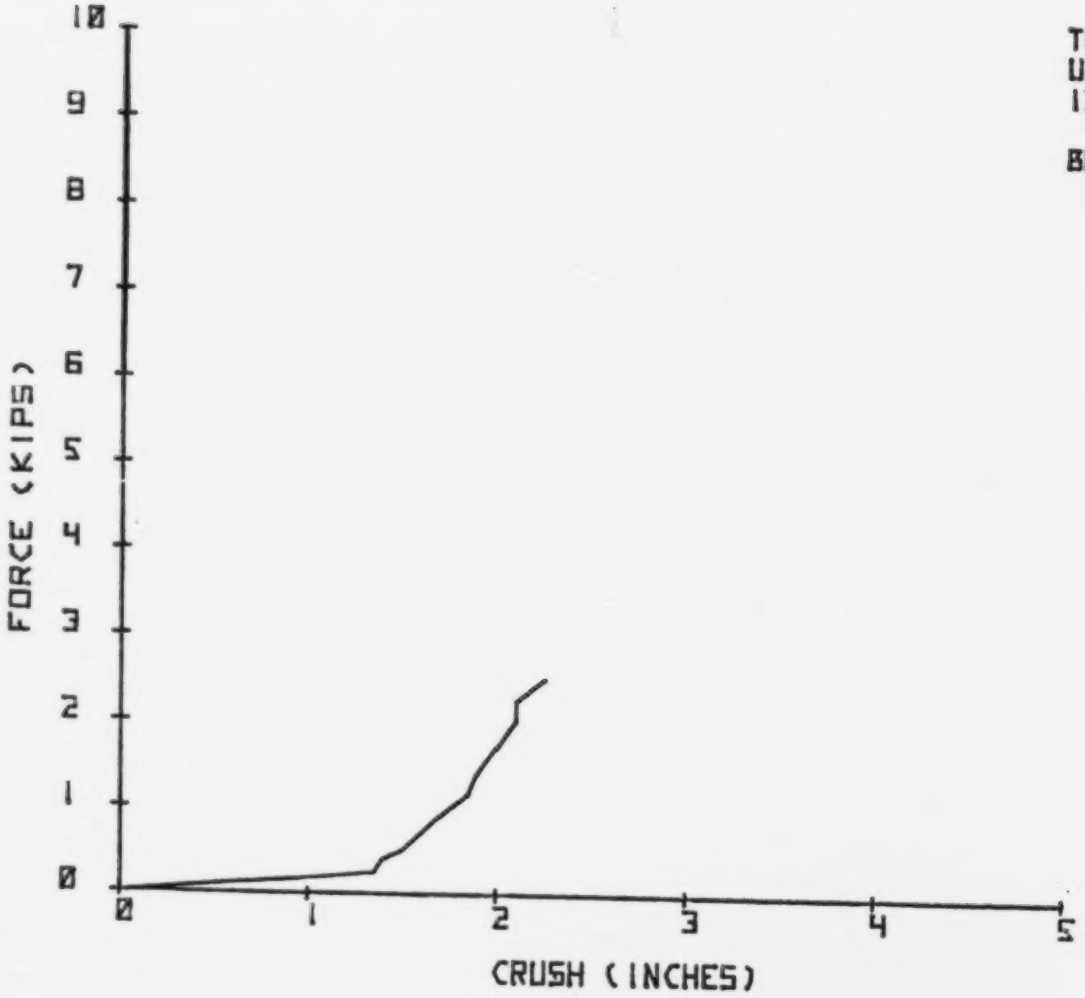

TEST 20
UPPER BODY FORM
13.5 IN. CRUSH AT
THE HIP POINT
BASELINE DOOR

STATIC CRUSH PROPERTIES

BEST DOCUMENT AVAILABLE

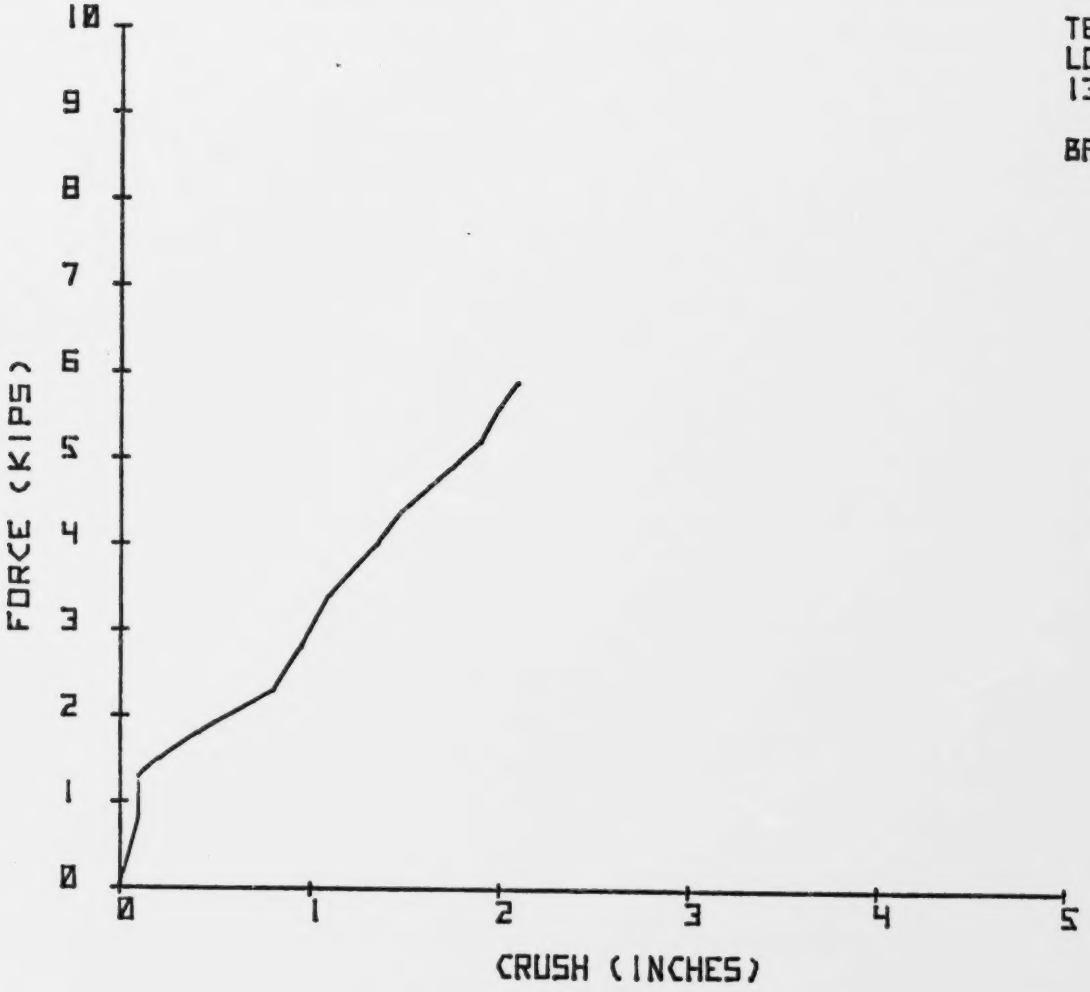

BEST DOCUMENT AVAILABLE

STATIC CRUSH PROPERTIES

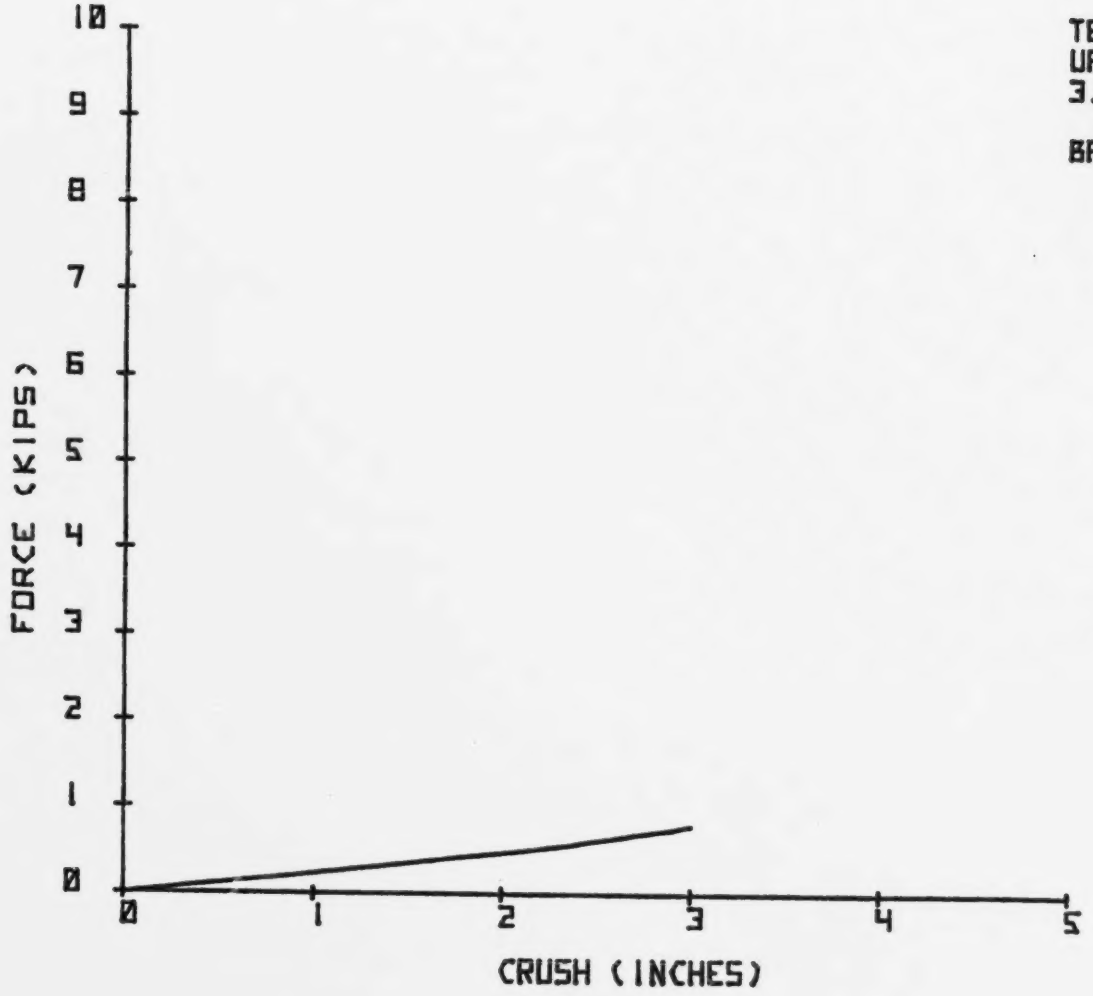

STATIC CRUSH PROPERTIES

BEST DOCUMENT AVAILABLE

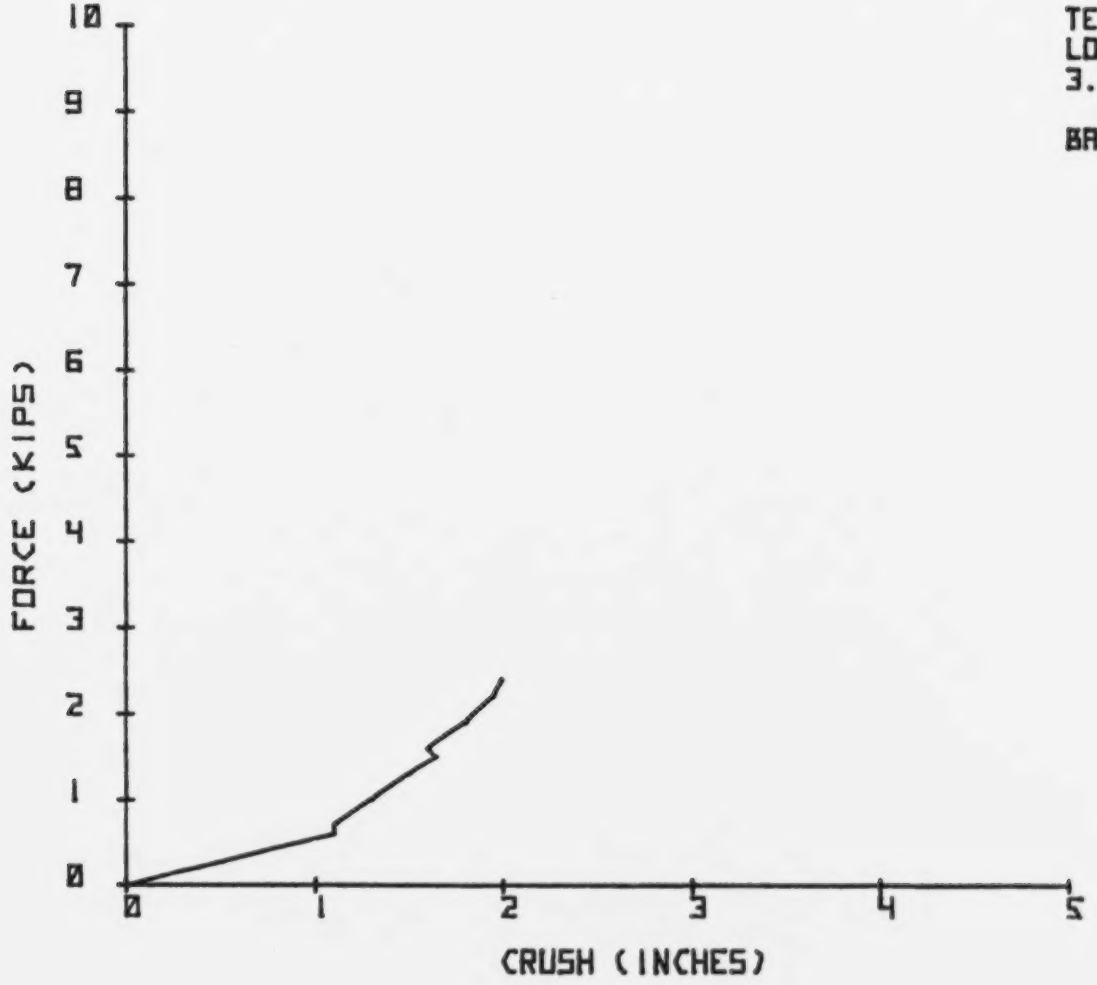

BEST DOCUMENT AVAILABLE

STATIC CRUSH PROPERTIES

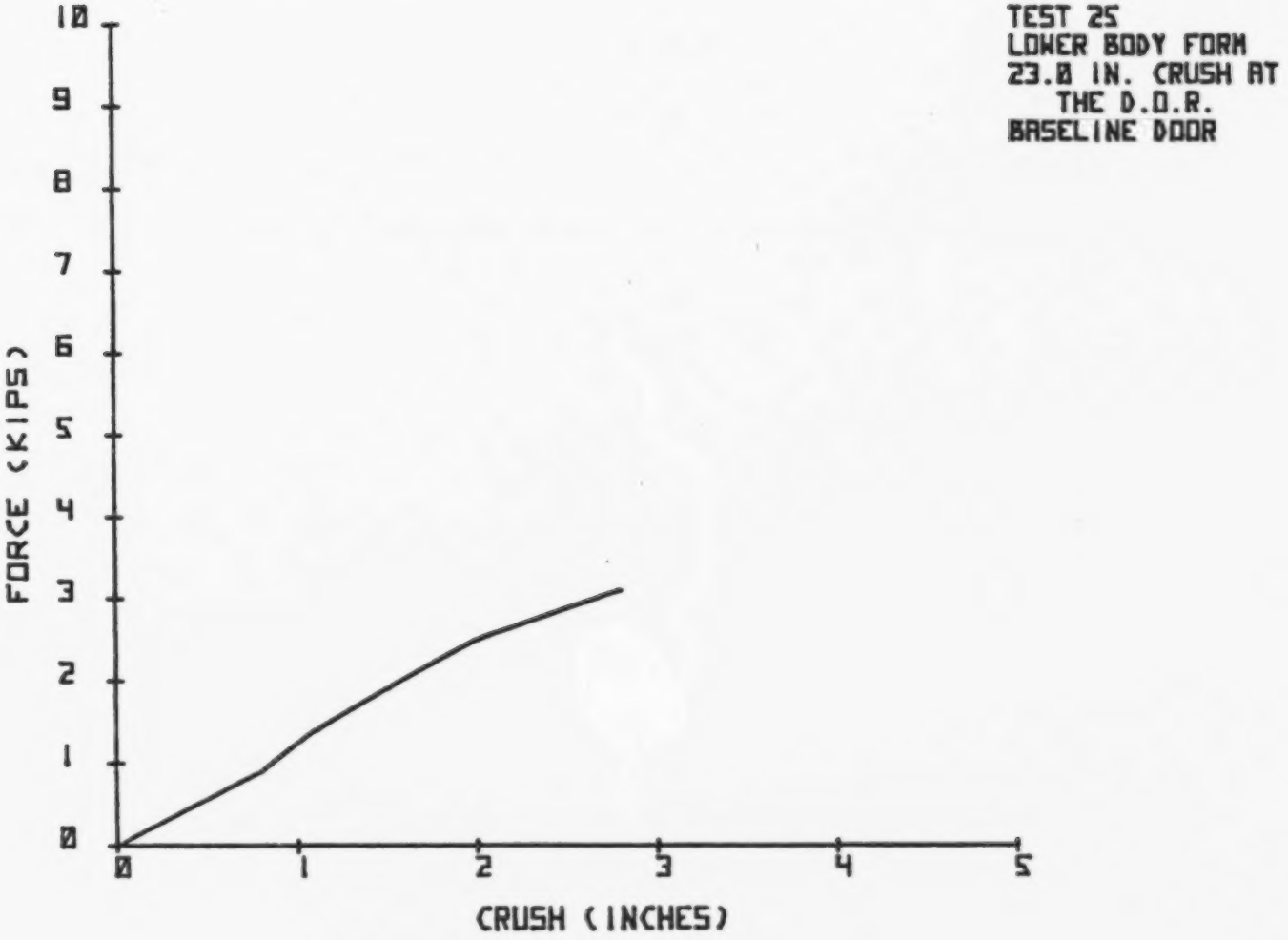

BEST DOCUMENT AVAILABLE

DYNAMIC CRUSH PROPERTIES

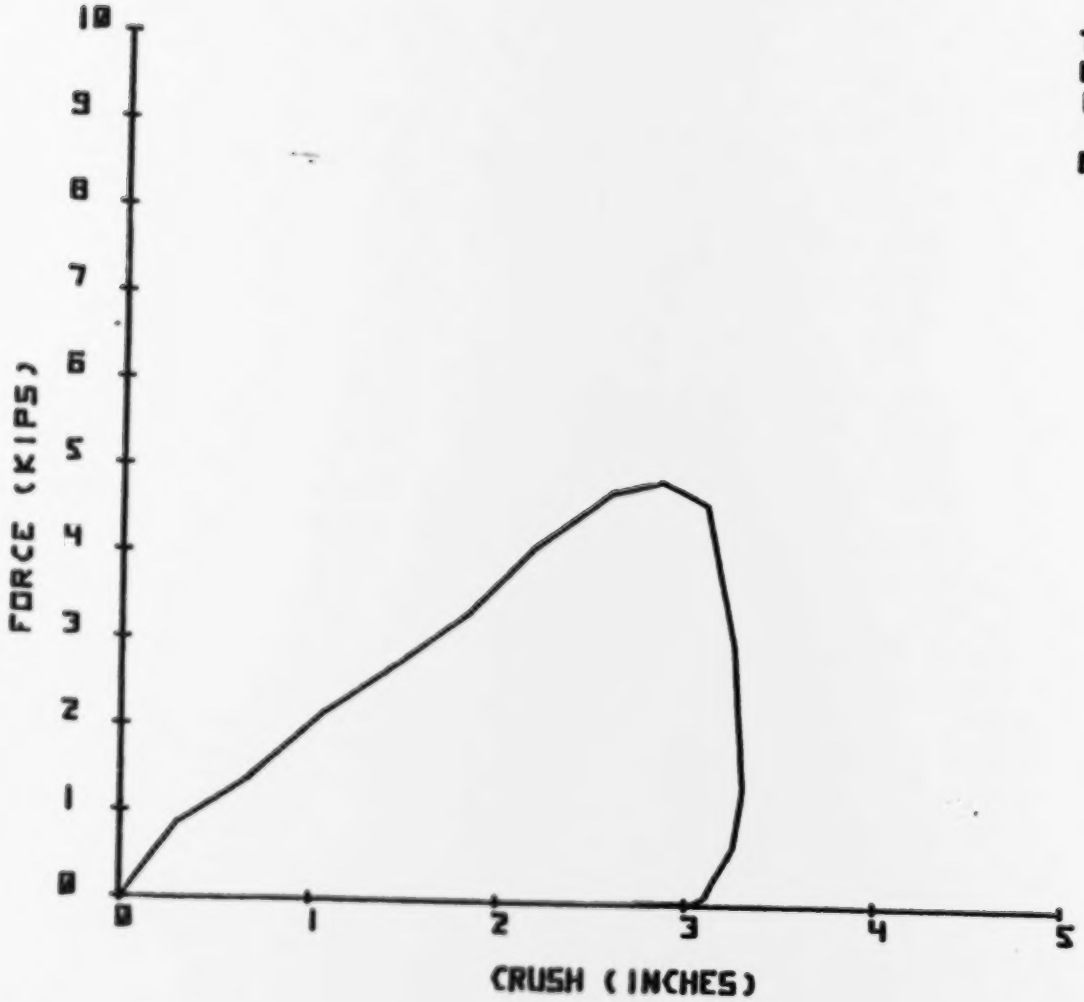

BEST DOCUMENT AVAILABLE

DYNAMIC CRUSH PROPERTIES

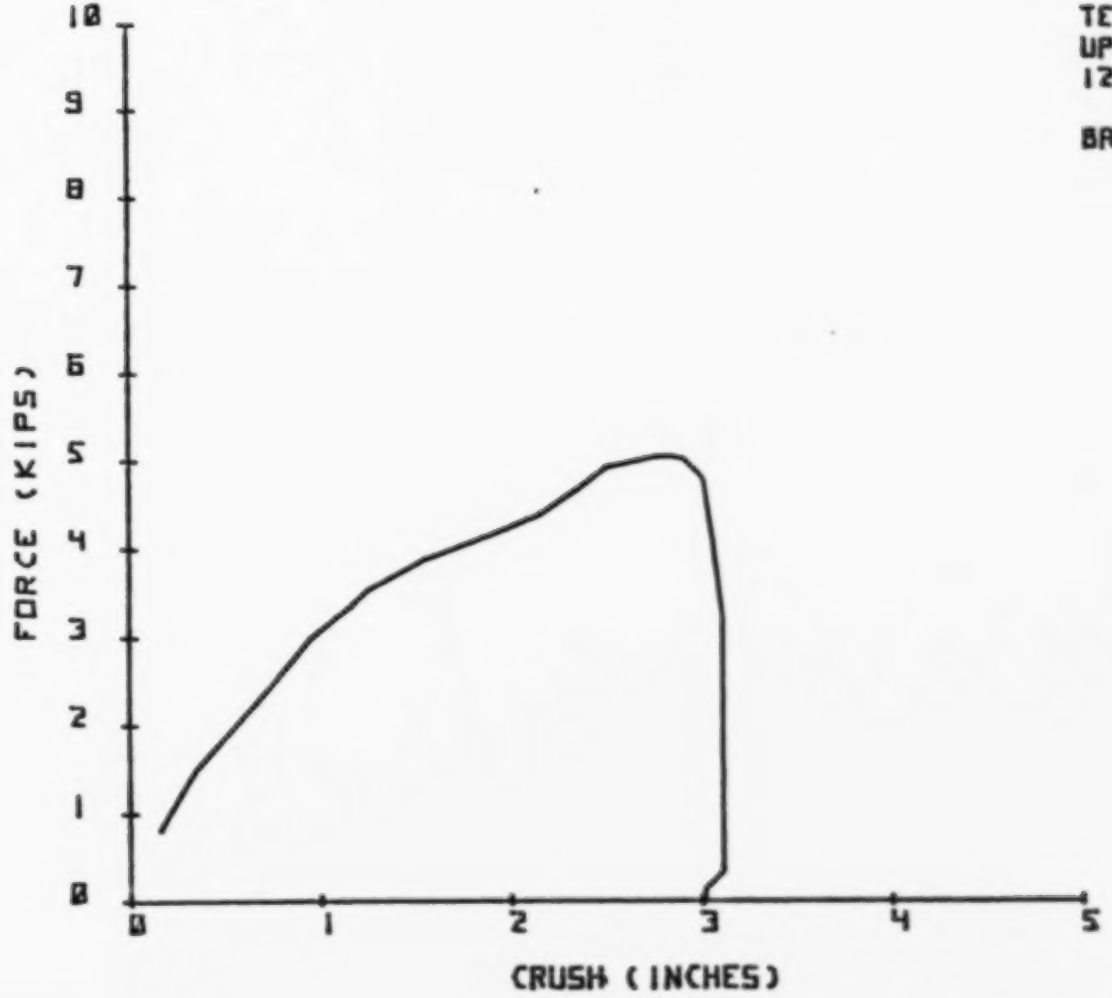

BEST DOCUMENT AVAILABLE

DYNAMIC CRUSH PROPERTIES

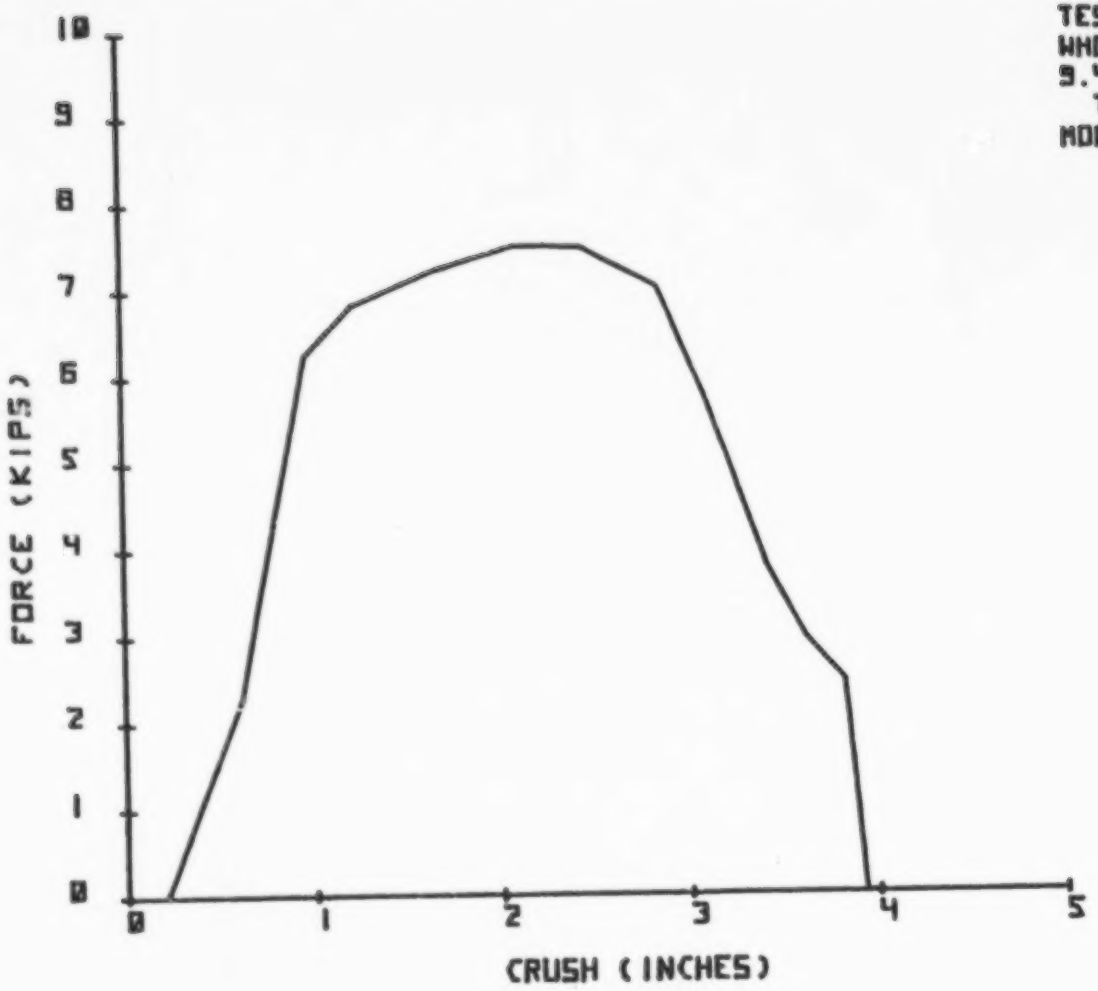

BEST DOCUMENT AVAILABLE

DYNAMIC CRUSH PROPERTIES

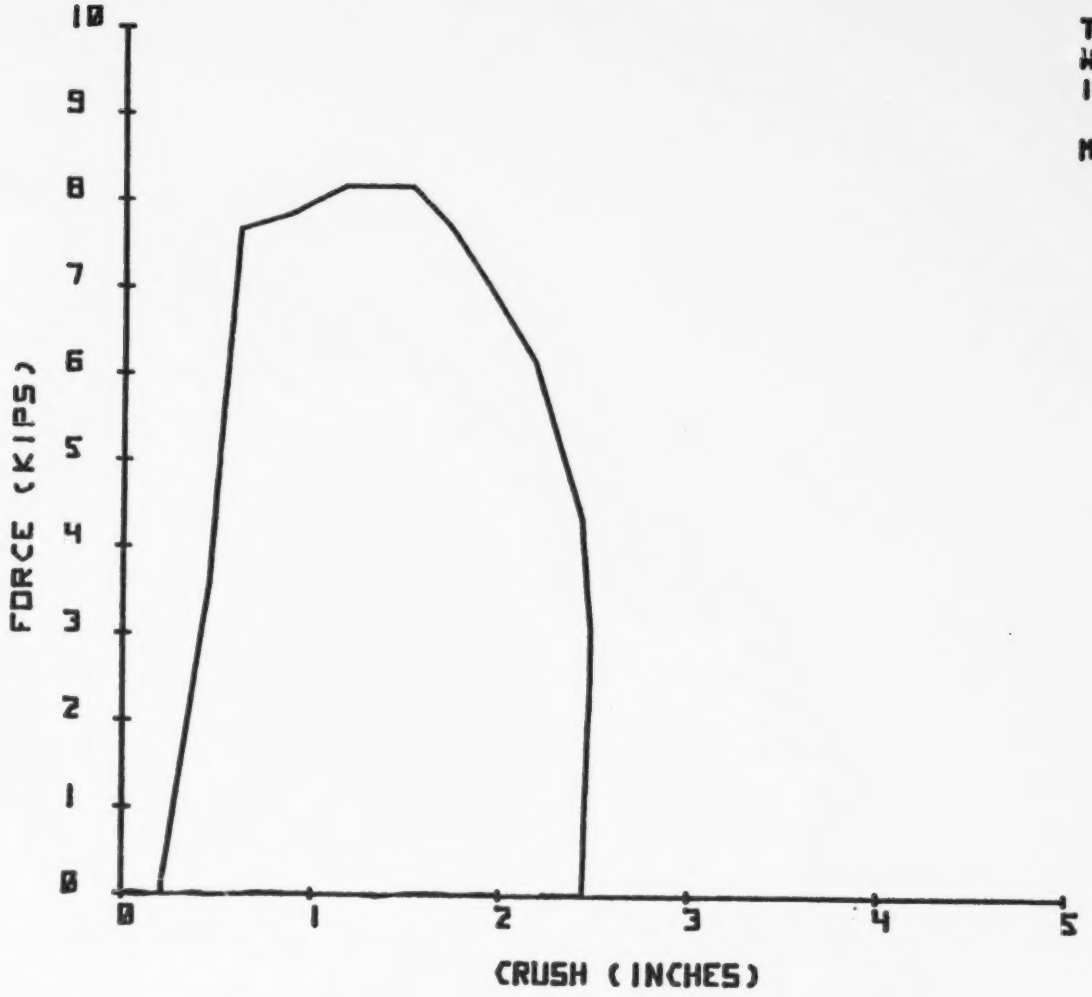

BEST DOCUMENT AVAILABLE

DYNAMIC CRUSH PROPERTIES

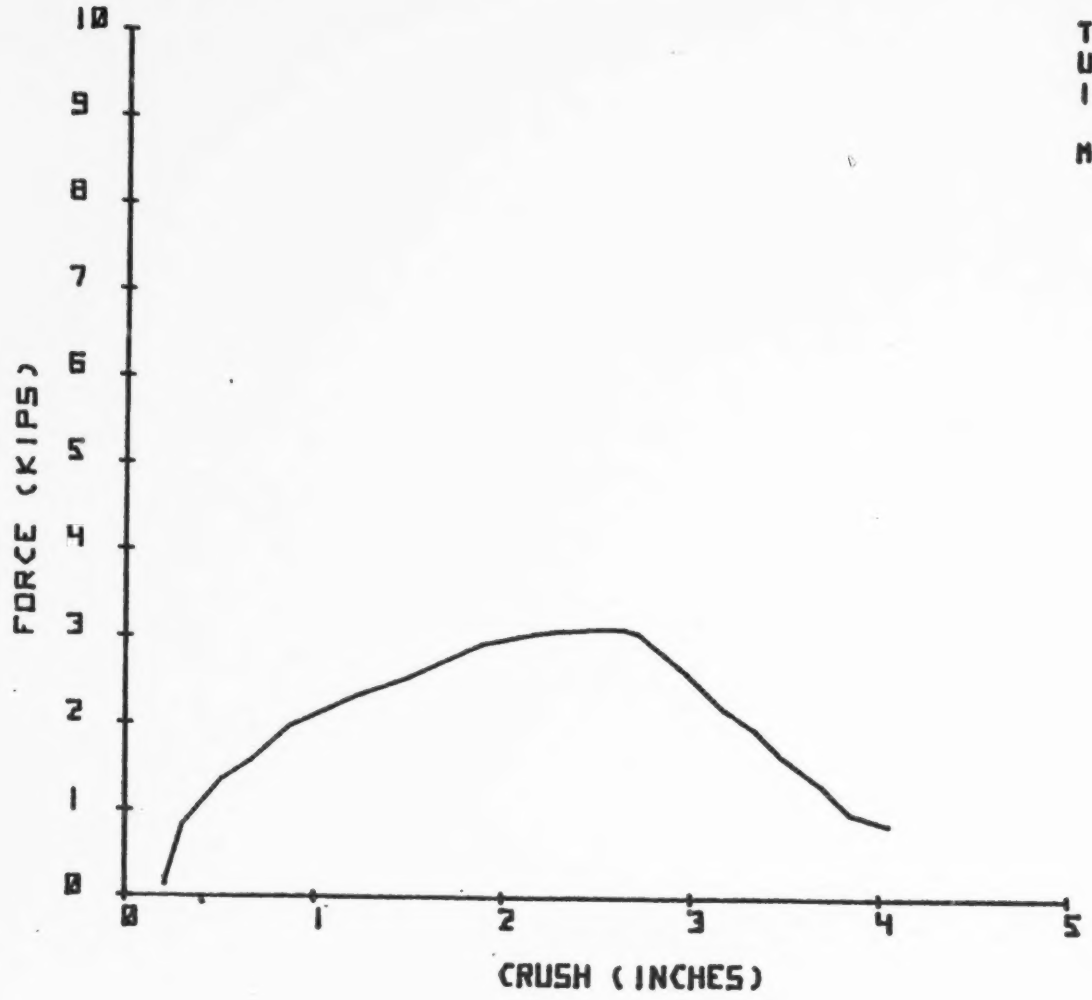

BEST DOCUMENT AVAILABLE

DYNAMIC CRUSH PROPERTIES

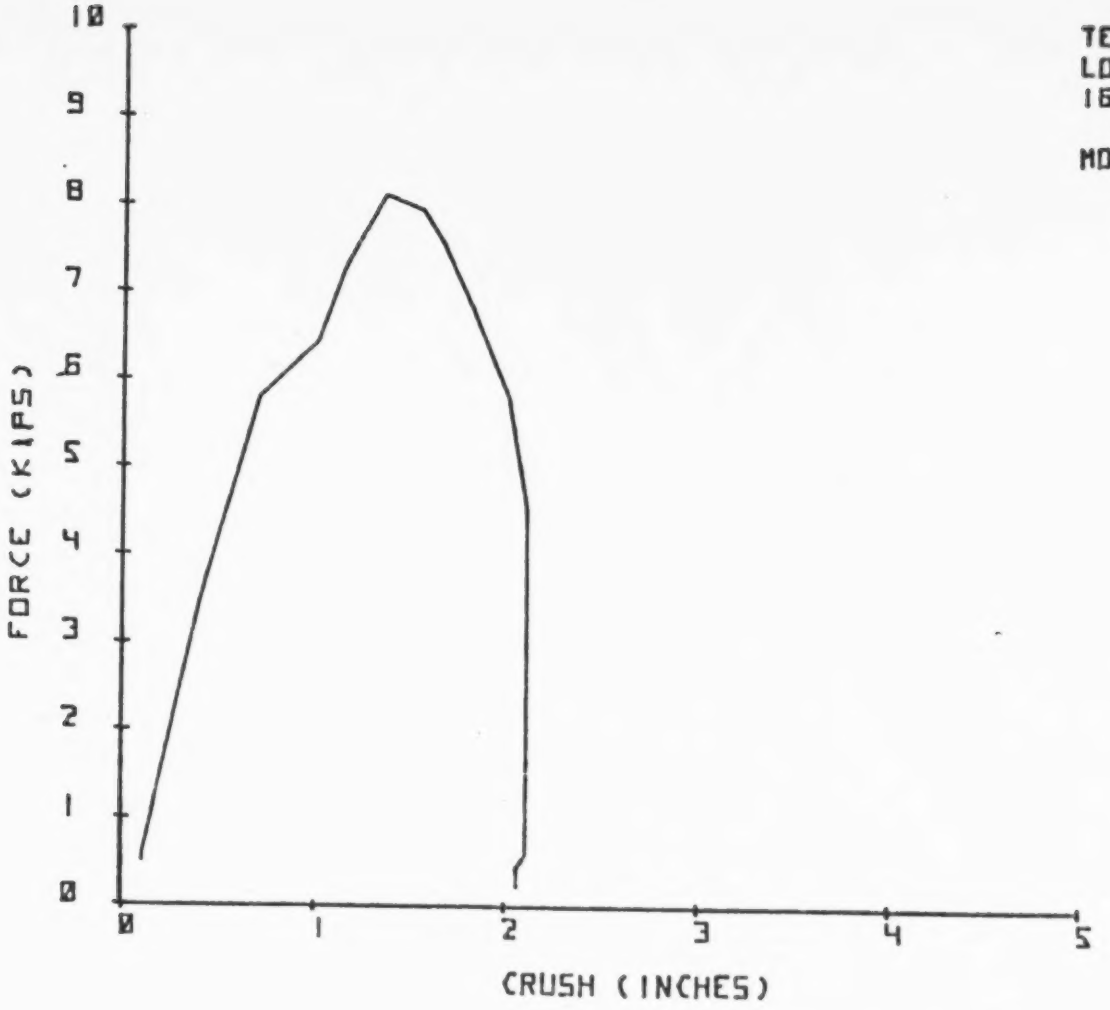

BEST DOCUMENT AVAILABLE

DYNAMIC CRUSH PROPERTIES

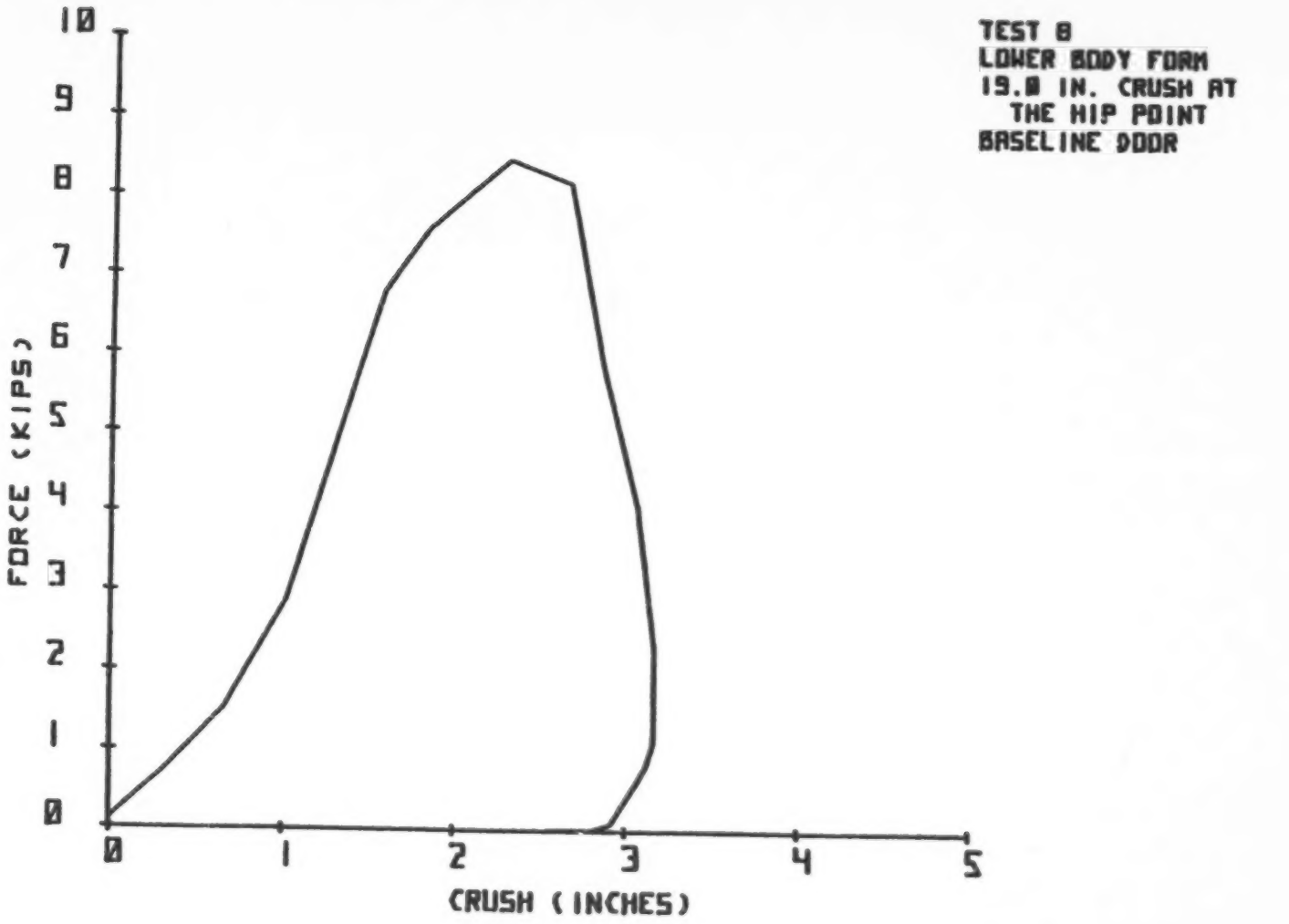

BEST DOCUMENT AVAILABLE

DYNAMIC CRUSH PROPERTIES

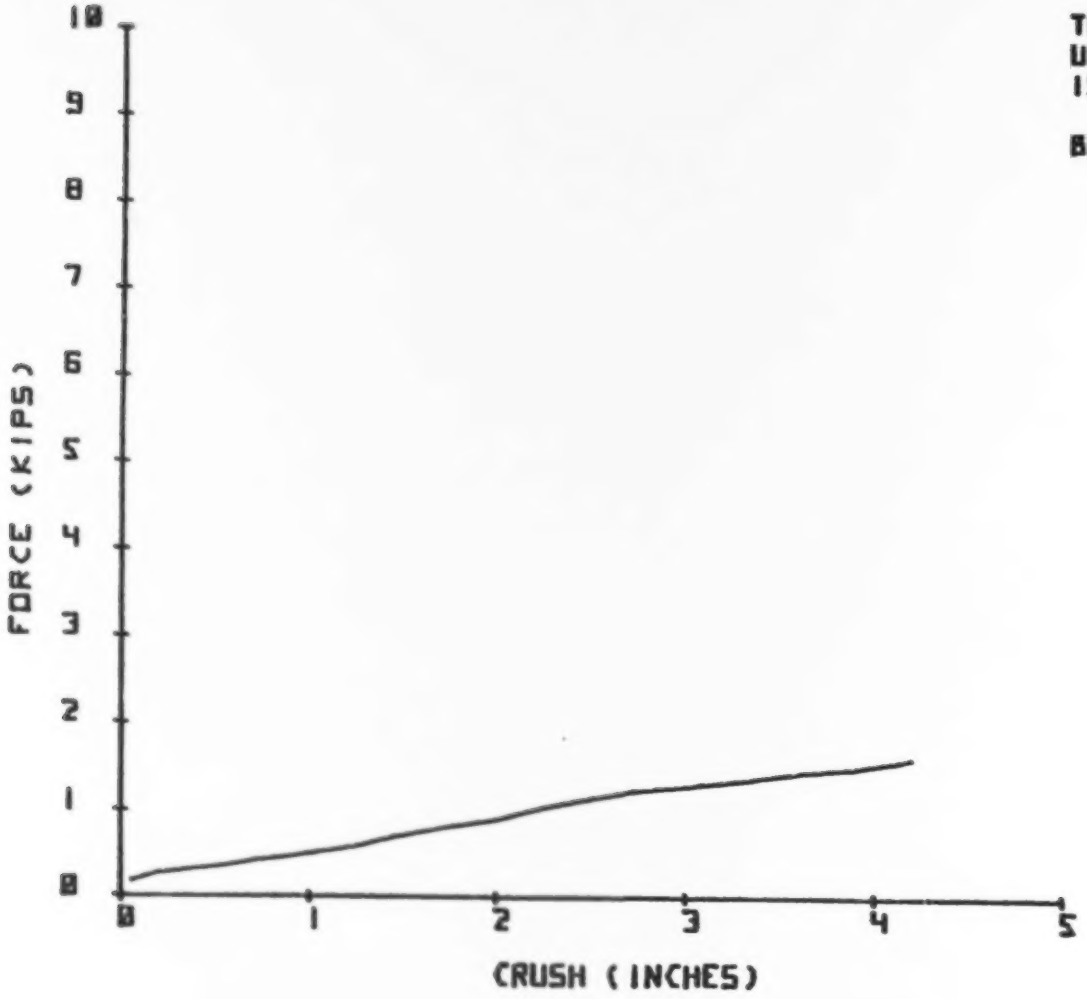

BEST DOCUMENT AVAILABLE

DYNAMIC CRUSH PROPERTIES

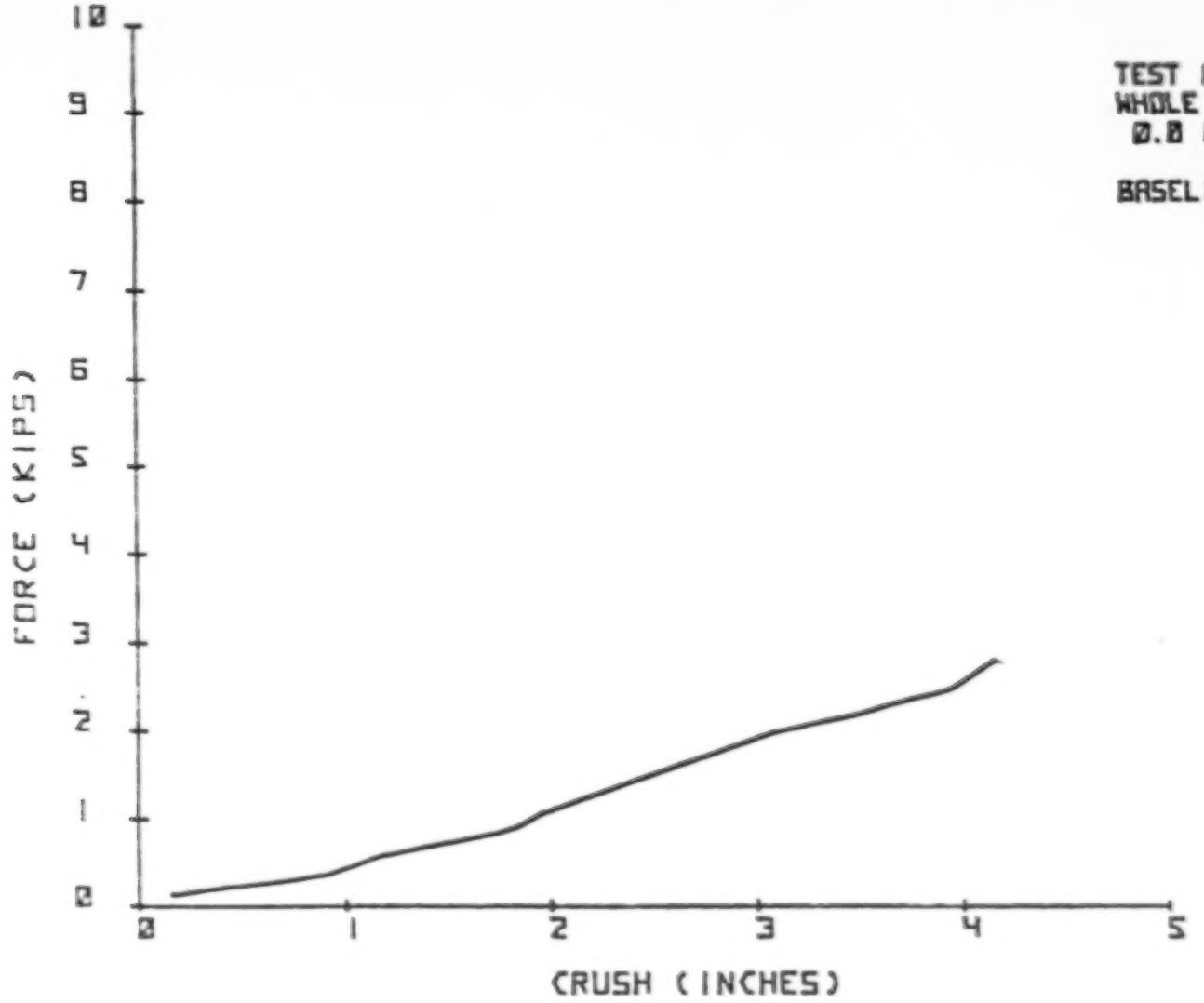

BEST DOCUMENT AVAILABLE

APPENDIX B

Interior Door Stiffness Trend Curves

BEST DOCUMENT AVAILABLE

DYNAMIC CRUSH PROPERTIES

WHOLE BODY FORM AT
CONSTANT INTERIOR CRUSH
VEHICLE PENETRATION ON
MOD.(REV. LT. WT.)DOOR
HIP PT. IMPACT

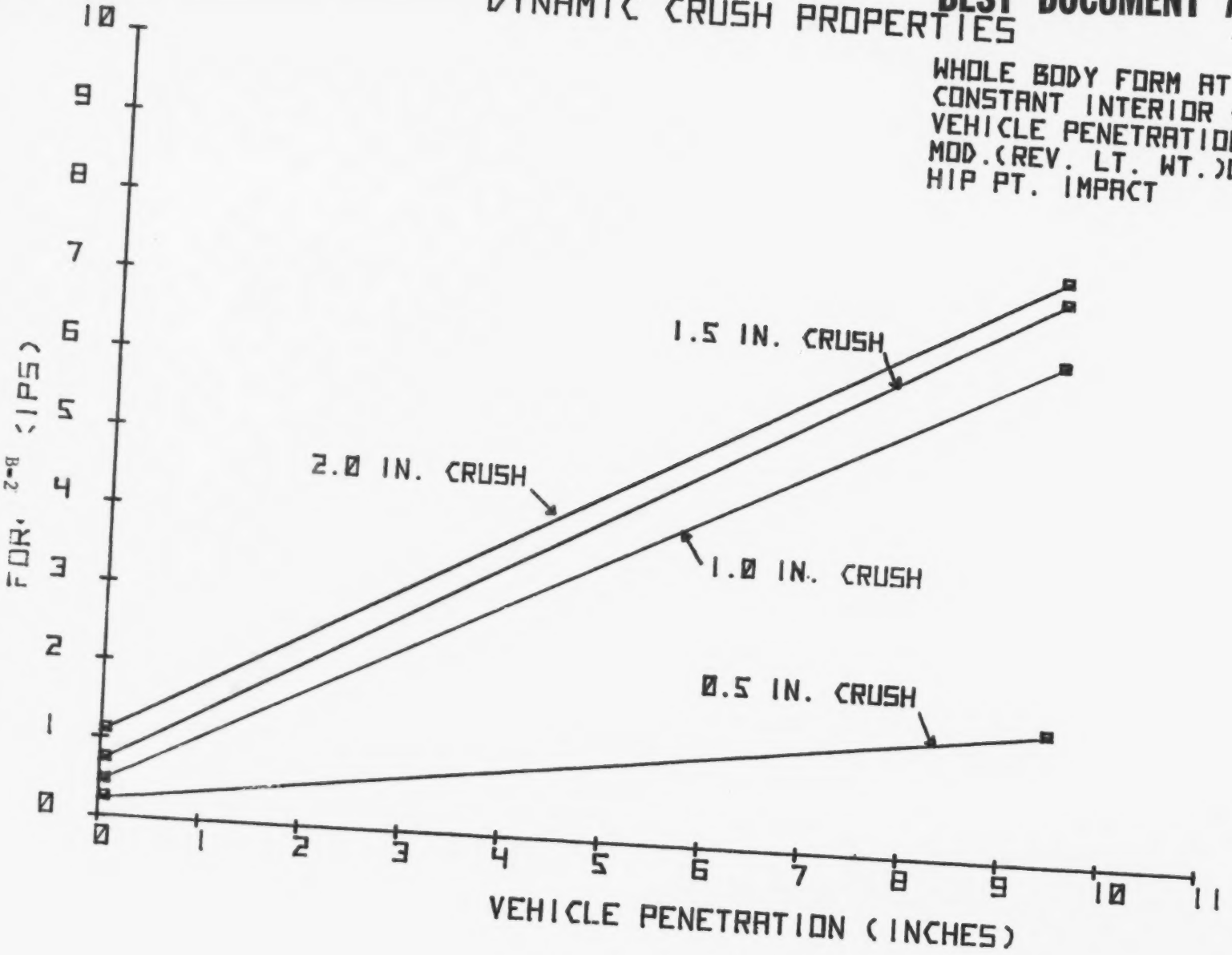

BEST DOCUMENT AVAILABLE

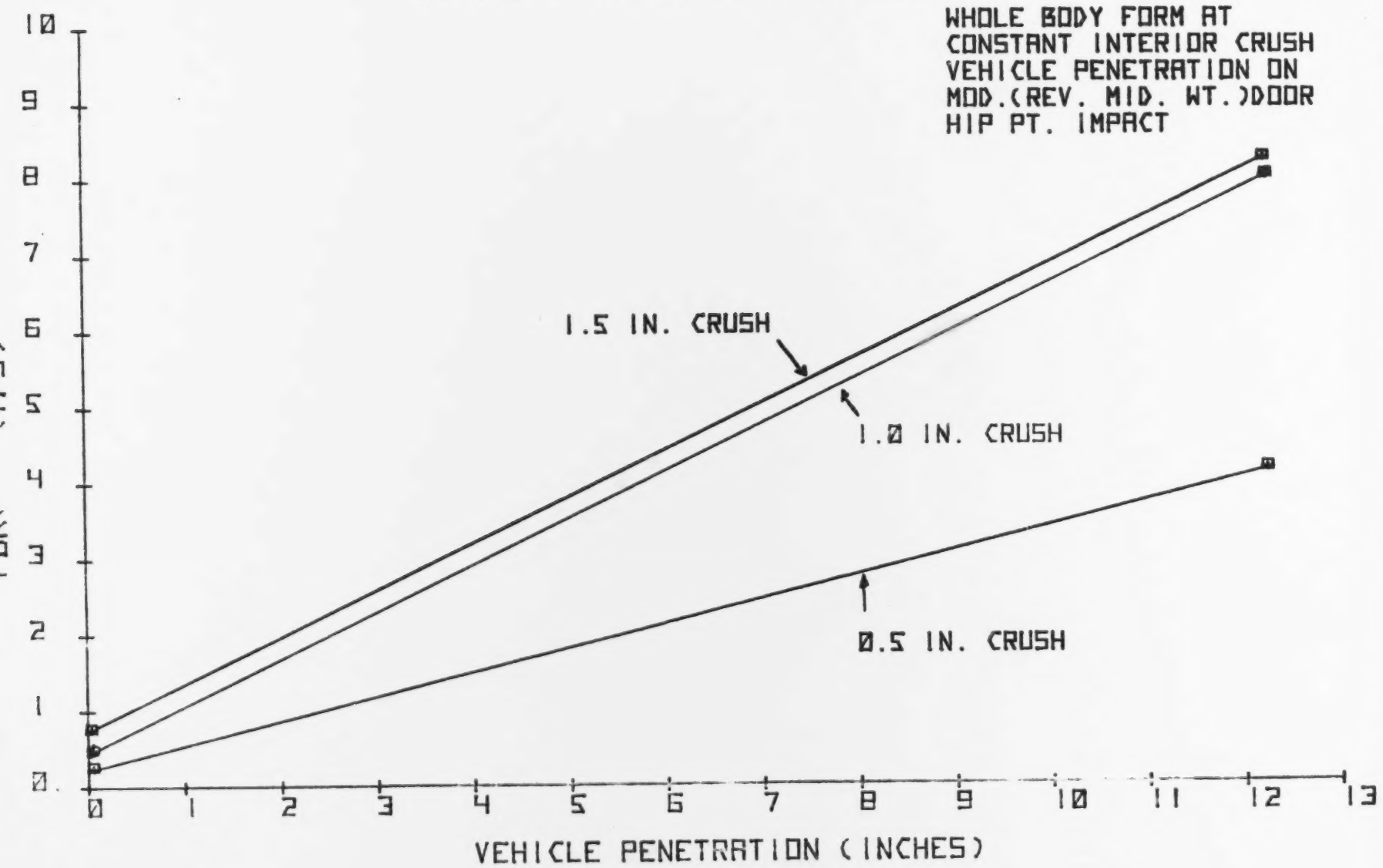

BEST DOCUMENT AVAILABLE

DYNAMIC CRUSH PROPERTIES

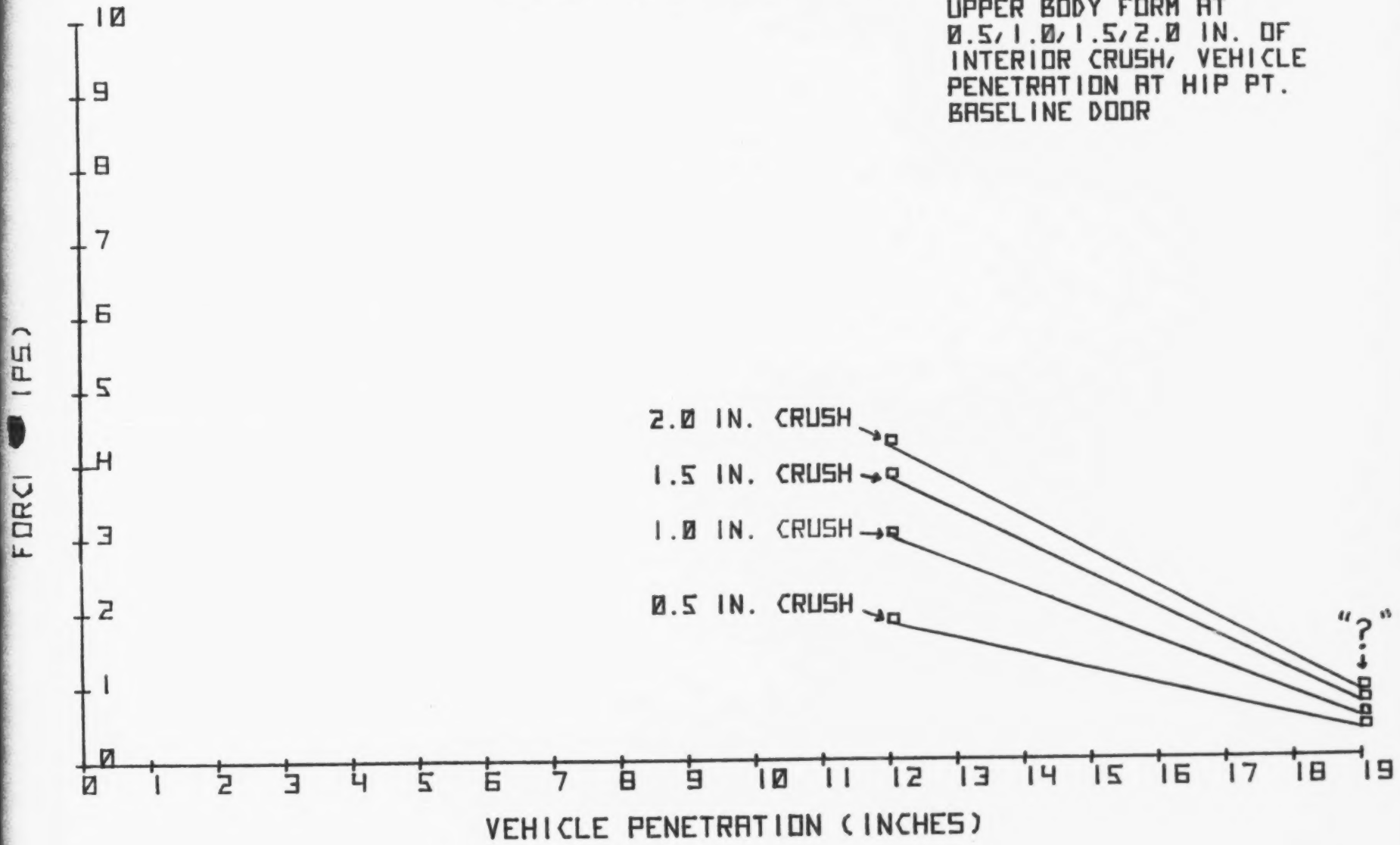
UPPER BODY FORM AT
0.5, 1.0, 1.5, 2.0 IN. OF
INTERIOR CRUSH, VEHICLE
PENETRATION AT HIP PT.
BASELINE DOOR
2.0 IN. CRUSH
1.5 IN. CRUSH
1.0 IN. CRUSH
0.5 IN. CRUSH
"?"
FORCE (PSI)
0 1 2 3 4 5 6 7 8 9 10
0 1 2 3 4 5 6 7 8 9 10 11 12 13 14 15 16 17 18 19
VEHICLE PENETRATION (INCHES)

BEST DOCUMENT AVAILABLE

DYNAMIC CRUSH PROPERTIES

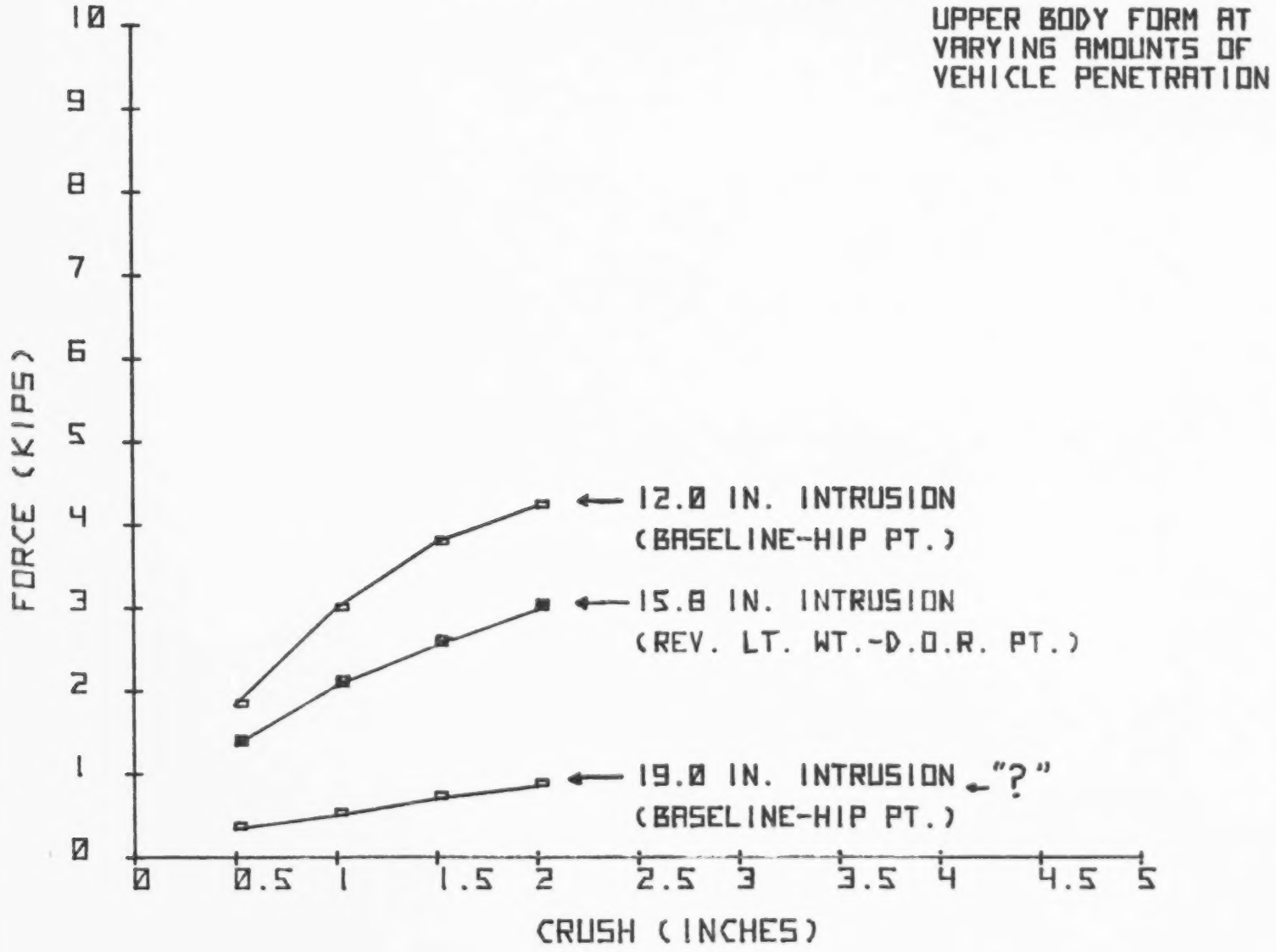

BEST DOCUMENT AVAILABLE

DYNAMIC CRUSH PROPERTIES

LOWER BODY FORM AT
0.5, 1.0, 1.5 IN. OF
INTERIOR CRUSH, VEHICLE
PENETRATION AT HIP PT.
BASELINE DOOR

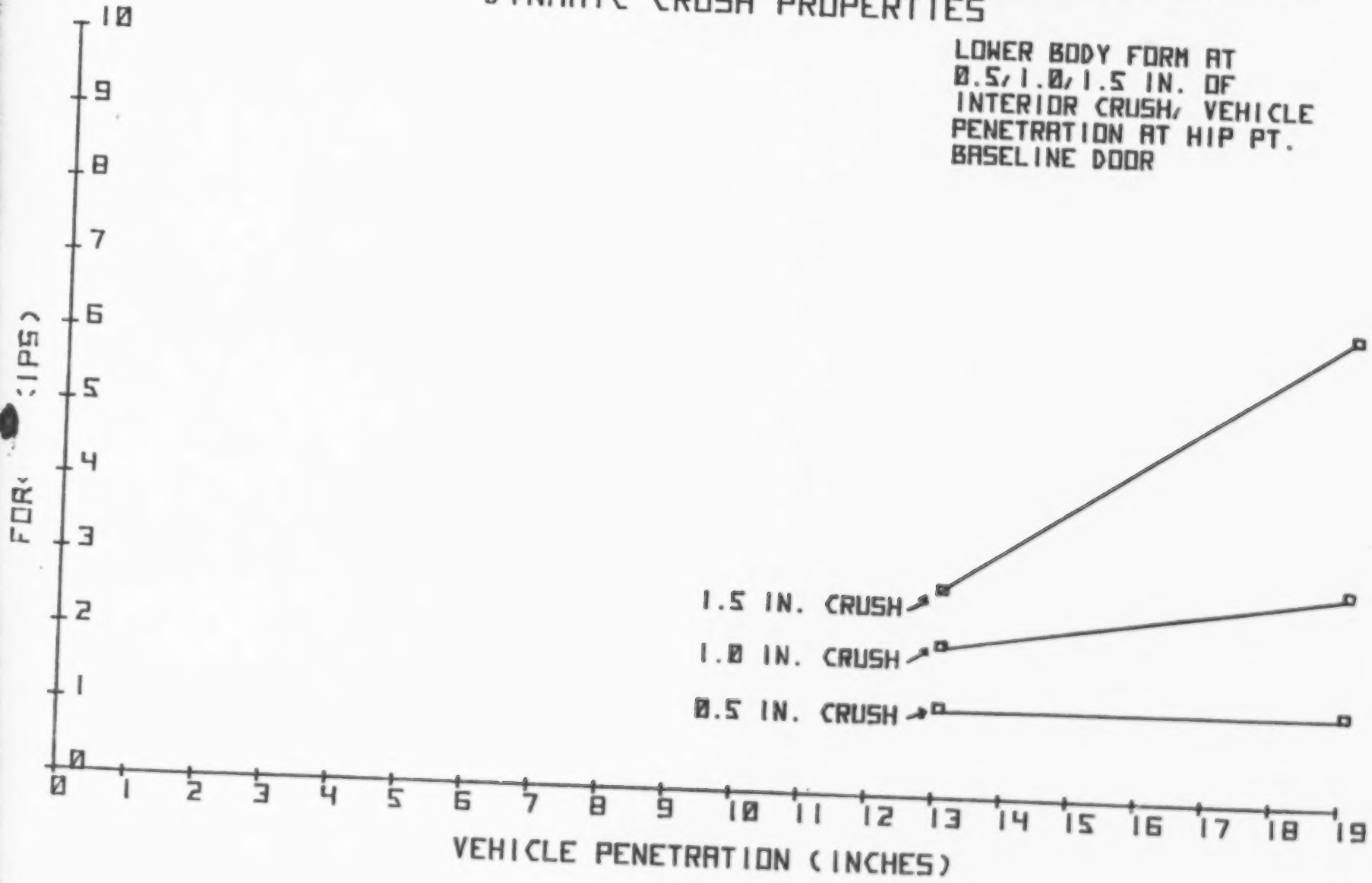

BEST DOCUMENT AVAILABLE

DYNAMIC CRUSH PROPERTIES

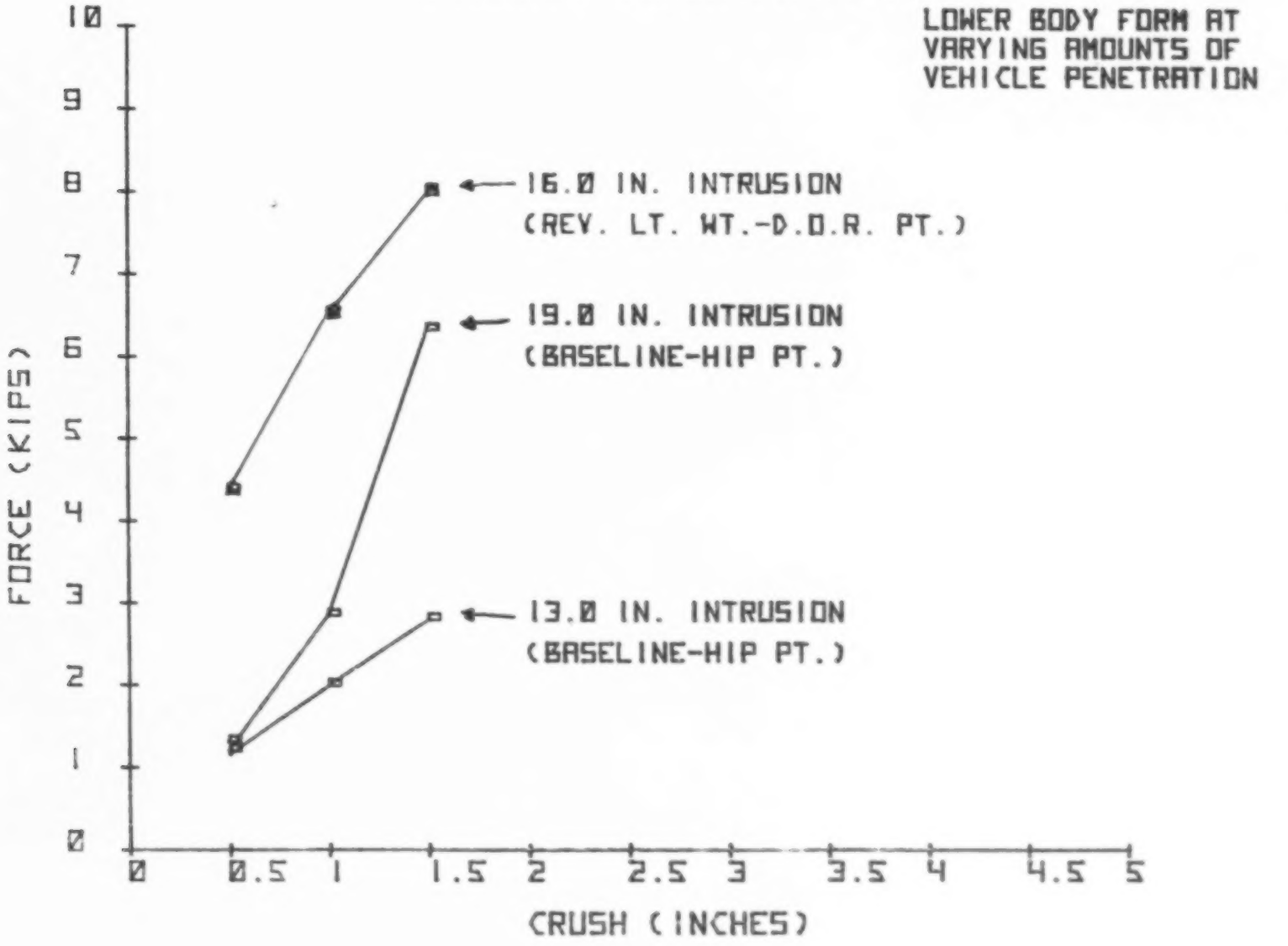

Blank Page

BEST DOCUMENT AVAILABLE

DYNAMIC CRUSH PROPERTIES

D.O.R. PT. IMPACT
AT 15.8 TO 16.0 INCHES
OF VEHICLE PENETRATON
MOD.(REV. LT. WT.)DOOR

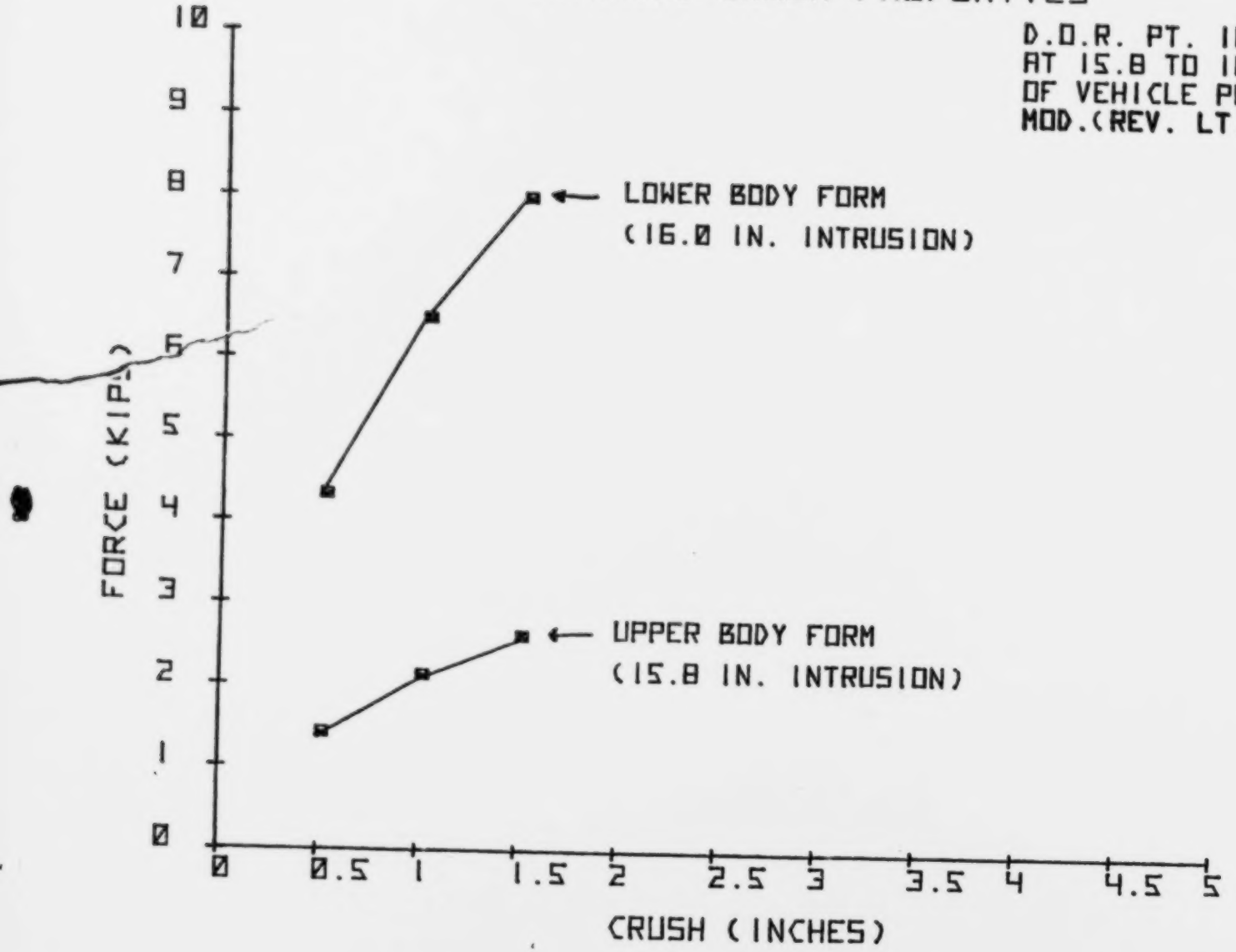

BEST DOCUMENT AVAILABLE

DYNAMIC CRUSH PROPERTIES

HIP PT. IMPACT AT
12.0 TO 13.0 INCHES OF
VEHICLE PENETRATION
BASELINE DOOR

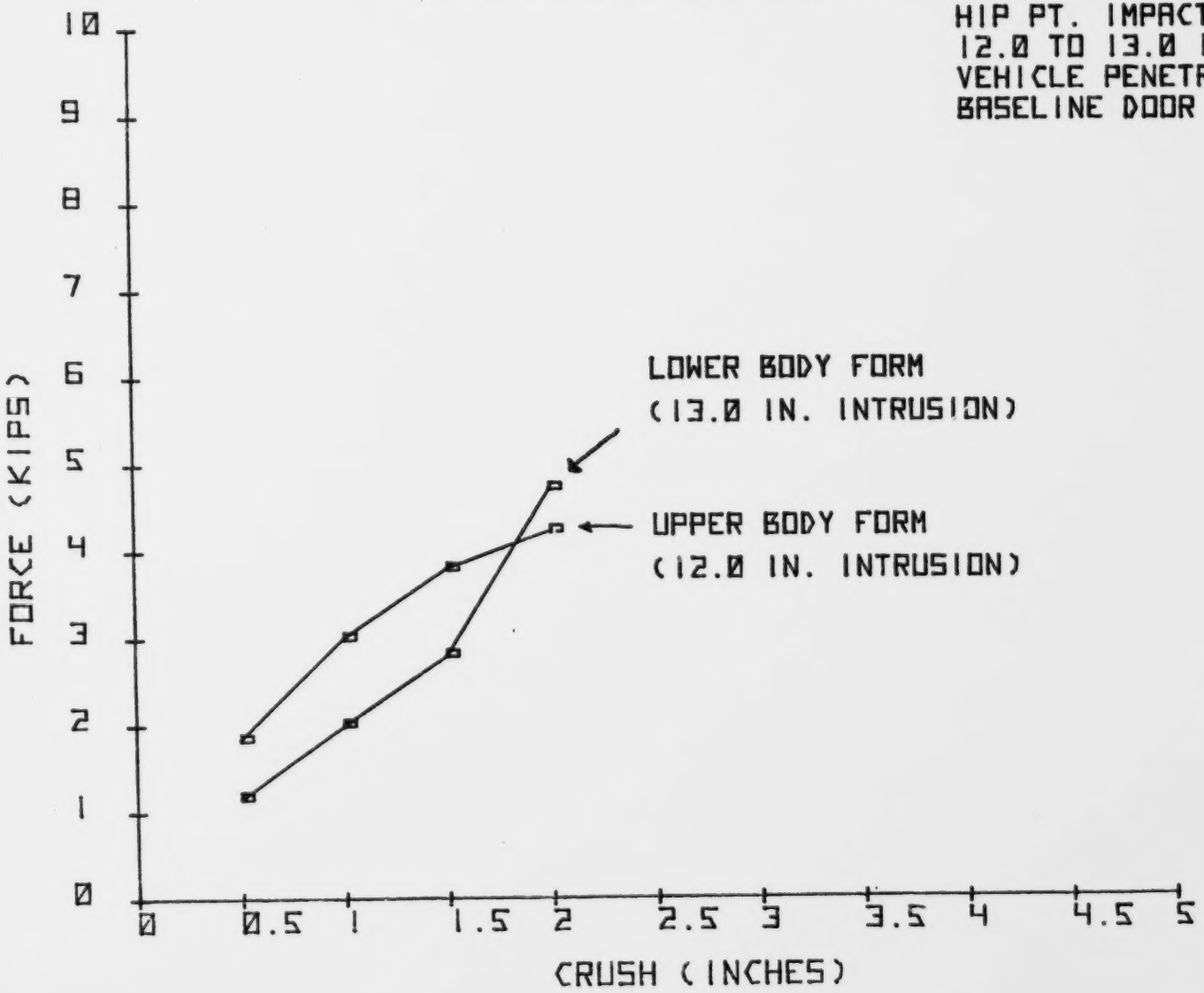

BEST DOCUMENT AVAILABLE

STATIC CRUSH PROPERTIES

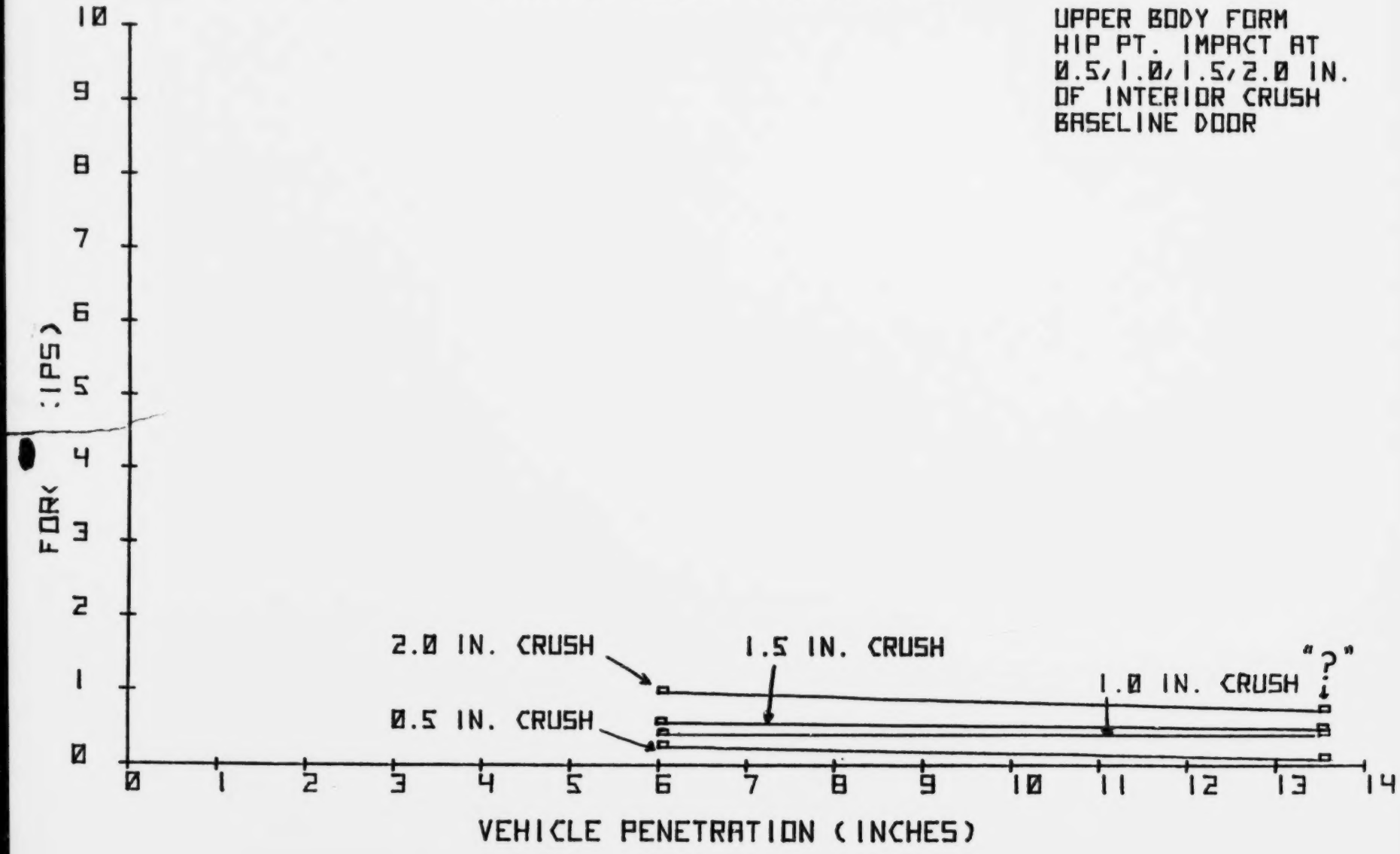

BEST DOCUMENT AVAILABLE

STATIC CRUSH PROPERTIES

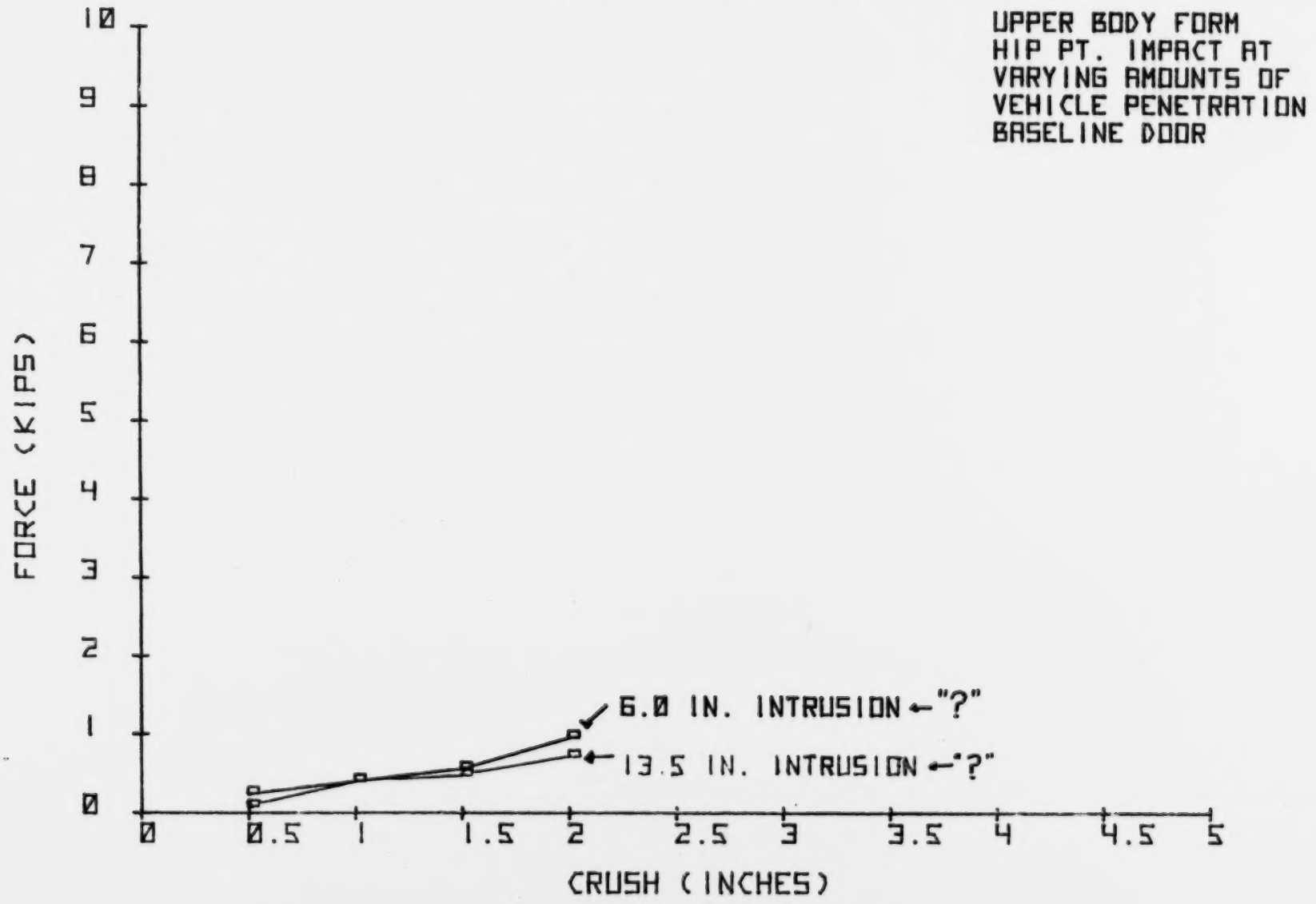

STATIC CRUSH PROPERTIES

BEST DOCUMENT AVAILABLE

UPPER BODY FORM
D.O.R. PT. IMPACT AT
0.5, 1.0, 1.5, 2.0 IN. OF
INTERIOR CRUSH
BASELINE DOOR

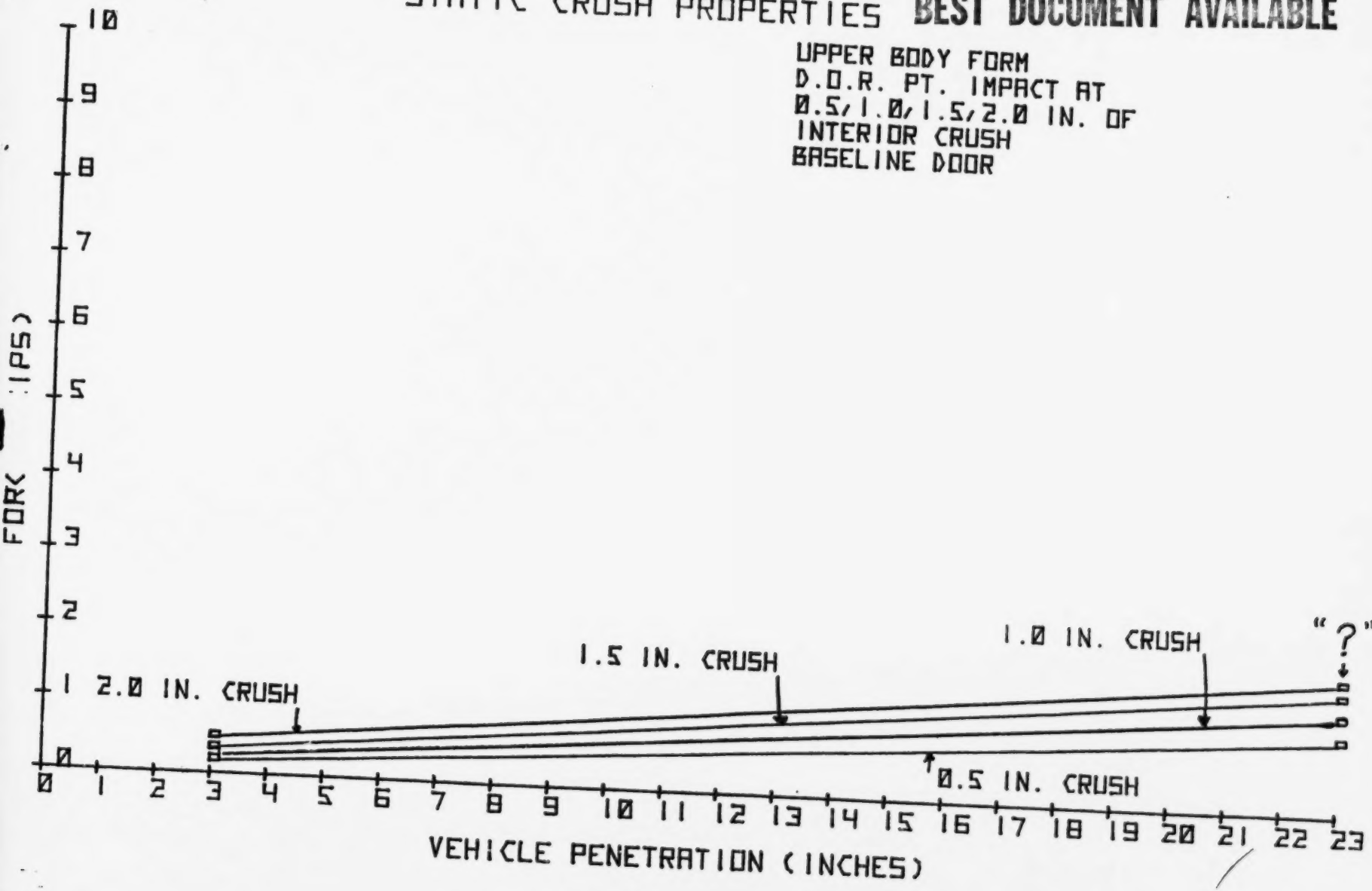

BEST DOCUMENT AVAILABLE

STATIC CRUSH PROPERTIES

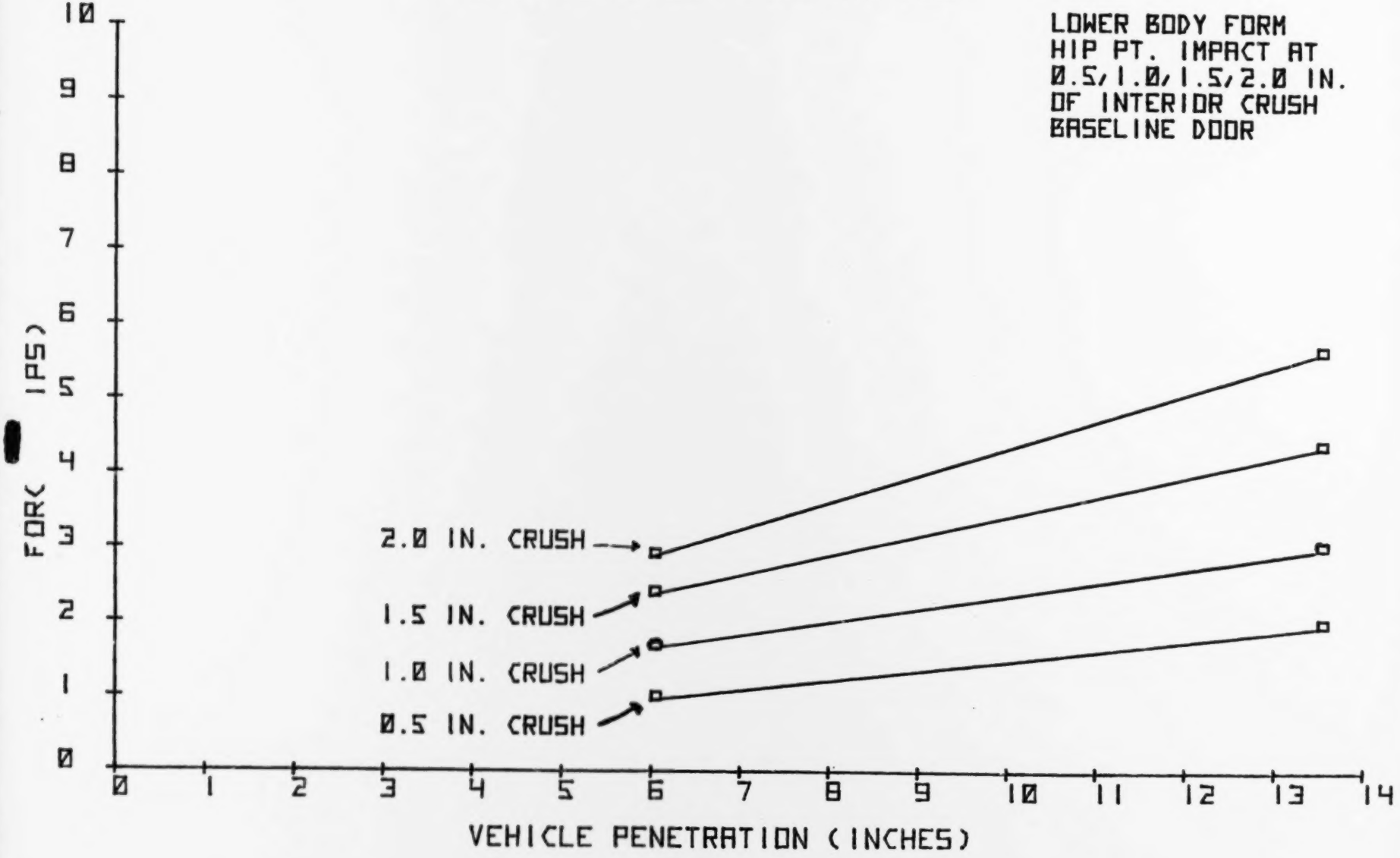

BEST DOCUMENT AVAILABLE

STATIC CRUSH PROPERTIES

LOWER BODY FORM
HIP PT. IMPACT
AT VARYING AMOUNTS OF
VEHICLE PENETRATION
BASELINE DOOR

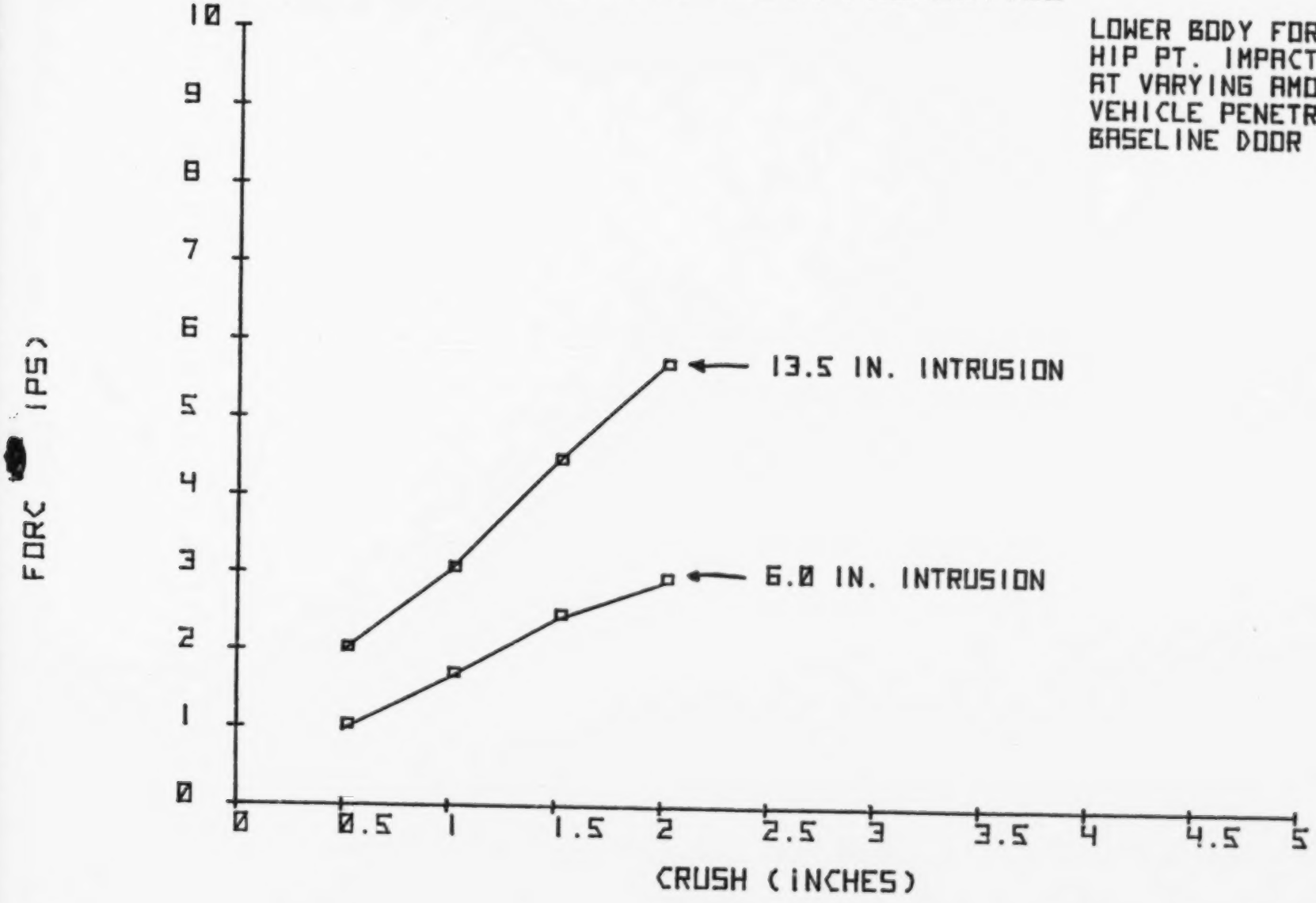

BEST DOCUMENT AVAILABLE

STATIC CRUSH PROPERTIES

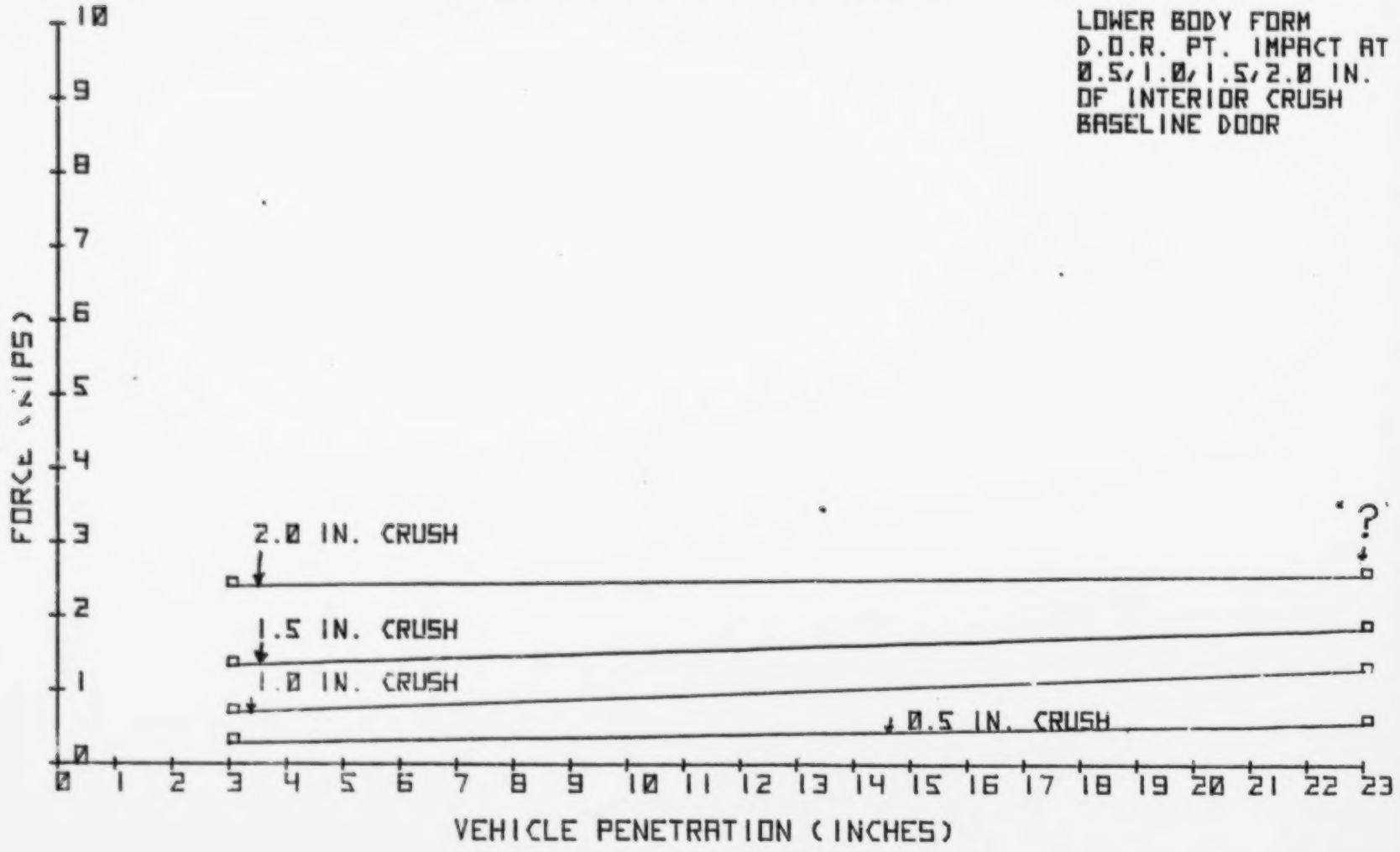

BEST DOCUMENT AVAILABLE

STATIC CRUSH PROPERTIES

HIP PT. IMPACT
AT 13.5 IN. OF
VEHICLE PENETRATION
BASELINE DOOR

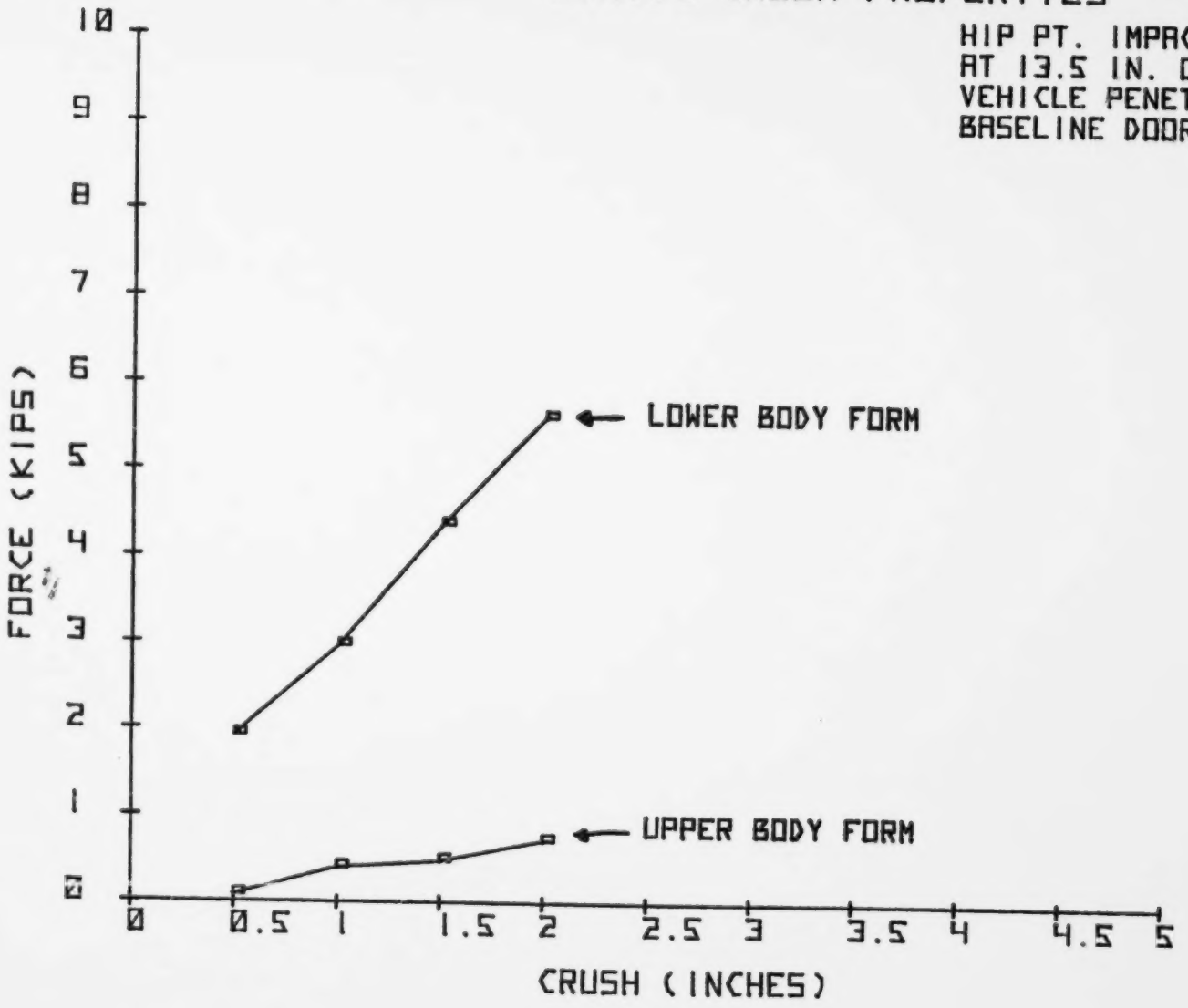

BEST DOCUMENT AVAILABLE

STATIC CRUSH PROPERTIES

D.O.R. PT. IMPACT
AT 3.0 IN. OF
VEHICLE PENETRATION
BASELINE DOOR

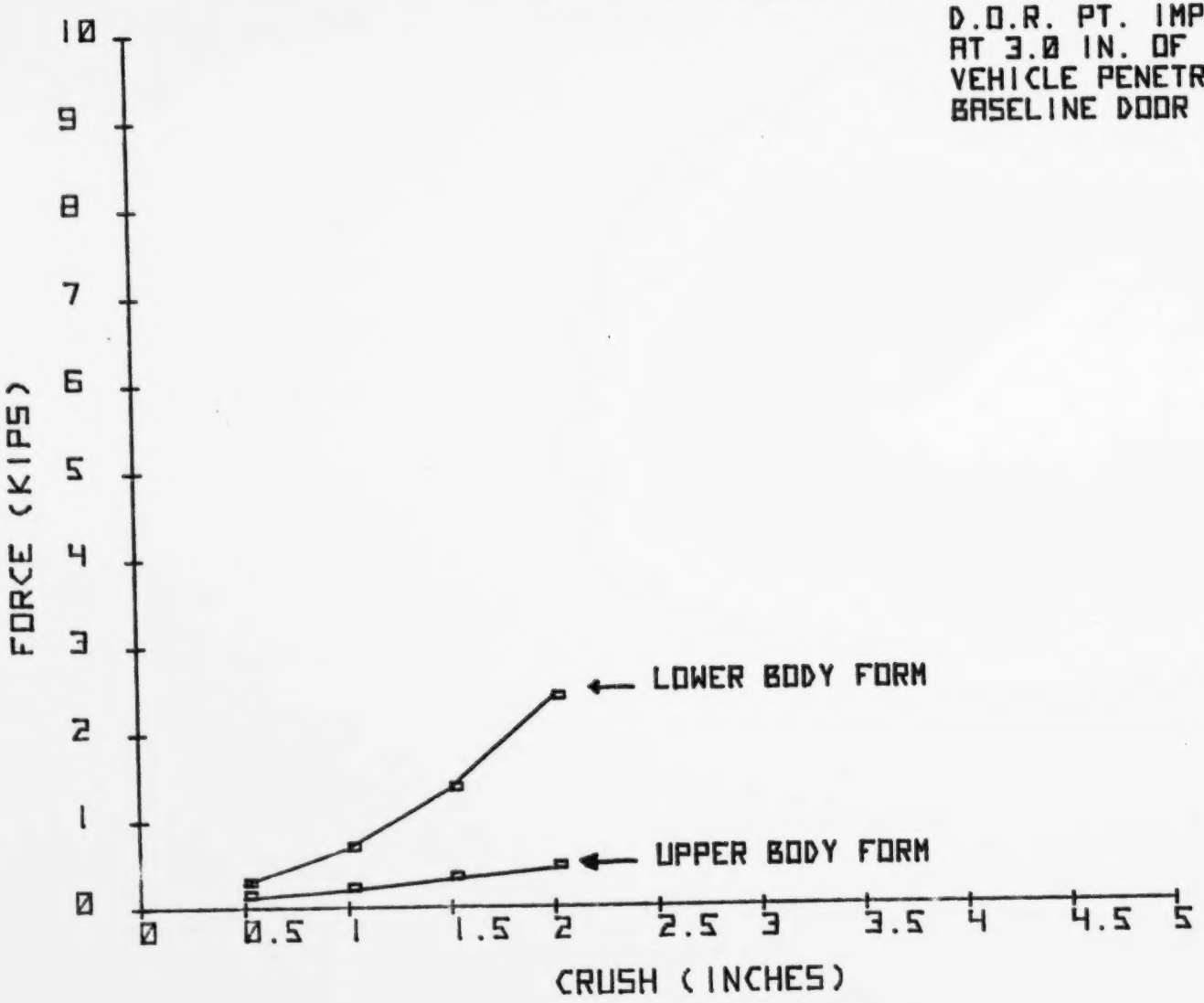

BEST DOCUMENT AVAILABLE

STATIC CRUSH PROPERTIES

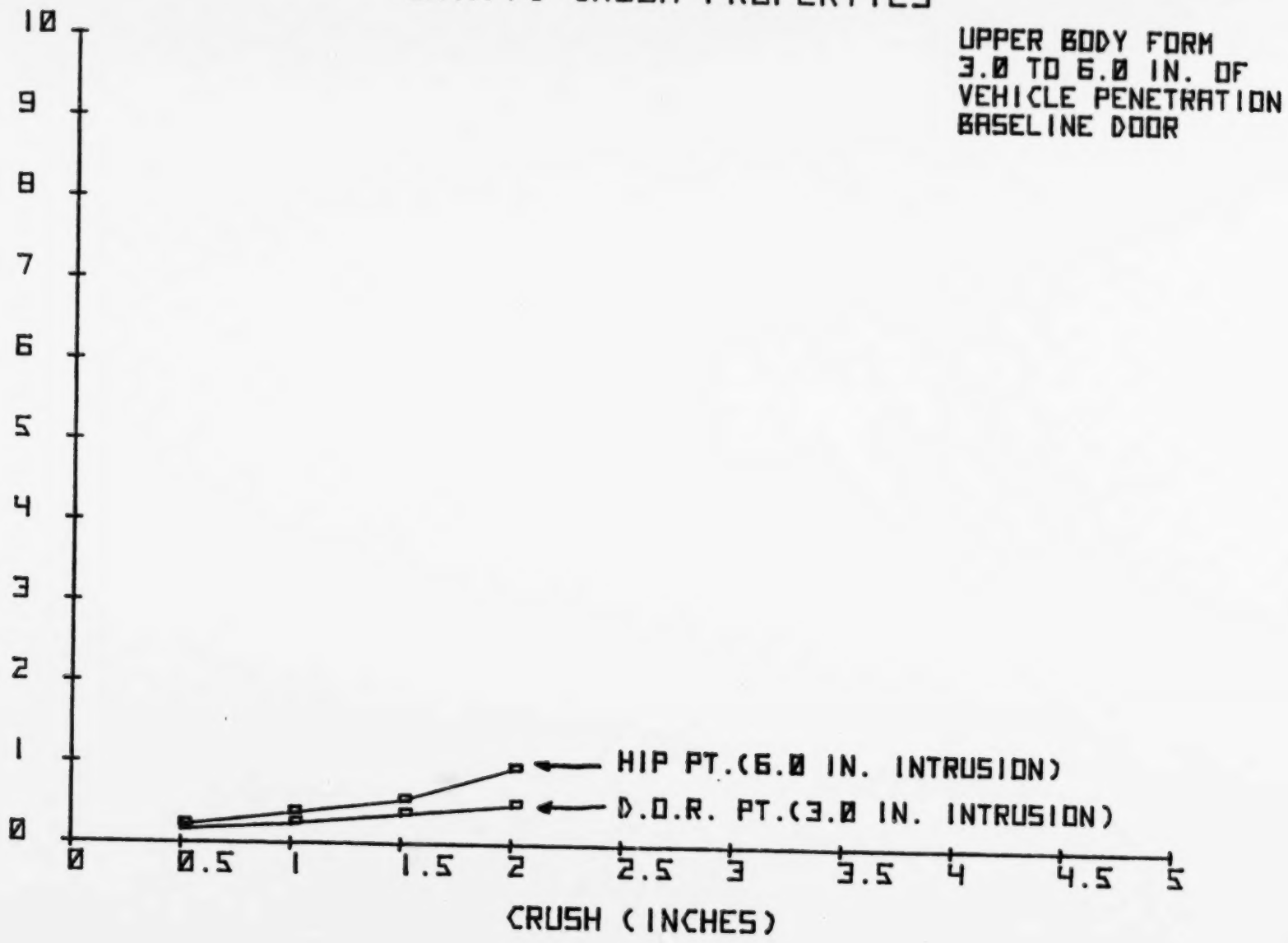

BEST DOCUMENT AVAILABLE

STATIC CRUSH PROPERTIES

LOWER BODY FORM
3.0 TO 6.0 IN. OF
VEHICLE PENETRATION
BASELINE DOOR

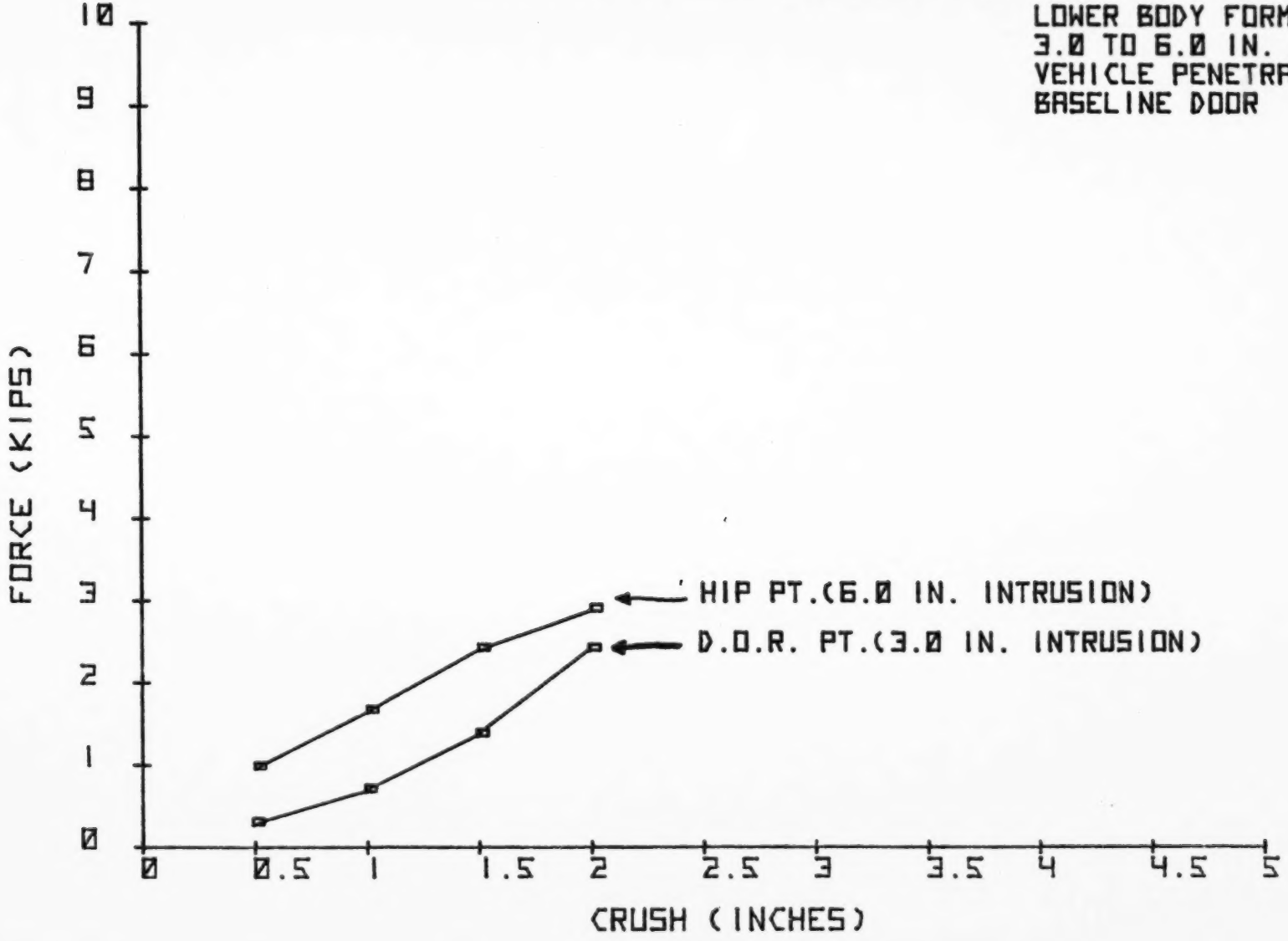

BEST DOCUMENT AVAILABLE

APPENDIX C

Discussion of Roller Tape Mechanisms

BEST DOCUMENT AVAILABLE

Fitzpatrick Engineering
RESTRAINT SYSTEMS DESIGN AND DEVELOPMENT
ROUTE 5, BOX 495A • WARSAW, IN 46580 PHONE: 219-267-4437

General Discussion of Mechanics of Tape Roller Energy Absorption Mechanism

Prepared by: Michael Fitzpatrick

Prepared for: Mr. Mike Monk and,
Mr. Rick Morgan; NHTSA

Date: October 31, 1979

BEST DOCUMENT AVAILABLE

The Tape-Draw Force Limiter

A highly efficient way to utilize a given stroke distance by converting kinetic energy into strain energy of deformation is to design the deformable vehicle structure so as to exhibit a relatively constant force over the stroking distance. If this is done, the g-loads imparted to the vehicle(s) will be essentially constant over the stroke length, thereby eliminating spurious effects, such as instantaneously high deceleration loads that are potentially harmful to the vehicle occupant.

The idea of force limiting mechanism is not new and, in fact, much development work has taken place in an effort to develop a light-weight, low cost, reliable, force limiting mechanism. Although vehicles modified with such a force-limiter have exhibited significant improvements over unmodified vehicles, a large percentage of the solutions were expensive, heavy, and, unfortunately, not reliable. A case in point is the plastic hinge concept. Although, as mentioned, its use results in energy absorption improvements over an unmodified vehicle, it is heavy, rather costly, and due to its ever-changing moment arm during the stroking motion, does not have a constant force-deflection relationship.

To investigate these points a bit further, consider the weight. The plastic hinge concept, by definition, is plastic only at the hinge point, and during the stroking motion, only this section of the member is being utilized to its full potential, while the rest of the member merely goes along for the ride. It, therefore, has a high ratio of weight to absorbed energy.

Consider cost and relaibility. The hinge is rather difficult to fabricate at low cost due to the high degree of manufacturing care required to ensure that it does not fail at the hinge joint in a brittle fashion rather than plastically as designed. In addition, the hinge concept has been shown to have erratic results even when tested on the component level under tightly controlled laboratory conditions. Sometimes cracks appear at the joints and on occasion the failure mode has been simply a buckling of the compression flange. These characteristics when coupled with the fact that the deforming force varies with stroke instead of being constant as would be desired, show the need for a more optimal energy management system.

BEST DOCUMENT AVAILABLE

A system has been designed and tested that shows significant improvements in the areas mentioned. It consists of using the stroking force to pull a metal tape over a system of rollers as shown in Figure 1 . As the tape progresses over the rollers, it is plastically deformed, thereby converting kinetic energy into strain energy of deformation. Since each element of tape passing over the rollers is forced to conform to the roller, each element is strained the same way and in the same amount so that an equal amount of strain energy is absorbed by each element. For a tape of constant geometry, this is equivalent to saying that the drawing force required to pull the tape over the rollers is constant over the stroke length.

Since every bit of the tape is being plastically deformed instead of only a local area as on the plastic hinge, it has the optimum ratio of weight to absorbed energy.

It can be shown that, up to a certain limit, the force required to draw the tape across the roller is directly proportional to the number of rollers, the width of the tape,the thickness of tape squared, the yield strength of the material and is inversely proportional to the roller diameter. This gives a large degree of design latitude in choosing a tape system, thereby making a change in design force a matter of merely selecting another tape thickness, adding or subtracting a roller, etc.

The cost of such a system is obviously minimal. Material costs are low and fabrication costs are limited to fastening the required number of rollers to a support point. Reliability also is good. We have conducted numerous impact sled tests using the tape-draw system as an upper torso restraint and also as a knee restraint. To date no failures have occurred and the results have been very repeatable.

If for any reason, it is desired to design a system with a force that varies with stroke in a predetermined manner, this requirement can be met by, say, trimming the tape so that the tape width varies with length. In this way, almost any force deflection relationship could be realized. A slightly different aspect of this versatility would be realized, for example, in a tape system whose length was normal to the impacting force. This relationship

BEST DOCUMENT AVAILABLE

between force and stroke is definitely not a constant force relationship, and in fact, is usually highly non-linear. However, by proper adjustment of the tape width and/or other parameters that will be discussed later, a substantially constant force during the stroking length could be realized. Thus, the roller-tape system exhibits a high degree of versatility in that the tape axis need not be co-linear with stroking direction.

Specific Applications

Let us now discuss some specific applications of the tape-roller system.

The writer is familiar with several applications in which the tape-roller system has been successfully used as an energy absorption device; however two stand out as prime examples of how such a device might be used.

Force limiting in belt systems has been accomplished by pulling a mild steel tape through a set of rollers as shown in Figure 1. Force limiting in impact sled decelerator design, has been accomplished in a similar method but with the tape draw axis at ninety degrees to the impact direction (Figure 2)..The equations that describe the tension in the metal tape are identical for the two cases; however the force required to produce tape drawing is different since the direction of force application is different. In the following we will discuss the general operation of the device in some detail. After this discussion it will be apparent as to how the designer would proceed in each of the two general cases cited above.

Let us examine the type of application shown in Figure 1 in some

BEST DOCUMENT AVAILABLE

detail.

The maximum force that can be developed from a given metal tape occurs when the tape is strained to its maximum amount without breaking. The most compact roller system that could attain this maximum strain is a single small roller. For mild steel, the ultimate strain is found to be approximately 30 percent. Experience has shown that a mild steel tape 0.045 inches thick will break or begin to break when passed over three rollers of 7/16-inch diameter. Applying the strain equation found in Figure 3, the strain works out to be .28 at the outer fibers. This agrees well with the expected ultimate strain of .30.

The tape tension force produced by a tape and roller mechanism has been shown theoretically to obey the following relationship:

(1) $$F = \frac{N W t^2 S_y}{D+t}$$

where roller friction and strain rate effects have been neglected (these effects will be discussed later), F is the force, N is the number of rollers, t is the tape thickness, D is the roller diameter, and S_y is the effective yield strength of the tape material. A derivation of this equation may be found in Appendix A. If a wire or rod is used instead of a tape the proper equation is found in Appendix B.

Static pull tests show this relationship to hold fairly well over a-wide range of the equation parameters, especially when the effect of strain hardening as the material passes over the rollers is taken into account. If strain hardening is a factor, Eqn. 1 should be modified accordingly by increasing the normal yield strength of the material by an amount dS_y given by the equation below,

(2) $$dS_y = \sum_{i=1}^{N} \frac{(130{,}500 - 381{,}000t)\ln(1+\frac{t}{D})\, i}{N}$$

BEST DOCUMENT AVAILABLE

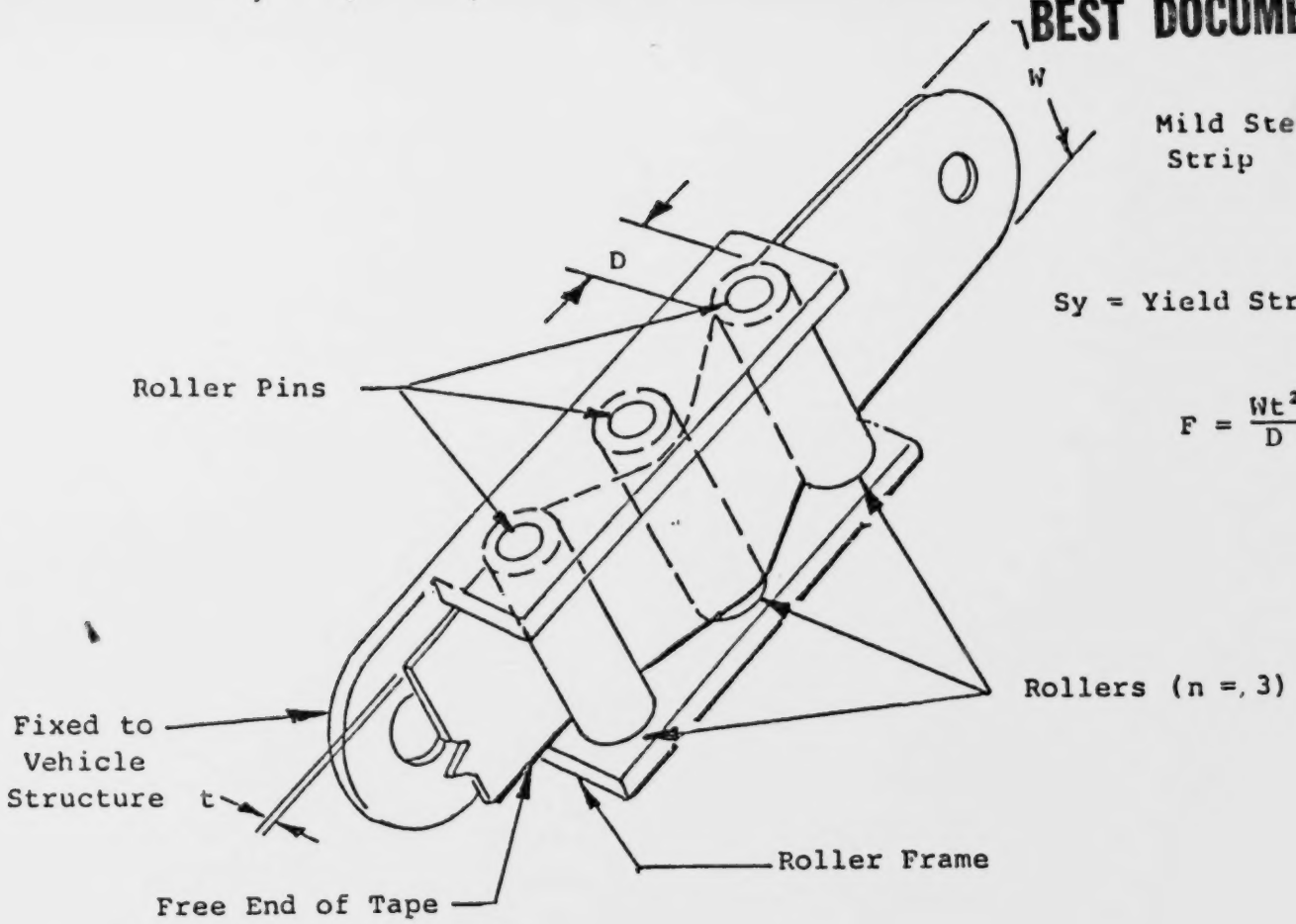

FIGURE 1 FORCE LIMITER

BEST DOCUMENT AVAILABLE

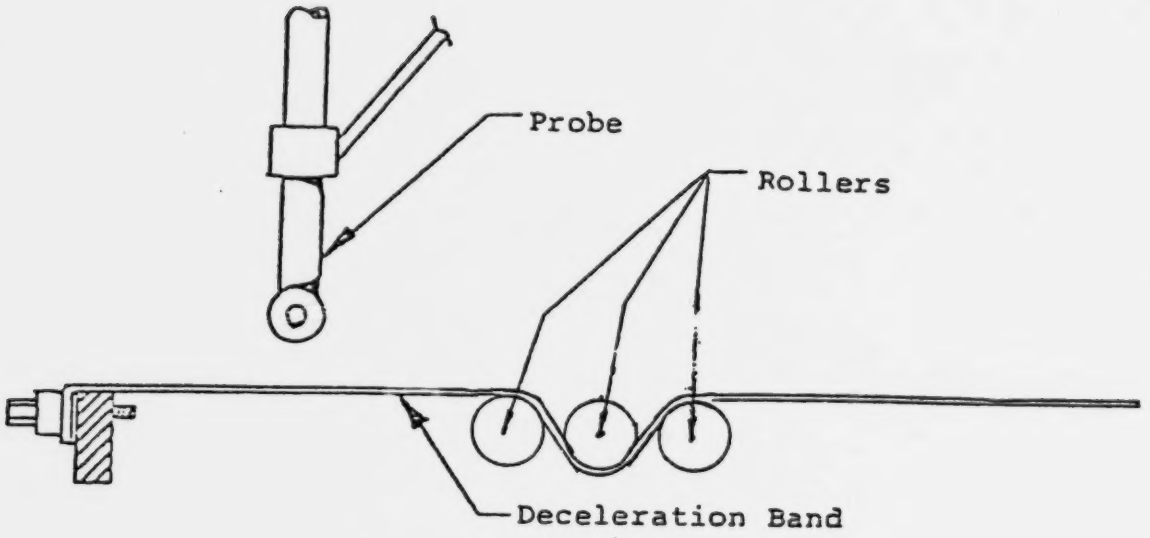

(a) Probe about to strike deceleration band.

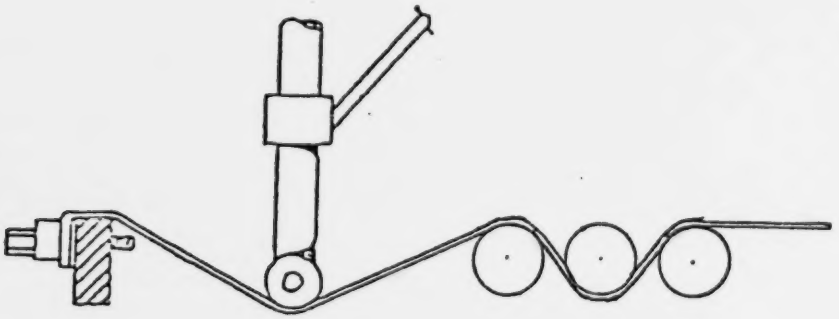

(b) Probe in contact with deceleration band.

Figure 2. Deceleration Mechanism Diagram.

BEST DOCUMENT AVAILABLE

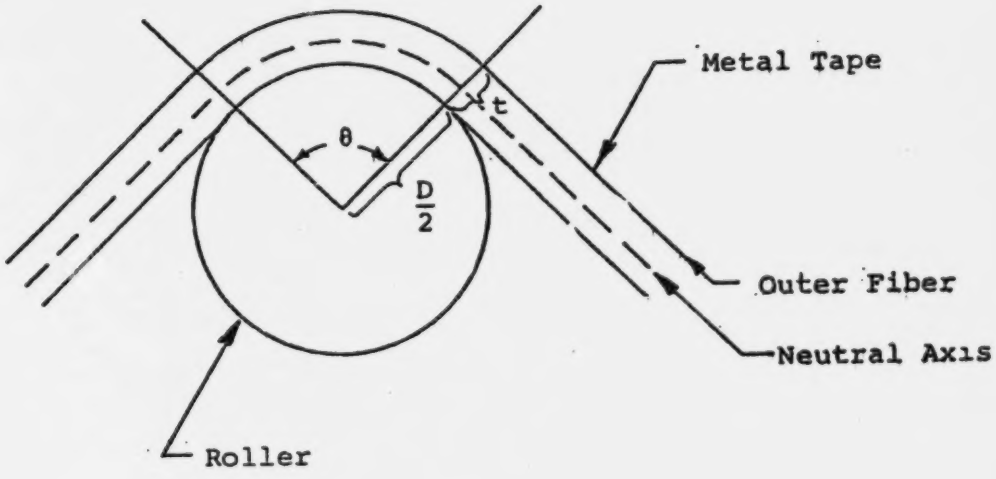

$$\text{Strain } (\varepsilon) = \frac{\text{length of outer fiber - length of neutral axis}}{\text{length of neutral axis}}$$

$$\varepsilon = \frac{\theta(\frac{D}{2} + t) - \theta(\frac{D+t}{2})}{\theta \frac{D+t}{2}}$$

$$\varepsilon = \frac{t}{D+t} \quad \text{for one roller}$$

$$\varepsilon = \frac{Nt}{D+t} \quad \text{where N is the number of rollers}$$

STRAIN EQUATION

Figure 3

BEST DOCUMENT AVAILABLE

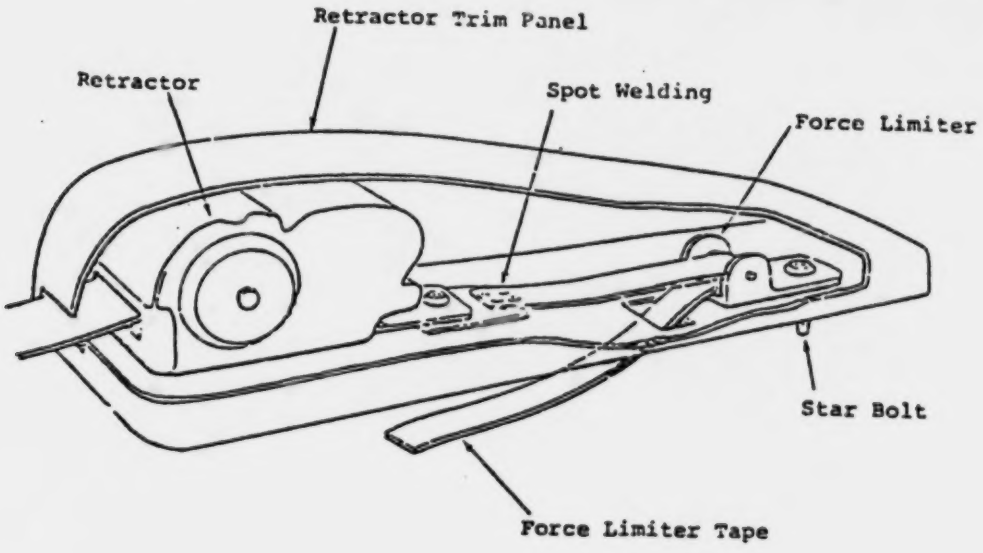

Figure 4. Torso Belt Force Limiter Assembly

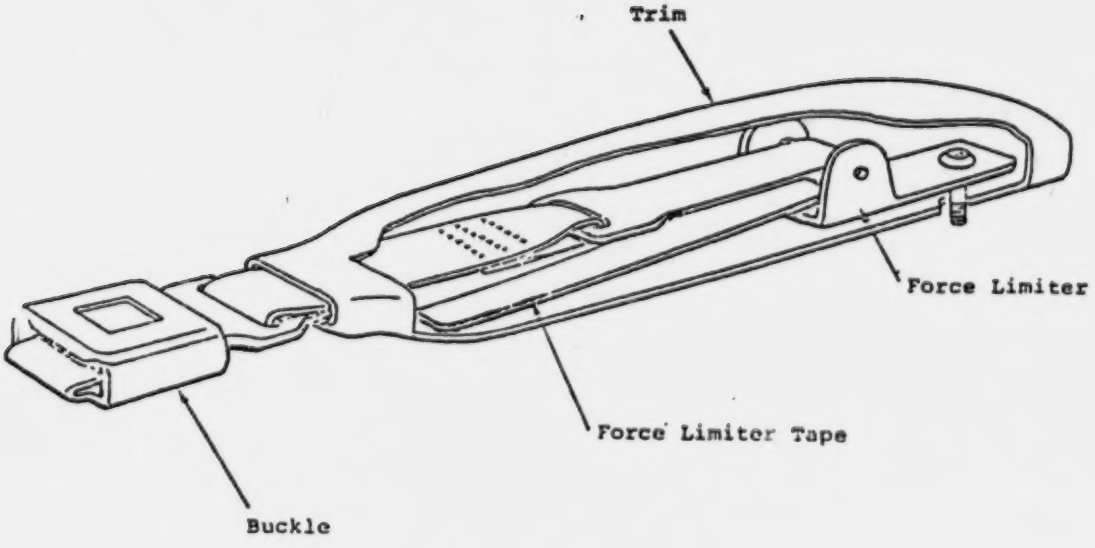

Figure 5. Lap Belt Force-Limiter Assembly

BEST DOCUMENT AVAILABLE

where t and D are in inches and dS_y in lbs/sq. in.. It should be noted that the equation is only valid up to a total stress, S_y plus dS_y = the ultimate strength of the material.

Friction can be assumed to be negligible in all true roller applications and, even when the roller is replaced with a non-rolling pin, the coefficient of friction is usually low varying from approximately 0.12 for completely unlubricated surfaces to 0.04 for lubricated surfaces (see Ref. 1, Appendix A).

Experience has shown that a good estimate on strain rate effects can be obtained by multiplying the basic equation by strain rate factor equal to:

(3) $$SRF = 1 + 0.08*\log(V)$$

where V is the strain velocity in in/min. Using all the relationships previously derived, we end up with a general equation for the force required to pull the tape through the rollers equal to:

(4) $$F = \frac{N\ W\ t^2\ (S_y + dS_y)(SRF)}{D + t}$$

where all the values have been defined above.

This discussion completes a general description of how the tape-roller force limiter functions. With a little imagination the designer should be able to visualize many more applications. Figures 4 through 6 show a few more variations for belt restraint system applications.

BEST DOCUMENT AVAILABLE

FORCE LIMITER

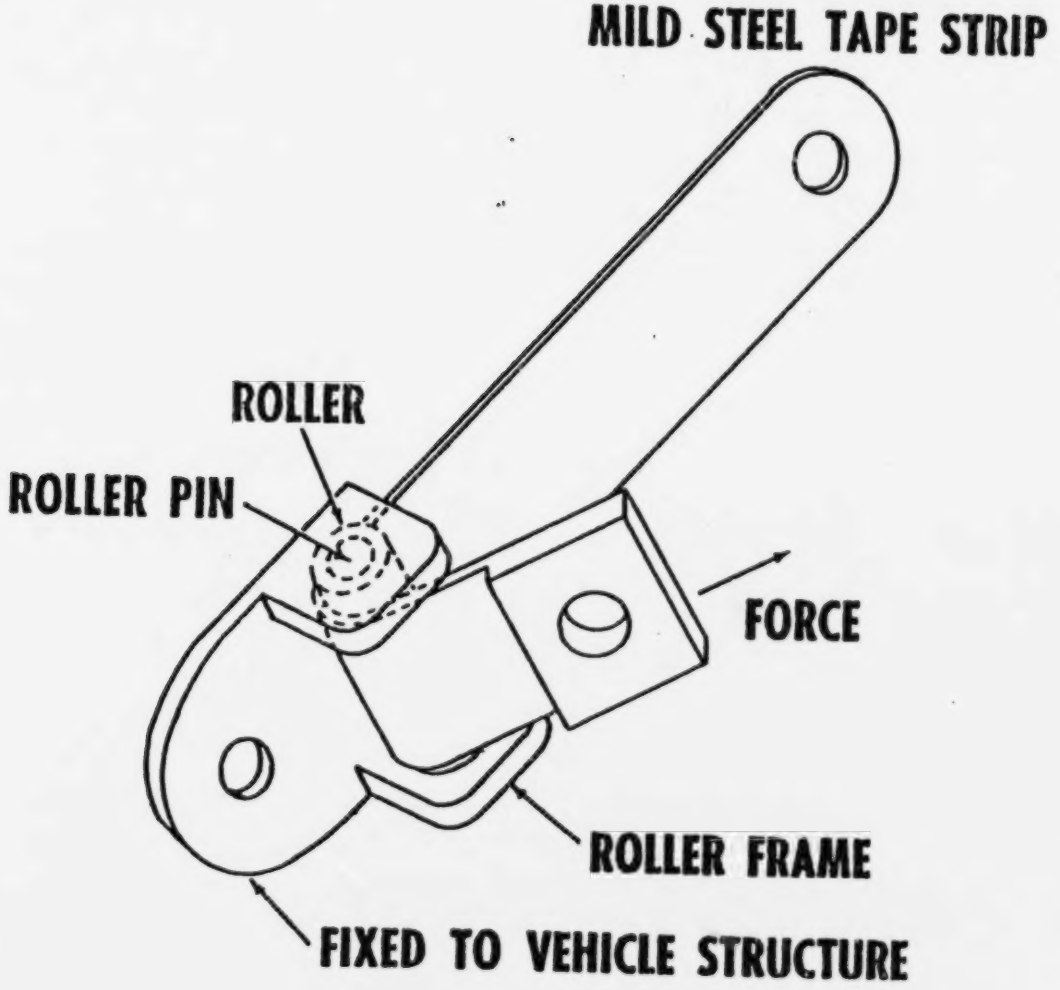

Figure 6. Single Roller System

BEST DOCUMENT AVAILABLE

ATTACHMENT A

Force Limited Tape/Roller Analysis

Prepared by: Michael Fitzpatrick

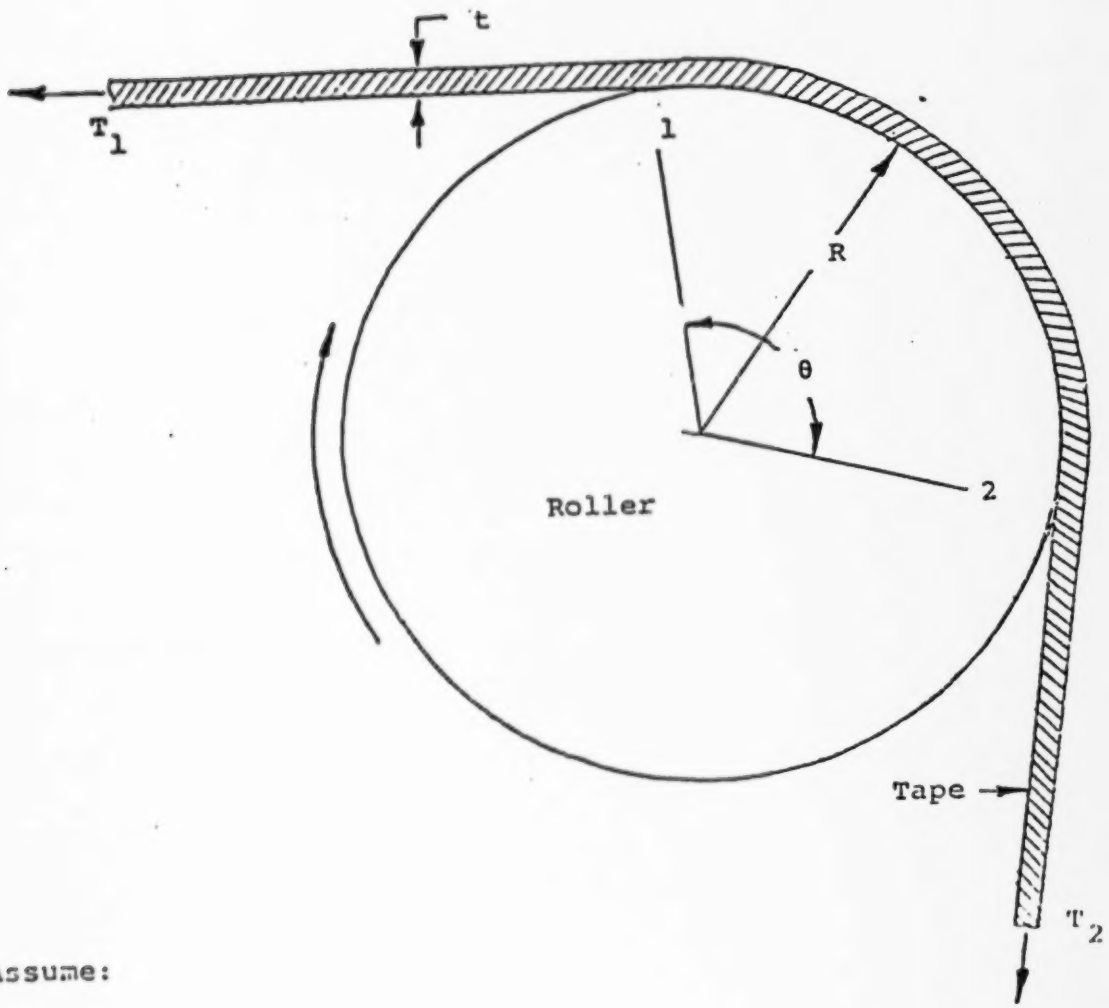

Assume:

1. No friction between tape and roller
2. Neutral axis of tape at t/2
3. Strain energy absorbed in exceeding elastic limit of material is negligible when compared to energy absorbed during plastic deformation.

[redacted]

[redacted]

BEST DOCUMENT AVAILABLE

4. Strain energy due to axial stretching of tape negligible when compared to strain energy of bending.

5. Roller radius <the radius of curvature of tape at the elastic limit.

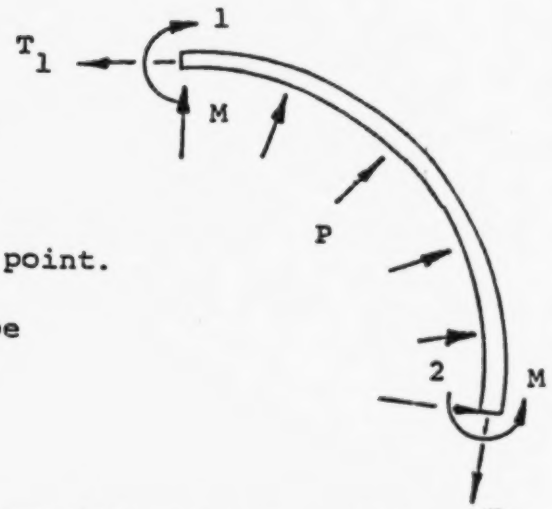

As the tape approaches the roller it is subjected to a constantly increasing bending moment, until at some point the stress in the outermost fiber reaches its yield point.

The radius of curvature of the tape at the elastic limit is:

$$R = \frac{EI}{Mo}$$

Since tension is also present, we may determine the radius of curvature when the outer fiber at 1 begins to yield in the following manner.

$$T_{y.p.} = \frac{M_o C}{I} + \frac{T_1}{A}$$

$$M_o = \frac{I}{C}\left[T_{y.p.} - \frac{T_1}{A}\right] \qquad \text{so that}$$

(1) $$R_{y.p.} = \frac{EC}{T_{y.p.} - \frac{T_1}{A}}$$

At a radius of curvature somewhat less than this (approximately 2/3 $R_{y.p.}$ for a rectangular tape), the tape will become fully plastic.

Assuming the roller diameter is much less than this (assumption 5) the tape will be fully plastic when it conforms to the roller at Point 1.

BEST DOCUMENT AVAILABLE

Between Points 1 and 2, the strain in the tape is constant since the radius of curvature and stress condition is constant. After leaving Point 2,however, the tape must straighten so that more strain energy is absorbed by the tape. In the absence of strain hardening effects and for tape tensile stresses small compared with bending stresses this energy will be the same as that at Point 1.

Equating the work done in pulling the tape over the roller to the strain energy stored in the tape, we have:

$$(T_2 - T_1)R\phi = 2M_p\phi \quad \text{or}$$

(2) $$T_2 - T_1 = \frac{2M_p}{R}$$ (The factor "2" comes from energy being absorbed at two places on the roller.)

For a fully plastic section and the initial assumptions:

$$M_p = 2\int_o^{t/2} WT_y y\,dy$$

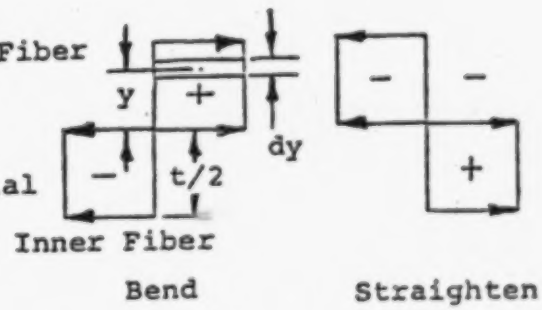

Where: W = tape width
T_y = yield stress of material
y^y = distance to centroid of dy
dy= thickness of element

(3) $$M_p = 2WT_y \left[\frac{y^2}{2}\right]_o^{t/2} = \frac{WT_y t^2}{4}$$

Substituting (2) into (3)

(4) $$T_2 - T_1 = \frac{T_y W t^2}{2R}$$

BEST DOCUMENT AVAILABLE

This equation was modified to include the effects of strain hardening and, assuming a mild steel tape, would be:

$$(5) \quad T = \frac{N W t^2}{D+t} \left[Ty + \Delta Ty\right] \qquad \text{where:}$$

$$\Delta Ty = \sum_{i=1}^{N} \frac{(130{,}500 - 381{,}000t) \ln(1+\frac{t}{D}) i}{N}$$

The denominator in the multiplicative term in Equation 2 has been changed from 2R to D + t to increase the effective bend radius to the neutral axis of the tape.

To determine the validity of the derived equations, a series of static pull tests were conducted in which the parameters in the equation were varied one at a time to determine their individual effect on the drawing force required to move the tape over the rollers.

The actual force required to pull the metal tape over the rollers was compared to the force calculated with Equation 5 for each test so that a percent difference between calculated and actual values was obtained.

Calculating an overall average percent difference for all the tests showed this average percent difference to be -5%; i.e., the calculated force was on the average 5% lower than the test force.

Therefore, it was concluded that the relationship previously derived was qualitatively correct and should be multiplied by a factor of 1.05 to be as quantitatively accurate as possible.

BEST DOCUMENT AVAILABLE

LIST OF REFERENCES

1. Swift, H.W., "Plastic Bending Under Tension", paper presented at the Seventh International Congress for Applied Mechanics, London, September 5-11, 1948.

2. Hayden, H.W., "The Structure and Properties of Materials", Volume III "Mechanical Behavior", John Wiley and Sons, Inc., New York. 1965.

3. Fitzpatrick, M.V., "Approximate Analysis of Plastic Deformation of Tape-Draw Mechanism", unpublished analysis for Minicars, Inc. 1972.

BEST DOCUMENT AVAILABLE

Fitzpatrick Engineering	CALCULATION SHEET	Page ____ Of ___

Project	Job Order No	Calculation Serial No

ATTACHMENT B

Derivation of Equation For the Force Required to Pull a Wire or Rod over a Roller

Prepared By		Date
Checked By		Date

BEST DOCUMENT AVAILABLE

Fitzpatrick Engineering	CALCULATION SHEET	PAGE 1 OF
PROJECT	JOB ORDER NO	CALCULATION SERIAL N

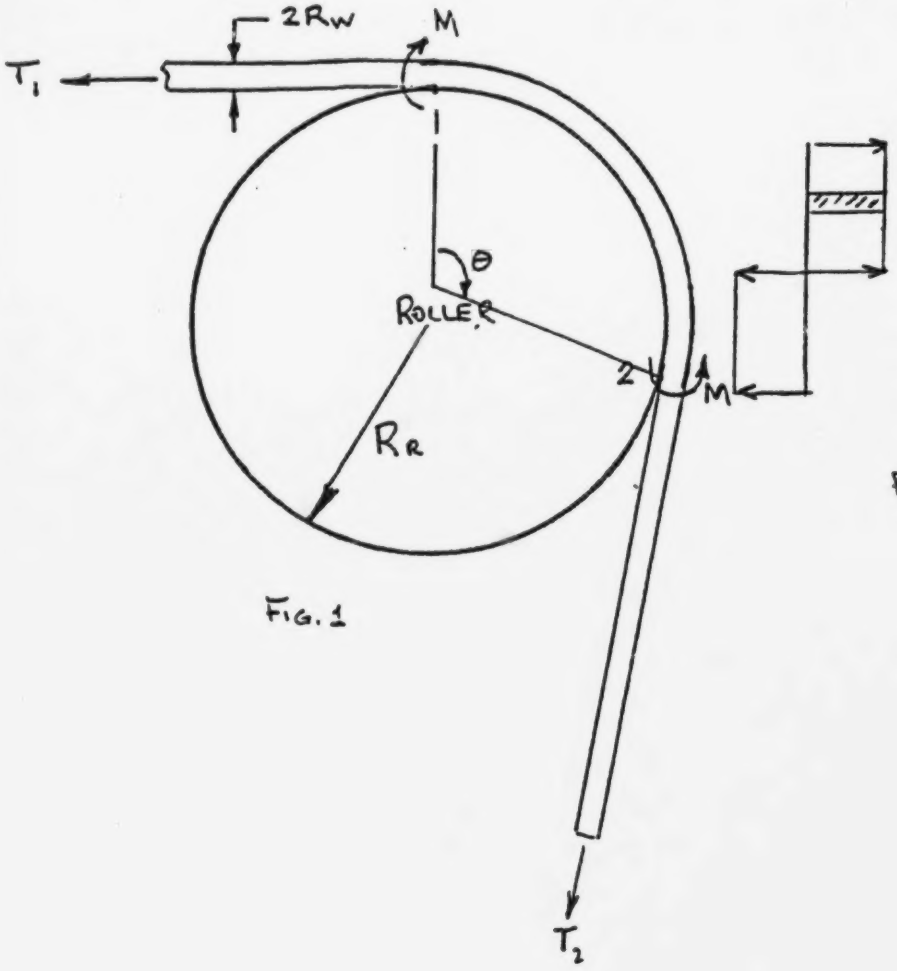

FIG. 1

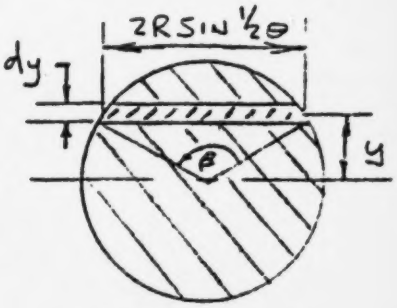

WIRE OR ROD
CROSS-SECTION

FIG. 2

AS THE WIRE APPROACHES THE ROLLER IT IS SUBJECTED TO A CONSTANTLY INCREASING BENDING MOMENT UNTIL AT SOME POINT THE STRESS IN THE OUTERMOST FIBERS REACHES THE YIELD POINT. THE RADIUS OF CURVATURE OF THE WIRE AT THIS POINT IS:

$$R = \frac{EI}{M_o}$$

PREPARED BY MICHAEL FITZPATRICK	DATE 11/1/19
CHECKED BY	DATE

SINCE TENSION IS ALSO PRESENT WE MAY DETERMINE THE RADIUS OF CURVATURE WHEN OUTER FIBER AT PT. 1 BEGINS TO YIELD IN THE FOLLOWING MANNER:

$$\sigma_{y.p.} = \frac{M_o R_w}{I} + \frac{T_1}{A_w} \quad \text{OR,}$$

$$M_o = I/c \left[\sigma_{y.p.} - T_1/A\right] \text{ SO THAT,}$$

(1) $$R_{y.p.} = \frac{E R_w}{\sigma_{y.p.} - \frac{T_1}{A_w}}$$

AT A RADIUS OF CURVATURE SOMEWHAT LESS THAN THIS, APPROX-IMATELY 0.6 $R_{y.p.}$ FOR A WIRE OR ROD, THE WIRE WILL BE-COME FULLY PLASTIC. THUS TO DETERMINE THE UPPER LIMIT OF THE ROLLER DIA FOR WHICH THE ENERGY ABSORBER WILL OPERATE ACCORDING TO THE EQN. THAT IS DERIVED IN THE FOLLOWING WE MAY WRITE:

(2) $$R_{ROLLER} < \frac{0.6\, E R_w}{\sigma_{y.p.} - \frac{T_1}{A_w}}$$

NOW LET US DERIVE THE BASIC EQN. THAT DESCRIBES THE WIRE-ROLLER SYSTEM.

BETWEEN POINTS 1 & 2 THE STRAIN IN THE TAPE IS CONSTANT SINCE THE RADIUS OF CURVATURE IS CONSTANT AT THE ROLLER RADIUS. HOWEVER AT BOTH PTS, 1 & 2, THE WORK IS DONE ON THE WIRE AS

BEST DOCUMENT AVAILABLE

THE WIRE FIRST CONFORMS TO THE ROLLER AND THEN AGAIN AS IT LEAVES THE ROLLER.

EQUATING THE WORK DONE IN PULLING THE WIRE OVER THE ROLLER TO THE STRAIN ENERGY STORED IN THE WIRE WE HAVE:

$$(T_2 - T_1) R_R \theta = 2 M_p \theta$$

WHERE M_p IS THE MOMENT IN THE WIRE FOR A FULLY PLASTIC CONDITION.

FOR A FULLY PLASTIC SECTION (SEE FIG. 2) WE HAVE

$$M_p = 2 \tau_{y.p.} \int_0^{R_w} y \, dA \quad \text{WHERE}$$

$$dA = 2 R_w \sin \tfrac{1}{2}\beta \, dy$$

WE MAY REWRITE $\tfrac{1}{2}\beta$ AS $\cos^{-1} y/R$ OR $\sin^{-1} \dfrac{\sqrt{R_w^2 - y^2}}{R_w}$

$\therefore$,

$$dA = 2\sqrt{R_w^2 - y^2}\, dy \quad \text{SO THAT,}$$

$$M_p = 4 \tau_{y.p.} \int_0^{R_w} y \sqrt{R_w^2 - y^2}\, dy = 4 \tau_{y.p.} \left[-\tfrac{1}{3} (R_w^2 - y^2)^{3/2} \right]_0^R$$

$$M_p = \frac{4 \tau_{y.p.} R_w^3}{3}$$

$\therefore$,

$$(:) \quad T_2 - T_1 = \frac{8 \tau_{y.p.} R_w^3}{3 R_R}$$ WHICH IS THE BASIC EQN (NEGLECTING STRAIN HARDENING) FOR A ONE-ROLLER SYSTEM.

BEST DOCUMENT AVAILABLE

APPENDIX D

Occupant/Door Comparisons from Budd No. 11 Simulation

BEST DOCUMENT AVAILABLE

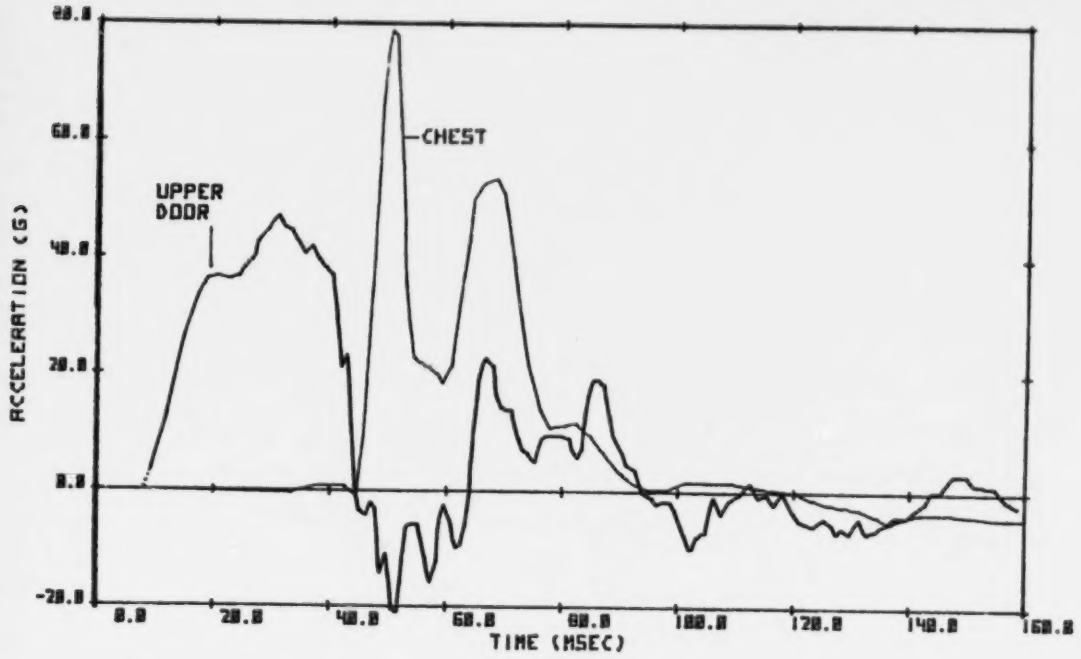

SRL 17-5 TEST #1-VEHICLE/OCCUPANT-CHEST ACC.

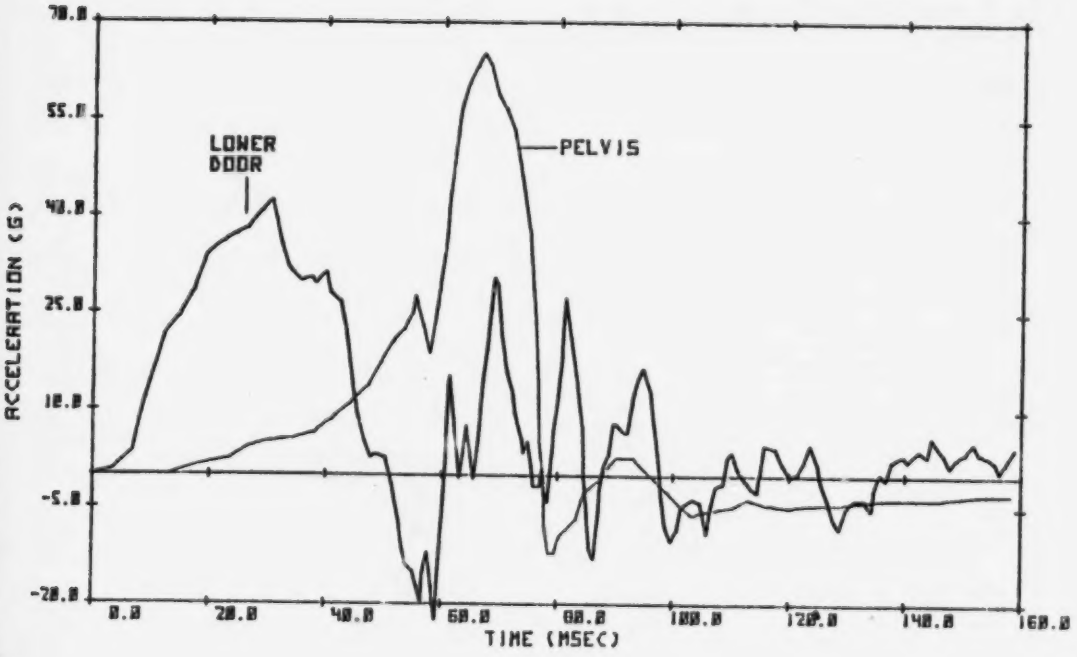

SRL 17-5 TEST #1-VEHICLE/OCCUPANT-PELVIS ACC

BEST DOCUMENT AVAILABLE

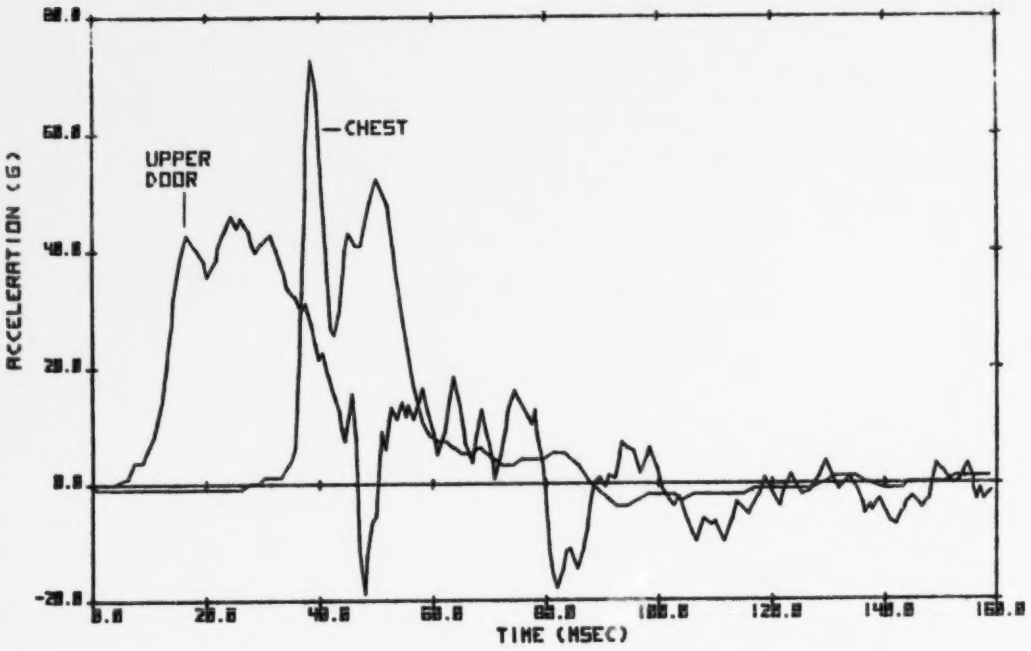

SRL 17-5 TEST #2 -VEHICLE/OCCUPANT-CHEST ACC.

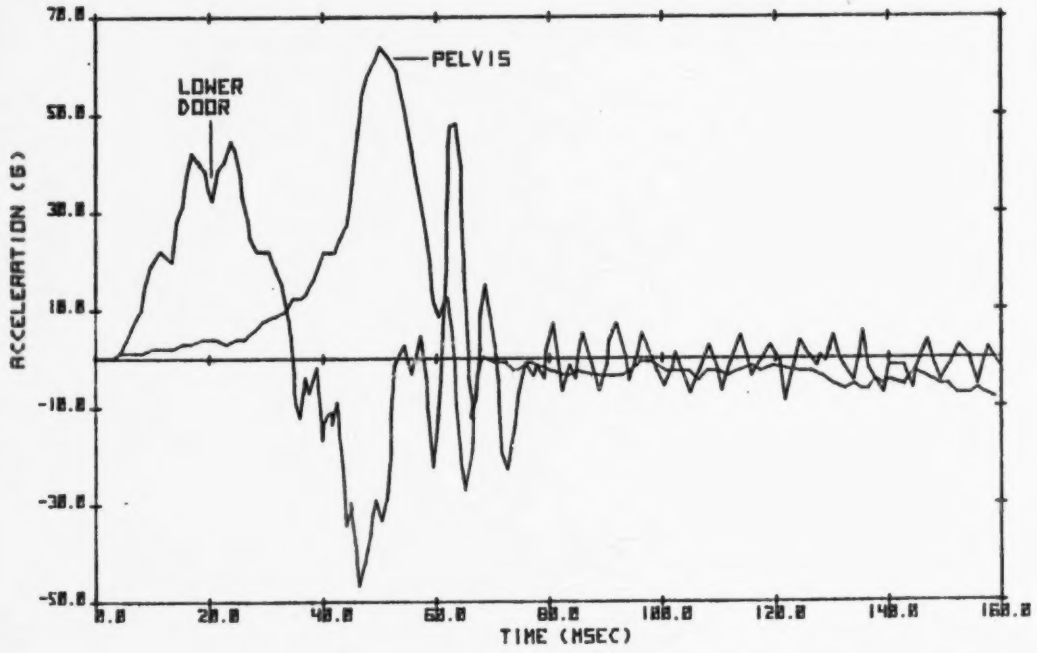

SRL 17-5 TEST #2 - VEHICLE/OCCUPANT-PELVIS ACC.

BEST DOCUMENT AVAILABLE

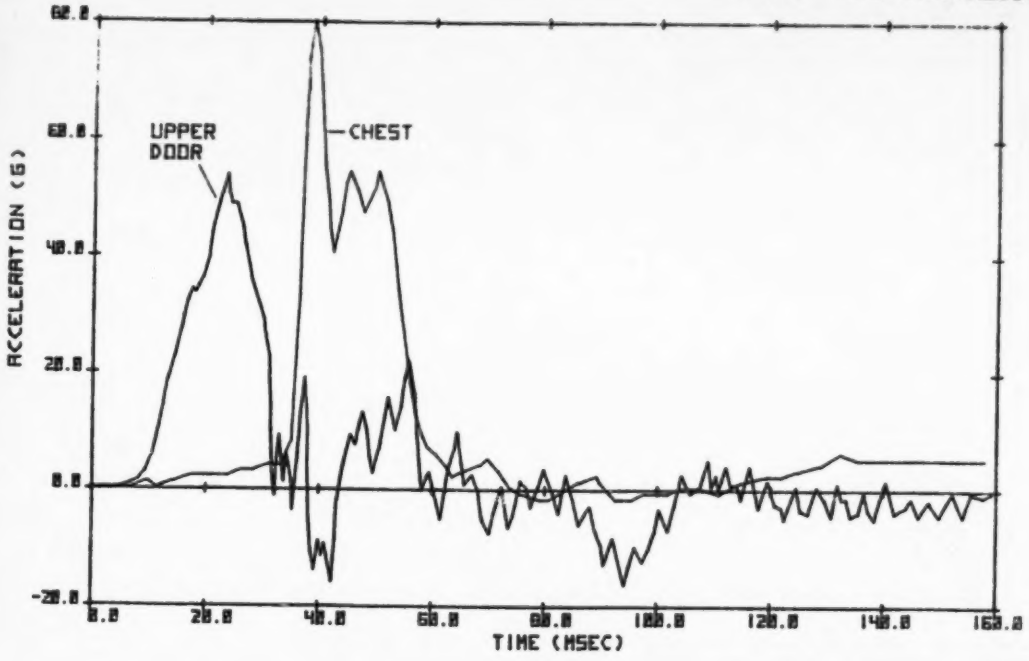

SRL 17-5 TEST #3 - VEHICLE/OCCUPANT-CHEST ACC.

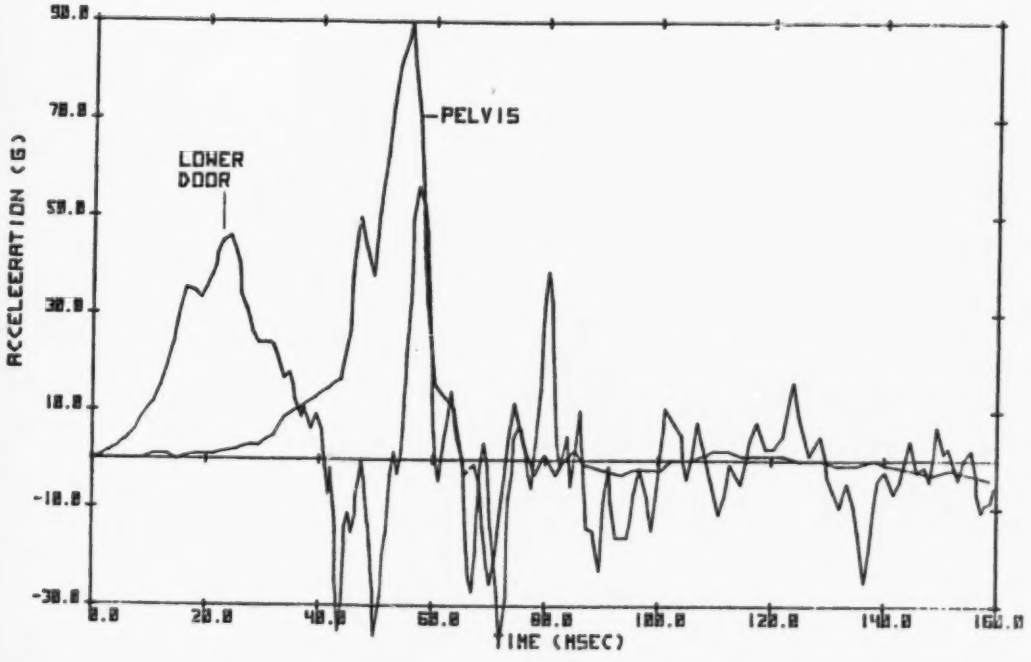

SRL 17-5 TEST #3 - VEHICLE/OCCUPANT-PELVIS ACC.

BEST DOCUMENT AVAILABLE

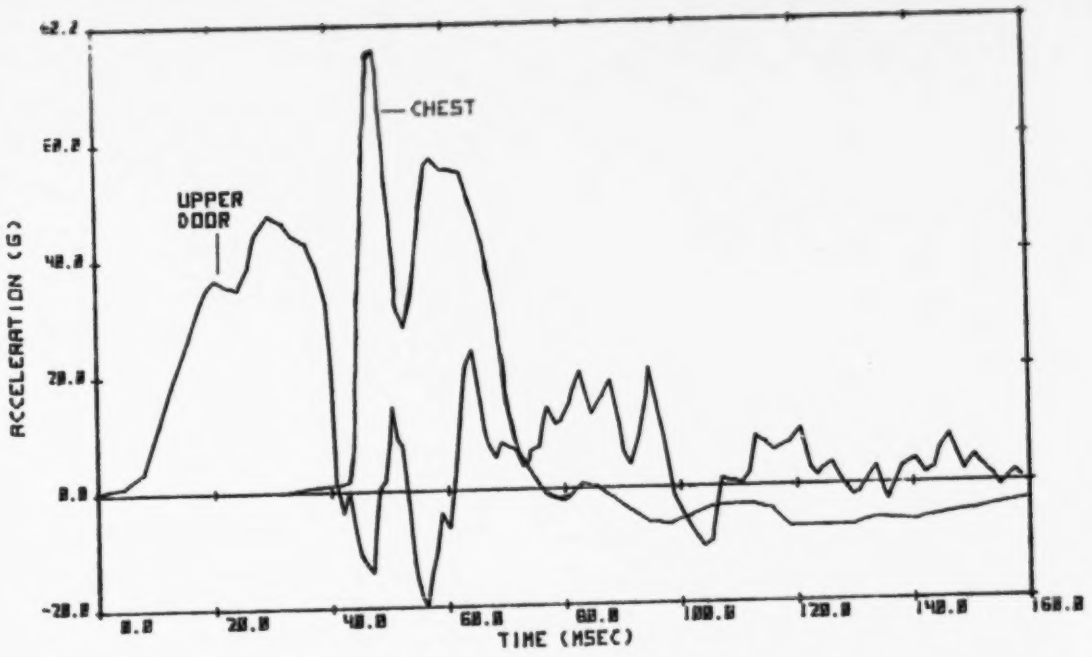

SRL 17-5 TEST #4-VEHICLE/OCCUPANT-CHEST ACC.

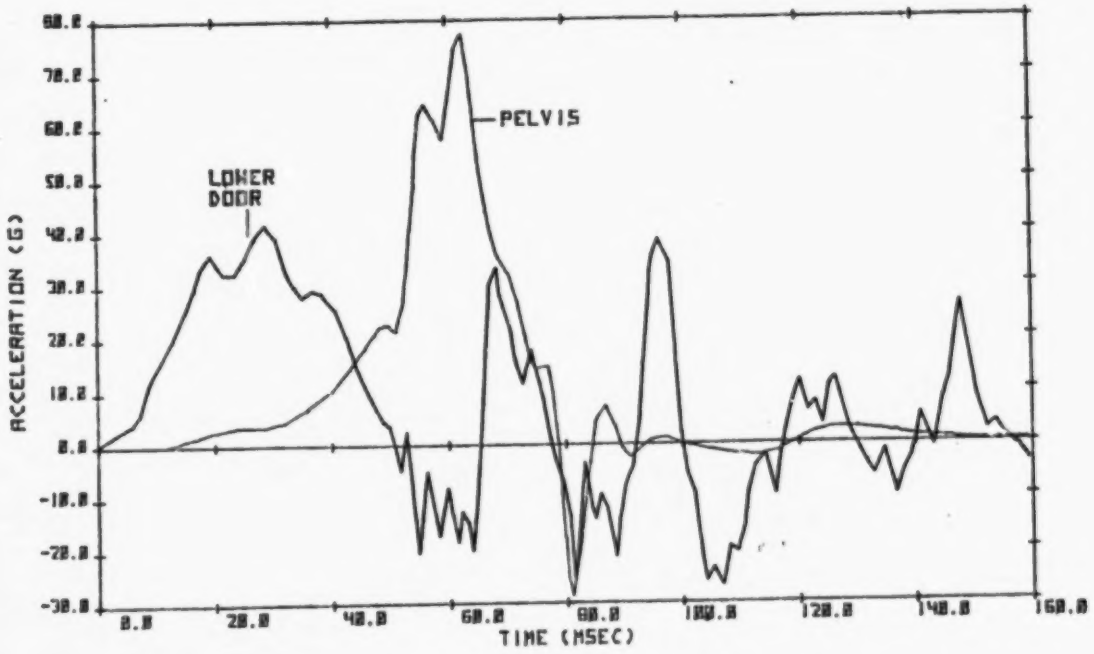

SRL 17-5 TEST #4-VEHICLE/OCCUPANT-PELVIS ACC

BEST DOCUMENT AVAILABLE

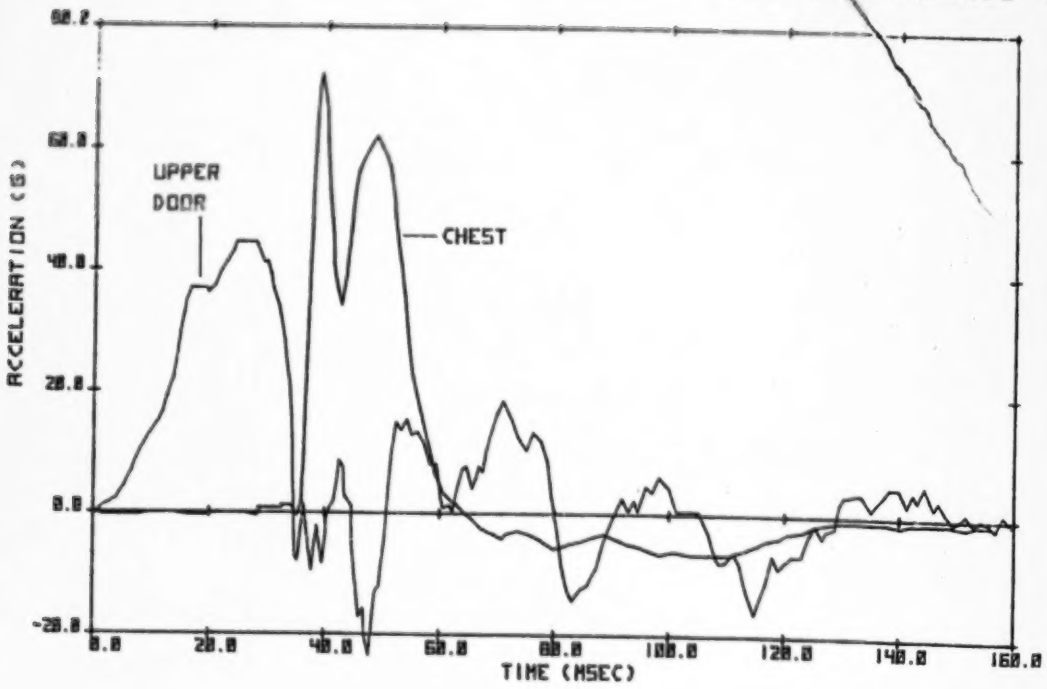

SRL 17-5 TEST #5 - VEHICLE/OCCUPANT-CHEST ACC.

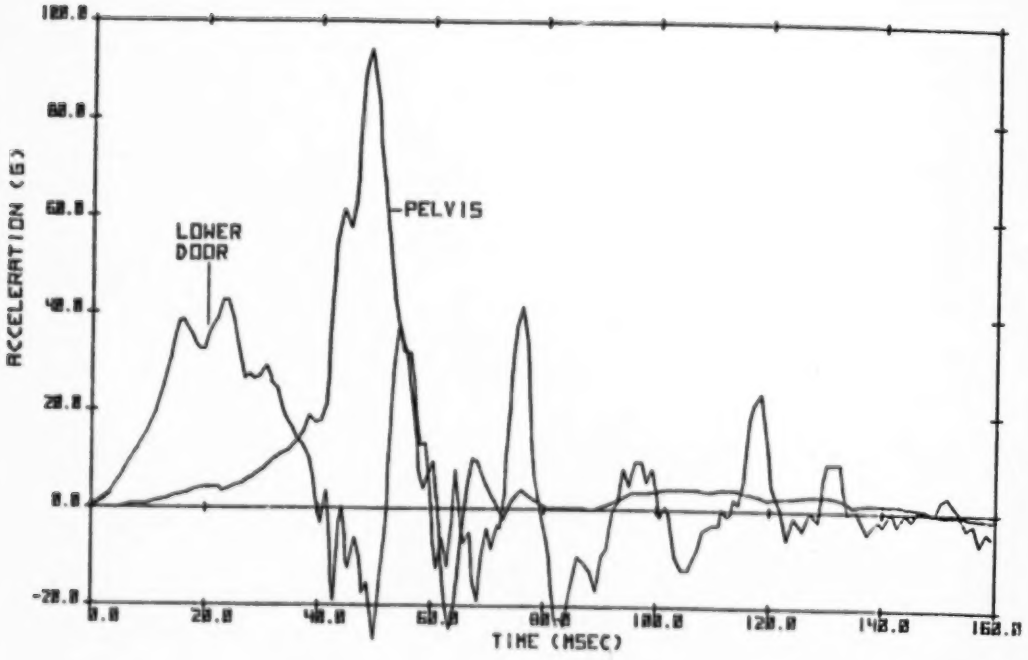

SRL 17-5 TEST #5 - VEHICLE/OCCUPANT-PELVIS ACC.

BEST DOCUMENT AVAILABLE

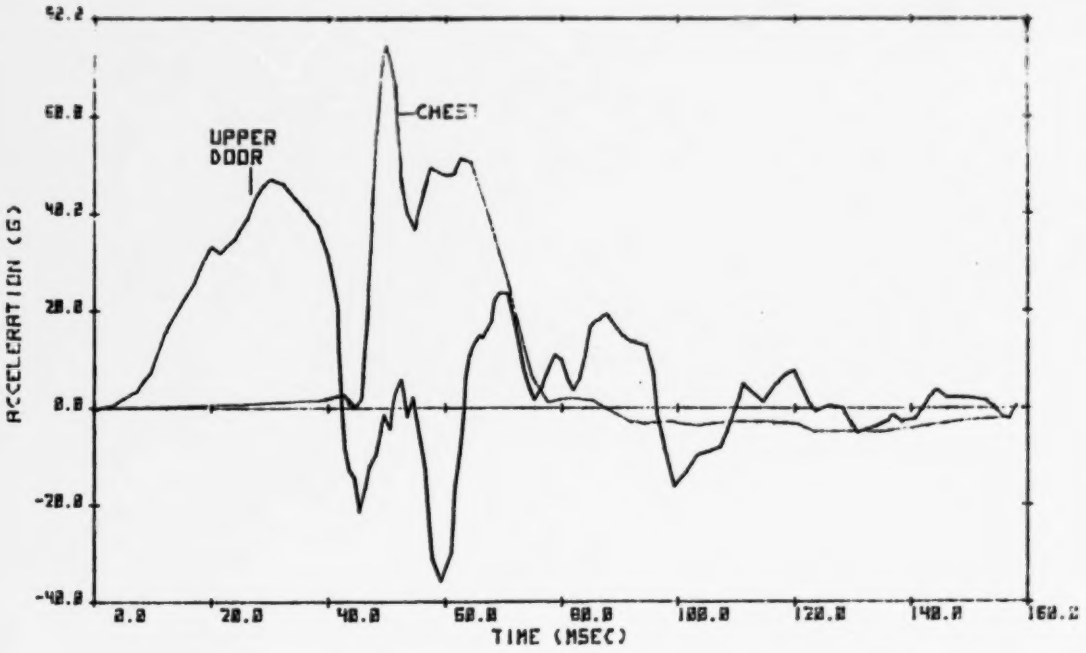

SRL 17-5 TEST #6-VEHICLE/OCCUPANT-CHEST ACC.

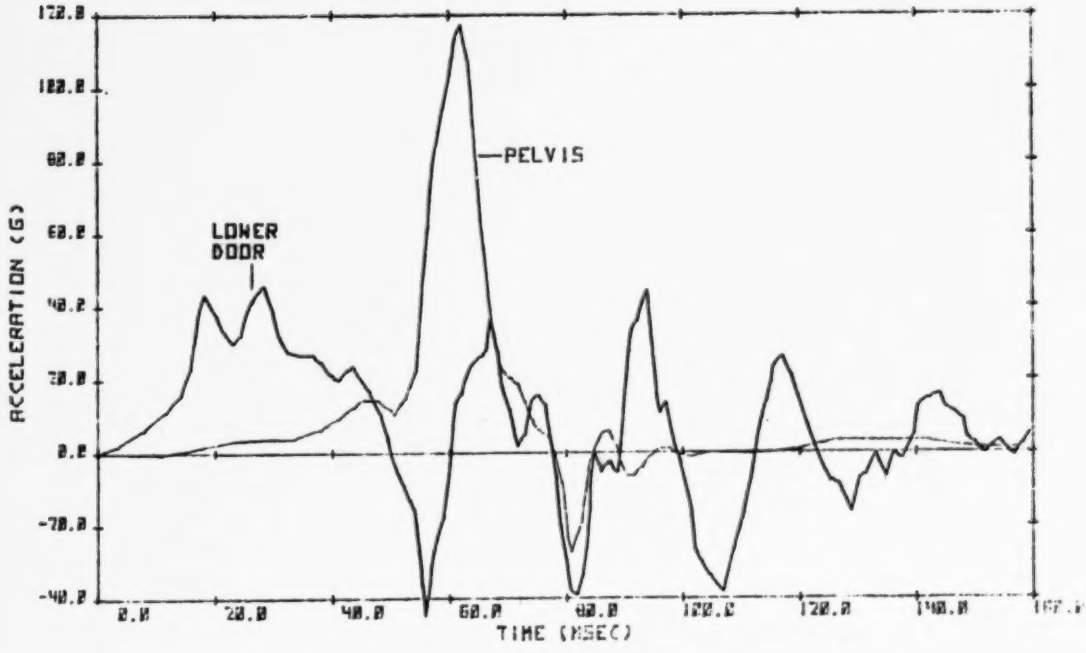

SRL 17-5 TEST #6-VEHICLE/OCCUPANT-PELVIS ACC

BEST DOCUMENT AVAILABLE

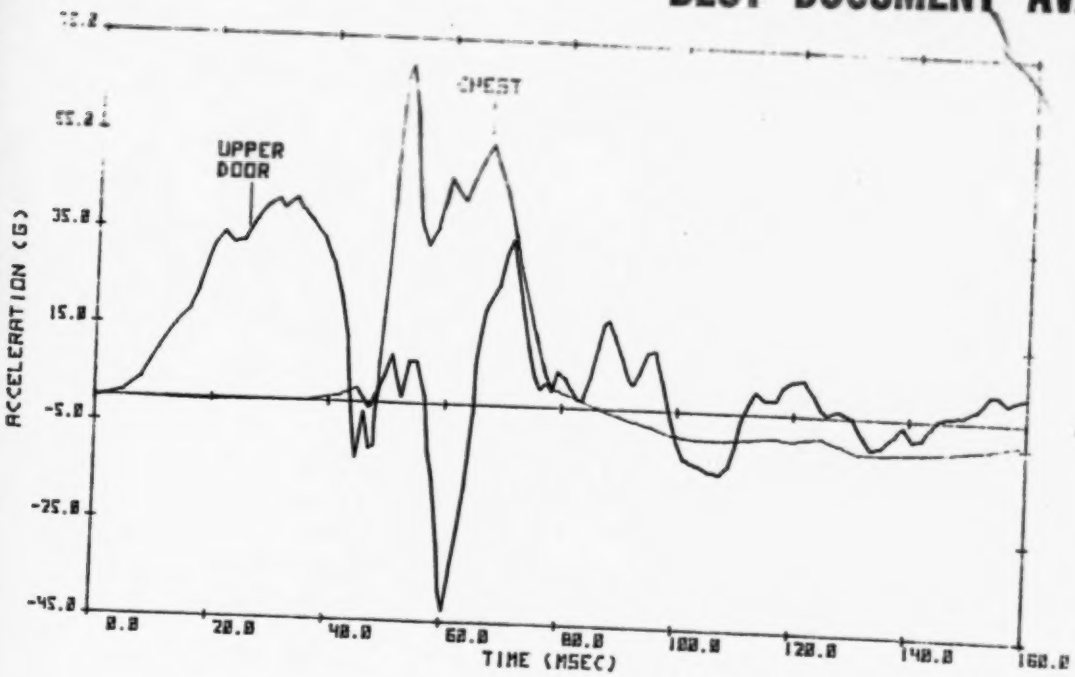

SRL 17-S TEST #7-VEHICLE/OCCUPANT-CHEST ACC.

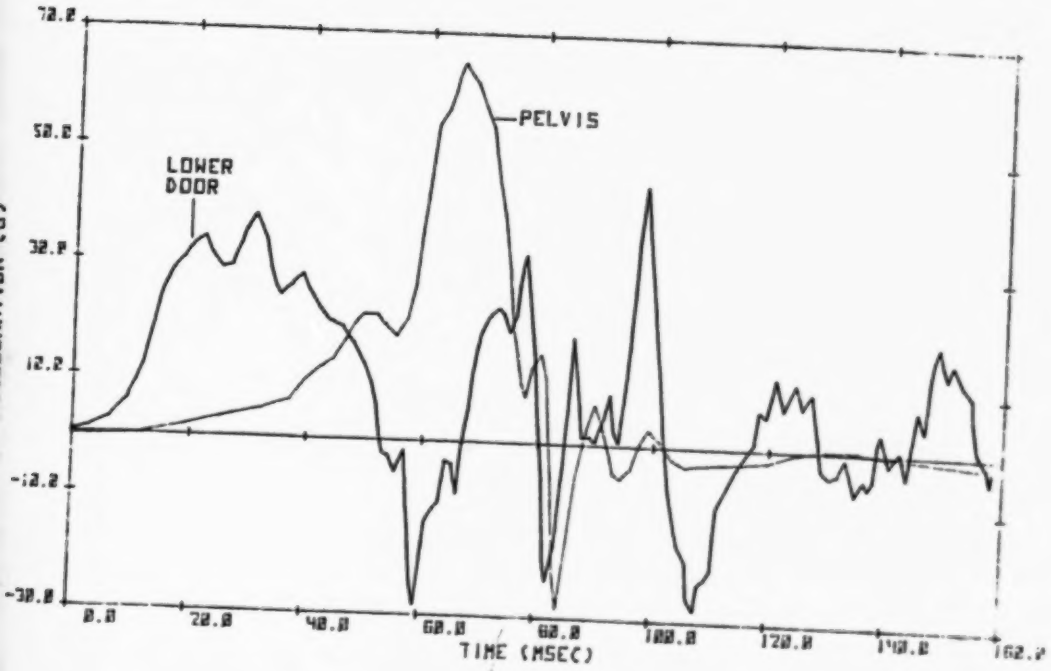

SRL 17-S TEST #7-VEHICLE/OCCUPANT-PELVIS ACC

BEST DOCUMENT AVAILABLE

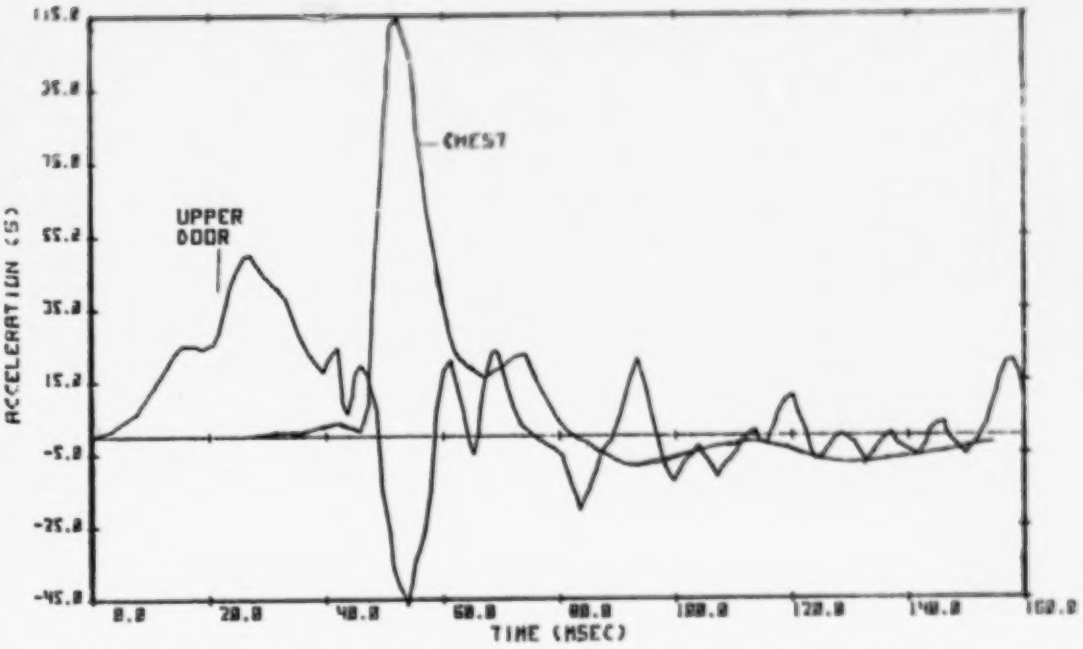

SRL 17-5 TEST #8-VEHICLE/OCCUPANT-CHEST ACC.

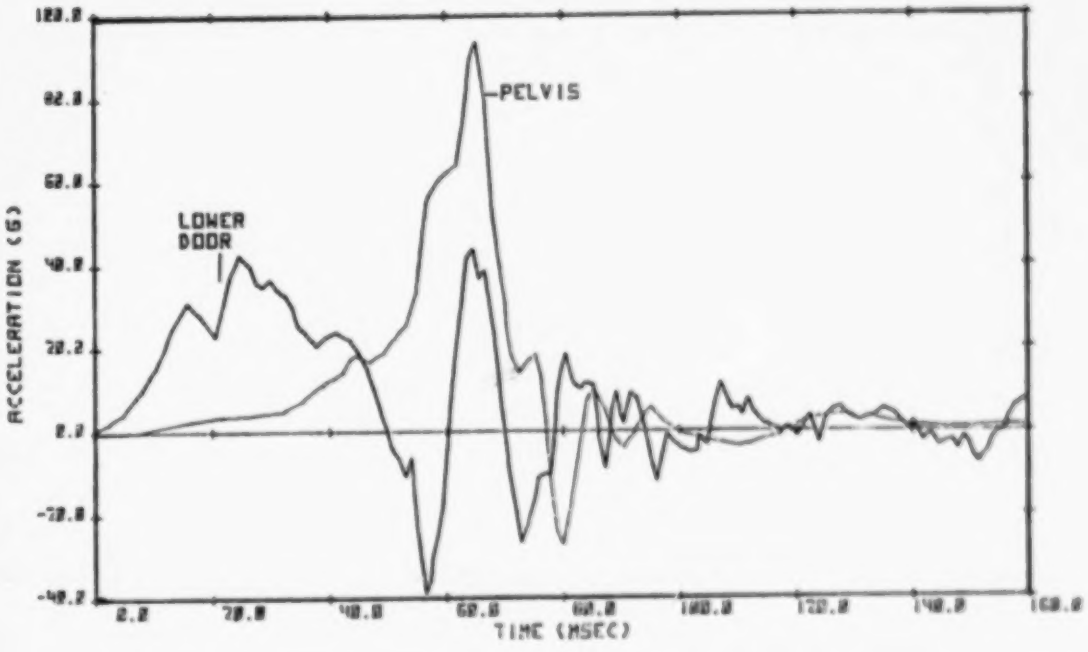

SRL 17-5 TEST #8-VEHICLE/OCCUPANT-PELVIS ACC

BEST DOCUMENT AVAILABLE

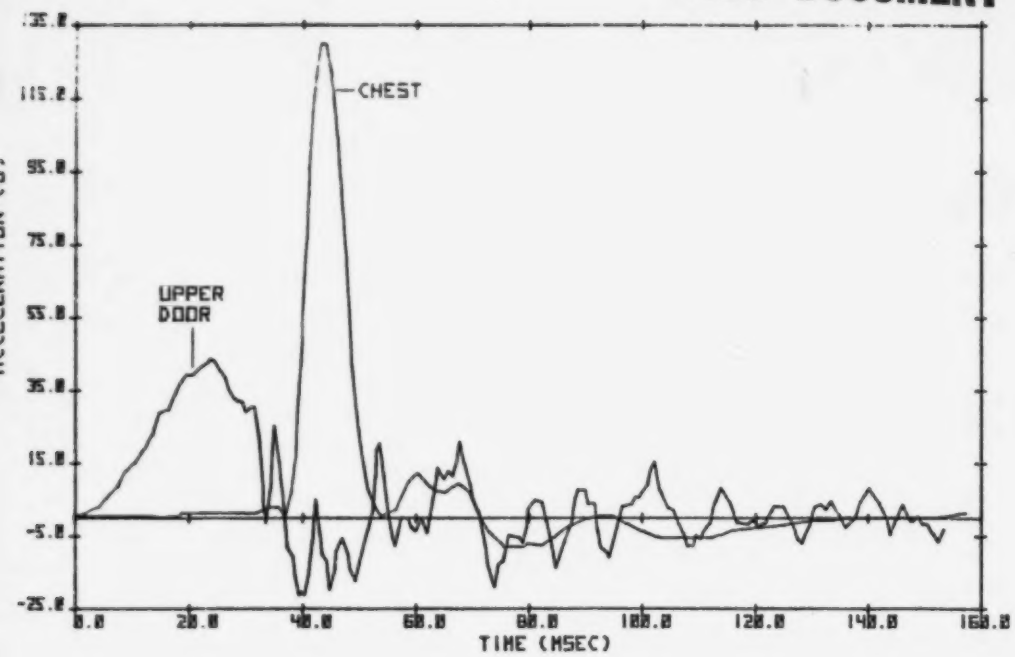

SRL 17-5 TEST #9 - VEHICLE/OCCUPANT-CHEST ACC.

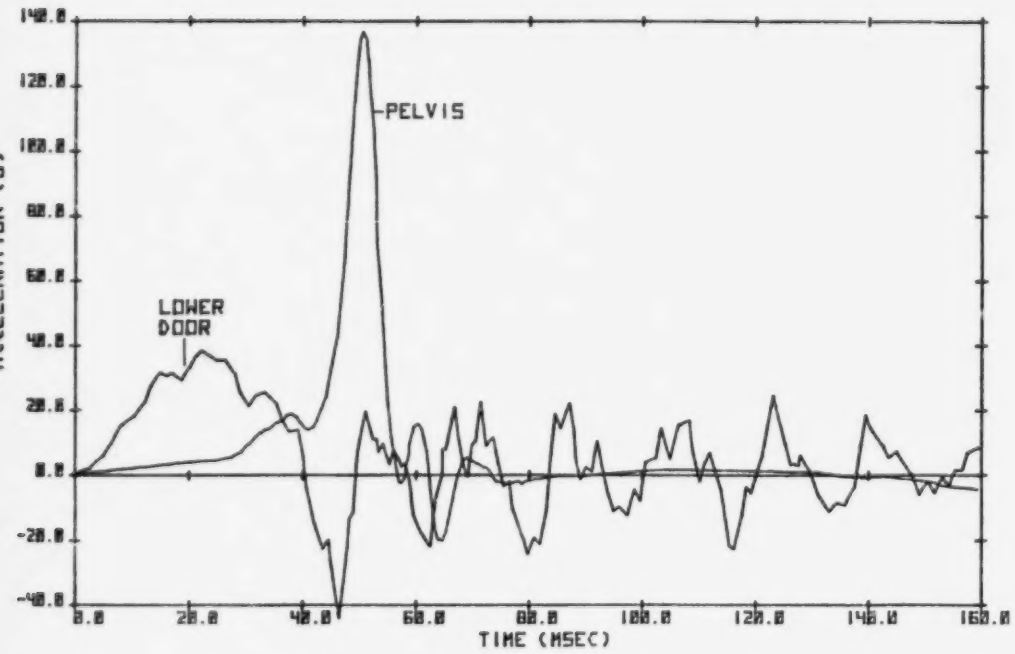

SRL 17-5 TEST #9 - VEHICLE/OCCUPANT-PELVIS ACC.

BEST DOCUMENT AVAILABLE

APPENDIX E

Body Form Responses from Dynamic Science Test No. 8330-2 Simulation

BEST DOCUMENT AVAILABLE

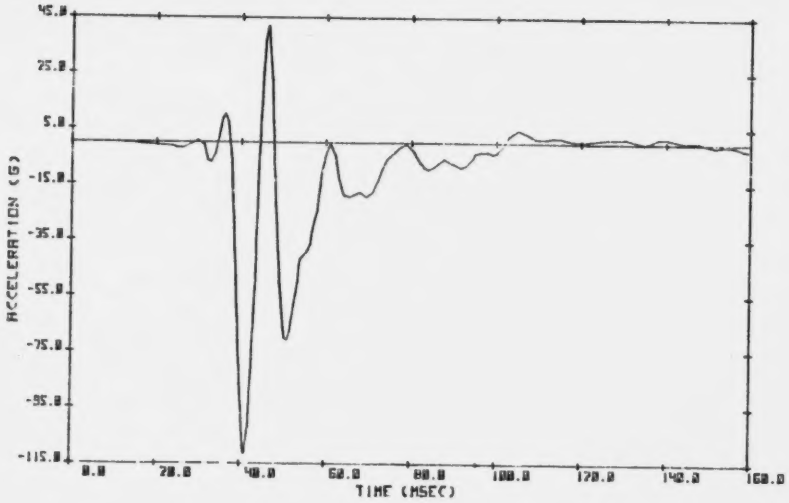

SRL 17-5 TEST #10 - LEFT UPPER RIB

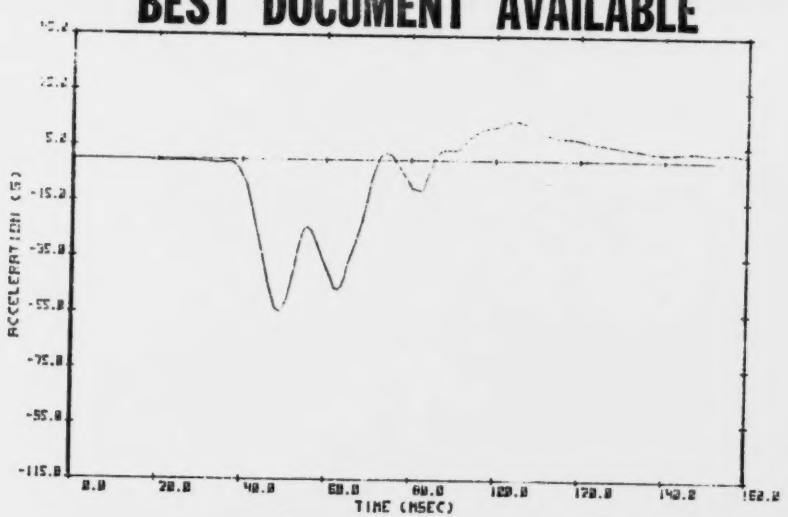

SRL 17-5 TEST #10 - RIGHT UPPER RIB

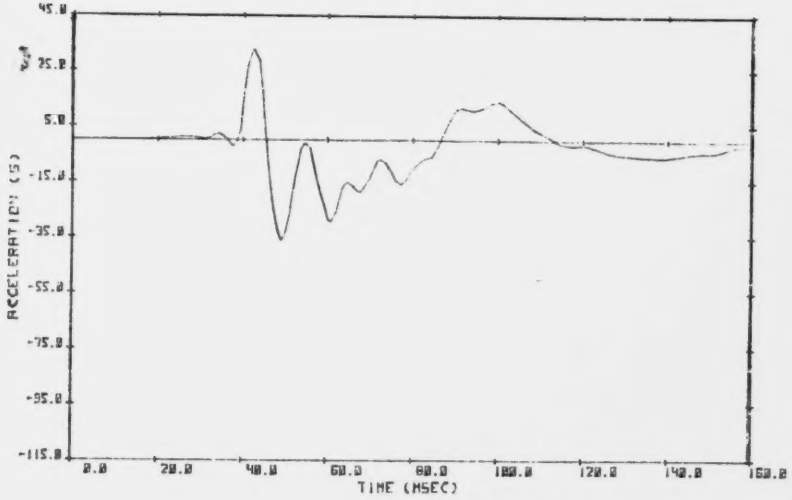

SRL 17-5 TEST #10 - UPPER STERNUM

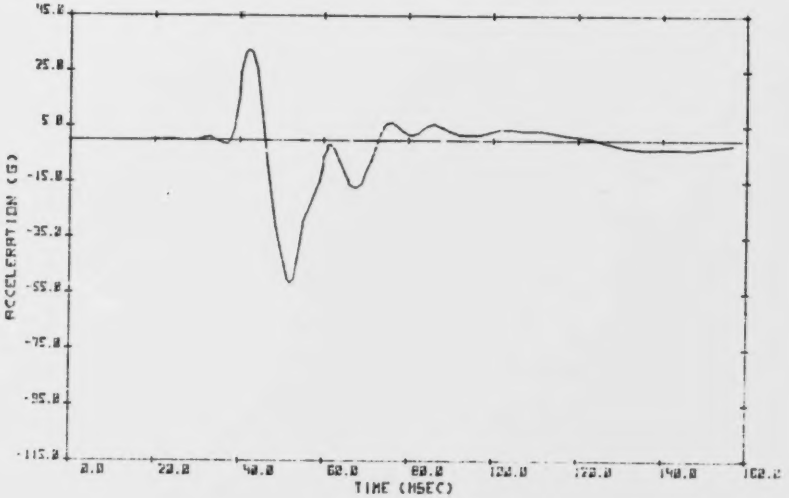

SRL 17-5 TEST #10 - LOWER STERNUM

BEST DOCUMENT AVAILABLE

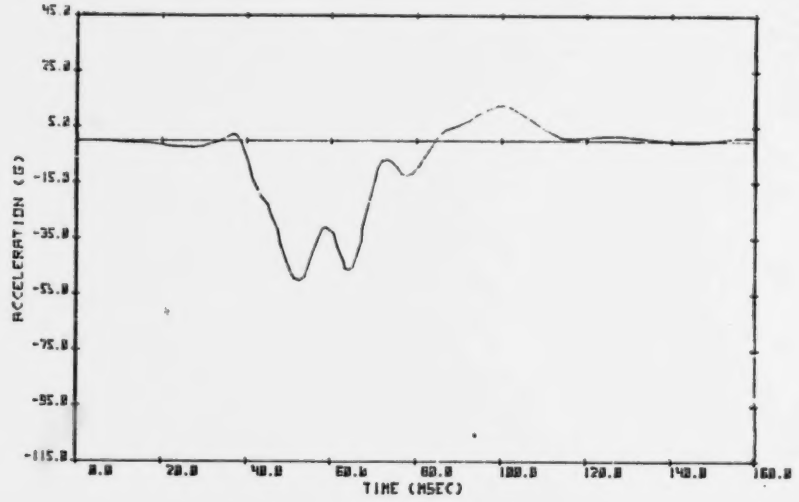

SRL 17-5 TEST #10 - UPPER SPINE

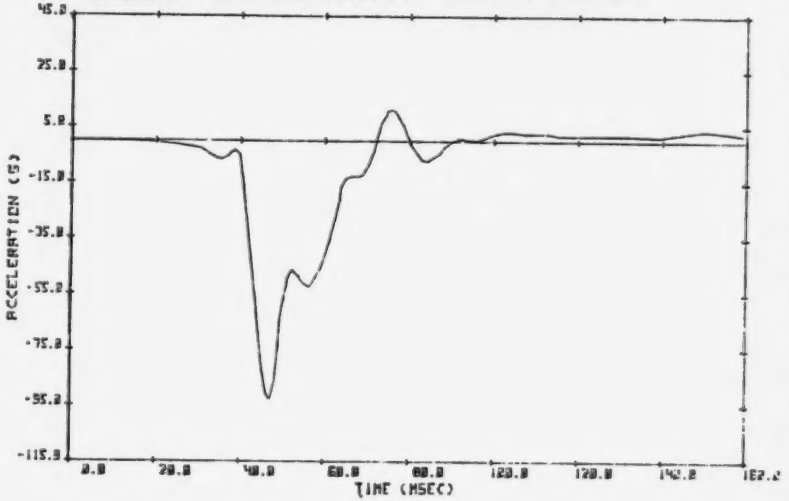

SRL 17-5 TEST #10 - LOWER SPINE

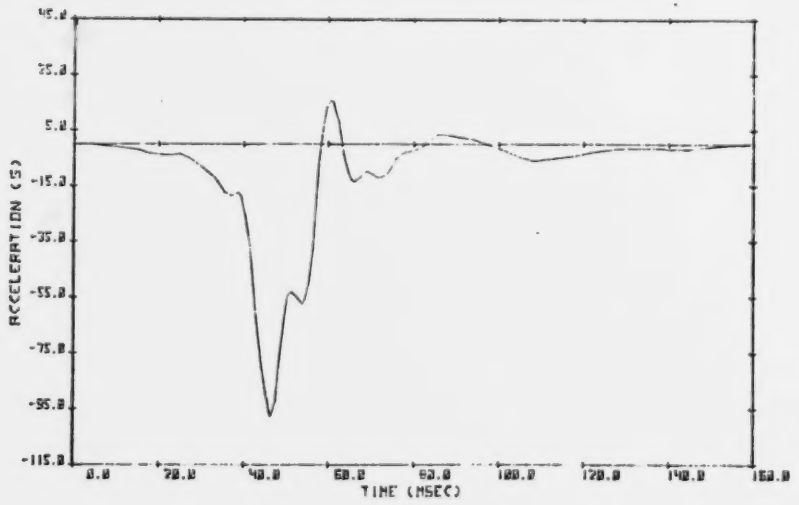

SRL 17-5 TEST #10 - PELVIS

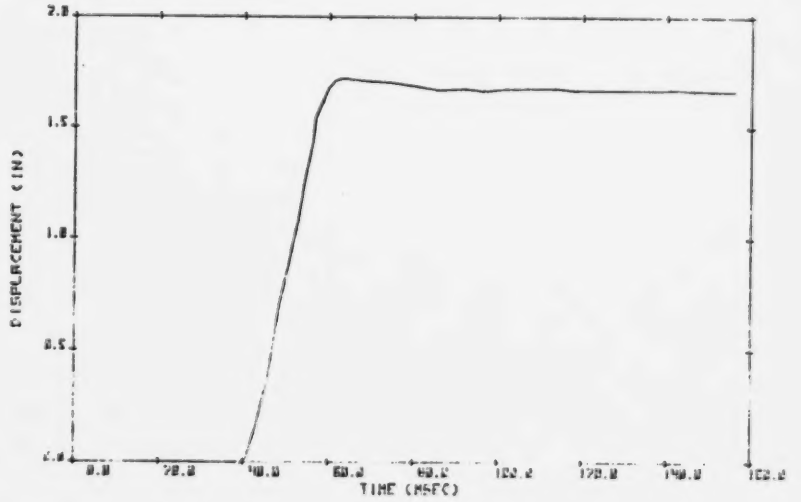

SRL 17-5 TEST #10 - CHEST DEFLECTION

BEST DOCUMENT AVAILABLE

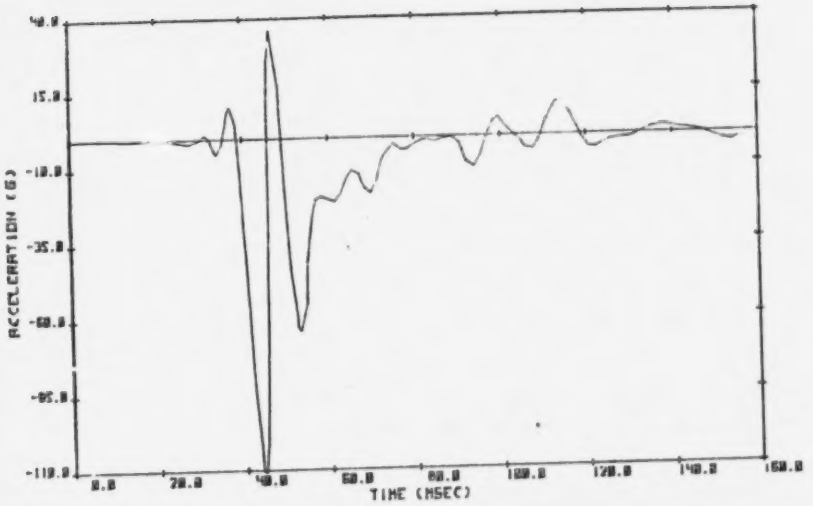

SRL 17-5 TEST #11 - LEFT UPPER RIB

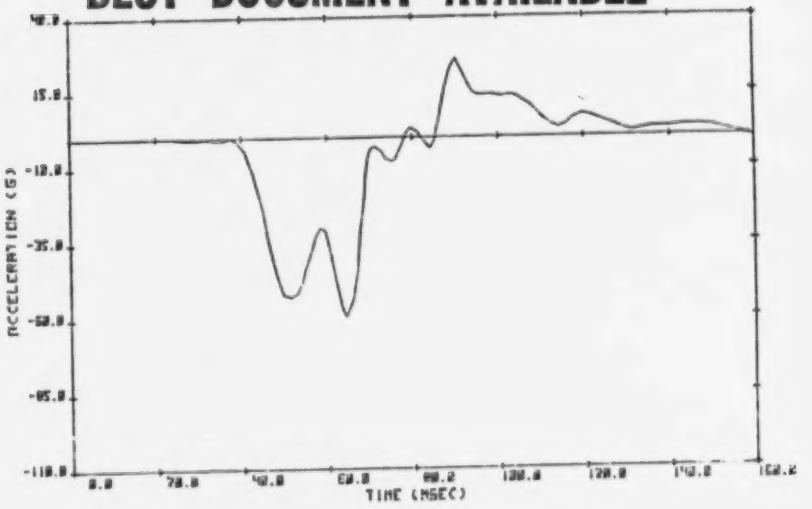

SRL 17-5 TEST #11 - RIGHT UPPER RIB

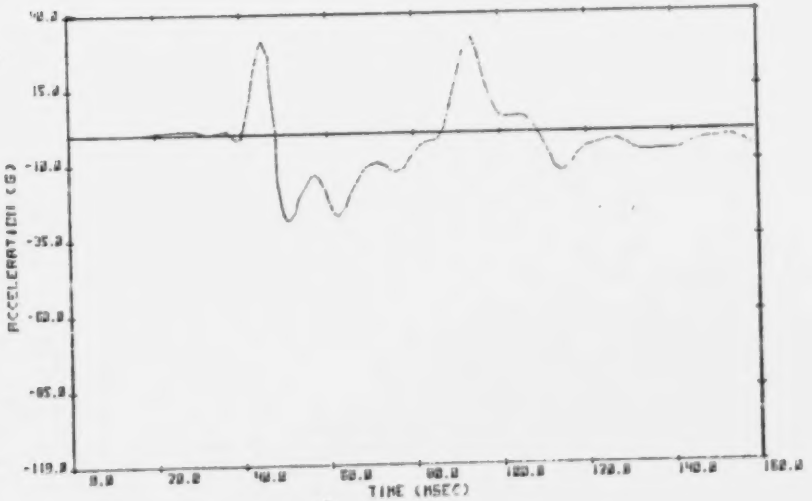

SRL 17-5 TEST #11 - UPPER STERNUM

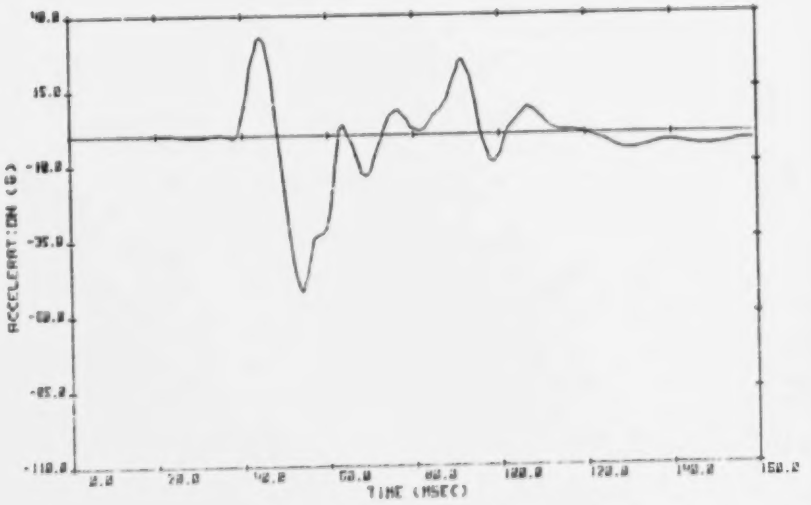

SRL 17-5 TEST #11 - LOWER STERNUM

BEST DOCUMENT AVAILABLE

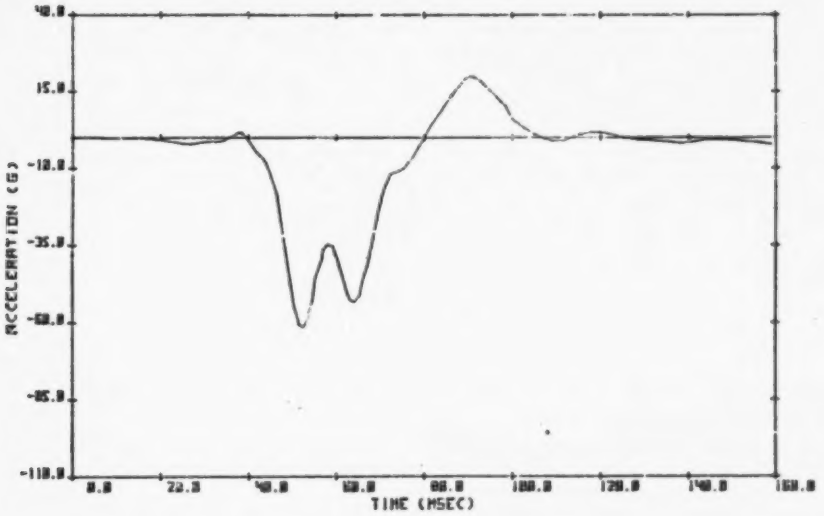

SRL 17-5 TEST #11 - UPPER SPINE

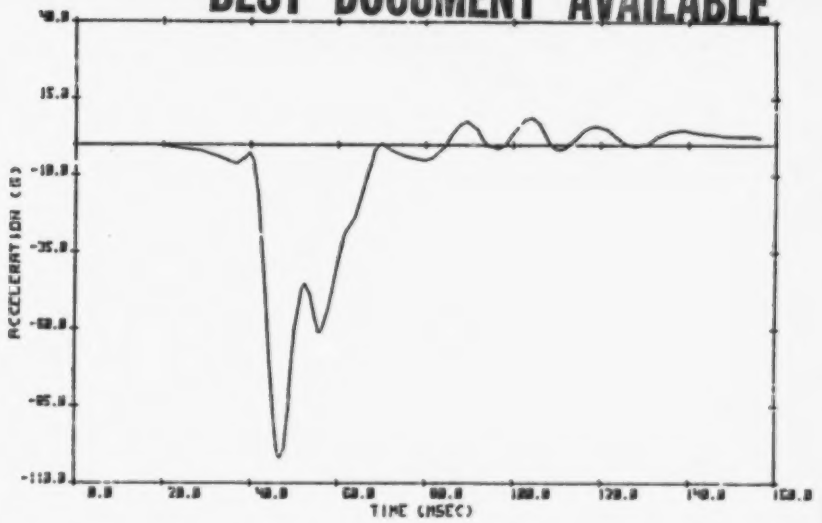

SRL 17-5 TEST #11 - LOWER SPINE

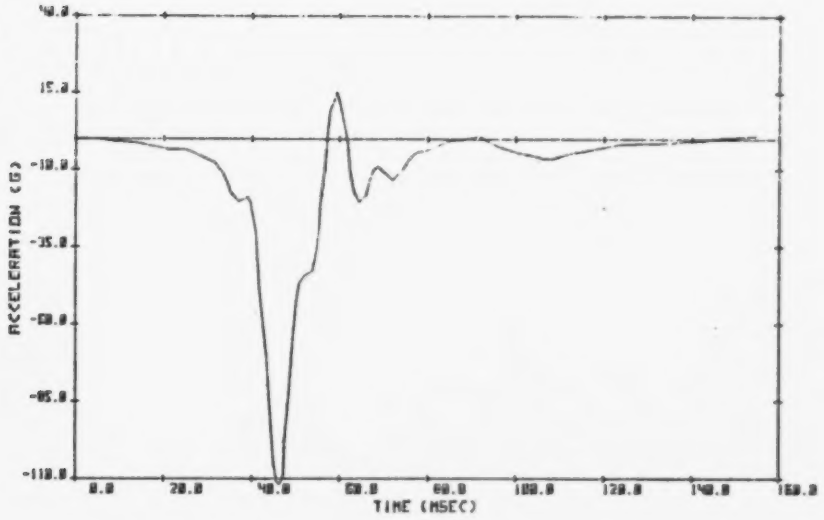

SRL 17-5 TEST #11 - PELVIS

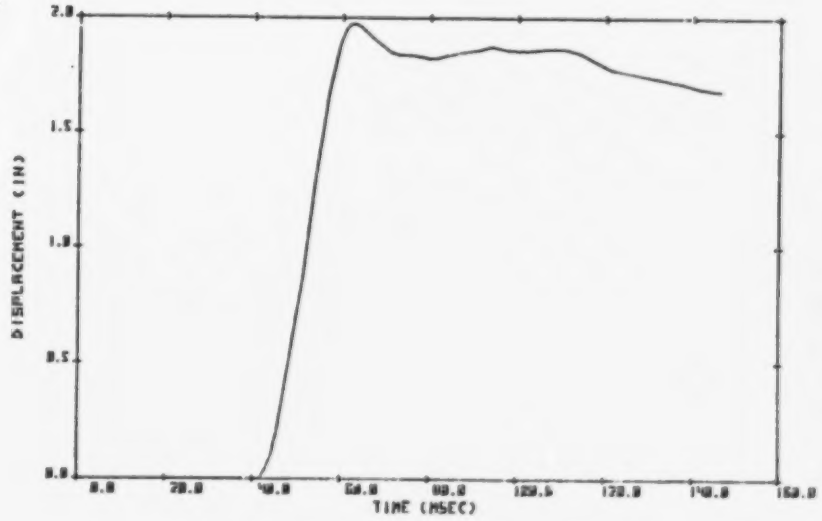

SRL 17-5 TEST #11 - CHEST DEFLECTION

BEST DOCUMENT AVAILABLE

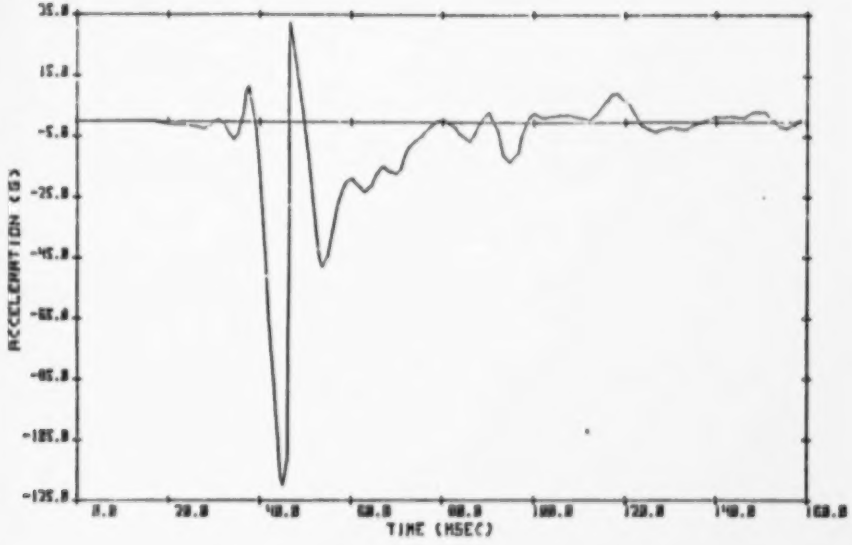

SRL 17-5 TEST #12 - LEFT UPPER RIB

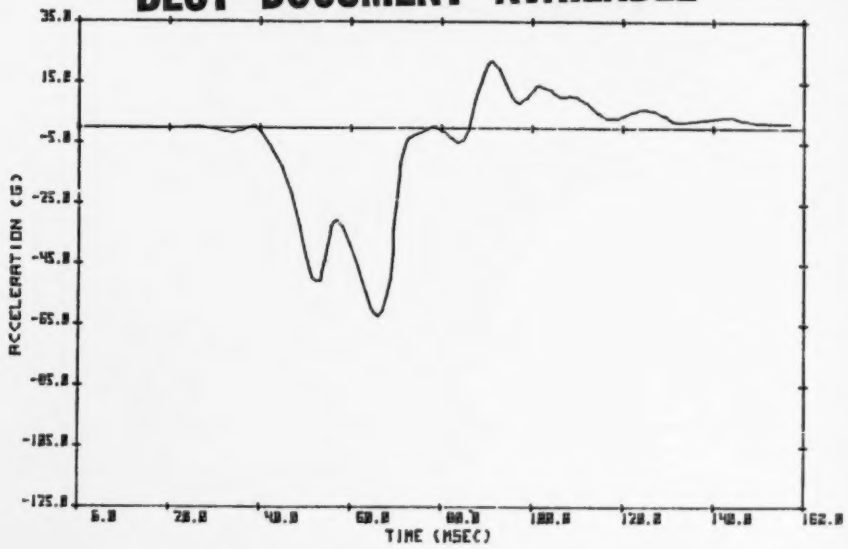

SRL 17-5 TEST #12 - RIGHT UPPER RIB

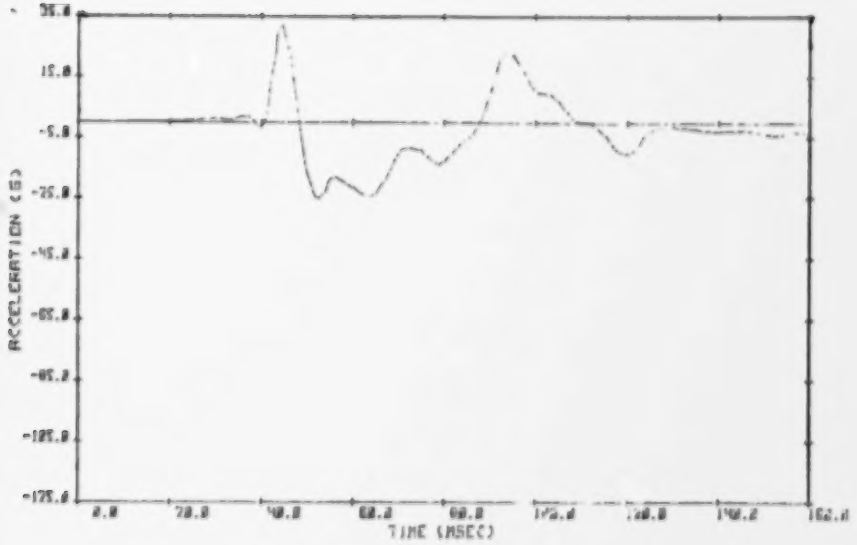

SRL 17-5 TEST #12 - UPPER STERNUM

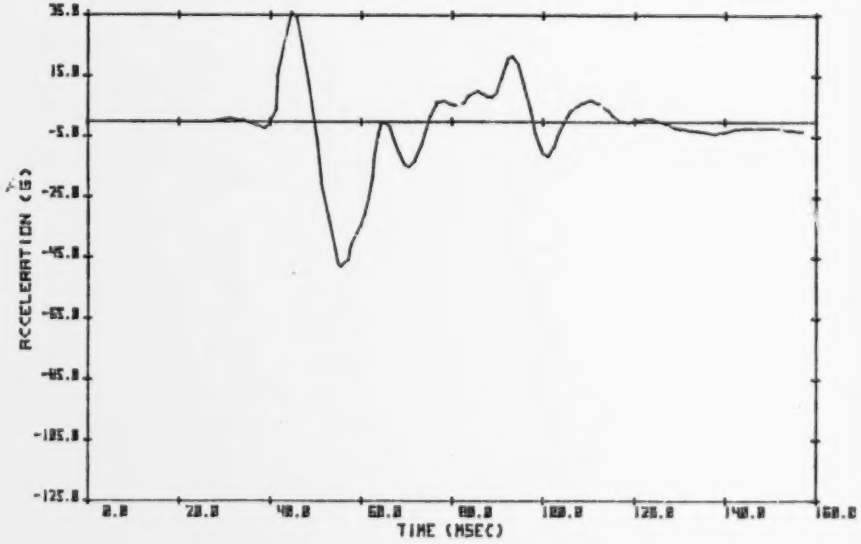

SRL 17-5 TEST #12 - LOWER STERNUM

BEST DOCUMENT AVAILABLE

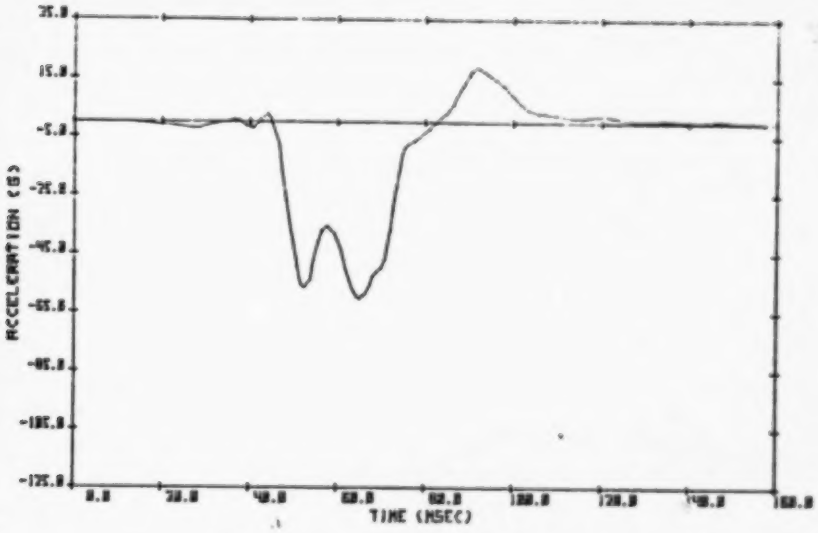

SRL 17-5 TEST #12 - UPPER SPINE

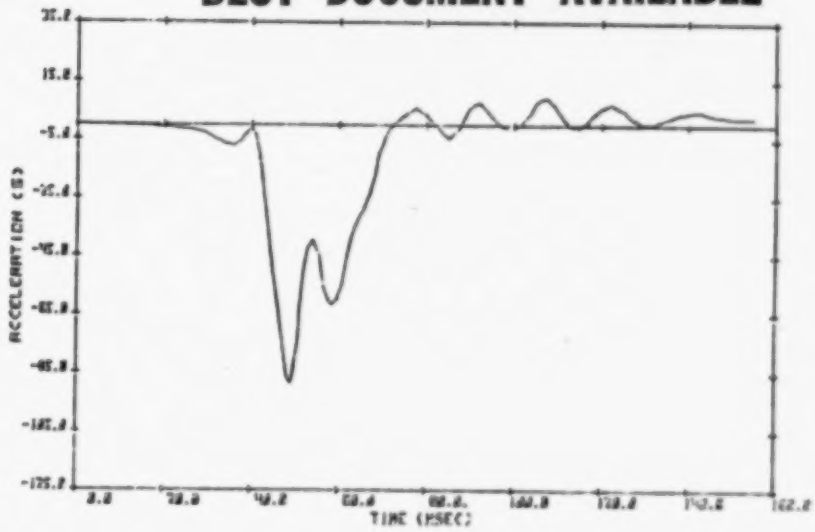

SRL 17-5 TEST #12 - LOWER SPINE

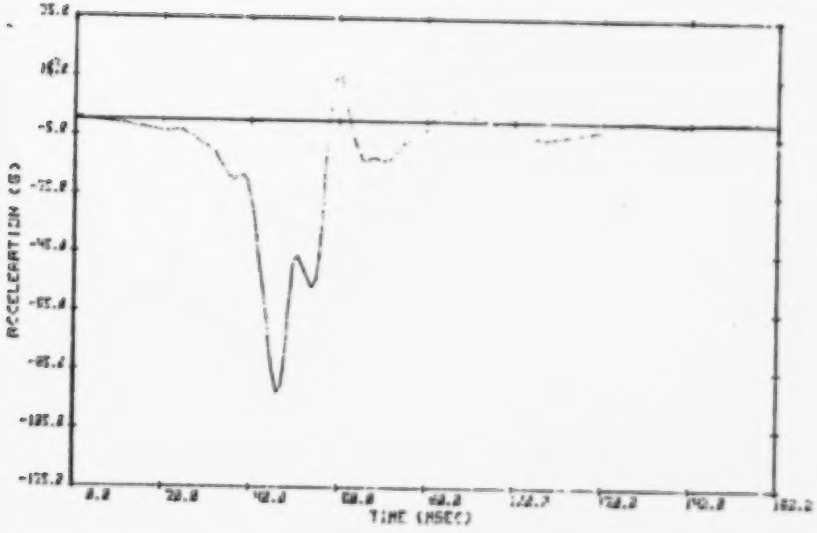

SRL 17-5 TEST #12 - PELVIS

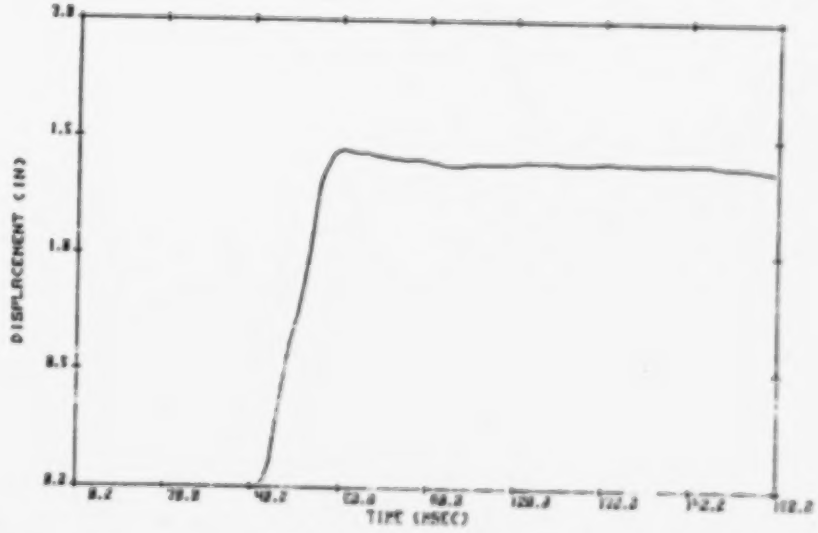

SRL 17-5 TEST #12 - CHEST DEFLECTION

BEST DOCUMENT AVAILABLE

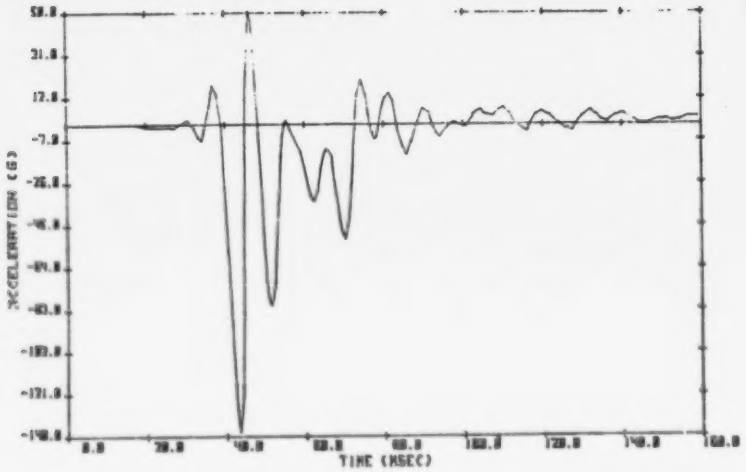

SRL 17-S TEST #13 - LEFT UPPER RIB

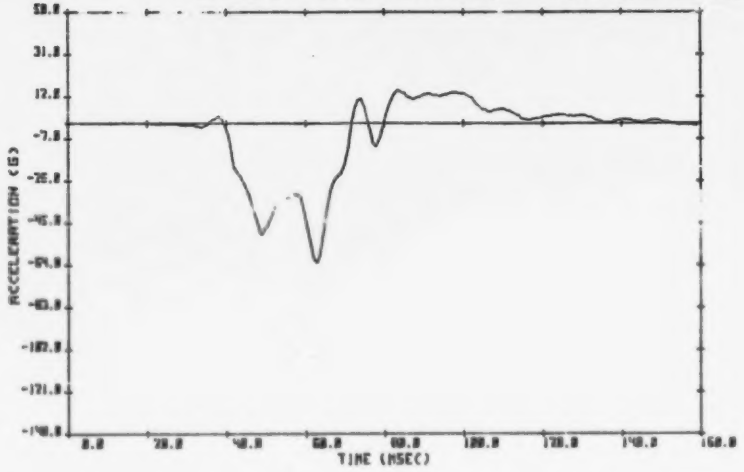

SRL 17-S TEST #13 - RIGHT UPPER RIB

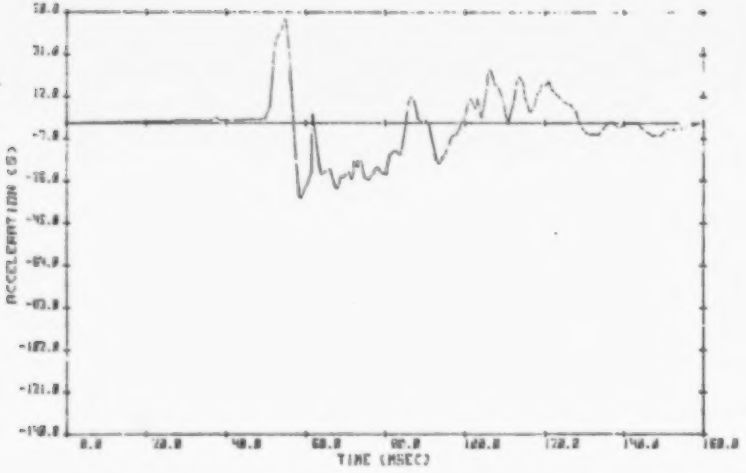

SRL 17-S TEST #13 - UPPER STERNUM

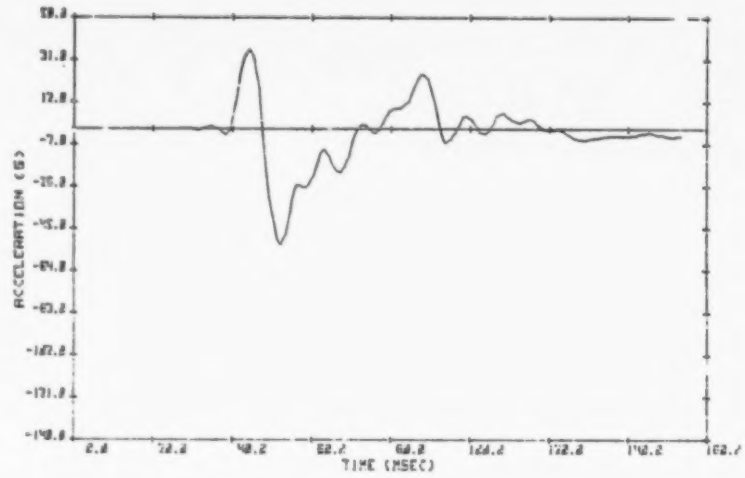

SRL 17-S TEST #13 - LOWER STERNUM

BEST DOCUMENT AVAILABLE

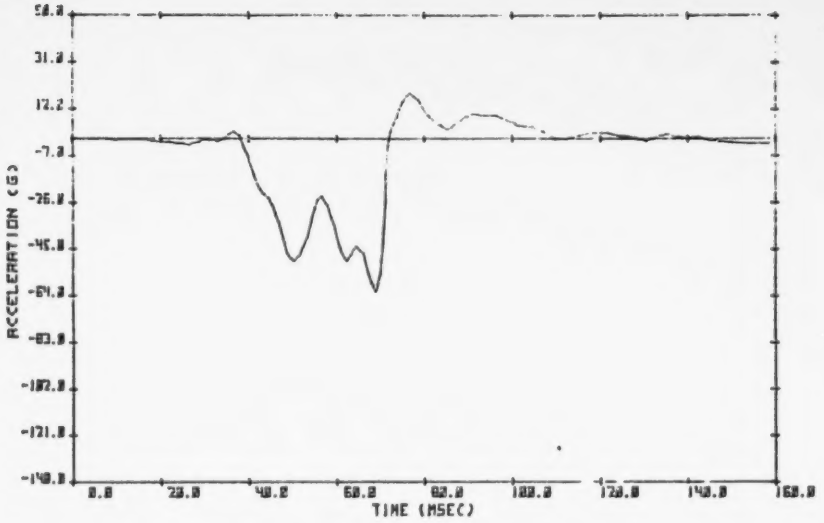

SRL 17-S TEST #13 - UPPER SPINE

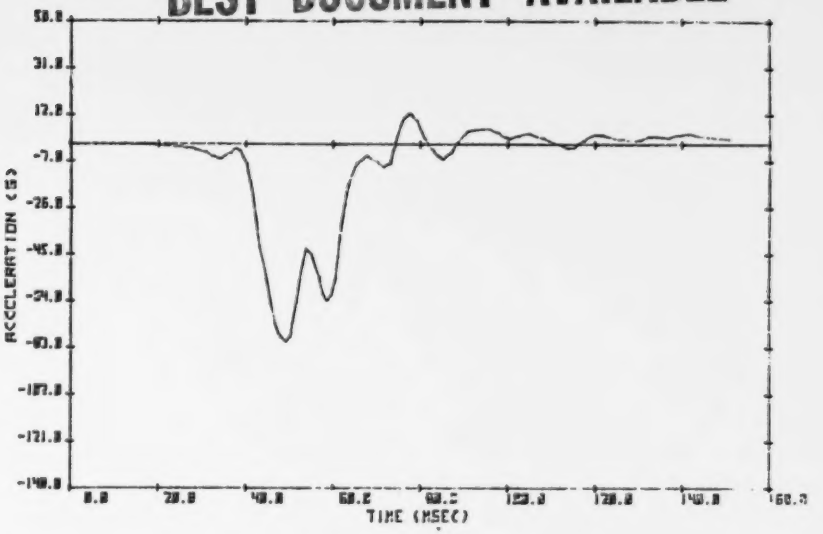

SRL 17-S TEST #13 - LOWER SPINE

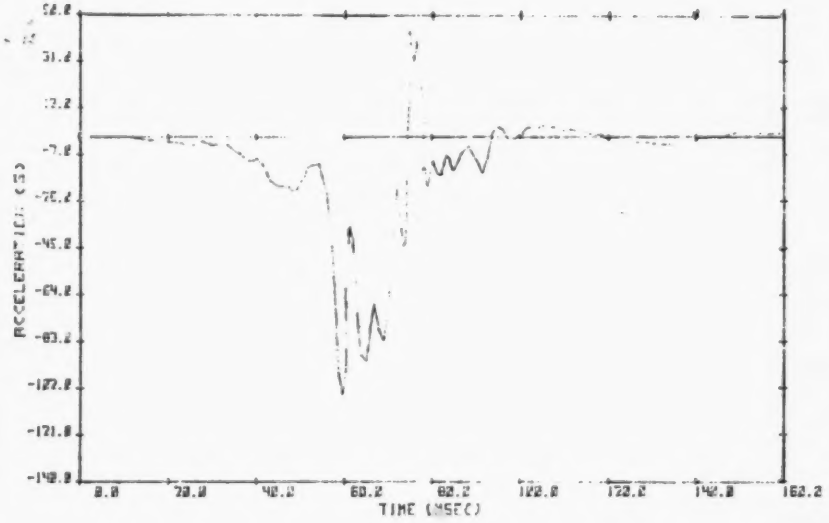

SRL 17-S TEST #13 - PELVIS

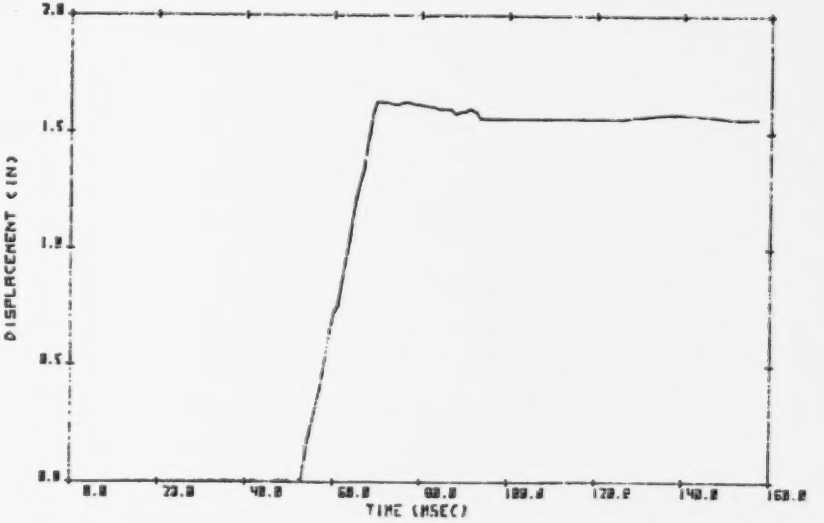

SRL 17-S TEST #13 - CHEST DEFLECTION

BEST DOCUMENT AVAILABLE

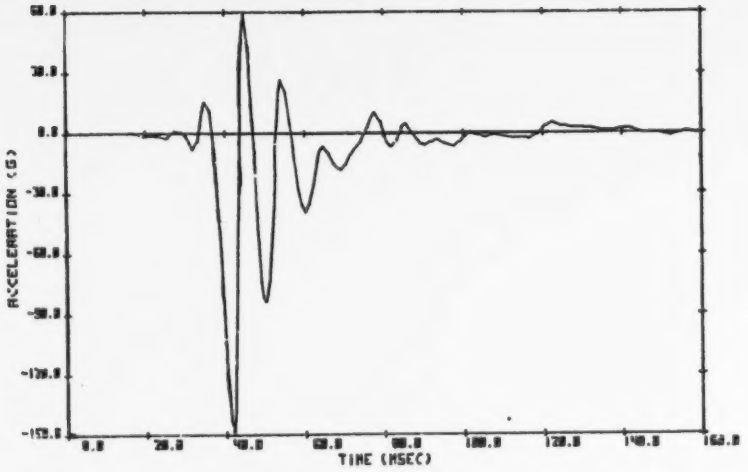

SRL 17-5 TEST #14 - LEFT UPPER RIB

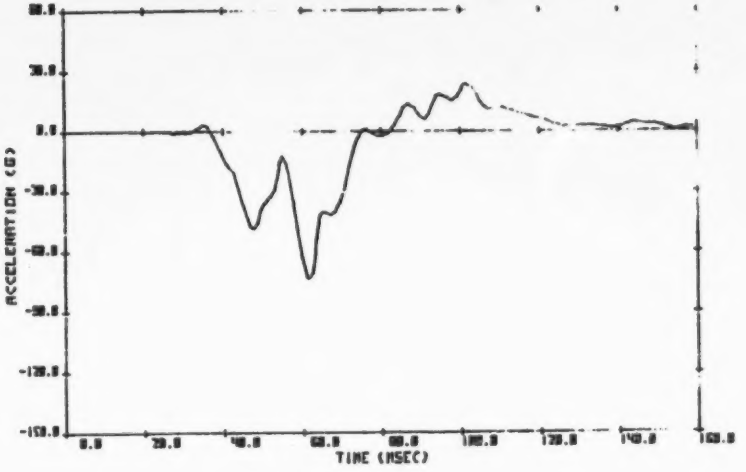

SRL 17-5 TEST #14 - RIGHT UPPER RIB

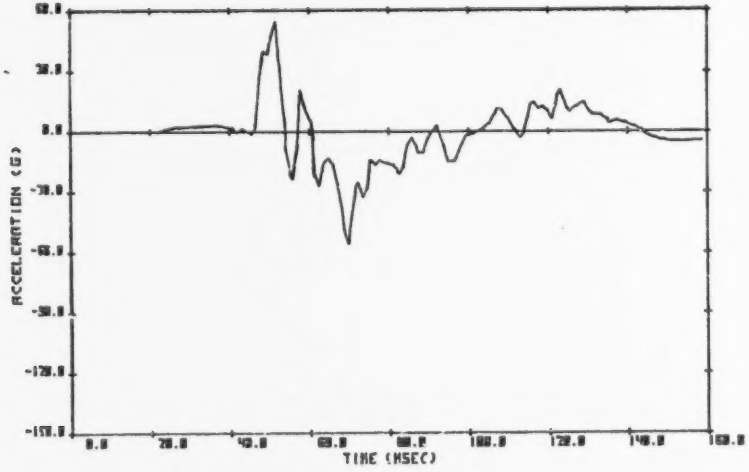

SRL 17-5 TEST #14 - UPPER STERNUM

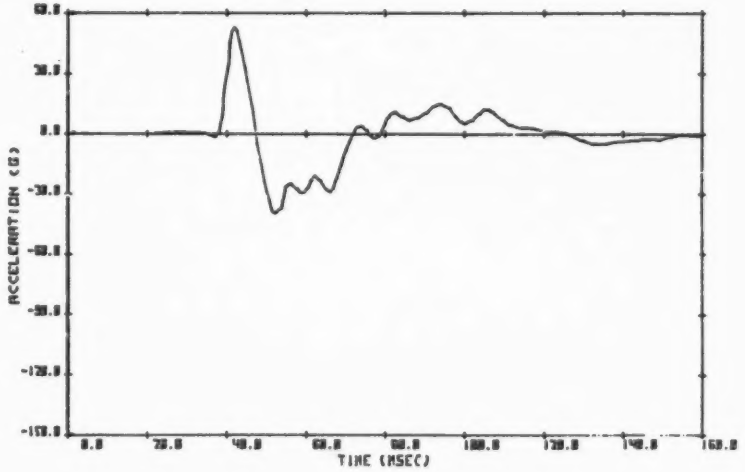

SRL 17-5 TEST #14 - LOWER STERNUM

BEST DOCUMENT AVAILABLE

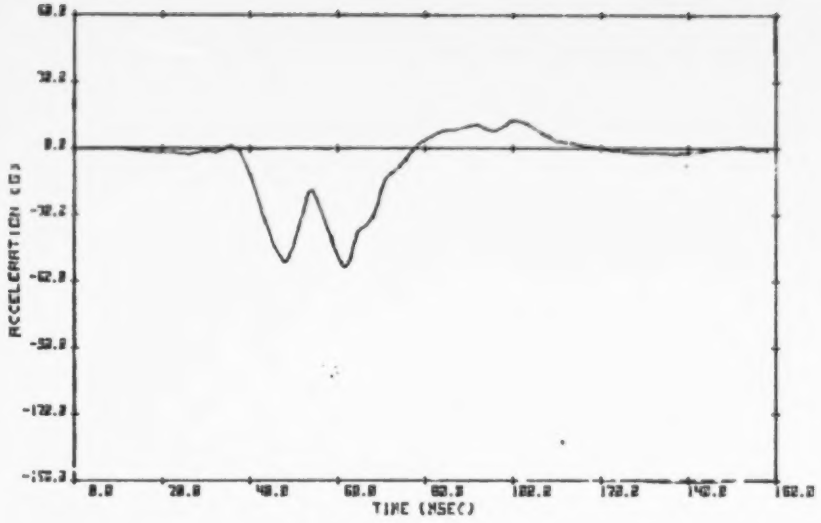

SRL 17-5 TEST #14 - UPPER SPINE

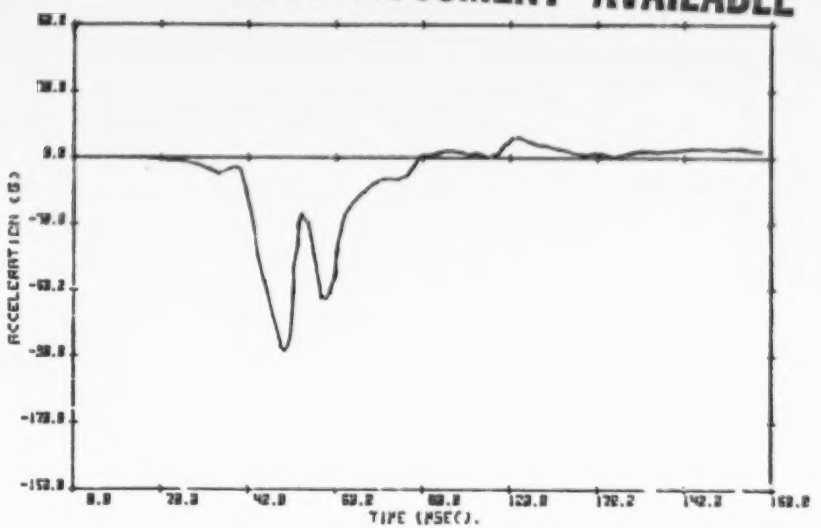

SRL 17-5 TEST #14 - LOWER SPINE

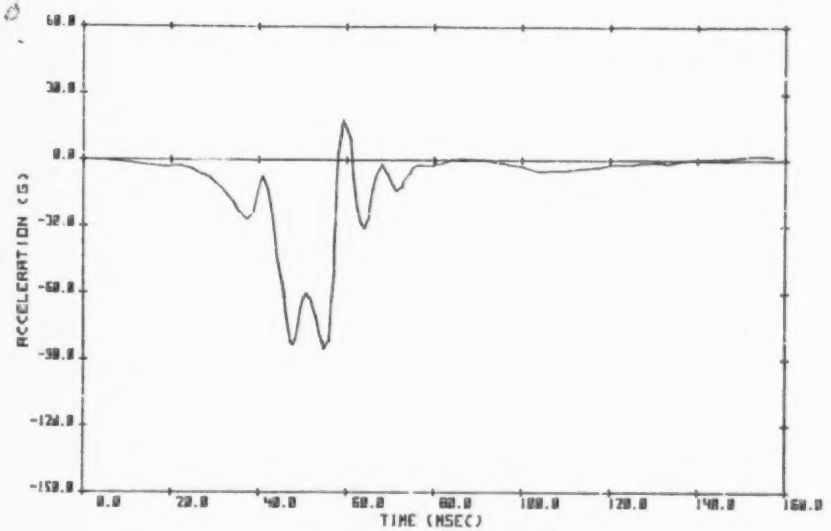

SRL 17-5 TEST #14 - PELVIS

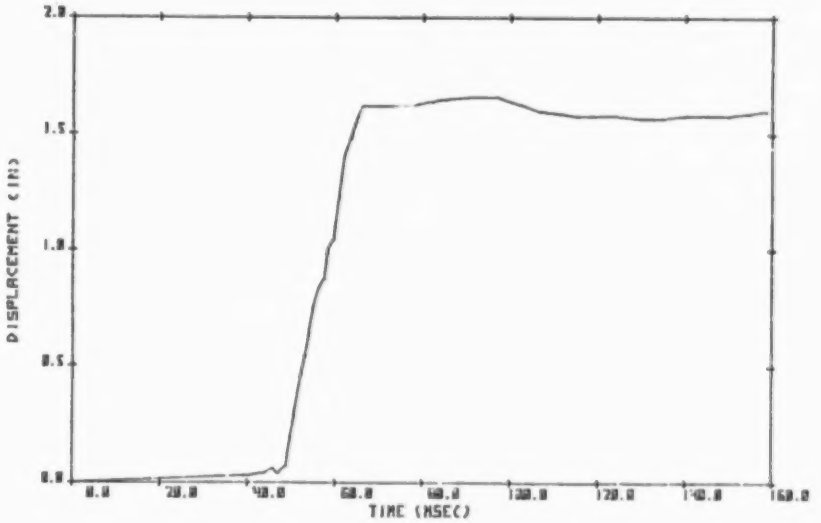

SRL 17-5 TEST #14 - CHEST DEFLECTION

BEST DOCUMENT AVAILABLE

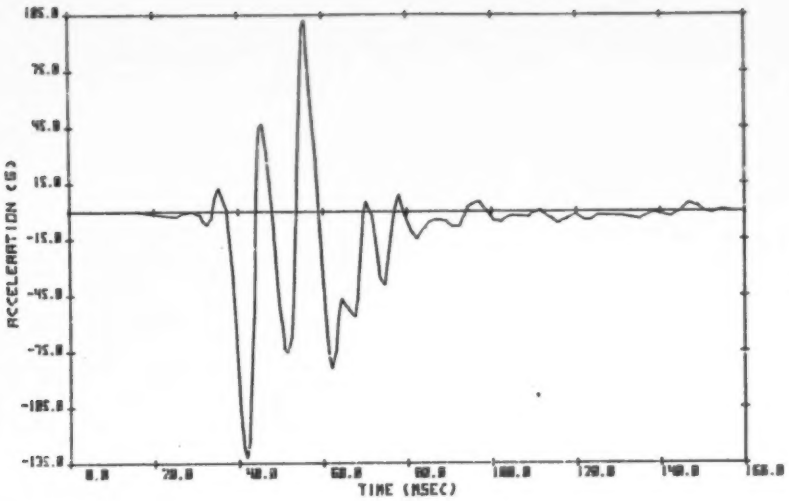

SRL 17-5 TEST #15 - LEFT UPPER RIB

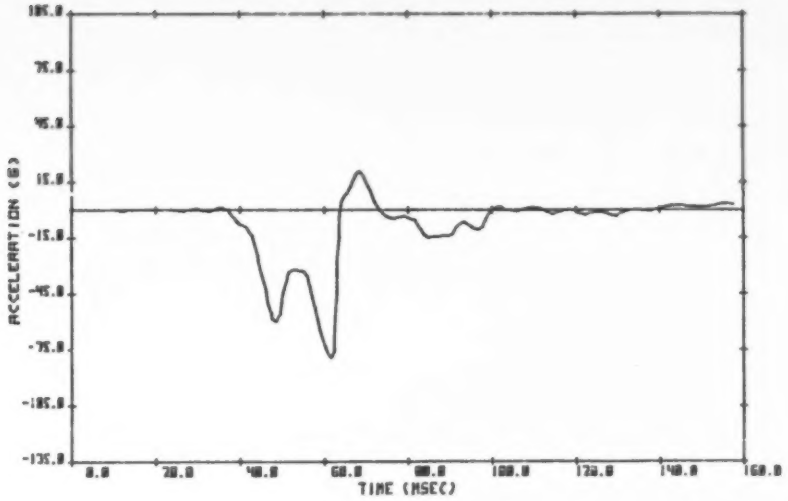

SRL 17-5 TEST #15 - RIGHT UPPER RIB

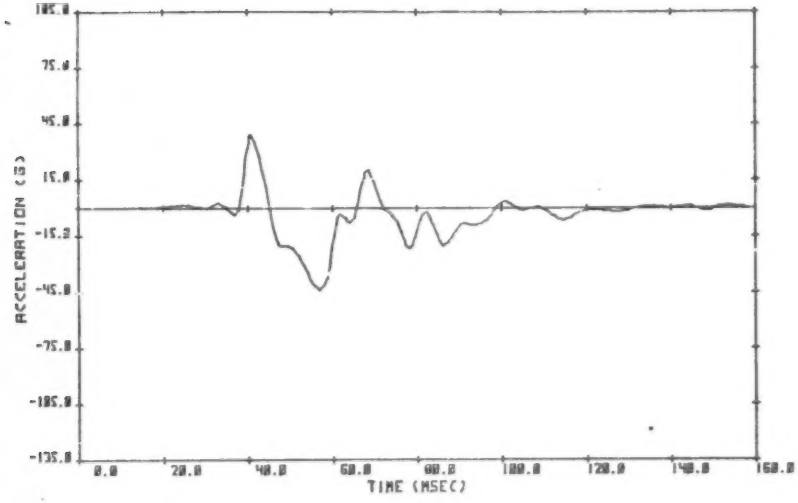

SRL 17-5 TEST #15 - UPPER STERNUM

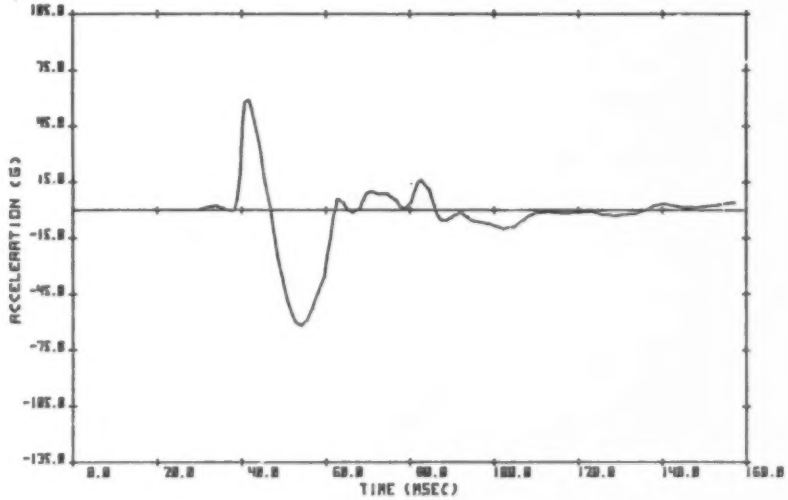

SRL 17-5 TEST #15 - LOWER STERNUM

BEST DOCUMENT AVAILABLE

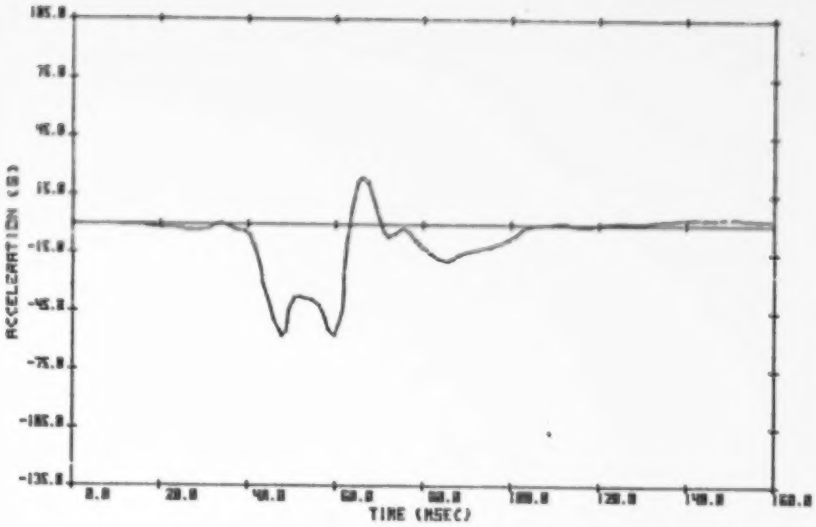

SRL 17-S TEST #15 - UPPER SPINE

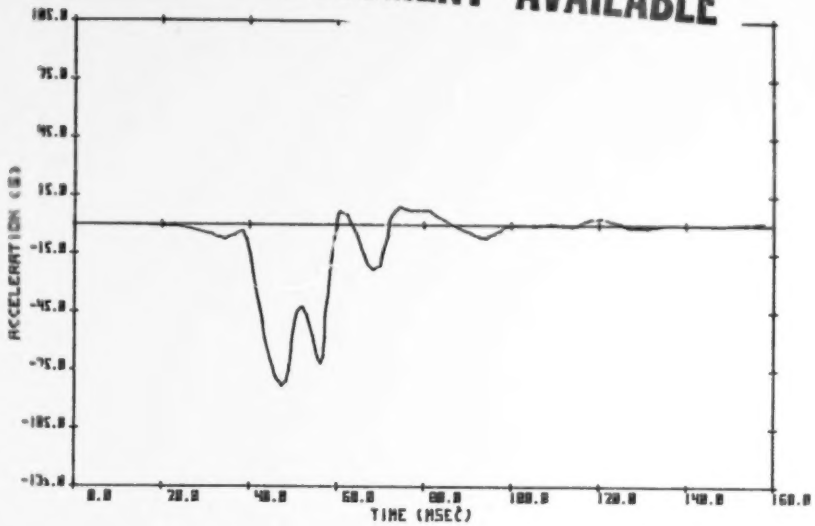

SRL 17-S TEST #15 - LOWER SPINE

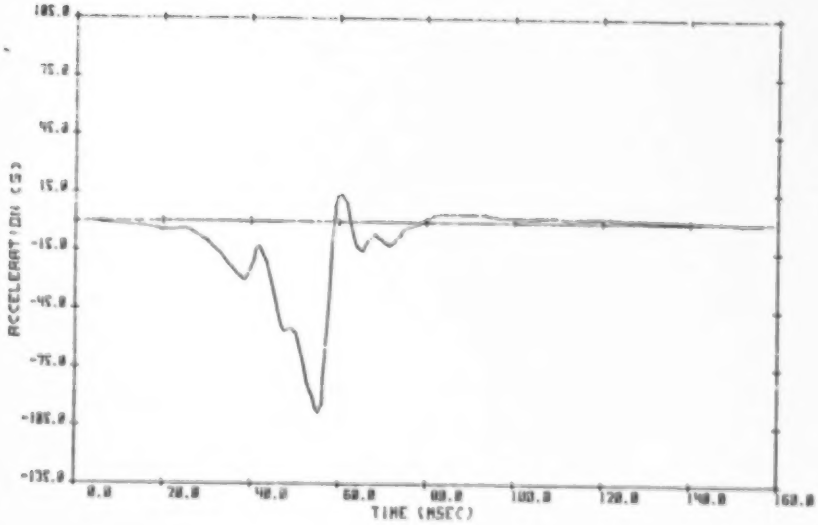

SRL 17-S TEST #15 - PELVIS

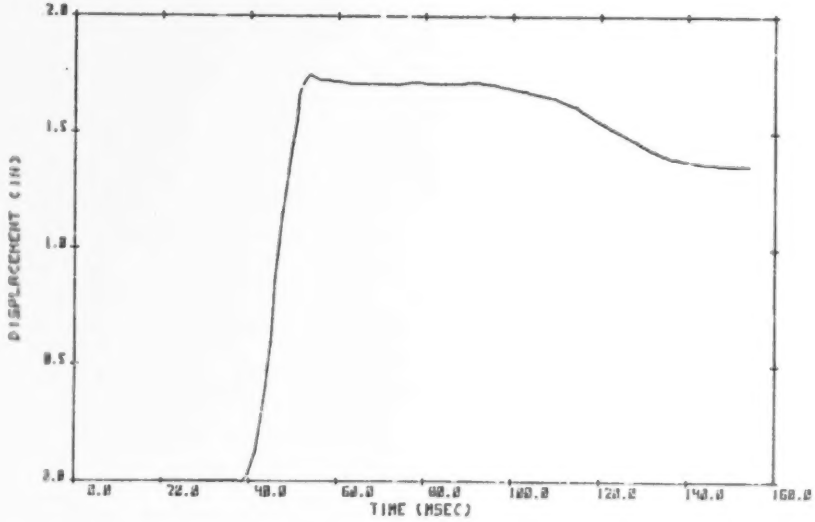

SRL 17-S TEST #15 - CHEST DEFLECTION

BEST DOCUMENT AVAILABLE

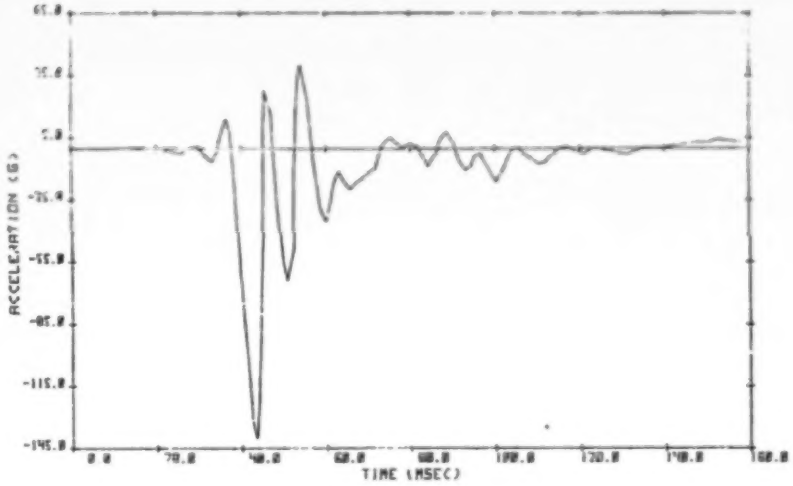

SRL 17-S TEST #16 - LEFT UPPER RIB

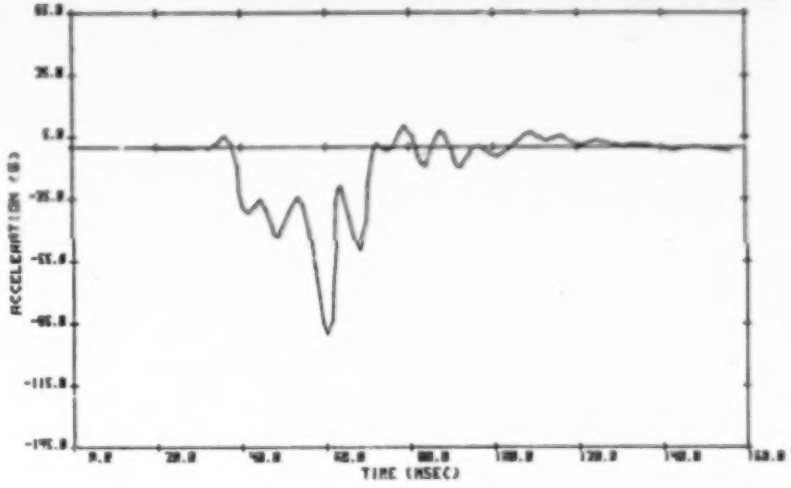

SRL 17-S TEST #16 - RIGHT UPPER RIB

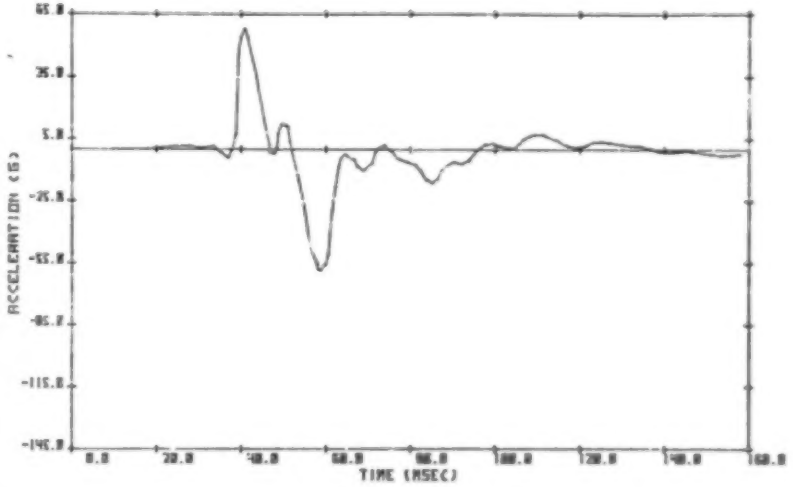

SRL 17-S TEST #16 - UPPER STERNUM

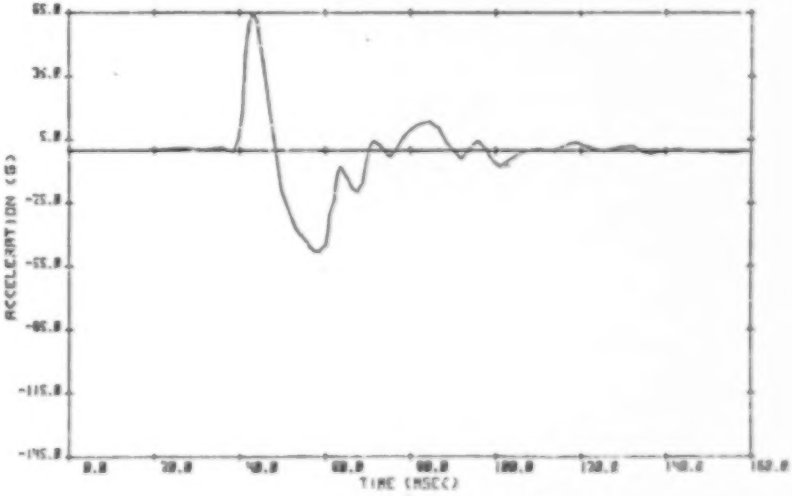

SRL 17-S TEST #16 - LOWER STERNUM

BEST DOCUMENT AVAILABLE

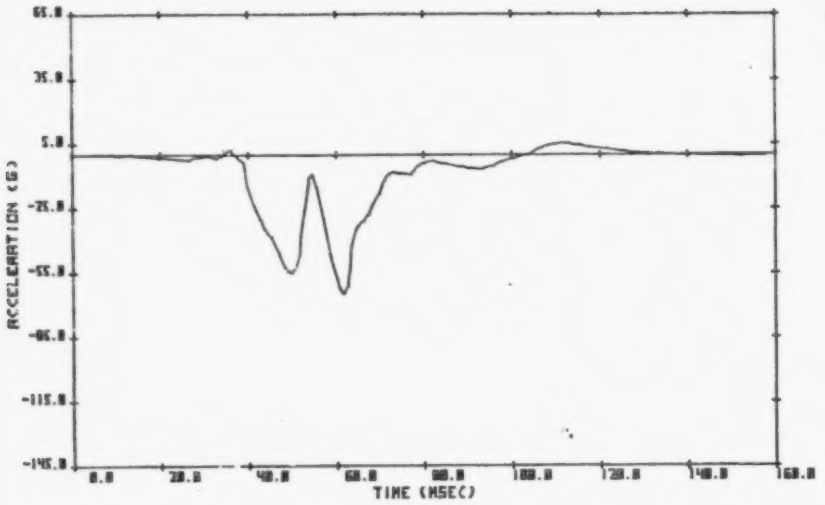

SRL 17-S TEST #16 - UPPER SPINE

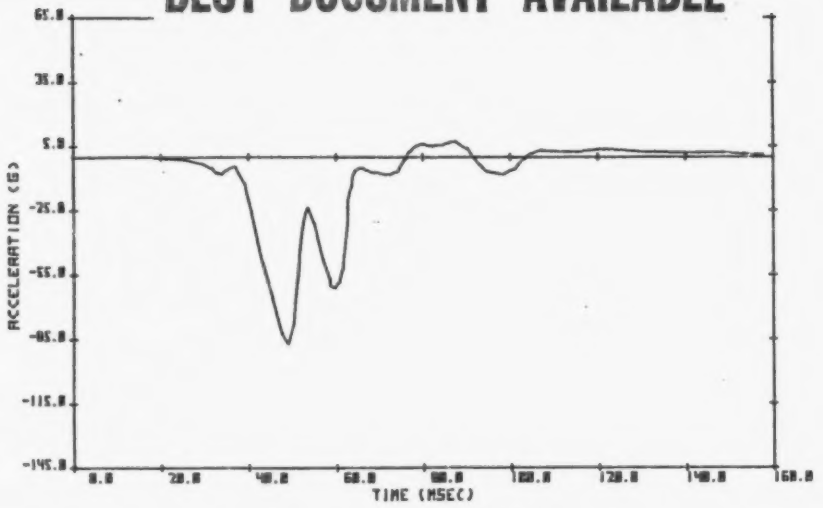

SRL 17-S TEST #16 - LOWER SPINE

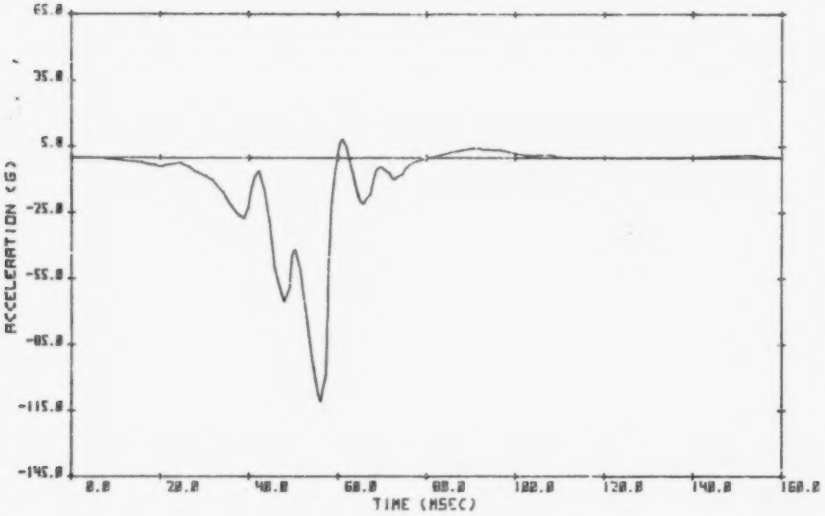

SRL 17-S TEST #16 - PELVIS

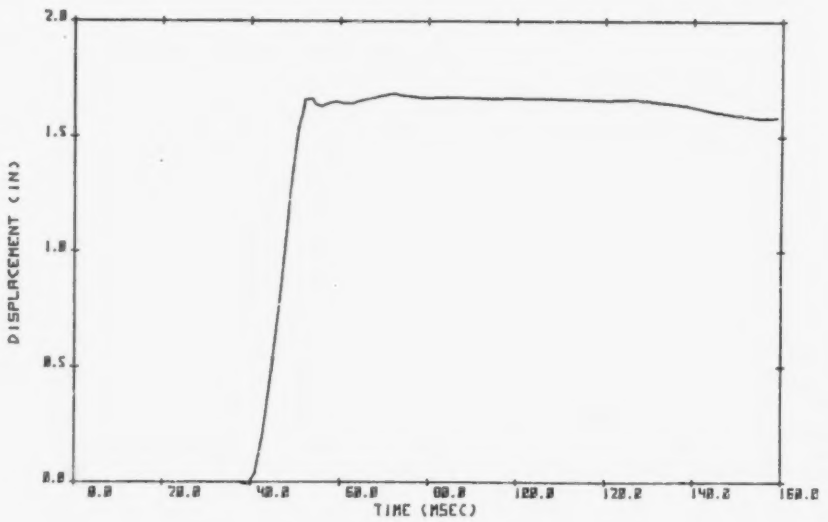

SRL 17-S TEST #16 - CHEST DEFLECTION

BEST DOCUMENT AVAILABLE

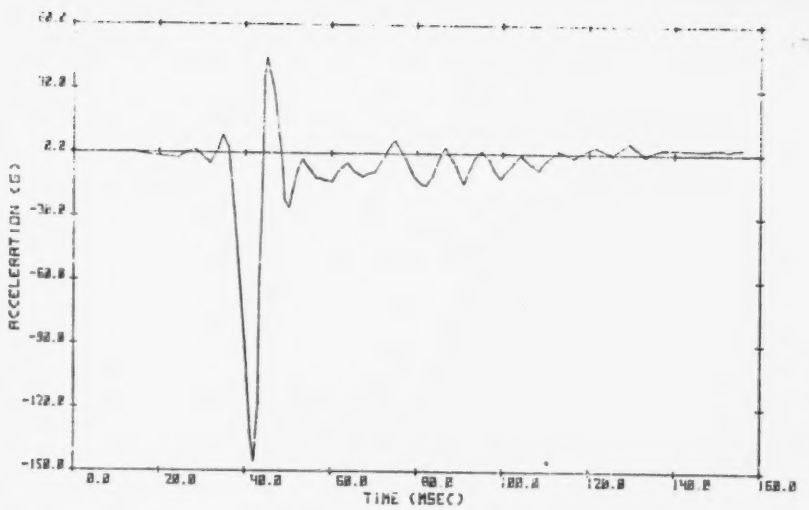

SRL 17-5 TEST #17 - LEFT UPPER RIB

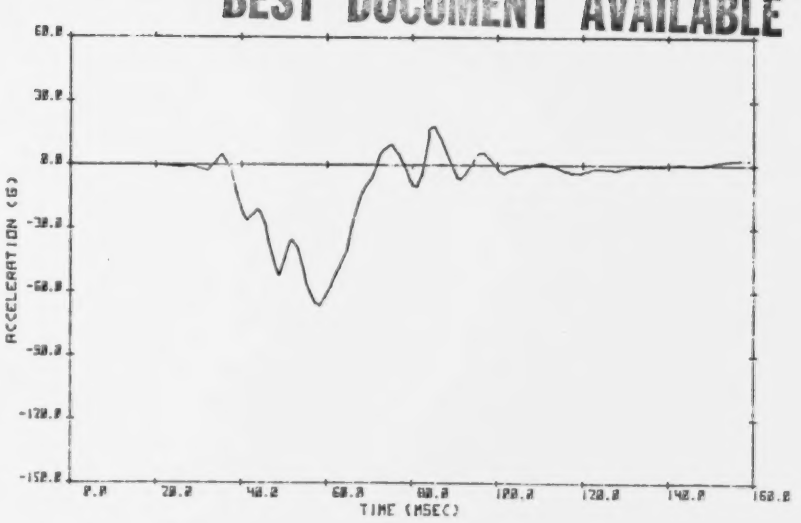

SRL 17-5 TEST #17 - RIGHT UPPER RIB

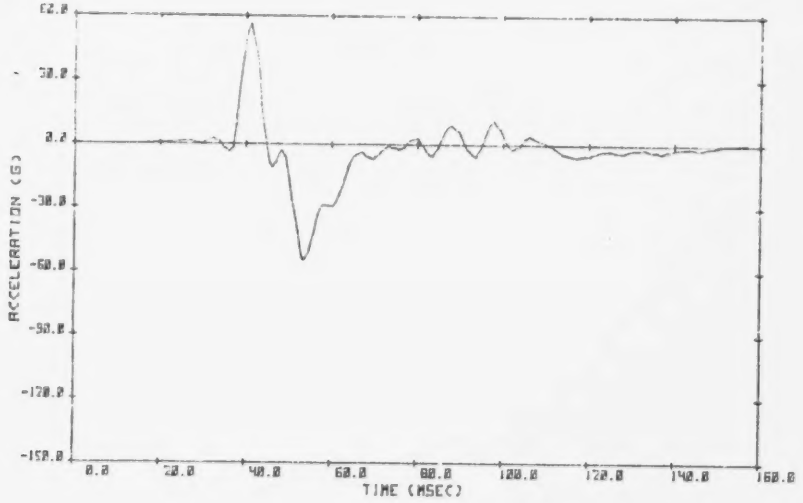

SRL 17-5 TEST #17 - UPPER STERNUM

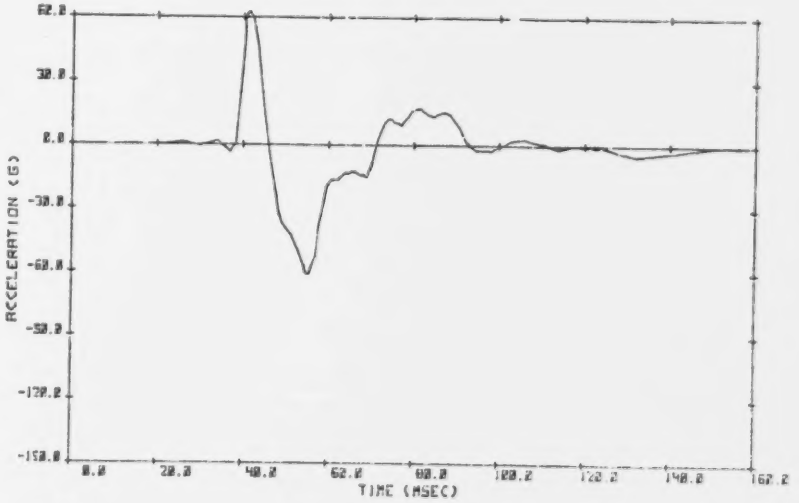

SRL 17-5 TEST #17 - LOWER STERNUM

BEST DOCUMENT AVAILABLE

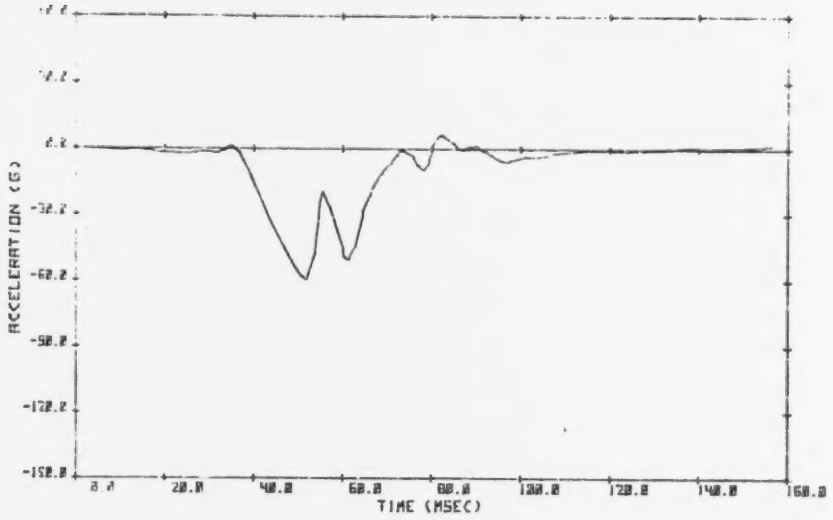

SRL 17-5 TEST #17 - UPPER SPINE

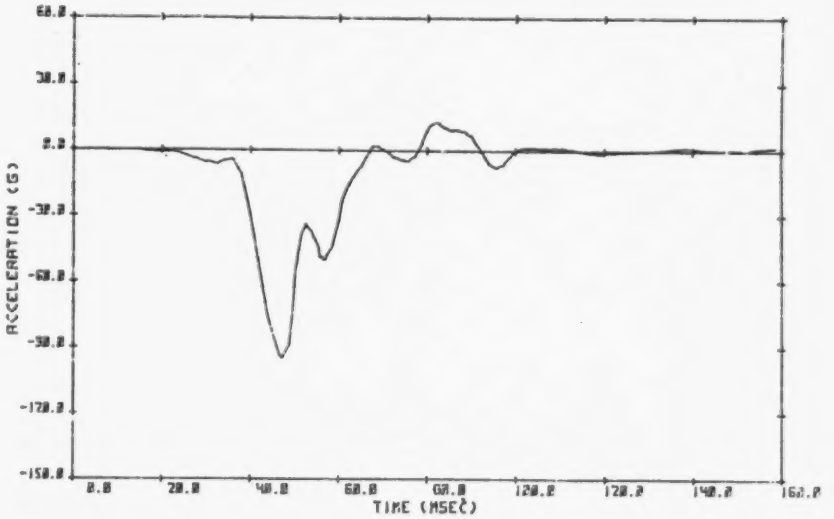

SRL 17-5 TEST #17 - LOWER SPINE

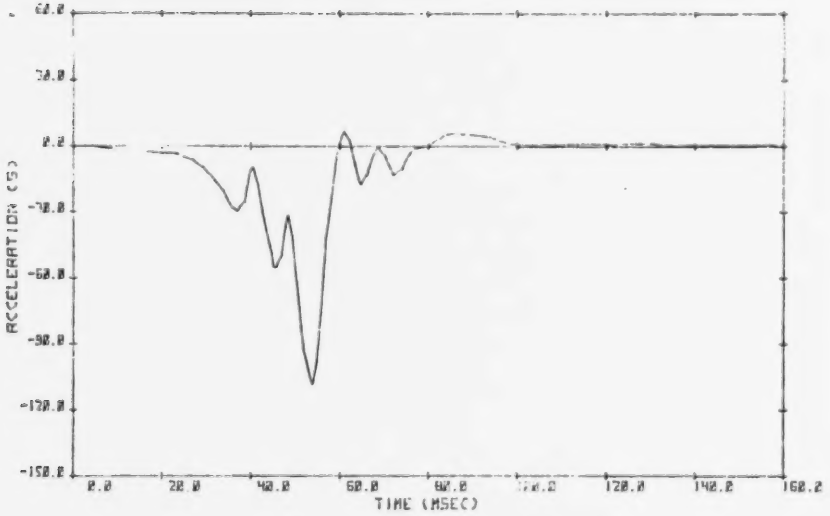

SRL 17-5 TEST #17 - PELVIS

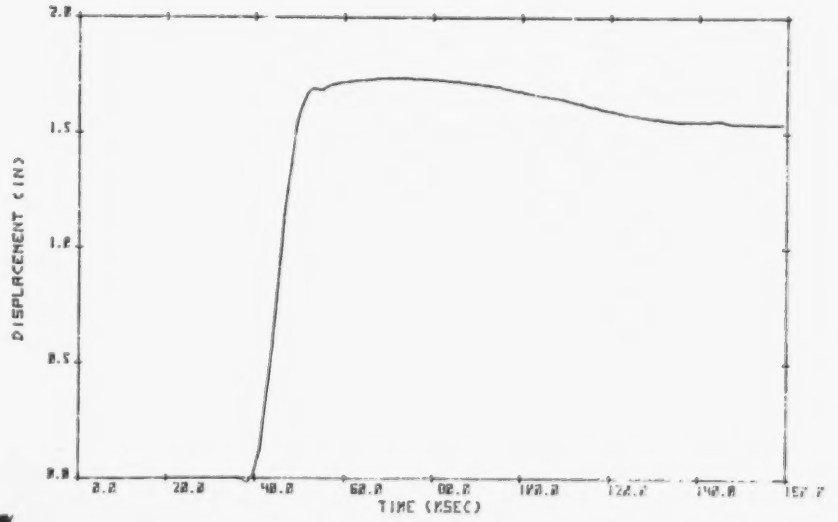

SRL 17-5 TEST #17 - CHEST DEFLECTION

BEST DOCUMENT AVAILABLE

APPENDIX F

Force vs. Deflection Curves for Phase I
Padding Component Tests

TEST NO.7 ENSOLITE ARC

VELOCITY = 14.99 MPH
THICKNESS = 5.6 IN
TEMP = 63 F

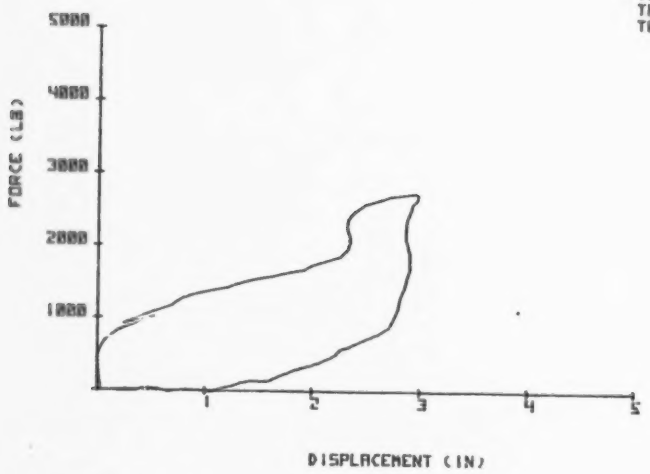

BEST DOCUMENT AVAILABLE

TEST NO.10 APR

VELOCITY = 14.99 MPH
THICKNESS = 5.6 IN
TEMP. = 64 F

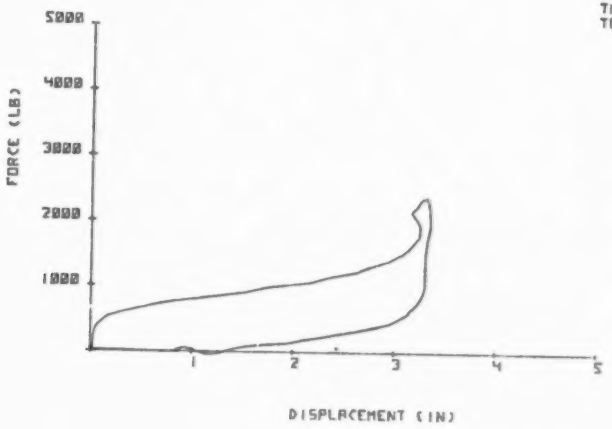

TEST NO.13 RUBATEX R-4991-T

VELOCITY=15.15 MPH
THICKNESS=5.25 IN
TEMP=64 F

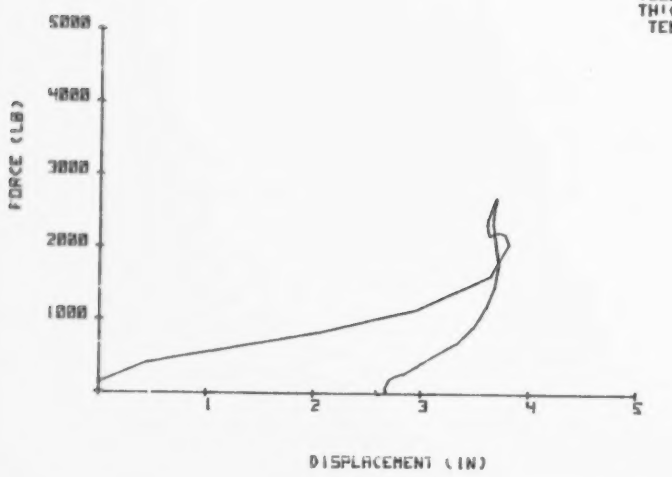

TEST NO.15 RUBATEX R-310-V

VELOCITY=14.99 MPH
THICKNESS=5.25 IN
TEMP=67 F

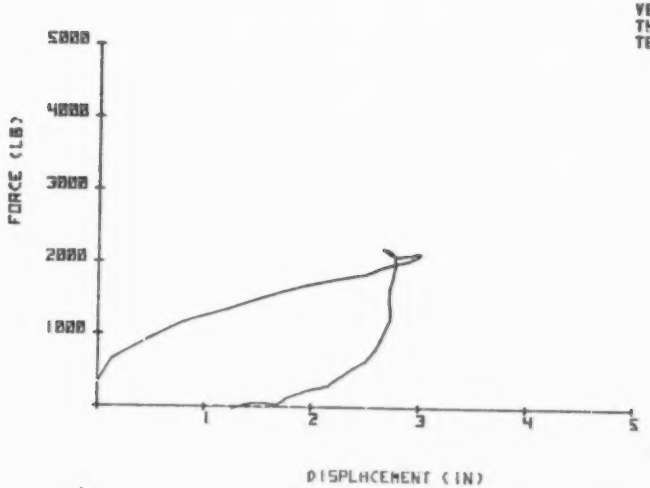

BEST DOCUMENT AVAILABLE

TEST NO.23 ENSOLITE HCR

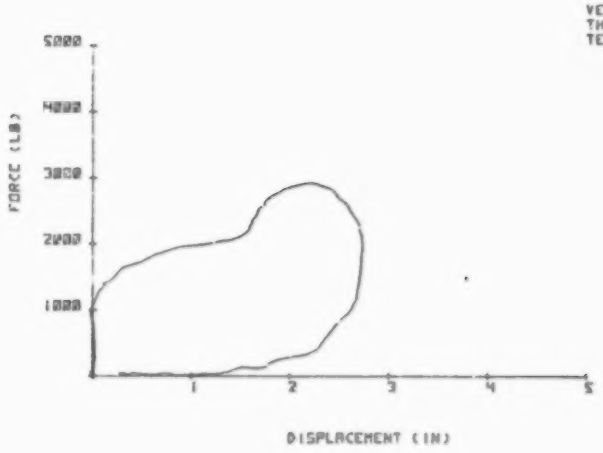

TEST NO.25 FIBERGLASS TYPE G

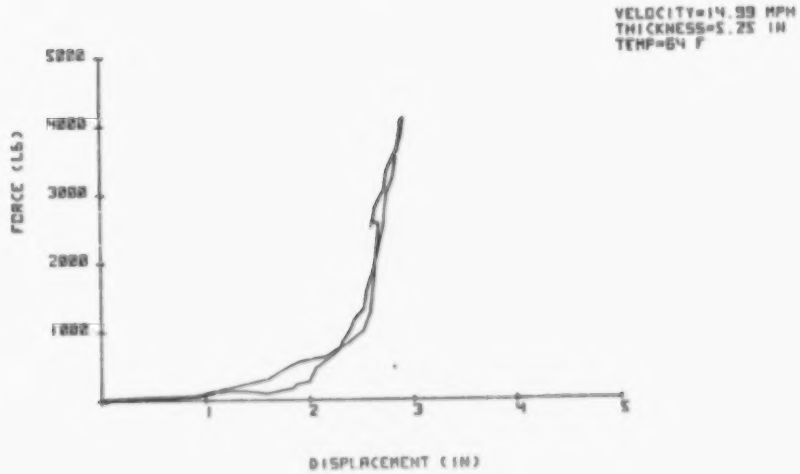

TEST NO.26 NEOPRENE LS 200

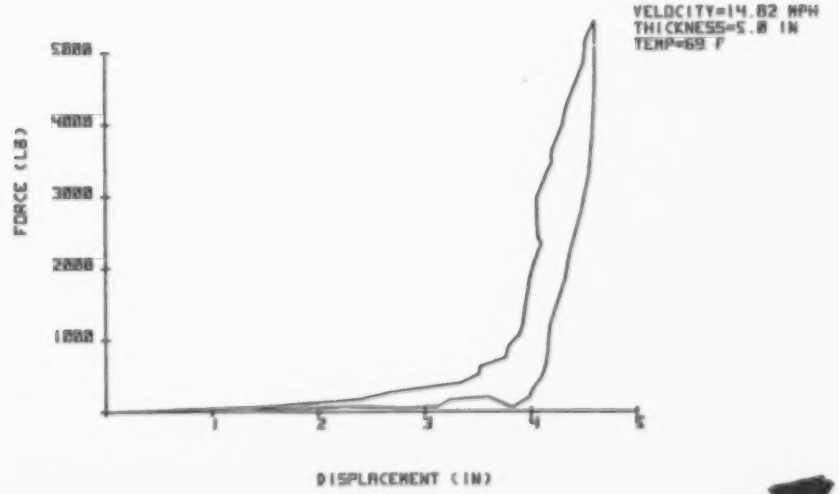

TEST NO.28 NEOPRENE UDRP

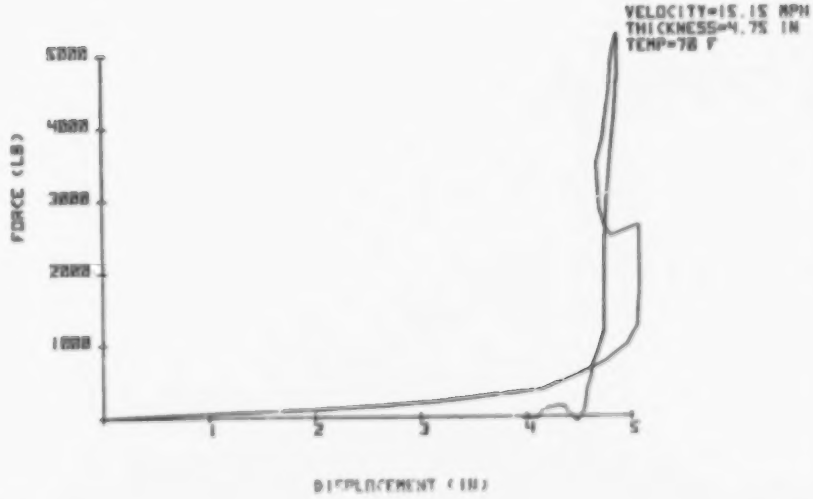

TEST NO.30 ETHAFOAM

BEST DOCUMENT AVAILABLE

VELOCITY=14.99 MPH
THICKNESS=5.0 IN
TEMP=71 F

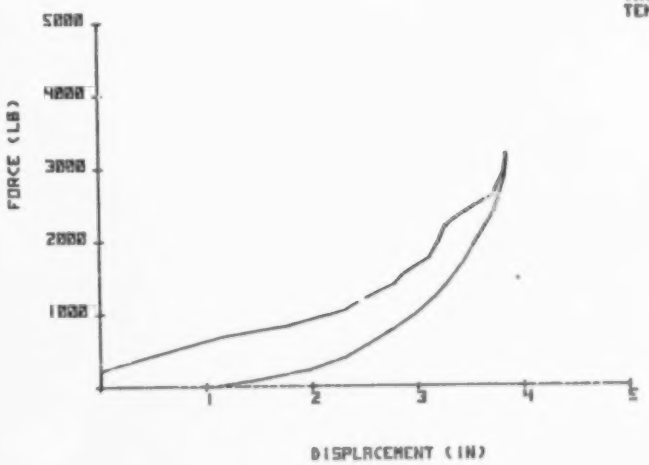

TEST NO.32 ETHAFOAM 600

VELOCITY=14.92 MPH
THICKNESS=5.13 IN
TEMP=72 F

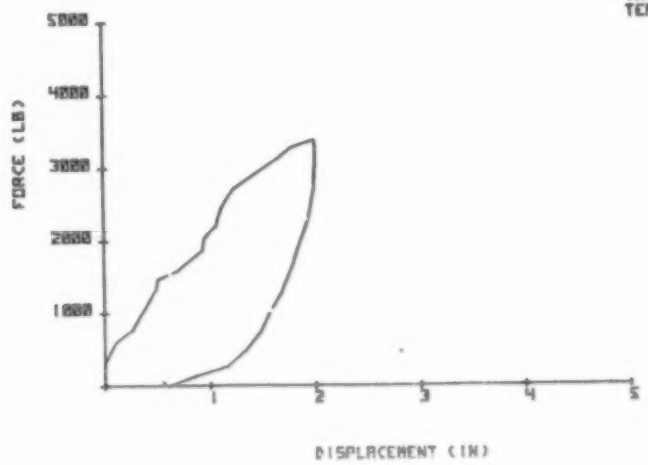

TEST NO 35 ETHAFOAM 400

VELOCITY=14.62 MPH
THICKNESS=5.25 IN
TEMP=71 F

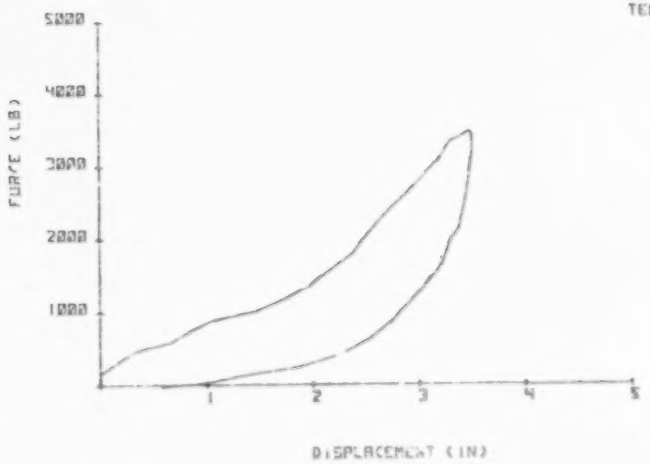

TEST NO. 36 NEOPRENE (JL)

VELOCITY = 14.99 MPH
THICKNESS = 5.3 IN.
TEMP. = 71 F

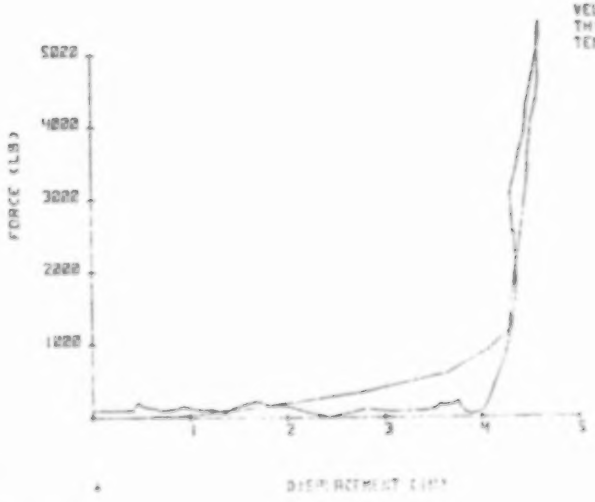

Blank Page

TEST NO.40 RUBATEX R8407-5

TEST NO.42 ETHAFOAM 900

BEST DOCUMENT AVAILABLE

VELOCITY=15.15 MPH
THICKNESS=5.0 IN
TEMP=71 F

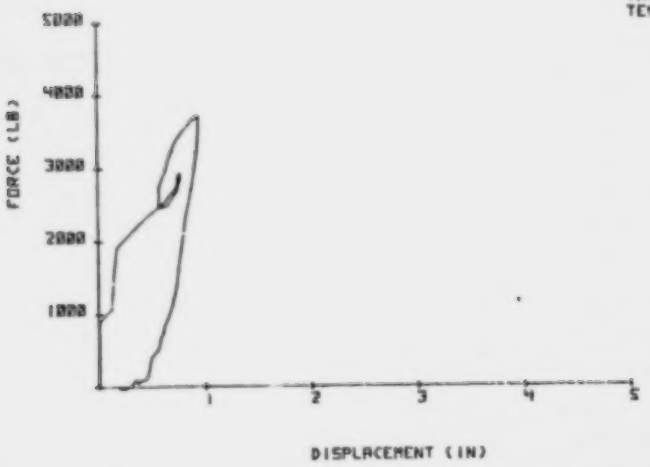

VELOCITY=15.15 MPH
THICKNESS=5.0625 IN
TEMP=71 F

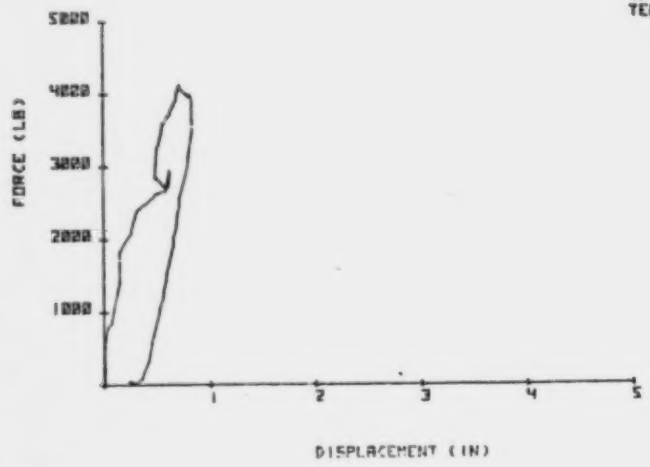

TEST NO.45 ENSOLITE BCR

TEST NO.47 DURAFOAM C 222 A

VELOCITY = 15.25 MPH
THICKNESS = 5.125 IN.
TEMP. = 71 F

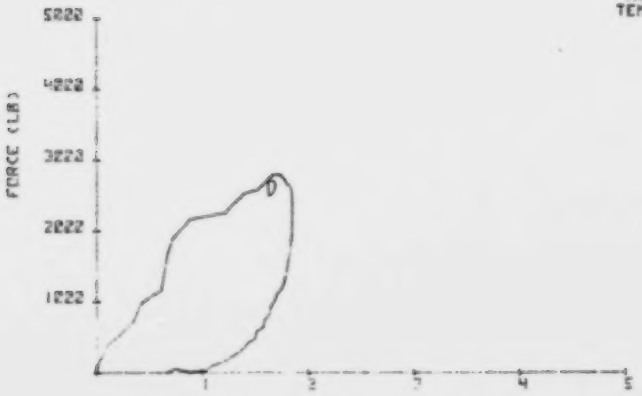

VELOCITY=15.25 MPH
THICKNESS=4.0625 IN
TEMP=70 F

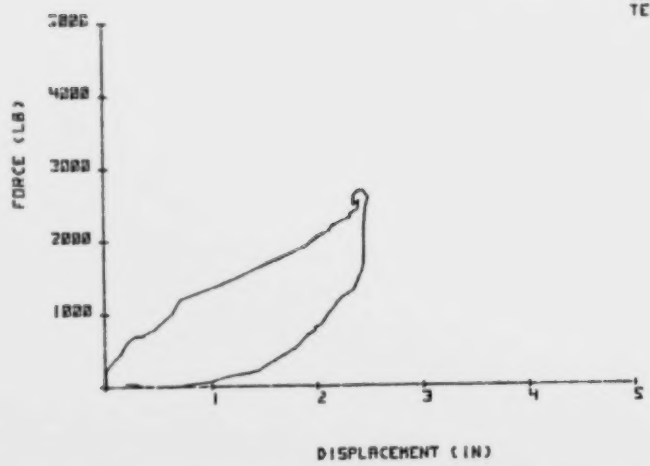

TEST NO.49 DURAFOAM C111A

VELOCITY = 15.25 MPH
THICKNESS = 4.125 IN
TEMP. = 69 F

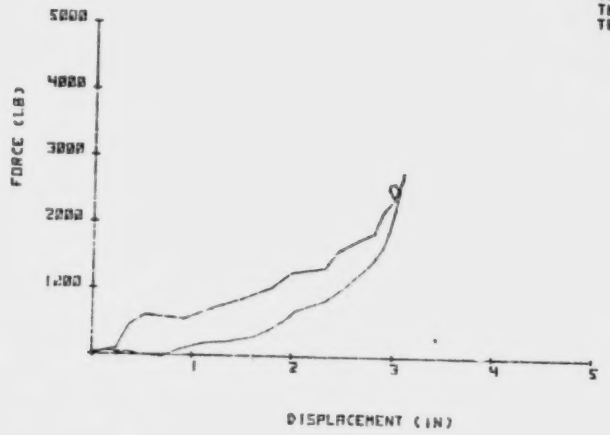

TEST NO.51 DURAFOAM C191XLDS

BEST DOCUMENT AVAILABLE

VELOCITY = 15.32 MPH
THICKNESS = 4.25 IN
TEMP. = 71 F

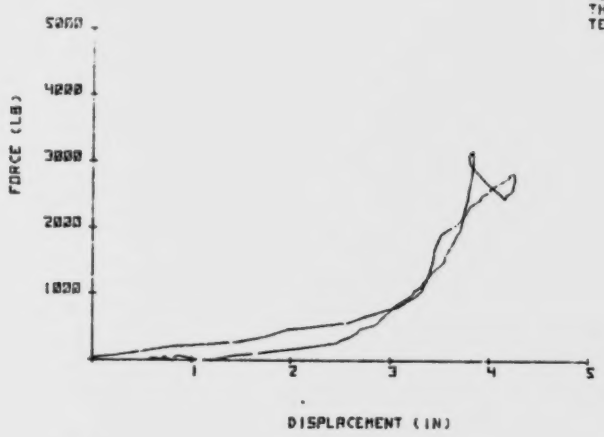

TEST NO.52 DURAFOAM C191LD

VELOCITY = 15.15 MPH
THICKNESS = 4.0625 IN
TEMP. = 71 F

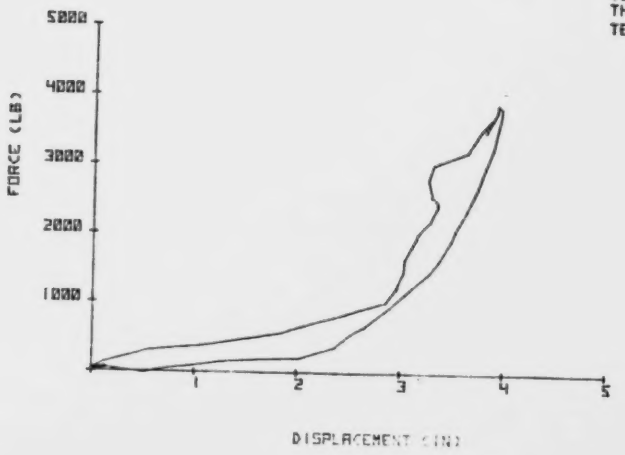

TEST NO.54 FIBERGLAS 4-5 PCT

VELOCITY = 14.97 MPH
THICKNESS = 5.25 IN
TEMP. = 78 F

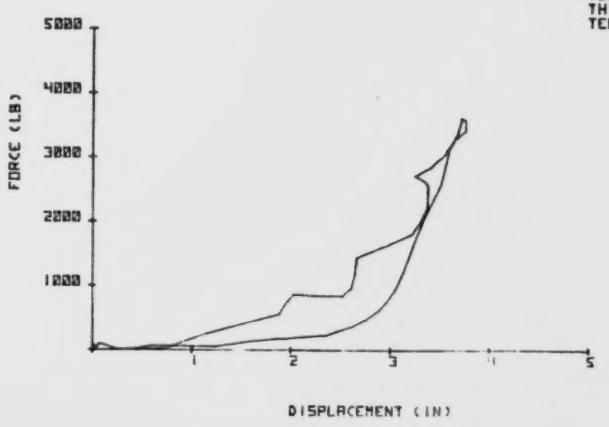

TEST NO.57 FIBERGLAS (D.D.)

VELOCITY = 14.28 MPH
THICKNESS = 4.25 IN
TEMP. = 78 F

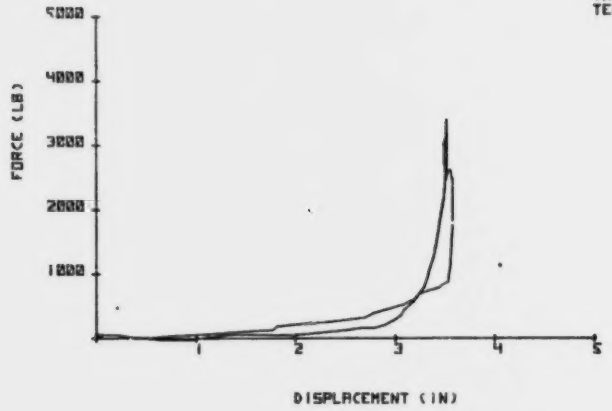

TEST NO.58 FIBERGLAS TYPE L

VELOCITY = 15.25 MPH
THICKNESS = 4.75 IN
TEMP. = 69 F

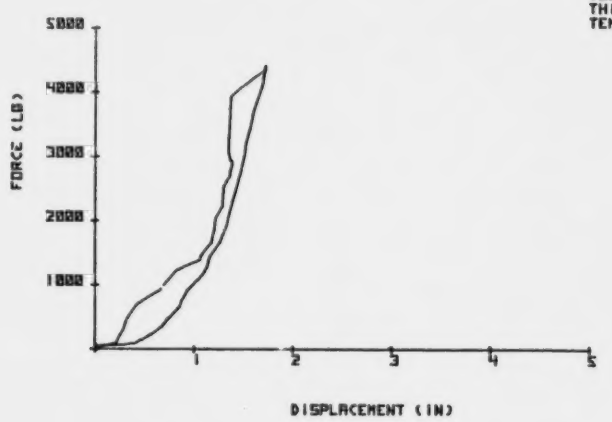

TEST NO.59 FIBERGLAS TYPE Q

VELOCITY = 15.25 MPH
THICKNESS = 4.625 IN
TEMP. = 78 F

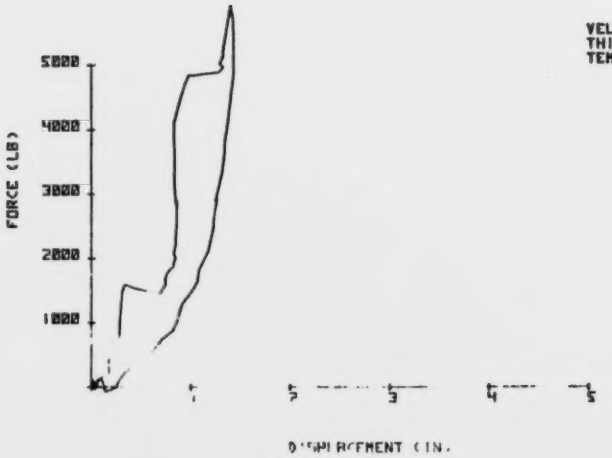

TEST NO.64 ENSOLITE MLC (WHT)

VELOCITY = 14.75 MPH
THICKNESS = 5.5 IN
TEMP. = 78 F

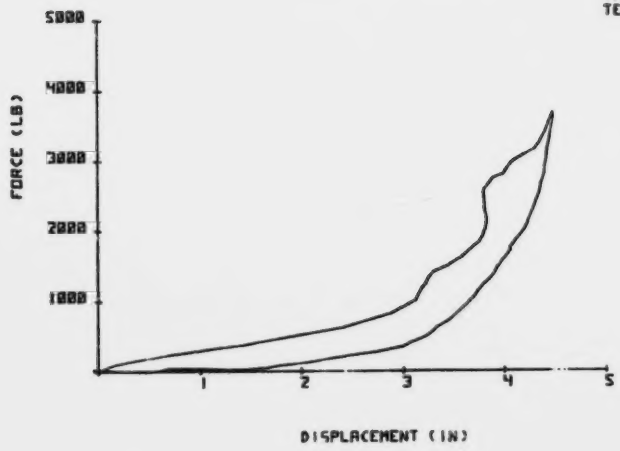

BEST DOCUMENT AVAILABLE

TEST NO.65 ENSOLITE MLC (W-20)

BEST DOCUMENT AVAILABLE

VELOCITY = 14.75 MPH
THICKNESS = 5.5 IN
TEMP. = 70 F

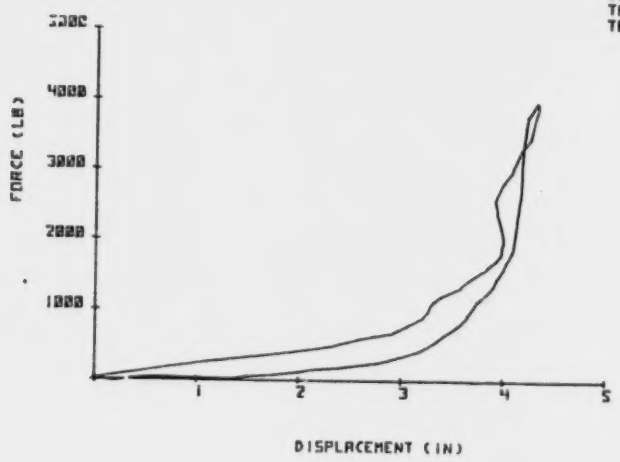

TEST NO.68 ENSOLITE MLC (BLK)

VELOCITY = 14.75 MPH
THICKNESS = 5.25 IN
TEMP. = 67 F

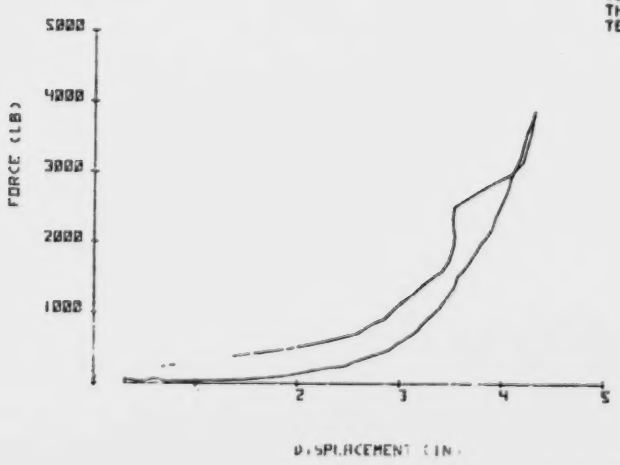

TEST NO.69 ENSOLITE MLC (B-20)

VELOCITY = 15.15 MPH
THICKNESS = 5.25 IN
TEMP. = 66 F

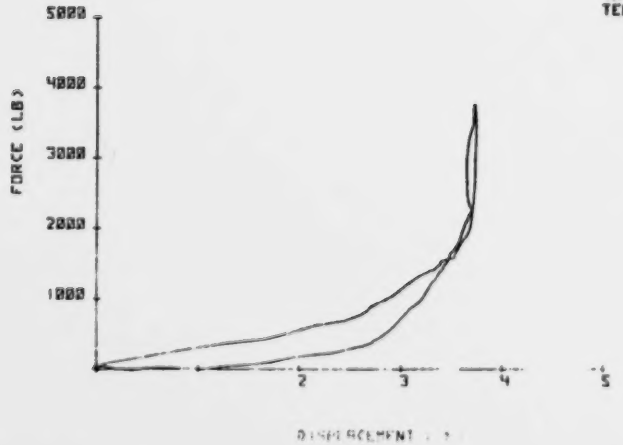

TEST NO.72 ENSOLITE LPC

VELOCITY = 15.37 MPH
THICKNESS = 5.25 IN
TEMP. = 63 F

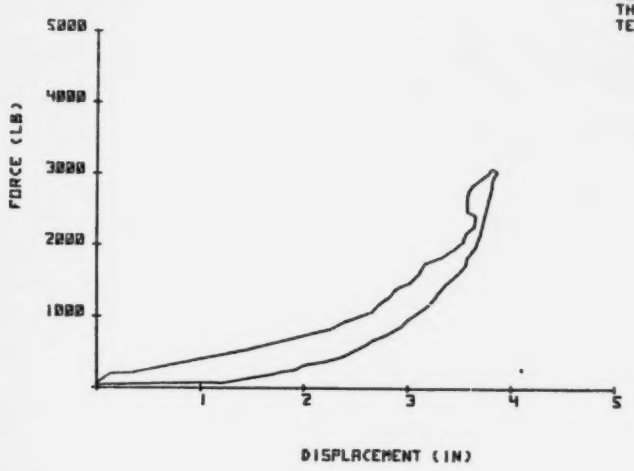

TEST NO.73 ENSOLITE LPC (20)

VELOCITY = 15.25 MPH
THICKNESS = 5.25 IN
TEMP. = 66 F

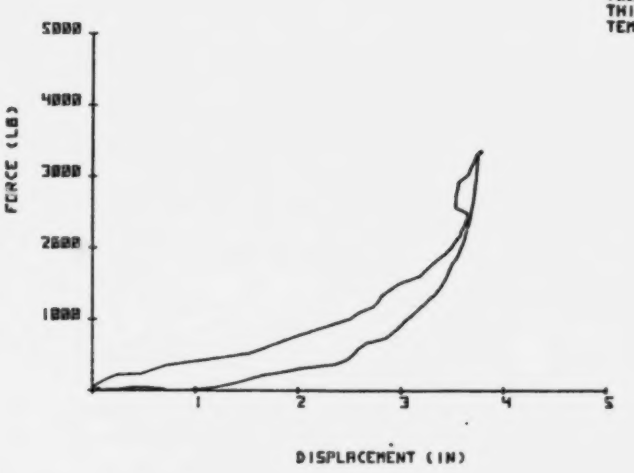

TEST NO.74 ENSOLITE FBC

VELOCITY = 15.25 MPH
THICKNESS = 5.25 IN
TEMP. = 67 F

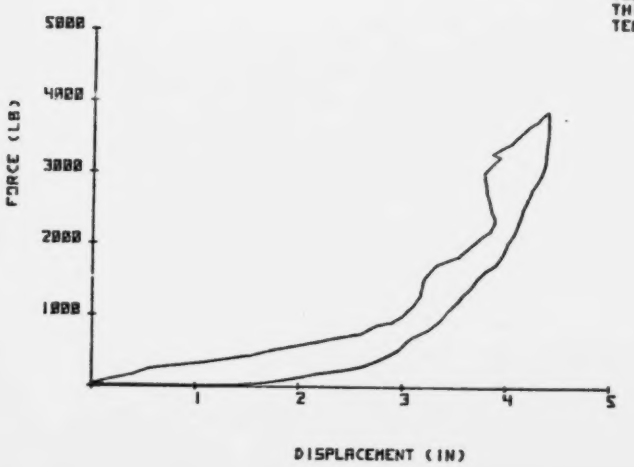

TEST NO.75 ENSOLITE FBC (20)

VELOCITY = 15.25 MPH
THICKNESS = 5.25 IN
TEMP. = 67 F

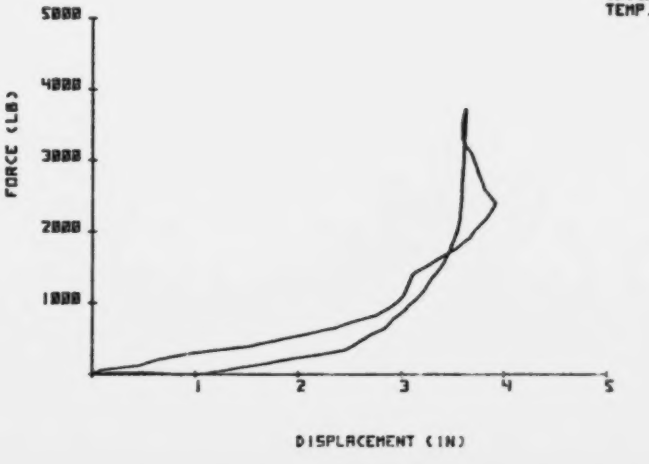

BEST DOCUMENT AVAILABLE

BEST DOCUMENT AVAILABLE

APPENDIX G

Force vs. Deflection Curves for Phase II
Padding Component Tests

BEST DOCUMENT AVAILABLE

Padding Force Deflection Properties

Viewing force deflection curves is an easy way to visualize the efficiency with which the padding uses the available distance to stop the body form. A 100 pound body form traveling at 15 mph has approximately 750 ft/lb of kinetic energy. If a 5 inch padding sample is used, and it is assumed that 4.5 inches of compression are available before the material "bottoms out", then a constant force of about 2000 pounds will be sufficient to stop the mass. Figure G-1, then, shows the ideal padding force deflection curve for the 15 mph, ½ inch test. The peak force is kept to a minimum by maintaining a constant force over the entire distance. Also, the rebound velocity is zero since the force level drops to zero as soon as the deflection level decreases. Important padding factors include both the force level over the distance and the unloading or rebound shape of the curve. Figures G-2 and G-3 show the two extremes of bad force levels. In Figure G-2, the padding is too stiff and in Figure G-3, the padding is too soft and bottoms out. Figure G-4 illustrates a poor rebound characteristic. The body form would rebound at nearly the same speed that it impacted the padding in the case shown in Figure G-4. In any force-deflection curve, the area enclosed by the curve (increasing and decreasing deflection) is the amount of energy dissipated by the padding. The area under the unloading portion of the curve is the energy released back into the impactor, usually in the form of rebound velocity. Figure G-5 is a force deflection curve from one of the thorax experiments. The shaded areas indicate the amount of energy that was stored and the amount that was released back into the body form.

The force vs. deflection properties for the various paddings used in the Phase II mini sled testing are shown in Figures G-6 through G-23.

BEST DOCUMENT AVAILABLE

HYPOTHETICAL CASE IDEAL MATERIAL PROPERTY

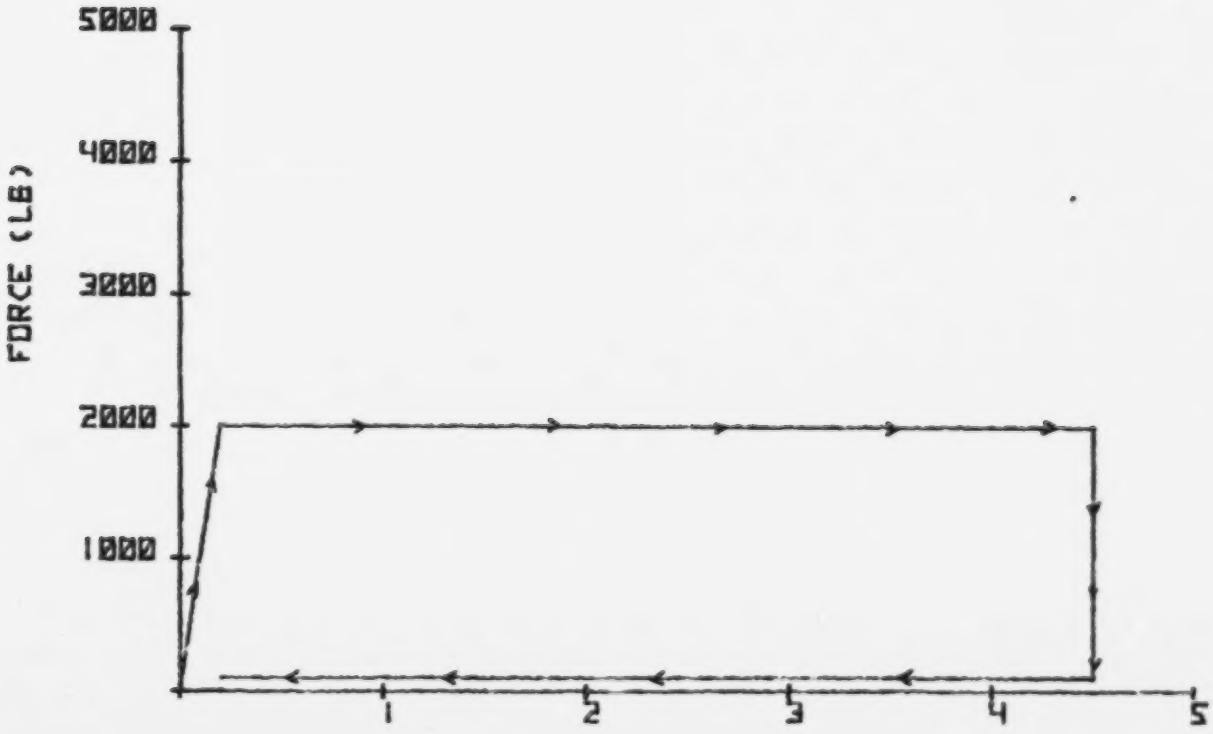

FIGURE G-1

BEST DOCUMENT AVAILABLE

HYPOTHETICAL CASE STIFF MATERIAL

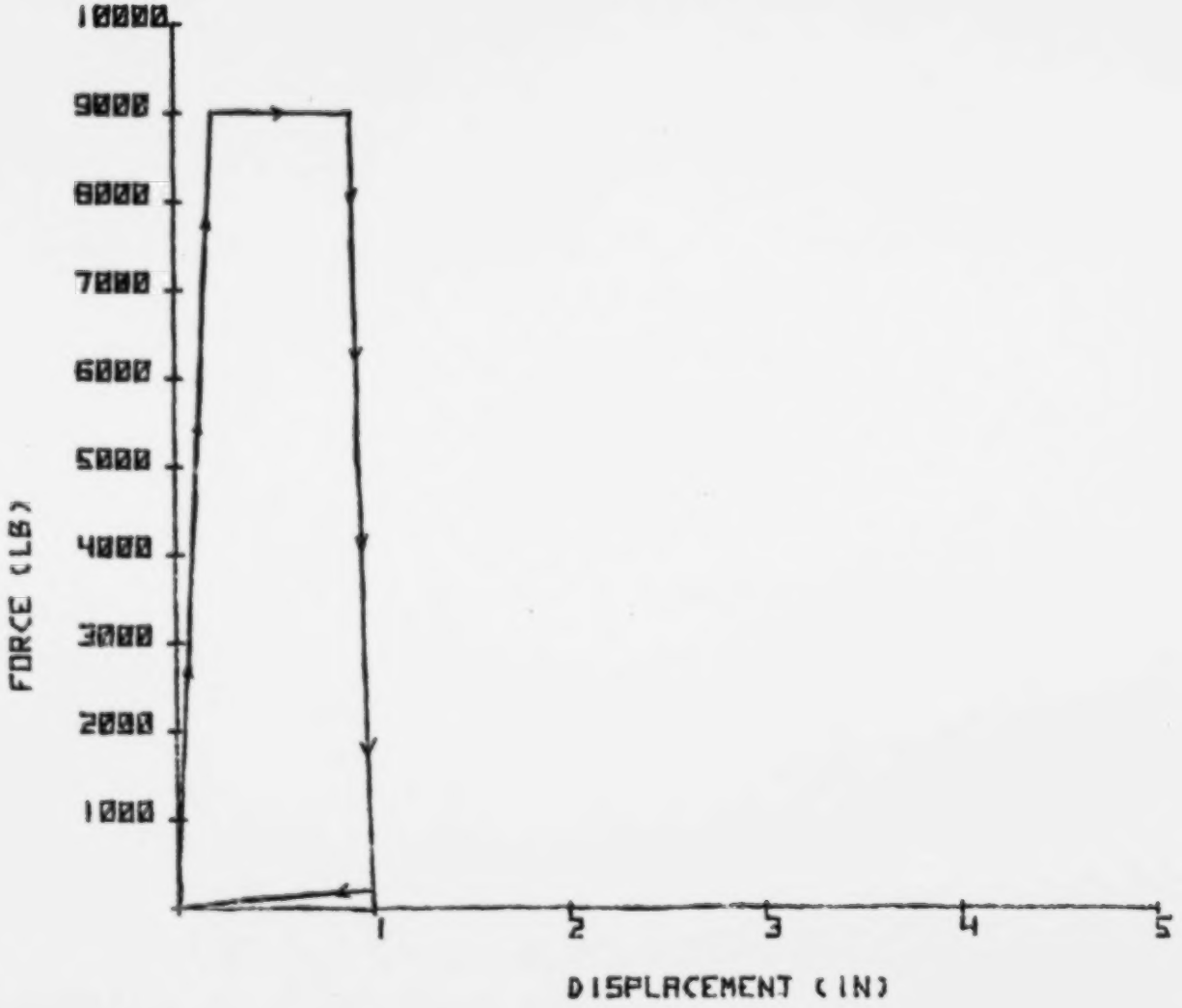

FIGURE G-2

BEST DOCUMENT AVAILABLE

HYPOTHETICAL CASE SOFT MATERIAL

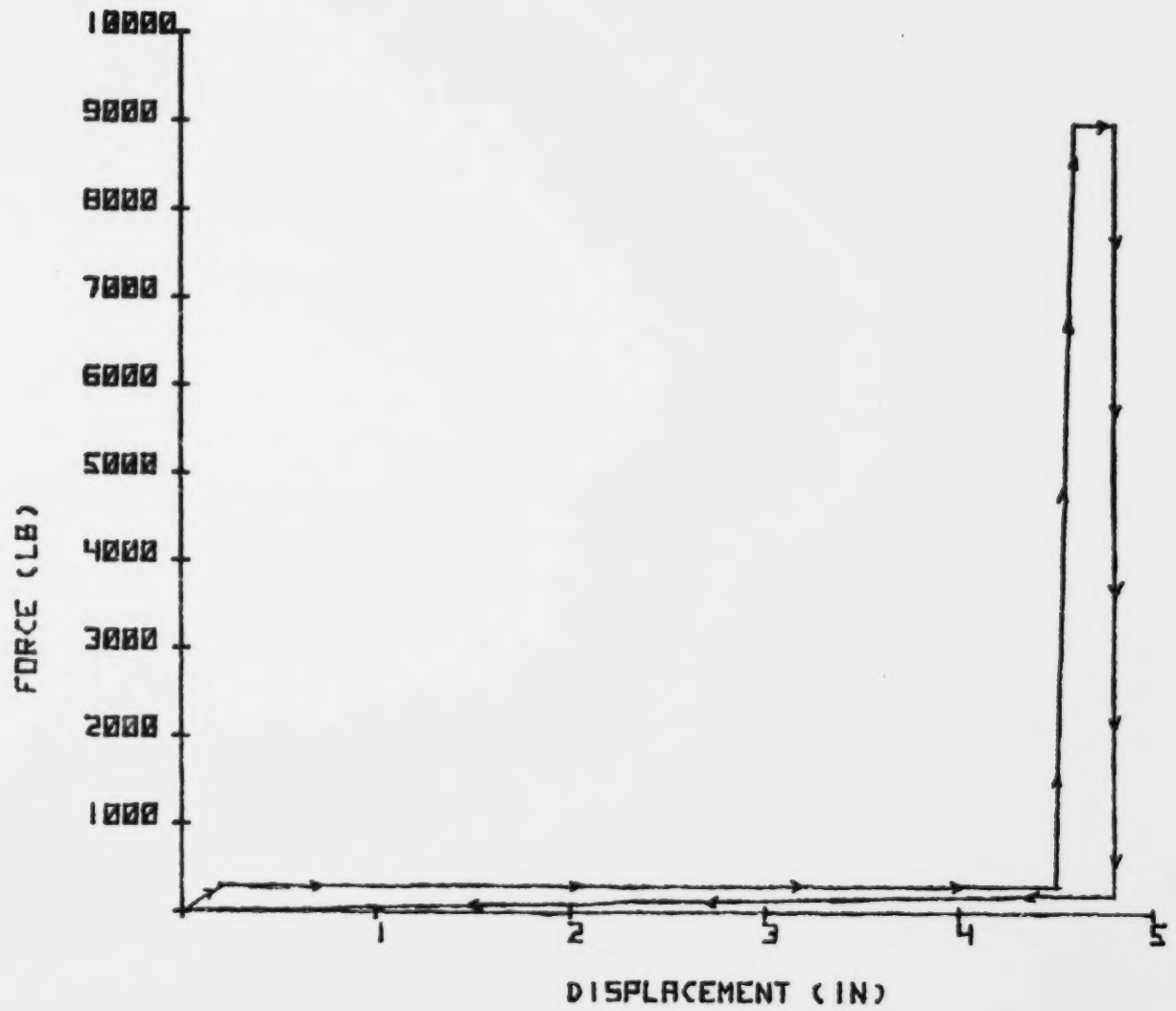

FIGURE C-3

BEST DOCUMENT AVAILABLE

HYPOTHETICAL CASE POOR ENERGY ABSORPTION

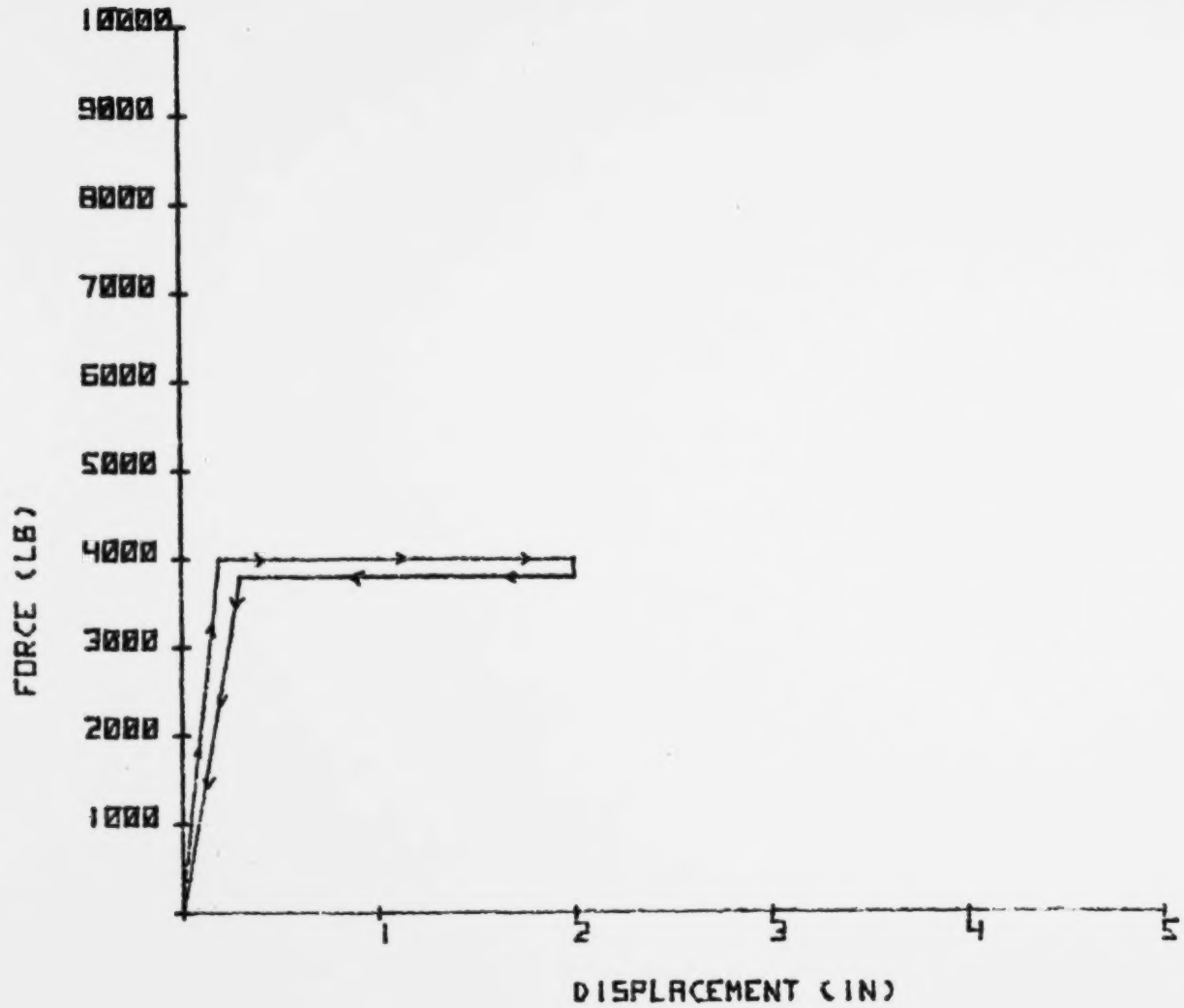

FIGURE G-4

TEST NO.45 ENSOLITE BCR

BEST DOCUMENT AVAILABLE

VELOCITY=15.25 MPH
THICKNESS=5.125 IN
TEMP=71 F

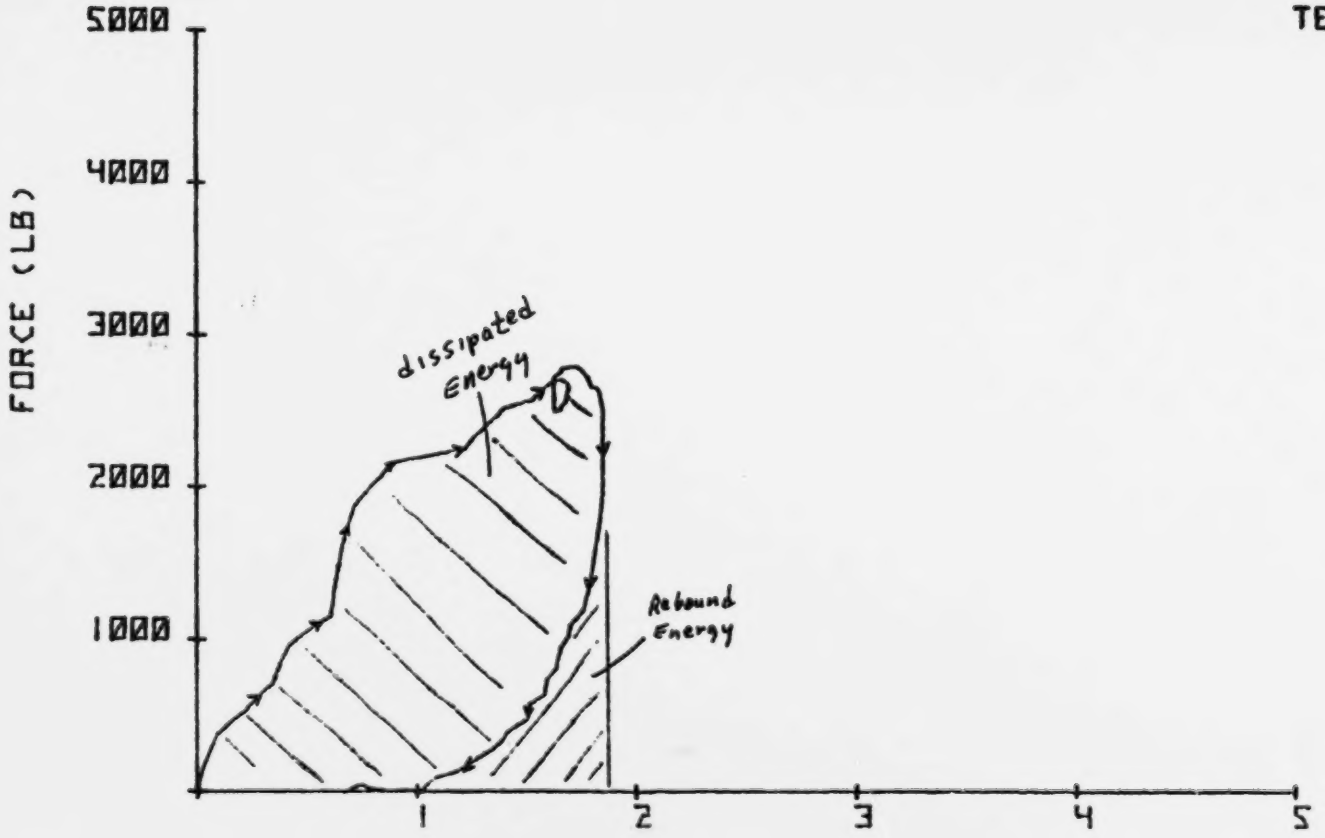

FIGURE G-5

BEST DOCUMENT AVAILABLE

Additional component tests at 15 mph were performed on a new variation of the Fiberglas honeycomb (Test #93) and on Ensolite (Test #96) and Rubatex (Test #95) samples. The purpose of the honeycomb test was to aid the supplier in developing a better configuration. The Ensolite and Rubatex were tested again to investigate the effect of a different bonding material and a long cure time after bonding. The force-deflection curve for the Fiberglas honeycomb is shown in Figure G-24. As can be seen, the force level to collapse the cells is now around 1500 pounds which is an improvement over previous samples. The AIS computed from the "B" parameter of the left upper rib is 2.47.

The force-deflection curves for the Rubatex and Ensolite materials are shown in Figures G-25 and G-26. No substantial benefit in energy absorption was seen by the new bonding material or the long cure time.

BEST DOCUMENT AVAILABLE

TEST NO.93 FIBERGLAS H38C

VELOCITY = 14.82 MPH
THICKNESS = 3.5 IN.
TEMP. = 78 F

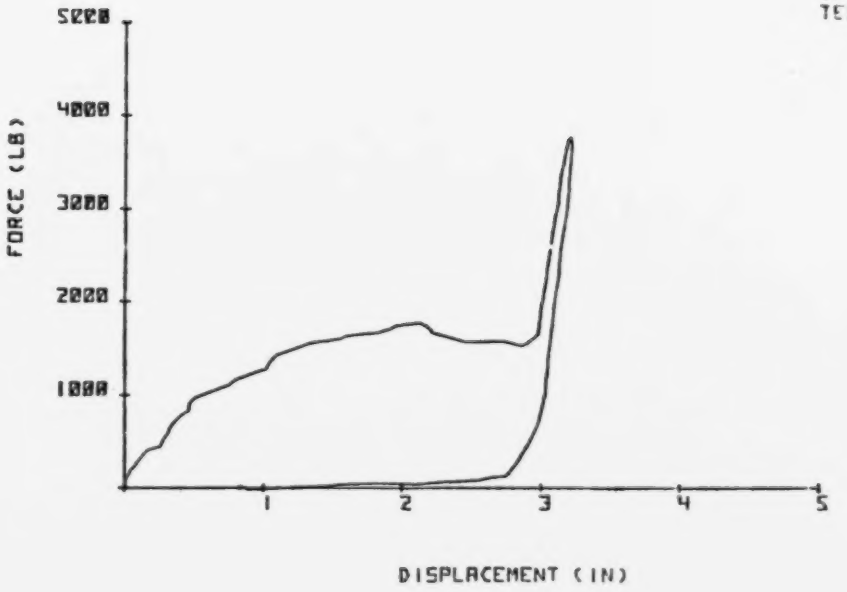

FIGURE G-24

BEST DOCUMENT AVAILABLE

VELOCITY = 14.99 MPH
THICKNESS = 3.0 IN.
TEMP. = 78 F

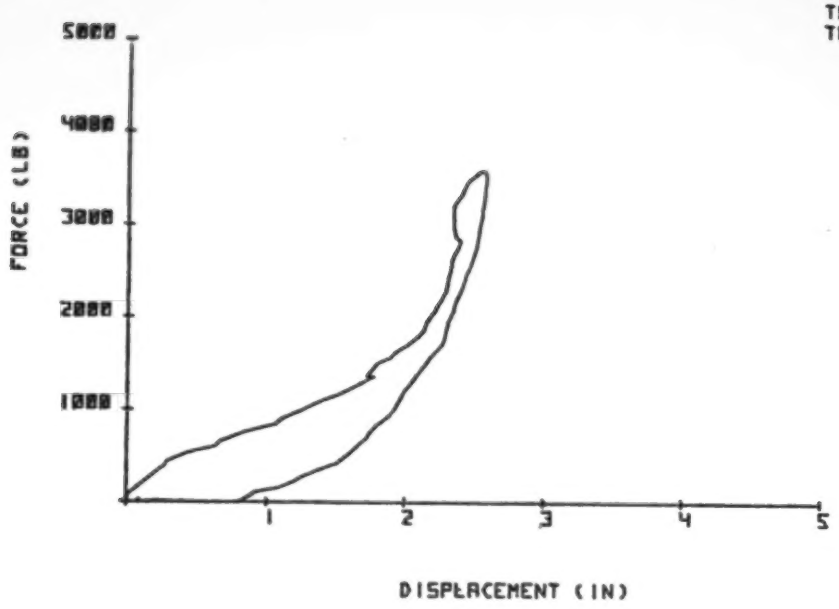

FIGURE G-25

TEST NO.96 ENSOLITE ABC

VELOCITY = 15.25 MPH
THICKNESS = 3.75 IN.
TEMP. = 79 F

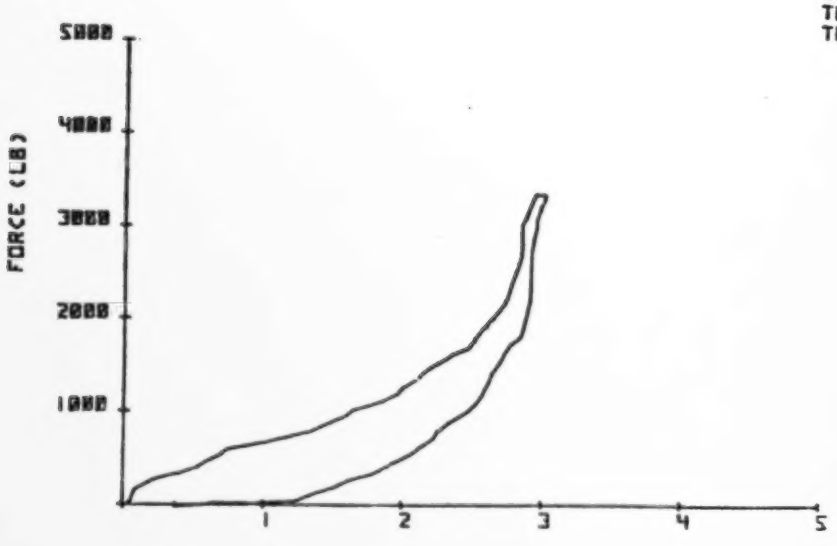

FIGURE G-26

[redacted] 212

BEST DOCUMENT AVAILABLE

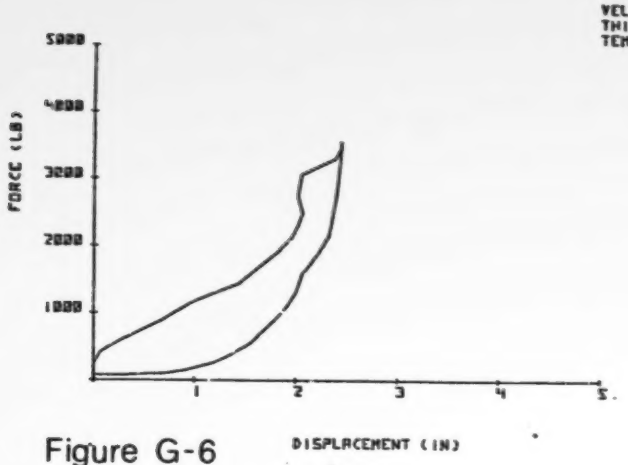

Figure G-6

TEST NO.62 ENSOLITE HCR

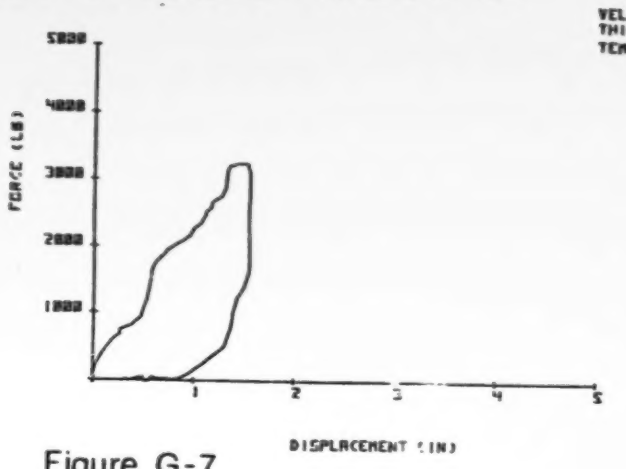

Figure G-7

TEST NO.63 ETHAFOAM 600

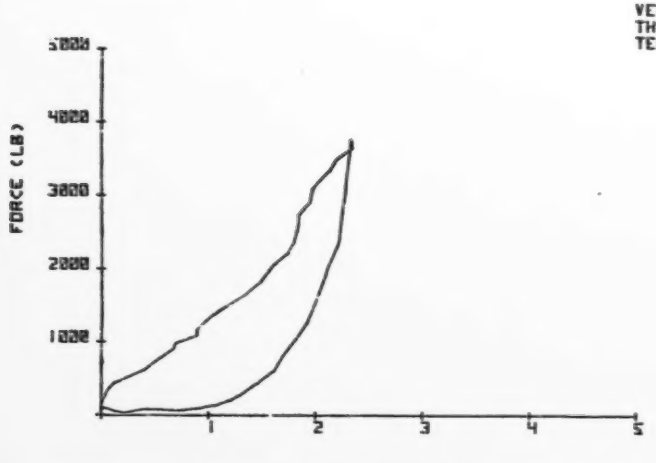

Figure G-8

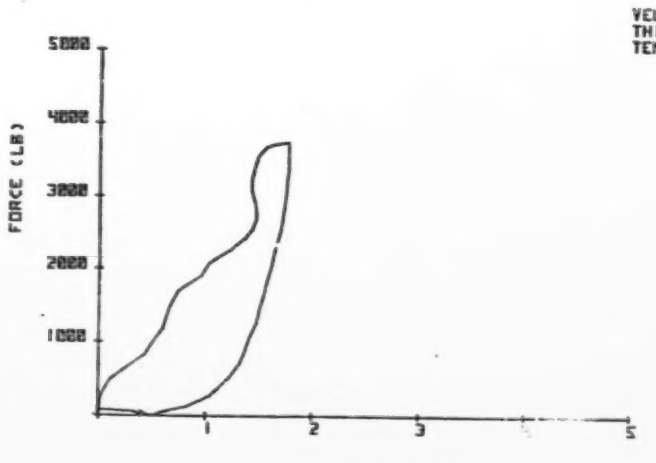

Figure G-9

Blank Page

TEST NO.76 FIBERGLAS H

BEST DOCUMENT AVAILABLE

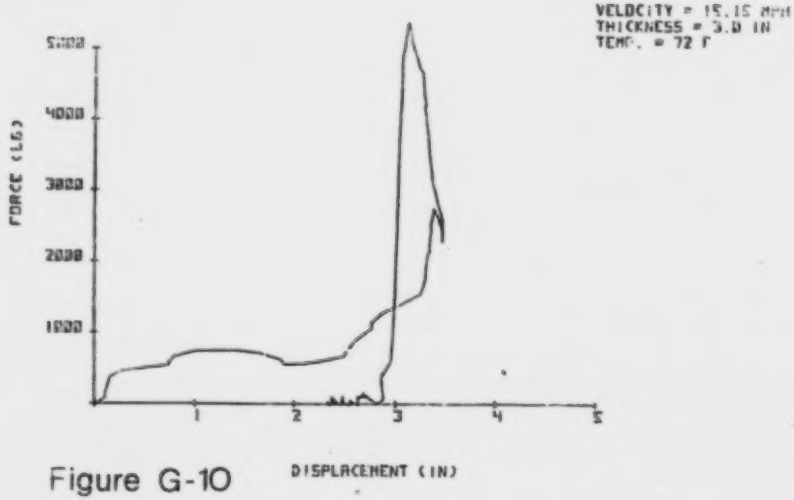

Figure G-10

TEST NO.77 RUBATEX R-318-V

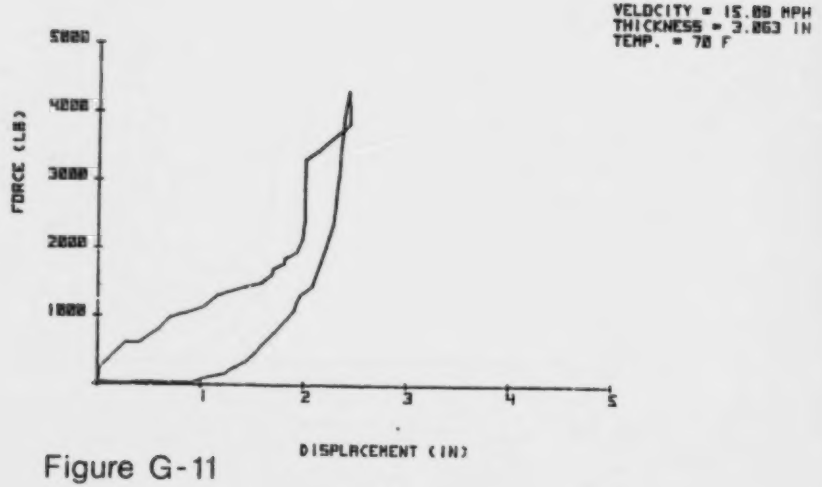

Figure G-11

TEST NO.78 DURAFOAM C111A

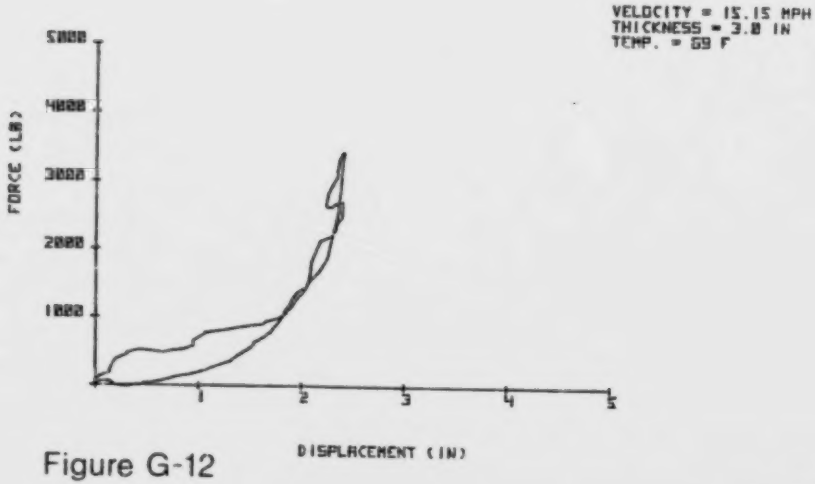

Figure G-12

TEST NO.79 DURAFOAM C222A

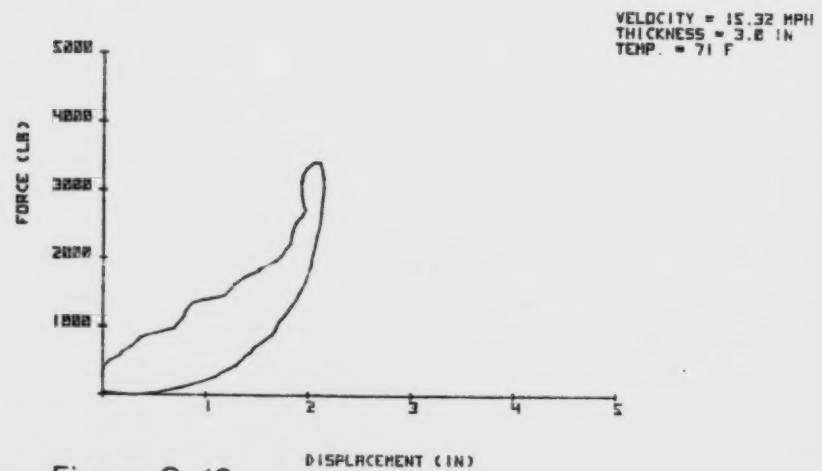

Figure G-13

BEST DOCUMENT AVAILABLE

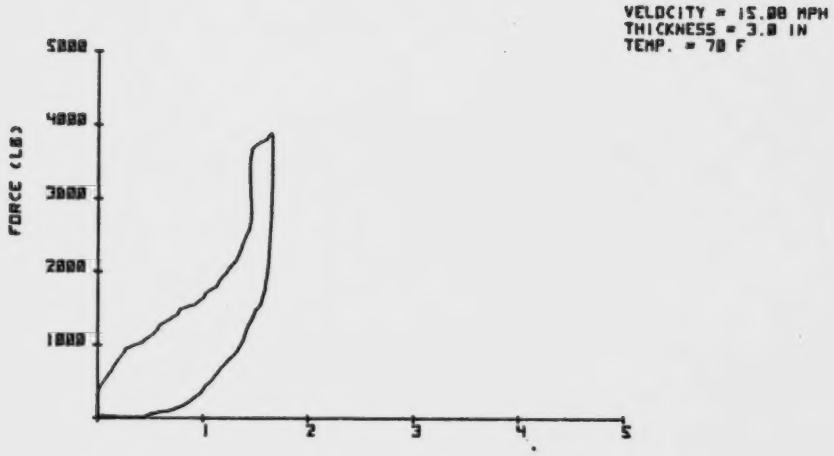

Figure G-14

TEST NO.82 FIBERGLAS HBC

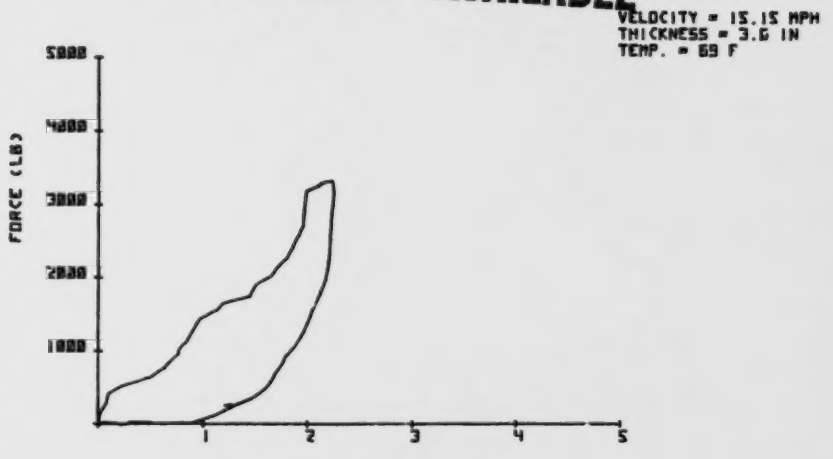

Figure G-15

TEST NO.86 FIBERGLAS HBC

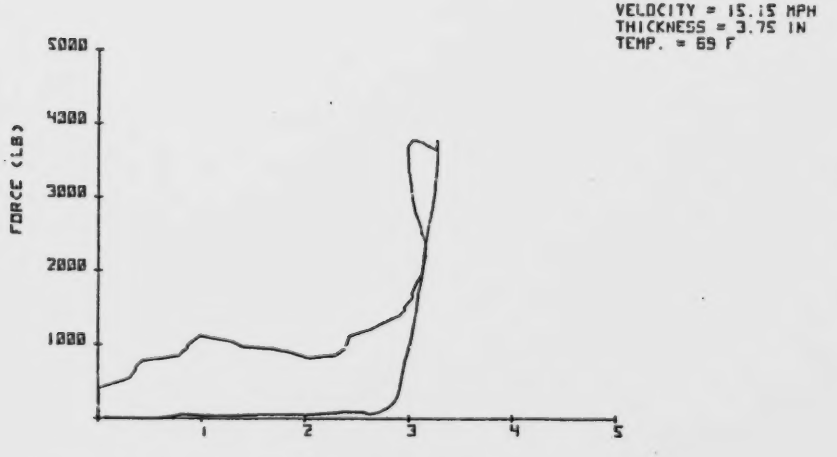

Figure G-16

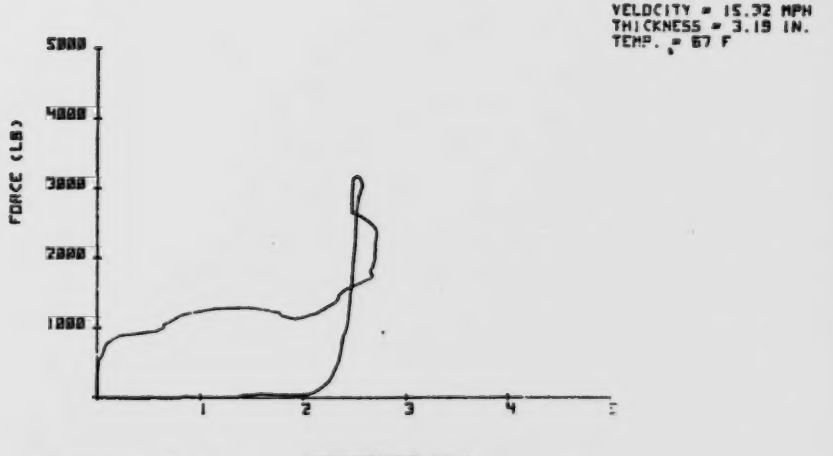

Figure G-17

BEST DOCUMENT AVAILABLE

TEST NO.87 [illegible]

VELOCITY = 15.32 MPH
THICKNESS = 3.8 IN
TEMP = 67 F

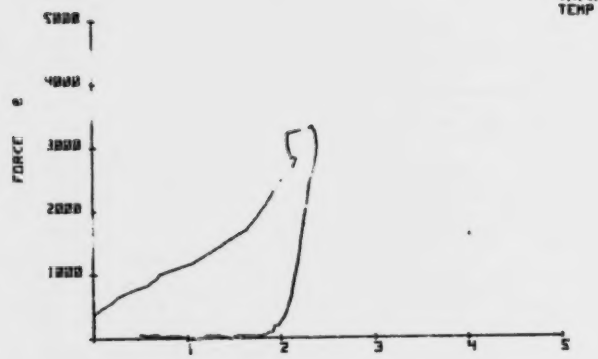

Figure G-18

TEST NO HH GTREM 041101

VELOCITY = 15.15 MPH
THICKNESS = 3.8 IN
TEMP = 69 F

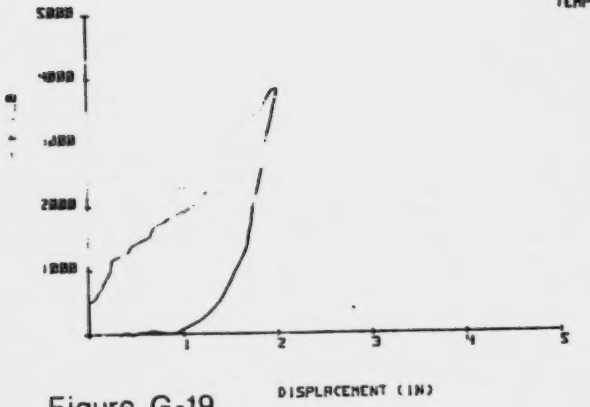

Figure G-19

TEST NO.89 ENSOLITE ABC

VELOCITY = 15.22 MPH
THICKNESS = 3.75 IN.
TEMP. = 65 F

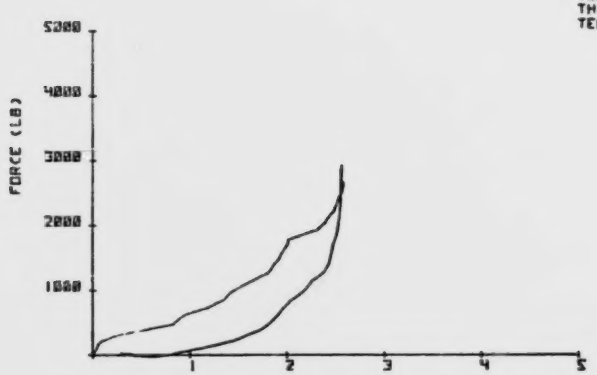

Figure G-20

TEST NO.90 RUBATEX R-310-V

VELOCITY = 15.15 MPH
THICKNESS = 3.19 IN.
TEMP. = 68 F

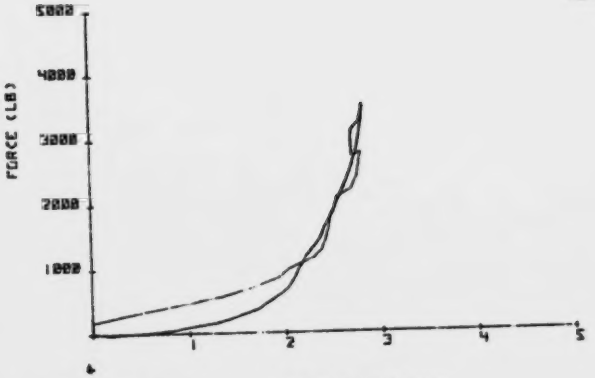

Figure G-21

BEST DOCUMENT AVAILABLE

TEST NO.91 RPR

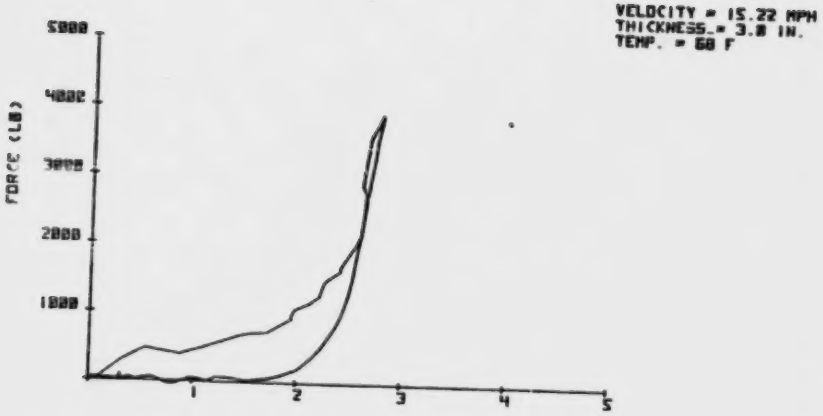

Figure G-22

TEST NO.92 RUBATEX 2VS

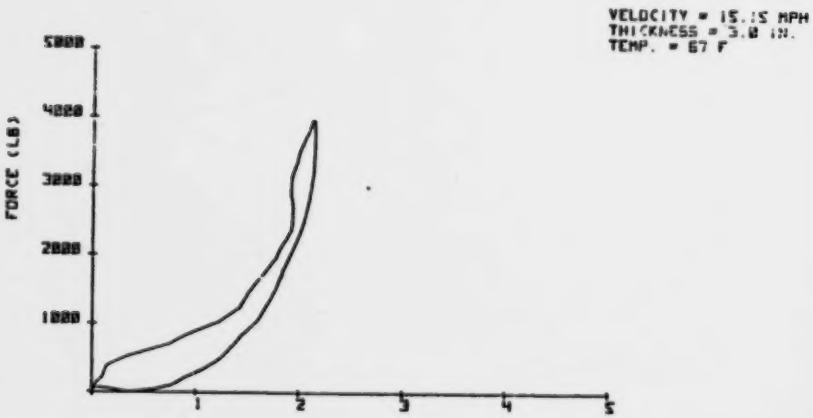

Figure G-23

BEST DOCUMENT AVAILABLE

APPENDIX H

Body Form Responses from HYGE Sled Padding Evaluation Tests

BEST DOCUMENT AVAILABLE

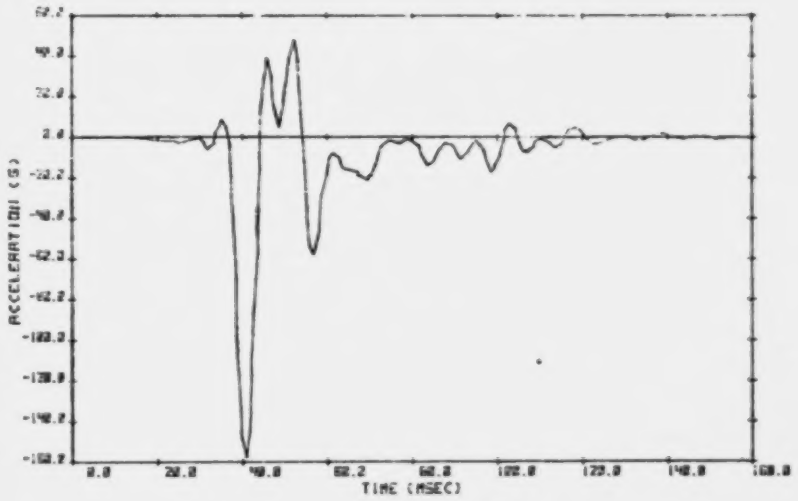

SRL 17-5 TEST #18 - LEFT UPPER RIB

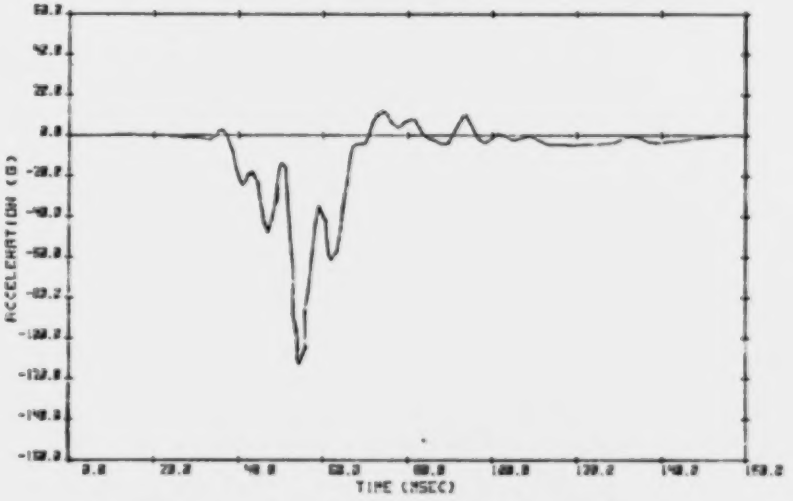

SRL 17-5 TEST #18 - RIGHT UPPER RIB

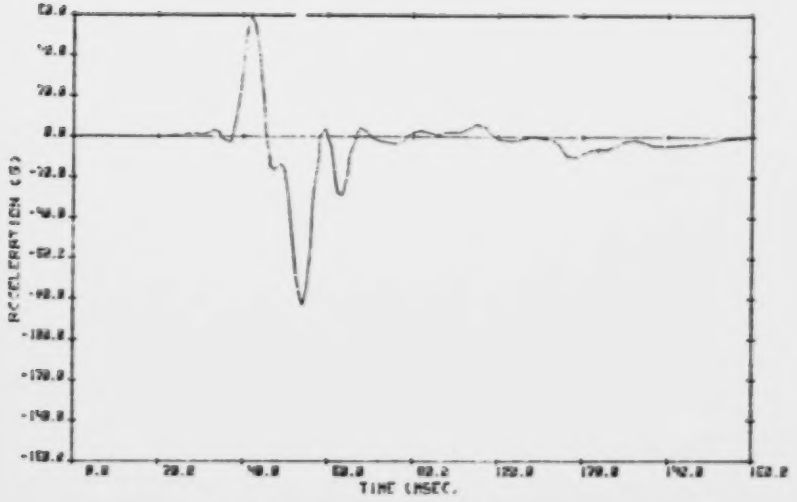

SRL 17-5 TEST #18 - UPPER STERNUM

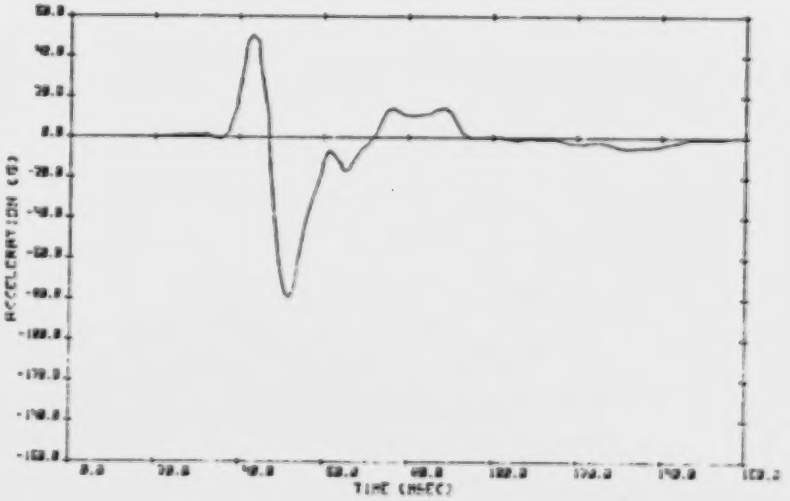

SRL 17-5 TEST #18 - LOWER STERNUM

BEST DOCUMENT AVAILABLE

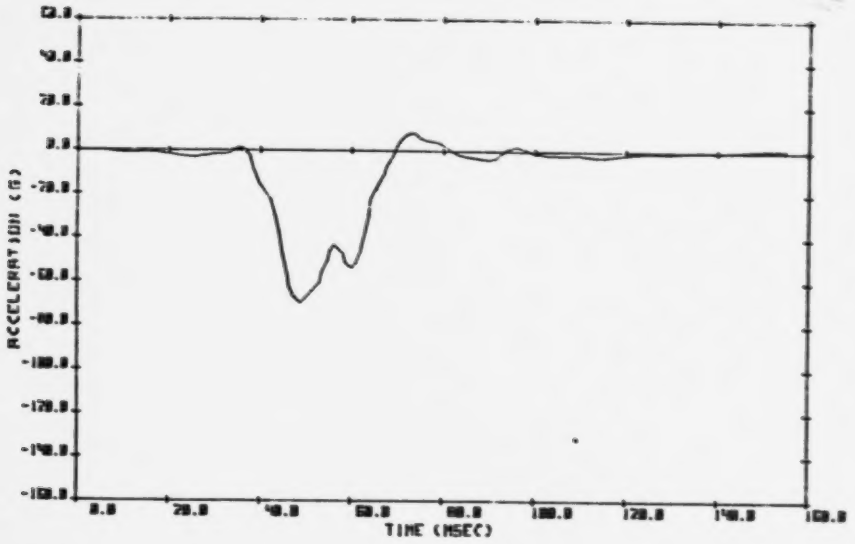

SRL 17-5 TEST #18 - UPPER SPINE

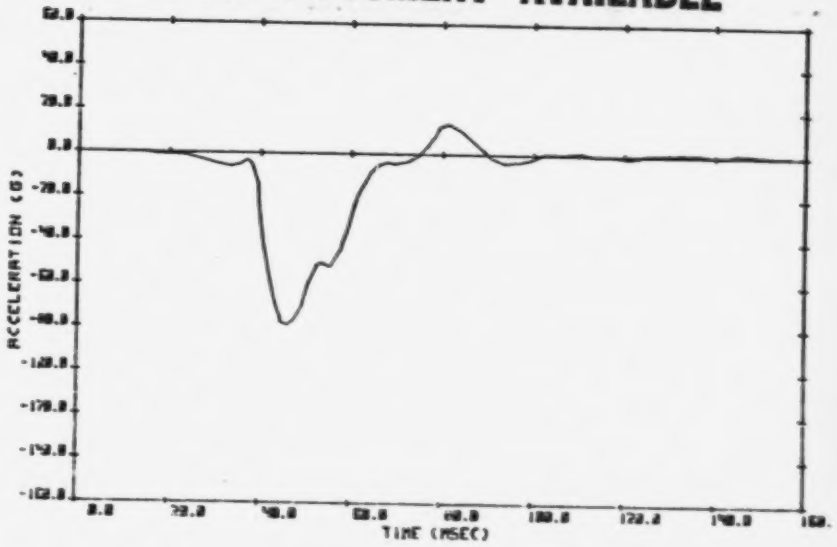

SRL 17-5 TEST #18 - LOWER SPINE

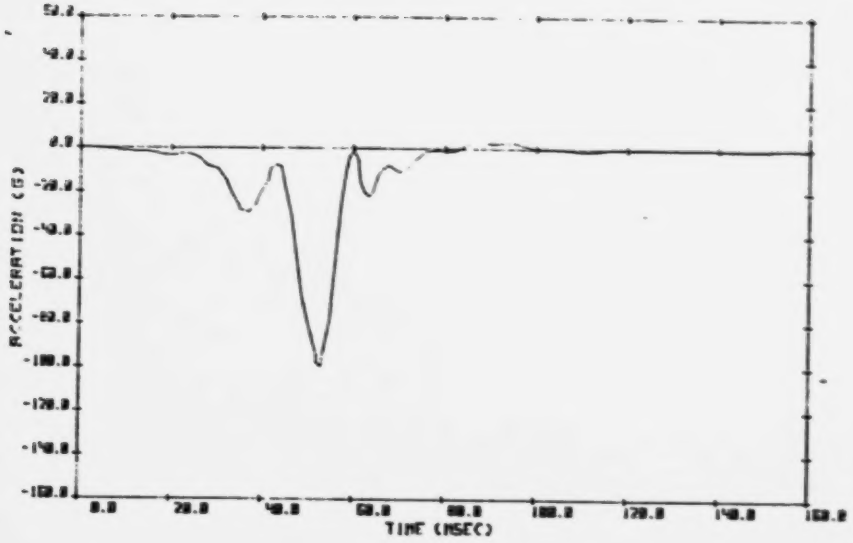

SRL 17-5 TEST #18 - PELVIS

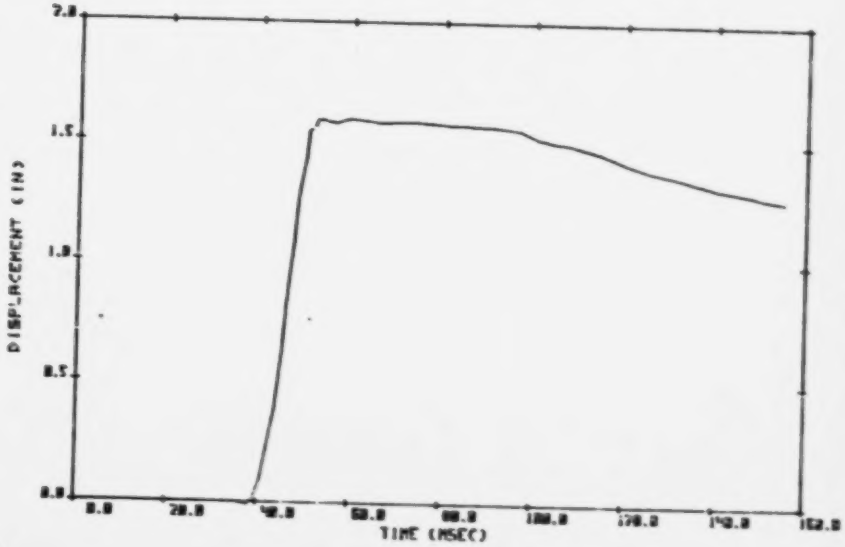

SRL 17-5 TEST #18 - CHEST DEFLECTION

Blank Page

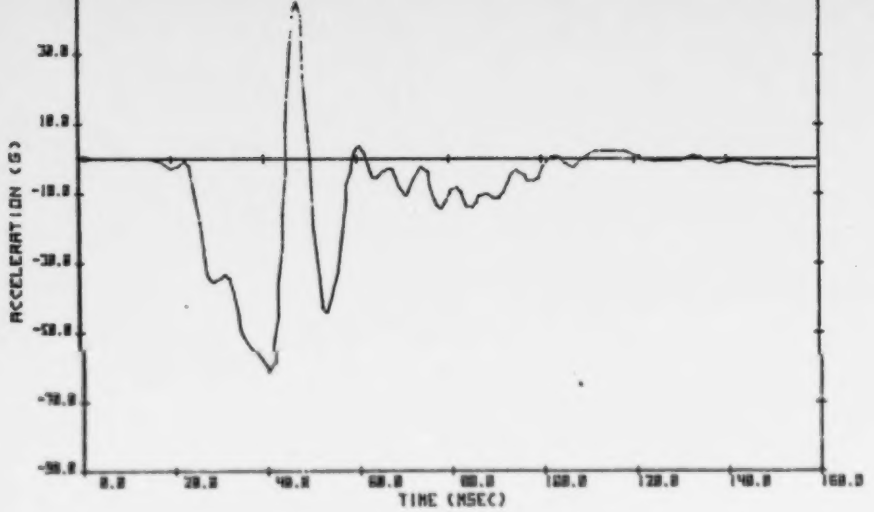

SRL 17-S TEST #19 (ABC) - LEFT UPPER RIB

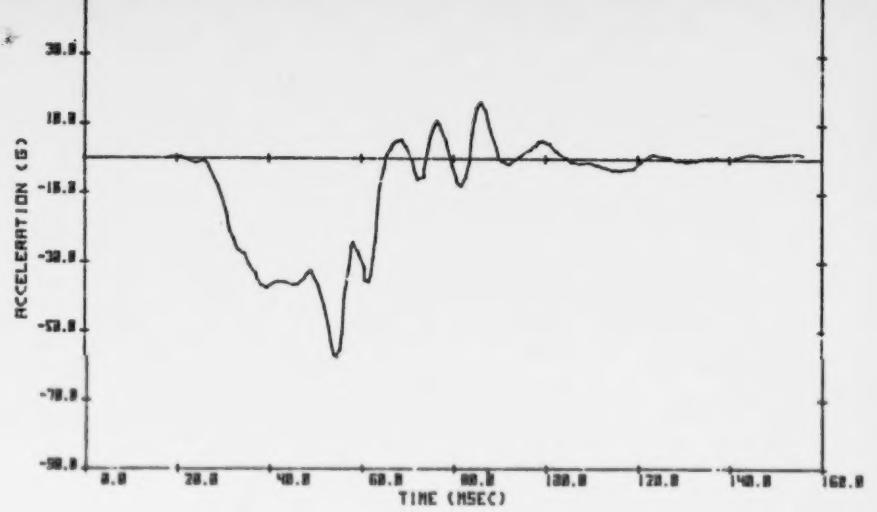

SRL 17-S TEST #19 (ABC) - RIGHT UPPER RIB

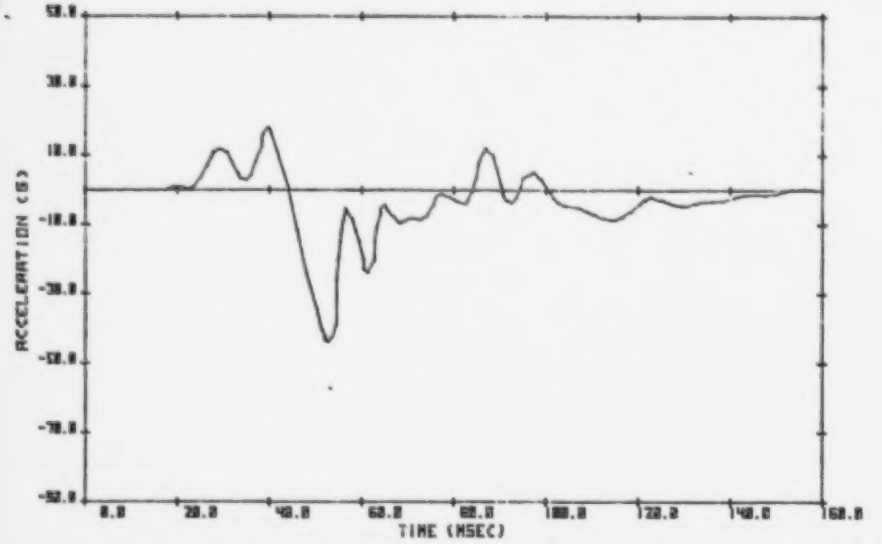

SRL 17-S TEST #19 (ABC) - UPPER STERNUM

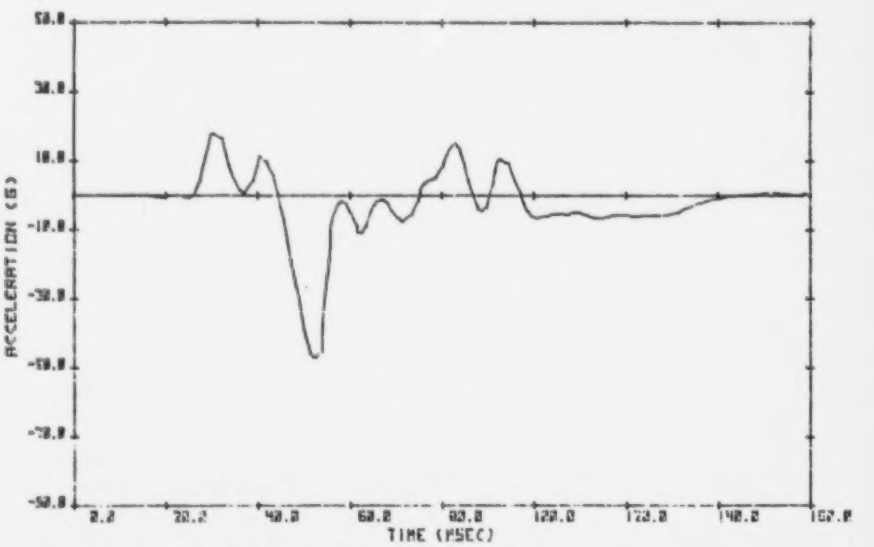

SRL 17-S TEST #19 (ABC) - LOWER STERNUM

[redacted]

221

BEST DOCUMENT AVAILABLE

BEST DOCUMENT AVAILABLE

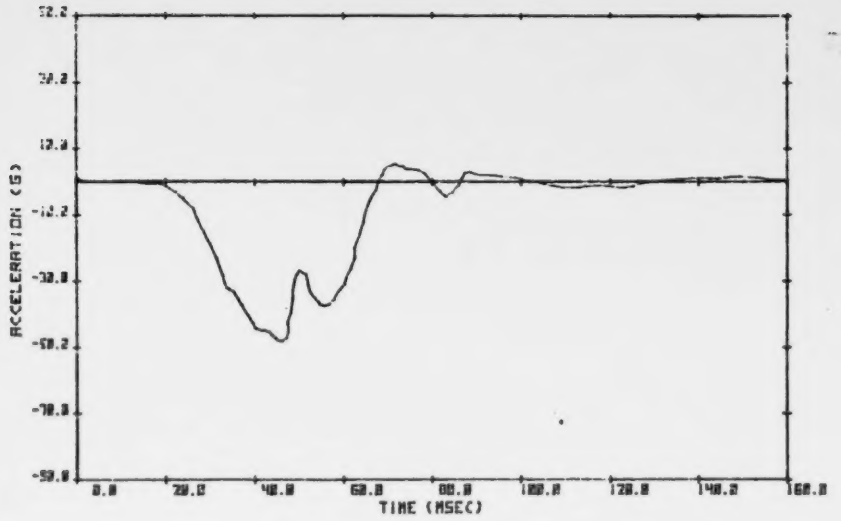

SRL 17-5 TEST #19 (ABC) - UPPER SPINE

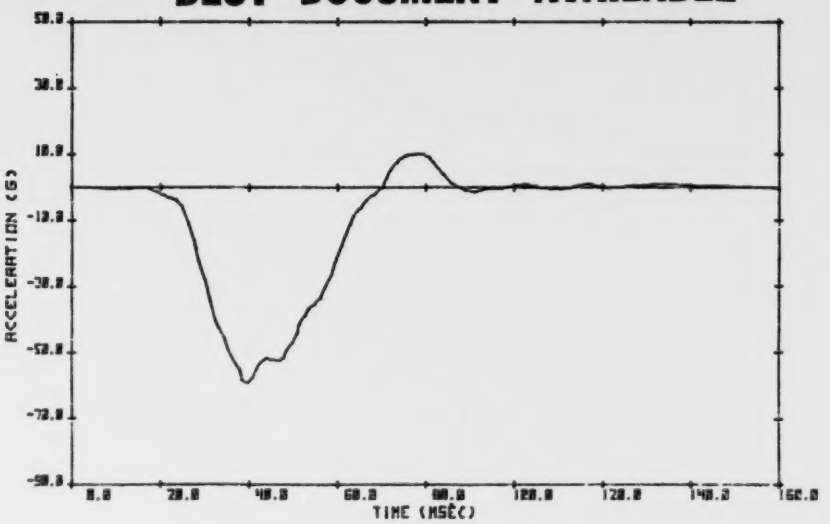

SRL 17-5 TEST #19 (ABC) - LOWER SPINE

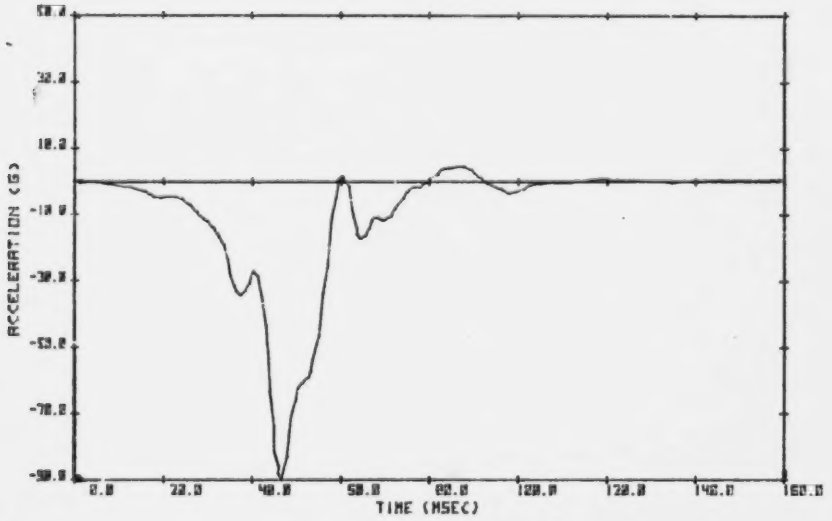

SRL 17-5 TEST #19 (ABC) - PELVIS

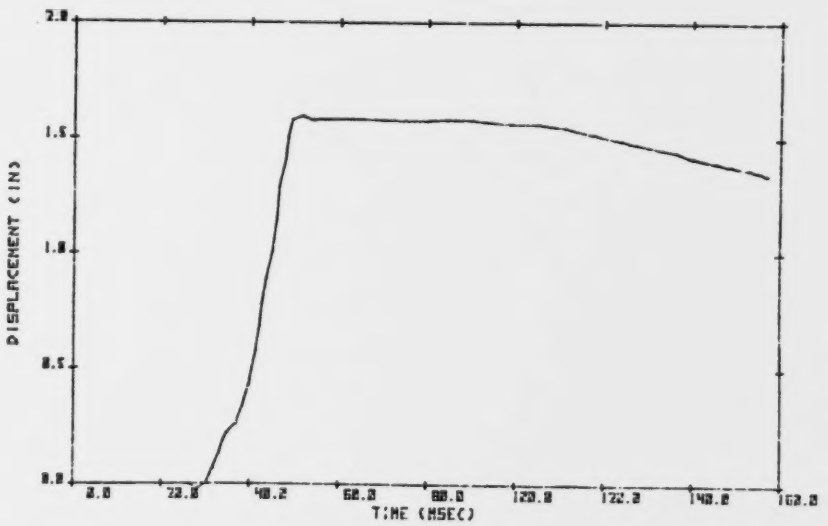

SRL 17-5 TEST #19 (ABC) - CHEST DEFLECTION

BEST DOCUMENT AVAILABLE

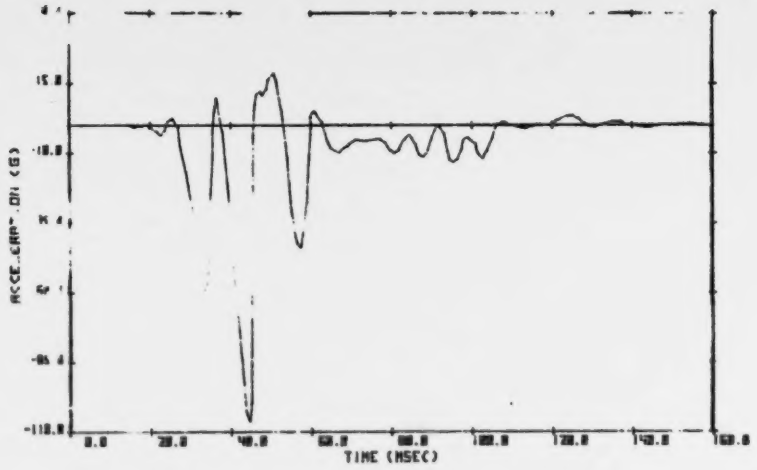

SRL 17-S TEST #20 (H2BC) - LEFT UPPER RIB

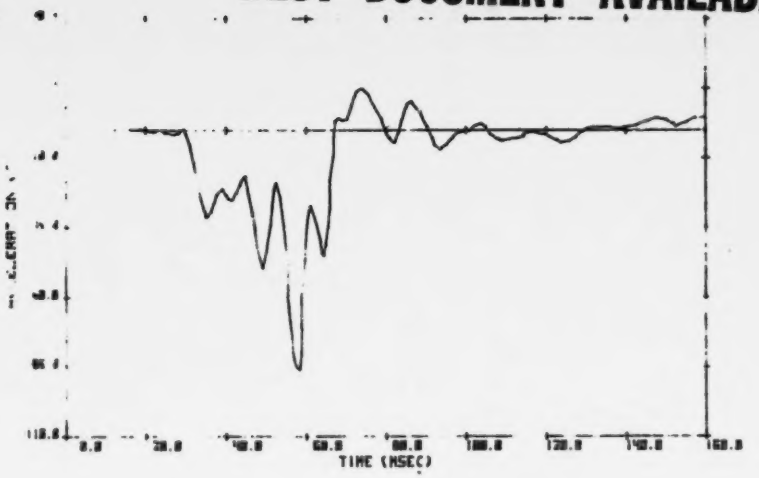

SRL 17-S TEST #20 (H2BC) - RIGHT UPPER RIB

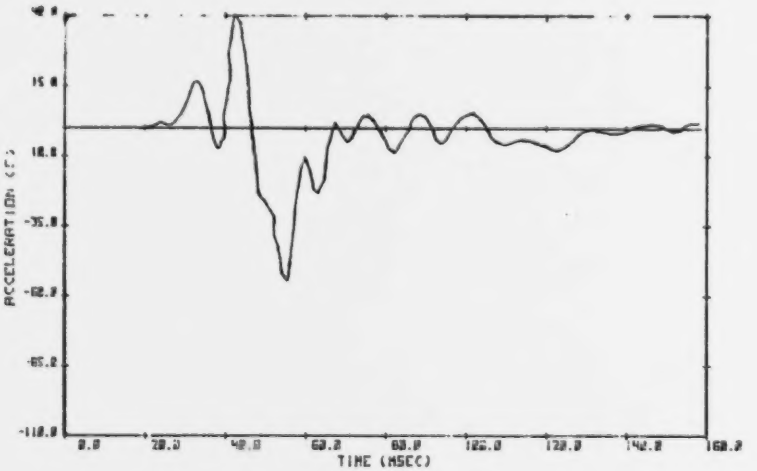

SRL 17-S TEST #20 (H2BC) - UPPER STERNUM

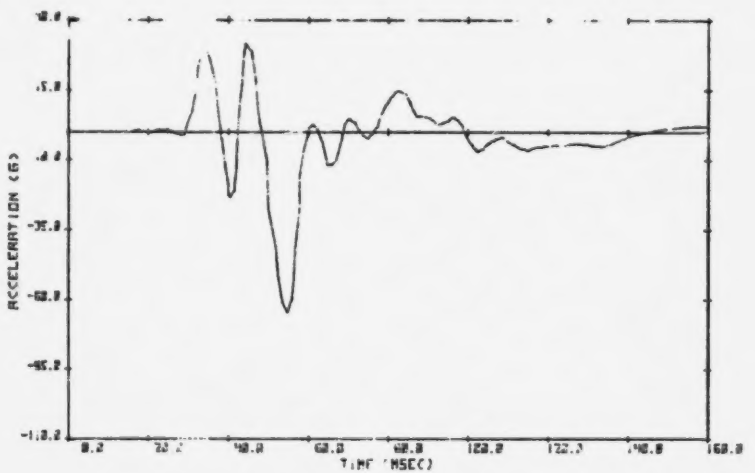

SRL 17-S TEST #20 (H2BC) LOWER STERNUM

BEST DOCUMENT AVAILABLE

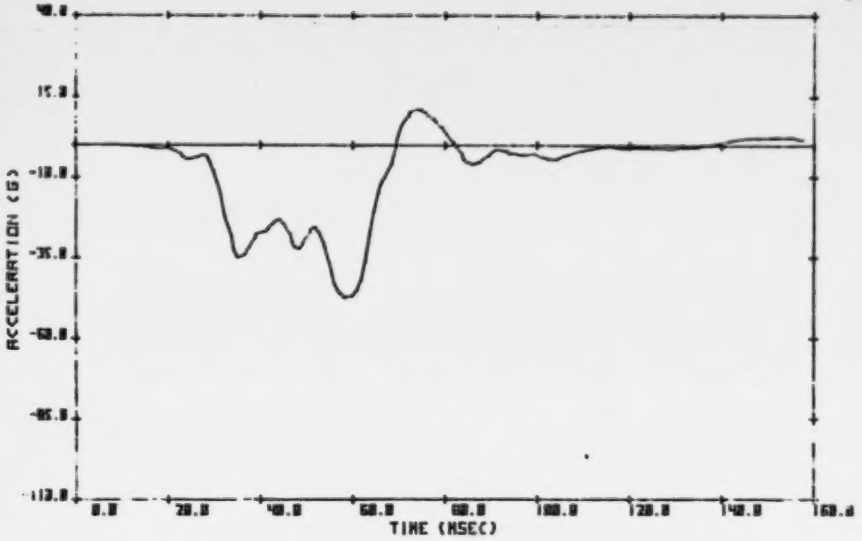

SRL 17-S TEST #20 (H2BC) - UPPER SPINE

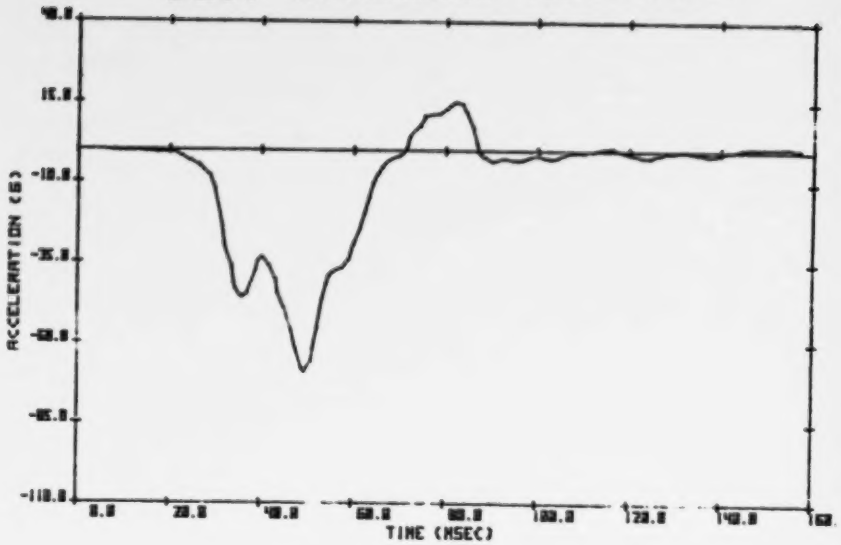

SRL 17-S TEST #20 (H2BC) - LOWER SPINE

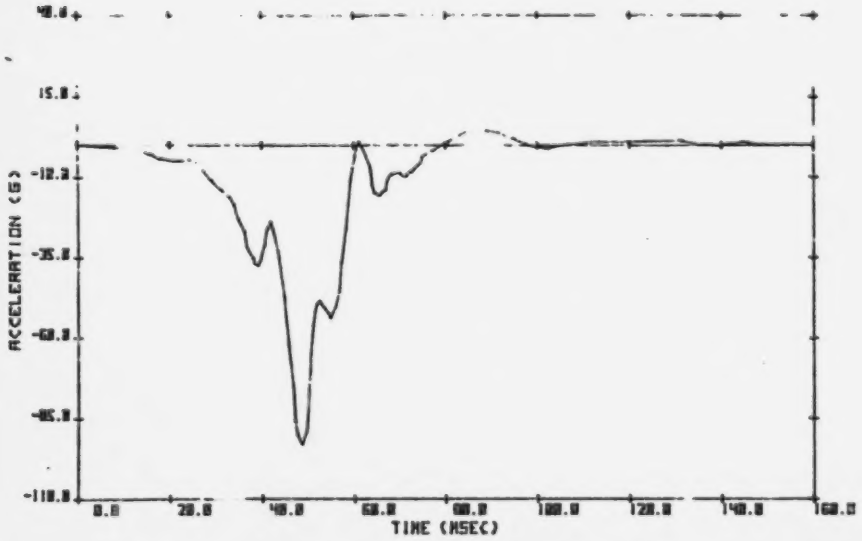

SRL 17-S TEST #20 (H2BC) - PELVIS

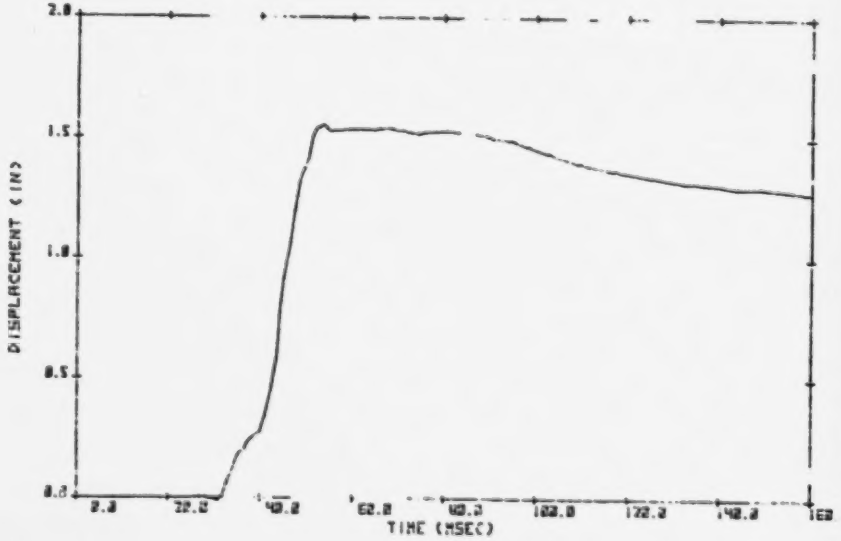

SRL 17-S TEST #20 (H2BC) - CHEST DEFLECTION

BEST DOCUMENT AVAILABLE

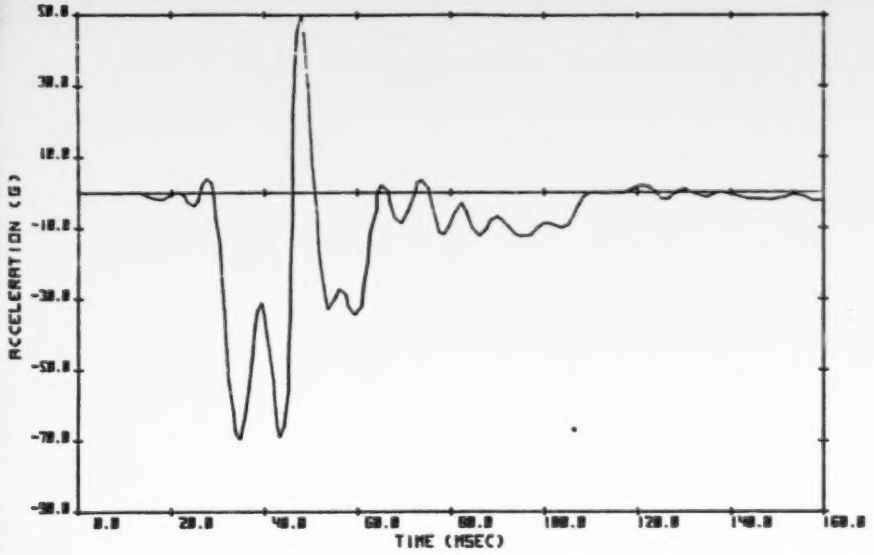

SRL 17-5 TEST #21 (GTREM) - LEFT UPPER RIB

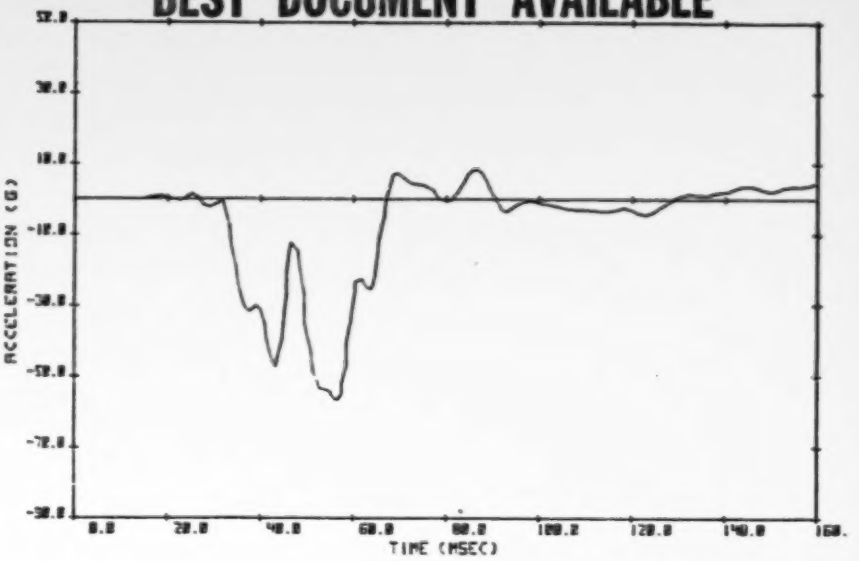

SRL 17-5 TEST #21 (GTREM) - RIGHT UPPER RIB

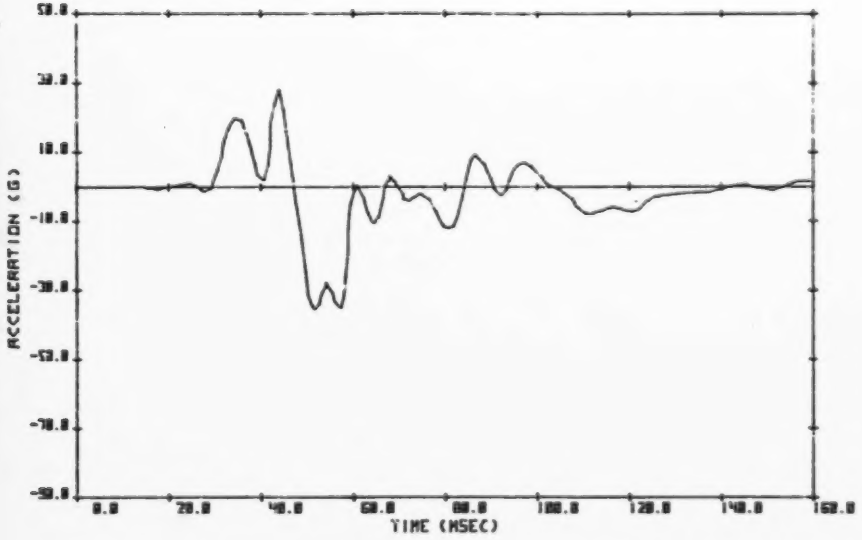

SRL 17-5 TEST #21 (GTREM) - UPPER STERNUM

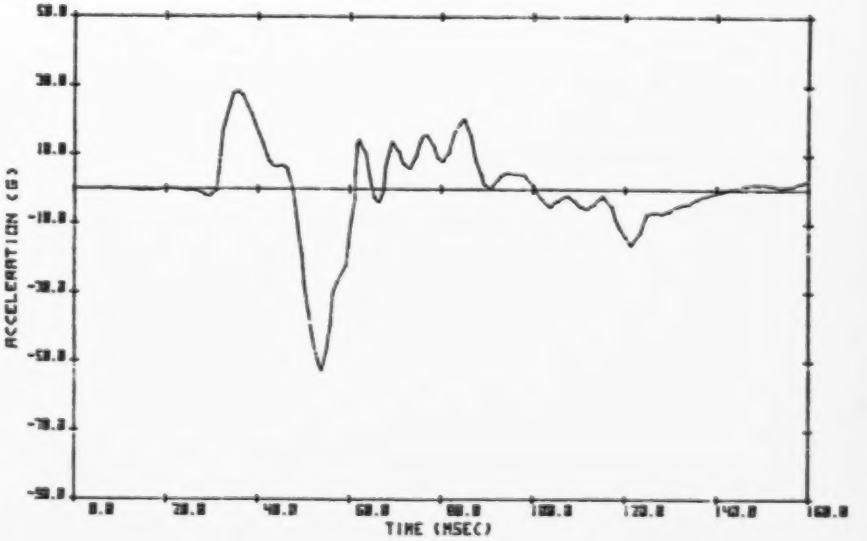

SRL 17-5 TEST #21 (GTREM) - LOWER STERNUM

BEST DOCUMENT AVAILABLE

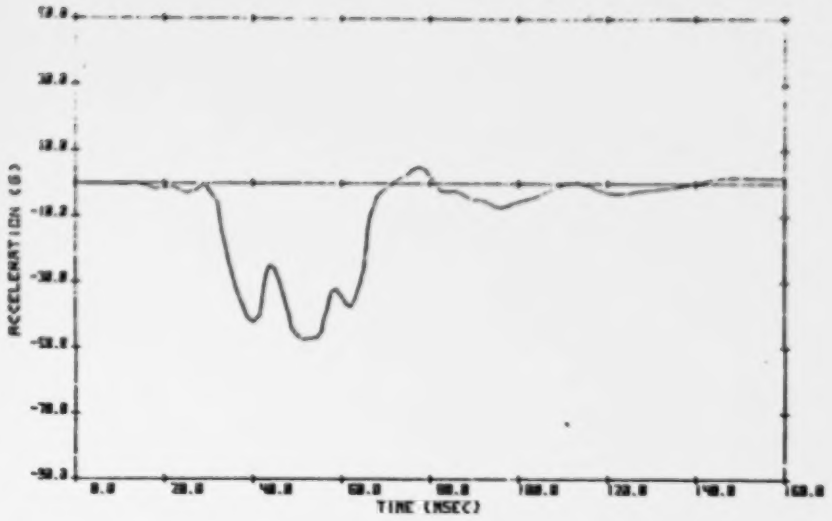

SRL 17-S TEST #21 (GTREM) - UPPER SPINE

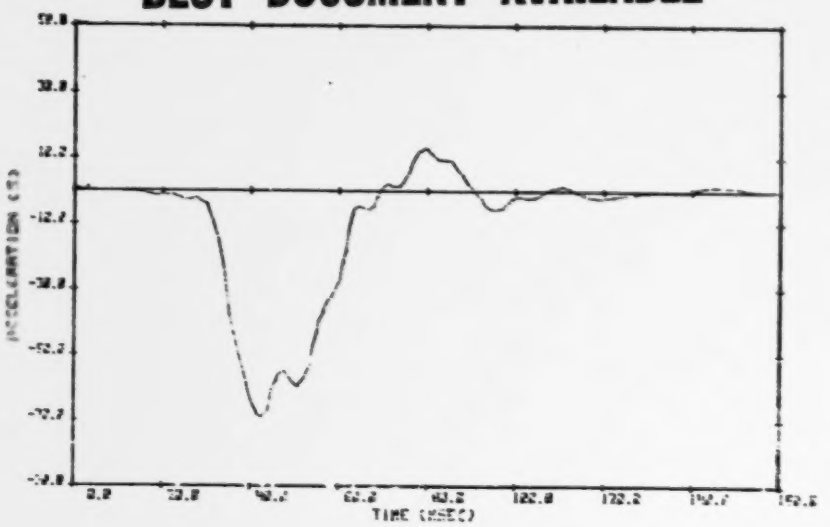

SRL 17-S TEST #21 (GTREM) - LOWER SPINE

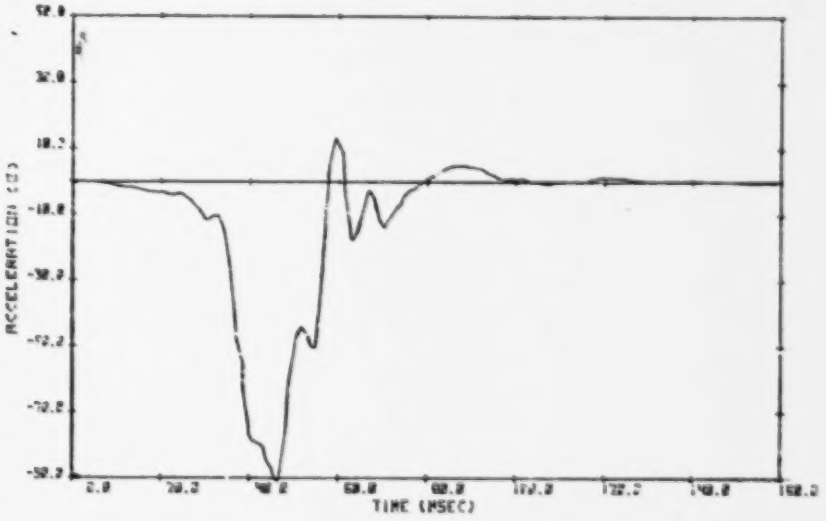

SRL 17-S TEST #21 (GTREM) - PELVIS

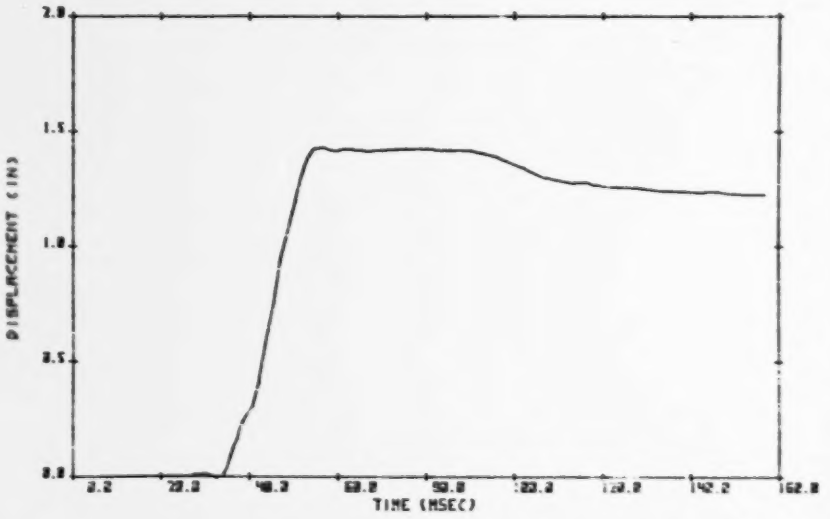

SRL 17-S TEST #21 (GTREM) - CHEST DEFLECTION

BEST DOCUMENT AVAILABLE

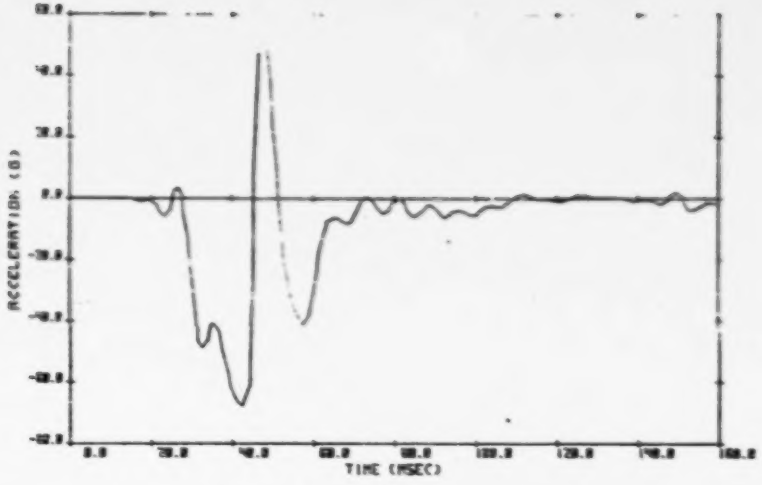

SRL 17-S TEST #22 (2VS) - LEFT UPPER RIB

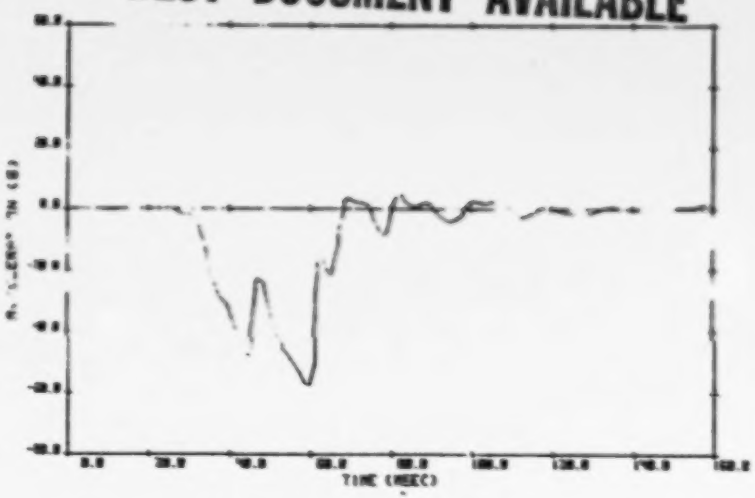

SRL 17-S TEST #22 (2VS) - RIGHT UPPER RIB

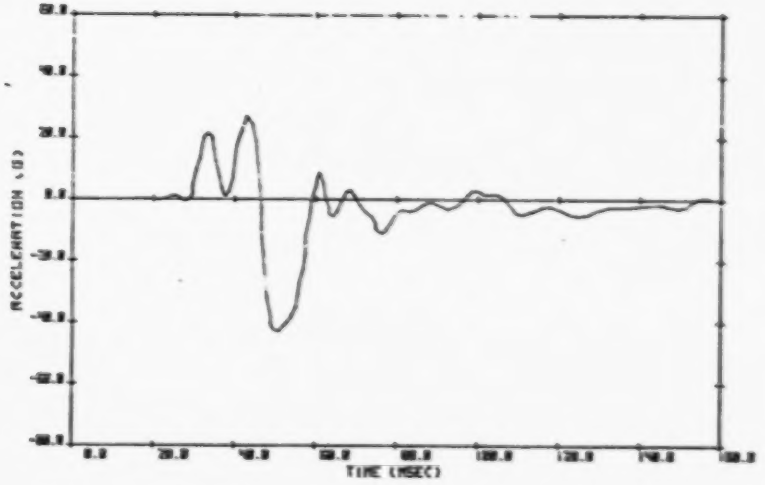

SRL 17-S TEST #22 (2VS) - UPPER STERNUM

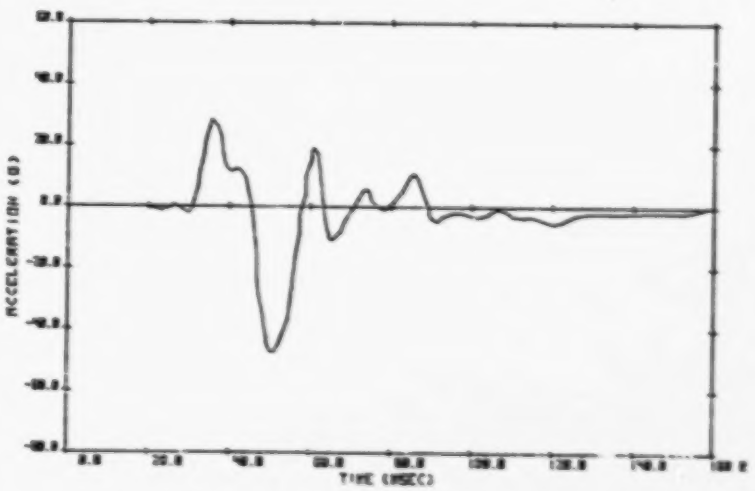

SRL 17-S TEST #22 (2VS) - LOWER STERNUM

BEST DOCUMENT AVAILABLE

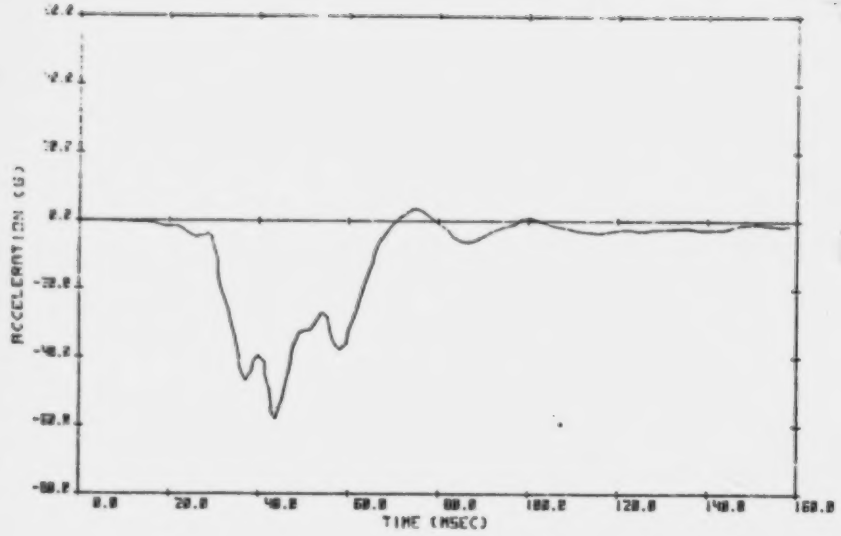

SRL 17-S TEST #22 (2VS) - UPPER SPINE

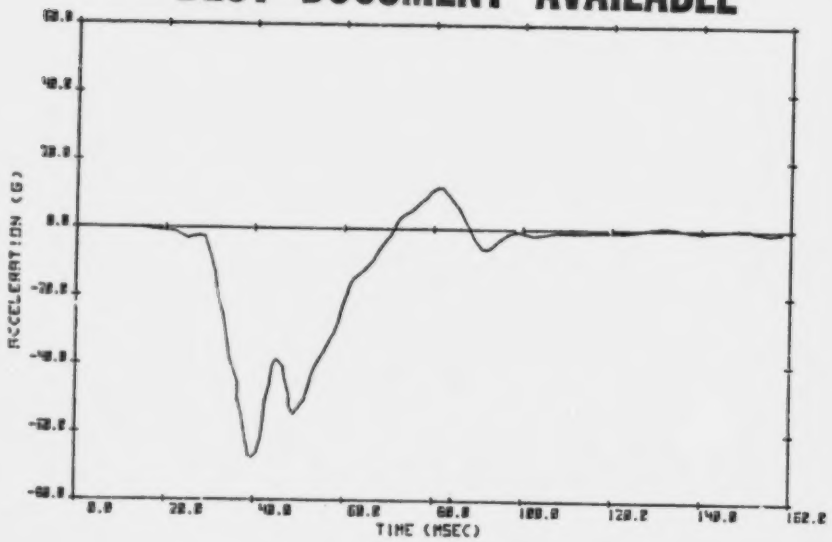

SRL 17-S TEST #22 (2VS) - LOWER SPINE

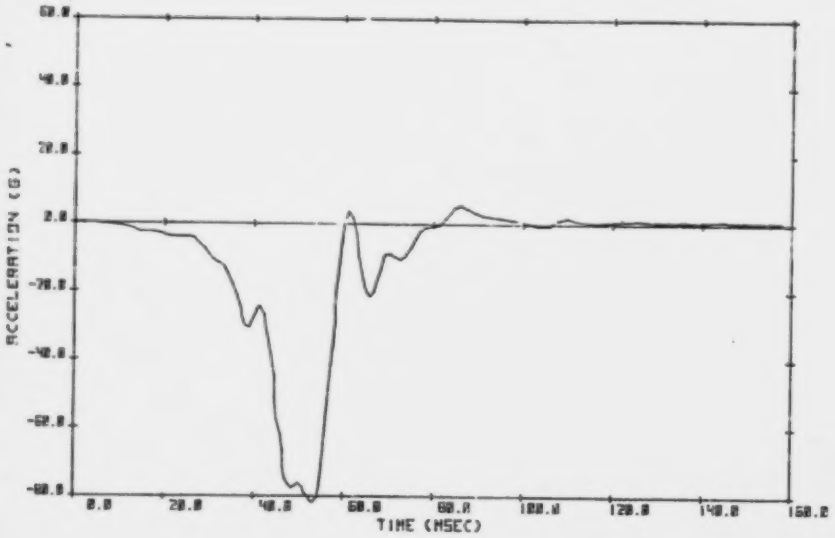

SRL 17-S TEST #22 (2VS) - PELVIS

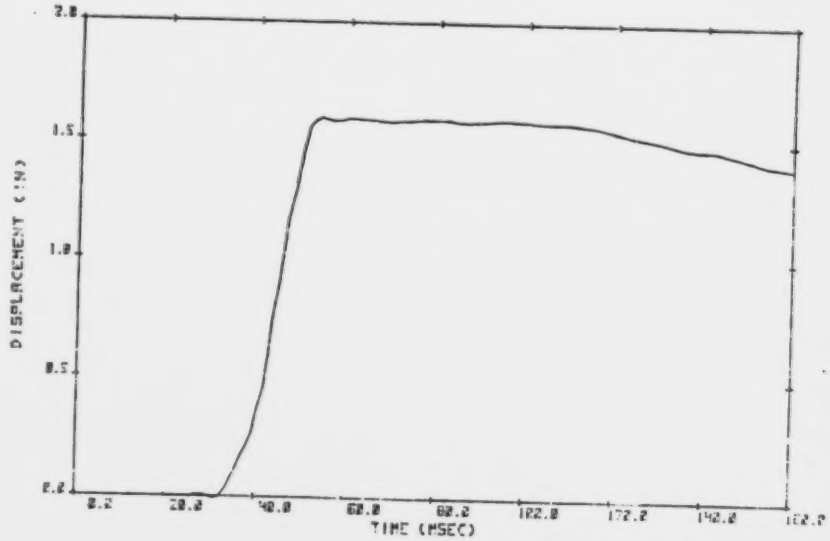

SRL 17-S TEST #22 (2VS) - CHEST DEFLECTION

[redacted]

228

BEST DOCUMENT AVAILABLE

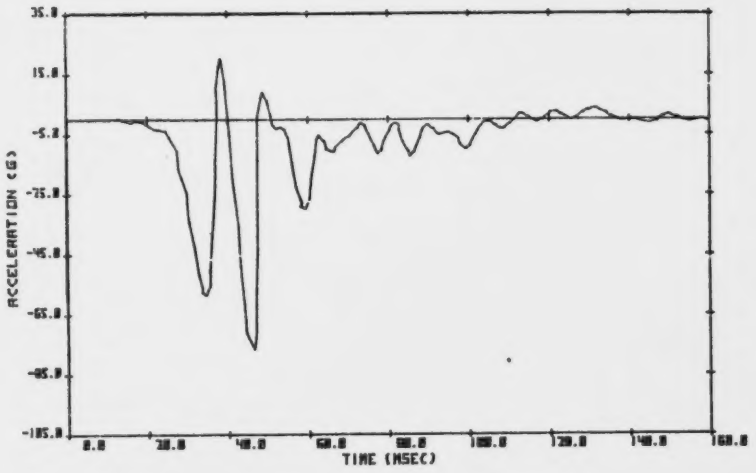

SRL 17-5 TEST #23 (H3BC) - LEFT UPPER RIB

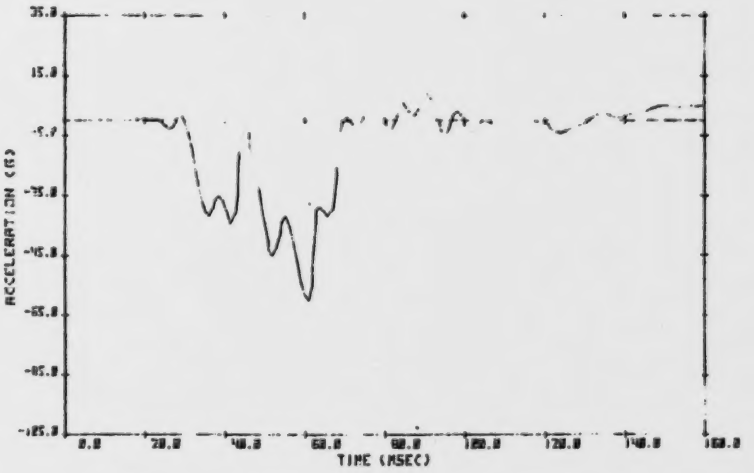

SRL 17-5 TEST #23 (H3BC) - RIGHT UPPER RIB

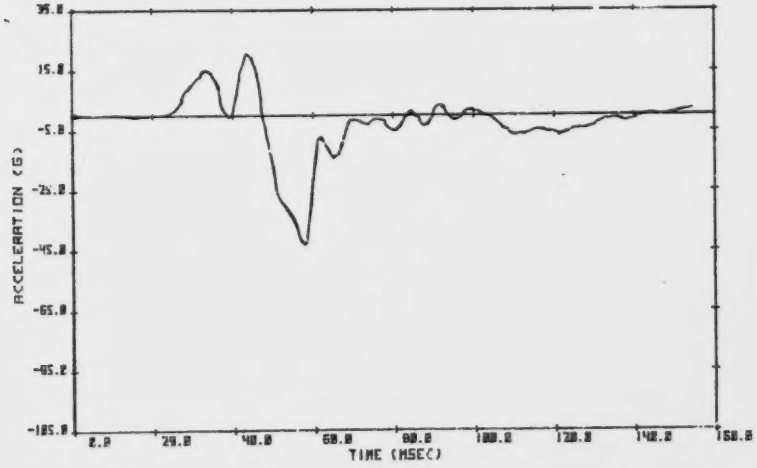

SRL 17-5 TEST #23 (H3BC) - UPPER STERNUM

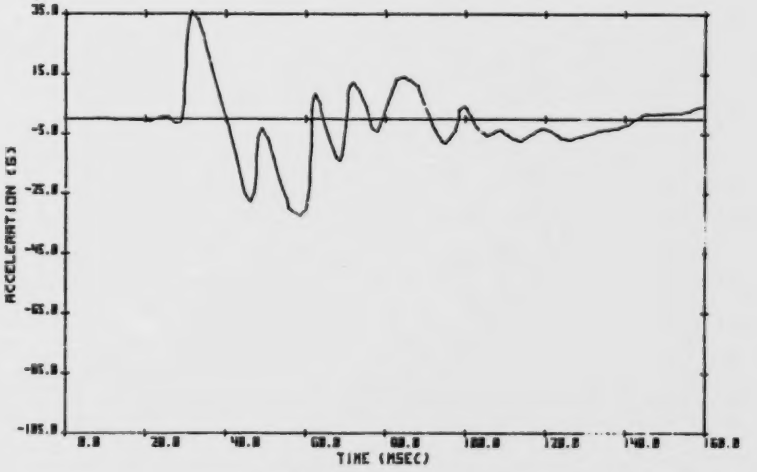

SRL 17-5 TEST #23 (H3BC) - LOWER STERNUM

BEST DOCUMENT AVAILABLE

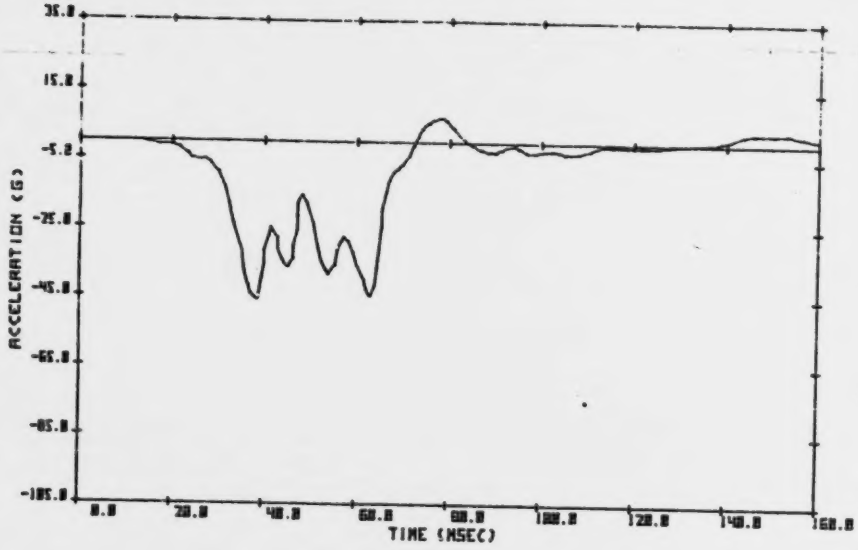

SRL 17-5 TEST #23 (H3BC) - UPPER SPINE

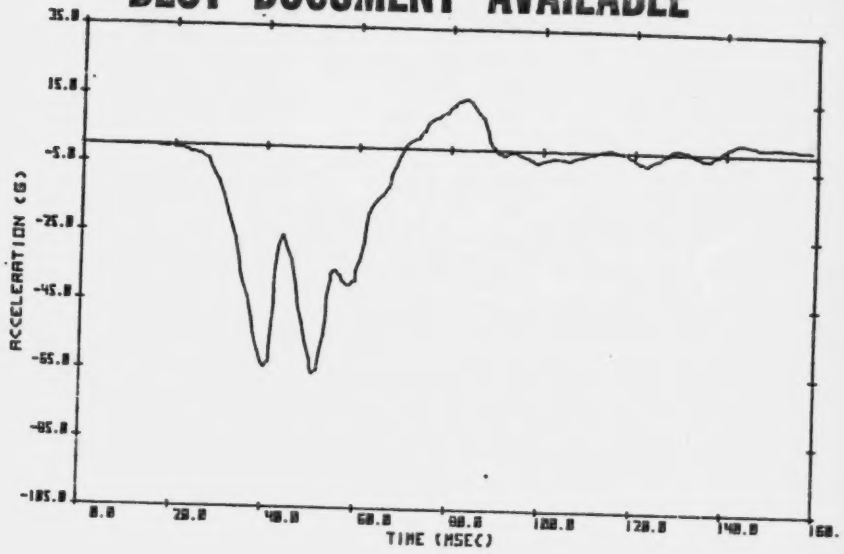

SRL 17-5 TEST #23 (H3BC) - LOWER SPINE

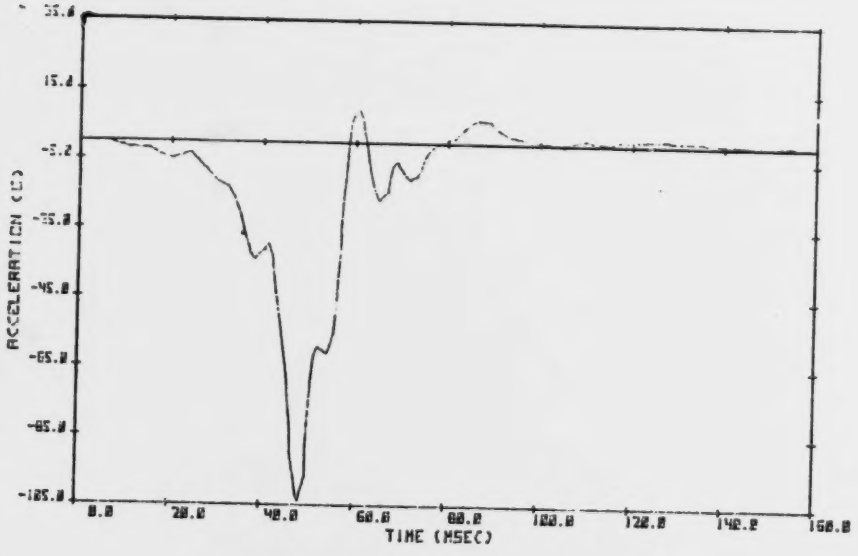

SRL 17-5 TEST #23 (H3BC) - PELVIS

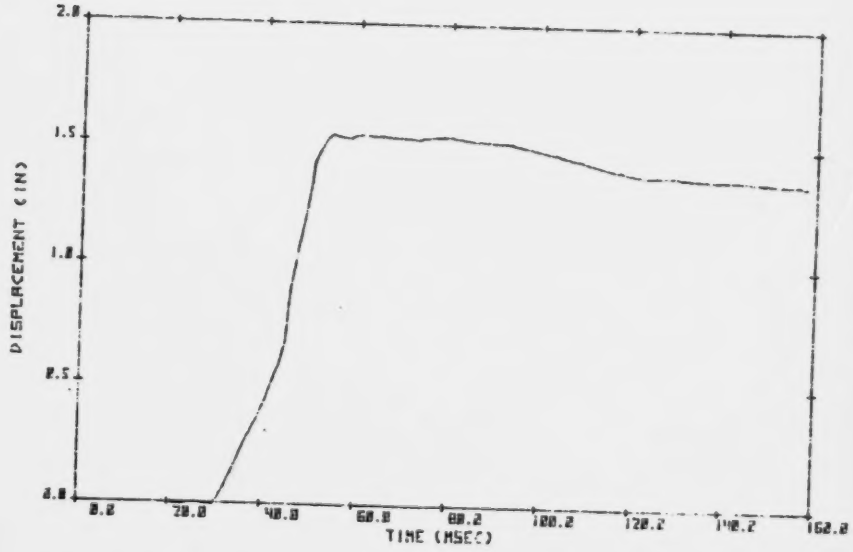

SRL 17-5 TEST #23 (H3BC) - CHEST DEFLECTION

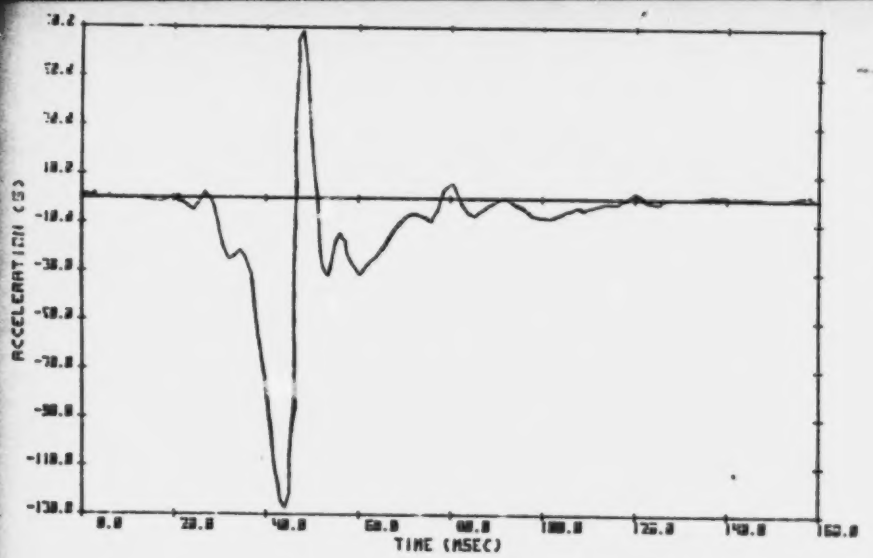

SRL 17-5 TEST #24 (C111A) - LEFT UPPER RIB

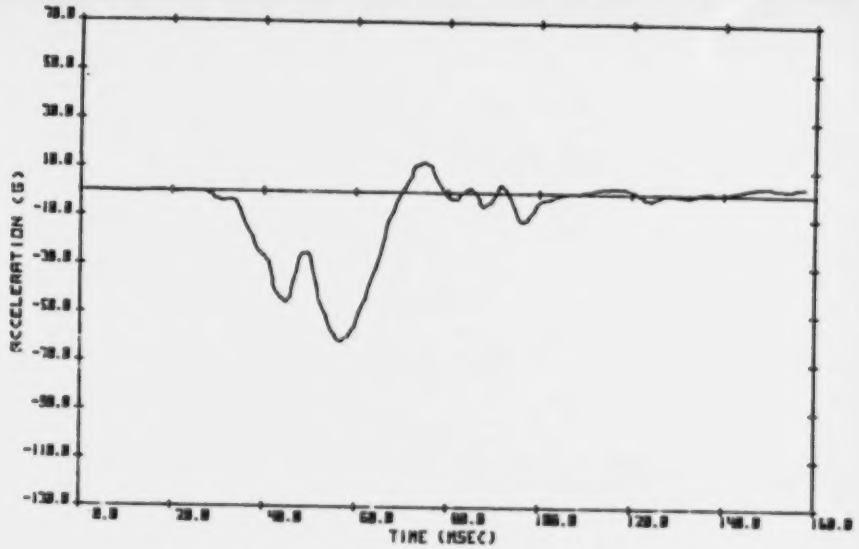

SRL 17-5 TEST #24 (C111A) - RIGHT UPPER RIB

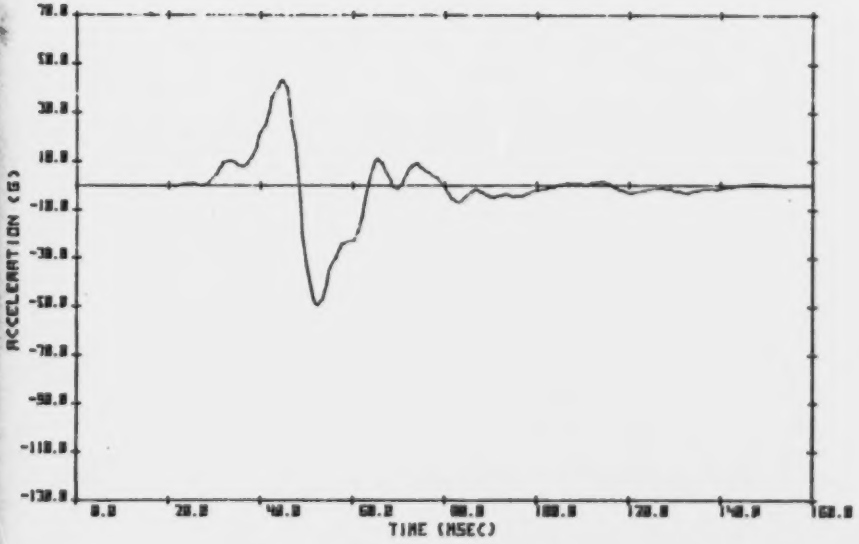

SRL 17-5 TEST #24 (C111A) - UPPER STERNUM

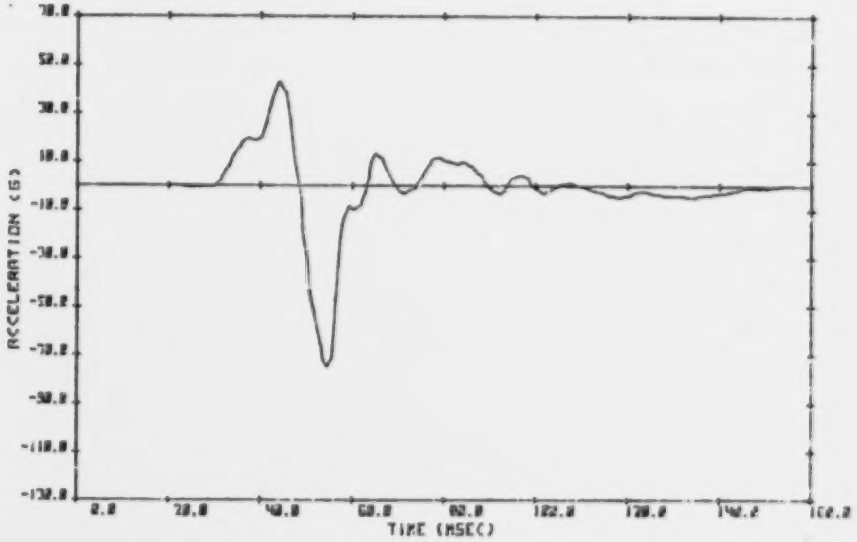

SRL 17-5 TEST #24 (C111A) - LOWER STERNUM

BEST DOCUMENT AVAILABLE

BEST DOCUMENT AVAILABLE

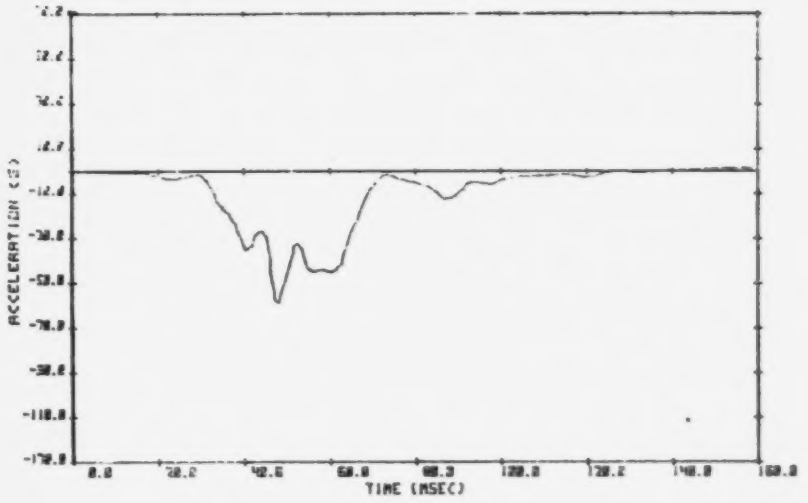

SRL 17-S TEST #24 (C1111A) - UPPER SPINE

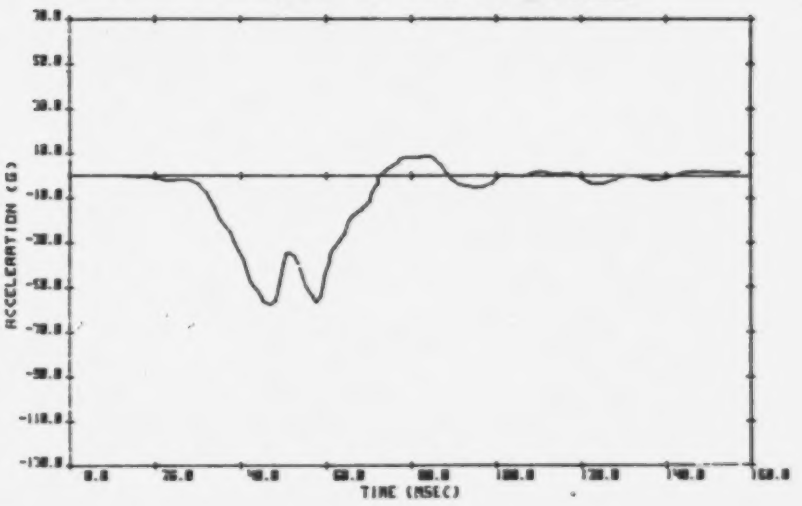

SRL 17-S TEST #24 (C1111A) - LOWER SPINE

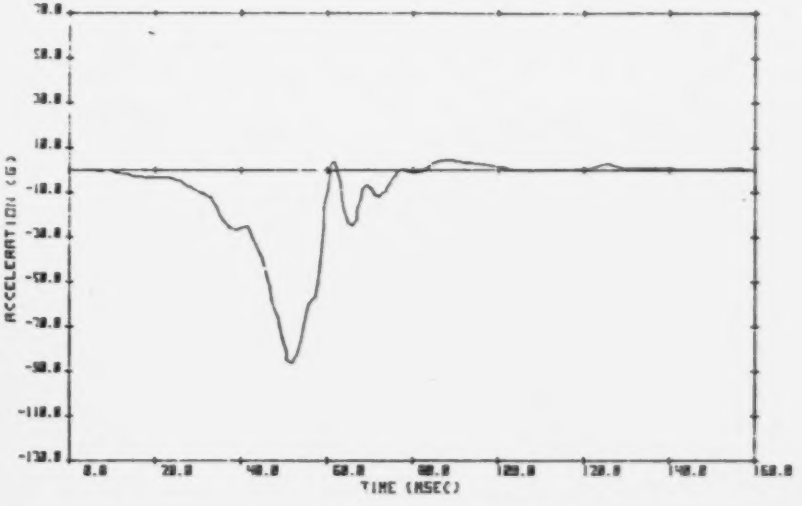

SRL 17-S TEST #24 (C1111A) - PELVIS

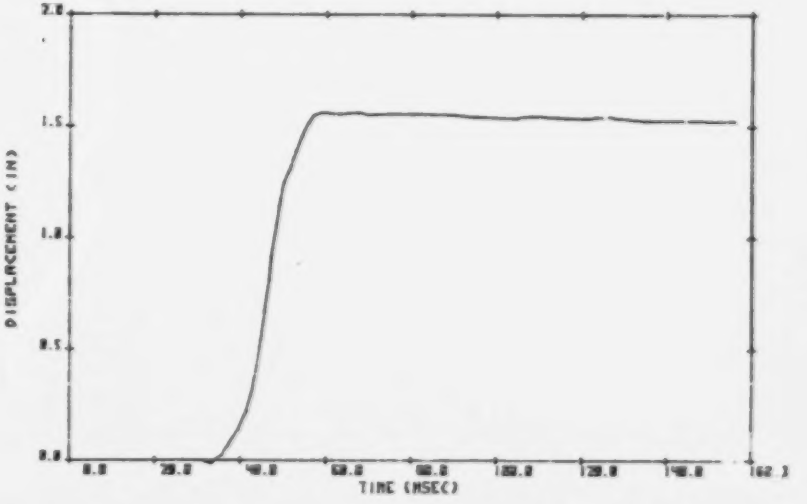

SRL 17-S TEST #24 (C1111A) - CHEST DEFLECTION

BEST DOCUMENT AVAILABLE

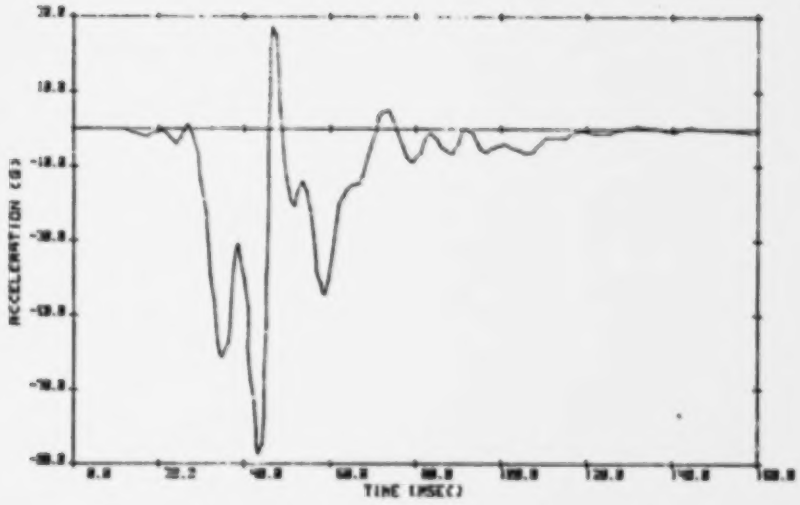

SRL 17-S TEST #25 (C222A) - LEFT UPPER RIB

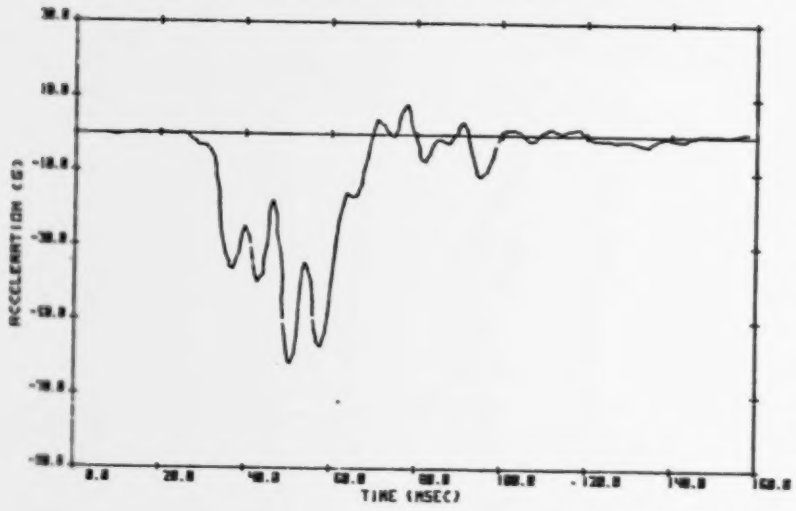

SRL 17-S TEST #25 (C222A) - RIGHT UPPER RIB

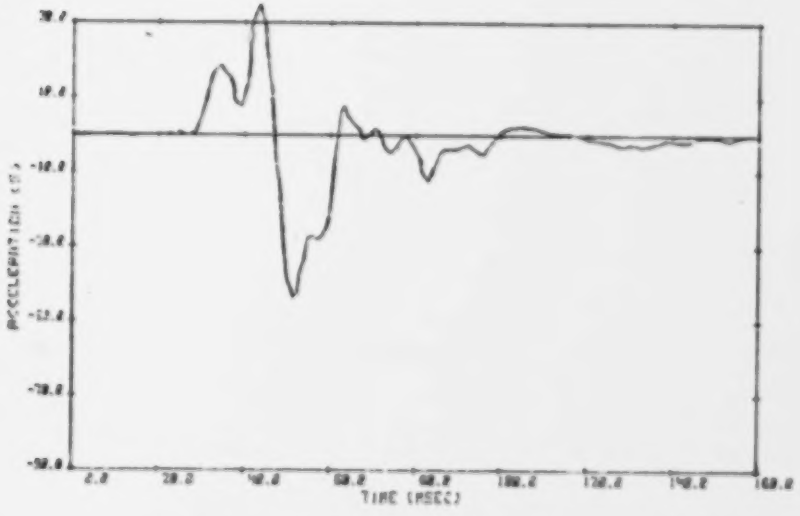

SRL 17-S TEST #25 (C222A) - UPPER STERNUM

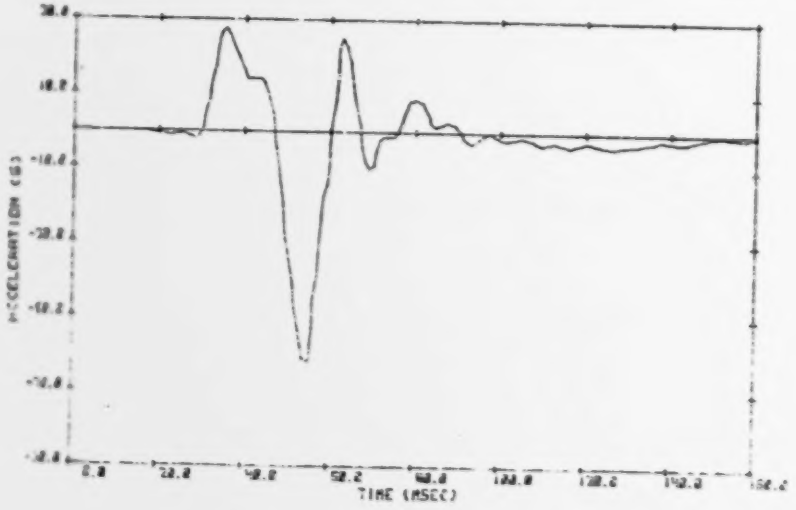

SRL 17-S TEST #25 (C222A) - LOWER STERNUM

BEST DOCUMENT AVAILABLE

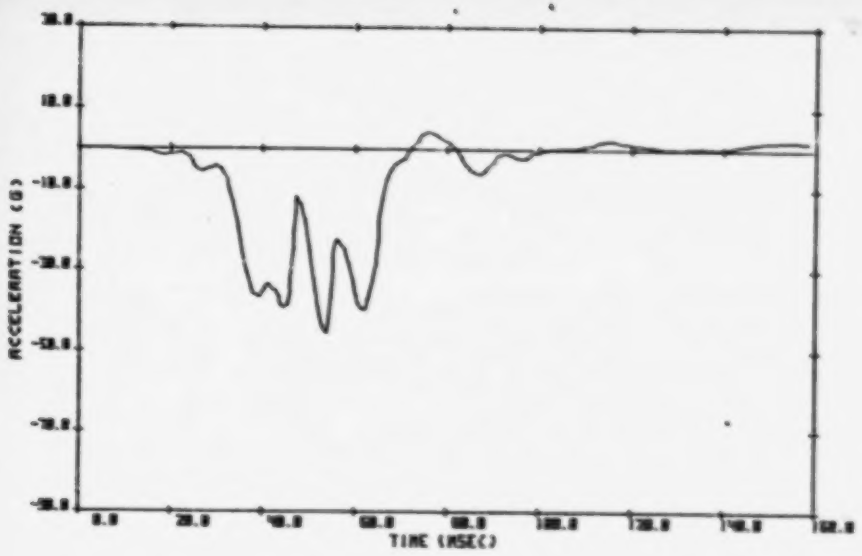

SRL 17-S TEST #25 (C222A) - UPPER SPINE

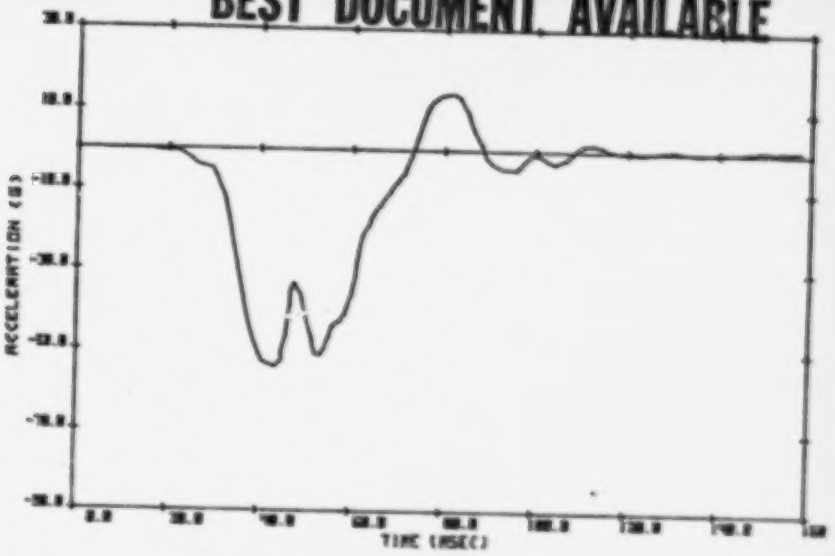

SRL 17-S TEST #25 (C222A) - LOWER SPINE

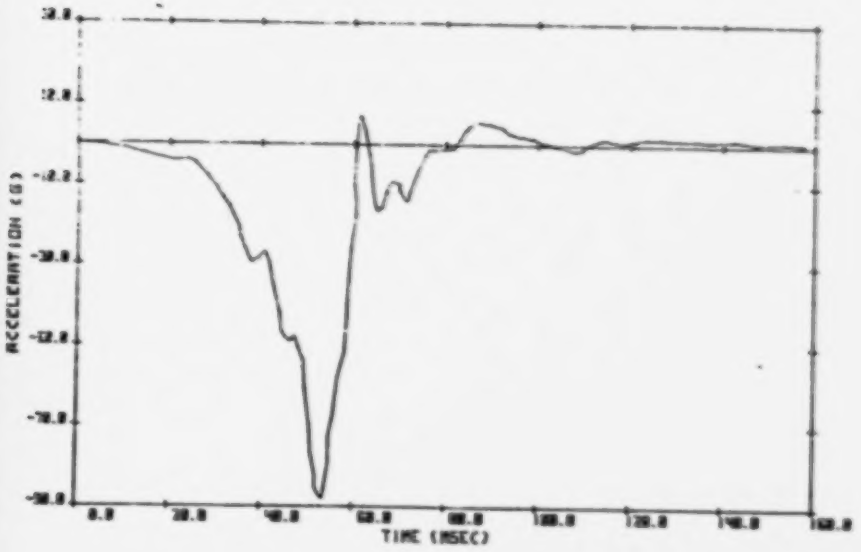

SRL 17-S TEST #25 (C222A) - PELVIS

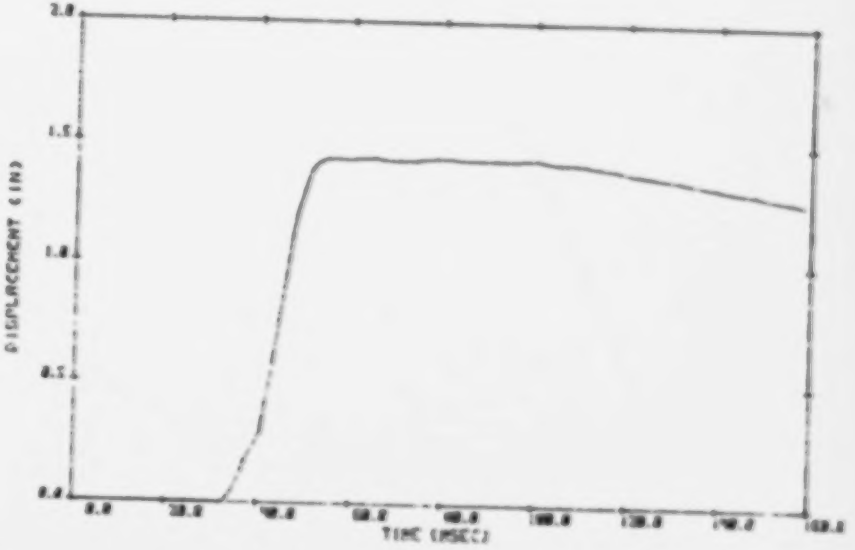

SRL 17-S TEST #25 (C222A) - CHEST DEFLECTION

BEST DOCUMENT AVAILABLE

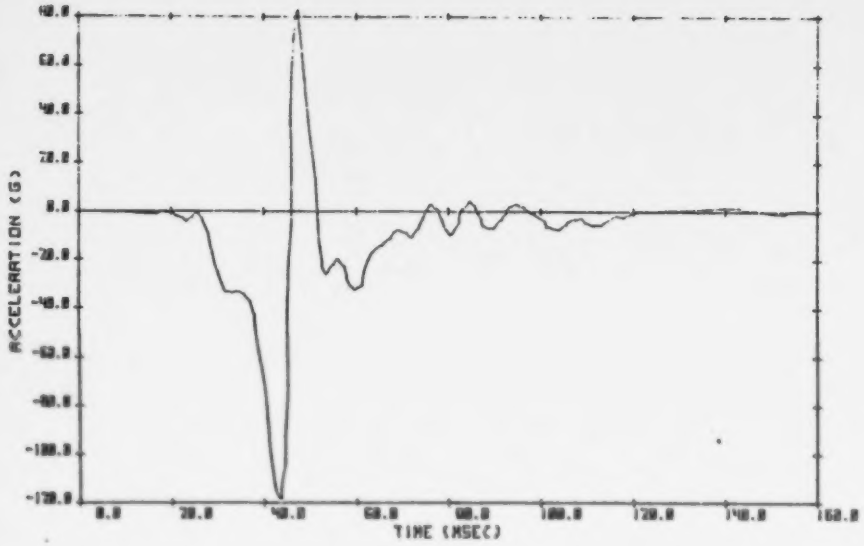

SRL 17-S TEST #26 (R-310-V) - LEFT UPPER RIB

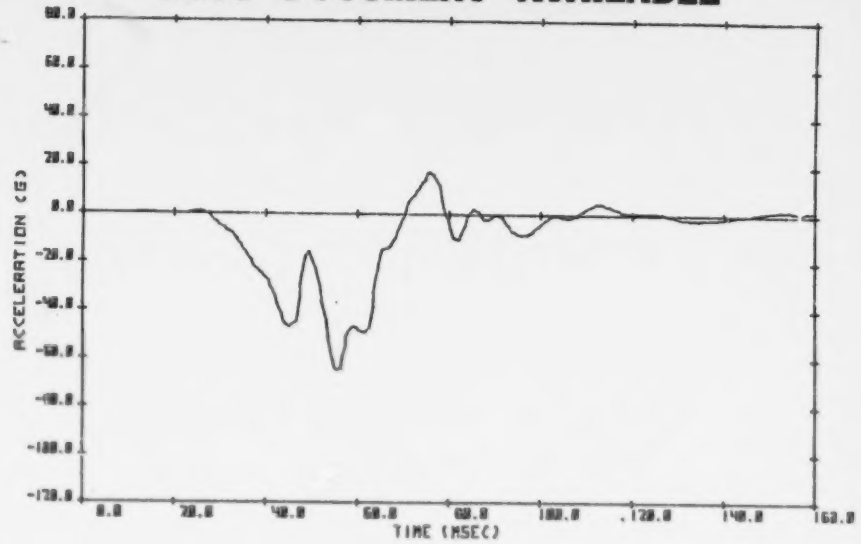

SRL 17-S TEST #26 (R-310-V) - RT. UPPER RIB

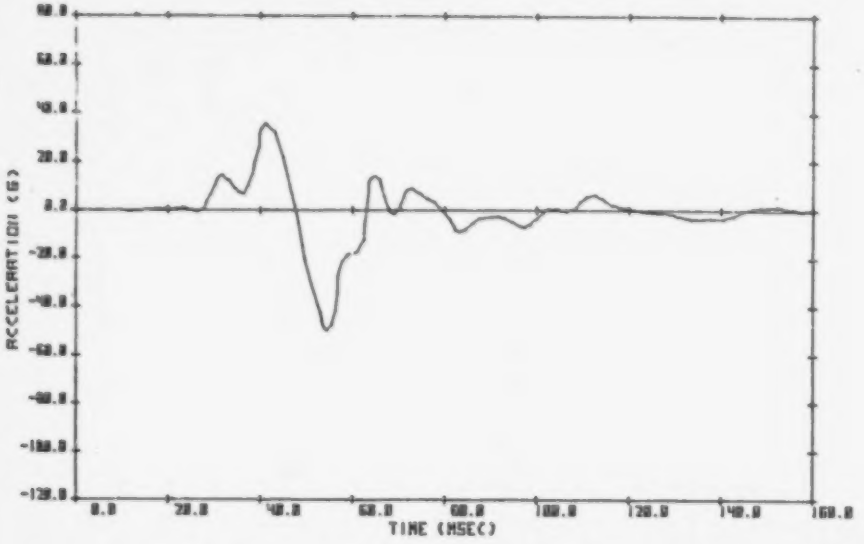

SRL 17-S TEST #26 (R-310-V) - UPPER STERNUM

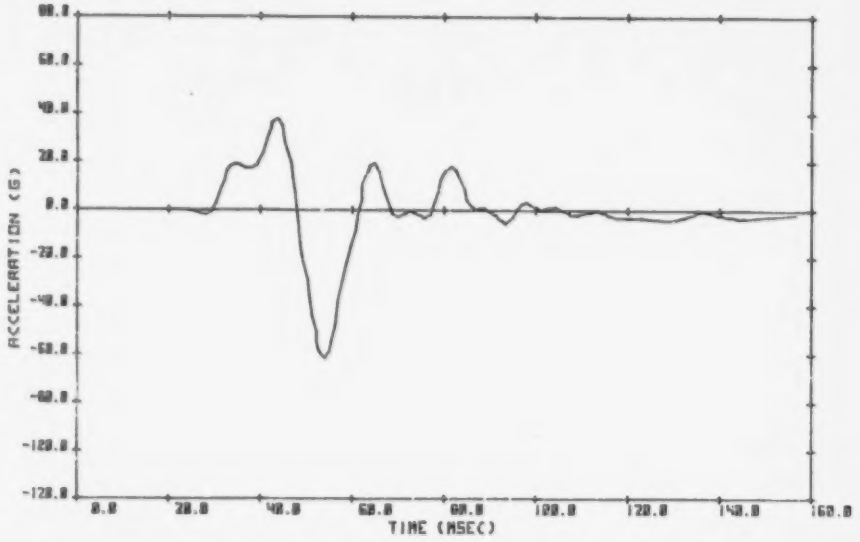

SRL 17-S TEST #26 (R-310-V) - LOWER STERNUM

BEST DOCUMENT AVAILABLE

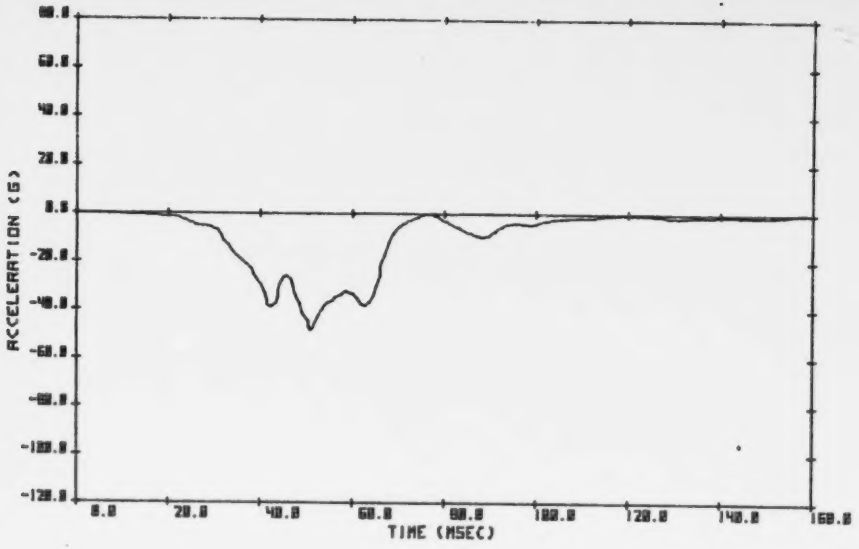

SRL 17-5 TEST #26 (R-310-V) - UPPER SPINE

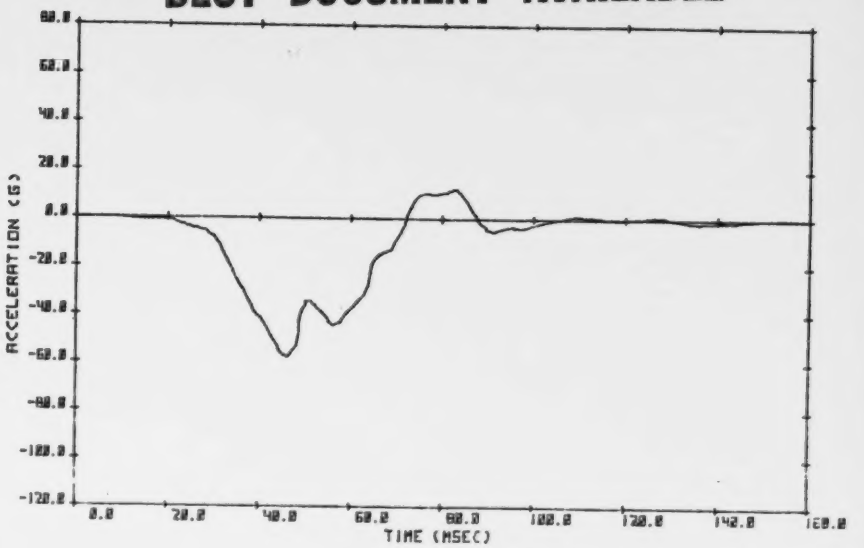

SRL 17-5 TEST #26 (R-310-V) - LOWER SPINE

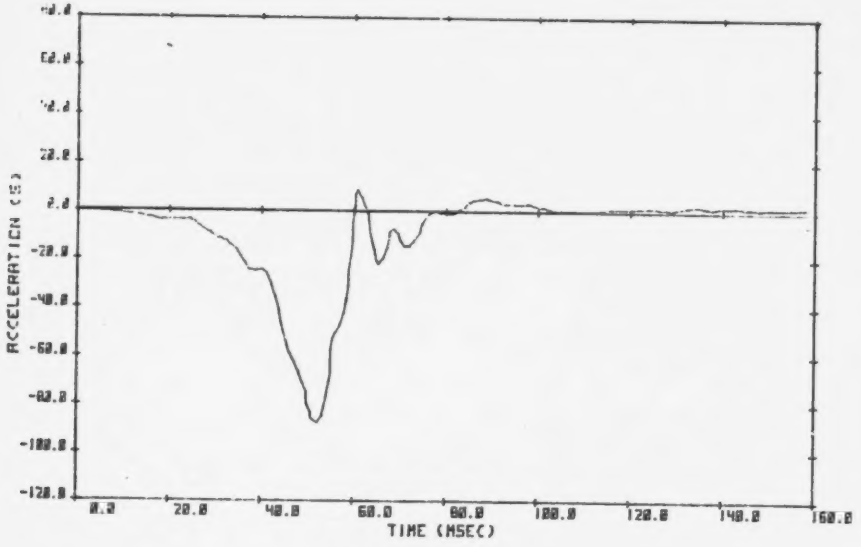

SRL 17-5 TEST #26 (R-310-V) - PELVIS

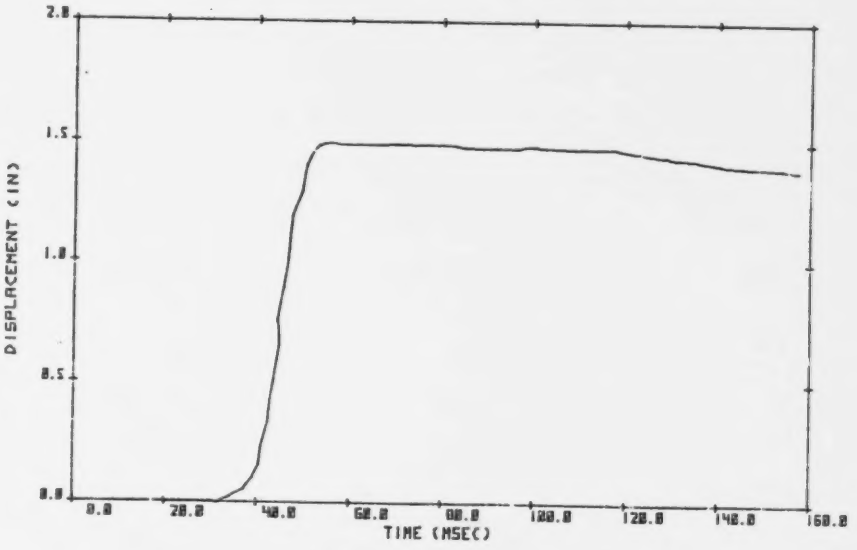

SRL 17-5 TEST #26 (R-310-V) - CHEST DEFL'N

BEST DOCUMENT AVAILABLE

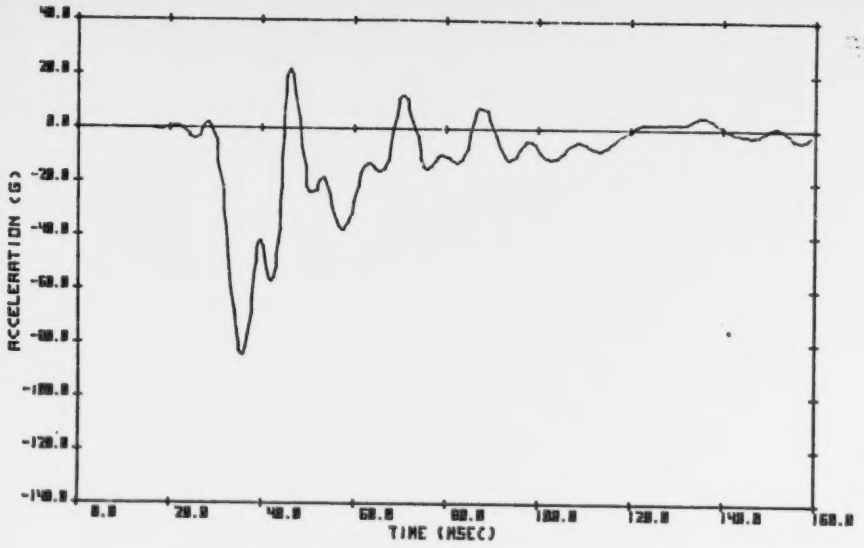

SRL 17-5 TEST #27 (GTREM) - LEFT UPPER RIB

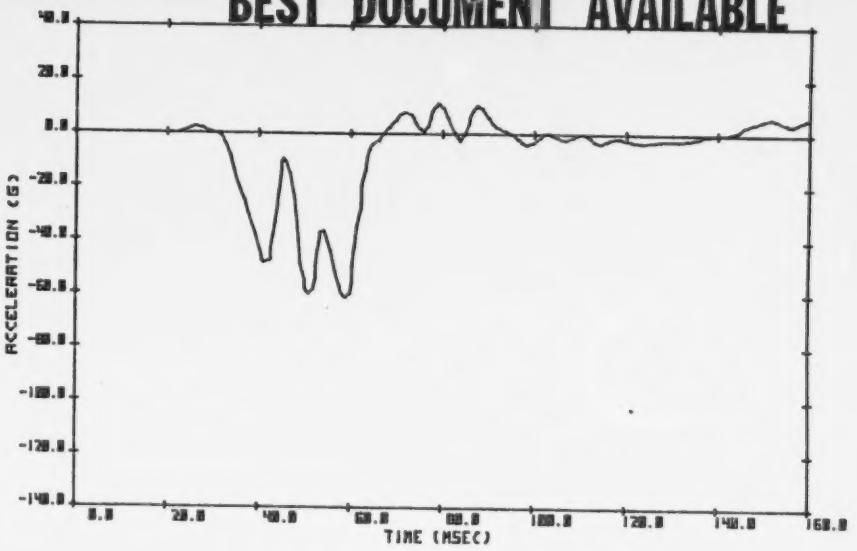

SRL 17-5 TEST #27 (GTREM) - RIGHT UPPER RIB

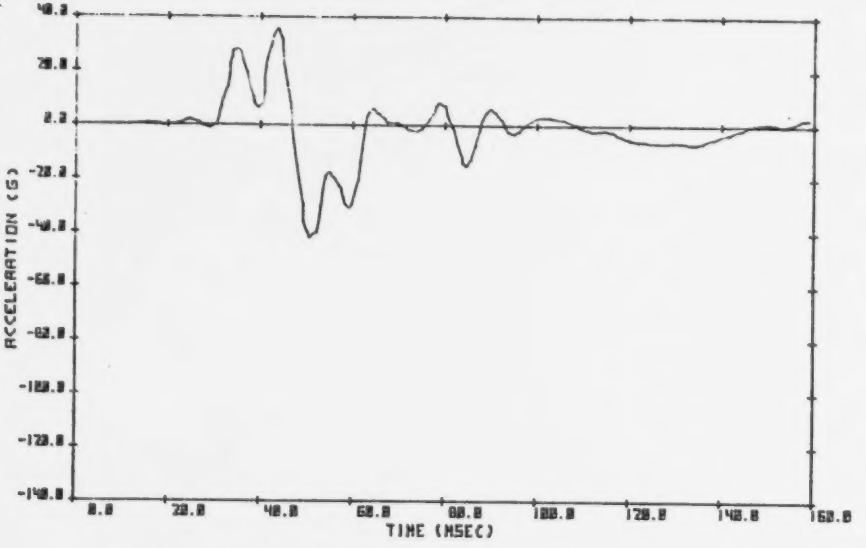

SRL 17-5 TEST #27 (GTREM) - UPPER STERNUM

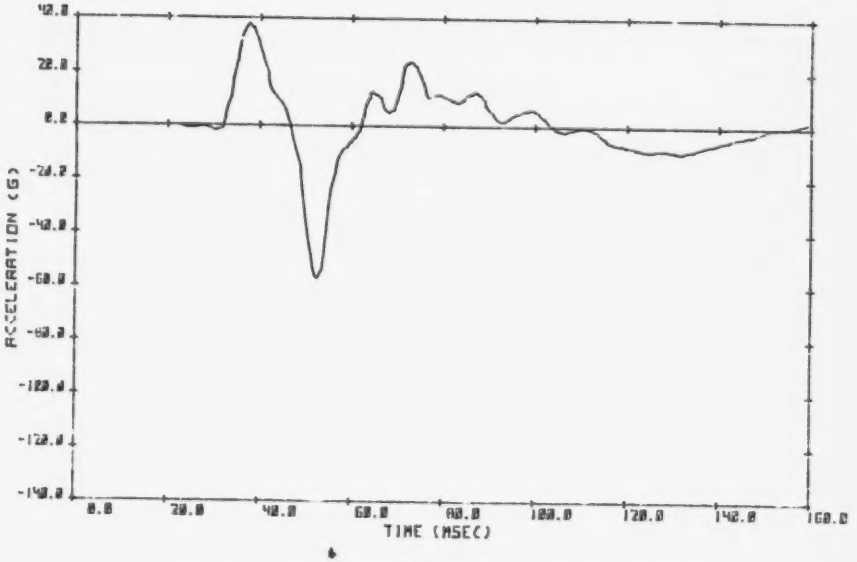

SRL 17-5 TEST #27 (GTREM) - LOWER STERNUM

BEST DOCUMENT AVAILABLE

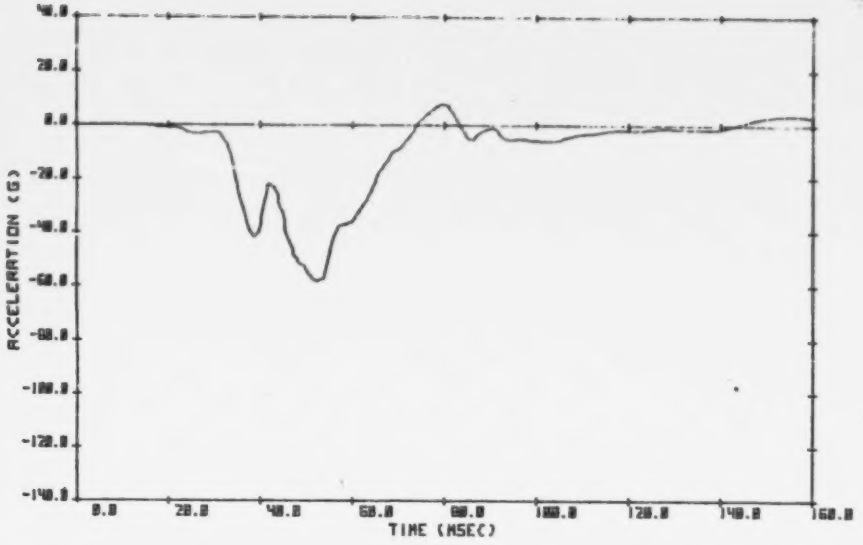

SRL 17-S TEST #27 (GTREM) - UPPER SPINE

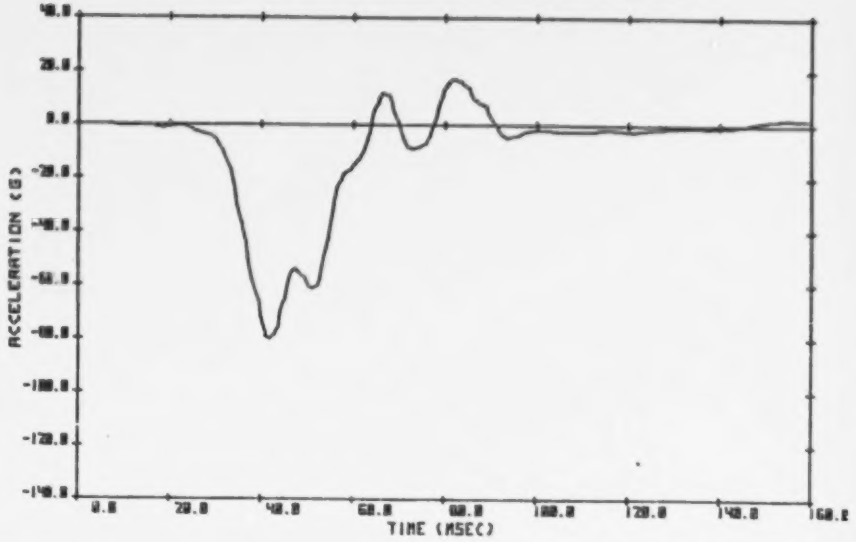

SRL 17-S TEST #27 (GTREM) - LOWER SPINE

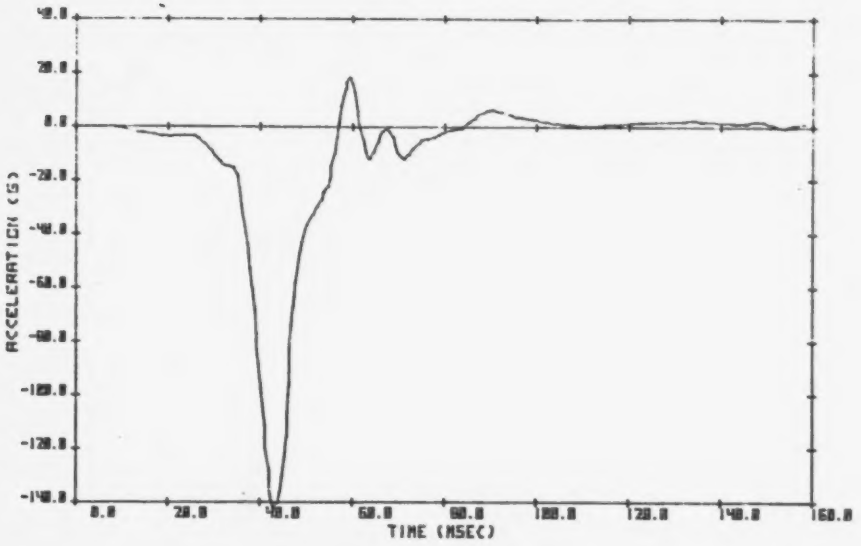

SRL 17-S TEST #27 (GTREM) - PELVIS

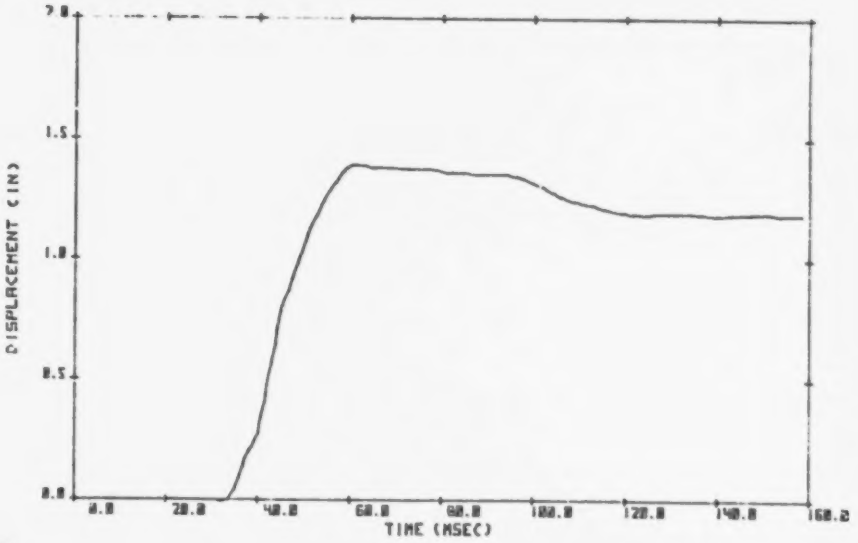

SRL 17-S TEST #27 (GTREM) - CHEST DEFLECTION

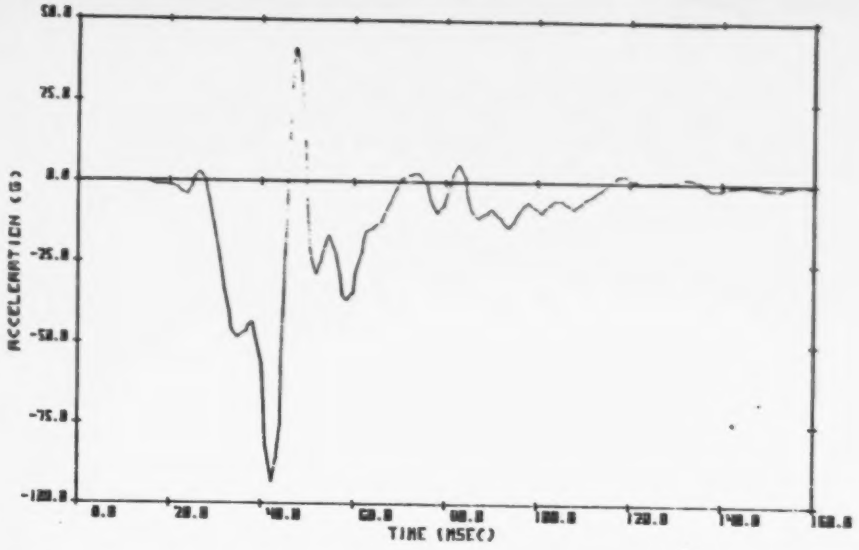

SRL 17-5 TEST #28 (APR) - LEFT UPPER RIB

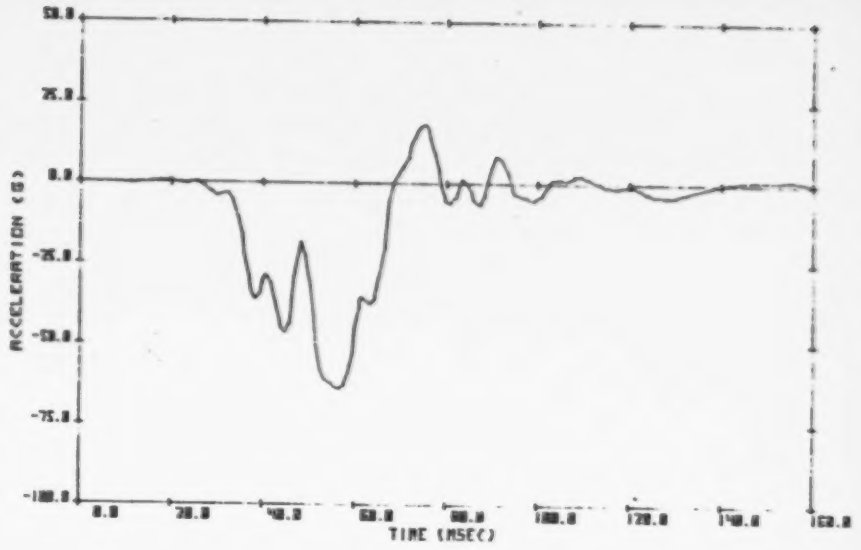

SRL 17-5 TEST #28 (APR) - RIGHT UPPER RIB

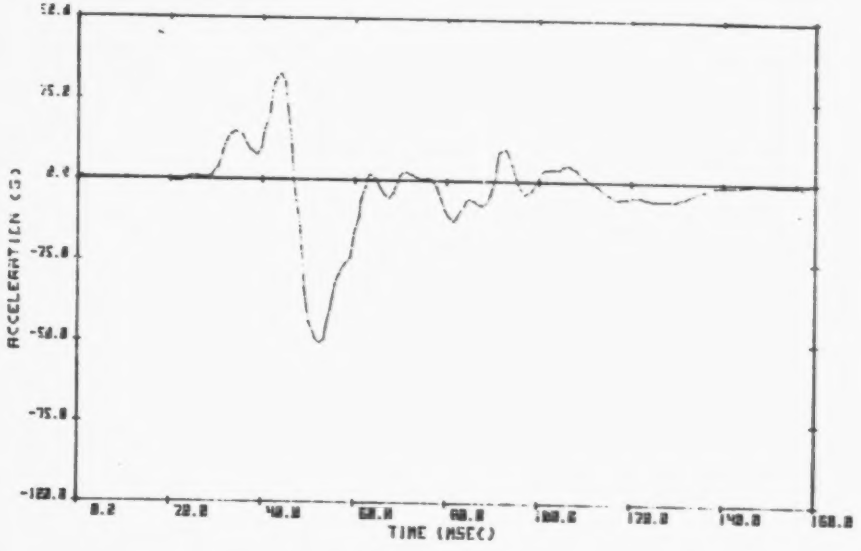

SRL 17-5 TEST #28 (APR) - UPPER STERNUM

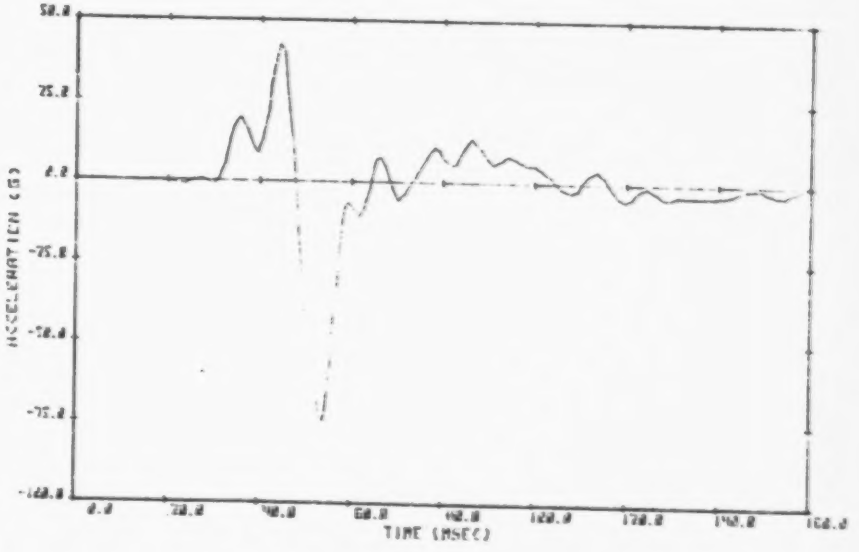

SRL 17-5 TEST #28 (APR) - LOWER STERNUM

BEST DOCUMENT AVAILABLE

BEST DOCUMENT AVAILABLE

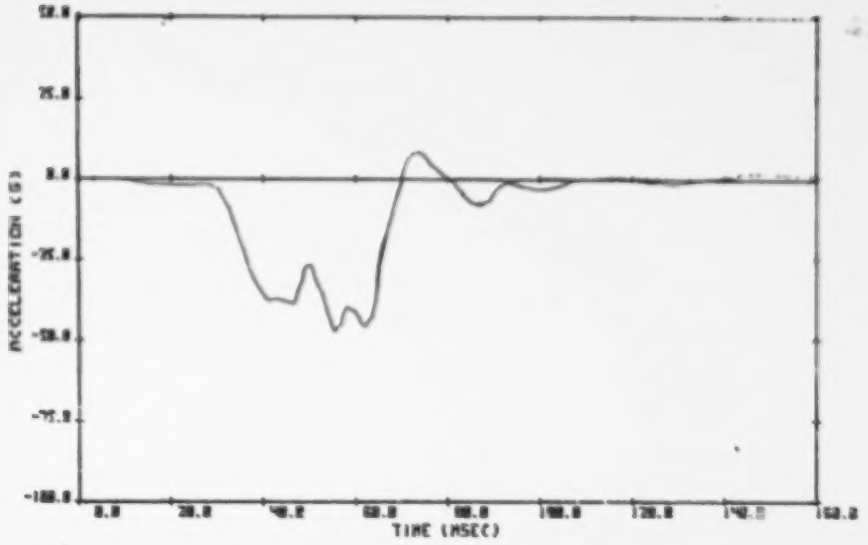

SRL 17-5 TEST #28 (APR) - UPPER SPINE

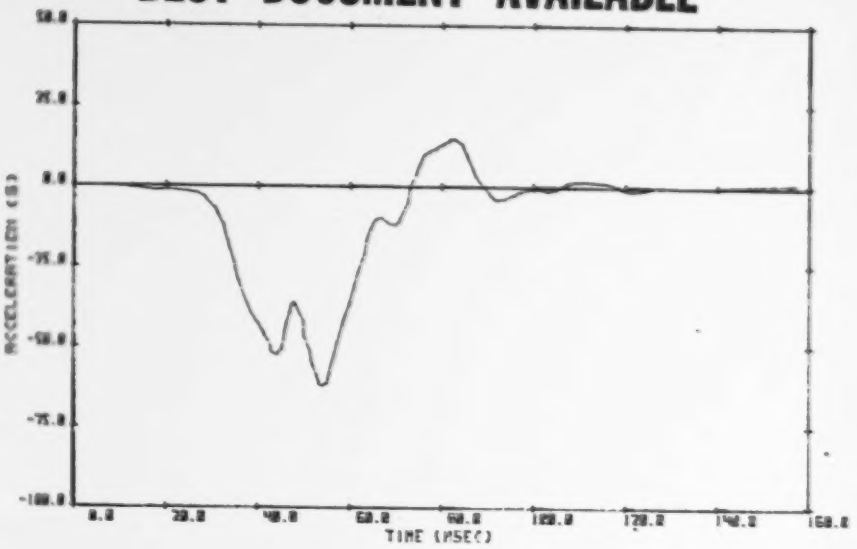

SRL 17-5 TEST #28 (APR) - LOWER SPINE

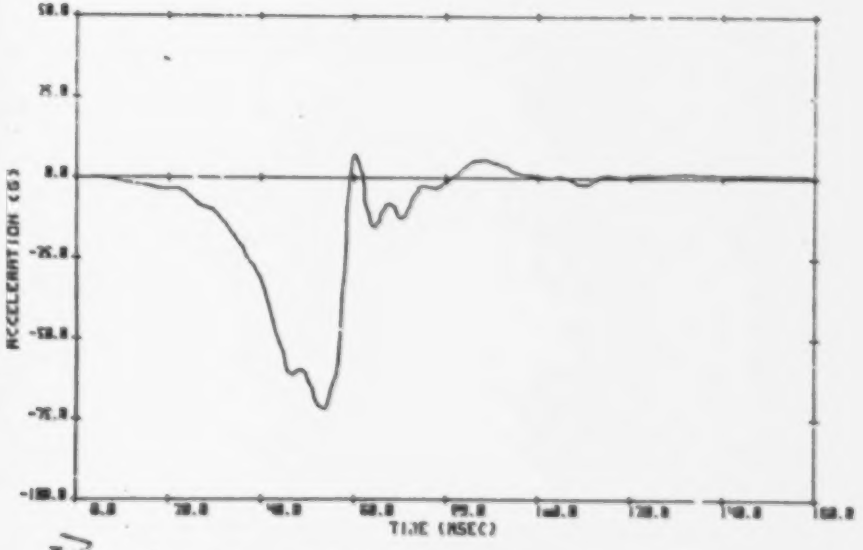

SRL 17-5 TEST #28 (APR) - PELVIS

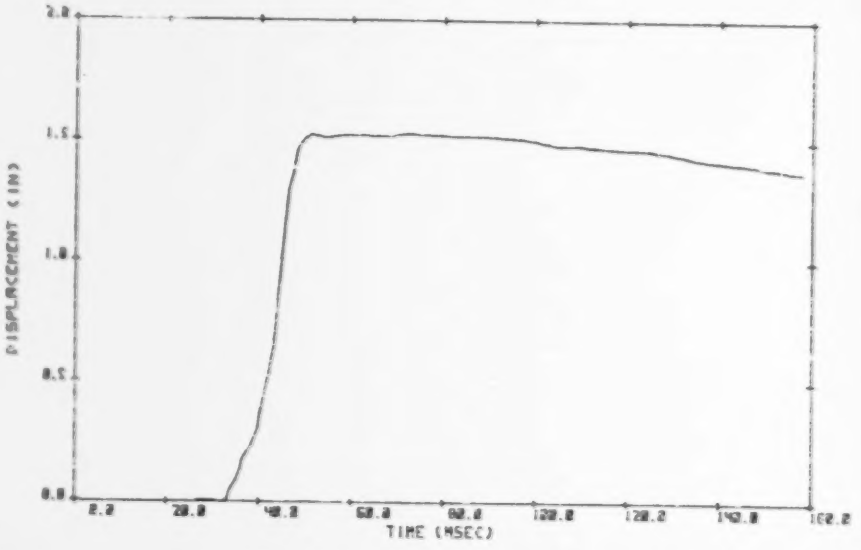

SRL 17-5 TEST #28 (APR) - CHEST DEFLECTION

BEST DOCUMENT AVAILABLE

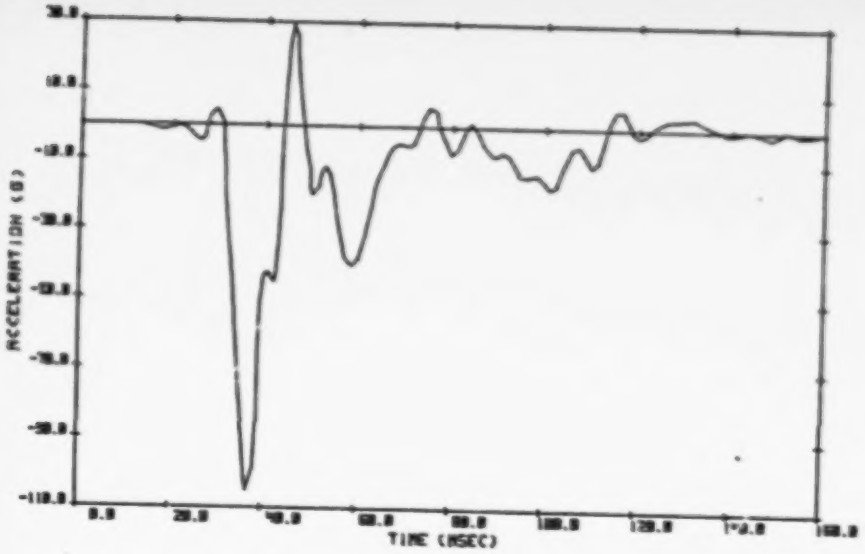

SRL 17-S TEST #29 (C311A) - LT. UPPER RIB

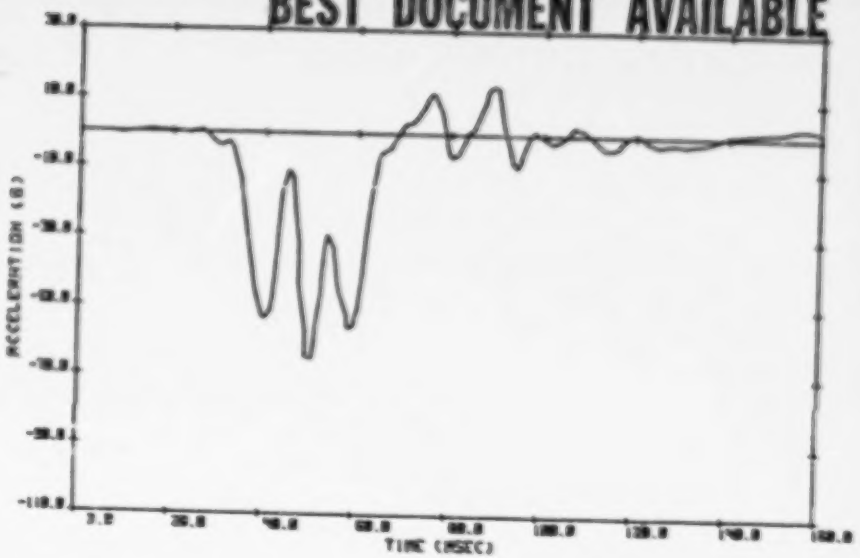

SRL 17-S TEST #29 (C311A) - RT. UPPER RIB

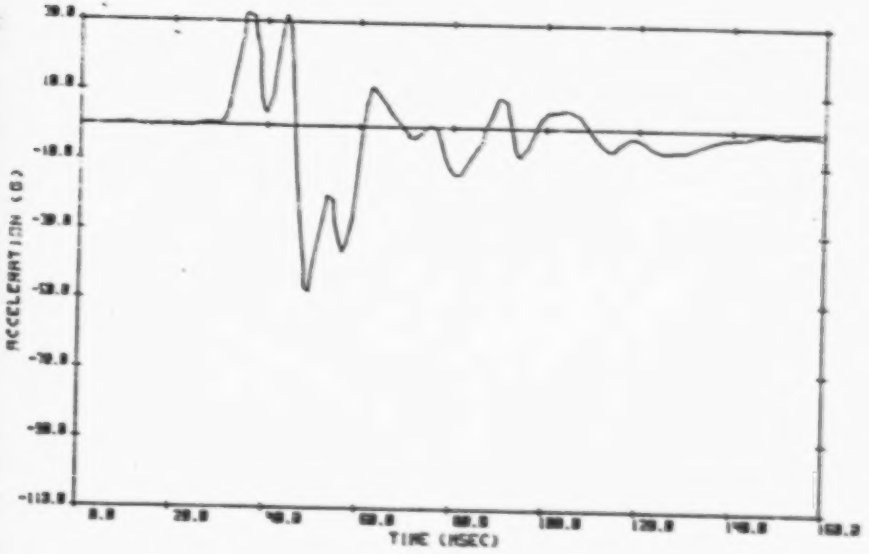

SRL 17-S TEST #29 (C311A) - UPPER STERNUM

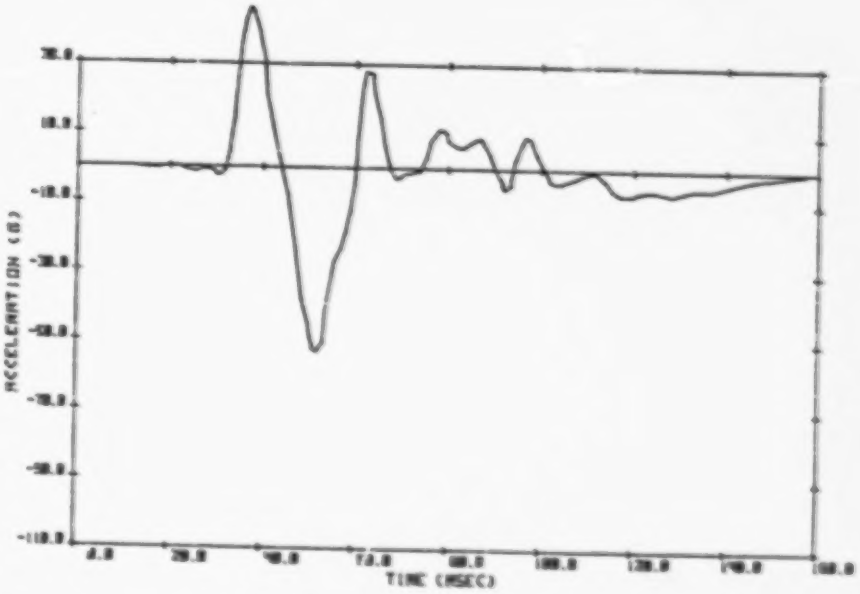

SRL 17-S TEST #29 (C311A) - LOWER STERNUM

BEST DOCUMENT AVAILABLE

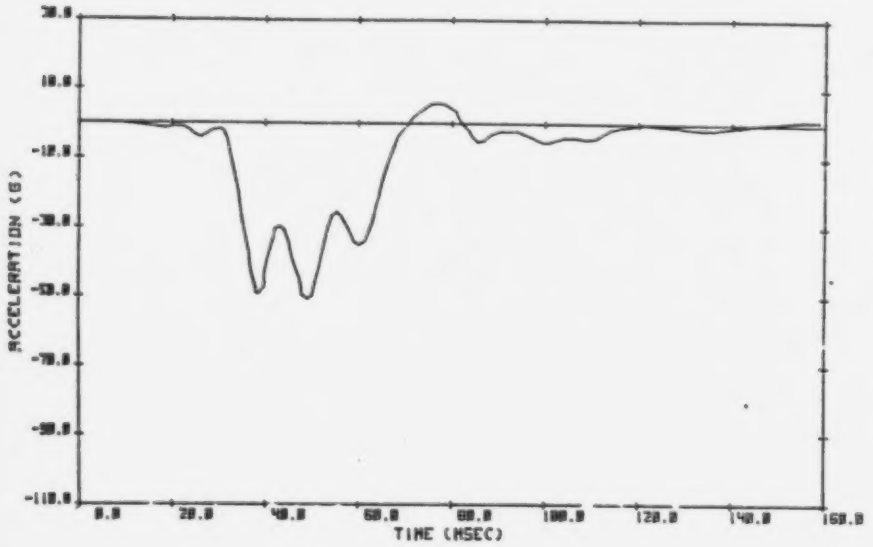

SRL 17-S TEST #29 (C311A) - UPPER SPINE

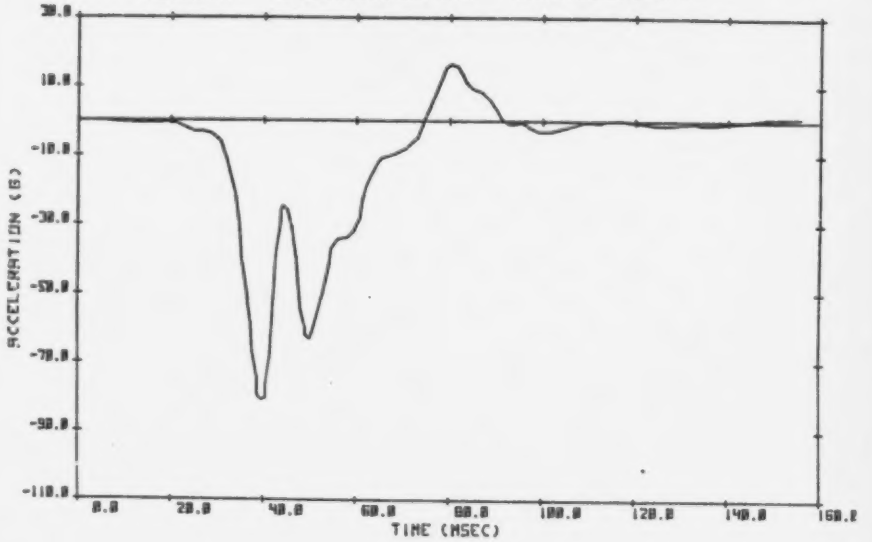

SRL 17-S TEST #29 (C311A) - LOWER SPINE

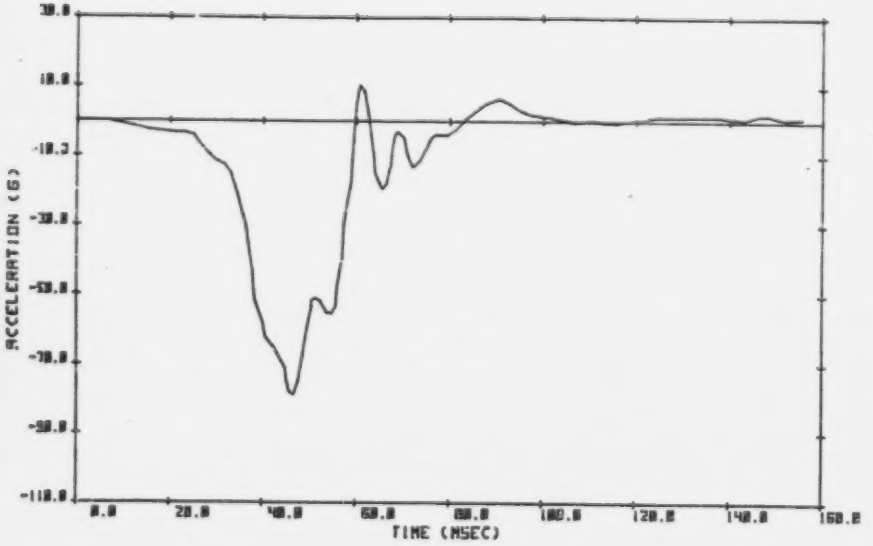

SRL 17-S TEST #29 (C311A) - PELVIS

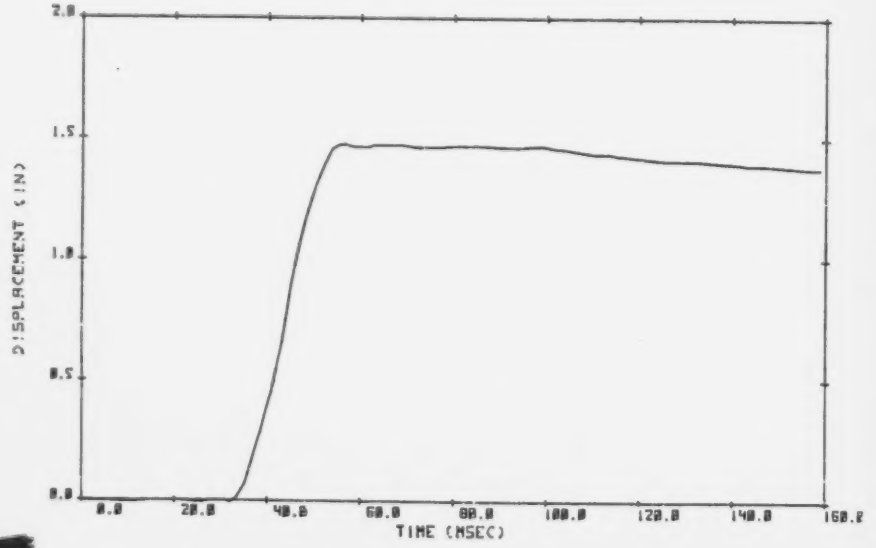

SRL 17-S TEST #29 (C311A) - CHEST DEFLECTION

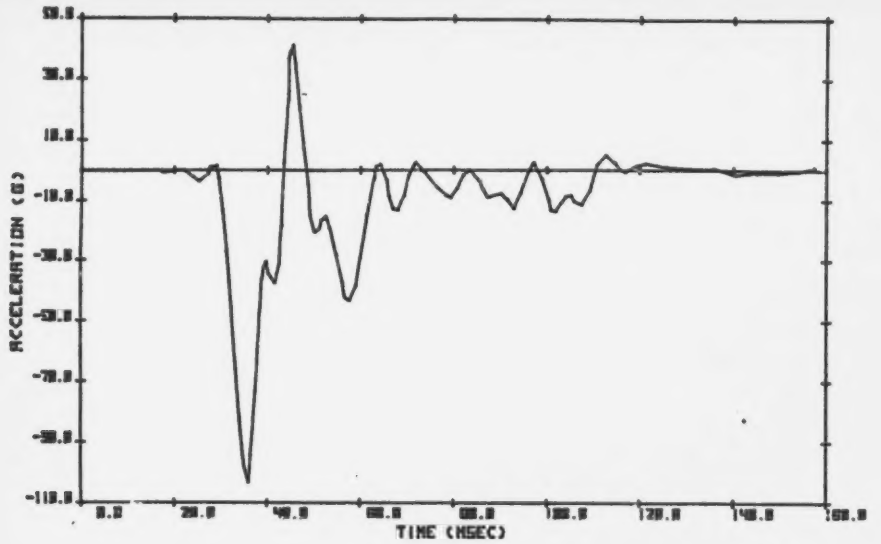

SRL 17-5 TEST #30 (ETH 600) - LT. UPPER RIB

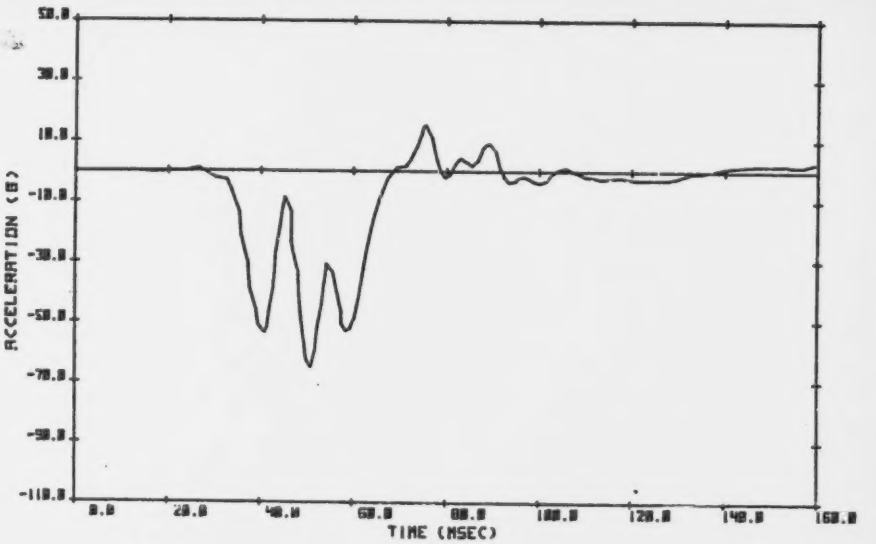

SRL 17-5 TEST #30 (ETH 600) - RT. UPPER RIB

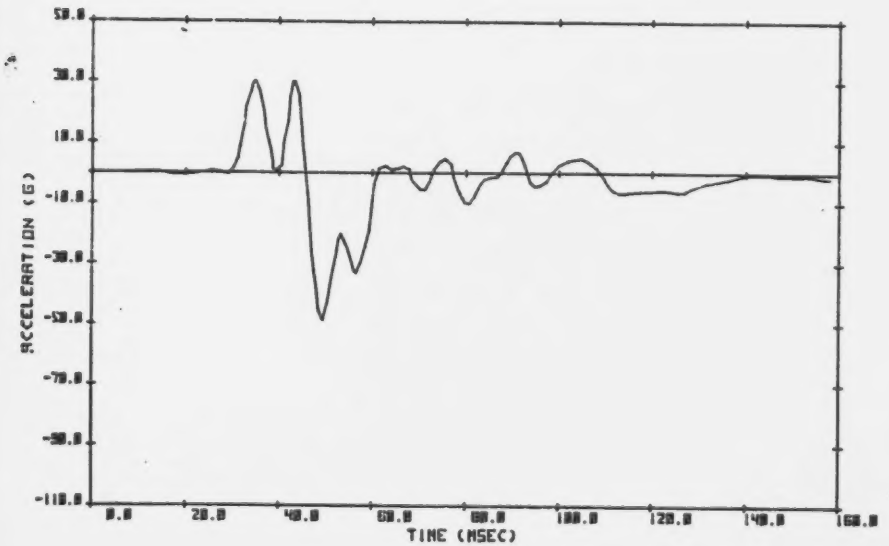

SRL 17-5 TEST #30 (ETH 600) - UPPER STERNUM

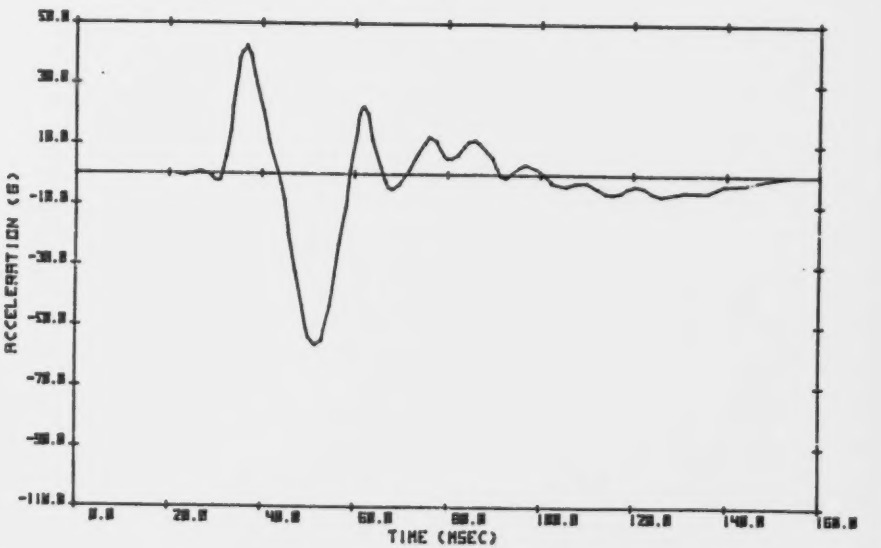

SRL 17-5 TEST #30 (ETH 600) - LOWER STERNUM

BEST DOCUMENT AVAILABLE

BEST DOCUMENT AVAILABLE

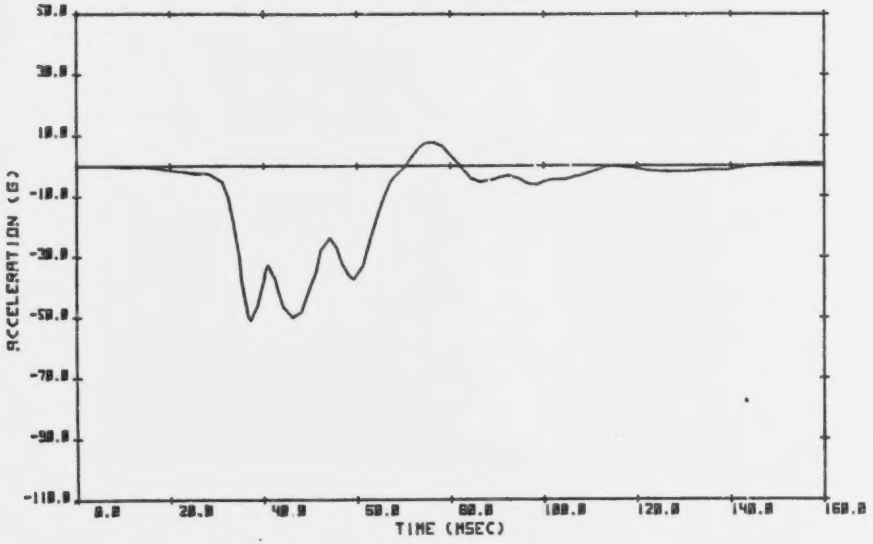

SRL 17-S TEST #30 (ETH 600) - UPPER SPINE

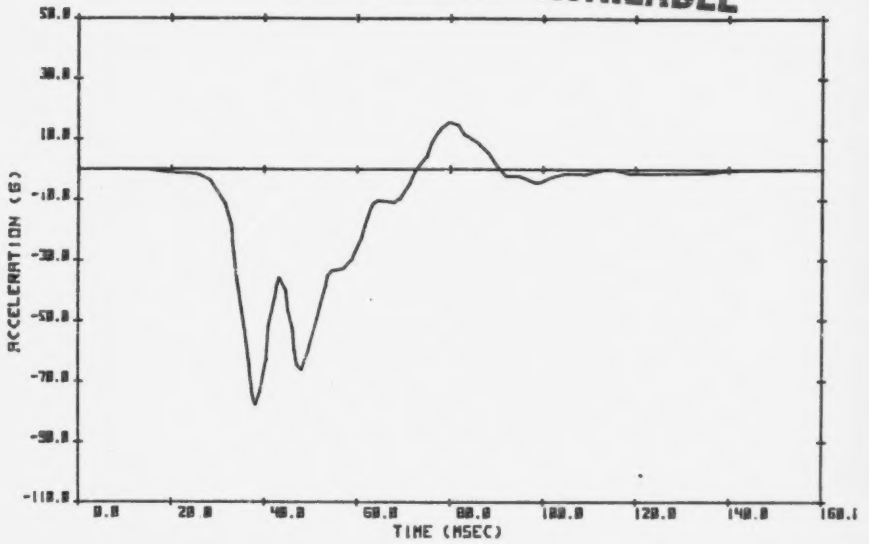

SRL 17-S TEST #30 (ETH 600) - LOWER SPINE

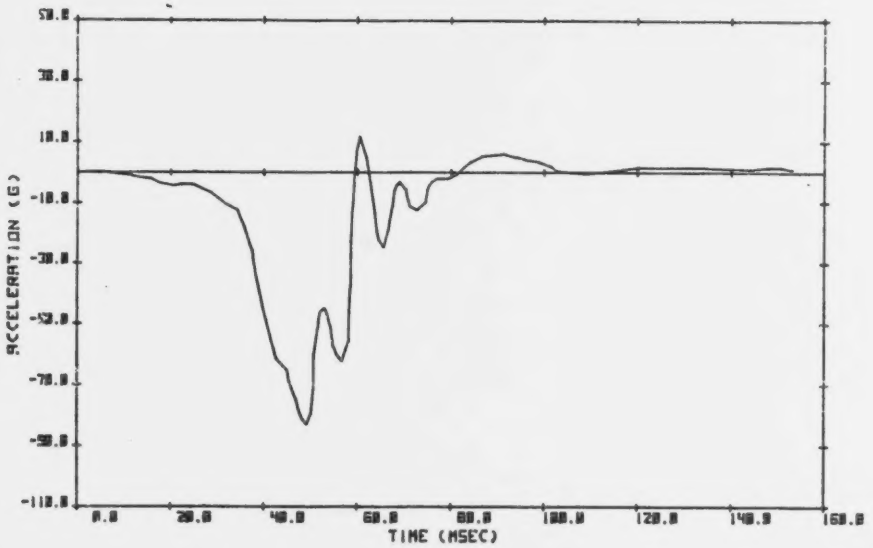

SRL 17-S TEST #30 (ETH 600) - PELVIS

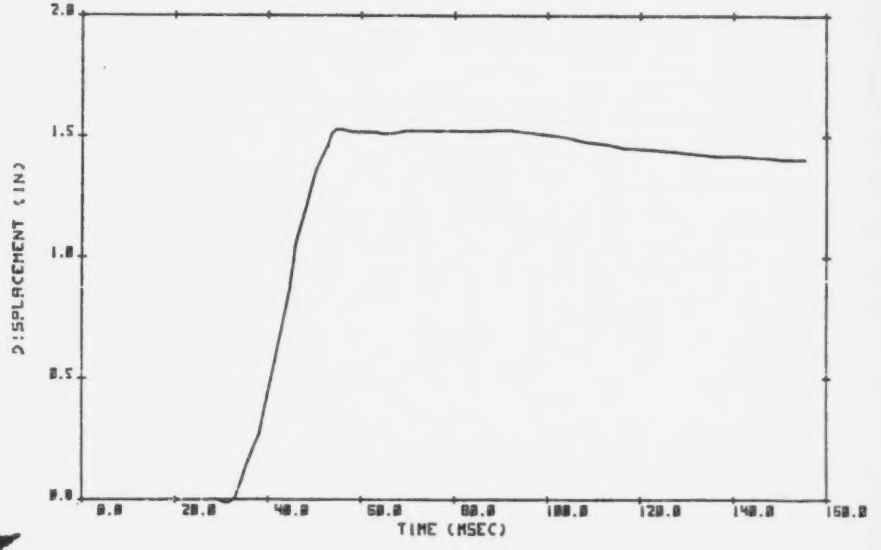

SRL 17-S TEST #30 (ETH 600) - CHEST DEFL'N

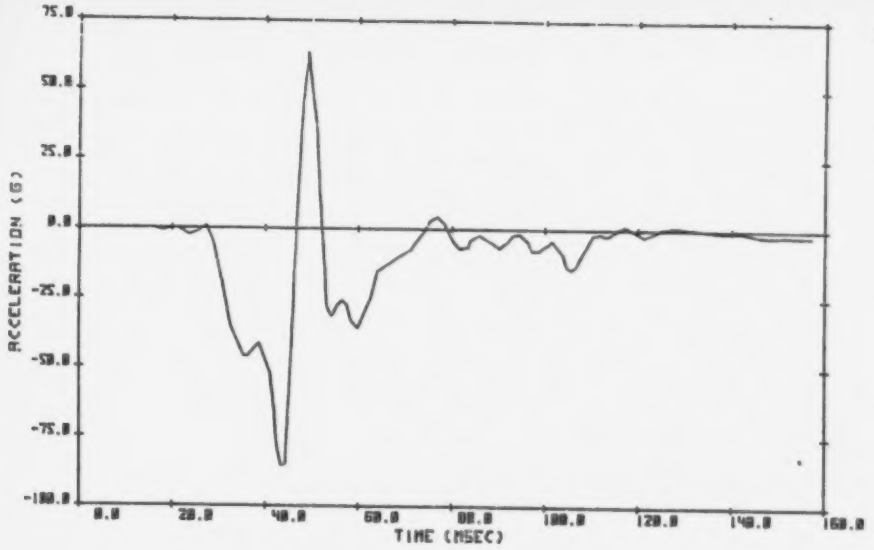

SRL 17-S TEST #31 (R-310-V) - LT. UPPER RIB

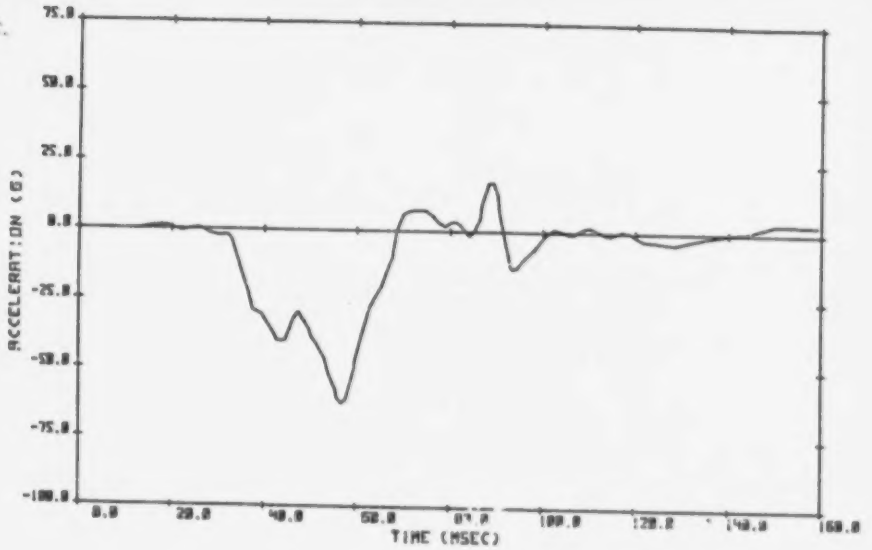

SRL 17-S TEST #31 (R-310-V) - RT. UPPER RIB

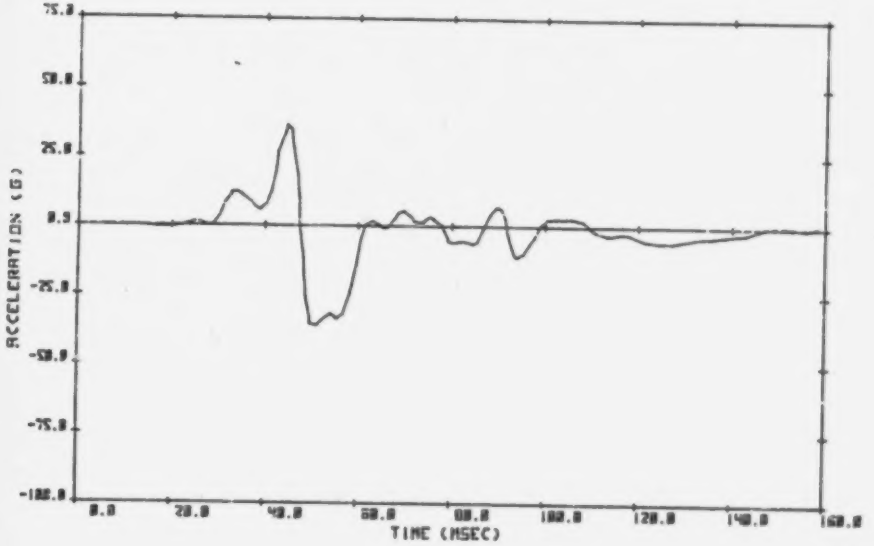

SRL 17-S TEST #31 (R-310-V) - UPPER STERNUM

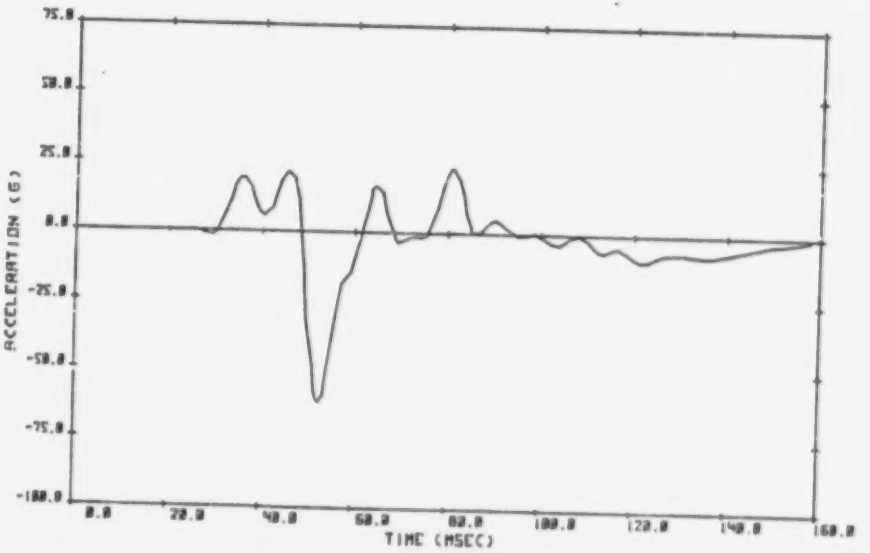

SRL 17-S TEST #31 (R-310-V) - LOWER STERNUM

BEST DOCUMENT AVAILABLE

BEST DOCUMENT AVAILABLE

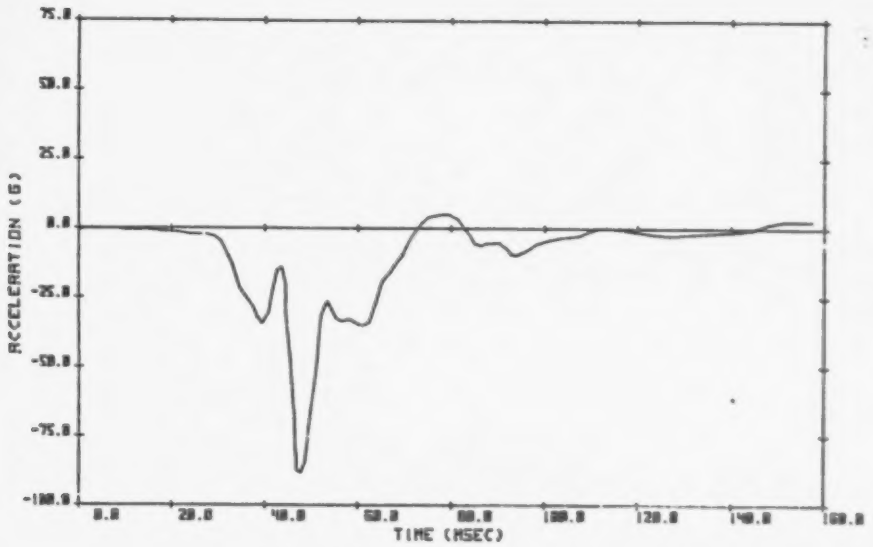

SRL 17-S TEST #31 (R-310-V) - UPPER SPINE

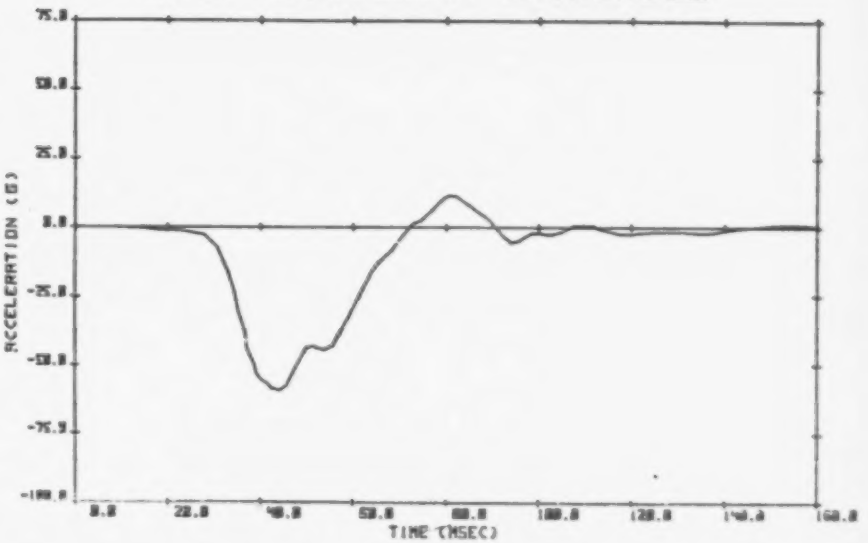

SRL 17-S TEST #31 (R-310-V) - LOWER SPINE

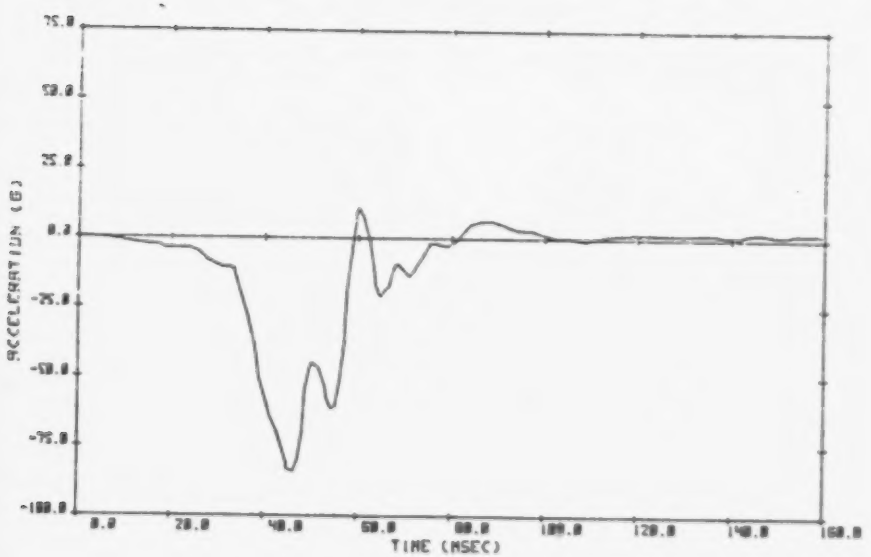

SRL 17-S TEST #31 (R-310-V) - PELVIS

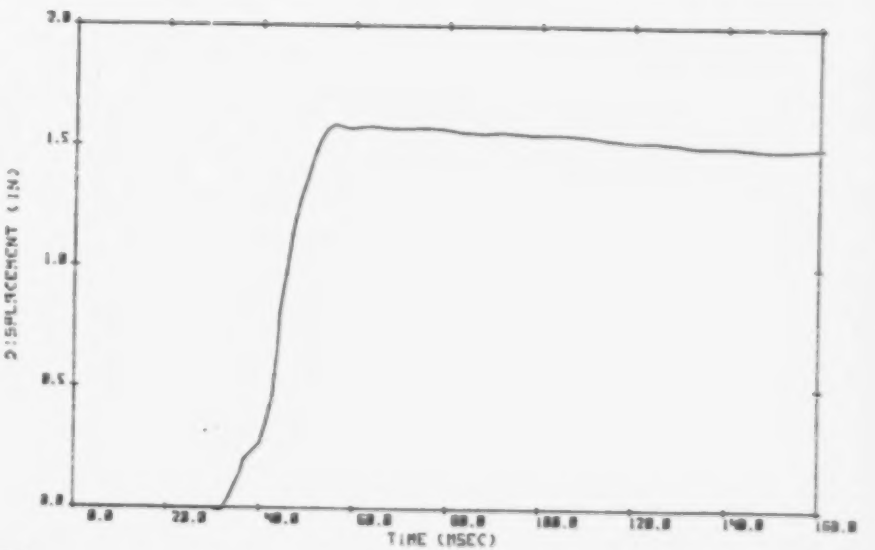

SRL 17-S TEST #31 (R-310-V) - CHEST DEFL'N

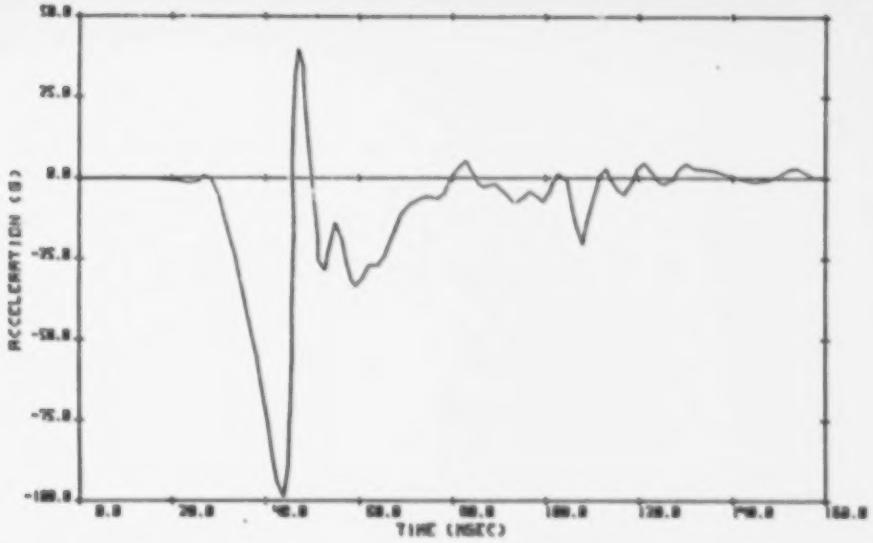

SRL 17-S TEST #32 (AAC) - LEFT UPPER RIB

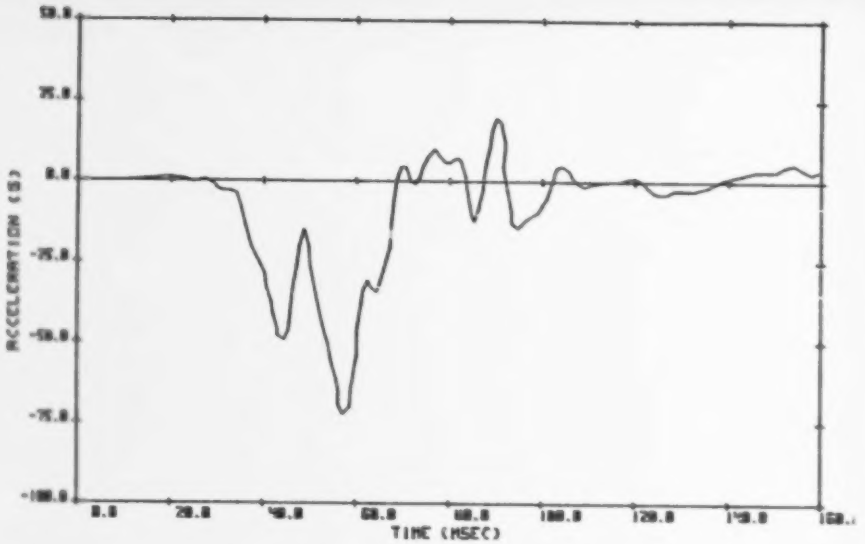

SRL 17-S TEST #32 (AAC) - RIGHT UPPER RIB

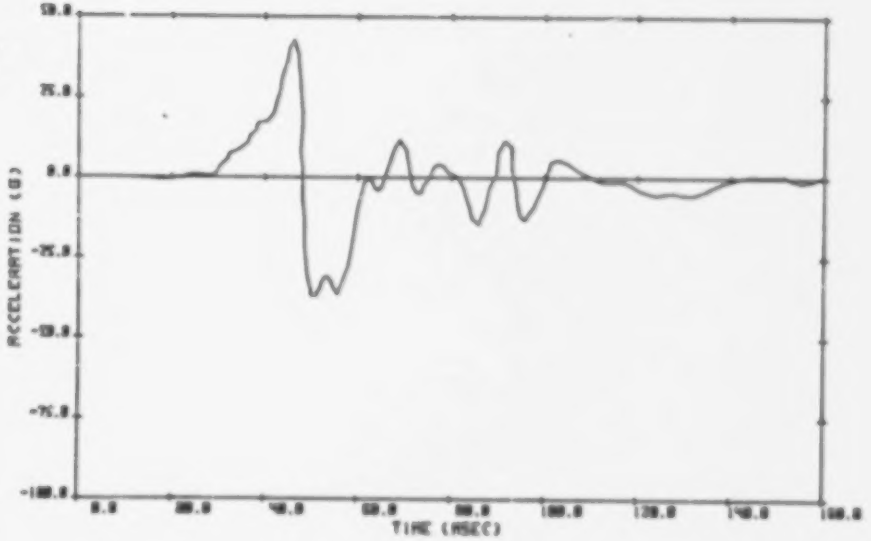

SRL 17-S TEST #32 (AAC) - UPPER STERNUM

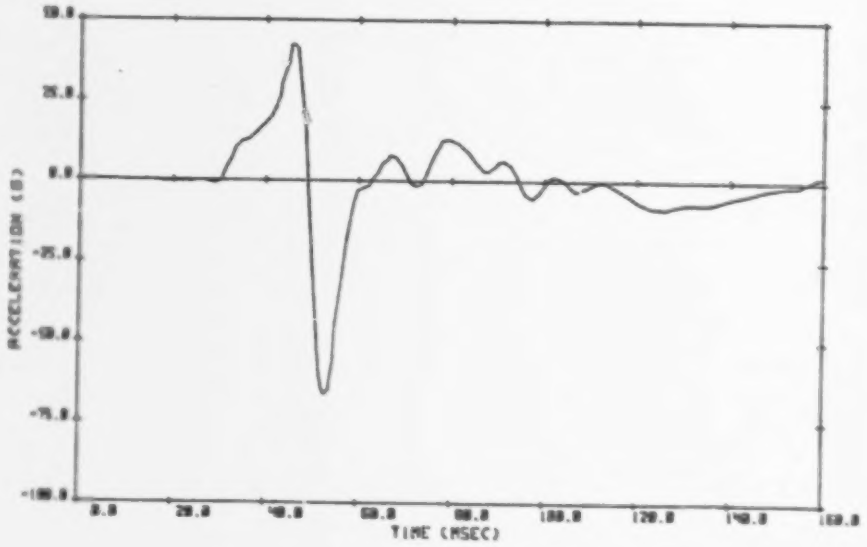

SRL 17-S TEST #32 (AAC) - LOWER STERNUM

BEST DOCUMENT AVAILABLE

BEST DOCUMENT AVAILABLE

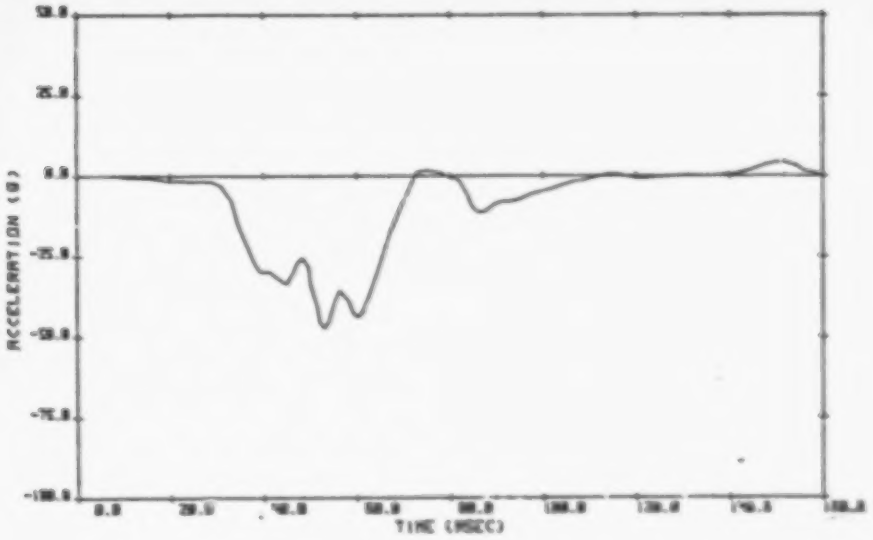

SRL 17-S TEST #32 (AAC) - UPPER SPINE

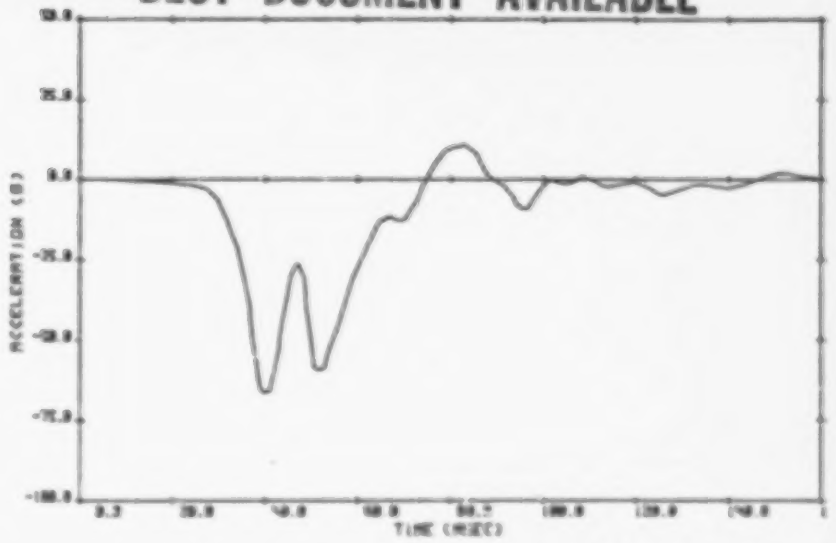

SRL 17-S TEST #32 (AAC) - LOWER SPINE

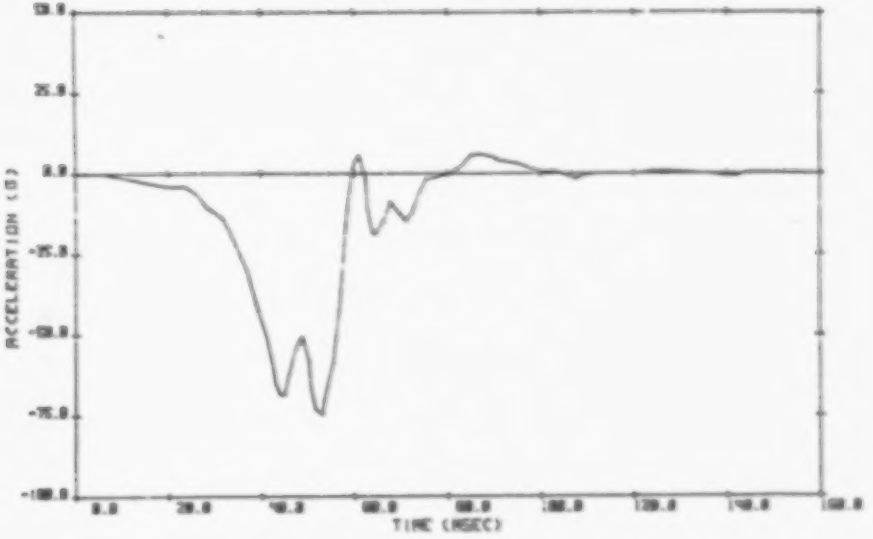

SRL 17-S TEST #32 (AAC) - PELVIS

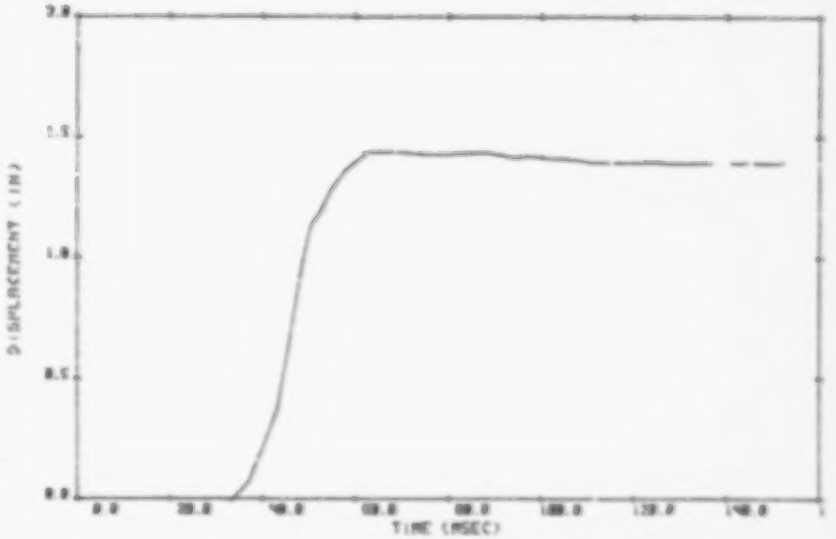

SRL 17-S TEST #32 (AAC) - CHEST DEFLECTION

BEST DOCUMENT AVAILABLE

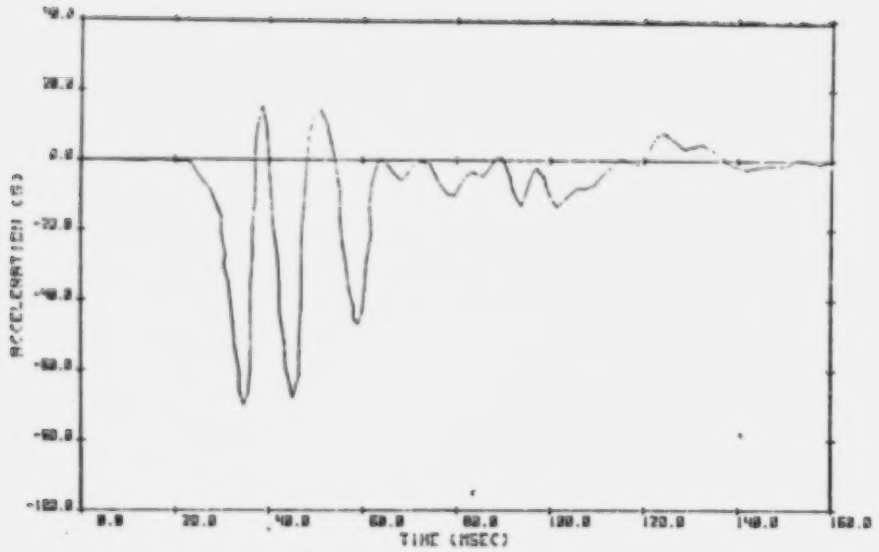

SRL 17-5 TEST #33 (H38C) - LT. UPPER RIB

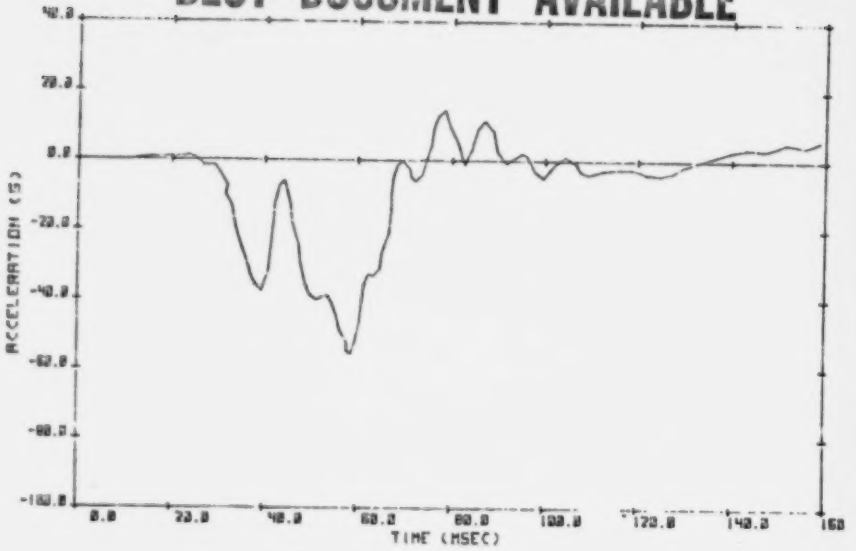

SRL 17-5 TEST #33 (H38C) - RT. UPPER RIB

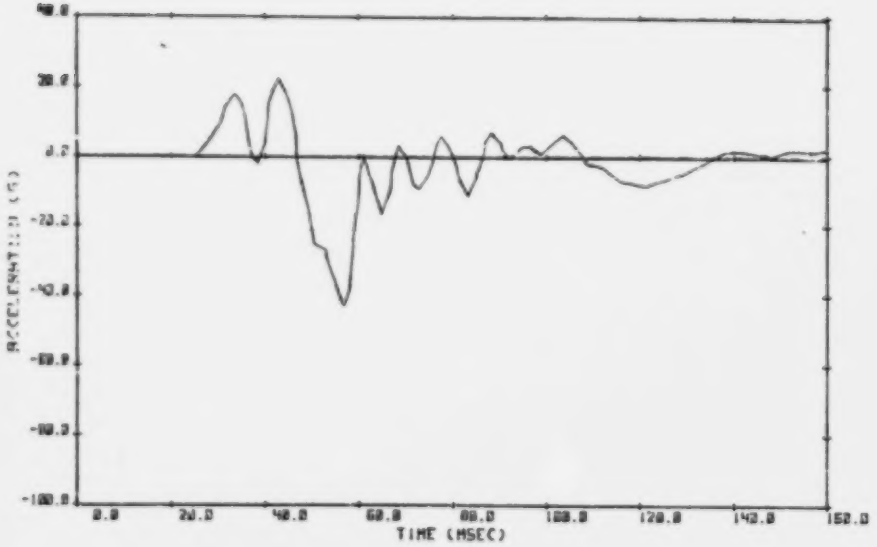

SRL 17-5 TEST #33 (H38C) - UPPER STERNUM

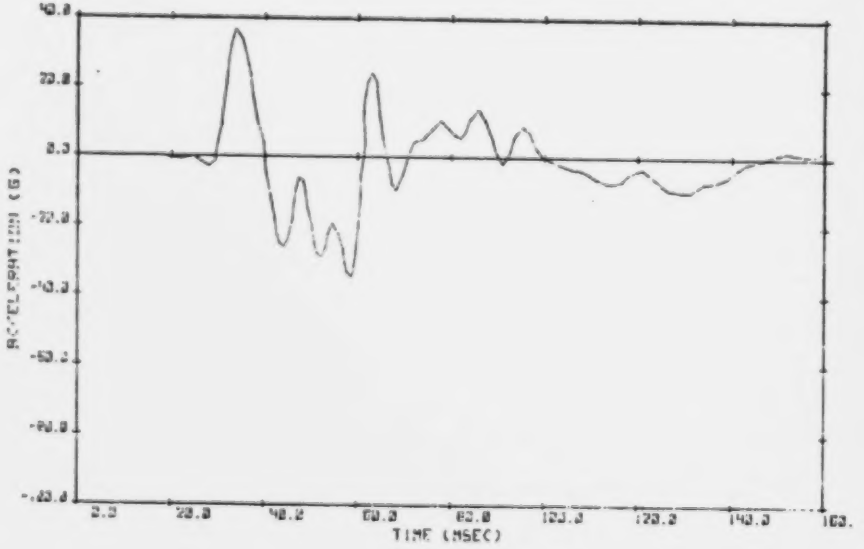

SRL 17-5 TEST #33 (H38C) - LOWER STERNUM

BEST DOCUMENT AVAILABLE

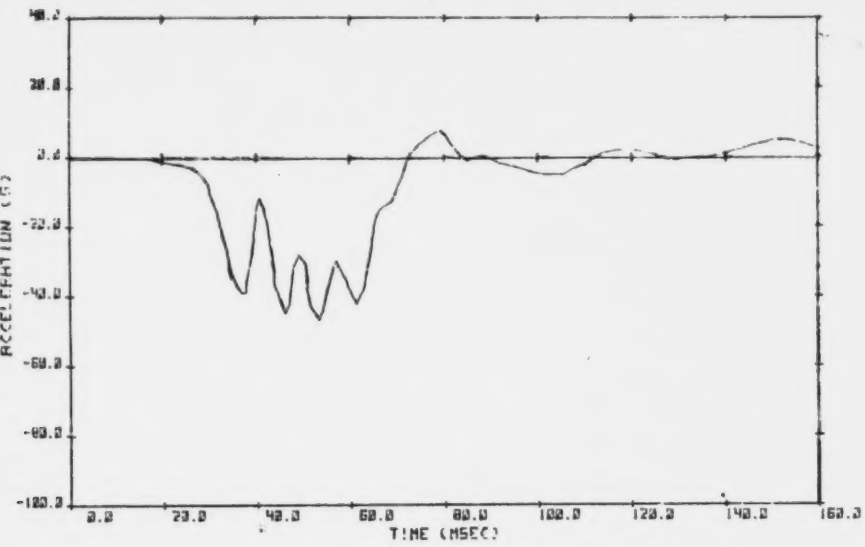

SRL 17-5 TEST #33 (H3BC) - UPPER SPINE

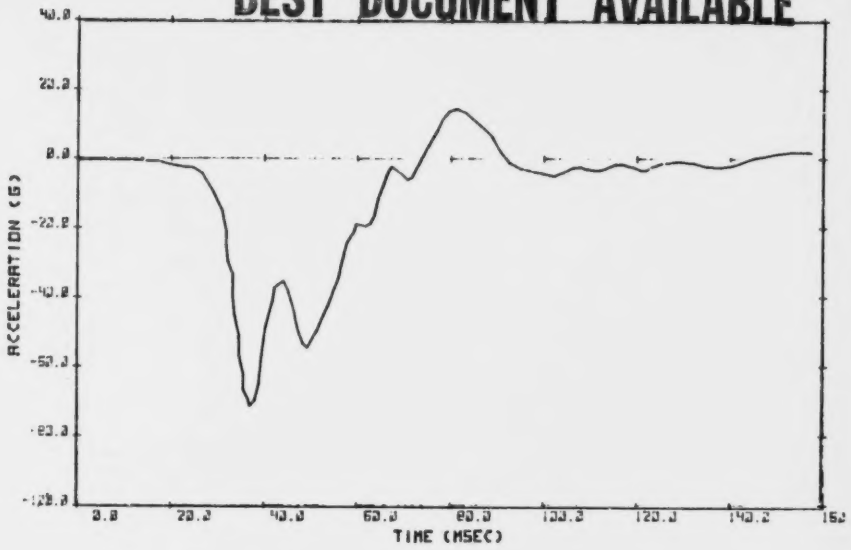

SRL 17-5 TEST #33 (H3BC) - LOWER SPINE

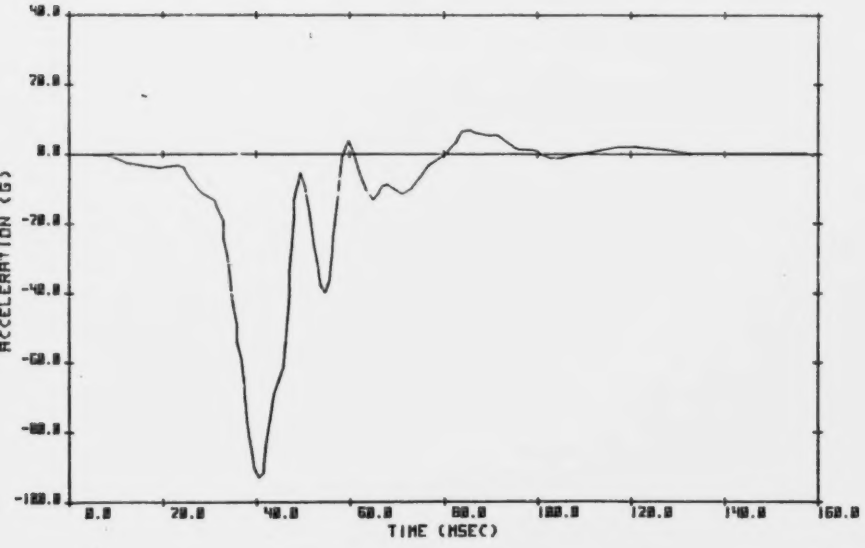

SRL 17-5 TEST #33 (H3BC) - PELVIS

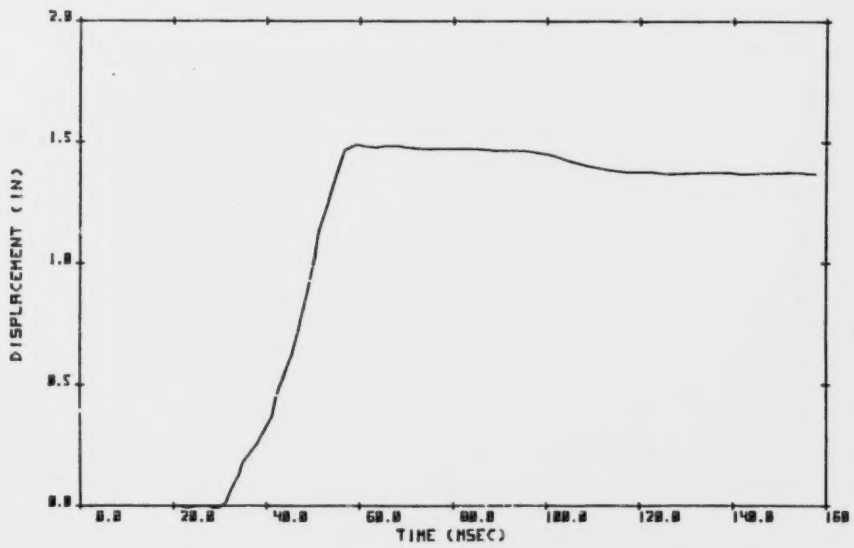

SRL 17-5 TEST #33 (H3BC) - CHEST DEFLECTION

[redacted]

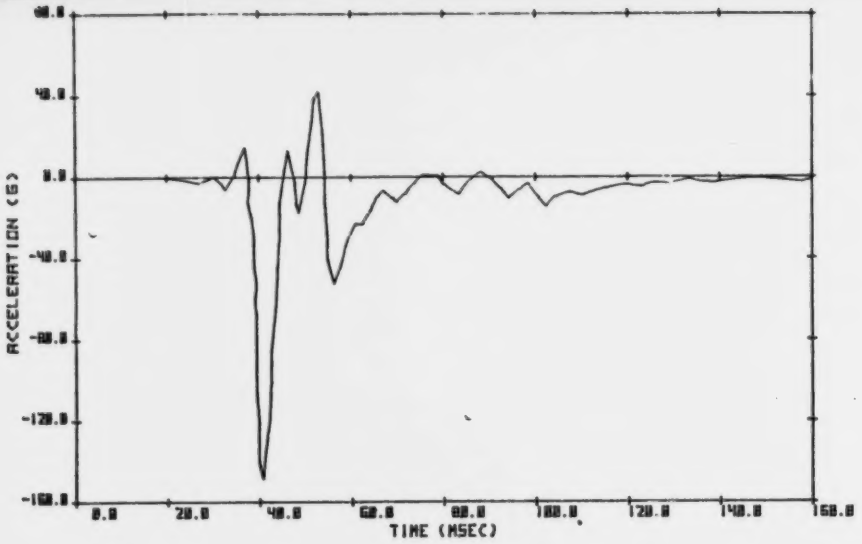

SRL 17-5 TEST #34 - LEFT UPPER RIB

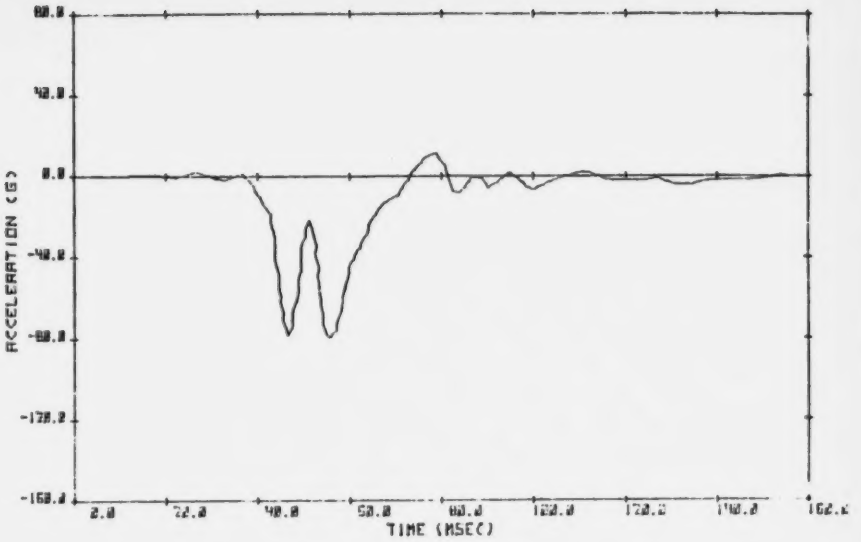

SRL 17-5 TEST #34 - RIGHT UPPER RIB

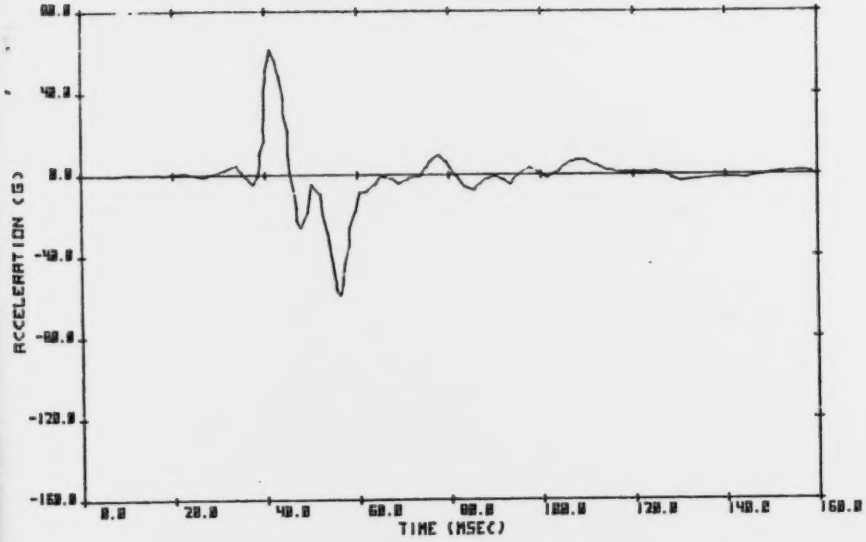

SRL 17-5 TEST #34 - UPPER STERNUM

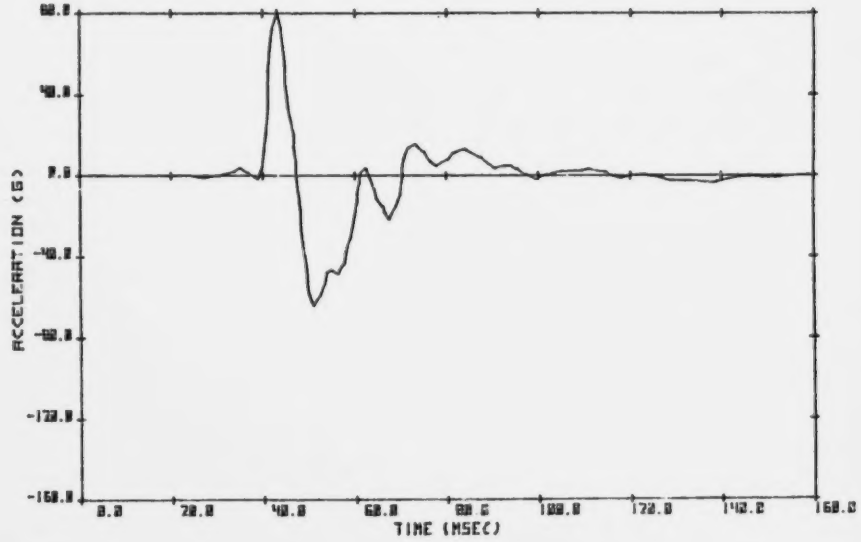

SRL 17-5 TEST #34 - LOWER STERNUM

BEST DOCUMENT AVAILABLE

BEST DOCUMENT AVAILABLE

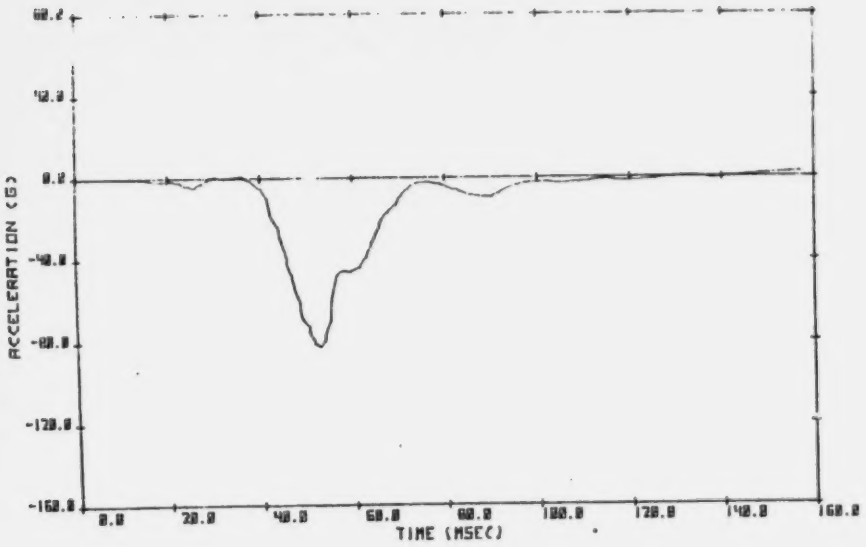

SRL 17-S TEST #34 - UPPER SPINE

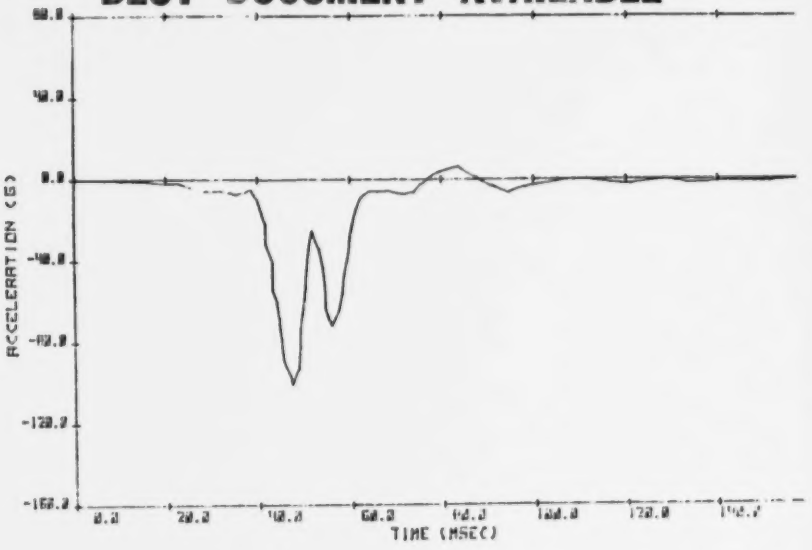

SRL 17-S TEST #34 - LOWER SPINE

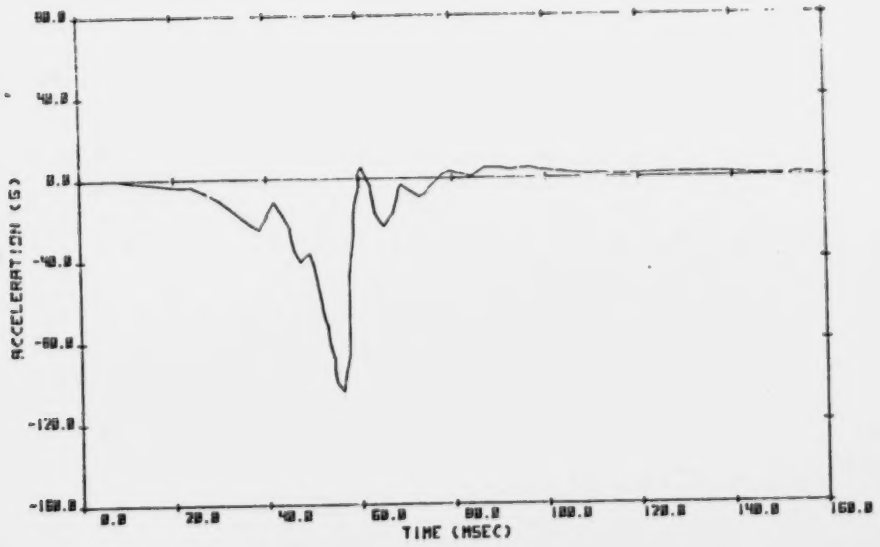

SRL 17-S TEST #34 - PELVIS

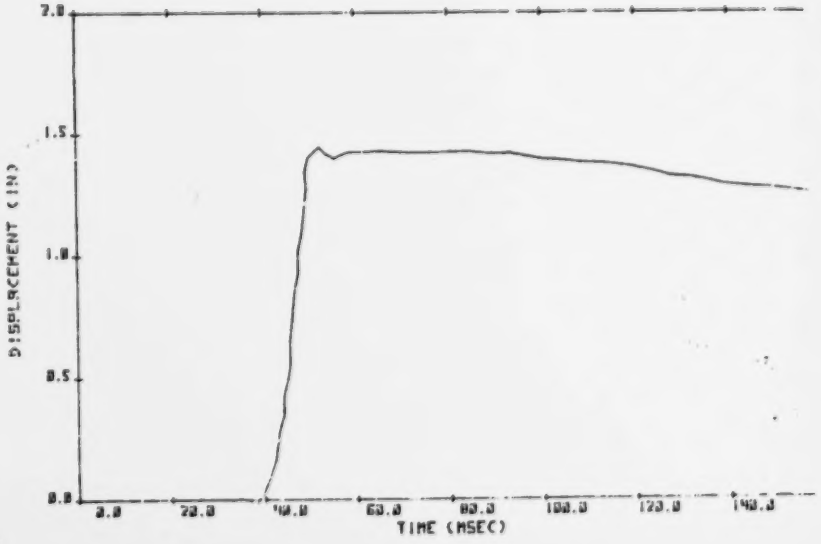

SRL 17-S TEST #34 - CHEST DEFLECTION

BEST DOCUMENT AVAILABLE

APPENDIX I

Drawing & Description of Fluid Impact Accelerator

BEST DOCUMENT AVAILABLE

This description is intended to give an overview of the main components of the accelerator and to tell how it operates. The schematic diagram of Figure I-I shows the components. These are:

1. piston and chamber
2. accumulator
3. hydraulic pump
4. fire valve
5. piston snubber

The accumulator, piston and chamber and piston snubber are all enclosed in the main casing. Only the pump and the fire valve with associated tubing and wiring are external to the device.

The operation of the impactor is as follows:

1) the air valve to the hydraulic pump is opened, initiating the pumping action

2) fluid is compressed into the accumulator until the desired charge pressure is reached (typical pressures of 10,000 psi are reached in a few seconds). The pump is turned off.

3) the fire valve is opened electronically expanding the fluid into the chamber

4) the piston is pushed out until all of the energy from the fluid is transferred to kenetic energy

5) the piston is "snubbed" to zero velocity.

BEST DOCUMENT AVAILABLE

The device has many advantages over more commonly used pneumatic devices. Safety is a key factor. The hydraulic fluid only compresses to levels of less than 10%, so a fracture of the main casing should not throw fragments to the surrounding area. Compact size (5" x 5" x 36") and large capacity are also positive factors for the device.

The design drawings of the device are contained on the following pages.

BEST DOCUMENT AVAILABLE

FLUID IMPACT ACCELERATOR

SCHEMATIC DIAGRAM

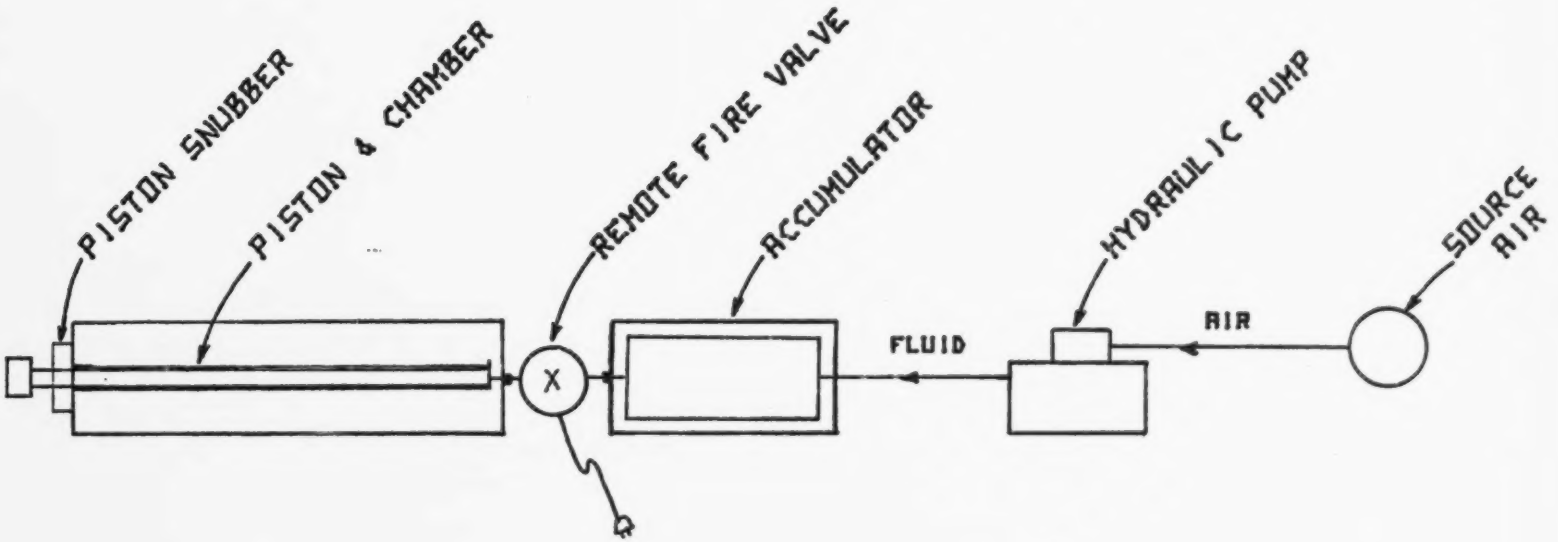

FIGURE I-1

Blank Page

BEST DOCUMENT AVAILABLE

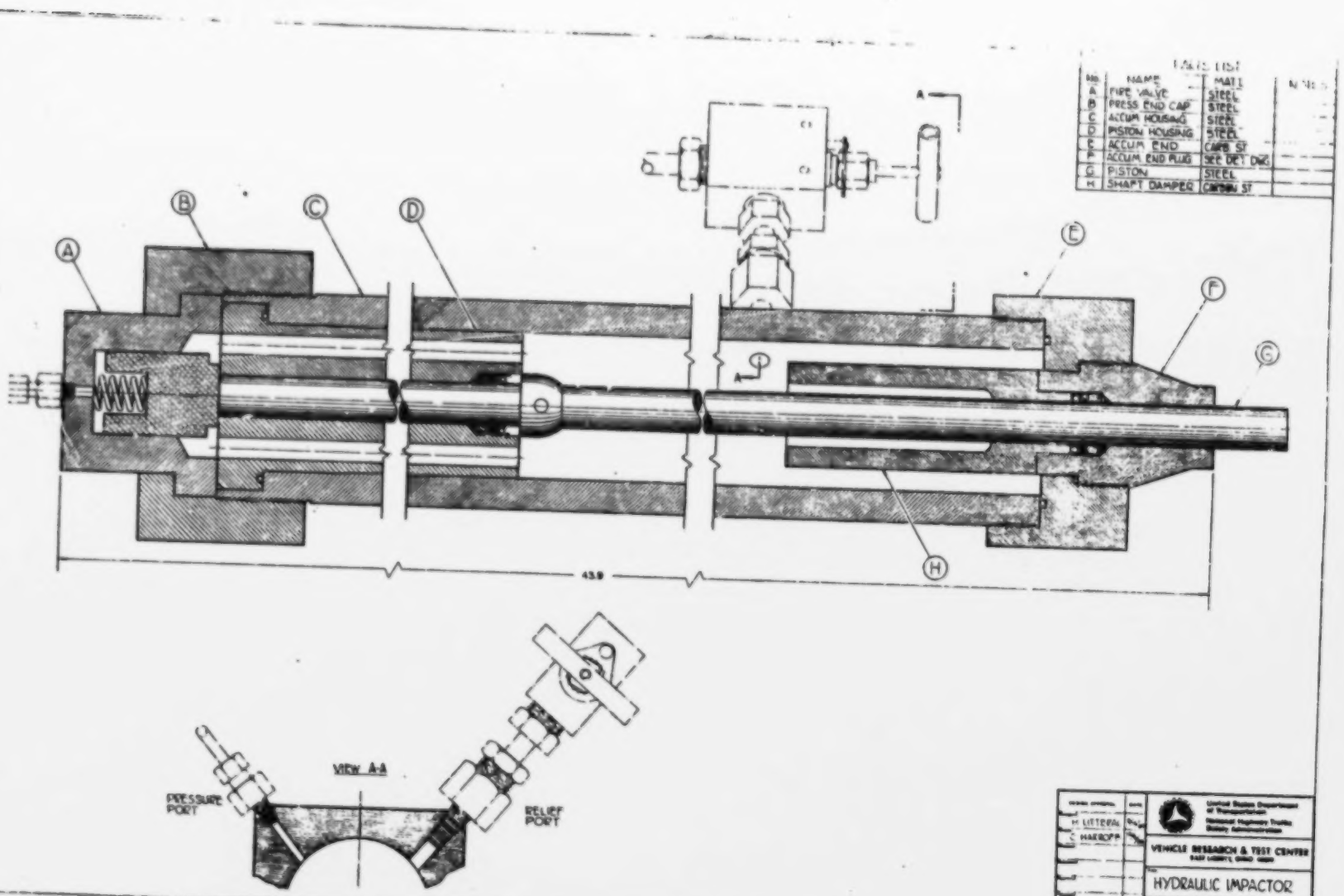

BEST DOCUMENT AVAILABLE

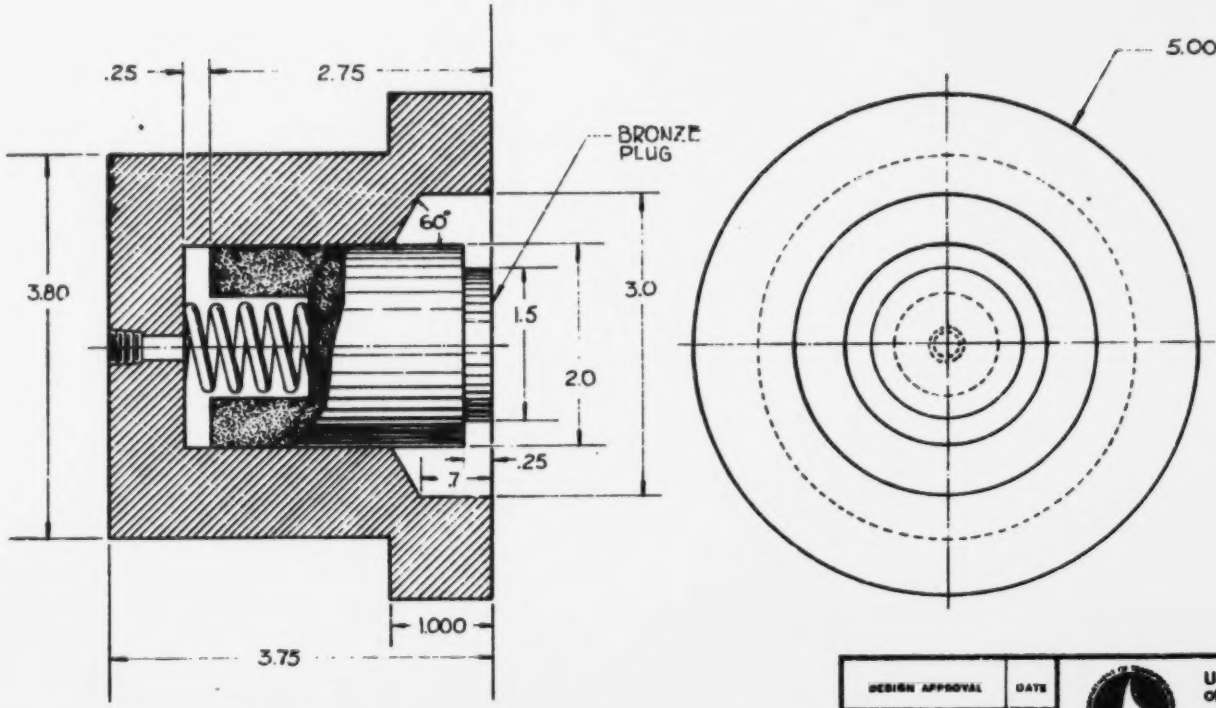

NOTE:
SPRING IS 10 LBS.
15/16 DIAM. x 2" L.

DESIGN APPROVAL	DATE
Designed H. LITTERAL	2/12/80
Drawn C HARROFF	12/9/80
Checked	
Submitted	
Approved	
Approved	
Approved	

United States Department of Transportation
National Highway Traffic Safety Administration

VEHICLE RESEARCH & TEST CENTER
EAST LIBERTY, OHIO 43319

Title: FIRE VALVE

Scale: FULL | Drawing Number: SRL 17-A

File Number | Sheet 2 of 9

BEST DOCUMENT AVAILABLE

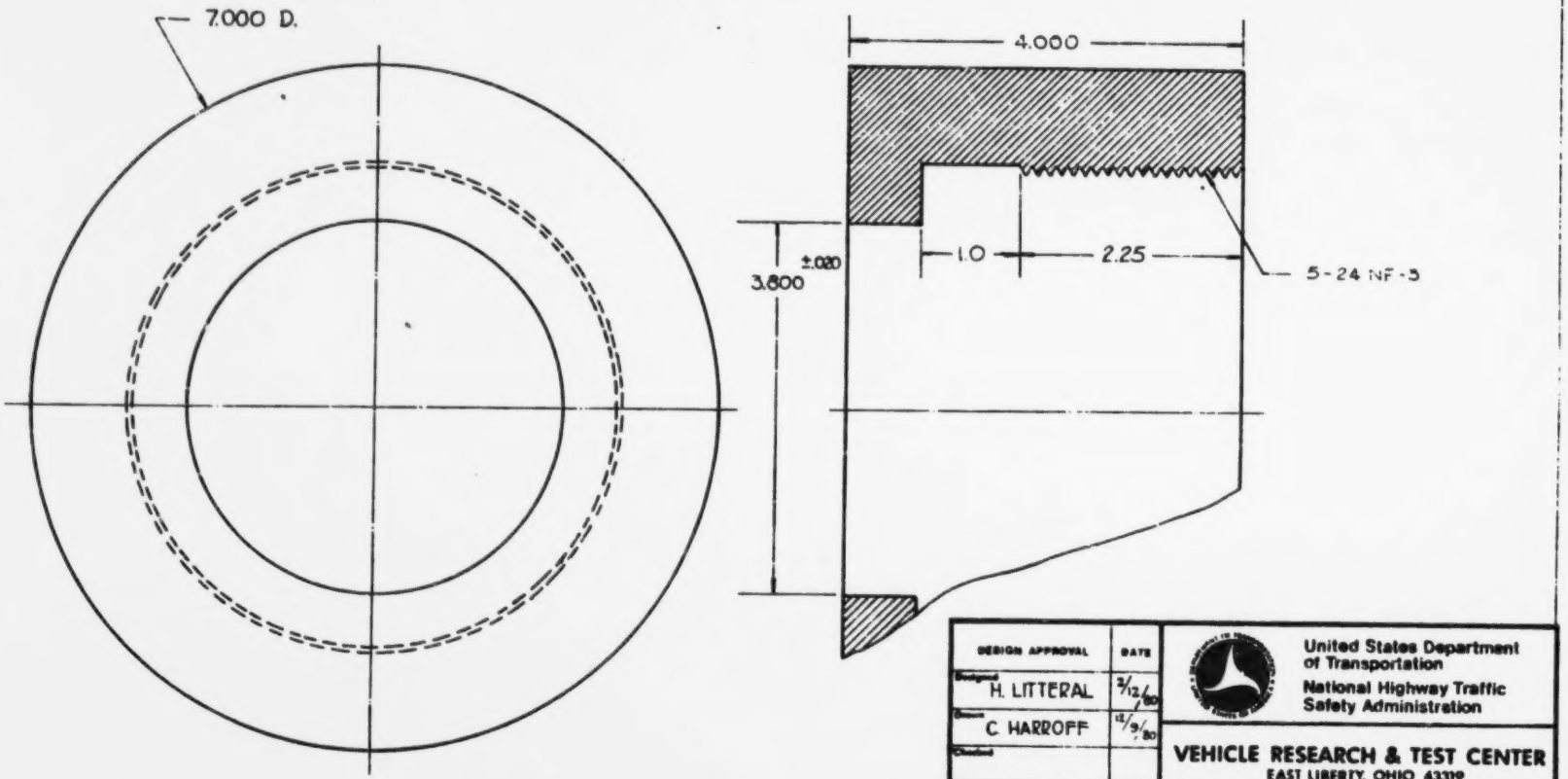

DESIGN APPROVAL	DATE
H. LITTERAL	3/12/80
C. HARROFF	12/9/80

United States Department of Transportation
National Highway Traffic Safety Administration

VEHICLE RESEARCH & TEST CENTER
EAST LIBERTY, OHIO 43319

Title: PRESSURE END CAP

Scale: FULL | Drawing Number: SRL 17-B | Sheet 3 of 9

BEST DOCUMENT AVAILABLE

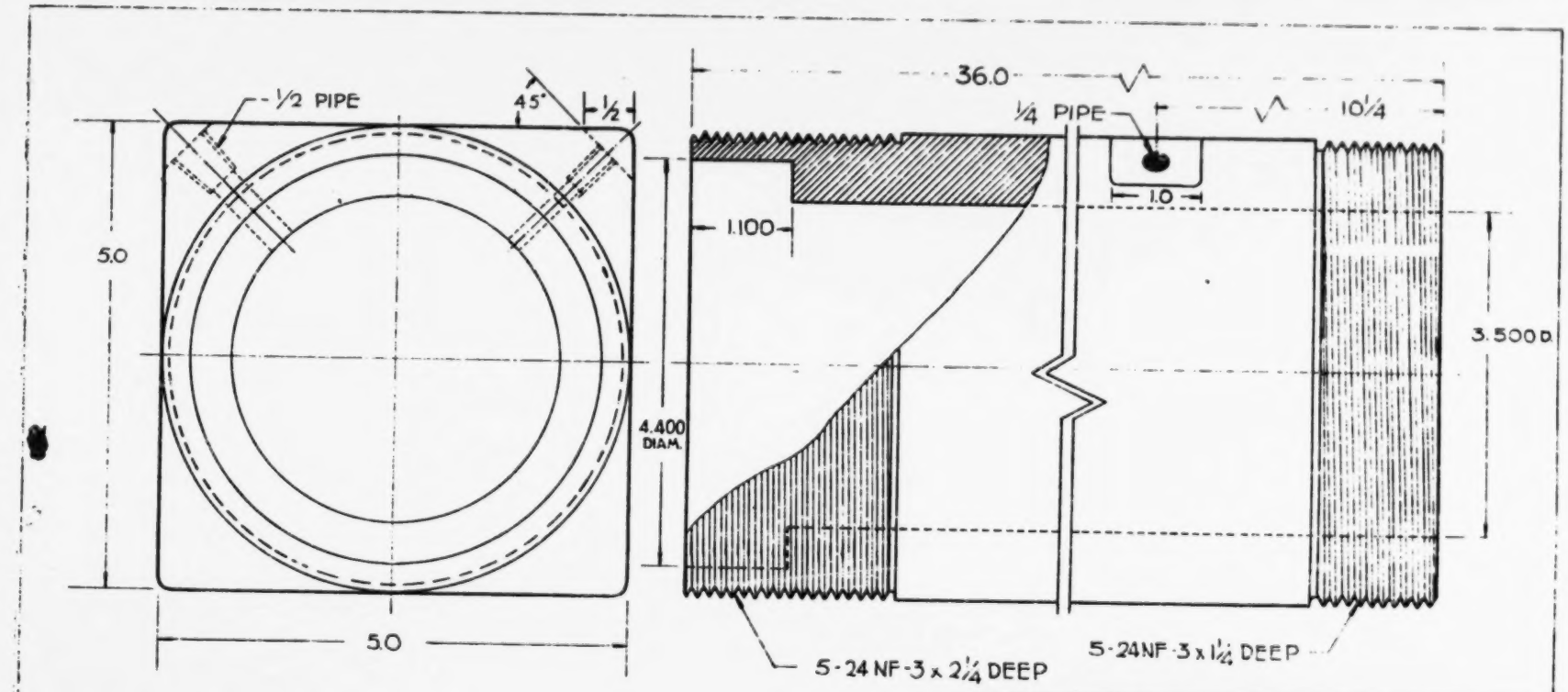

DESIGN APPROVAL	DATE
Designed H. LITTERAL	3/12/80
Drawn C. HARROFF	11/3/80
Checked	
Submitted	
Approved	
Approved	
Approved	

United States Department of Transportation
National Highway Traffic Safety Administration

VEHICLE RESEARCH & TEST CENTER
EAST LIBERTY, OHIO 43319

Title: ACCUMULATOR HOUSING

Scale: FULL | Drawing Number: SRL 17-C

File Number | Sheet 1 of 9

[redacted]
260

BEST DOCUMENT AVAILABLE

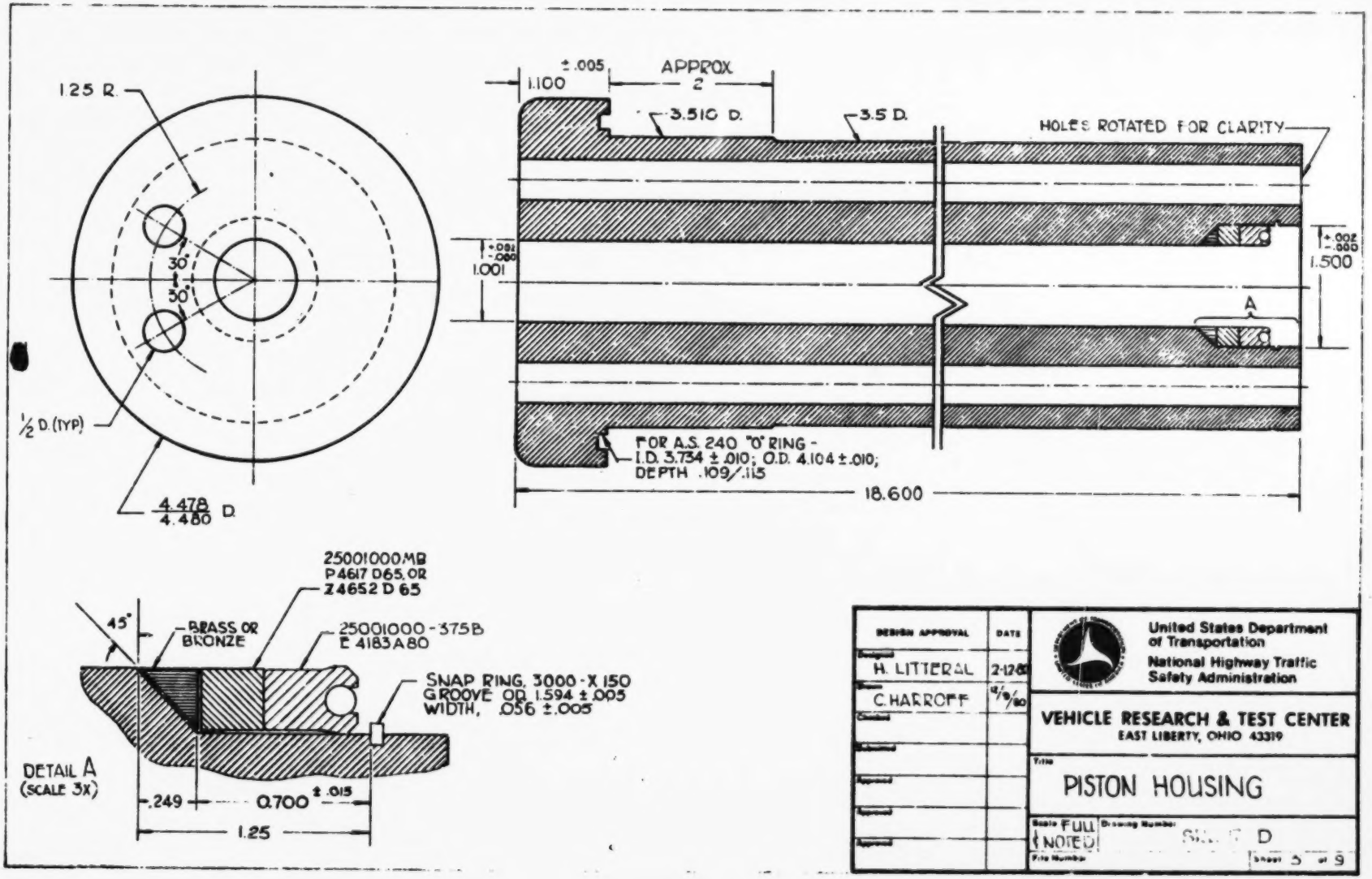

DESIGN APPROVAL	DATE
H. LITTERAL	2-12-60
C. HARROFF	4/9/60

United States Department of Transportation
National Highway Traffic Safety Administration

VEHICLE RESEARCH & TEST CENTER
EAST LIBERTY, OHIO 43319

Title: PISTON HOUSING

Scale: FULL (NOTED) Drawing Number: SK... D

File Number:

Sheet 5 of 9

BEST DOCUMENT AVAILABLE

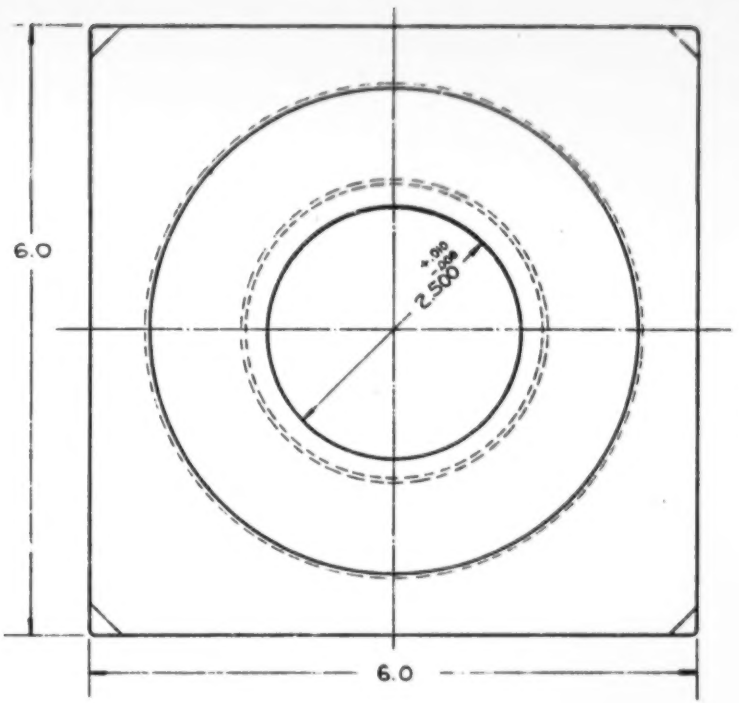

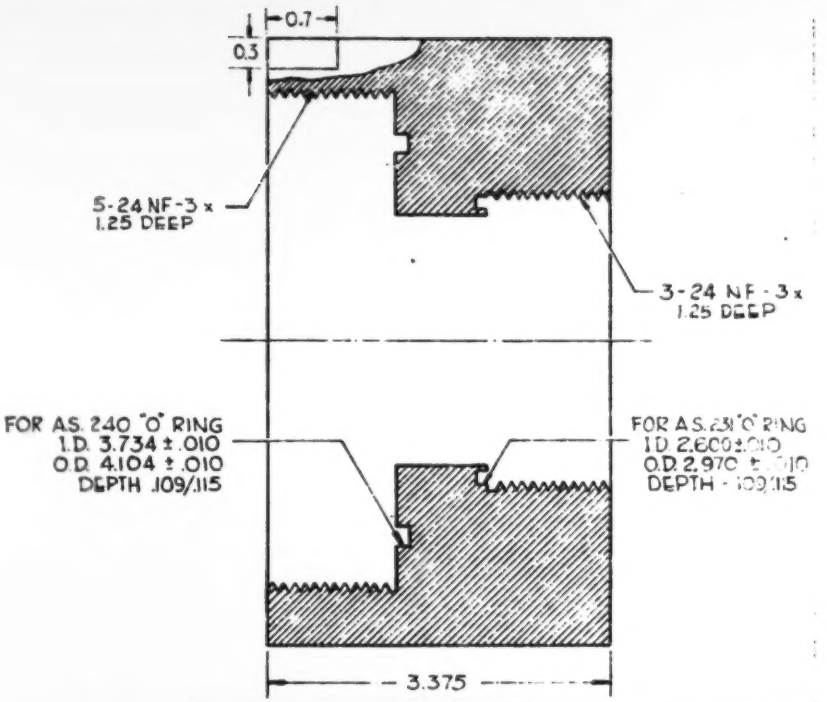

DESIGN APPROVAL	DATE
Designed H. LITTERAL	2/12/80
Drawn C. HARROFF	12/9/80
Checked	
Submitted	
Approved	
Approved	
Approved	

United States Department of Transportation
National Highway Traffic Safety Administration

VEHICLE RESEARCH & TEST CENTER
EAST LIBERTY, OHIO 43319

Title: ACCUMULATOR END

Scale: FULL | Drawing Number: SRL 17-E

File Number | Sheet 6 of 9

BEST DOCUMENT AVAILABLE

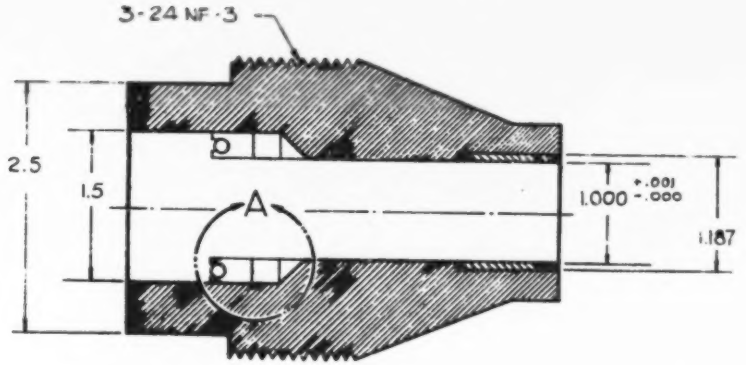

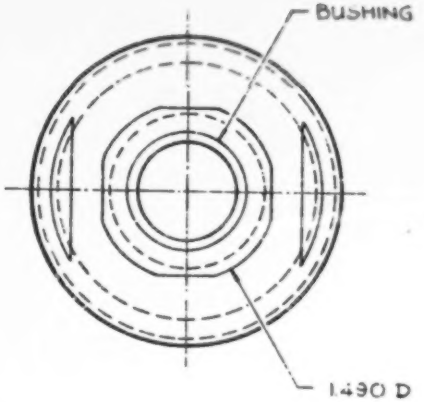

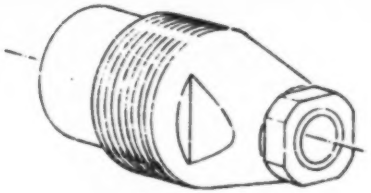

(NO SCALE)

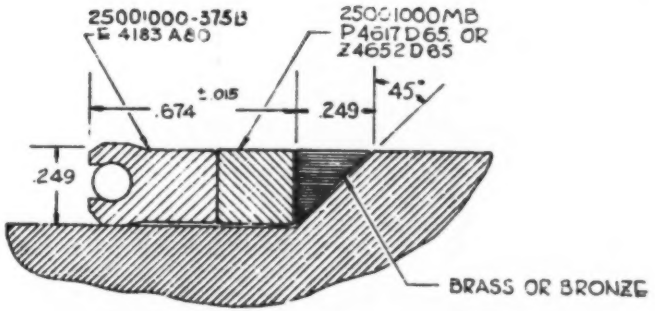

DETAIL A
(SCALE 3x)

DESIGN APPROVAL	DATE
Designed H. LITTERAL	9/12/80
Drawn C. HARROFF	12/3/80
Checked	
Submitted	
Approved	
Approved	
Approved	

United States Department of Transportation
National Highway Traffic Safety Administration

VEHICLE RESEARCH & TEST CENTER
EAST LIBERTY, OHIO 43319

Title: ACCUMULATOR END PLUG & DETAIL

Scale: FULL & NOTED | Drawing Number: [illegible]-F

File Number | Sheet 1 of 9

BEST DOCUMENT AVAILABLE

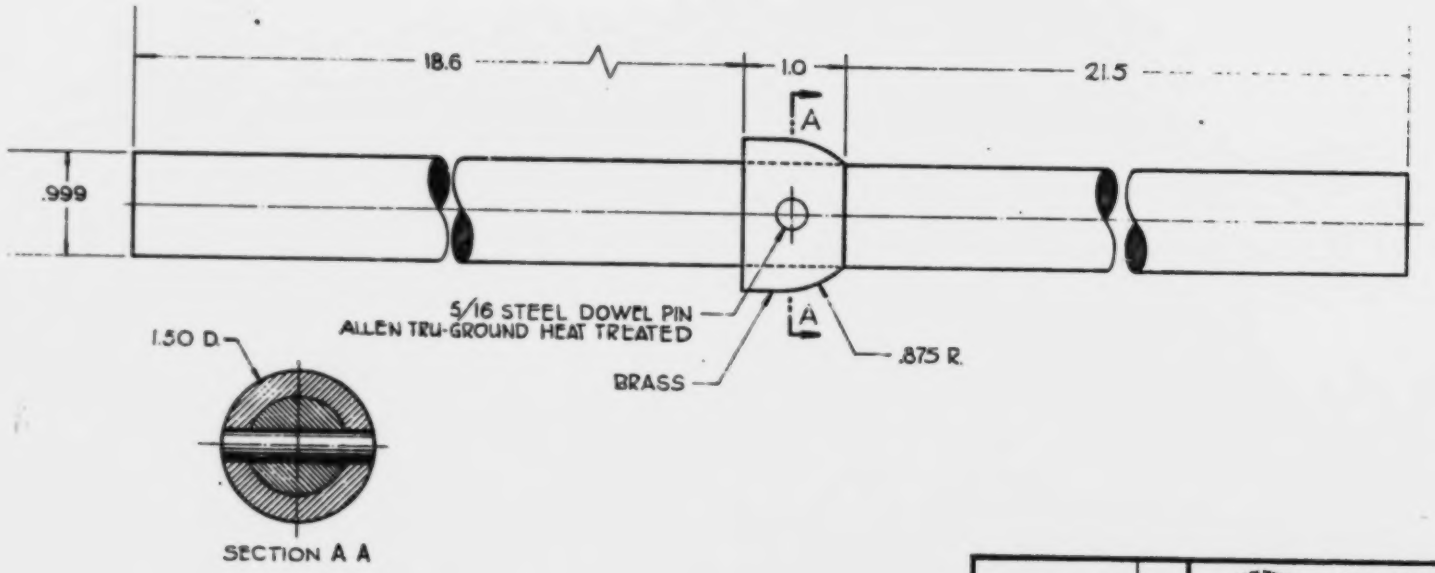

SECTION A A

DESIGN APPROVAL	DATE
Designed: H. LITTERAL	2/12/80
Drawn: C. HARROFF	12/9/80
Checked	
Released	
Approved	
Approved	
Approved	

United States Department of Transportation
National Highway Traffic Safety Administration

VEHICLE RESEARCH & TEST CENTER
EAST LIBERTY, OHIO 43319

Title: PISTON

Scale: FULL | Drawing Number: SRL 17-G | File Number | Sheet 8 of 9

BEST DOCUMENT AVAILABLE

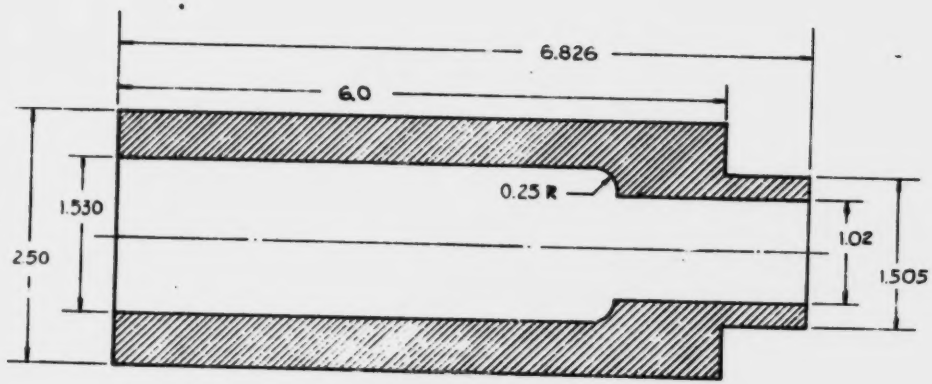

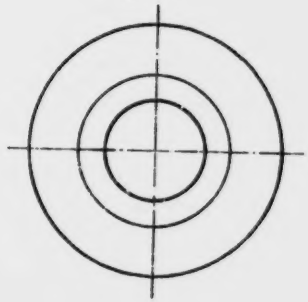

MATERIAL - CARBON STEEL

DESIGN APPROVAL	DATE
Designed H. LITTERAL	3/13/80
Drawn C. HARROFF	11/9/80
Checked	
Submitted	
Approved	
Approved	
Approved	

United States Department of Transportation
National Highway Traffic Safety Administration

VEHICLE RESEARCH & TEST CENTER
EAST LIBERTY, OHIO 43319

Title: SHAFT DAMPER

Scale: FULL | Drawing Number: SRL 17-H

File Number:

Sheet 9 of 9

[redacted]
265

BEST DOCUMENT AVAILABLE

APPENDIX J

Tarriere Drop Tests

BEST DOCUMENT AVAILABLE

Two types of drop tests were performed using the prototype side impact dummy. The first type was a one meter drop test onto a rigid surface. The second type was a two meter drop test into the Tarriere padding samples.

Three one (1) meter drop tests onto a rigid surface were performed. Figure J-1 is a photo of the test setup for the rigid drop tests. The drop test instrumentation consisted of 15 accelerometer (2264-2000) channels on the dummy, 1 force plate, 1 deflection potentiometer, 1 timing channel and 2 high speed cameras. Figures J-2 through J-5 are overlay plots of the three tests for the accelerometer readings of the left upper rib, the right upper rib, the upper spine and the lower spine, respectively. Dummy responses were fairly repeatable, with some unexpected variation in spinal accelerations. Manual calculations of the injury values were performed based on the spinal accelerations and on the "Q" and "B" parameters. The drop tests were performed prior to the installation of the AIS computer software, thereby necessitating manual injury calculations.

Following the 1 meter rigid drop tests, four two (2) meter drop tests into the Tarriere padding samples were performed. Figure J-6 is the test setup for the padded drop tests. Two drops were conducted into the full 5 1/2 inch padding samples. The padding samples were replaced after each test. The same condition was then repeated with the thoracic flesh removed from the dummy to allow film analysis of the padding stroke. Finally, 3 inch padding samples were cut and the 2 meter test was repeated (dummy flesh was on). It was estimated from the films that the dummy stroked slightly over half way into the 5 1/2 inch sample, and nearly all the way through the 3 inch samples. A summary of the test results for both the 1 meter and 2 meter tests are contained in Table J-1.

BEST DOCUMENT AVAILABLE

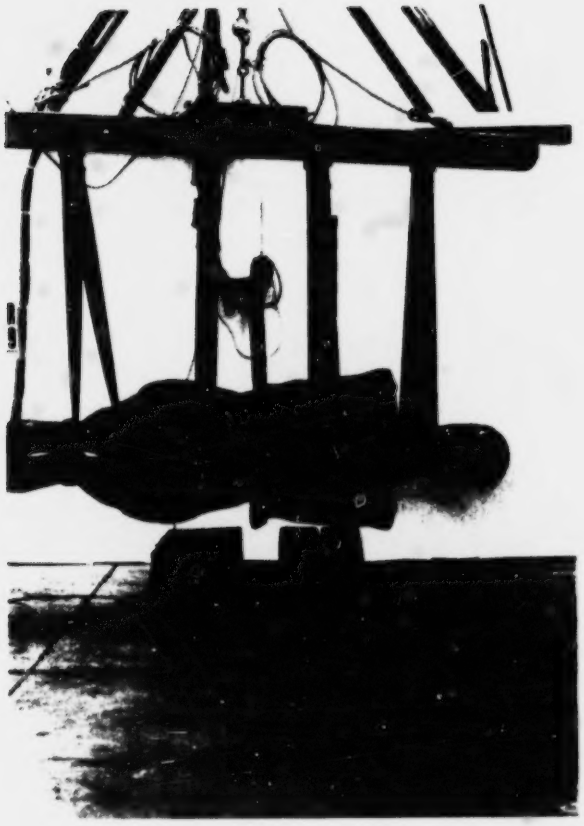

FIGURE J-1

Rigid Drop Test Set-up

BEST DOCUMENT AVAILABLE

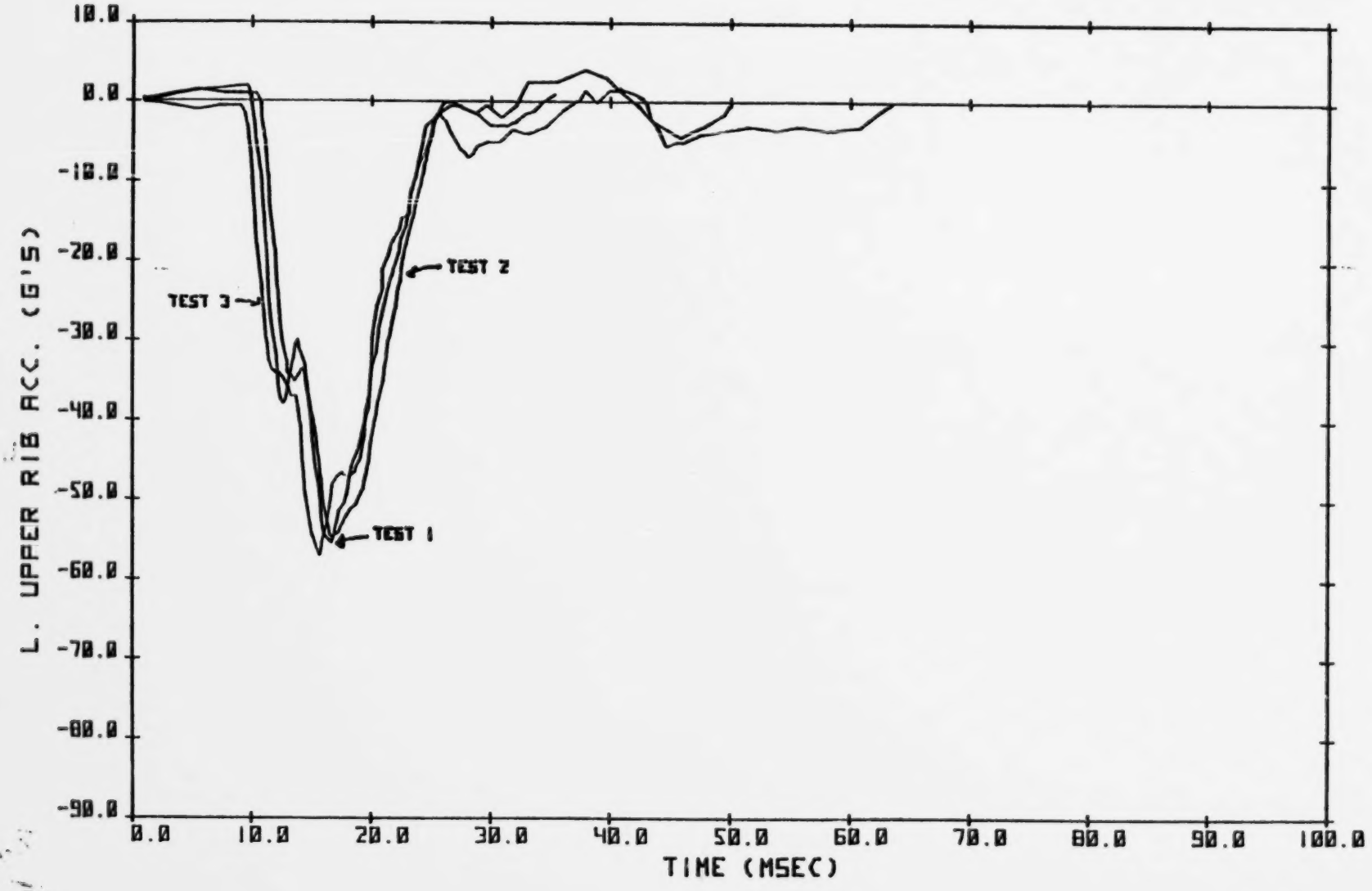

FIGURE J-2

RIGID DROP TESTS (1 METER)

BEST DOCUMENT AVAILABLE

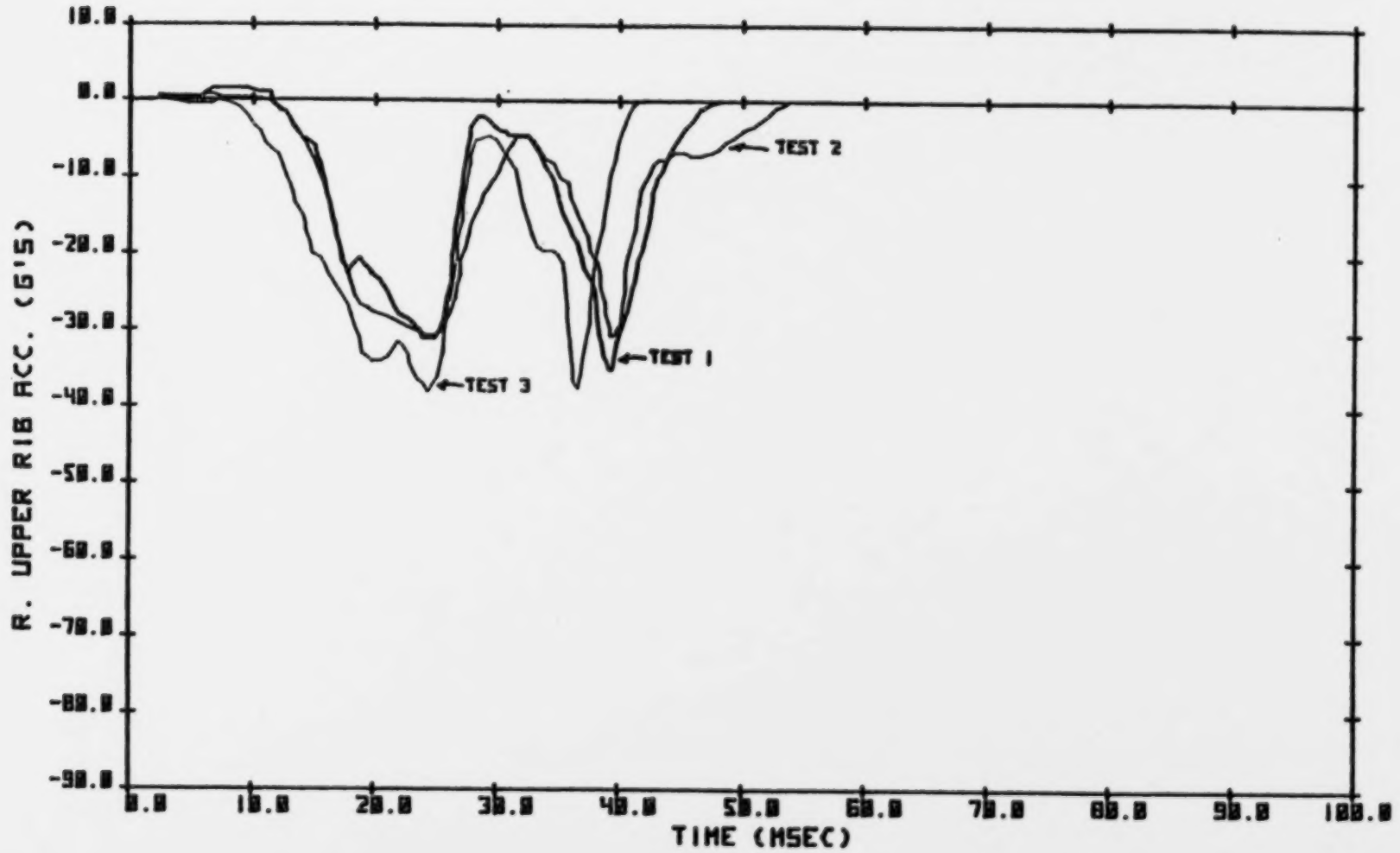

FIGURE J-3 RIGID DROP TESTS (1 METER)

BEST DOCUMENT AVAILABLE

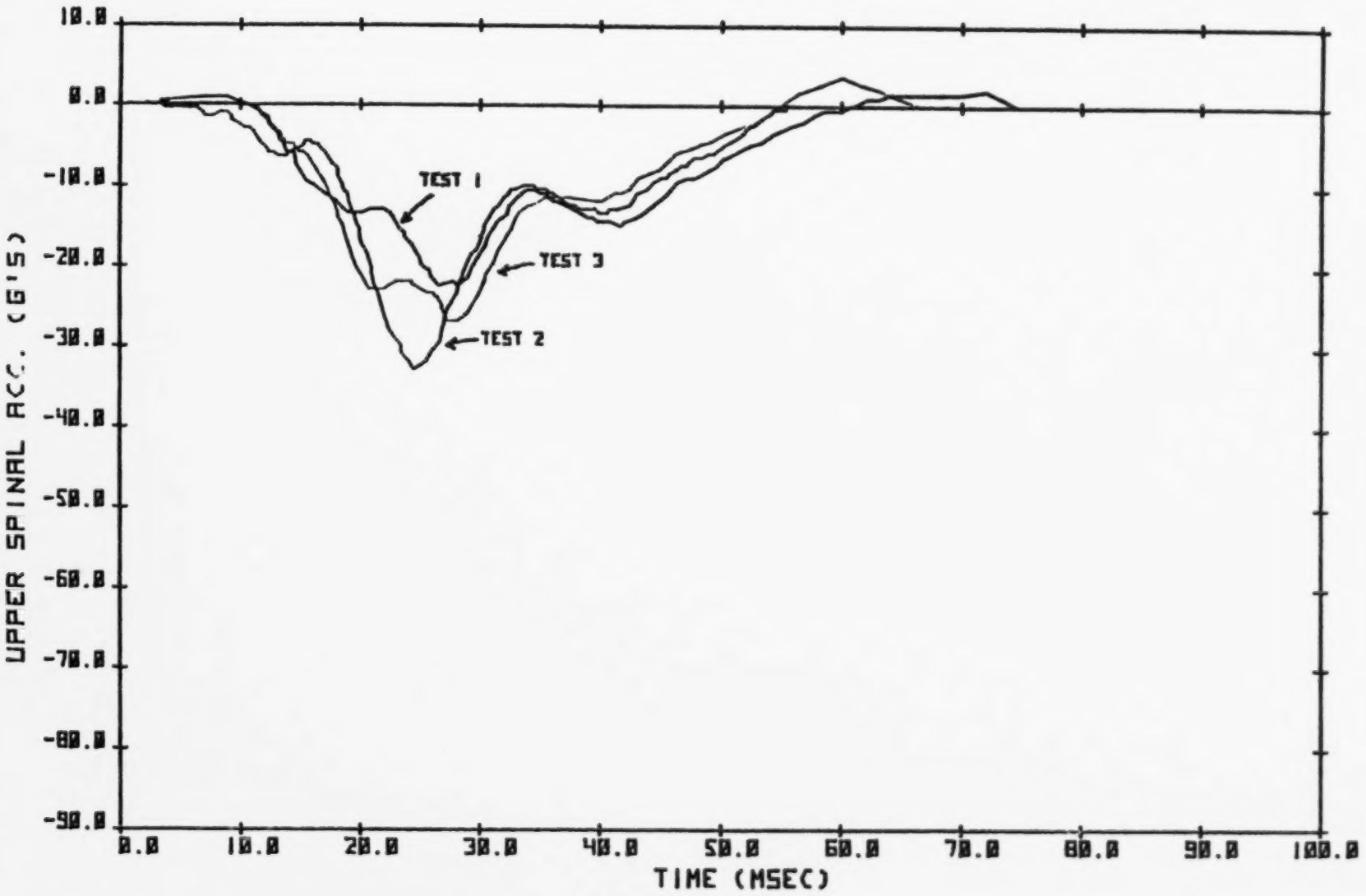

FIGURE J-4

RIGID DROP TESTS (1 METER)

Blank Page

BEST DOCUMENT AVAILABLE

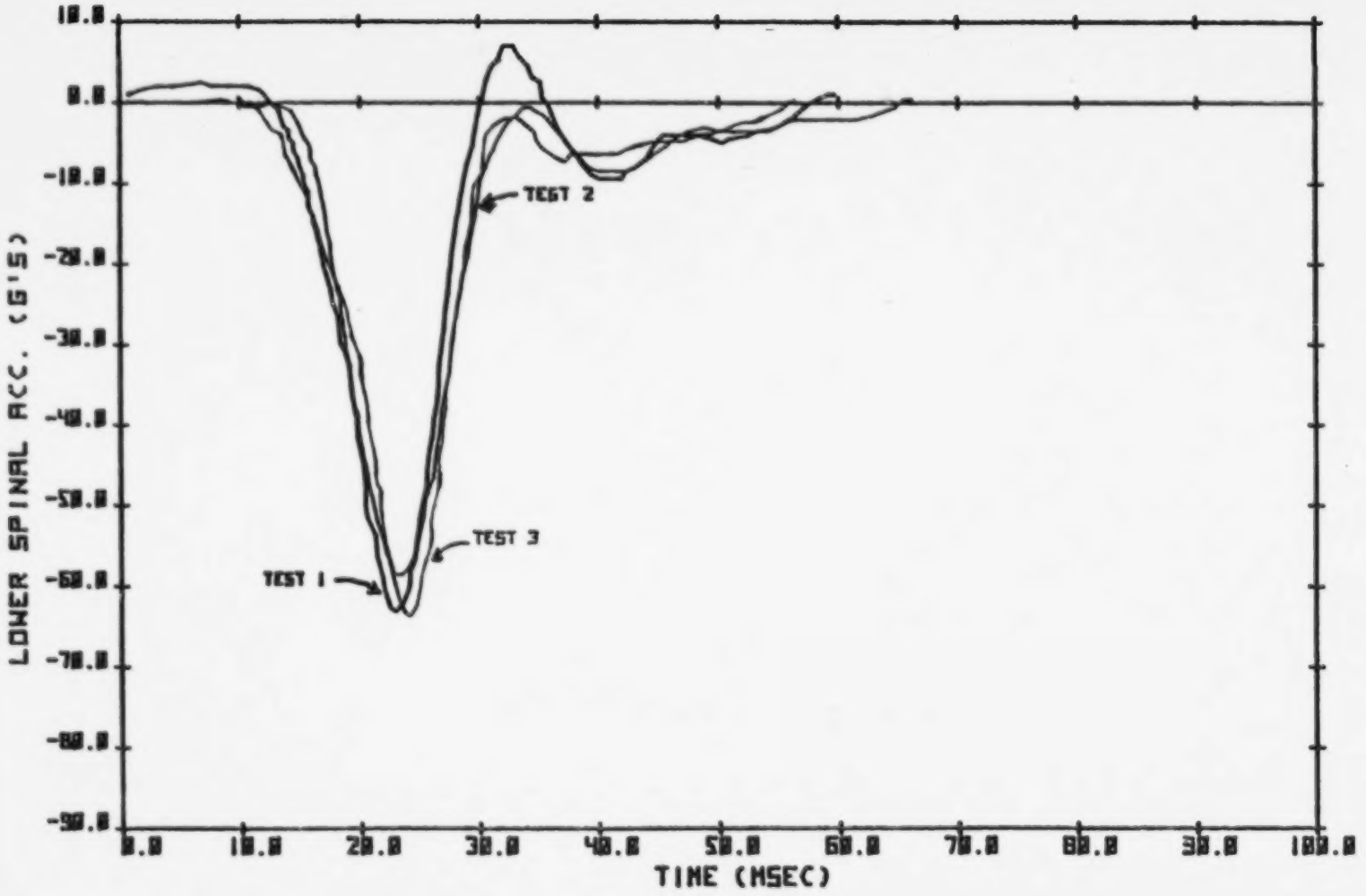

FIGURE 3-5

RIGID DROP TESTS (1 METER)

BEST DOCUMENT AVAILABLE

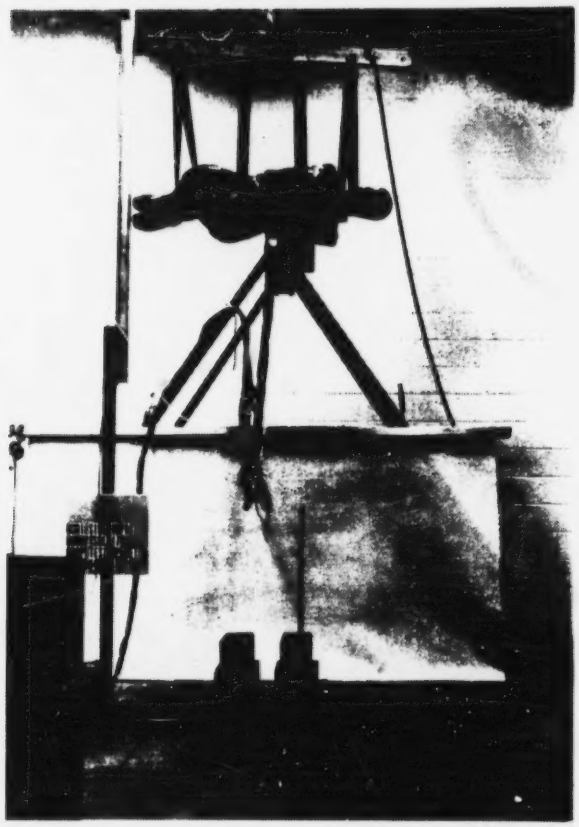

FIGURE J-6

Padding Drop Test Set-up

BEST DOCUMENT AVAILABLE

TABLE J-1

Tarriere Drop Test Results

Test No.	Test Cond'n	Upper Spine Accel'n (G's)	Lower Spine Accel'n (G's)	Left Upper Rib (G's)	Half Chest Deflection (in)	AIS (HSRI)"Q"	AIS (HSRI)"B"	Rib Fracture (Burgett)
1	1 meter Rigid Drop	22.6	62.8	55.4	1.51	2.32	2.15	US Accel - 3.52 LS Accel - 13.17
2	1 meter Rigid Drop	32.4	58.8	54.9	1.51	2.48	2.45	US Accel - 5.87 LS Accel - 12.21
3	1 meter Rigid Drop	26.5	63.5	55.8	1.71	2.6	2.44	US Accel - 4.46 LS Accel - 13.34
4	2 meter 5 1/2" Padding	31.2	36.9	39.3	1.94	2.07	3.10	US Accel - 5.59 LS Accel - 6.95
5	2 meter 5 1/2" Padding	26.5	30.9	21.7	-	1.89	3.35	US Accel - 4.46 LS Accel - 5.52
6	2 meter 5 1/2" Padding No Skin on Thorax	32.9	32.0	39.8	-	2.07	2.89	US Accel - 5.99 LS Accel - 5.78
7	2 meter 3" Padding	37.6	45.8	52.6	-	2.43	2.95	US Accel - 7.12 LS Accel - 9.09

BEST DOCUMENT AVAILABLE

Differences were noted between the displacement transducer readings and the displacements calculated from the rib and spinal accelerometers. The difference approached 0.5 inch for some tests (based on the left upper rib signal and the upper spine signal). When the geometric configuration of the dummy was taken into account (i.e., interpolating between the displacements of the upper and lower spine to find the displacement at the upper rib) the two methods agreed more closely. The upper spine accelerometer is 3.2 inches above the upper rib. The lower spine mount is 5.4 inches below the upper rib.

A method for determining the chest half deflection of the SID was developed based on the interpolation between the upper and lower spine distances. The interpolation was subtracted from the left upper rib displacement to obtain the chest deflection. Two other methods were tested, these being the differences between the left upper rib displacement and the upper spine displacement and the left upper rib displacement and the lower spine displacement. These three methods were then compared with the transducer readings for each of the three types of tests (pendulum, rigid drop and padded drop). Figure J-7 is the comparison between the three methods and the chest potentiometer for pendulum Test No. 2. Figure J-8 is the same comparison for drop Test No. 2 (1 meter rigid). Figure J-9 is the comparison for drop Test No. 4 (2 meters padded). It is apparent that the type of test performed has an effect on which method works best for determining the chest half deflection. It is therefore recommended that a displacement transducer be used in most test applications in addition to using integrals of the accelerometer signals.

[redacted]

[redacted]

BEST DOCUMENT AVAILABLE

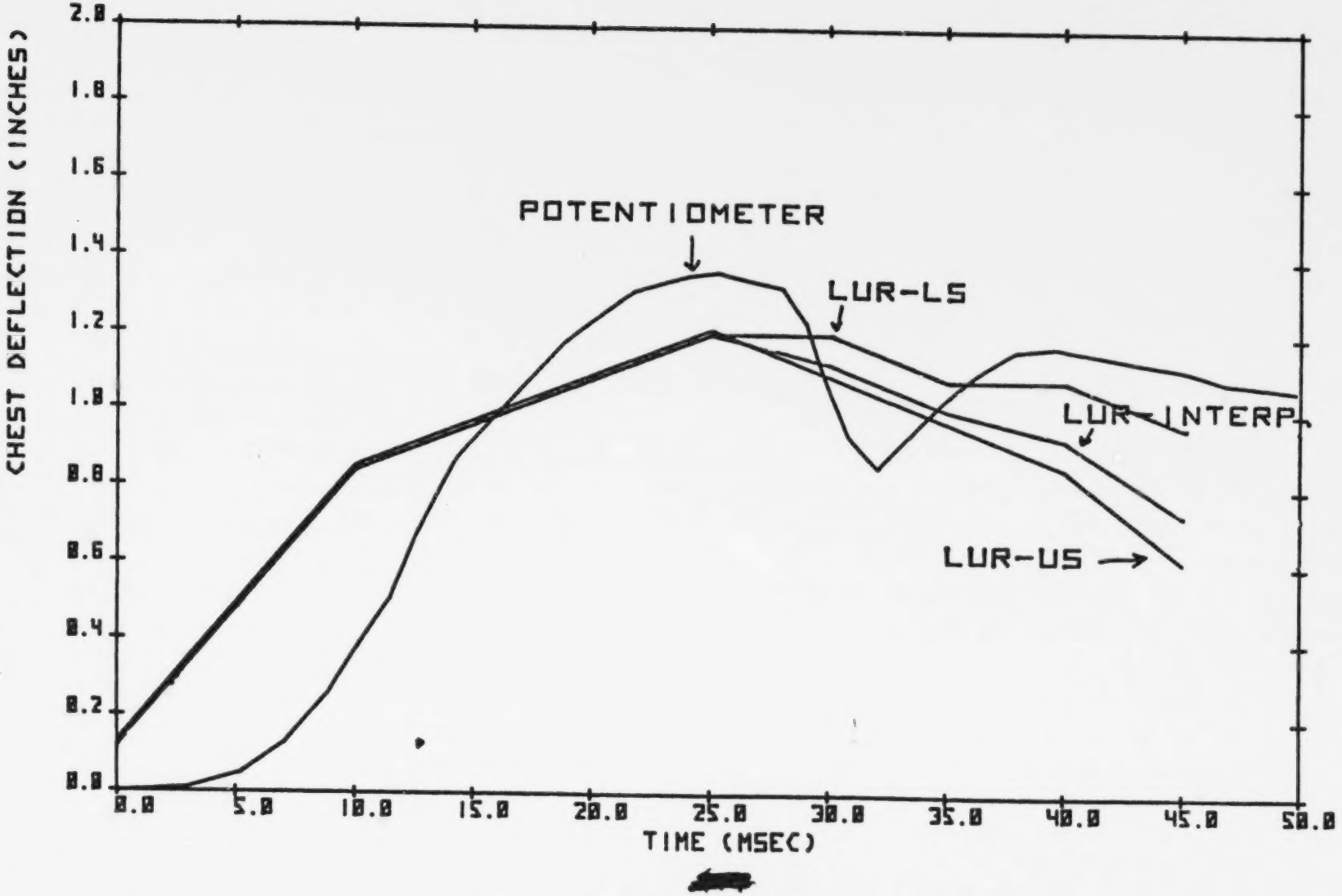

FIGURE J-7

CHEST DEFLECTION (PEND. #2)

BEST DOCUMENT AVAILABLE

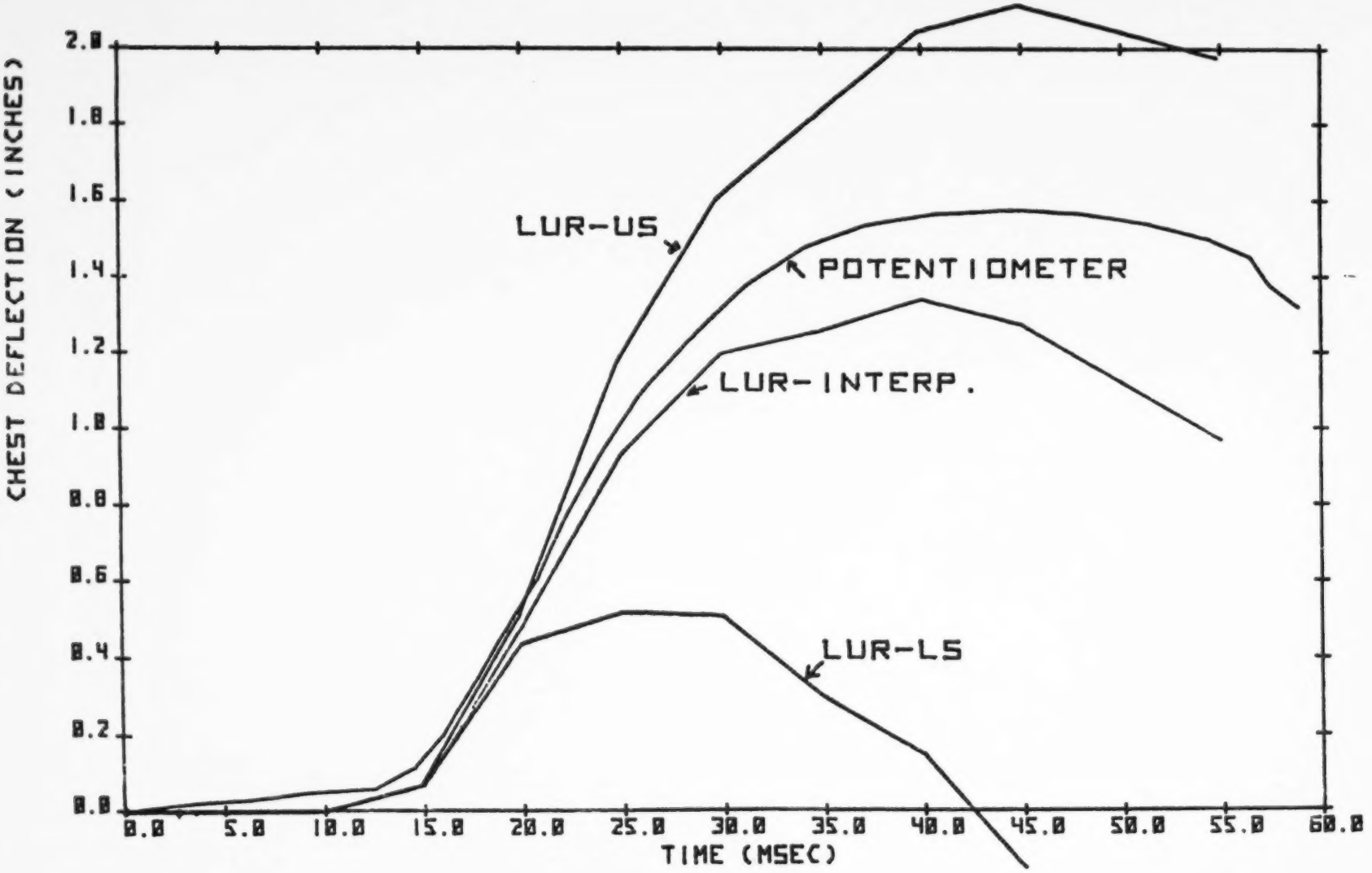

FIGURE J-8

CHEST DEFLECTION TEST #2

BEST DOCUMENT AVAILABLE

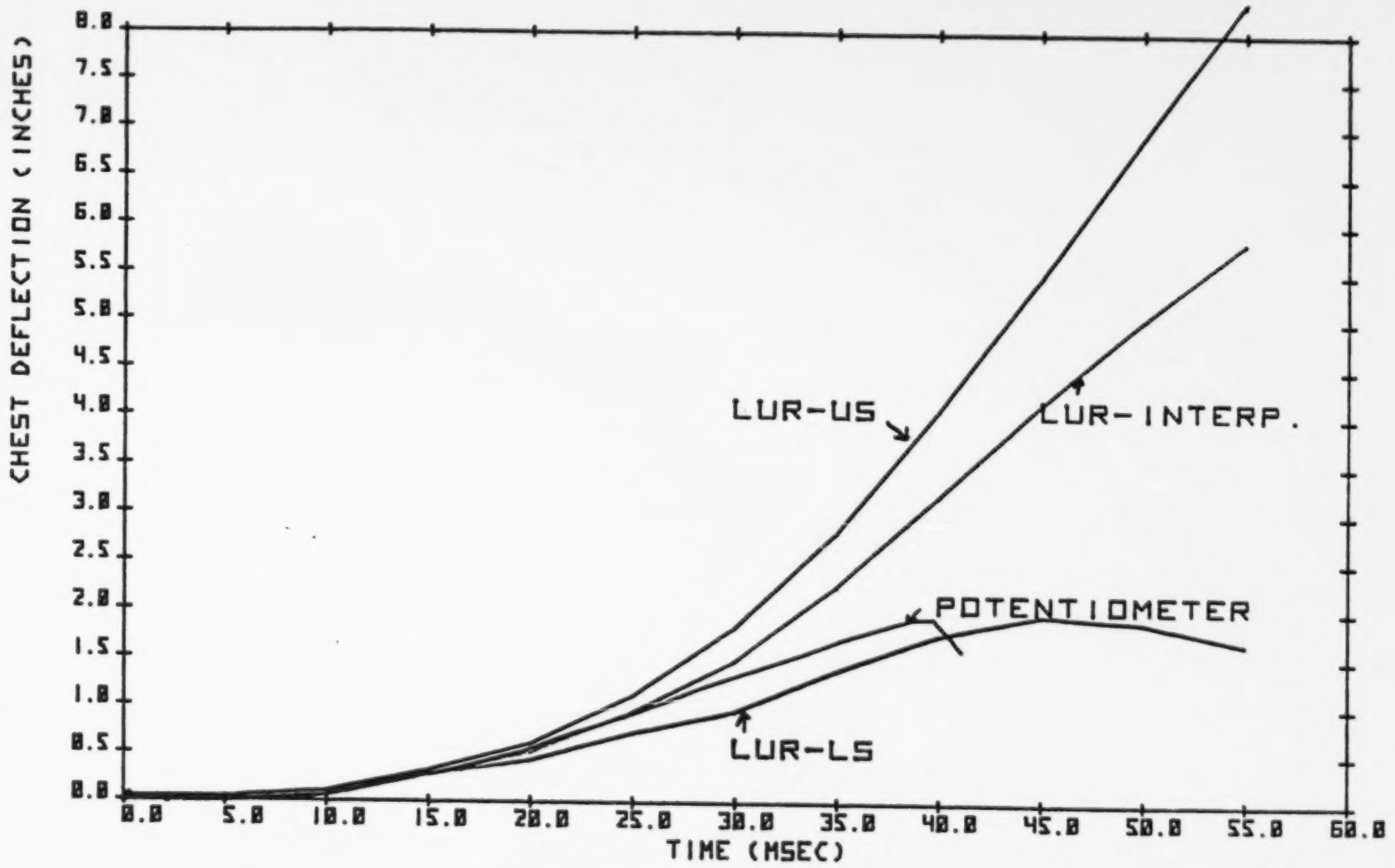

FIGURE J-9

CHEST DEFLECTION TEST #4